HELIOS FINAL REPORT

Nasa Contract NAS5-11279*

by

Roger R. Anderson

Approved for submission by:

Donald A. Gurnett
Principal Investigator

Dept. of Physics and Astronomy
The University of Iowa
Iowa City, IA 52242

Contract Time Period: February 12, 1969 to May 31, 1985

HELIOS FINAL REPORT

NASA Contract NAS5-11279

May 1986

INTRODUCTION

This document is the Final Report for the University of Iowa HELIOS Solar Wind Plasma Wave Experiment [E5a] supported under contract NAS5-11279 with Goddard Space Flight Center. This contract provided for the design, construction, testing, integration, and pre-launch activities of our instrumentation and the post-launch operations and data reduction and analysis activities. The objective of this experiment was the investigation of naturally occurring plasma instabilities and electrostatic and electromagnetic waves in the solar wind. To carry out this investigation, instrumentation consisting of a 16-channel spectrum analyzer connected to the electric field antennas, an antenna potential measurement system, a shock alarm system, and supporting electronics was designed, constructed, tested, and flown on the two HELIOS spacecraft. Five units were constructed under this contract: an engineering test model, a prototype, two flight units, and one flight spare unit. HELIOS 1 was launched on December 10, 1974, and HELIOS 2 was launched on January 15, 1976. The University of Iowa HELIOS Solar Wind Plasma Wave Experiments operated perfectly throughout the entire life of the mission which lasted much longer than the planned 18 months originally expected. The useful life of HELIOS 2 lasted until March 21, 1980 when an automatic switching of the onboard power system killed the travelling wave tube amplifier and severely damaged the spacecraft's data handling subsystem. HELIOS 2 was finally commanded off on January 8, 1981. HELIOS 1 continued to operate until March of 1986 when its command receiver failed.

As a part of this contract, we have acquired, processed, and analyzed much valuable data from our experiments during the 11+ years of HELIOS 1 and 4+ years of HELIOS 2. Below we will describe the scientific objectives of the HELIOS University of Iowa Solar Wind Plasma Wave Experiment, describe the instrumentation designed and constructed to meet these objectives, discuss the significant results obtained from the analysis of the data from this experiment, describe research in progress and future research, and discuss the major problems and anomalies encountered. Appendix A contains a copy of the technical description of the instrumentation and Appendix B contains a list of the scientific reports and publications resulting from this contract along with copies of those reports and publications.

SCIENTIFIC OBJECTIVES

The objective of the University of Iowa HELIOS Solar Wind Plasma Wave Experiment was the investigation of naturally occurring plasma instabilities and electrostatic and electromagnetic waves in the solar wind. In the solar wind a wide variety of electromagnetic and electrostatic wave phenomena can be expected in the frequency range from a few tens of Hz to several hundred kHz. These phenomena include Type III solar radio noise bursts and associated longitudinal electrostatic waves down to the solar wind plasma frequency (from about 20 kHz at 1 AU to 100 kHz at 0.3 AU), intense (30 mV/m) electrostatic electron plasma oscillations of the type observed with the Pioneer 8 spacecraft, electrostatic waves associated with interplanetary shock waves and solar particle emissions, whistler-mode instabilities related to anisotropic solar wind electron distributions ($T_{\parallel}/T_{\perp} > 1$), and electrostatic ion sound waves. Characteristic frequencies at which emissions or cutoffs might be expected include the upper and lower hybrid resonances, the electron and proton plasma frequencies, and the electron and proton gyrofrequencies.

Wave-particle interactions can lead to many important effects in the solar wind. Of particular interest on the HELIOS mission is the investigation of instabilities which make the solar wind behave like a fluid. If the solar wind had no collective effects, the ratio $T_{\parallel}/T_{\perp}$ for the protons would be 100 to 1 or more at the Earth, contrary to observation. It is generally believed that a plasma instability, possibly the whistler-mode, alters the proton pitch-angle distribution. Because of the large radial variation in the solar wind properties (density, magnetic field, $T_{\parallel}/T_{\perp}$, etc.) from the Earth to 0.3 AU, the stability criteria and wave phenomena occurring in the solar wind at 0.3 AU may be quite different compared to near the Earth. The spatial distribution of instabilities may influence the propagation of solar and galactic cosmic rays, slowing down times for super thermal particles can be drastically modified, waves generated in shocks can carry energy and momentum away from the shock region, and many more examples can be cited. Also of great importance is the direct observation of the electron plasma oscillations which are believed to give rise to Type III solar radio bursts through non-linear effects.

INSTRUMENTATION

The University of Iowa HELIOS Solar Wind Plasma Wave Experiment [E5a] was jointly planned with the University of Minnesota [P. Kellogg, E5b] and Goddard Space Flight Center [R. Weber and R. Stone, E5c] so that the combined experiments would provide complementary measurements. The frequency range of our experiment (E5a) and the University of Minnesota experiment (E5b), nominally 20 Hz to 200 kHz, was chosen to include most of the characteristic frequencies for plasma waves in the solar wind mentioned above. The upper frequency limit (200 kHz) is approximately the maximum electron plasma frequency expected and was also chosen to provide some overlapping frequency

coverage with the Goddard Space Flight Center HELIOS Radio Astronomy Experiment (E5c) frequency range (26 kHz to 3 MHz). The lower frequency limit for the plasma wave experiments (20 Hz) was influenced by the large spacecraft spin rate (1 rotation per second). Since strong electric field signals are expected at harmonics of the spacecraft spin rate due to the assymmetrical photoelectron sheath around the spacecraft, the lower frequency limit of the experiment has been chosen to be well above the frequencies of the expected spin rate interference. Although the University of Iowa and the University of Minnesota experiments cover the same frequency range, the two experiments are complementary but not redundant. The University of Iowa experiment was designed for high temporal resolution while the University of Minnesota experiment was designed for high frequency resolution. Past experience with plasma wave data from the Alouette, OGO, Injun, and IMP satellites has shown that it is very important to have both electric and magnetic field measurements so that electromagnetic and electrostatic waves can be distinguished. It is expected, therefore, that the AC electric field measurements provided by the plasma wave experiments and the AC magnetic field measurements provided by the HELIOS Search Coil Magnetometer Experiment [F. Neubauer, E4] will provide complementary data for the identification and understanding of certain phenomena.

The sensor for the University of Iowa HELIOS Solar Wind Plasma Wave Experiment is the HELIOS electric field/radio astronomy antenna. The electric field antenna and the associated erection mechanism were provided by the spacecraft. The antenna is an extendible cylindrical dipole 32 meters tip-to-tip, similar to antennas used on the Alouette, OGO, IMP, and RAE satellites. In order to reduce the capacitance between the antenna and the spacecraft photo-electron sheath to an acceptable level, an insulating sleeve approximately 2.0 meters long was placed over the antenna where the antenna passes through the spacecraft photo-electron sheath region. The antenna diameter was as small as possible (0.25 inch) in order to minimize the ratio of resistive-to-capacitive coupling to the surrounding plasma. The erection mechanism was designed to minimize the antenna to erection mechanism capacitance. This capacitance does not exceed approximately 30 pf in the extended configuration. Also, special consideration was given to electrostatically shielding the antenna from spacecraft related interference, such as through the erection mechanism, deployment length indicators, etc. Each element of the electric dipole was connected to three preamplifiers which provided signals to the respective University of Iowa, University of Minnesota, and Goddard Space Flight Center experiments. The University of Iowa constructed the housing for the two sets of three preamplifiers and the University of Iowa preamplifiers themselves. The housing for each set of preamplifiers measured 4.4" by 7.4" by 1.5". The total weight for each set of preampifiers was 0.45 kg.

The main elements of the University of Iowa HELIOS Solar Wind Plasma Wave Experiment consist of (1) a differential amplifier, (2) a 16-channel spectrum analyzer, (3) an antenna potential monitor, (4) a shock alarm, and (5) a power supply. These elements are all packaged inside a main electronics box of dimensions 8.4" by 9.7" by 4.3" which weighed 2.44 kg. Details of these experiment elements, the Data Processing Unit (DPU), and the shock memory will be discussed below. We will also describe the commands and the analog and digital housekeeping data and engineering parameters pertinent to our experiment.

The differential amplifier provides AC signals proportional to the potential difference between the antenna elements to the measurement electronics. It provides a high order of common mode rejection to reduce the response to interference signals present on both antenna elements. The differential amplifier is followed by a narrow band notch filter which provides approximately 30 dB of attenuation at frequencies of 20 kHz, 40 kHz, and 60 kHz (harmonics of the power supply frequency).

The 16-channel spectrum analyzer is the basic element of the University of Iowa experiment. This analyzer provides relatively coarse frequency coverage and rapid temporal resolution with essentially continuous coverage of all frequencies (20 Hz to 200 kHz) and all times (using peak detectors). The lowest eight frequency channels (31.1 Hz to 1.78 kHz) use active filters spaced with four filters per decade of frequency and have sine-wave bandwidths approximately ± 19% of their center frequencies. The highest eight frequency channels (3.11 kHz to 178 kHz) use passive filters spaced with four filters per decade of frequency and have sine-wave bandwidths approximately ±11% of their center frequencies. A detector and log compressor in each channel rectifies and logarithmically compresses signals from the filter and produces an output DC voltage approximately proportional to the logarithm of the signal intensity in each filter channel. The dynamic range of the compressors extends from 10 μV to 1V RMS. The log compressors provide three outputs each: (1) a peak output, (2) an average output, and (3) a short time constant shock output. The peak output provides a DC voltage (0.00 to 5.10 Volts) proportional to the logarithm of the peak signal observed since the preceding reading. The peak detector is reset after readout by a signal from the DPU. The average output provides an RC average output with either (1) a time constant τ which depends on the bit rate and science format mode or (2) a forced short time constant, τ_s,. Which time constant is used is determined by the shock alarm channel number. The forced short time constant for the average output is selected when Bit 0 of the shock alarm channel number is commanded to level "1". The short time constant shock outputs provide short-time-constant determinations of the logarithms of the field strengths to the shock mode memory. One channel of short time constant outputs (called the rapid sample output) is continuously available in the normal science data. The channel selected for this rapid sampling is determined by the shock alarm channel number. The output from this channel is sampled 16 times in one spacecraft rotation by the DPU and stored for later readout. On HELIOS 1 the selected channel was equal to the shock alarm channel number. On HELIOS 2 provisions were made to sequentially step through all 16 channels in 16 consecutive readout periods when Bit 1 of the shock alarm channel number was commanded to level "1". A Shadow Blanking Pulse was provided by the DPU to the experiment to open the input to the eight lowest frequency compressors for one eighth of a spin period twice per rotation to reduce the effects of large voltage pulses generated as the antenna sweeps through the spacecraft shadow. This blanking pulse could be eliminated by command.

The average potential, V_{avg}, and the difference potential, V_{diff}, between the antenna elements are measured with operational amplifiers in the main electronics package. The frequency range of the V_{diff} measurement is from 0.2 to 10.0 Hz. The dynamic range of the V_{diff} measurement can be controlled by command to be either ±8.0, ±2.0, ±0.5, or ±0.125 Volts. The dynamic range of the V_{avg} measurement is ±20.00 Volts. These data are needed for a complete understanding of the antenna operation in the plasma surrounding the spacecraft.

A shock alarm signal is to be sent to the spacecraft when the plasma wave experiment senses electric field noise associated with an interplanetary shock wave or other transient events. The shock alarm circuit permits the selection of any one of the 16 spectrum analyzer channels, by command, for shock identification. The threshold field strength required to trigger the shock alarm has 16 levels and is controlled by a four bit binary counter. The shock threshold level, which we call Shock Value E, is reset whenever any shock channel command is received. After reset, the threshold is advanced upward every time the threshold is exceeded. In each case the new threshold level is set to the peak value of the electric field strength observed. This procedure, therefore, results in the storage of the "best" event observed over the shock search interval. Inhibit lines from E5b and E5c prevent the threshold from advancing while the E5b impedance measurement is on or while E5c is calibrating. The shock level value is available on two outputs. The first is a four bit parallel binary word sent to the DPU. The DPU sends this value and other data to the spacecraft data handling system as serial words. The shock level value is also sent in the form of a single analog voltage (0.00 to 5.10 Volts) directly to the spacecraft as an engineering parameter. The higher voltages represent higher values of the shock level. This line was included as a backup to provide some useful data via the engineering subsystem if there were ever a major failure in the science data handling subsystem.

The experiment power supply provides regulated voltages of ±6 Volts and ±12 Volts to the experiment electronics. The power supply operates at a frequency of 20 kHz and is synchronized by a 40 kHz synchronization signal provided by the spacecraft. The total power consumed by our main electronics package and our two preamps is 2.66 Watts at a nominal input voltage of 28 Volts.

The Data Processing Unit (DPU) for the Plasma Wave Experiment is separate from the main experiment electronics and was provided by Goddard Space Flight Center through an industrial contractor. The purpose of the DPU is to (1) provide interface connections between the experiment and the spacecraft, (2) provide A/D conversion of all scientific analog data, and (3) provide buffer storage, as necessary, to adapt to the spacecraft data transmission format. Experiment E5a has 50 analog output lines which must be sampled by the DPU. These lines are the 16 spectrum analyzer peak outputs, the 16 spectrum analyzer average outputs, the 16 short time constant shock outputs, the rapid sample output, and the V_{diff} output. For real time data transmission of the normal science data these outputs

are sampled in a basic data block consisting of 16 6-bit Peak samples, 16 6-bit Average samples, and 8 8-bit V_{diff} or Rapid Sample samples. The 16 Peak spectrum analyzer outputs are sampled simultaneously to within 0.25 seconds. The 16 Average spectrum analyzer outputs are also sampled simultaneously to within 0.25 seconds, but these Average samples are taken at a different time than the Peak samples. The Peak and Average sampling of a given channel are equally spaced in time between successive data blocks. The DPU A/D converter converts these samples into digital words and stores them in a buffer storage for later transfer to the spacecraft telemetry. The DPU also provides a signal to our experiment which resets the Peak detectors immediately after the 16 Peak samples are obtained. 16 V_{diff} or Rapid Sample samples are acquired at 16 equally spaced angles covering one complete spin. Two consecutive data blocks are required to transmit either the complete 16 V_{diff} or 16 Rapid Sample samples. The spin synchronized sampling alternates between V_{diff} and Rapid Sample in each two consecutive data blocks. The time required to transmit each basic data block is determined by the spacecraft bit rate and telemetry format. It varies from 1.125 seconds to 576 seconds.

Sampling of data for shock mode storage occurs concurrently with the real time data sampling described above. When a shock or other large transient event occurs, data from both before and after the shock are stored in the spacecraft shock mode memory for later readout. Our experiment has 17 analog output lines which are sampled by the DPU for the shock mode memory read-in. They are the 16 short time constant shock outputs and V_{diff}. For the shock mode data transfer these outputs are sampled in a basic data block consisting of 16 6-bit short time constant spectrum analyzer samples and four 8-bit V_{diff} samples. The sampling rate for the 16 short time constant spectrum analyzer samples is such that all the samples occur within the time to transmit each basic data block. The times to transmit a basic data block are 0.281 seconds, 0.141 seconds, and 0.070 seconds, respectively, for the three shock mode memory read-in bit rates. The V_{diff} samples are equally spaced in time, both within a basic data block and between successive data blocks. Thus the time between V_{diff} samples is one quarter the basic data block transmission times just listed above. Spin synchronized sampling of the V_{diff} data is not used in the shock data because the sampling rates obtained in the shock mode data are sufficiently high to permit direct real time resolution of spin effects.

The onboard shock mode memory contained on each HELIOS spacecraft has a capcity of 2^{19} (524,288) bits. Each shock mode data block consists of 1152 bits acquired from the shock mode experiments (the magnetic field experiments, E2 and E3, the search coil magnetometer experiment, E4, and the plasma wave experiments, E5a and E5b) plus relevant spacecraft and engineering data. 1120 bits from each block (the 32-bit synchronization word is not stored) are stored in the memory which can hold 468 full blocks. The memory is divided into three parts, A, B, and C. Parts A and B each hold 108 blocks while part C holds 252 blocks. Read-in rates to the memory are 4096 bps, 8192 bps, and 16,384 bps. Thus the times to transmit each 1152-bit block are 0.281 seconds, 0.141 seconds, and 0.070 seconds, respectively, for the three bit rates. The shock mode data are read

continuously into either part A or part B of the memory which are cyclic. Once the part is filled, new data are written over beginning at the beginning of that memory part. When a shock alarm signal is received from either E2 or E5a (the choice is determined by a spacecraft command) the data are immediately routed to part C of the memory which is filled just once. From then on until another shock alarm signal is received, the shock mode data are read into either part B or part A, whichever one was not being used just before. The above shock mode memory read-in processes continue until commanded to stop. Then the shock mode memory data are transmitted to the ground. Data from part C of the memory are data immediately following the last shock alarm triggering and the data from either part A or part B are the data immediately preceding the last shock alarm triggering. The remaining part of memory data (either part B or part A) contains the data acquired just before the memory was commanded to stop read-in. The time periods covered by the data in part C of the memory are 70.9 seconds, 35.4 seconds, and 17.7 seconds, respectively, for the three shock memory read-in rates. The time periods covered by the data in part A and part B of the memory are 30.4 seconds each, 15.2 seconds each , and 7.6 seconds each, respectively, for the three shock memory read-in rates.

The University of Iowa HELIOS Solar Wind Plasma Wave Experiment has five Shock Alarm Channel Number commands, three V_{diff} Gain commands, and a Shadow Blanking Override command. Command 006 resets all four bits of the Shock Alarm Channel Number to level "0" and turns off the Shadow Blanking Override Command. Command 371 sets Bit 0 of the Shock Alarm Channel Number to level "1" and also sets the average output of the spectrum analyzers to the forced short time constant. Command 027 sets Bit 1 of the Shock Alarm Channel Number to level "1" and on HELIOS 2 causes the Rapid Sample electronics to sequentially step through all 16 channels. Command 350 sets Bit 2 of the Shock Alarm Channel Number to level "1". Command 216 sets Bit 3 of the Shock Alarm Channel Number to level "1". Each of these five commands also resets the Shock Value E to zero. Because the noise level amplitude in each channel is sufficient to raise the Shock Value E one step above zero, the Shock Value E will immediately jump at least one step above zero unless it is inhibited. Thus these commands can be used to generate an artificial shock for a shock mode memory read-in if E5a is controlling the triggering of the shock mode memory (spacecraft command 275) and if E5a is not being inhibited by E5b or E5c during their calibrations.

Command 161 resets both V_{diff} Gain bits to level "0". Command 237 resets V_{diff} Gain bit 0 to level "1". Command 140 resets V_{diff} Gain bit 1 to level "1". V_{diff} Gain = 0 is the least sensitive gain setting and covers the range from -8 Volts to +8 Volts. The V_{diff} output is linearly proportional to the input but it has a DC offset such that 0 Volts in equals 2.50 Volts out. Since the 8-bit V_{diff} output has a conversion ratio of one data number per 20 millivolts, the data number corresponding to 0 Volts in is 125. Each higher gain step is four times more sensitive than the gain step below it.

Command 223, the Shadow Blanking Override command, removes the shadow blanking of the lowest eight spectrum analyzer channels discussed earlier in the spectrum analyzer section.

The University of Iowa HELIOS Solar Wind Plasma Wave Experiment has three Analog Housekeeping words and one Digital Housekeeping word in the engineering data transmitted along with the normal science formats plus one Digital Housekeeping word stored in every block of the shock mode memory data.

The three Analog Housekeeping parameters are the Shock Value E, the Low Voltage Power Supply Monitor, and the Antenna Average Potential. The Shock Value E (SHOC-E) is found in Subcom Channel B-040. This parameter is an analog voltage proportional to the logarithm of the peak intensity measured by the selected shock channel since reset. The Low Voltage Power Supply Monitor (LVPSM) is found in Subcom Channel C-038. This parameter is an analog voltage equal to 2/3 of the regulated +6 Volt power supply line in the experiment. The Antenna Average Potential (V-AVG) is found in Subcom Channel C-039. This parameter is an analog voltage proportional to the average antenna potential, but it has a DC offset such that 0 Volts in equals 2.50 Volts out (Data number = 125). It measures the antenna potential from -20 Volts to +20 Volts.

The Digital Housekeeping word, given the designation DSEDB4, is found in Subcom Channel B-009. Bit 1 of this word is equal to Shock Alarm Channel Number Bit 3. Bit 2 of this word is equal to Shock Alarm Channel Number Bit 2. Bit 3 of this word is equal to Shock Alarm Channel Number Bit 1. Bit 4 of this word is equal to Shock Alarm Channel Number Bit 0. Bit 5 of this word is equal to V_{diff} Gain Bit 1. Bit 6 of this word is equal to V_{diff} Gain Bit 0. Bit 7 of this word is a logical "1" if the Shadow Blanking Override is on or if the E5a shock alarm triggering is inhibited by E5b or E5c.

The Digital Housekeeping word (designated 5E) in the shock mode memory data blocks contains the binary representations of the Shock Alarm Channel Number and the Shock Value E. The Shock Alarm Channel Number is given by bits 0-3 of 5E. Bits 0-3 of 5E are equivalent to bits 3-0 of the Shock Alarm Channel Number. The binary representation of the Shock Value E are given by bits 4-7 of 5E. Bits 4-7 of 5E are equivalent to bits 3-0 of the binary representation of the Shock Value E.

SIGNIFICANT RESULTS

Many significant advances in the study of plasma waves in the solar wind have been made with data from the University of Iowa Plasma Wave Experiments on HELIOS 1 and 2. The first observations of intense electron plasma oscillations associated with Type III solar radio bursts were made with data from these instruments. These observations confirmed the basic electron plasma oscillation mechanism proposed by Ginzburg and Zheleznyakov in 1958 for the generation of the Type III solar radio emissions. A study of electron plasma oscillation events associated with Type III solar radio bursts, using data from HELIOS 1 and 2, IMP 6 and 8, and Voyager 1 and 2, found that these events showed a pronounced increase in both intensity and frequency of occurrence with decreasing heliocentric radial distance. Only the HELIOS spacecraft, with their close approaches to the sun (about 0.3 AU perehelion) have been able to provide in situ measurements of these events in the region of their highest occurrence.

The Type III solar radio burst itself has been studied extensively using data from the HELIOS spacecraft. Stereoscopic radio direction-finding measurements from the HELIOS 1 and 2, IMP 8, and Hawkeye 1 spacecraft were used to track a Type III solar radio burst in three dimensions, independent of modeling assumptions concerning the emission frequency as a function of radial distance from the Sun. By combining these radio direction-finding measurements with direct in situ measurements of the solar wind plasma density near the Sun, it was found that the dominant emission occurs at the second harmonic, $2f_p$, of the electron plasma frequency. The results of this study confirmed earlier results by other investigations which had to rely on assumed models for the radial dependence of the emission frequency or on average statistical properties of the solar wind.

Further work has also been done on the association of Type III solar radio bursts and electron plasma oscillations in order to provide important new information on nonlinear plasma processes of considerable current interest. A study of the volume emissivity of Type III solar radio bursts showed that although the emissivities varied over a large range, all the emissivities decreased rapidly with increasing heliocentric radial distance. The best fit power law for the events analyzed found the emissivity, J, proportional to $R^{-6.0\pm0.3}$. When the observed electron plasma oscillation intensitites and variation with radial distance (E was proportional to $R^{-1.4\pm0.5}$) were used in two current models for the conversion of electrostatic plasma oscillations to electromagnetic radiation, the observed emissivities were shown to be in good agreement with the predicted emissivities.

The most commonly observed plasma wave detected by HELIOS is a sporadic emission between the electron and ion plasma frequencies. These waves are thought to be ion acoustic waves which are Doppler-shifted upwards in frequency from below the ion plasma frequency by the motion of the solar wind. Wavelength measurements fron IMP 6 support this conclusion. Comparison of HELIOS results with measurements from this Earth-orbiting spacecraft show that the ion acoustic wave turbulence detected in interplanetary space has characteristics essentially identical to those bursts of electrostatic turbulence generated by protons streaming into the solar wind from the Earth's bow shock. In a few cases, ion acoustic wave enhancements have been observed in direct association with abrupt increases in the anisotropy of the solar wind electron distribution. Comparisons with the overall solar wind corotational structure show that the most intense ion acoustic waves usually occur in the low-velocity regions ahead of high-speed solar wind streams. Of the detailed plasma parameters investigated, the ion acoustic wave intensities are found to be most closely correlated with the electron-to-proton temperature ratio, T_e/T_p, and with the electron heat flux. Investigations of the the detailed electron and proton distribution functions also show that the ion acoustic waves usually occur in regions with highly non-Maxwellian distributions characteristic of double-proton streams. Two main mechanisms, an electron heat flux instability and a double-ion beam instability, have been extensively studied as possible generation mechanisms for the ion-acoustic-like waves observed in the solar wind. More recently the electrostatic lower hybrid instability has been studied as a possible generation mechanism when T_e/T_p is near one. The possible macroscopic consequences of the solar wind ion acoustic waves detected by HELIOS is uncertain. It has been suggested that ion acoustic waves in the solar wind could have important consequences for controlling heat conduction in the solar wind. However, the ion acoustic waves detected by HELIOS are usually very weak. The ratio of the electric field energy density to the plasma energy density, $E^2/8\pi nkT$, is only about 10^{-5} to 10^{-7} during intense bursts, and much smaller on the average. Whether such low intensities can have significant macroscopic effects on the solar wind still needs to be explored in more detail.

Plasma wave turbulence associated with interplanetary shocks has also been studied using the HELIOS plasma wave data. Three types of plasma waves are usually detected in association with a strong interplanetary shock: (1) electron plasma oscillations, (2) electrostatic ion-acoustic or Buneman mode turbulence from about 1 to 30 kHz, and (3) whistler-mode electromagnetic noise. The primary burst of electric and magnetic field noise at the shock occurs a few seconds after the jump in the magnetic field, with a broad maximum in the electric field intensitites at a few kHz and a monotonically decreasing magnetic field spectrum below about 1 kHz. Many of the characteristics of strong interplanetary shocks are found to be closely similar to previous observations of plasma wave turbulence associated with the Earth's bow shock.

RESEARCH IN PROGRESS AND FUTURE RESEARCH

The University of Iowa Plasma Wave Experiments on HELIOS 1 and 2 operated satisfactorily for the entire lives of the HELIOS spacecraft and have provided us with much valuable data that is still important to space physics researchers. HELIOS 1 operated for an entire 11 year solar cycle and HELIOS 2 operated from about solar minimum until solar maximum. As the HELIOS mission approached solar maximum, the number of solar radio bursts and interplanetary shock waves detected increased dramatically. This increase in activity provided many valuable opportunities for correlative studies with ISEE 1, 2, and 3 and IMP 8 to provide triangulation measurements of Type III solar radio bursts and other plasma wave events. Current research efforts are concentrating on the study of plasma waves associated with interplanetary shocks using a large number of events to investigate the dependence of the plasma wave intensities on the Mach number, magnetic field direction, and shock normal angle. Other studies of electron plasma oscillations associated with Type III solar radio bursts and electron plasma oscillations and ion acoustic waves in the solar wind are continuing. We have produced 24-hour survey plots of all of our HELIOS 1 and 2 plasma wave data and have submitted microfilm copies of them to the National Space Science Data Center. In support of our current research efforts we have produced and will continue to produce expanded time-scale plots for ourselves and for a number of colleagues including Professor H. Kikuchi (Nihon University and Max Planck Institut fur Aeronomie, Lindau), Professor F. M. Neubauer (University of Cologne), Drs. E. Marsch and A. Richter (Max Planck Institut fur Aeronomie, Lindau), and Dr. C. Dum (Max Planck Institut fur extraterrestrische Physik, Garching).

We have not been able to pursue new research topics using the HELIOS data to the extent that we would have liked because of the limited amount of funds that have been available for HELIOS data reduction and analysis in the past several years. Since the beginning of FY82, we have been funded at an average rate of about $13,000 per year. This funding has been adequate only to carry out the necessary HELIOS computer processing for the generation of the survey plots, to do a minimal amount of data analysis in support of the research topics listed above, and to provide special processing upon request to other HELIOS investigators.

MAJOR PROBLEMS AND ANOMALIES ENCOUNTERED

Shortly after the launch of HELIOS 1 it was discovered that one of the two antenna elements which make up the electric dipole antenna did not extend properly and was electrically shorted to the spacecraft structure. The resulting antenna configuration was therefore an electric monopole, the spacecraft body and associated booms acting as a ground plane. Although this was not the intended antenna configuration, the effects of this failure were not particularly serious. Monopole antennas of this type have been successfully used on several previous spacecraft plasma wave and radio wave experiments. The primary detrimental effects for the HELIOS 1 Plasma Wave Experiment were a loss of 6 dB in the electric field sensitivity because of the shorter antenna length and an increase in the noise level of the 178 kHz channel by about 25 dB because of an interference signal conducted into the experiment from the shorted antenna. It was also thought that the reduced common mode rejection caused by the asymmetrical antenna configuration would result in larger interference levels, particularly from the spacecraft solar array. However, comparisons with the HELIOS 2 spacecraft, for which both antennas extended properly, showed that the background noise voltages were essentially the same in all except the 178 kHz channel. One disadvantage of a monopole antenna is that the effective length cannot be estimated as well as for a dipole antenna because of the complicated geometry of the spacecraft body. To calculate electric field strengths from the HELIOS 1 data, we assumed that the spacecraft body acted as a perfect ground plane, in which case the effective length is one half of the length of the monopole element, or $l_{eff} = 8.0$ meters. The assumption is justified mainly on the grounds that the spacecraft body and associated booms have a rather large capacitance to the surrounding plasma which should maintain the spacecraft potential essentially constant with respect to the local plasma potential. At higher frequencies, above the electron plasma frequency where plasma effects are not important, the effective length is probably somewhat smaller, by about 15-20%, because of the finite size of the ground plane. Because of the large range of electric field strengths encountered in the solar wind, uncertainties of this magnitude are not considered serious. The calculated electric field strengths also rely on the assumption that the wavelengths are longer than the antenna length. In most cases, specific tests based on spin modulation measurements of the antenna pattern and Doppler shift estimates can be performed to verify this assumption. The power flux for auroral kilometric radiation and electric field strengths for electron plasma oscillations observed by HELIOS 1 as it passed through the Earth's bow shock were in good quantitative agreement with previous similar measurements from the IMP 6 and 8 spacecraft. This showed that the assumptions regarding the effective antenna length were reasonable.

Below 1 kHz, the noise levels on HELIOS 1 and 2 were noticeably higher than what we had found on IMP 6 and 8. The rapid increase in the HELIOS noise levels below 1 kHz is caused by interference from the solar array. Because of the spacecraft rotation, large voltage transients, as

large as 70 Volts, occur as the solar panels rotate into and out of the sunlight. These voltage transients are coupled to the antenna through the plasma sheath surrounding the spacecraft and produce strong interference over a very broad range of frequencies. This same type of interference also occurs at low frequencies in the IMP 6 and 8 electric field measurements but is more intense on HELIOS 1 and 2 because of the higher spin rate (1.0 rps) in comparison to the spin rates of IMP 6 and 8 (0.083 and 0.4 rps).

The sensitivity of the HELIOS 1 instrument was about a factor of two poorer than that of the HELIOS 2 instrument at all frequencies (except at 178 kHz where it was a factor of 16 poorer) due to the factor of two difference in antenna lengths. The sensitivities of both HELIOS instruments were poorer at all frequencies than the IMP 6 and 8 sensitivities mainly due to the fact the IMP spacecraft had longer antennas. The effective antenna lengths on HELIOS 1 and 2 were 8.0 and 16.0 meters, respectively, while the effective antenna lengths on IMP 6 and 8 were 46.2 and 60.9 meters, respectively. Since during much of the time, especially during solar minimum, many of the receiver channels remained near their noise levels, it would certainly have been desireable to have had longer antennas on HELIOS.

A highly unusual and unexpected interference problem was encountered on HELIOS 1 when the S band telemetry signal was switched from the medium gain to high gain telemetry antenna about 10 days after launch. When the telemetry transmitter was switched to the high gain antenna, a very intense broadband interference occurred, with an increase in noise level of nearly 50 dB in some channels. This interference was also accompanied by a number of other dramatic effects indicating a major disturbance in the plasma around the spacecraft, the most notable being a large increase in the $E \simeq 100$ eV electron flux detected by the solar wind plasma experiment and a charging of the electric antenna element to -30 to -40 Volts with respect to the spacecraft structure. Subsequent investigations of these effects have led to the conclusion that the interference and electron heating are caused by a multipacting breakdown of the high gain antenna feed. This breakdown is essentially a transit time resonance for electrons accelerated across the gap in the antenna feed and occurs when the secondary emission coefficient is sufficiently large to cause a rapid buildup of electron density in the gap. Since the resonance condition is highly sensitive to gap spacing, the antenna feed on HELIOS 2 was redesigned with a larger gap spacing to eliminate this problem. As a result of this modification, no similar interference problems were observed on HELIOS 2. Because of the multipacting problem with the high gain antenna, useful plasma wave data could initially be obtained only by using the medium gain antenna. Since operation with the medium gain antenna resulted in a significant bit rate penalty to the other experiments, this mode of operations was quite limited, usually consisting of only a few 8-hour passes per week. Fortunately, shortly after the first perehelion passage, the multipacting interference completely disappeared, and it has not reappeared except for a short

period during the second perehelion passage. The disappearance of the multipacting breakdown is not understood in detail but is generally thought to be caused by modifications of the surface properties (secondary electron coefficient) of the high gain antenna feed due to the high temperatures encountered near perehelion or to the wearing down of sharp edges on the feed by the continuous bombardment of electrons.

ACKNOWLEDGEMENTS

We are extremely grateful to the many individuals and groups at Goddard Space Flight Center without whose support this project could not have been so successfully accomplished. We especially want to thank Dr. James H. Trainor, the U.S. Project Scientist, Gilbert Ousley and Charlie White from the HELIOS Project Office, James Kunst and his integration support team, Earl Beard from the Information Processing Division, and Pat Corrigan and his team from the Operating Satellites Project.

APPENDIX A

"Updated Scientific and Technical Description of the HELIOS Solar Wind Plasma Wave Experiment"

by

Donald A. Gurnett, Roger R. Anderson, and Daniel L. Odem

Department of Physics and Astronomy
The University of Iowa
Iowa City, Iowa 52242

May 1974

TABLE OF CONTENTS

1.0 Scientific Objectives

This document describes the University of Iowa solar wind plasma wave experiment for the HELIOS missions (Experiment 5a). This experiment has been jointly planned with the University of Minnesota [P. Kellogg] and GSFC [R. Weber and R. Stone] so that the combined experiments provide complementary measurements.

The objective of this experiment is the investigation of naturally occurring plasma instabilities and electromagnetic waves in the solar wind. In the solar wind a wide variety of electromagnetic and electrostatic wave phenomena can be expected in the frequency range from a few tens of Hz to several hundred kHz. These phenomena may include Type III radio noise bursts and associated longitudinal electrostatic waves down to the solar wind plasma frequency (from about 20 kHz at 1 AU to 100 kHz at 0.3 AU), intense (30 mV/m) electrostatic waves of the type observed by Scarf with the Pioneer 8 spacecraft, electrostatic waves associated with interplanetary shock waves and solar particle emissions, and whistler-mode instabilities related to anisotropic solar wind electron distributions ($T_{||}/T_{\perp} > 1$). Figure 1 summarizes the frequency range and characteristics of various plasma noise phenomena which could be expected in the solar wind and Figure 2 illustrates the expected radial variation of the solar wind electron plasma frequency, ion plasma frequency, electron gyrofrequency, and lower-hybrid resonance frequency from the earth to 0.3 AU.

Wave-particle interactions can lead to many important effects in the solar wind. Of particular interest on this mission is the investigation of instabilities which make the solar wind behave like a fluid. If the solar wind had no collective effects, the ratio $T_{||}/T_{\perp}$ for the protons would be 100 to 1 or more at the earth, contrary to observation. It is generally believed that a plasma instability, possibly the whistler-mode, alters the proton pitch angle distribution. Because of the large radial variation in the solar wind properties (density, magnetic field, $T_{||}/T_{\perp}$, etc.) from the Earth to 0.3 AU, the stability criteria and wave phenomena occurring in the solar wind at 0.3 AU may be quite different compared to near the Earth. The spatial distribution of instabilities may influence the propagation of solar and galactic cosmic rays, slowing down times for super thermal particles can be drastically modified, waves generated in shocks can carry energy and momentum away from the shock region, and many more examples can be cited. Also of great importance is the direct observation of the electron plasma oscillations which are believed to give rise to Type III radio noise bursts through non-linear effects.

The frequency range of this experiment, nominally 20 Hz to 200 kHz, has been chosen to include most of the characteristic frequencies for plasma waves in the solar wind (see Figures 1 and 2). The upper frequency limit (200 kHz) is approximately the maximum electron plasma frequency (f_{pe}) expected and was chosen to provide some overlapping frequency coverage with the radio astronomy experiment (50 kHz to 2 MHz). The lower frequency limit for the plasma waves experiment

(20 Hz) is influenced by the spacecraft spin rate (1 rev/second). Since strong electric field signals are expected at harmonics of the spacecraft spin rate, due to the asymmetrical photoelectron sheath around the spacecraft, the lower frequency limit of this experiment has been chosen to be well above the frequencies of the expected spin rate interference.

Past experience with radio noise data from the Alouette, OGO, Injun, and IMP satellites has shown that it is very important to have both electric and magnetic field measurements so that electromagnetic and electrostatic waves can be distinguished. It is expected, therefore, that the AC electric field measurements provided by this experiment and the AC magnetic field measurements provided by Dr. Neubauer's search coil magnetometer experiment will provide complementary data for the identification and understanding of certain phenomena.

2.0 Technical Description of the Experiment

2.1 Electric Field Antenna

Figure 3 shows a sketch of the electric field/radio astronomy antenna used on the HELIOS spacecraft. The antenna is an extendible cylindrical dipole 32 meters tip-to-tip, similar to the antennas used on the Alouette, OGO, IMP, and RAE satellites. In order to reduce the capacity between the antenna and the spacecraft photo-electron sheath to an acceptable value, an insulating sleeve approximately 2.0 meters long is placed over the antenna where the antenna passes through the spacecraft photo-electron sheath region. The antenna diameter is as small as possible (0.25 inch) in order to minimize the ratio of resistive-to-capacitive coupling to the surrounding plasma.

The electric field antenna and associated erection mechanism are provided by the spacecraft for this experiment. The antenna erection mechanism is designed to minimize the antenna to erection mechanism capacitance. This capacitance does not exceed approximately 30 pf in the extended configuration. Also, special consideration has been given to electrostatically shielding the antenna from spacecraft related interference, such as through the erection motor, deployment length indicators, etc.

2.2 Electric Antenna Preamplifier

Each element of the electric dipole is connected to three

preamplifiers which provide signals to the respective University of Iowa, University of Minnesota, and GSFC experiments.

2.3 Main Electronics Package (Iowa)

A block diagram of the main experiment electronics is shown in Figure 4. The main elements of the experiment electronics consists of (1) a differential amplifier, (2) a 16-channel spectrum analyzer, (3) an antenna potential monitor, (4) a shock alarm, and (5) a power supply.

2.3.1 Differential Amplifier. The differential amplifier provides AC signals proportional to the potential difference between the antenna elements. It provides a high order of common mode rejection to reduce the response to interference signals present on both antenna elements. The differential amplifier is followed by a narrow band notch filter which provides approximately 30 db of attenuation at frequencies of 20 kHz, 40 kHz, and 60 kHz (harmonics of the power supply frequency).

2.3.2 16-Channel Spectrum Analyzer. The 16-channel spectrum analyzer is the basic element of the University of Iowa experiment. This analyzer is to provide relatively coarse frequency coverage and rapid temporal resolution with essentially continuous coverage of all frequencies (20 Hz to 200 kHz) and all times (using peak detectors). The nominal frequency response of the various spectrum analyzer channels is shown in Figure 5 and the corresponding center frequencies

and bandwidths are given in Table 1. The lowest 8 frequency channels use active filters spaced with four filters per decade of frequency. The highest 8 frequency channels use passive filters spaced with four filters per decade. The detector and log compressor in each channel will rectify and log compress signals from the filter and produce an output proportional to the logarithm of the noise intensity in each filter channel. The log compressor output is used to provide three outputs (1) a peak output (P), (2) an average output (A), and (3) a short time constant output (S).

2.3.2.1 Peak Output (P). The peak output provides a voltage (0-5 volts) proportional to the logarithm of the peak signal since the preceding reading. The peak detector is reset after readout by a signal from the DPU (described in section 3).

2.3.2.2 Average Output (A). The average output provides an RC average output with either (1) a time constant τ which depends on the bit rate and science format mode or (2) a forced short time constant, τ_s. Which time constant is used is determined by the shock alarm channel number. The forced short time constant is used whenever the shock alarm channel number is odd, i.e., whenever Shock Alarm Bit 0 is "ON". Command 371 selects the forced short time constant τ_s while the reset command 006 selects the normal time constant

τ. The normal spectrum analyzer time constants τ are listed in Table 2. The forced short time constants τ_s are listed in Table 1.

2.3.2.3 Short Time Constant Output (S). The short time constant outputs provide short-time-constant field strength voltages to the shock mode memory. One channel of short time constant outputs is continuously available in the science data and is labeled S_N. This channel is determined by the shock alarm channel number. The output from this channel is sampled 16 times in one spacecraft revolution by the DPU and stored for later readout. The time constants τ_s for the short-time-constant measurements are given in Table 1 for the various frequency channels.

2.3.2.4. Shadow Blanking. The DPU provides a Shadow Blanking Pulse to the experiment to open the input to the 8 lowest frequency compressors for 4 sectors twice per revolution to reduce the effects of the large voltage pulses generated as the antennas sweep through the spacecraft shadow. Command 223 overrides this shadow blanking. Reset command 006 allows shadow blanking.

2.3.3 Antenna Potential Monitor. The average potential, $V_{average}$, and the difference potential, $V_{difference}$, between the antenna elements are measured with operational amplifiers

in the main electronics package. The frequency range of the V_{diff} measurement is from 0.2 to 10.0 Hz. The dynamic range of the V_{diff} measurement can be controlled by command to be either $\pm$8.0, $\pm$2.0, $\pm$0.5, or $\pm$0.125 volts. The dynamic range of the V_{ave} measurement is $\pm$20.00 volts. This data is needed for a complete understanding of the antenna operation in the plasma surrounding the spacecraft.

2.3.4 Shock Alarm. A shock alarm signal is to be sent to the spacecraft when the electric field experiment senses noise associated with an interplanetary shock wave. The shock alarm circuit will permit the selection of any one of the 16 spectrum analyzer channels, by command, for shock identification. The threshold field strength required to trigger the shock alarm has 16 levels and is controlled by a 4 bit binary counter. The shock threshold level is reset whenever any shock channel command is received (bit 0, 1, 2, 3 or reset). No information concerning satellite mode lines is required for reset. After reset, the threshold is advanced upward every time the threshold is exceeded, in each case the new threshold level is set to the peak value of the electric field strength observed. This procedure, therefore, results in the storage of the "best" event observed over the shock search interval. This "shock level value E" is available on two outputs. The first is a 4 bit parallel binary word sent to the DPU. The DPU sends this value and other

data to the spacecraft as serial words. The "shock level value E" is also sent directly to the spacecraft (through the DPU plugs). This connection is a single analog voltage line, 0 to 5.0 VDC with higher voltages representing higher values of the shock. This line has a time constant of 0.10 second. Inhibit lines from E5b and E5c prevent the threshold from advancing while the E5b impedance measurement is on or while E5c is calibrating.

2.3.5 Power Supply. The experiment power supply provides regulated voltages of ±6 volts and ±12 volts to the experiment electronics. The power supply operates at a frequency of 20 kHz and is synchronized by a 40 kHz synchronization signal provided by the spacecraft.

2.4 Summary of Weight, Power, Etc.

2.4.1 Weight.

2 Preamplifiers (Experiments 5a, 5b, and 5c each assessed 0.15 kg)	0.45 Kg
Main Electronics Package (Experiment 5a only)	2.44 Kg

2.4.2 Power.

Main Electronics Package and 2 of the 6 Preamplifiers.	2.6 watts

3.0 Plasma Waves Data Processing Unit

3.1 General Description

The Data Processing Unit (DPU) for the Plasma Waves Experiment is separate from the main experiment electronics and is provided by GSFC through an industrial contractor. The purpose of the DPU is to (1) provide interface connections between the experiment and the spacecraft, (2) provide A/D conversion of all scientific analog data, (3) provide buffer storage, as necessary, to adapt to the spacecraft data transmission format.

3.2 Data Format (Real Time Modes)

Experiment 5a has 50 analog (0-5 volt) output lines which must be sampled by the DPU. In Figure 4 these outputs are P_0, P_1, ..., P_{15}, A_0, A_1, ..., A_{15}, S_0, S_1, ..., S_{15}, S_N and V_{diff}. For real time data transmission these outputs are to be sampled in a basic data block consisting of 256 bits, broken down as follows:

(1) 16 6-bit Peak Samples (P_0, P_1, ..., P_{15})	96 bits
(2) 16 6-bit Average Samples (A_0, A_1, ..., A_{15})	96 bits
(3) 8 8-bit V_{diff} or S_N samples (spin synchronized)	64 bits
BASIC DATA BLOCK SIZE	256 bits

The 16 peak spectrum analyzer samples above are sampled simultaneously to within 0.25 seconds. The 16 average spectrum analyzer samples are also sampled simultaneously to within 0.25 seconds, but these average samples are taken at a different time than the peak samples. The peak and average sampling of a given channel are equally spaced in time between successive data blocks. The DPU A/D converts these samples and stores them in a buffer storage for later transfer to the spacecraft telemetry. The DPU also provides a signal to the experiment which resets the peak detectors immediately after the 16 peak samples are obtained. The 16 V_{diff} or S_N samples in (3) above occur at sixteen equally spaced angles covering one complete spin. The spin synchronized sampling alternates between V_{diff} and S_N in each 2 successive data blocks. The S_N channel number is determined by the channel number of the shock alarm circuit.

The time required to transmit each basic data block is determined by the spacecraft bit rate and telemetry format. The basic data block time and corresponding normal time constant τ for the average field strength measurements are given in Table 2 for each spacecraft bit rate and telemetry format.

3.3 Data Format (Shock Mode)

Sampling of data for shock mode storage occurs concurrently with the real time data sampling described in the previous section. When a shock occurs data both before and after the shock are stored in the spacecraft shock mode memory for later readout.

Experiment 5a has 17 analog (0-5 volt) output lines which are sampled by the DPU for the shock mode readout. In Figure 4 these outputs are S_0, S_1, ..., S_{15}, and V_{Diff}. For the shock mode data transfer these outputs are to be sampled in a basic data block consisting of 128 bits, broken down as follows:

(1) 16 6-bit Short Time Constant Spectrum Analyzer Samples (S_0, S_1, ..., S_{15})	96 bits
(2) 4 8-bit V_{Diff} Samples	32 bits
BASIC BLOCK SIZE	128 bits

The sampling rate for the 16 short time constant spectrum analyzer samples is not critical except that all 16 channels must, of course, be sampled within the time required to transmit each basic data block. The V_{Diff} samples are equally spaced in time, both within a basic data block and between successive data blocks. Spin synchronized sampling of V_{Diff} is not used in the shock data because the sampling rates obtained in the shock mode data are sufficiently high to permit direct (real time) resolution of spin effects.

The time to transmit each basic data block is determined by the spacecraft bit rate and telemetry format. The approximate data block times for the shock mode sampling are given in Table 2 for each shock mode bit rate. T_0 is the duration of shock mode data stored in part C of the shock memory.

4.0 E5a Commands

4.1 Command 006.

Cmd 006 resets all four bits of the Shock Alarm Channel Number to level "0" and turns off the Shadow Blanking Override Command.

4.2 Command 371

Cmd 371 sets Bit 0 of the Shock Alarm Channel Number to level "1". The command also sets the average output of the spectrum analyzers to the forced short time constant.

4.3 Command 027

Cmd 027 sets Bit 1 of the Shock Alarm Channel Number to level "1".

4.4 Command 350

Cmd 350 sets Bit 2 of the Shock Alarm Channel Number to level "1".

4.5 Command 216

Cmd 216 sets Bit 3 of the Shock Alarm Channel Number to level "1".

Each of the above five commands also resets the Shock Value E to zero. Because the noise level amplitude in each channel is sufficient to raise the Shock Value E one step above zero, the Shock Value E will immediately jump at least one step above zero unless it is inhibited. Thus these commands can be used to generate an artificial shock if E5a

is controlling the input to the shock memory (Cmd 275) and if E5a is not being inhibited by E5b or E5c during their calibrations.

4.6 Command 161

Cmd 161 resets both V-Diff Gain bits to level "0".

4.7 Command 237

Cmd 237 sets V-Diff Gain Bit 0 to level "1".

4.8 Command 140

Cmd 140 sets V-Diff Gain Bit 1 to level "1".

V-Diff Gain = 0 is the least sensitive gain setting and covers the range from -8 volts to +8 volts. The V-Diff output is linearly proportional to the input but it has a DC offset such that 0 volts in equals 2.50 volts out. Each higher gain step is four times more sensitive than the gain step below it.

4.9 Command 223.

Cmd 223 removes the shadow blanking of the lowest eight spectrum analyzer channels.

5.0 Analog Housekeeping Data

5.1 Shock Value Level E (SHOC-E)

Channel B040

This channel is an analog voltage proportional to the logarithm of the peak intensity measured by the selected shock channel since reset.

5.2 Low Voltage Power Supply Monitor (LVPSM)

Channel C038

This channel is an analog voltage equal to 2/3 of the regulated +6 volt power supply line in the experiment.

5.3 Antenna Average Potential (V-AVG)

Channel C039

This channel is an analog voltage linearly proportional to the average antenna potential, but it has a DC offset such that 0 volts in equals 2.50 volts out. It measures the antenna potential from -20 volts to +20 volts.

6.0 Digital Housekeeping Data

Channel B-009 (DSEDB4)

6.1 Bit 1 is Shock Alarm Channel Number Bit 3

6.2 Bit 2 is Shock Alarm Channel Number Bit 2

6.3 Bit 3 is Shock Alarm Channel Number Bit 1

6.4 Bit 4 is Shock Alarm Channel Number Bit 0

6.5 Bit 5 is V-Diff Gain Bit 1

6.6 Bit 6 is V-Diff Gain Bit 0.

6.7 Bit 7 is a logical "1" if the Shadow Blanking Override is on or if the E5a shock alarm system is inhibited by E5b or E5c.

7.0 Housekeeping Data in Format 6

The 5E word in Format 6 contains the binary representations of the Shock Alarm Channel Number and the Shock Value E. The Shock Alarm Channel Number is given by bits 0-3 of 5E. Bit 0 of 5E is equivalent to Bit 3 of the Shock Alarm Channel Number. Bit 3 of 5E is equivalent to Bit 0 of the Shock Alarm Channel Number. Bit 4 of 5E is equivalent to Bit 3 of the Binary representation of the Shock Value E. Bit 7 of 5E is equivalent to Bit 0 of the binary representation of the Shock Value E.

8.0 Thermistor Locations

8.1 E5a Box

The thermistor in the E5a experiment box is located approximately in the middle of the box on the shock alarm board.

8.2 E5 Preamps

The thermistors in the preamps are attached to the walls of the connector compartments.

TABLE 1

Filter Number	Center Frequency	Bandwidth	Type of Filter	Short Time Constant
0	31.1 Hz	±19%	Active	0.2 sec.
1	56.2	±19%	Active	0.1 sec.
2	100.0	±19%	Active	0.05 sec.
3	178.0	±19%	Active	0.05 sec.
4	311	±19%	Active	0.05 sec.
5	562	±19%	Active	0.05 sec.
6	1.0 kHz	±19%	Active	0.05 sec.
7	1.78	±19%	Active	0.05 sec.
8	3.11	±11%	Passive (UTC)	0.05 sec.
9	5.62	±11%	Passive (UTC)	0.05 sec.
10	10.0	±11%	Passive (UTC)	0.05 sec.
11	17.8	±11%	Passive (UTC)	0.05 sec.
12	31.1	±11%	Passive (UTC)	0.05 sec.
13	56.2	±11%	Passive (UTC)	0.05 sec.
14	100.0	±11%	Passive (UTC)	0.05 sec.
15	178.0	±11%	Passive (UTC)	0.05 sec.

TABLE 2

Format	Spacecraft Bit Rate	Experiment 5a Words/Frame	Experiment 5a Block Length	Experiment 5a Bit Rate	Block Time	Spectrum Analyzer Time Constant	DC Field Angular Resolution
1 (High Data Rate)	512 bits/sec	16	256 bits	56.9 bits/sec	4.500 sec.	4.500	22.5°
	1024	16	256	113.8	2.250	2.250	22.5°
	2048	16	256	227.6	1.125	1.125	22.5°
2 (Normal Data Rate)	32	4	256	0.89	288.0	18.0	22.5°
	64	4	256	1.78	144.0	18.0	22.5°
	128	4	256	3.56	72.0	18.0	22.5°
	256	4	256	7.11	36.0	18.0	22.5°
	512	4	256	14.22	18.0	18.0	22.5°
3 (Reduced)	8	8	256	0.44	576.0	18.0	22.5°
	16	8	256	0.89	288.0	18.0	22.5°
	32	8	256	1.78	144.0	18.0	22.5°
	64	8	256	3.56	72.0	18.0	22.5°
5 (Very High Data Rate)	4096	8	256	227.6	1.125	1.125	22.5°
	2048	8	256	113.8	2.25	2.25	22.5°
6 (Shock Mode)**	4096 (T_o=70.9)	16	128	455.1*	0.281	0.05***	25.3°
	8192 (T_o=35.4)	16	128	910.2*	0.141	0.05***	12.7°
	16384 (T_o=17.7)	16	128	1820.4*	0.070	0.05***	6.3°

* Not transmitted, but stored bit rate.
** Not general S/C format, but used only by shock expts. on special shock line.
*** The short time constants for channels 0 and 1 are 0.2 and 0.1 seconds, respectively.

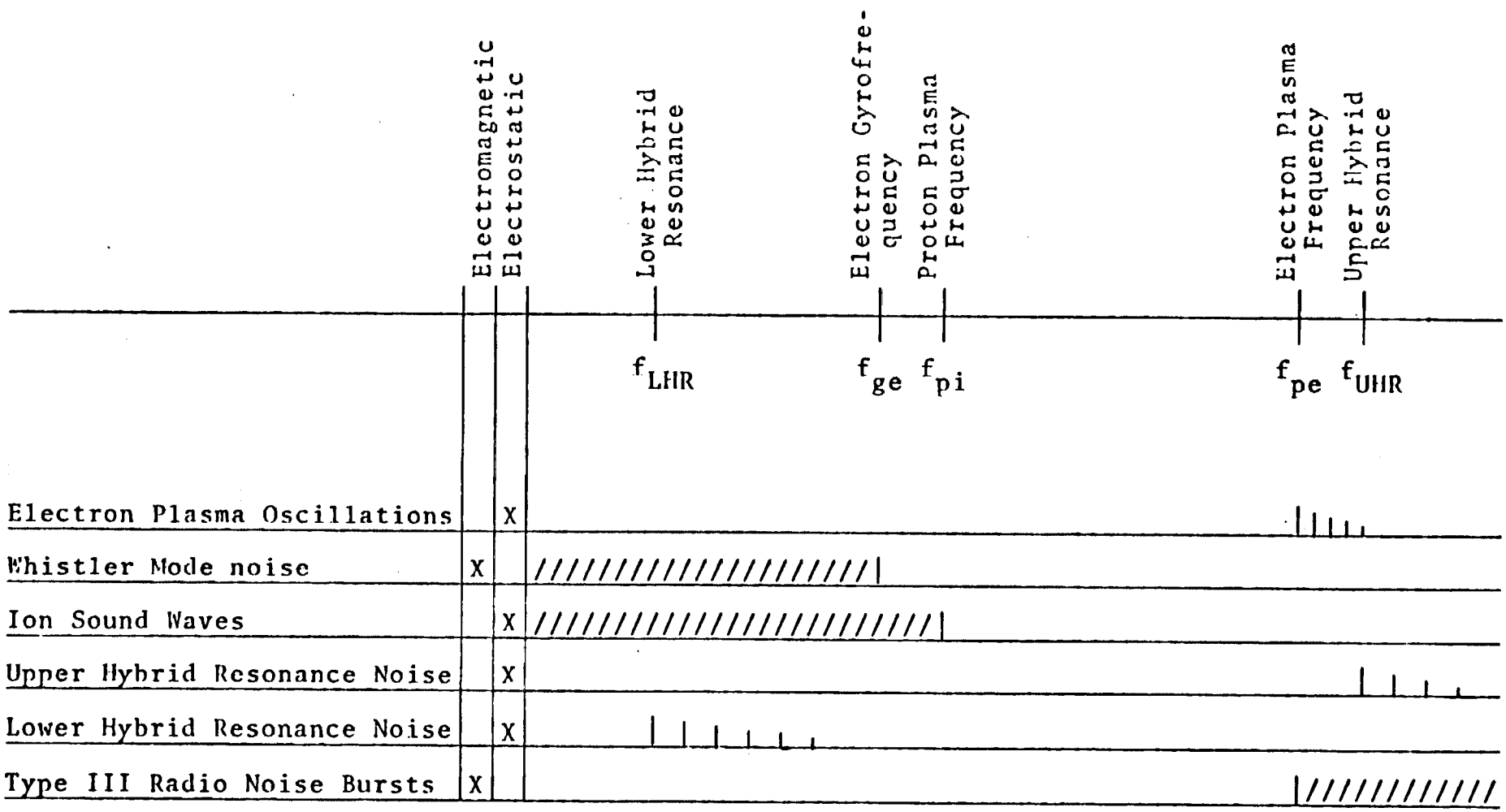
Electromagnetic
Electrostatic
Lower Hybrid Resonance
Electron Gyrofre-quency
Proton Plasma Frequency
Electron Plasma Frequency
Upper Hybrid Resonance
f_{LHR}
f_{ge}
f_{pi}
f_{pe}
f_{UHR}
Electron Plasma Oscillations
Whistler Mode noise
Ion Sound Waves
Upper Hybrid Resonance Noise
Lower Hybrid Resonance Noise
Type III Radio Noise Bursts

Figure 1

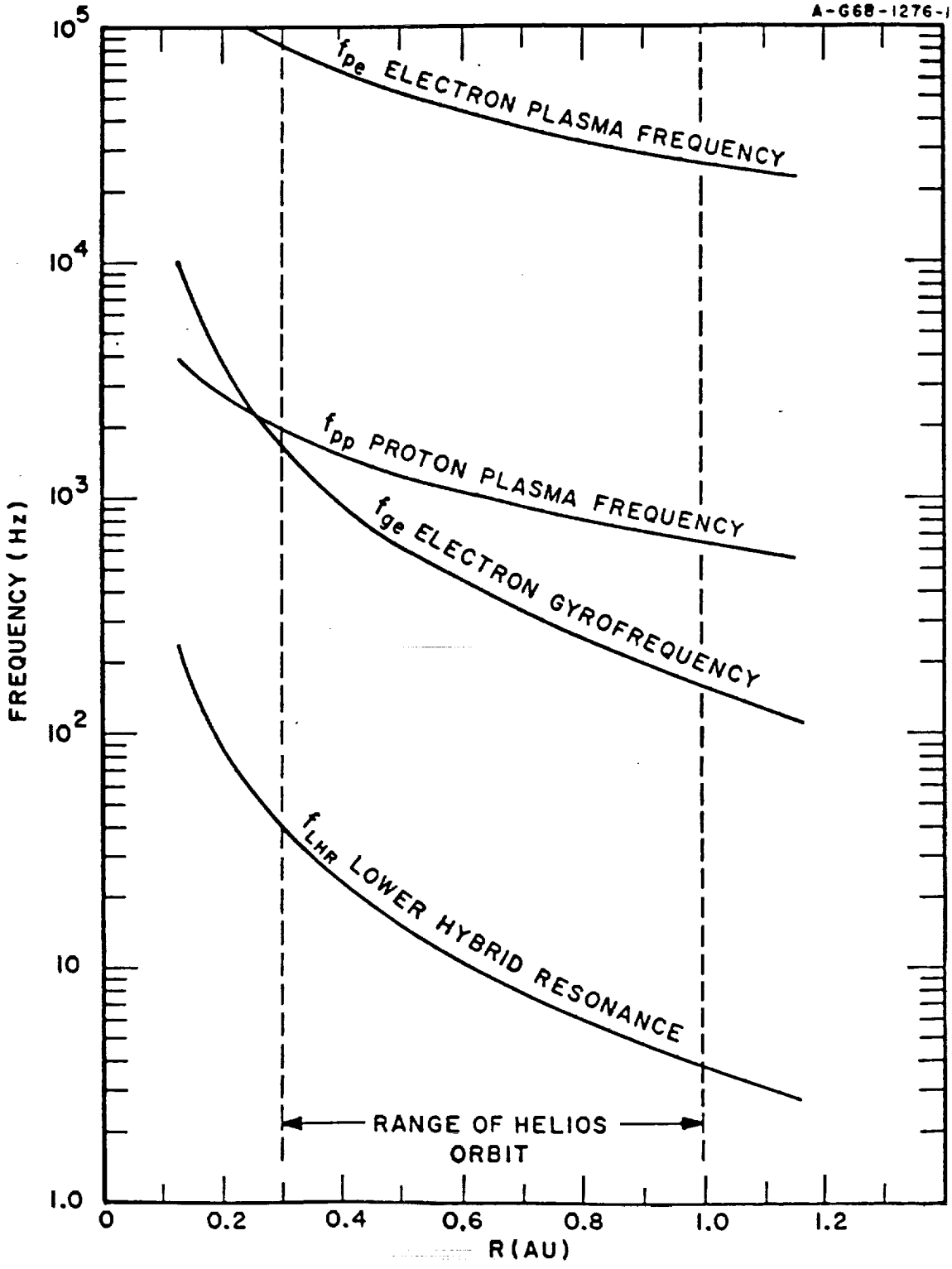
A-G68-1276-1
10^5
10^4
10^3
10^2
10
1.0
FREQUENCY (Hz)
f_{pe} ELECTRON PLASMA FREQUENCY
f_{pp} PROTON PLASMA FREQUENCY
f_{ge} ELECTRON GYROFREQUENCY
f_{LHR} LOWER HYBRID RESONANCE
RANGE OF HELIOS ORBIT
0
0.2
0.4
0.6
0.8
1.0
1.2
R(AU)

Figure 2

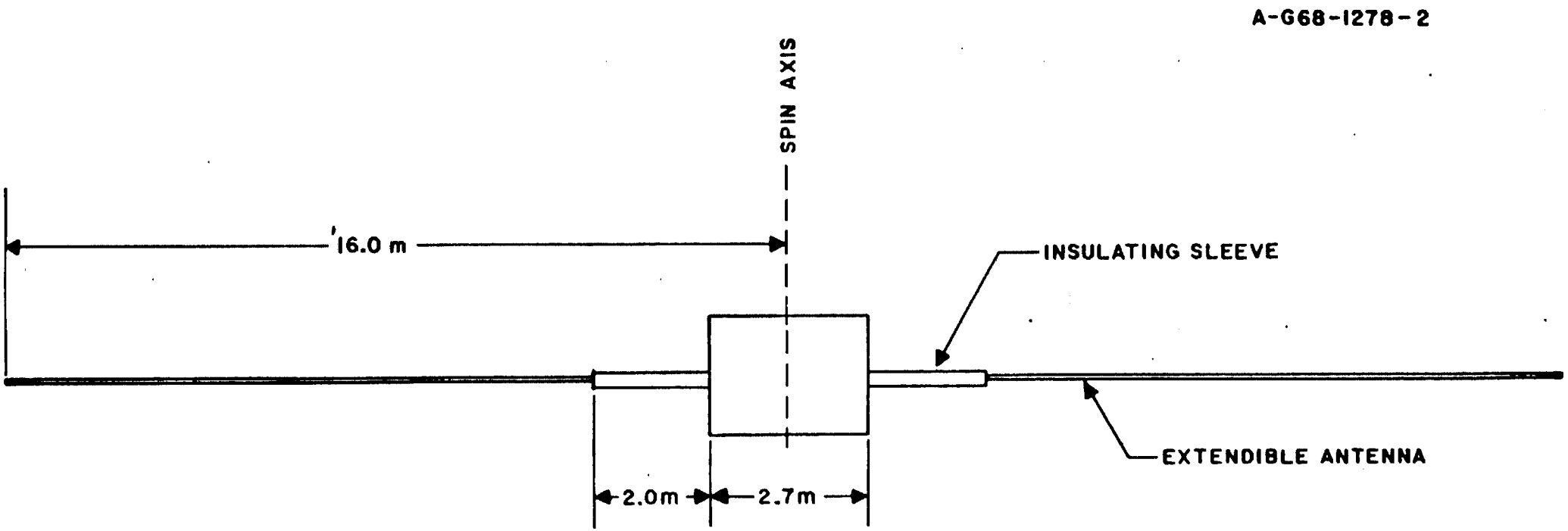
A-G68-1278-2
SPIN AXIS
16.0 m
INSULATING SLEEVE
EXTENDIBLE ANTENNA
2.0m
2.7m

FIGURE 3

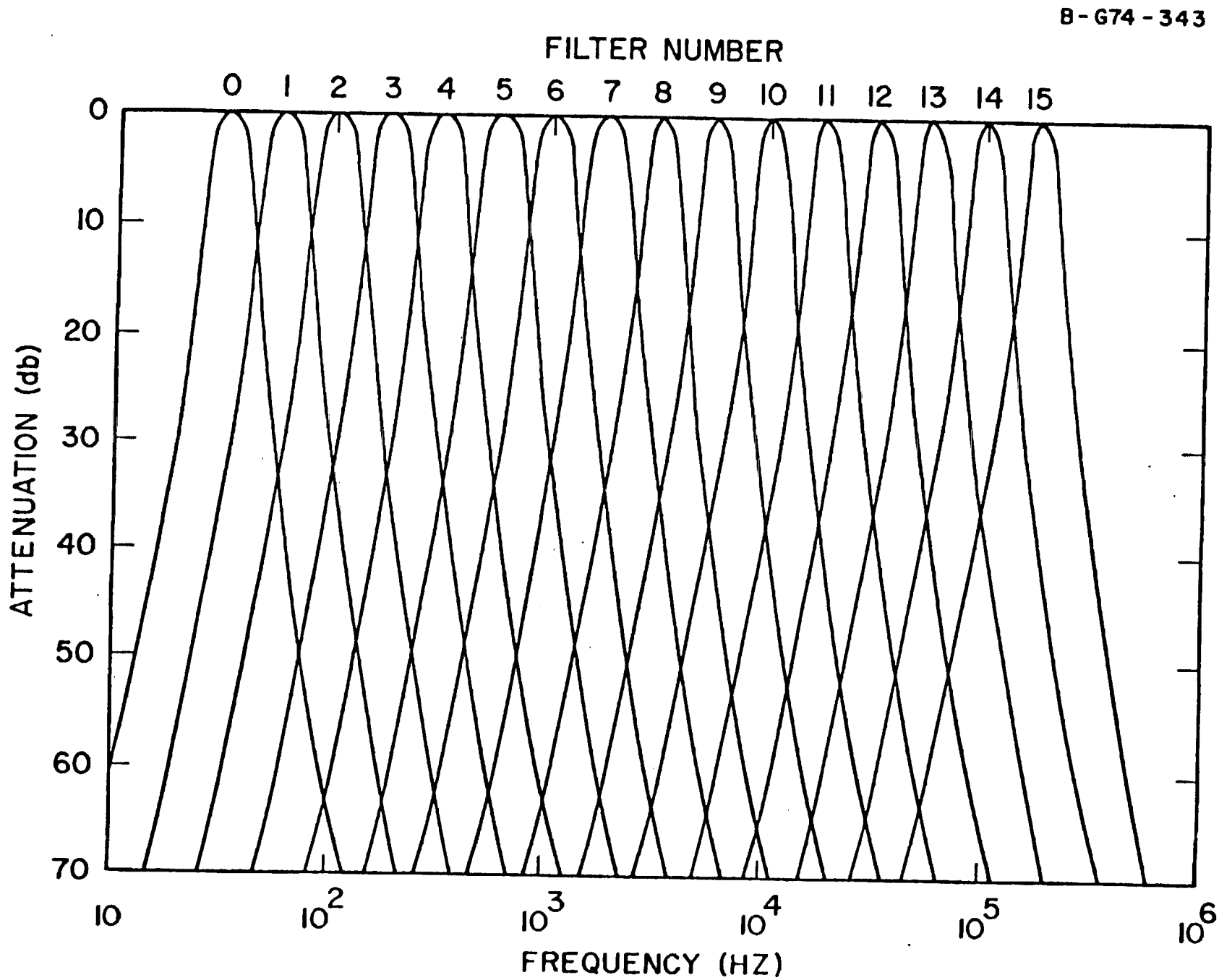
B-G74-343
FILTER NUMBER
0 1 2 3 4 5 6 7 8 9 10 11 12 13 14 15
0
10
20
30
40
50
60
70
ATTENUATION (db)
10
10^2
10^3
10^4
10^5
10^6
FREQUENCY (HZ)

FIGURE 6

FOLDOUT FRAME

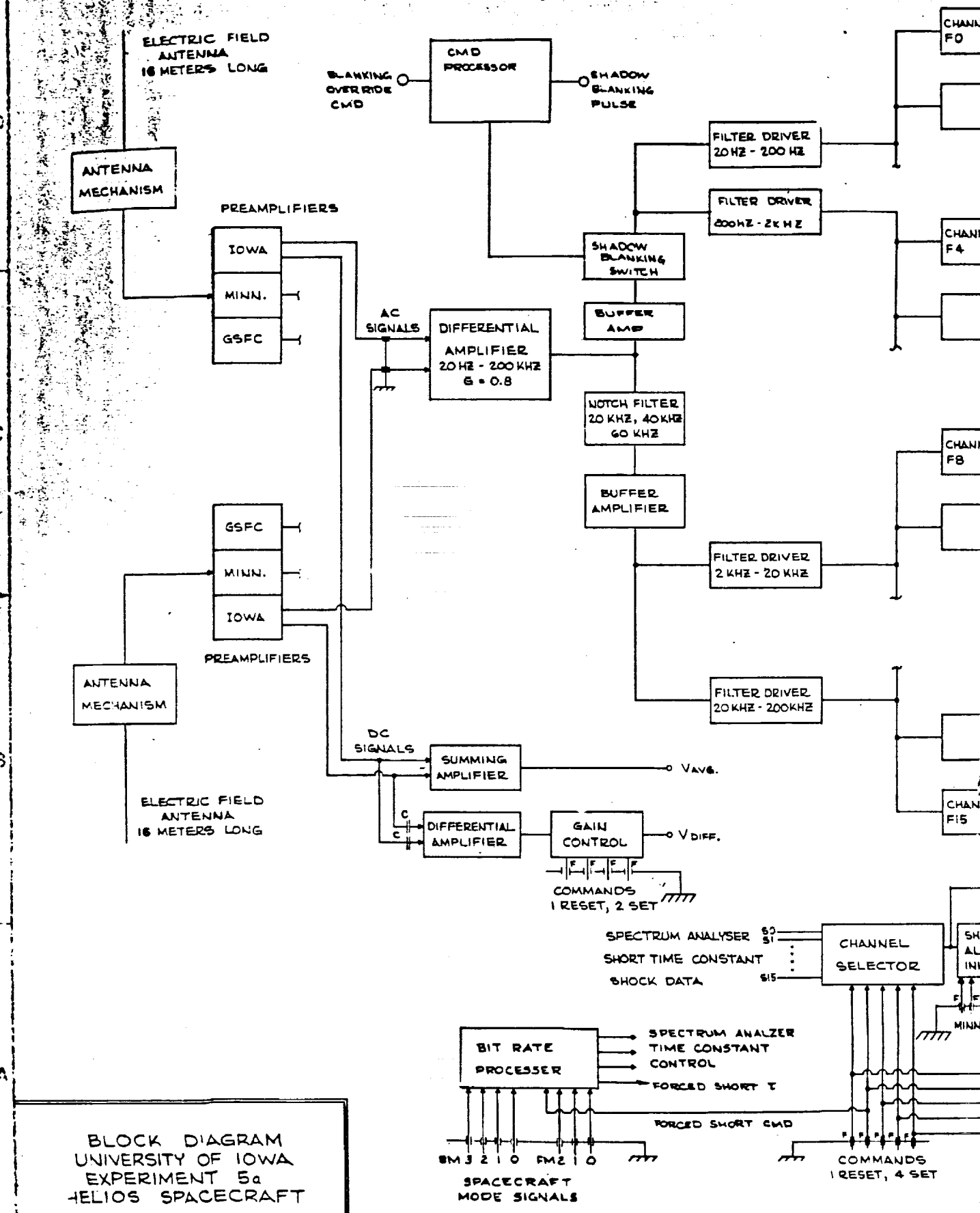

BLOCK DIAGRAM
UNIVERSITY OF IOWA
EXPERIMENT 5a
HELIOS SPACECRAFT

ORIGINAL PAGE IS
OF POOR QUALITY

NO.	REVISIONS	DATE	INITIAL
1	ADDED BLANKING	12 JAN 72	MDS

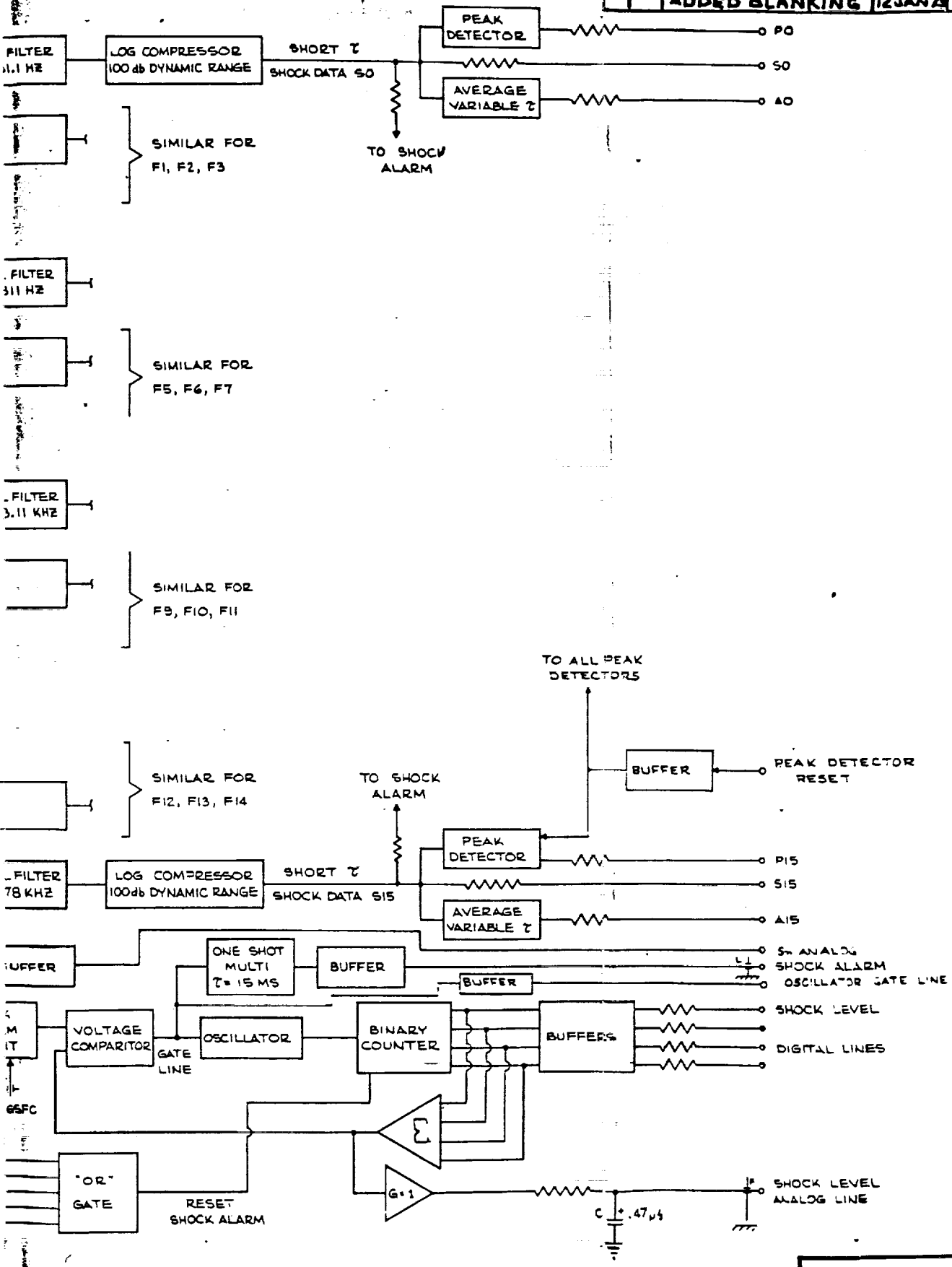

FIGURE 4

APPENDIX B

Scientific Reports and Publications
Involving the University of Iowa
HELIOS Solar Wind Plasma Wave Experiments
and Produced under Contract NAS5-11279

Bibliography of Published Papers

Following is a list of all publications involving The University of Iowa HELIOS Solar Wind Plasma Wave Experiment:

Gurnett, D. A., R. R. Anderson, and D. L. Odem, "The HELIOS solar wind plasma wave experiment (E5a), "RAUMFAHRTFORSCHUNG, Band 19, Heft 5, 245, 1975.

Gurnett, D. A. and R. R. Anderson, "Electron plasma oscillations associated with type III radio bursts," Science, 194, 1159, 1976.

Gurnett, D. A. and R. R. Anderson, "Plasma wave electric fields in the solar wind: Initial results from HELIOS-1," J. Geophys. Res., 82, 632, 1977.

Gurnett, D. A., M. M. Baumback, and H. Rosenbauer, "Stereoscopic direction finding analysis of a type III solar radio burst: Evidence for emission at $2f_g^-$," J. Geophys. Res., 83, 616, 1978

Gurnett, D. A. and L. A. Frank, "Ion-acoustic waves in the solar wind," J. Geophys. Res., 82, 58, 1978.

Gurnett, D. A., R. R. Anderson, F. L. Scarf, and W. S. Kurth, "The heliocentric radial variation of plasma oscillations associated with type III radio bursts," J. Geophys. Res., 83, 4147, 1978.

Gurnett, D. A., F. M. Neubauer, and R. Schwenn, "Plasma wave turbulence associated with an interplanetary shock," J. Geophys. Res., 84, 541, 1979.

Gurnett, D. A., E. Marsch, W. Pilipp, R. Schwenn, and H. Rosenbauer, "Ion-acoustic waves and related plasma observations in the solar wind," J. Geophys. Res., 84, 2029, 1979.

Burlaga, L., R. Lepping, R. Weber, T. Armstrong, C. Goodrich, J. Sullivan, D. Gurnett, P. Kellogg, E. Keppler, F. Mariani, F. Neubauer, H. Rosenbauer, and R. Schwenn, "Interplanetary particles and fields, November 22 - December 7, 1977: Helios, Voyager, and IMP observations between 0.6 AU and 1.6 AU," J. Geophys. Res., 85, 2227, 1980.

Gurnett, D. A., R. R. Anderson and R. L. Tokar, "Plasma oscillations and the emissivity of type III radio bursts," Radio Physics of the Sun, ed. by M. Kundu, Reidel, Dordrecht, Netherlands, p. 369, 1980.

Tokar, R. L. and D. A. Gurnett, "The volume emissivity of type III radio bursts," J. Geophys. Res., 85, 2353, 1980.

Gurnett, D. A. and R. R. Anderson, "A summary of progress in space physics made with Helios plasma wave instrument data (E5a)," HELIOS solar probes science summaries, NASA Technical Memorandum TM82005, p. 27, August, 1980.

Gurnett, D. A., Plasma waves in the solar wind: A review of observations, Solar Wind, 4, ed. by H. Rosenbauer, Max Institut Report No. MPAE-2-100-81-31, Lindau, Germany, p. 286, 1981.

Dum, C. T., E. Marsch, W. Pilipp, and D. A. Gurnett, Ion sound turbulence in the solar wind, Solar Wind, 4, ed., by H. Rosenbauer, Max Institut Report No. MPAE-W-100-81-31, Lindau, Germany, p. 299, 1981.

Kikuchi, H., D. A. Gurnett, R. R. Anderson, E. Keppler, A. K. Richter, R. Schwenn, E. Marsch, K. Richter,and H. Rosenbauer, Solar radio bursts and electron plasma oscillations associated with interplanetary shocks waves and energetic protons, International Union of Geodesy and Geophysics, International Association of Geomagnetism and Aeronomy, Bulletin No. 48, August 1983.

Denskat, K. U. and D. A. Gurnett, Physics of the inner heliosphere: Waves and discontinuities, Physics of the Inner Heliosphere, submitted for publication, 1984.

Gurnett, D. A. and R. R. Anderson, Plasma waves in the solar wind: 10 years of HELIOS observations, 10 Years of HELIOS, 20 Years of US-Germany Cooperation in Space, ed. by H. Porsche, Oberpfaffenhoven, DFVLR, p. 100, 1984.

RAUMFAHRTFORSCHUNG

BAND 19 · HEFT 5 · September/Oktober 1975

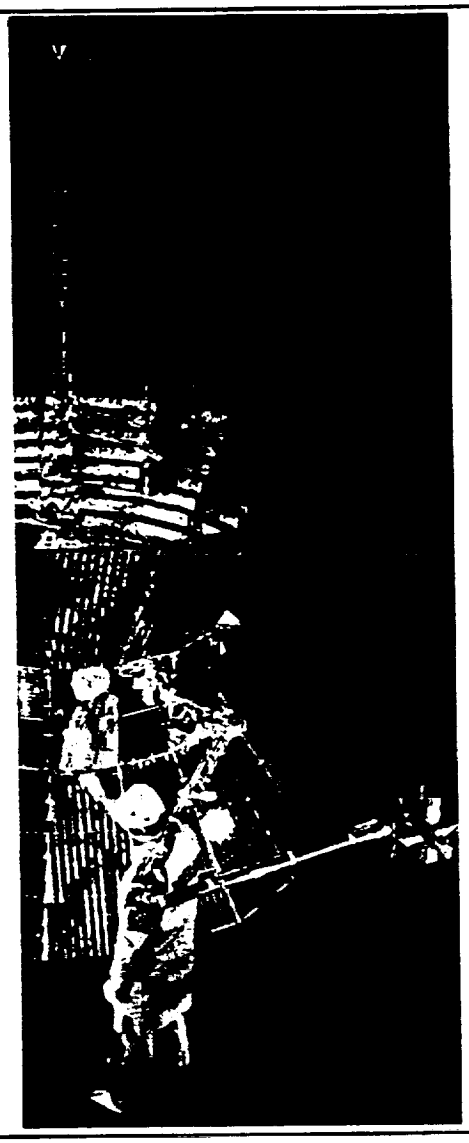

Themenheft HELIOS-EXPERIMENTE

ZEITSCHRIFT FÜR RAKETENANTRIEBE, RAUMFAHRZEUG- UND RAUMKÖRPERTECHNIK, ASTRIONIK ASTRODYNAMIK, RAUMFAHRTMEDIZIN UND BIOTECHNIK, HÖHENFORSCHUNG UND ASTROPHYSIK

HERAUSGEGEBEN VON DER

DGLR · Deutsche Gesellschaft für Luft- und Raumfahrt e. V.

The University of Iowa HELIOS Solar Wind Plasma Wave Experiment (E 5a)

*Donald A. GURNETT, Roger R. ANDERSON and Daniel L. ODEM, University of Iowa**/USA*

This document describes the University of Iowa solar wind plasma wave experiment for the HELIOS missions (Experiment 5a). The objective of this experiment is the investigation of naturally occurring plasma instabilities and electromagnetic waves in the solar wind. To carry out this investigation, the experiment consists primarily of a 16-channel spectrum analyzer connected to the electric field antennas. The spectrum analyzer covers the frequency range from 20 Hz to 200 kHz and has an amplitude dynamic range which extends from · 3 μV/m to 30 mV/m per channel. This spectrum analyzer, the antenna potential measurements, the shock alarm system and the supporting electronics are discussed in detail.

Dieser Bericht beschreibt das Solarwind-Plasmawellen-Experiment der Universität Iowa für die HELIOS-Mission (Experiment 5a). Aufgabe dieses Experimentes ist die Untersuchung der auftretenden Plasma-Instabilitäten und der elektromagnetischen Wellen im Solaren Wind. Um diese Messungen durchführen zu können, besteht das Experiment hauptsächlich aus einem Spektral-Analysator mit 16 Kanälen, der mit den Antennen zur Messung des elektrischen Feldes verbunden ist. Der Spektral-Analysator deckt einen Frequenzbereich von 20 Hz bis 200 kHz ab und hat eine Amplitudenweite von 0,3 μV/m bis 30 mV/m pro Kanal. Der Spektral-Analysator, die Messungen des Antennenpotentials, das Stoßwellen-Alarmsystem und die dazugehörige Elektronik werden im Detail diskutiert.

1. SCIENTIFIC OBJECTIVES

The University of Iowa solar wind plasma wave experiment for the HELIOS missions has been jointly planned with the University of Minnesota [P. Kellogg] and GSFC [R. Weber and R. Stone] so that the combined experiments provide complementary measurements.

The objective of this experiment is the investigation of naturally occurring plasma instabilities and electromagnetic waves in the solar wind. In the solar wind a wide variety of electromagnetic and electrostatic wave phenomena can be expected in the frequency range from a few tens of Hz to several hundred kHz. These phenomena may include Type III radio noise bursts and associated longitudinal electrostatic waves down to the solar wind plasma frequency (from about 20 kHz at 1 AU to 100 kHz at 0.3 AU), intense (30 mV/m) electrostatic waves of the type observed by Scarf **et al.** [1] with the Pioneer 8 spacecraft, electrostatic waves associated with interplanetary shock waves and solar particle emissions, and whistler-mode instabilities related to anisotropic solar wind electron distributions ($T_{II}/T_{\perp} > 1$). Figure 1 summarizes the frequency range and characteristics of various plasma wave phenomena which could be expected in the solar wind and FIG. 2 illustrates

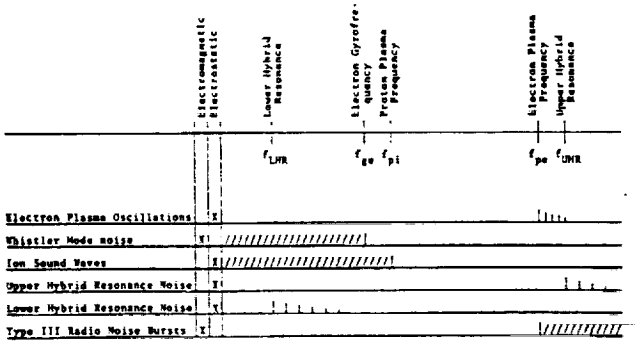

FIG. 1: **Frequency range and characteristics of various plasma wave phenomena which could be expected in the solar wind**

* This experiment was supported by NASA Contract NAS5-11279.

** Department of Physics and Astronomy, The University of Iowa, Iowa City, Iowa 52242 USA.

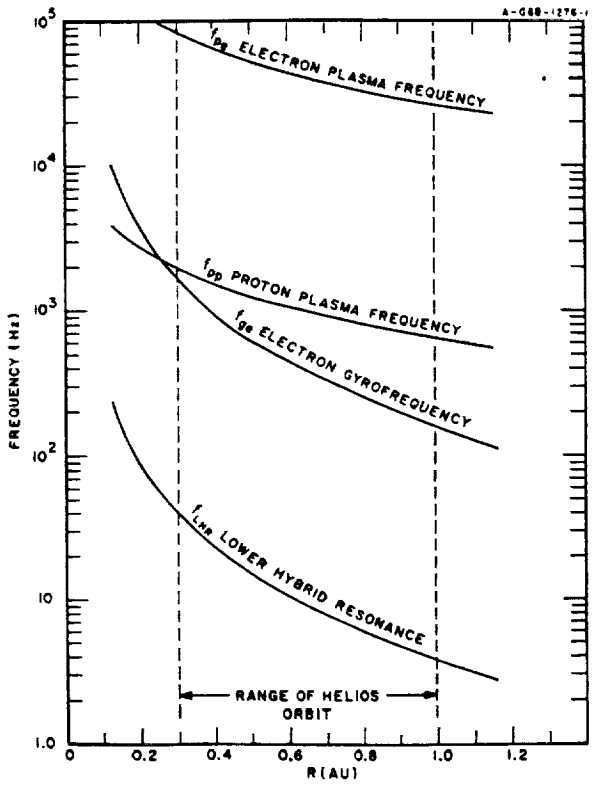

FIG. 2: **The expected radial variation of the solar wind electron plasma frequency, ion plasma frequency, electron gyro-frequency, and lower-hybrid resonance frequency from the Earth to 0.3 AU**

the expected radial variation of the solar wind electron plasma frequency, ion plasma frequency, electron gyrofrequency, and lower-hybrid resonance frequency from the Earth to 0.3 AU.

Wave-particle interactions can lead to many important effects in the solar wind. Of particular interest on this mission is the investigation of instabilities which make the solar wind behave like a fluid. If the solar wind had no collective effects, the ratio $T_{II}/T_{\perp}$ for the protons would be 100 to

1 or more at the Earth, contrary to observation. It is generally believed that a plasma instability, possibly the whistler-mode, alters the proton pitch angle distribution. Because of the large radial variation in the solar wind properties (density, magnetic field, $T_{II}/T_{\perp}$, etc.) from the Earth to 0.3 AU, the stability criteria and wave phenomena occuring in the solar wind at 0.3 AU may be quite different compared to near the Earth. The spatial distribution of instabilities may influence the propagation of solar and galactic cosmic rays, slowing down times for super thermal particles can be drastically modified, waves generated in shocks can carry energy and momentum away from the shock region, and many more examples can be cited. Also of great importance is the direct observation of the electron plasma oscillations which are believed to give rise to Type III radio noise bursts through non-linear effects.

The frequency range of this experiment, nominally 20 Hz to 200 kHz, has been chosen to include most of the characteristic frequencies for plasma waves in the solar wind (see FIGs. 1 and 2). The upper frequency limit (200 kHz) is approximately the maximum electron plasma frequency (f_{pe}) expected and was chosen to provide some overlapping frequency coverage with the radio astronomy experiment (26 kHz to 3 MHz). The lower frequency limit for the plasma waves experiment (20 Hz) is influenced by the spacecraft spin rate (1 rev/second). Since strong electric field signals are expected at harmonics of the spacecraft spin rate, due to the asymmetrical photoelectron sheath around the spacecraft, the lower frequency limit of this experiment has been chosen to be well above the frequencies of the expected spin rate interference.

2. TECHNICAL DESCRIPTION OF THE EXPERIMENT

2.1 Electric Field Antenna

FIG. 3 shows a sketch of the electric field/radio astronomy antenna used on the HELIOS spacecraft. The antenna is an extendible cylindrical dipole 32 meters tip-to-tip, similar to the antennas used on the Alouette, OGO, IMP, and RAE satellites. In order to reduce the capacity between the antenna and the spacecraft photo-electron sheath to an acceptable value, an insulating sleeve approximately 2.0 meters long is placed over the antenna where the antenna passes through the spacecraft photoelectron sheath region. The antenna diameter is as small as possible (0.635 cm) in order to minimize the ratio of resistive-to-capacitive coupling to the surrounding plasma.

The electric field antenna and associated erection mechanism are provided by the spacecraft for this experiment. The antenna erection mechanism is designed to minimize the antenna to erection mechanism capacitance. This capacitance does not exceed approximately 30 pf in the extended configuration. Also, special consideration has been given to electrostatically shielding the antenna from spacecraft related interference, such as through the erection motor, deployment length indicators, etc.

2.2 Electric Antenna Preamplifier

Each element of the electric dipole is connected to three preamplifiers which provide signals to the respective University of Iowa, University of Minnesota, and GSFC experiments.

2.3 Main Electronics Package

A block diagram of the main experiment electronics is shown in FIG. 4. The main elements of the experiment electronics consist of (1) a differential amplifier, (2) a 16-channel spectrum analyzer, (3) an antenna potential monitor, (4) a shock alarm, and (5) a power supply.

The differential amplifier provides AC signals proportional to the potential difference between the antenna elements. It provides a high order of common mode rejection to reduce the response to interference signals present on both antenna elements. The differential amplifier is followed by a narrow band notch filter which provides approximately 30 db of attenuation at frequencies of 20 kHz, 40 kHz, and 60 kHz (harmonics of the power supply frequency).

The 16-channel spectrum analyzer is the basic element of the University of Iowa experiment. This analyzer is to provide relatively coarse frequency coverage and rapid temporal resolution with essentially continuous coverage of all frequencies (20 Hz to 200 kHz) and all times (using peak detectors). The nominal frequency response of the various spectrum analyzer channels is shown in FIG. 5. The lowest 8 frequency channels use active filters spaced with four filters per decade of frequency. The highest 8 frequency channels use passive filters spaced with four filters per decade. The detector and log compressor in each channel will rectify and log compress signals from the filter and produce an output proportional to the logarithm of the noise intensity in each filter channel. The dynamic range of the compressors extends from 10 μV to 1 V rms. The log compressor output is used to provide three outputs: (1) a peak output (P), (2) an average output (A), and (3) a short time constant output (S).

The peak output provides a voltage (0-5 volts) proportional to the logarithm of the peak signal since the preceding reading. The peak detector is reset after readout by a signal from the Data Processing Unit (DPU).

The average output provides an RC average output with either (1) a time constant τ which depends on the bit rate and science format mode or (2) a forced short time constant, τ_s. Which time constant is used is determined by the shock alarm channel number.

The short time constant outputs provide short-time-constant field strength voltages to the shock mode memory. One channel of short time constant outputs is continuously available in the science data. This channel is determined by the shock alarm channel number. The output from this channel is sampled 16 times in one spacecraft revolution by the DPU and stored for later readout.

The DPU provides a Shadow Blanking Pulse to the experiment to open the input to the 8 lowest frequency compressors for 4 sectors twice per revolution to reduce the

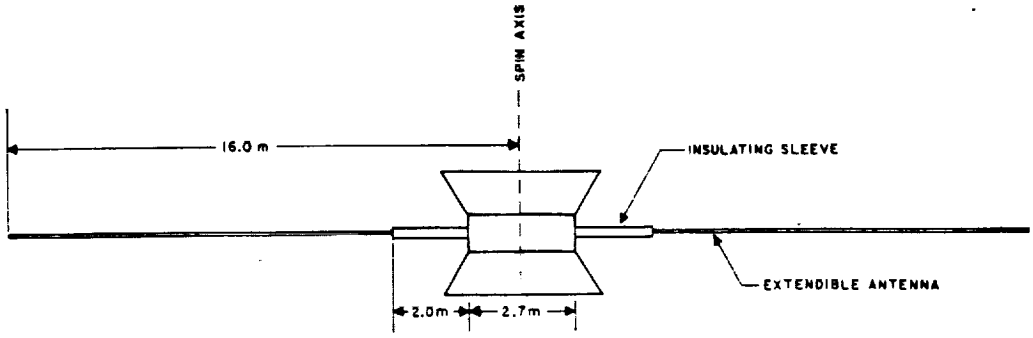

FIG. 3:
Sketch of the electric field/radio astronomy antenna used on the HELIOS spacecraft

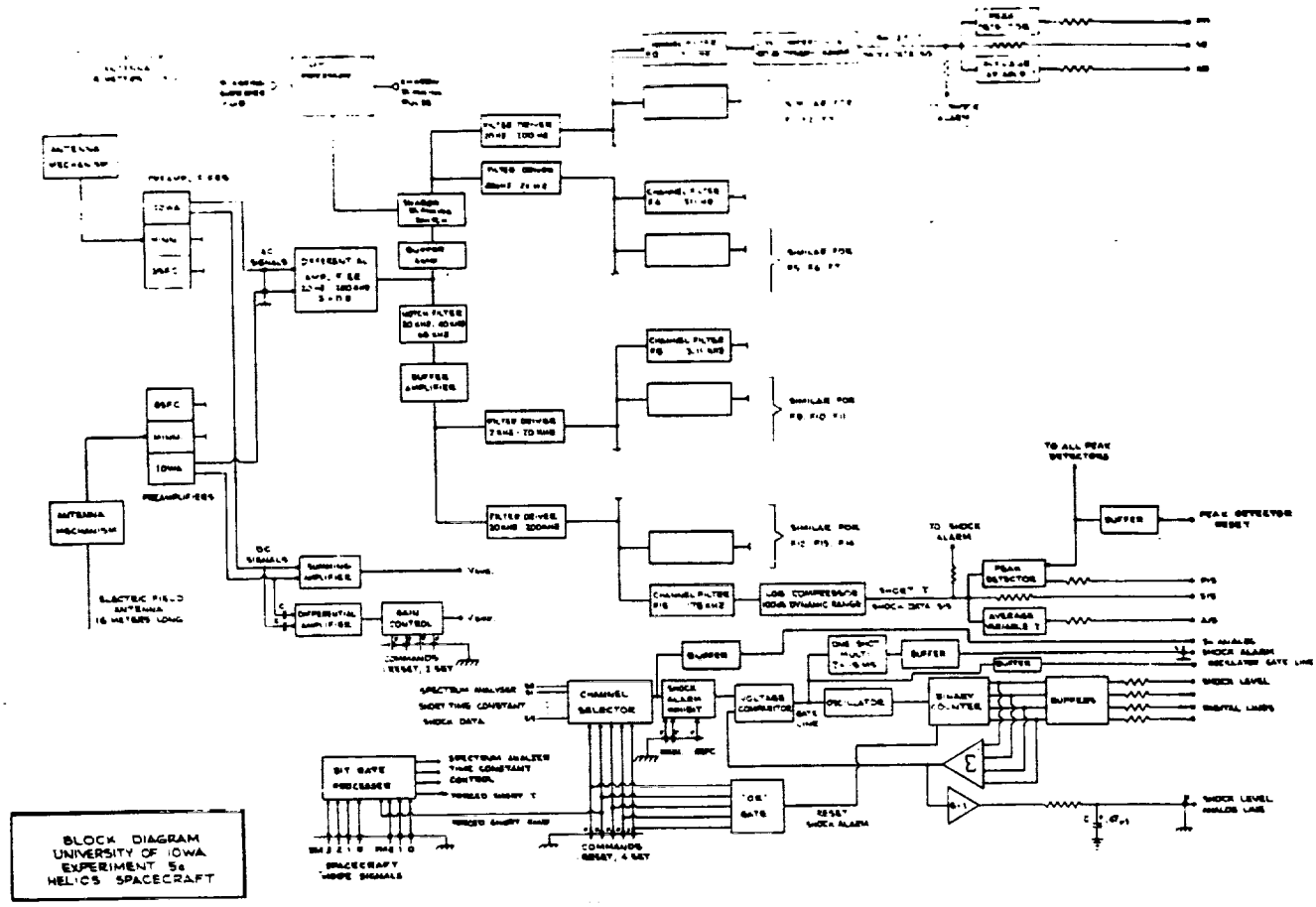

FIG. 4: **Block diagram of the University of Iowa HELIOS solar wind plasma wave experiment**

effects of the large voltage pulses generated as the antennas sweep through the spacecraft shadow. This blanking pulse can be eliminated by command.

The average potential, V_{avg} and the difference potential, V_{diff}, between the antenna elements are measured with operational amplifiers in the main electronics package. The frequency range of the V_{diff} measurement is from 0.2 to 10.0 Hz. The dynamic range of the V_{diff} measurement can be controlled by command to be either $\pm$ 8.0, $\pm$ 2.0, $\pm$ 0.5, or $\pm$ 0.125 volts. The dynamic range of the V_{avg} measurement is $\pm$ 20.00 volts. These data are needed for a complete understanding of the antenna operation in the plasma surrounding the spacecraft.

A shock alarm signal is to be sent to the spacecraft when the electric field experiment senses noise associated with an interplanetary shock wave. The shock alarm circuit will permit the selection of any one of the 16 spectrum analyzer channels, by command, for shock identification. The threshold field strength required to trigger the shock alarm has 16 levels and is controlled by a 4 bit binary counter. The shock threshold level is reset whenever any shock channel command is received. After reset, the threshold is advanced upward every time the threshold is exceeded, in each case the new threshold level is set to the peak value of the electric field strength observed. This procedure, therefore, results in the storage of the "best" event observed over the shock search interval.

The experiment power supply provides regulated voltages of $\pm$ 6 volts and $\pm$ 12 volts to the experiment electronics. The power supply operates at a frequency of 20 kHz and is synchronized by a 40 kHz synchronization signal provided by the spacecraft.

2.4 Data Processing Unit

The Data Processing Unit (DPU) for the Plasma Waves Experiment is separate from the main experiment electronics and is provided by GSFC through an industrial contractor. The purpose of the DPU is to (1) provide interface connections between the experiment and the spacecraft, (2) provide A/D conversion of all scientific analog data, (3) provide buffer storage, as necessary, to adapt to the spacecraft data transmission format.

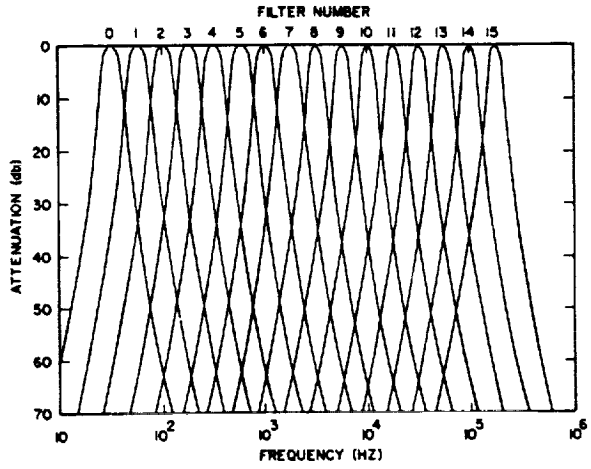

FIG. 5: **Frequency response curves for the 16 spectrum analyzer channels**

REFERENCE:

[1] SCARF, F. L., G. M. CROOK, I. M. GREEN and P. F. VIROBIK: Initial results of the Pioneer 8 VLF electric field experiment, **J. Geophys. Res., 73**, 6665, 1968.

Reprinted from
10 December 1976, volume 194, pages 1159-1162

SCIENCE

Electron Plasma Oscillations Associated with Type III Radio Bursts

Abstract. *Plasma wave electric field measurements with the solar orbiting Helios spacecraft have shown that intense (approximately 10 millivolts per meter) electron plasma oscillations occur in association with type III solar radio bursts. These observations confirm the basic mechanism, proposed in 1958, that type III radio emissions are produced by intense electron plasma oscillations excited in the solor corona by electrons ejected from a solar flare.*

Plasma wave electric field instruments on the German-American Helios 1 and Helios 2 spacecraft, in orbit around the sun, have detected intense electron plasma oscillations in association with type III solar radio bursts. These observations confirm a well-known mechanism, proposed by Ginzburg and Zheleznyakov (*1*) in 1958, for the generation of these radio emissions. In this report we briefly describe the essential features of the plasma oscillation mechanism for generating type III radio bursts and present the recent Helios results, which show the occurrence of intense electron plasma oscillations in association with type III radio bursts.

Type III radio bursts are produced by particles ejected from a solar flare and are characterized by an emission frequency which decreases with increasing time. These radio bursts are observed

over a very broad frequency range, from as high as several hundred megahertz to as low as 10 khz. The characteristic frequency variation of type III radio bursts was explained by Wild (2) in 1950, who proposed that the radio emissions are generated at a local oscillation frequency of plasma in the solar corona called the electron plasma frequency: $f_p = 9n^{\frac{1}{2}}$ (khz), where n is the electron density (cm $^{-3}$). The decreasing emission frequency with increasing time is attributed to the decreasing electron density, hence plasma frequency, encountered by the solar flare particles as they move outward through the solar corona and solar wind. Measurements with satellite-borne instruments have shown that the particles responsible for the type III radio emissions are electrons with energies ranging from a few kiloelectron volts to several tens of kiloelectron volts (3).

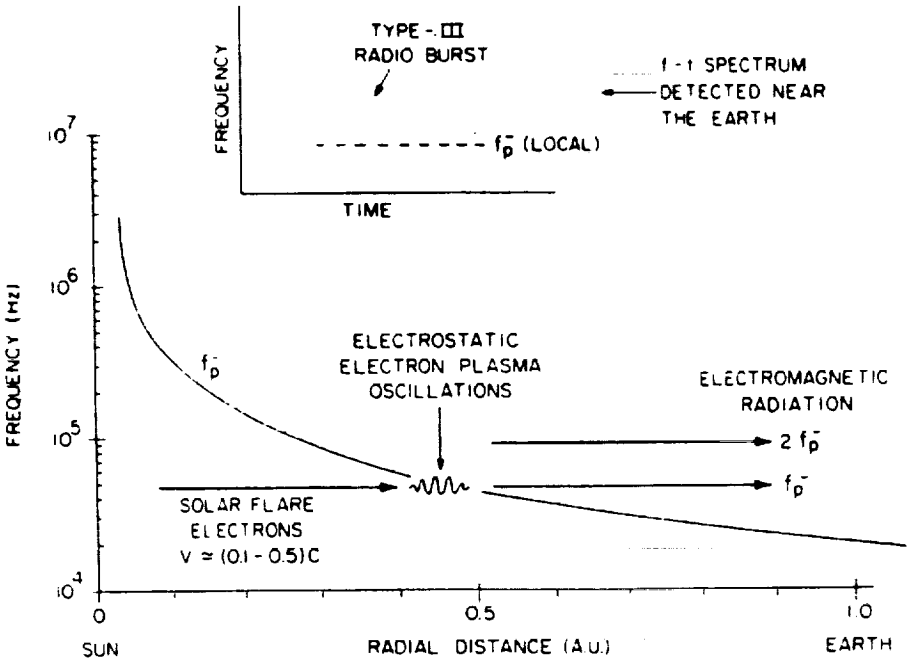

Fig. 1. Radial variation of the electron plasma frequency, f_p^-, between the sun and the earth. Type III solar radio bursts are believed to be generated by a two-step process in which (i) localized electron plasma oscillations at f_p^- are produced by solar flare electrons streaming outward from the sun, and (ii) these plasma oscillations are converted to escaping electromagnetic radiation by nonlinear wave-wave interactions. The characteristic frequency variation of the type III burst is caused by the decreasing plasma frequency encountered by the solar flare electrons as they move away from the sun. Abbreviations: v, electron velocity; c, speed of light.

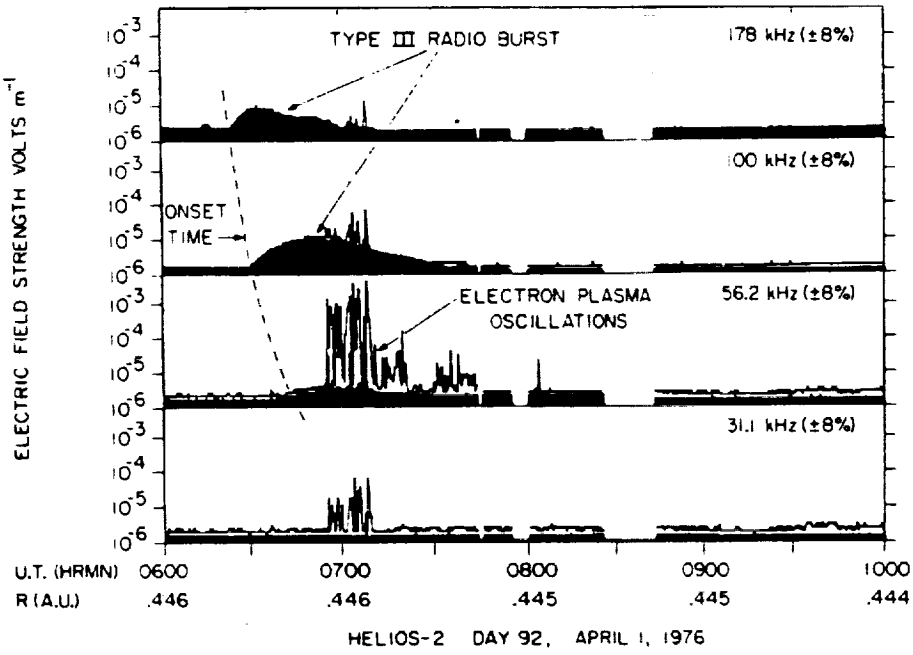

Fig. 2. Example of the intense electron plasma detected by Helios 2 in association with a type III solar radio burst. Note the characteristic increasing onset time of the type III burst with decreasing frequency and the narrow bandwidth of the electron plasma oscillations in the 56.2-khz channel. The electron plasma frequency determined by the solar-wind plasma experiment on Helios is $f_p^- = 54$ khz, which is very close to the observed frequency of the electron plasma oscillations. The solid lines give the peak electric field intensities, and the solid black area indicates the average intensities.

According to the mechanism proposed by Ginzburg and Zheleznyakov, and subsequently refined and modified by other investigators (4, 5), the generation of type III radio emissions is a two-step process in which (i) electrostatic plasma oscillations are first produced at the local electron plasma frequency by a two-stream instability excited by the solar flare electrons, and (ii) the plasma oscillations are converted to electromagnetic radiation by nonlinear wave-wave interactions. This mechanism is illustrated schematically in Fig. 1, which shows a model for the radial variation of the electron plasma frequency from the sun to the earth. According to current ideas, the electrostatic energy of the plasma oscillations is transformed into electromagnetic radiation at either the fundamental (f_p^-) or the harmonic ($2f_p^-$) of the local electron plasma frequency. The radiation at the fundamental is caused by interactions of the plasma oscillations with ion sound waves, and the radiation at the second harmonic is caused by interactions between oppositely propagating electron plasma oscillations. Radiation at both the fundamental and the harmonic has been detected, although at low frequencies ($\leq$ 1 Mhz) the harmonic radiation appears to be the dominant component (6).

Since the electron plasma oscillations are local phenomena and cannot be detected remotely, in situ measurements must be obtained in the solar corona or solar wind to confirm the occurrence of these oscillations in association with type III bursts. Rough estimates, using the theoretical model of Papadopoulos *et al.* (5), indicate that plasma oscillations with field strengths of about 10 mv m^{-1} or larger are required to explain the power flux of a typical type III radio burst at low frequencies (7). Although it should be possible to detect such plasma oscillations in the solar wind with earth-orbiting satellites, considerable difficulty has been experienced in obtaining confirming observations. After nearly 4 years of measurements with the earth-orbiting IMP 6 and IMP 8 satellites, no elec-

ron plasma oscillations with intensities this large have been found in association with a type III radio burst (7). This difficulty can be attributed to two factors. First, since the plasma oscillations occur only in the source, whereas the type III radiation propagates over large distances, electron plasma oscillations are expected to be detected for only a small fraction of the observable type III radio bursts. If the source region is very small or filamentary, as appears to be the case, then it is very improbable that the spacecraft will be suitably located within the beam of electrons ejected by the flare to detect the plasma oscillations. Second, and probably more important, for satellite observations near the earth it is very difficult to distinguish plasma oscillations generated by electrons from a solar flare from similar plasma oscillations (8) generated in the vicinity of the earth by electrons emitted from the earth's bow shock. The noisy and very disturbed plasma environment near the earth makes it very difficult to identify the plasma oscillations expected in association with a type III radio burst.

The solar orbiting Helios 1 and Helios 2 spacecraft provided the first opportunity to obtain simultaneous measurements of plasma waves and radio emissions away from the disturbing effects of the earth and in the region close to the sun, where the solar radio bursts are most intense. These spacecraft were launched on 10 December 1974 and 15 January 1976 into eccentric orbits near the ecliptic plane with perihelion radial distances of 0.309 and 0.290 A.U., approaching closer to the sun than any previous spacecraft. The plasma wave and radio astronomy instrumentation on the Helios spacecraft consists of a 32-m electric dipole antenna and a combination of frequency spectrum analyzers provided by the University of Iowa, the University of Minnesota, and Goddard Space Flight Center. A more detailed description of this instrumentation is provided by Gurnett and Anderson (9).

During the first 18 months after the launch of Helios 1, a total of 24 type III radio bursts was detected by the two Helios spacecraft. Of these, three events have been found with unusually intense electron plasma oscillations, which are almost certainly associated with the type III radio emission. The basic parameters for these events are summarized in Table 1. All three of these events were detected by Helios 2 within a single 24-hour interval from 31 March to 1 April 1976, during a period of exceptional solar flare activity which lasted from 23 March to 2 April 1976. At the time of these events Helios 2 was at a radial distance of about 0.45 A.U. from the sun and in a position which placed the spacecraft within, or very near, the source region of the type III radio emission.

Table 1. Type III radio bursts associated with intense electron plasma oscillations detected by Helios 1 and Helios 2 spacecraft. The values in the last column are the plasma oscillation field strengths required to account for the observed radio emission intensities; they were computed by using the theory of Papadopoulos *et al.* (5) with $\alpha = 0.1$, $n = 36$ electron/cm^3, $T_e = 10$ ev, and $R = 0.44$ A.U. [see (7) for details of these calculations].

Type III burst			f_p^- (khz)	Electric field strength of plasma oscillations (mv m^{-1})	
Date (1976)	U.T.	Intensity at $2f_p^- = 100$ khz (watt m^{-2} hertz^{-1})		Observed	Calculated
31 March	1810	1.15×10^{-17}	58	14.8	6.01
1 April	0620	2.59×10^{-17}	54	5.26	7.37
1 April	1038	8.17×10^{-17}	56	2.35	9.82

The detailed electric field intensities for one of these events are shown in Fig. 2. The type III radio emission can be clearly seen in the 178- and 100-khz channels and is just barely detectable in the 56.2-khz channel. The smooth intensity variation and the increase of onset time with decreasing frequency provide a unique identification of this event as a type III radio burst. Starting at about 0655 U.T., and lasting to about 0720 U.T., a series of intense bursts of electric field noise is evident in the 56.2-khz channel. These bursts are very intense, reaching a peak electric field strength of 5.26 mv m^{-1}. This intensity is almost 60 db greater than the corresponding intensity of the type III radio emission in this channel. Comparisons with the solar wind plasma density measurements from Helios (10) show that the center frequency of these bursts, ~ 56.2 khz, is very close to the local electron plasma frequency, $f_p^- = 54$ khz. The bandwidth of these bursts is evidently very narrow, since the corresponding weak bursts in the adjacent 31.1- and 100-khz channels can be completely attributed to the frequency response of the spectrum analyzer filters, assuming a nearly monochromatic emission at $f_p^- = 54$ khz. The narrow bandwidth of the bursts and the close agreement of the emission frequency with the local electron plasma frequency provide convincing evidence that this electric field noise consists of electron plasma oscillations. The very close temporal correspondence between the occurrence of these plasma oscillations and the occurrence of the type III radio burst leaves essentially no doubt that the plasma oscillations are associated with the type III emission. A qualitatively similar relationship is also observed for the remaining two events.

The peak electric field strengths of the three intense plasma oscillation events detected by Helios and the corresponding type III radio emission intensities at $2f_p^- = 100$ khz are summarized in Table 1. For comparison, the computed plasma oscillation field strengths required to account for the observed radio emission intensities are also shown in Table 1. These electric field intensities have been calculated by using the theoretical model of Papadopoulos *et al.* (5) for the conversion of the plasma oscillation energy to electromagnetic radiation. Further details of the assumptions used in these calculations are given by Gurnett and Frank (7). As can be seen from Table 1, the observed plasma oscillation field strengths are in excellent quantitative agreement with the field strengths required by the theory.

The Helios observations have provided a firm confirmation that the basic plasma oscillation mechanism proposed by Ginzburg and Zheleznyakov is involved in the generation of type III radio emissions. However, many important questions still remain. Since intense plasma oscillations of the type detected by Helios are rarely observed compared to the number of type III radio bursts detected at the earth (7), it is generally concluded that the spatial distribution of plasma oscillations must be highly inhomogeneous, with the intense plasma oscillations confined to small isolated regions. Since the power radiated by the plasma oscillations is a very strong function (fourth power) of the electric field strength, the fraction of the total volume containing plasma oscillations could be quite small, < 1 percent, with only a moderate increase in the required field strengths. For each of the three cases detected by Helios the plasma oscillations are extremely impulsive, consisting of many short bursts lasting for only a few

seconds or less. These impulsive variations are clearly indicated by the large ratio of the peak to average field strengths evident in Fig. 2. The highly inhomogeneous structure indicated by these variations was not contemplated in the original model of Ginzburg and Zheleznyakov, which only dealt with the linear growth of the plasma oscillations, and has been studied only recently (5) in relation to the large-amplitude nonlinear evolution of the two-stream instability. Considerable further investigation, both theoretical and experimental, is still required to fully understand the spatial structure of these intense plasma oscillations and the implications with regard to the generation of radio emissions by the sun and other cosmic radio sources.

DONALD A. GURNETT
ROGER R. ANDERSON
Department of Physics and Astronomy, University of Iowa, Iowa City 52242

References and Notes

1. V. L. Ginzburg and V. V. Zheleznyakov, *Sov. Astron. AJ* **2**, 653 (1958).
2. J. P. Wild, *Aust. J. Sci. Res. Ser. A* **3**, 541 (1950).
3. L. A. Frank and D. A. Gurnett, *Sol. Phys.* **27**, 446 (1972); H. Alvarez, F. Haddock, R. P. Lin, *ibid.* **26**, 468 (1972); R. P. Lin, L. G. Evans, J. Fainberg, *Astrophys. Lett.* **14**, 191 (1973).
4. P. A. Sturrock, *Nature (London)* **192**, 58 (1961); D. A. Tidman, T. J. Birmingham, H. M. Stainer, *Astrophys. J.* **146**, 207 (1966); S. A. Kaplan and V. N. Tsytovich, *Sov. Astron. AJ* **11**, 956 (1968); D. F. Smith, *Space Sci. Rev.* **16**, 91 (1974).
5. K. Papadopoulos, M. L. Goldstein, R. A. Smith, *Astrophys. J.* **190**, 175 (1974).
6. M. L. Kaiser, *Sol. Phys.* **35**, 181 (1975).
7. D. A. Gurnett and L. A. Frank, *ibid.*, p. 477.
8. F. L. Scarf, R. W. Fredricks, L. A. Frank, M. Neugebauer, *J. Geophys. Res.* **76**, 5162 (1971).
9. D. A. Gurnett and R. R. Anderson, *ibid.*, in press.
10. We thank H. Rosenbauer and R. Schwenn from the Max-Planck-Institut for providing the plasma density data from Helios.
11. Research at the University of Iowa was supported by NASA contract NAS5-11279 and grant NGL-16-001-043. Research was performed by D.A.G. while on leave at the Max-Planck-Institut für Extraterrestrische Physik, Garching bei München, West Germany. Research at the Max-Planck-Institut was supported by the Alexander von Humboldt Foundation.

14 July 1976; revised 8 October 1976

Plasma Wave Electric Fields in the Solar Wind: Initial Results From Helios 1

DONALD A. GURNETT[1]

Max-Planck-Institut für extraterrestrische Physik, 8046 Garching, West Germany

ROGER R. ANDERSON

Department of Physics and Astronomy, University of Iowa, Iowa City, Iowa 52242

Plasma wave measurements provided by Helios 1 show that the electric field intensities in the solar wind are usually very low, much lower than those for comparable measurements near the earth, where particles moving upstream from the bow shock often cause large disturbances in the solar wind. The most commonly occurring plasma wave detected by Helios is a sporadic emission at frequencies from about 1 to 10 kHz, between the electron and ion plasma frequencies. These waves are thought to be ion sound waves which are Doppler-shifted upward in frequency from below the ion plasma frequency. The maximum electric field intensity of these waves is a few hundred microvolts per meter. At higher frequencies, from about 20 to 100 kHz, electron plasma oscillations are detected at frequencies near the local electron plasma frequency. These electron plasma oscillations are more intense, with field strengths sometimes as large as a few millivolts per meter, but occur very infrequently. Both the ion sound waves and the electron plasma oscillations show a tendency to occur at higher frequencies closer to the sun but no pronounced variation in intensity with radial distance from the sun. In four cases, electron plasma oscillations have been found in association with type III radio bursts.

INTRODUCTION

In this paper we survey and analyze the electric field measurements obtained from the University of Iowa plasma wave experiment on the Helios 1 spacecraft. Helios 1, which was launched on December 10, 1974, is in an eccentric solar orbit near the ecliptic plane with initial perihelion and aphelion radial distances of 0.309 and 0.985 AU, respectively. The University of Iowa plasma wave experiment on Helios 1 provides measurements of electric field intensities in the frequency range from 31 Hz to 178 kHz. This frequency range includes most of the characteristic frequencies of the plasma (the electron plasma frequency f_p^-, the ion plasma frequency f_p^+, and the electron gyrofrequency f_g^-) expected in the solar wind from 0.3 to 1.0 AU. The data obtained from this experiment provide the first observations of plasma waves in the region close to the sun ($R \simeq 0.3$ AU) and measurements with greatly improved sensitivity and frequency range in comparison to any previous solar wind plasma wave investigations performed at 1.0 AU.

Plasma waves play a crucial role in most, if not all, plasma interactions which take place in low-density collisionless plasmas. When the mean free path of the particles becomes much larger than the basic scale length of the system, as occurs in the solar wind and the earth's magnetosphere, collisions can no longer provide the mechanism for energy and momentum exchange between the particles. As the system evolves, deviations from thermal equilibrium occur which produce unstable particle distributions. In the region of instability, waves develop which grow to such large amplitudes that they directly affect the distribution function of the interacting particles. These wave-particle interactions usually tend to drive the distribution function toward thermal equilibrium, the waves playing a role similar to collisions in an ordinary fluid.

In the early solar wind models of *Parker* [1958] it was realized that microscopic collisionless interactions must be present to account for the fluidlike properties of the solar wind. The importance of these collisionless interactions was later confirmed in more detail by the two-fluid calculations of *Hartle and Sturrock* [1968], which showed that the solar wind protons must be heated somewhere inside 1 AU to account for the observed proton temperature and velocity at the earth. Because of the low collision frequency in the solar wind this heating must involve wave-particle interactions. Over the past 10 years, numerous theoretical studies have been performed to try to identify the most important and relevant plasma wave instabilities which occur in the solar wind. See, for example, the recent review by *Hollweg* [1975]. Most of these studies have concentrated on various types of low-frequency hydromagnetic (Alfvén) waves and instabilities which occur at frequencies below the ion gyrofrequency. The properties of these low-frequency hydromagnetic waves have now been extensively studied by using satellite-borne magnetometers on interplanetary spacecraft (see, for example, *Coleman* [1966], *Belcher and Davis* [1971], and *Burlaga* [1971]). At higher frequencies, in the range appropriate for comparison with the Helios plasma wave measurements, several types of electrostatic and electromagnetic instabilities have been suggested which may play an important role in controlling the macroscopic structure of the solar wind. *Fredricks* [1969] suggested that electrostatic ion sound waves, driven by currents at discontinuities in the solar wind, could heat the protons in the solar wind by resonant interactions. Substantial proton heating by waves of this type is only expected at radial distances of less than about 0.3 AU. *Forslund* [1970] considered the possible types of two-stream instabilities which could occur because of the skewing of the electron distribution function caused by heat conduction in the solar wind. Four types of instabilities were found which could be driven by electron heat conduction: electromagnetic ion cyclotron, electrostatic ion cyclotron, magnetoacoustic, and ion acoustic. Any of these modes could in principle be unstable in the solar wind at 1 AU.

[1] Permanent address: Department of Physics and Astronomy, University of Iowa, Iowa City, Iowa 52242.

Paper number 6A0740

Schulz and Eviatar [1972] and *Hollweg* [1975] have suggested that these heat conduction driven instabilities may significantly lower the heat conduction in the solar wind, with corresponding modifications of the radial temperature gradient. When streams of energetic electrons are ejected into the solar wind by a solar flare, electron plasma oscillations are expected to be produced by two-stream instabilities at frequencies near the electron plasma frequency. Electron plasma oscillations have received extensive theoretical study because of their presumed relationship to solar radio emissions, particularly type III solar radio bursts [*Ginzburg and Zheleznyakov*, 1958; *Sturrock*, 1961; *Tidman et al.*, 1966; *Smith*, 1974]. These waves are thought to play an important role in controlling the energy spectrum and temporal evolution of the energetic 1- to 100-keV solar flare electrons [*Papadopoulos et al.*, 1974].

Although plasma waves are thought to be of considerable importance in the solar wind, relatively little is known about the types of waves which occur in the solar wind at frequencies above the ion gyrofrequency. Near the earth many measurements of plasma wave electric and magnetic fields have been made in the solar wind with sensitive and reliable instruments. However, in the absence of interplanetary shocks or other large-scale disturbances the proper identification of the waves intrinsic to the solar wind from measurements near the earth is greatly complicated by the disturbing effects of particles arriving from the earth's bow shock and magnetosphere. By very careful investigation of the particle distribution functions to determine the origin of the particles producing an instability, it is possible to identify waves intrinsic to the solar wind. An example of an investigation of this type is given by *Gurnett and Frank* [1975], in which electron plasma oscillations associated with electrons from a solar flare are identified by the Imp 8 spacecraft near the earth. Because of the difficulty of separating out the effects caused by the earth's interaction with the solar wind, few measurements of this type have been made near the earth.

In interplanetary space, far away from the disturbing effects of the earth, the only previous measurements of high-frequency plasma waves ($f >> f_e$) are from the Pioneer 8 and 9 spacecraft [*Scarf et al.*, 1968; *Scarf and Siscoe*, 1971], which provided electric field measurements in the solar wind at radial distances between about 0.75 and 1.0 AU. Since the Pioneer 8 and 9 electric field experiments were relatively insensitive (they used a short telemetry antenna as an electric field sensor), only the most intense plasma waves could be detected. The principal results of the Pioneer 8 and 9 plasma wave experiments were the occasional detection of strong low-frequency ($f \approx 400$ Hz) electric field turbulence in the solar wind. Several different types of turbulence were identified depending on the detailed temporal variations and correlations with other parameters. Short-duration 'spikes' in the electric field intensity at ~400 Hz tended to occur at discontinuities in the magnetic field or plasma parameters (such as at interplanetary shocks) and were closely associated with the occurrence of sudden commencements and geomagnetic disturbances at the earth [*Siscoe et al.*, 1971]. Detailed studies of the electric field intensities during selected storm periods showed a significant variation in the broadband electric field intensity with radial distance from the sun, with maximum broadband intensities of nearly 50 mV m^{-1} (equivalent 100-Hz sine wave response) at 0.75 AU [*Scarf et al.*, 1973]. Longer-duration events, sometimes lasting for one to several days, were also occasionally observed in the broadband electric field measurements with amplitudes of typically 1–10 mV m^{-1} in the 400-Hz channel [*Siscoe et al.*, 1971]. These long-duration events were found to be correlated with regions of enhanced density, such as occur ahead of high-speed streams. Near the earth, electron plasma oscillations associated with the earth's bow shock were detected by Pioneer 8 and 9 [*Scarf et al.*, 1968]; however, comparable plasma oscillations were not observed in interplanetary space away from the effects of the earth [*Scarf et al.*, 1972].

As will be shown, the plasma wave electric field measurements provided by Helios 1 add considerably to the Pioneer 8 and 9 results by providing measurements over a wider range of frequencies and radial distances and with considerably better sensitivity. For most of the types of waves detected by Helios 1 the electric field intensities are below the sensitivity threshold of the Pioneer 8 and 9 instruments, so no direct comparisons can be made. Waves with intensities comparable to the intense low-frequency spikes and long-duration events observed by Pioneer 8 and 9 have not yet been detected by Helios 1.

Instrument Description

The plasma wave and radio astronomy experiment of Helios 1 consists of a combination of three instruments: a 16-channel spectrum analyzer from the University of Iowa to provide high

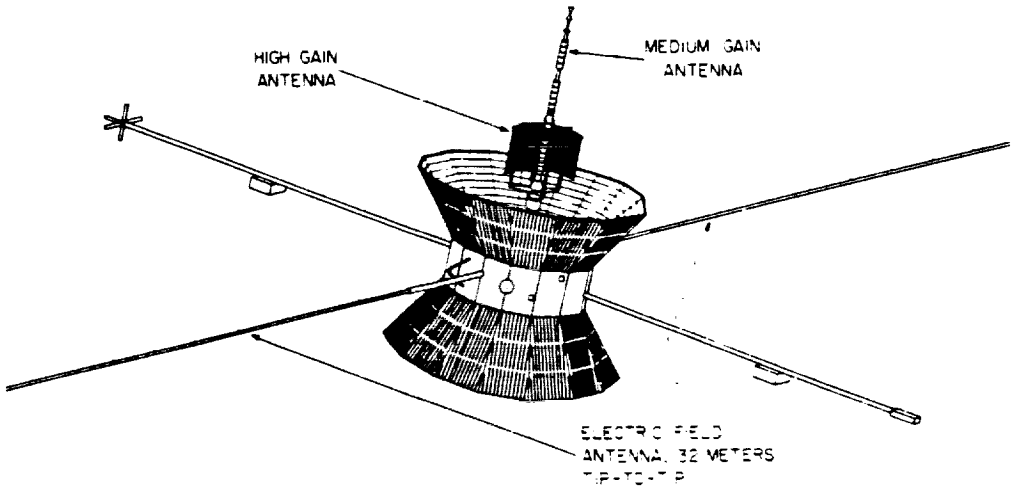

Fig. 1. The geometry of the electric field antenna used for the Helios plasma wave measurements. The spacecraft is spin-stabilized with the medium gain telemetry antenna axis oriented perpendicular to the ecliptic plane.

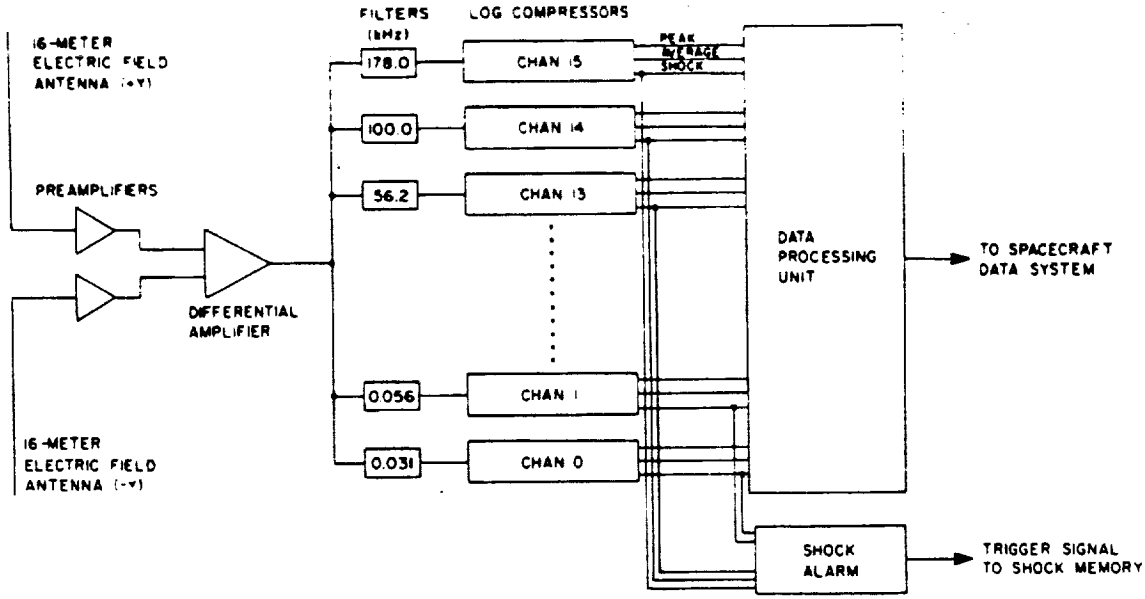

Fig. 2. A block diagram of the University of Iowa plasma wave experiment on Helios. The shock alarm is used to initiate a very rapid sampling rate mode using the spacecraft memory.

time resolution plasma wave measurements in the frequency range from 31 Hz to 178 kHz, a narrow bandwidth spectrum analyzer with 168 frequency steps from the University of Minnesota to provide high frequency resolution plasma wave measurements in the frequency range from 10.4 Hz to 209 kHz, and a 16-channel radiometer from Goddard Space Flight Center to provide solar radio wave measurements in the frequency range from 26.5 kHz to 3.0 MHz. Only results from the University of Iowa instrument are presented in this paper. All three instruments share a single electric dipole antenna with a nominal tip-to-tip length of 32 m, which is extended outward perpendicular to the spacecraft spin axis, as is shown in Figure 1. The spacecraft spin axis is oriented perpendicular to the ecliptic plane, and the nominal spin rate is 1.0 rps.

A block diagram of the University of Iowa plasma wave instrument is shown in Figure 2. This instrument consists of 16 continuously active receiver channels with four frequency channels per decade. The bandwidth of these channels is relatively wide, $\pm 10\%$ for the channels from 31 Hz to 1.78 kHz and $\pm 8\%$ for the channels from 3.11 to 178 kHz. The frequency passbands overlap to provide essentially continuous coverage of all frequencies from about 20 Hz to 200 kHz. The signal from each filter channel is processed by a logarithmic compressor which provides a voltage output proportional to the logarithm of the electric field strength. The dynamic range of the logarithmic compressor is 100 dB. Two types of field strength measurements, called the average and the peak, are made for each channel. The average field strength is the exponentially weighted average (a resistance-capacitance integrator) of the logarithm of the field strength with a time constant of 50 ms for all channels except 56 and 31 Hz, which have time constants of 100 and 200 ms, respectively. The peak field strength is obtained from a peak detector which gives the maximum field strength since the preceding sample. The continuously active channels, with peak detection and overlapping frequency response, assure that any wave which occurs within the frequency and sensitivity range of the instrument will be detected, even very short bursts with durations much shorter than the sampling period. The 16 peak and 16 average field strengths are sampled essentially simultaneously by a data processing unit which provides analog-to-digital conversion and formating for the spacecraft data system. A wide range of sampling rates is possible, depending in detail on the spacecraft bit rate and telemetry format. The fastest sampling rate in real-time operation provides a complete set of 16 peak and 16 average samples every 1.125 s. Even faster sampling rates, up to 14.2 samples per second for each channel, are possible when a rapid read-in to the spacecraft memory is used. The memory read-in is triggered by a 'shock alarm' circuit (see Figure 2) which responds to the field strength in a preselected channel. A shock alarm signal is generated whenever the field strength exceeds the largest field strength detected since the last memory readout. The memory is organized to store data both immediately before and immediately after the shock alarm signal occurs. The overall function of the shock alarm and memory read-in is to provide very rapid sampling of the electric field spectrum, as well as other magnetic field and plasma data, around the time of maximum field strength.

In-Flight Operation and Near-Earth Observations

Shortly after the launch of Helios 1 it was discovered that one of the two antenna elements which make up the electric dipole antenna did not extend properly and was electrically shorted to the spacecraft structure. The resulting antenna configuration is therefore an electric monopole, the spacecraft body and associated booms acting as a ground plane. Although this is not the intended antenna configuration, the effects of this failure are not particularly serious. Monopole antennas of this type have been successfully used on several previous spacecraft plasma and radio wave experiments [*Shvh*, 1965; *Benediktov et al.*, 1968; *Scarf et al.*, 1968]. The primary detrimental effects for the Helios 1 experiment are a loss of 6 dB in the electric field sensitivity because of the shorter antenna length and an increase in the noise level of the 178-kHz channel by about 25 dB because of an interference signal conducted into the experiment from the shorted antenna. It was also thought that the reduced common mode rejection caused by the asymmetrical antenna configuration would result in larger interference levels, particularly from the spacecraft solar array. However, comparisons with the Helios

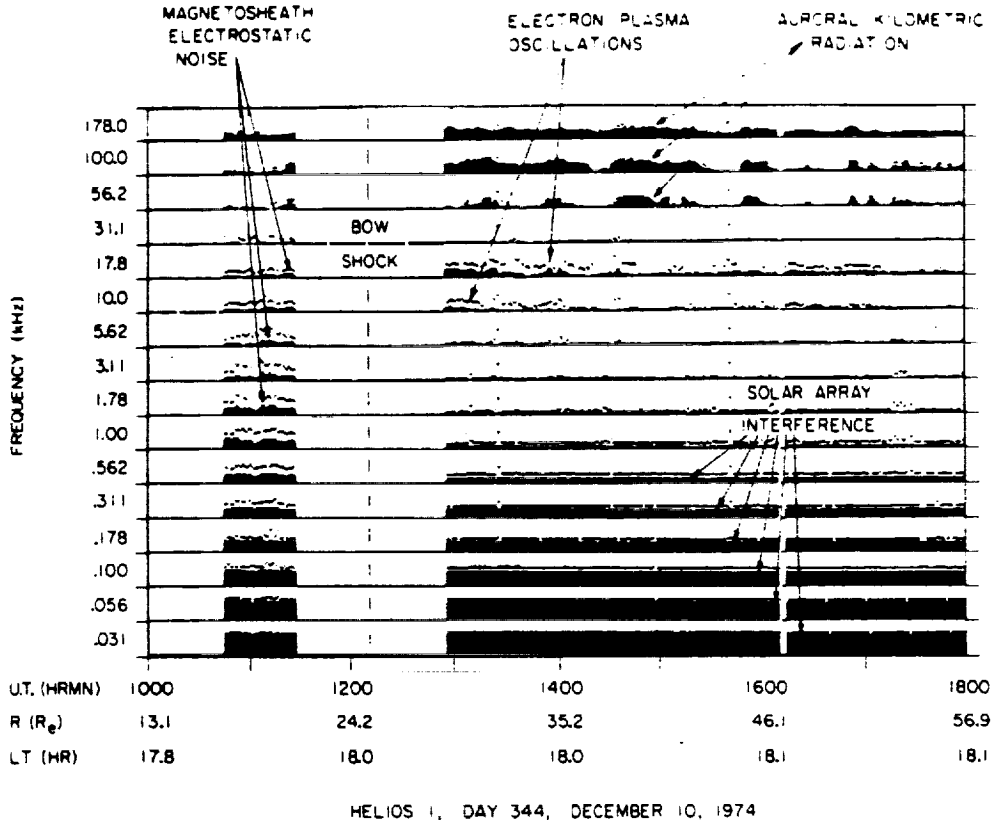

Fig. 3. The electric field intensities detected by Helios 1 during the outbound pass through the bow shock shortly after launch.

2 spacecraft, which was recently launched and for which both antennas extended properly, show that the background noise voltages are essentially the same in all except the 178-kHz channel.

One disadvantage of a monopole antenna is that the effective length cannot be estimated as well as for a dipole antenna because of the complicated geometry of the spacecraft body. To calculate electric field strengths from the Helios 1 data, we assume that the spacecraft body acts as a perfect ground plane, in which case the effective length is one half of the length of the monopole element, or l_{eff} = 8.0 m. This assumption is justified mainly on the grounds that the spacecraft body and associated booms have a rather large capacitance to the surrounding plasma which should maintain the spacecraft potential essentially constant with respect to the local plasma potential. At higher frequencies, above the electron plasma frequency where the plasma effects are not important, the effective length is probably somewhat smaller, by about 15–20%, because of the finite size of the ground plane. Because of the large range of electric field strengths encountered in the solar wind, uncertainties of this magnitude are not considered serious. The calculated electric field strengths also rely on the assumption that the wavelengths are longer than the antenna length. In most cases, specific tests based on spin modulation measurements of the antenna pattern and Doppler shift estimates can be performed to verify this assumption.

To demonstrate the operation of the experiment in an environment which has already been extensively investigated, we have analyzed the electric field intensities observed as Helios 1 passes through the region near the earth's bow shock shortly after launch. The electric field intensities in this region are shown in Figure 3 for all 16 channels, from 31 Hz to 178 kHz. The ordinate for each channel is proportional to the logarithm of the electric field strength, and the interval from the base line of one channel to the base line of the next higher channel represents a range of electric field strengths from about 1 μV m^{-1} to 100 mV m^{-1} for l_{eff} = 8.0 m. The peak electric field strengths are indicated by dots, and the average field strengths are indicated by vertical bars (the solid black areas) extending upward from the base line of each channel.

During the pass through the bow shock one of the strongest and most prominent types of noise detected by Helios 1 is a high-frequency (50–500 kHz) radio emission generated in the earth's auroral zones. This noise, which is called terrestrial (or auroral) kilometric radiation [*Gurnett*, 1974; *Kurth et al.*, 1975], is detectable for several weeks after launch and is clearly evident in the frequency channels above 50 kHz in Figure 3. Auroral kilometric radiation provides a useful source for verifying the effective length of the monopole antenna. During a period of maximum intensity, at a radial distance of 31.1 R_E from the earth (1315 UT), the power flux of the auroral kilometric radiation is found to be 2.98×10^{-15} W m^{-2} at 178 kHz for an effective length of 8.0 m. From a comparison with Figure 5 of *Gurnett* [1974] it is seen that this power flux is in good quantitative agreement with the typical maximum intensities of auroral kilometric radiation detected by the Imp 6 spacecraft at comparable radial distances from the earth.

Because of the data gap from 1128 to 1255 UT in Figure 3, no plasma wave measurements are available at the time of the actual bow shock crossing. Before the bow shock crossing, during the interval from about 1045 to 1128 UT, a broad spectrum of electric field noise is detected, extending from frequencies below 31 Hz to greater than 56.2 kHz. This noise is characteristic of the intense electrostatic turbulence which is

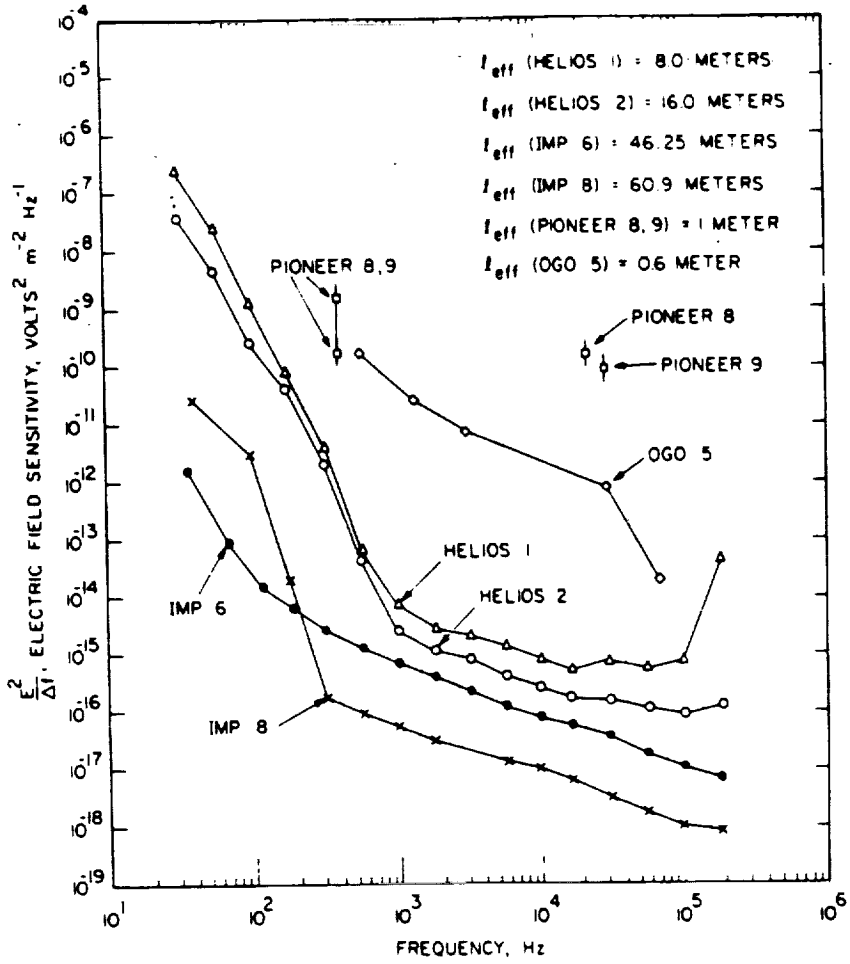

Fig. 4. The threshold electric field sensitivity of Helios 1 and Helios 2 compared to several other plasma wave experiments which have made electric field measurements in the solar wind. The rapid increase in the noise level at low frequencies is caused by interference from the spacecraft solar array.

commonly observed throughout the magnetosheath downstream of the bow shock [*Rodriguez and Gurnett*, 1975]. After the bow shock crossing, from about 1255 to 1425 UT and in several intervals thereafter, an intense narrow band electric field emission is evident in the 10.0- and 17.8-kHz channels. This narrow band emission consists of electron plasma oscillations of the type discussed by *Scarf et al.* [1971], excited by electrons streaming into the solar wind from the bow shock. For an effective length of 8.0 m the electric field strength of these plasma oscillations is found to range from about 100 μV m^{-1} to 1 mV m^{-1}, with occasional peaks as large as 3 mV m^{-1}. These field strengths are in good quantitative agreement with similar measurements obtained from the Imp 6 and 8 spacecraft [see *Gurnett and Frank*, 1975].

In Figure 4 we show the in-flight noise level of the Helios 1 plasma wave experiment (and also Helios 2) and compare these noise levels with several other similar experiments which have made electric field measurements in the solar wind. In each case the noise levels have been calculated by using the effective length determined from strictly geometrical considerations, without regard for errors caused by sheath effects or wavelengths shorter than the antenna. The rapid increase in the noise level of the Helios experiments at low frequencies, below about 1.0 kHz, is caused by interference from the spacecraft solar array. Because of the spacecraft rotation, large voltage transients, as large as 70 V, occur as the solar panels rotate into and out of the sunlight. These voltage transients are coupled to the antenna through the plasma sheath surrounding the spacecraft and produce strong interference over a very broad range of frequencies. This same type of interference also occurs at low frequencies in the Imp 6 and 8 electric field measurements but is more intense on Helios because of the higher spin rate (1.0 rps) in comparison to the spin rates of Imp 6 and 8 (0.083 and 0.4 rps). The difference in sensitivity between Helios 1 and Helios 2 is caused by the factor of 2 difference in the antenna lengths. The improved sensitivity of the Imp 6 and 8 experiments is mainly due to the longer antennas used on these spacecraft. Since comparisons are to be made later with the Pioneer 8 and 9 electric field measurements, the noise levels of the Pioneer 8 and 9 experiments are also shown in Figure 4, based on the instrument parameters given by *Scarf et al.* [1968] and *Scarf and Siscoe* [1971]. The noise levels of the Pioneer experiments assume an effective length of 1.0 m, which, as was pointed out by *Scarf et al.* [1968], is considered somewhat uncertain because of possible errors introduced by local sheath effects. Also shown for comparison are the noise levels of the Ogo 5 electric field experiment (F. Scarf, personal communication, 1976), which has made electric field measurements in the solar wind [*Scarf et al.*, 1972]. The noise levels of the Ogo 5 7.3- and 14.0-kHz channels are not shown because of the presence of strong spacecraft-generated interference in these channels.

A highly unusual and unexpected interference problem was encountered on Helios 1 when the *S* band telemetry signal was

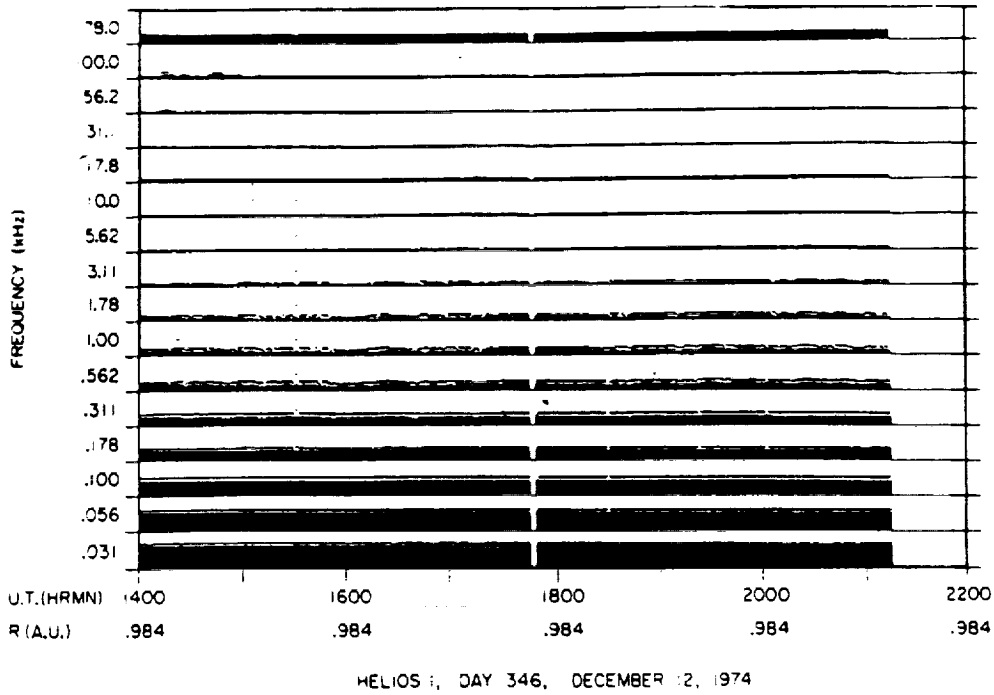

Fig. 5. An example of one of the many "quiet" periods observed in the Helios 1 plasma wave data.

switched from the medium to high gain telemetry antenna about 10 days after launch. When the telemetry transmitter was switched to the high gain antenna, a very intense broadband interference occurred, with an increase in noise level of nearly 50 dB in some channels. This interference was also accompanied by a number of other dramatic effects indicating a major disturbance in the plasma around the spacecraft, the most notable being a large increase in the $E \simeq 100$ eV electron flux detected by the solar wind plasma experiment (H. Rosenbauer, personal communication, 1976) and a charging of the electric antenna element to -30 to -40 V with respect to the spacecraft structure. Subsequent investigations of these effects have led to the conclusion that the interference and electron heating are caused by a multipacting breakdown of the high gain antenna feed. This breakdown is essentially a transit time resonance for electrons accelerated across the gap in the antenna feed and occurs when the secondary emission coefficient is sufficiently large to cause a rapid buildup of electron density in the gap [*Hatch and Williams*, 1954, 1958]. Since the resonance condition is highly sensitive to the gap spacing, the antenna feed on Helios 2 was redesigned with a larger gap spacing to eliminate this problem. As a result of this modification, no similar interference effects have yet been observed on Helios 2.

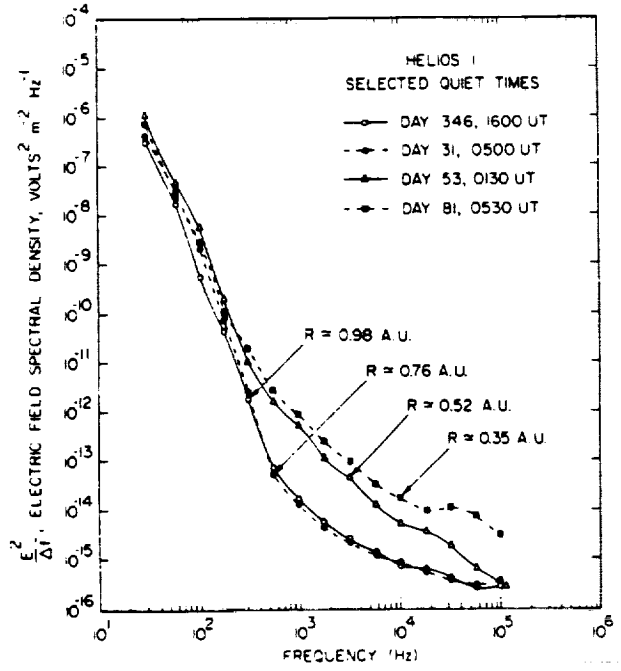

Fig. 6. The Helios 1 electric field noise levels at several selected quiet times between launch and first perihelion. These spectrums provide upper limits to the electric field intensities in the solar wind during quiet conditions. The enhanced noise levels near perihelion are believed to be caused by spacecraft-generated interference.

Because of the multipacting problem with the high gain antenna, useful plasma wave data could initially be obtained only by using the medium gain antenna. Since operation with the medium gain antenna resulted in a larger bit rate penalty to the other experiments, this mode of operation was quite limited, usually consisting of only a few 8-hour passes per week. Fortunately, shortly after the first perihelion passage the multipacting interference completely disappeared, and it has not reappeared again except for a short period during the second perihelion passage. The disappearance of the multipacting breakdown is not understood in detail but is generally thought to be caused by modifications of the surface properties (secondary electron emission coefficient) of the high gain antenna feed due to the high temperatures encountered near perihelion.

Since some of the results which will be presented involve the detection of relatively rare plasma wave phenomena, it is important to comment on the total quantity of data which has been analyzed. For this study all of the real-time data obtained from Helios 1 during the first 16 months of in-flight operation, consisting of approximately two and one-half orbits around the sun, have been processed and analyzed in detail. In addition, a survey has been made of the data currently available from Helios 2 during the first 2.5 months of in-flight operation.

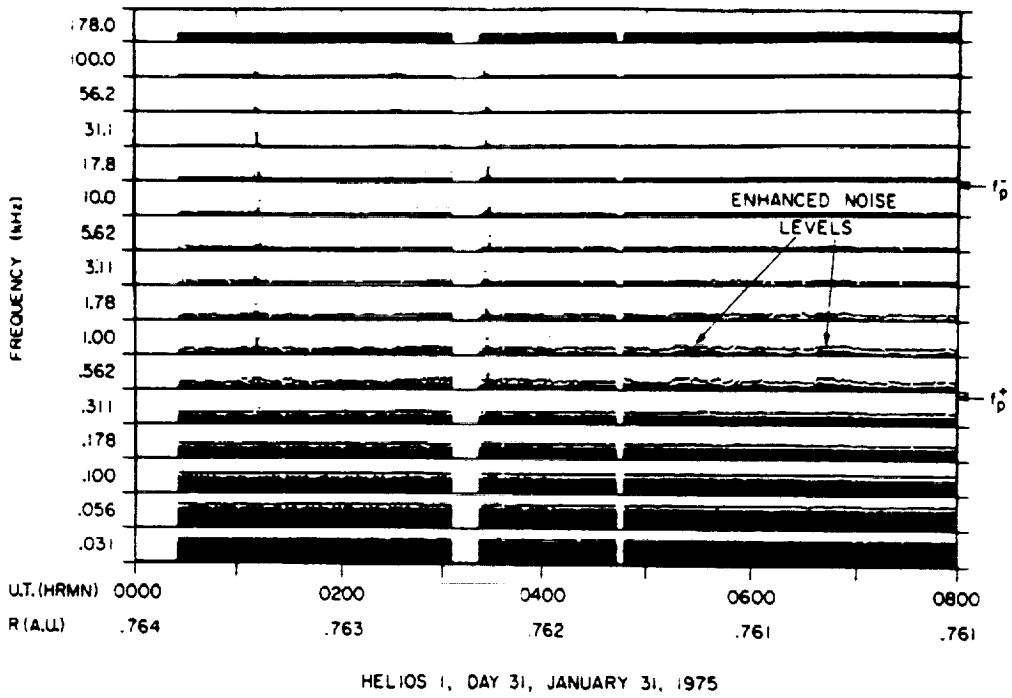

Fig. 7. Another example of a quiet period in which slightly enhanced noise levels are clearly evident in the 562-Hz to 3.11-kHz channels.

Because of the multipacting interference early in the flight of Helios 1 and the reduced telemetry coverage after the first perihelion the overall fraction of the time for which usable plasma wave data are available is only about 30%. This limitation in the available data significantly reduces the detection rate for relatively infrequent events such as type III solar radio bursts and interplanetary shocks. No interplanetary shocks have yet been identified in the Helios plasma wave data, although such events may be identified later when more detailed comparisons are made with the plasma and magnetic field data.

Quiescent Conditions in the Solar Wind

A characteristic feature of the Helios 1 plasma wave data is the almost complete absence of detectable electric fields for a substantial fraction of the time, 50% or more, and for long periods, sometimes lasting several days or longer. This is in striking contrast to measurements in the solar wind near the earth, where moderately intense plasma waves, produced by particles arriving from the bow shock and magnetosphere, are present a large fraction of the time. The electric field intensities during one such quiescent period are shown in Figure 5. Except for some very low intensity waves between about 562 Hz and 3.11 kHz, which will be discussed shortly, all of the electric field channels are near their minimum noise level, as determined by the solar array noise at frequencies below about 1.0 kHz and by the preamplifier noise at frequencies above 1.0 kHz. Comparable quiescent periods are a common feature of the Helios data at all radial distances from 1.0 to 0.3 AU. One notable effect, which was observed on both the first and the second perihelion passage, is a gradual increase in the background noise level with decreasing radial distance from the sun. This radial dependence is illustrated in Figure 6, which shows electric field spectrums selected at four representative radial distances during quiet times. The quiescent noise levels are seen to remain essentially constant from 0.98 to 0.76 AU but then to increase gradually by about 10–15 dB with decreasing radial distance, reaching maximum intensity near perihelion. Although the origin of the increased noise level near perihelion is not known, it is reasonably certain that this noise is not caused by plasma waves. The reason for this conclusion is that the noise intensity displays a pronounced variation with the spacecraft rotation, with a single maximum when the antenna is pointing away from the sun. To be interpreted as an electric field, the spin modulation must have two maximums per rotation. The most likely explanation is that the noise is caused by some type of spacecraft-generated interference which increases in intensity near perihelion. Numerous param-

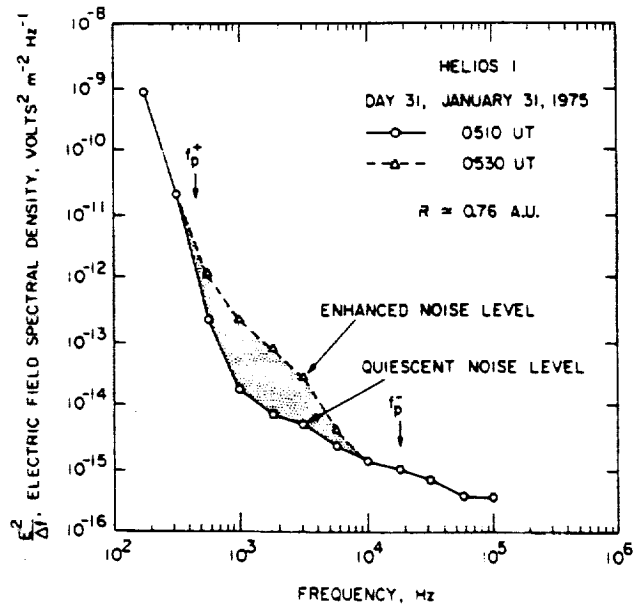

Fig. 8. An electric field spectrum during one of the periods of enhanced noise level evident in Figure 7. The broadband electric field strength of the waves which produce these enhancements is only about 10 μV m^{-1}.

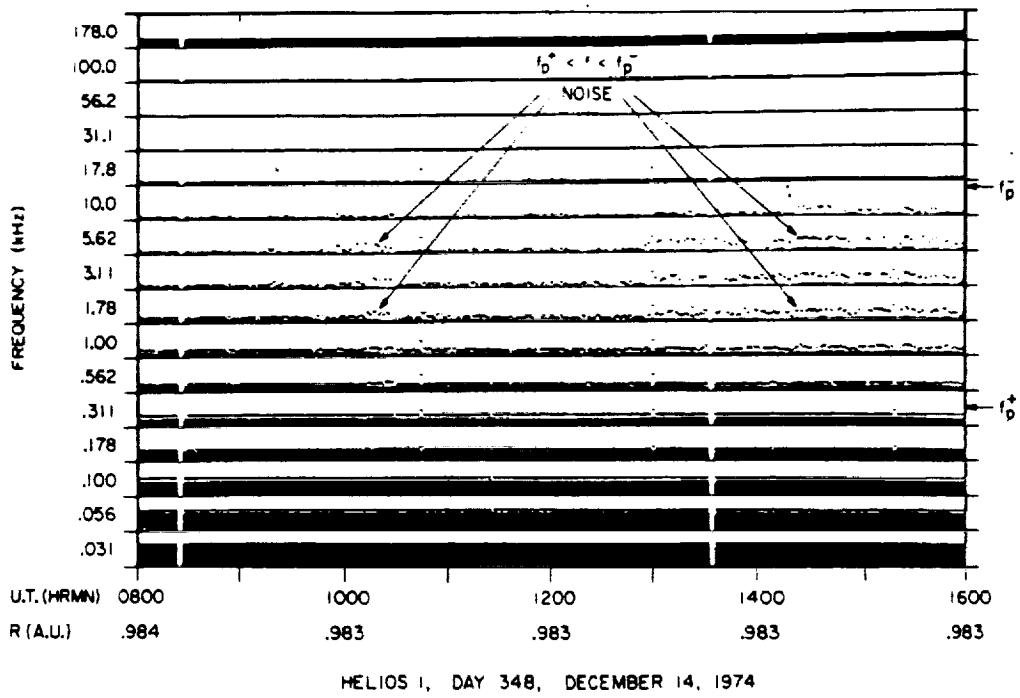

Fig. 9. A more disturbed period during which moderately intense electric fields are detected over a broad range of frequencies between electron and ion plasma frequencies f_p^- and f_p^+. The plasma frequencies are computed from the plasma densities measured simultaneously by the solar wind plasma experiment on Helios.

eters of the spacecraft power system, which could possibly affect the interference levels at high frequencies, vary considerably with radial distance from the sun.

During quiescent periods such as the one in Figure 5 there is often a slight irregular enhancement of the noise level in the 562-Hz to 3.11-kHz channels, suggesting that some very weak plasma waves may be present in this frequency range. An example of the otherwise quiescent interval during which these low-intensity enhancements are particularly evident is shown in Figure 7. The electric field spectrum during one of the periods of enhanced noise intensity, at 0530 UT, is shown in Figure 8 and is compared with the spectrum at a time of minimum noise level, at 0510 UT. Although it is very difficult to be certain that these periods of enhanced intensity are not caused by spacecraft interference, most of the evidence suggests that these enhancements are caused by plasma waves.

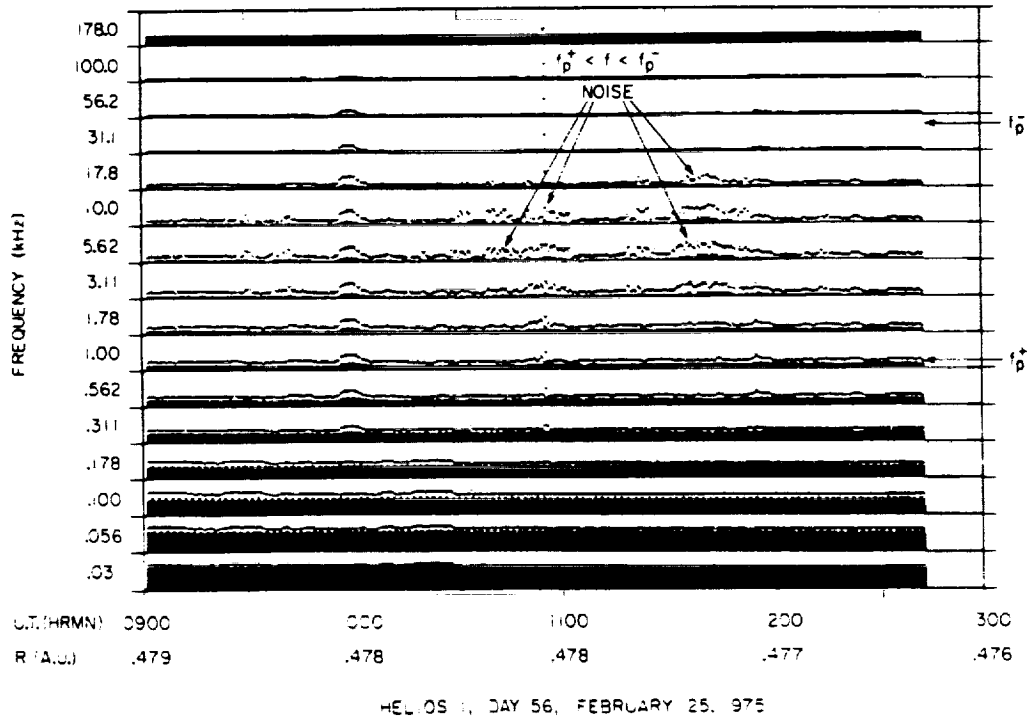

Fig. 10. Another example of the $f_p^+ < f < f_p^-$ noise, similar to Figure 9 but closer to the sun.

The fact that the enhancements appear in only a limited number of channels indicates that the noise is distinctly different from the multipacting interference and from the interference encountered near perihelion. Also, this same noise is detected even more clearly by Helios 2, which has better electric field sensitivity than Helios 1 and for which no multipacting interference has been detected.

If the very weak irregular enhancements in the 562-Hz to 3.11-kHz channels are due to plasma waves, then the electric field intensity of these waves is very small, the broadband electric field strength being only about 10 μV m^{-1}. Although these waves are very weak, they are apparently present a large fraction of the time, possible 50% or more, because they are almost always detectable, even during quiescent periods such as appear in Figures 5 and 7. Because of the difficulty of clearly resolving these very low intensities, further investigation of these waves will be delayed until more data are available from Helios 2, which has better sensitivity than Helios 1.

Waves Between the Electron and Ion Plasma Frequencies

Occasionally, intervals occur in the Helios 1 plasma wave data in which moderately intense electric field noise is detected in the frequency range from about 1 to 10 kHz. Two examples of this noise are shown in Figures 9 and 10, at radial distances of 0.98 and 0.47 AU, respectively. As will be shown, the frequency range of this noise consistently lies between the local electron and ion plasma frequencies f_p^- and f_p^+. We therefore refer to this noise as $f_p^+ < f < f_p^-$ noise. This terminology is adopted from a strictly observational viewpoint. It should be noted that if sizable Doppler shifts occur, then the actual wave frequencies in the rest frame of the plasma may not, in fact, be directly related to either of these frequencies.

Except for the extremely weak noise enhancements discussed in the previous section, the $f_p^- < f < f_p^+$ noise is the most commonly occurring type of plasma wave detected by Helios 1. When this noise occurs, it is usually observed with sporadic intensities for periods ranging from a few hours to several days. Such periods of enhanced $f_p^- < f < f_p^+$ noise intensities usually occur a few times per month. It seems likely that this noise is associated with a corotating feature of the solar wind which recurs for every solar rotation; however, at the present time the available data have not been analyzed in enough depth to establish a definite association. The noise has been detected at essentially all radial distances surveyed by Helios 1.

It is evident in Figures 9 and 10 that the peak intensities of the $f_p^- < f < f_p^+$ noise are larger than the average intensities by a factor of approximately 20–30 dB. This large ratio of the peak to average field strengths indicates that the noise is very impulsive, consisting of many brief bursts occurring on time scales that are short in comparison to the averaging interval (which is about 1 min for Figure 9 and 30 s for Figure 10). These impulsive temporal variations clearly distinguish this noise from the quiescent noise enhancements, as shown in Figure 7, which have a more nearly constant amplitude. To illustrate the temporal structure of the $f_p^- < f < f_p^+$ noise, Figure 11 shows a greatly expanded time scale, with 0.28-s resolution, from a shock mode memory read-in which occurred at about 1500 UT during the event in Figure 9. These high time resolution measurements show that the $f_p^- < f < f_p^+$ noise consists of many short bursts lasting for only a few tenths of a second. Even on this greatly expanded time scale the temporal structure of the individual bursts is sometimes not clearly resolved. Often when an individual burst occurs, it tends to occur simultaneously (within the time resolution available) across a broad range of frequencies.

Typical peak and average frequency spectrums of the $f_p^- < f < f_p^+$ noise are shown in Figure 12 at times of relatively high intensity selected from the events in Figures 9 and 10. The

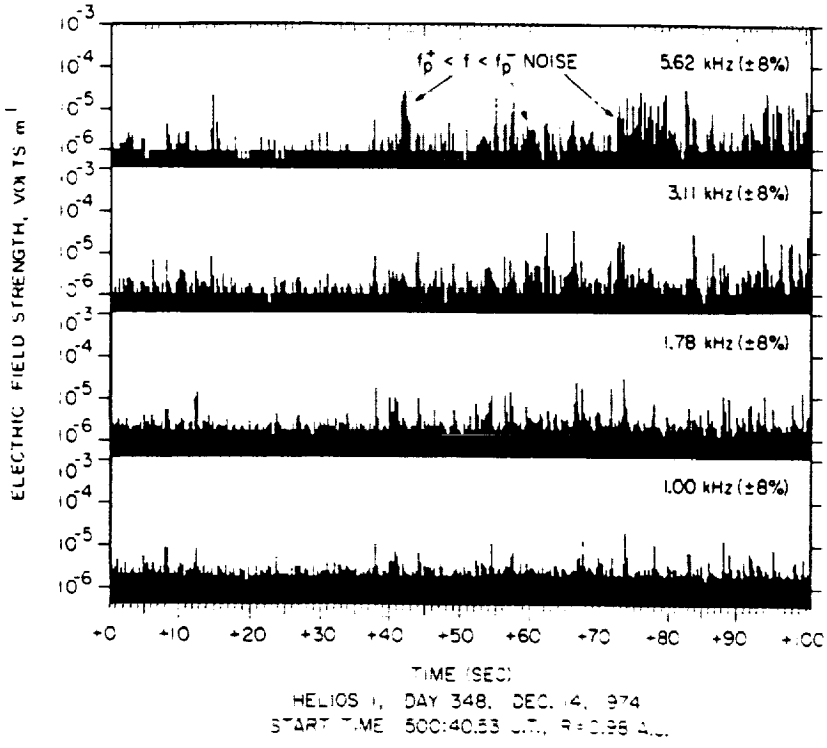

Fig. 11. High time resolution measurements of the $f_p^+ < f < f_p^-$ noise showing that the noise consists of many short bursts lasting only a few tenths of a second.

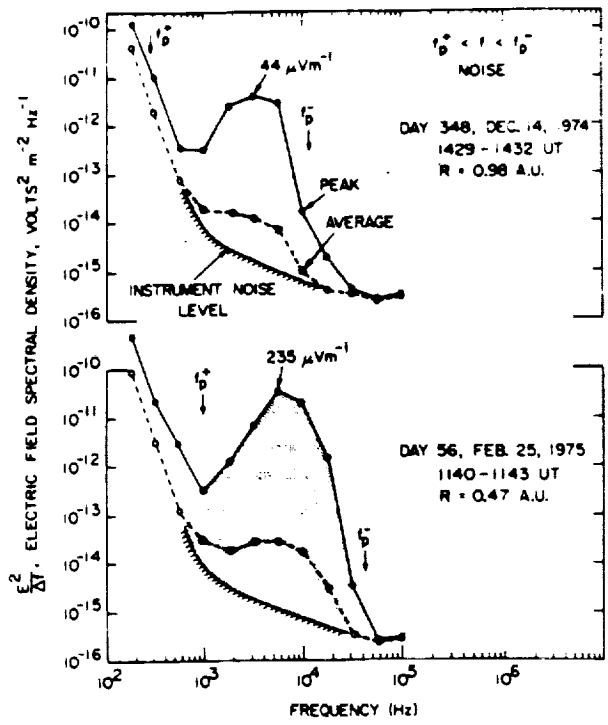

Fig. 12. Selected spectrums of the $f_p^+ < f < f_p^-$ noise showing the shift toward higher frequencies with decreasing radial distance from the sun. Also note the large ratio of the peak to average electric field strength, indicating very impulsive temporal variations.

large ratio between peak and average electric field intensities is clearly evident in these spectrums. Also shown are the electron and ion plasma frequencies as computed from the plasma densities given by the Helios 1 solar wind plasma experiment: f_p^- is computed from the total density of all ions, charge neutrality being assumed, and $f_p^+ = (m_e/m_p)^{1/2} f_p^-$, where m_e and m_p are the electron and proton masses. The spectrums are seen to consist of a single broad maximum between the electron and ion plasma frequencies. By comparing the spectrums for days 348 and 56, at $R = 0.98$ AU and $R = 0.47$ AU, it is seen that the frequency spectrum shifts toward higher frequencies, approximately in proportion to f_p^+ and f_p^-, as the spacecraft comes closer to the sun. Examination of other similar spectrums confirms the tendency evident in Figure 12 for the spectrum to shift toward higher frequencies with decreasing radial distance from the sun. This frequency shift is apparently directly associated with the increase in the electron and ion plasma frequencies as the solar wind density increases near the sun.

The spectrums in Figure 12 also show an increase in the peak electric field strength, from 44 to 235 μV m^{-1}, between day 348 and day 56, the largest field strength occurring closer to the sun. Although this comparison suggests that the electric field intensity of the $f_p^+ < f < f_p^-$ noise may increase with decreasing radial distance from the sun, examination of other similar cases shows that the electric strength variation from event to event is too large to provide any firm conclusion about the radial variation in the electric field intensity. The maximum single-channel electric field strength of the $f_p^+ < f < f_p^-$ noise is typically in the range from about 50 to 300 μV m^{-1} and seldom exceeds 500 μV m^{-1}.

To aid in identifying the plasma wave mode responsible for the $f_p^+ < f < f_p^-$ noise, it is of interest to establish the electric field direction of this noise relative to the magnetic field and solar wind velocity vectors. The electric field direction in the plane of rotation of the electric antenna can be determined from the spin modulation of the electric field intensities. Because the noise bursts usually occur on a time scale comparable to the time for one rotation (1 s), a statistical analysis must be performed over many events, usually for several hundred spacecraft rotations, to determine an average spin modulation pattern. This procedure is simplified on Helios by the fact that the average (50-ms time constant) field intensity measurements are always sampled in 16 equally spaced angular sectors. However, because of the very low average field strength of the $f_p^+ < f < f_p^-$ noise and the very impulsive intensity variations, simple averaging of the intensity as a function of the sector number does not give a good indication of the spin modulation. The approach used is to compute the frequency of occurrence of field intensities above a given threshold as a function of the threshold and the sector number. The spin modulation is then determined from the contours of constant frequency of occurrence as a function of the sector number. This method of analysis is less sensitive than simple averaging to errors introduced by a few exceptionally intense bursts.

An example of this spin modulation analysis for a $f_p^+ < f < f_p^-$ noise event detected at about 0.98 AU is shown in Figure 13. The accumulation interval for this frequency of occurrence determination is 1 hour. The antenna orientation angle ϕ_{SE}^A is the spacecraft-centered solar ecliptic longitude of the $+Y$ antenna axis, including a correction of 18° to account for the phase shift caused by the 50-ms receiver time constant. The solid and dashed lines give the electric field intensities at frequencies of occurrence of 5 and 10%, respectively. Even with a 1-hour accumulation interval, considerable scatter is still evident in the frequency of occurrence contours. Nevertheless, a consistent modulation pattern is clearly evident with the maximum intensities at about $\phi_{SE}^A \simeq -30°$ and $+150°$. During

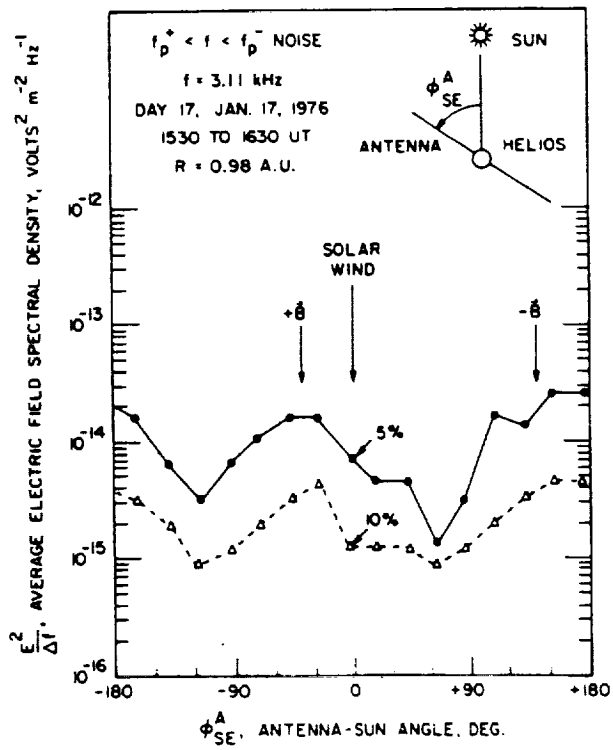

Fig. 13. The angular distribution of electric field intensities for the $f_p^+ < f < f_p^-$ noise. The electric field of this noise is oriented approximately parallel to the direction of the solar wind magnetic field.

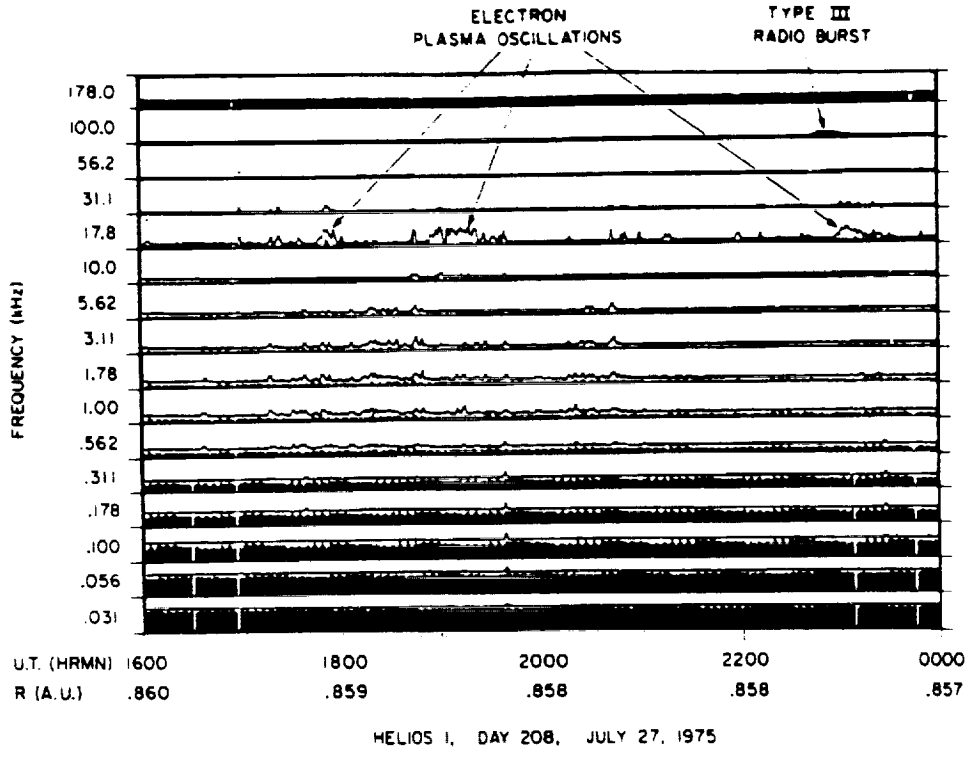

Fig. 14 Examples of electron plasma oscillations at $f \simeq f_p$ detected during a period of enhanced solar flare activity.

this interval the average spacecraft-centered solar ecliptic longitude and latitude of the magnetic field are approximately $\phi_{SE}{}^{B} = -40° \pm 10°$ and $\theta_{SE}{}^{B} = 0° \pm 20°$, respectively (F. Neubauer, personal communication, 1976). Because the magnetic field is oriented close to the spin plane of the electric antenna, this event provides a good case for determining the electric field orientation relative to the solar wind magnetic field direction. For comparison the magnetic field directions $+\mathbf{B}$ and $-\mathbf{B}$, projected into the plane of rotation of the antenna, are shown in Figure 13. The electric field intensities clearly have a symmetrical distribution with respect to the solar wind magnetic field direction, with the maximum intensity when the antenna axis is aligned parallel to the magnetic field. The sharp nulls in the electric field intensity, by about a factor of 10, indicate that the electric field of the $f_p^- < f < f_p$ noise is very closely aligned along the direction of the solar wind magnetic field, probably to within less than 15°.

Electron Plasma Oscillations

Occasionally, narrow band electric field emissions are detected in the frequency range from about 20 to 100 kHz which are almost certainly caused by electron plasma oscillations at the local electron plasma frequency f_p^-. An example of a period during which electron plasma oscillations are detected by Helios 1 is shown in Figure 14. The identification of these waves as electron plasma oscillations is based on the close similarity of the frequency spectrums and intensities to the electron plasma oscillations observed upstream of the bow shock, as seen in Figure 3. In contrast to the plasma oscillations detected near the earth, which are associated with electrons from the bow shock, the plasma oscillations shown in Figure 14 must be generated by particles of solar origin or by nonthermal particle distributions in the solar wind.

Typically, only one or two brief periods occur per month in which electron plasma oscillations are detected by Helios 1. In most cases the plasma oscillations are observed during a single isolated interval lasting from a few minutes to about half an hour. The plasma oscillation events which occur on day 208 (in Figure 14) and also continue to day 209 (not shown) represent an exceptionally active period with respect to the occurrence of electron plasma oscillations. This period corresponds to one of the few periods of substantial solar flare activity detected by Helios 1 during the first year of in-flight operation. On the basis of the previous association of electron plasma oscillations with low-energy (few keV) electrons ejected by a solar flare [*Gurnett and Frank*, 1975] it seems likely that the electron plasma oscillations detected during this period are associated with electrons from this flare activity. Preliminary comparisons with the data from the energetic particle and plasma experiments on Helios 1 (E. Keppler and H. Rosenbauer, personal communication, 1976) confirm that low-energy (1–20 keV) electrons of solar origin are present during this period. The type III radio burst associated with one of these flares is clearly evident in the 100-kHz channel of Figure 14, starting at about 2243 UT. This type III radio burst and others detected by Helios are discussed in the next section.

The electric field spectrum of the electron plasma oscillation detected on day 208, at a time of relatively high intensity, is shown in the top panel of Figure 15. Also shown are the spectrums for two other examples of electron plasma oscillations detected at closer radial distances to the sun. For comparison and confirmation of the identification of these waves as electron plasma oscillations, the local electron plasma frequencies determined from the solar wind plasma experiment are also given in Figure 15. The close correspondence between the emission frequency and the local electron plasma frequency is clearly evident. The spectrums in Figure 15 also show the expected increase in the electron plasma frequency as the solar wind density increases closer to the sun. This tendency, for increasing frequencies closer to the sun, is a general characteristic of all of the electron plasma oscillations detected by Helios 1.

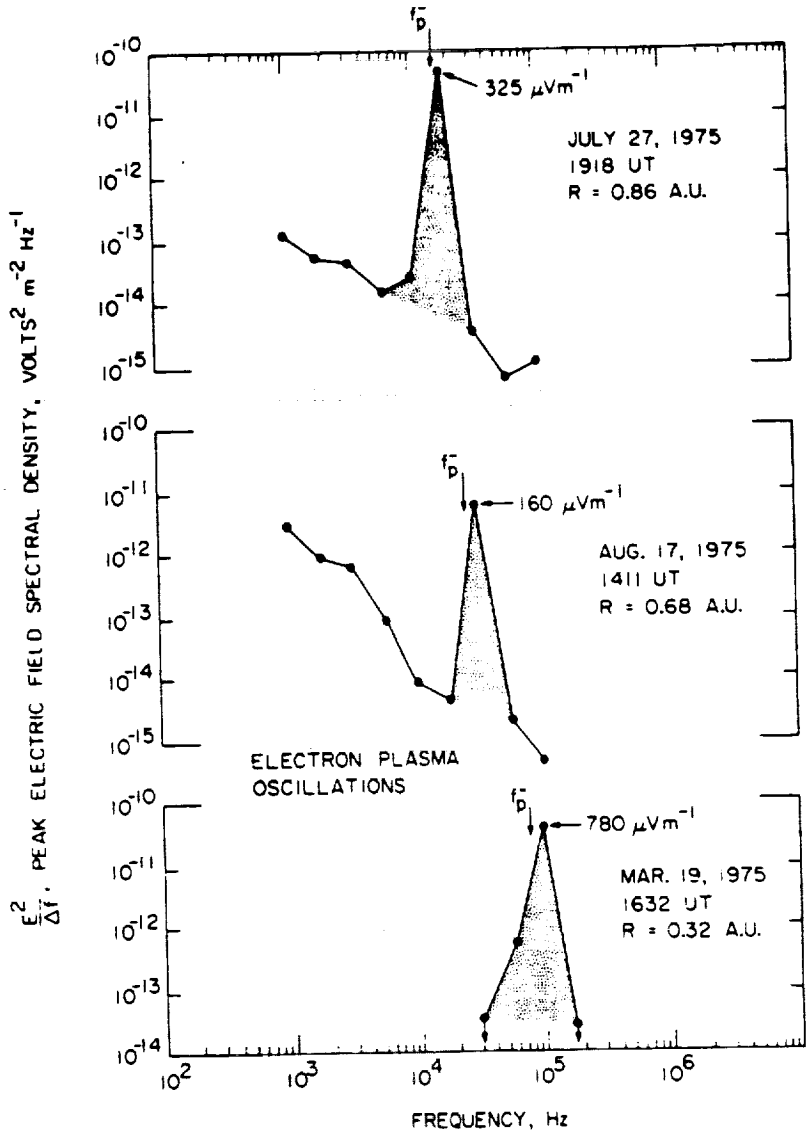

Fig. 15. Selected spectrums of electron plasma oscillations showing the tendency for increasing frequency with decreasing radial distance from the sun. The frequency of the plasma oscillations is in good agreement with the electron plasma frequency f_p determined from the solar wind plasma experiment.

As can be seen from Figure 14, the peak electric field intensities of the electron plasma oscillations are considerably larger than the average field intensities, which remain near the receiver noise level during the entire event. The large ratio of the peak to average field strengths indicates that the electron plasma oscillations, like the $f_p^- < f < f_p^-$ noise, consist of many brief bursts with durations that are short in comparison to the averaging interval. The temporal structure of a typical burst of electron plasma oscillations is illustrated in Figure 16, which shows a greatly expanded time scale for a series of plasma oscillation bursts detected during a shock mode memory read-in. The rise and decay times of the individual bursts are clearly resolved in these data and are typically in the range from about 0.25 to 1.0 s. In this case the durations of the bursts are only a few seconds. Occasionally, much longer bursts are observed lasting as long as several minutes. When multiple bursts occur, a moderately well defined upper limit to the field strength is often evident (as is true for the first three bursts in Figure 16) and is an indication that some nonlinear effect saturates the instability. The saturation level is usually in the range from about 100 to 500 μV m^{-1}, although occasionally, larger field strengths do occur, as will be discussed in the next section. Electron plasma oscillations with field strengths exceeding 1 mV m^{-1} are extremely rare. Because of the limited number of events available and the large variation in the intensity from event to event it is not known for certain whether the electric field strength has a significant variation with radial distance from the sun. Some of the most intense events have been observed at radial distances near the sun, as is shown in Figure 15.

As is true for the $f_p^- < f < f_p^-$ noise, the electric field orientation of electron plasma oscillations can be determined from spin modulation measurements. Because long-duration bursts sometimes occur with nearly constant (saturated) intensities, the spin modulation pattern can be determined very easily in these cases. Figure 17 shows the spin modulation observed during a single rotation for an unusually long (2 min) burst of plasma oscillations detected by Helios 1 near perihelion (R = 0.332 AU). During this event the solar wind magnetic field is oriented near the spin plane of the antenna: $\phi_{SE}^B = -15° \pm 3°$, and $\theta_{SE}^B = 19° \pm 1°$ (F. Neubauer, personal communication, 1976) in a direction favorable for determining

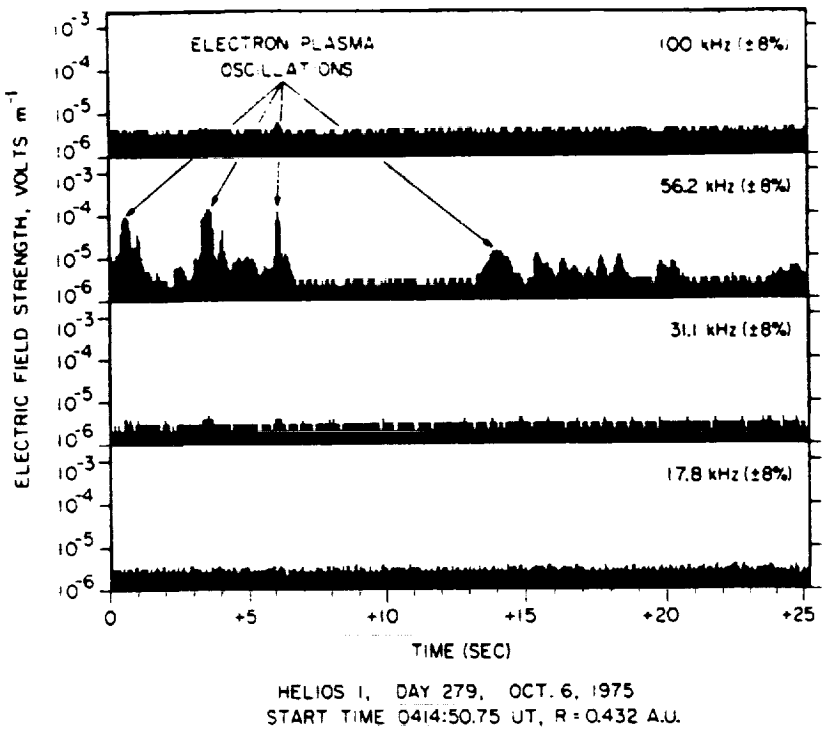

Fig. 16. High time resolution measurements showing several bursts of electron plasma oscillations with durations of only a few seconds. Note the nearly constant saturation amplitude of the first three bursts.

the electric field orientation relative to the magnetic field direction. As can be seen from Figure 17, the maximum electric field intensity occurs when the antenna axis is parallel to the magnetic field. The sharp nulls when the antenna axis is perpendicular to the magnetic field indicate that the electric field of the electron plasma oscillations is very closely aligned along the direction of the solar wind magnetic field, probably to within less than 20°.

Type III Solar Radio Bursts

One of our primary objectives in studying type III solar radio bursts is to determine whether electron plasma oscillations are involved in the generation of these radio emissions, as has been suggested for many years. In all of the data currently available a total of 18 type III solar radio bursts have been detected by Helios 1 and 2. Of these 18 type III radio bursts, 4 show clear evidence of electron plasma oscillations which could possibly be associated with the radio emission. Two of these events, shown in Figures 18 and 19, occur in association with the solar flare activity on days 208 and 209 (July 27 and 28), 1975, discussed in the previous section, and the second two events, shown in Figures 20 and 21, occur in association with the solar flare activity on day 92 (April 1), 1976.

Before detailed discussion of these events it is useful to consider the ideal 'signature' to be expected if electron plasma oscillations are involved in the generation of type III radio emissions. As is well known, type III radio bursts are produced by electrons ejected into the solar wind by a solar flare. At low frequencies ($\lesssim 1$ MHz), considerable evidence exists showing that the type III radio emissions occur at the harmonic $2f_p$ of the local electron plasma frequency [*Fainberg et al.*, 1972; *Haddock and Alvarez*, 1973; *Kaiser*, 1975]. The characteristic frequency-time dispersion of a type III radio burst, decreasing in frequency with increasing time, is caused by the decreasing electron plasma frequency encountered by the solar flare electrons as they propagate outward from the sun. If the type III radio emission is caused by the conversion of electron plasma oscillations to electromagnetic radiation at $2f_p$, as is widely believed, then the onset of the plasma oscillations at the local electron plasma frequency f_p should occur essentially simultaneously with the onset of the type III radio emission at $2f_p$ and should last for an interval comparable to the duration of

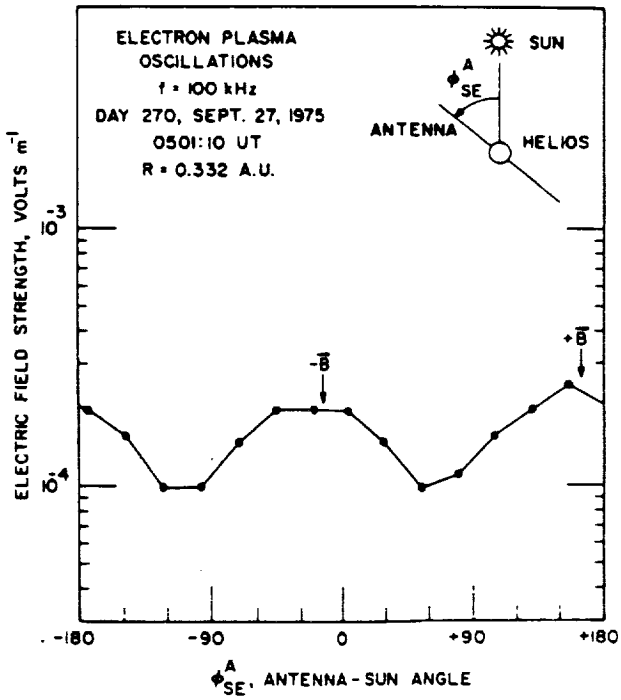

Fig. 17. Spin modulation measurements of electron plasma oscillations showing that the electric field of these waves is oriented nearly parallel to the solar wind magnetic field.

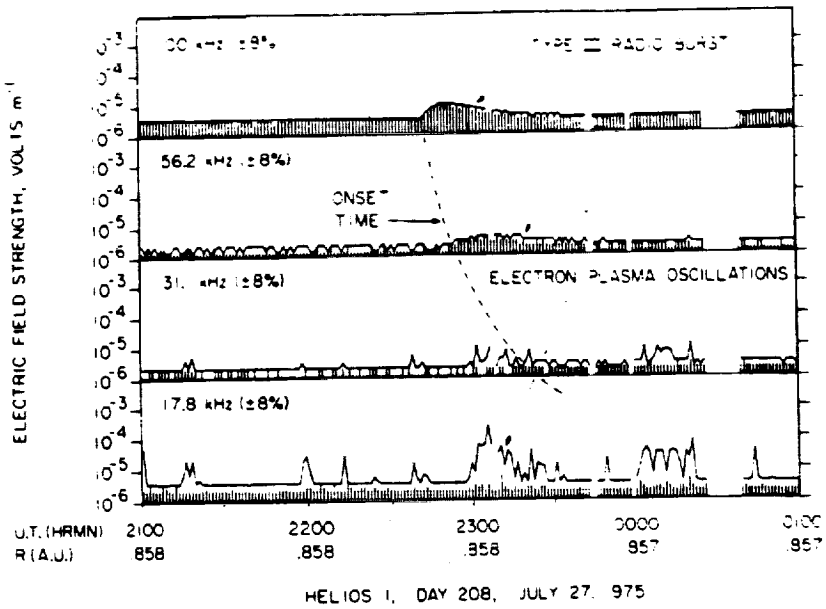

Fig. 18. A type III radio burst which is possibly associated with the electron plasma oscillations detected in the 17.8-kHz channel from about 2257 to 2335 UT. In this case the onset of the electron plasma oscillations at $f_p \simeq 20$ kHz is in good agreement with the estimated onset time of the type III radio emission (dashed line) at $2f_p \simeq 40$ kHz.

the type III burst at this frequency. Electron plasma oscillations are not expected to be observed for all type III bursts, since the spacecraft must be within the source region to detect the locally generated plasma oscillations.

From the standpoint of the expected plasma wave signature the event on day 208 in Figure 18 represents an excellent example of the expected relationship between electron plasma oscillations and type III radio emission. The onset time of the X ray flare associated with this event is 2232 UT, as determined from the soft X ray detector on Helios 1 (J. Trainor, personal communication, 1976). The type III radio emission produced by the electrons from this flare is first detected in the 100-kHz channel at 2243 UT and subsequently in the 56.2- and 31.1-kHz channels at 2251 and 2313 UT. The approximate onset times are indicated by the smooth dashed curve in Figure 18. Starting at about 2257 UT, a pronounced burst of electron plasma oscillations occurs in the 17.8-kHz channel, lasting for about half an hour. At the time of maximum intensity the peak electric field strength of these plasma oscillations is about 223 μV m^{-1}. Since the plasma oscillations are detected in the 31.1-kHz channel but not in the 10.0-kHz channel, the electron plasma frequency must be slightly greater than 17.8 kHz, probably about 20 kHz. From the dashed curve in Figure 18 the onset time of the type III radio emission at $2f_p \simeq 40$ kHz is estimated to be about 2254 UT, coincident within a few minutes with the onset time of the electron plasma oscillations at $f_p \simeq 20$ kHz. By using the 56.2-kHz channel as a guide the duration of the type III radio emission at $2f_p \simeq 40$ kHz is esti-

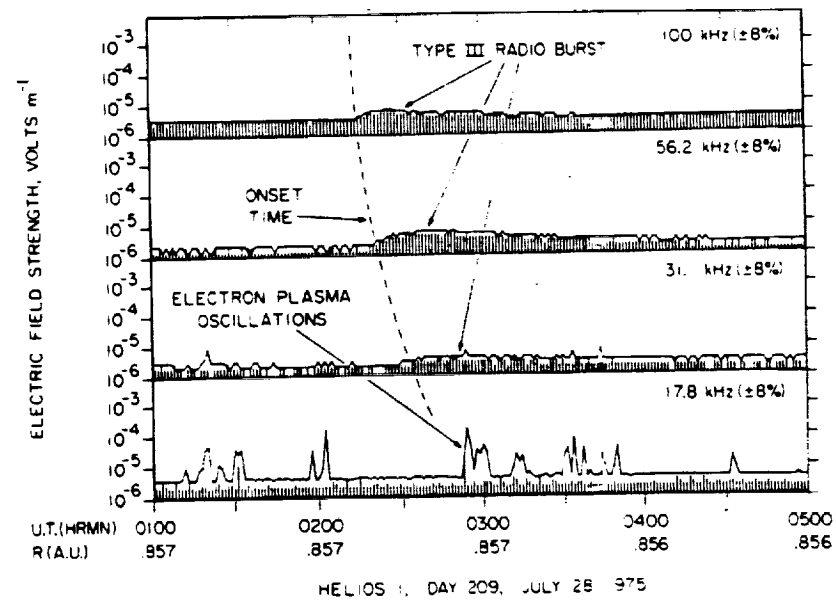

Fig. 19. A type III radio burst and associated electron plasma oscillations occurring a few hours after the event in Figure 18. In this case the onset time of the plasma oscillations is not in good agreement with the onset time of the radio emission at $2f_p$. However, the plasma oscillations do occur during the period when a significant level of radio emission is being detected at $2f_p$.

mated to be about 35 min, which is comparable to the duration of the electron plasma oscillations. These comparisons are all in excellent agreement with the signature expected for electron plasma oscillations associated with a type III radio burst.

About 3.5 hours after the event in Figure 18, another type III radio burst occurred with electron plasma oscillations. This event is shown in Figure 19. The electron plasma oscillations in this case consist of numerous sporadic bursts lasting for about 1 hour, from 0252 to 0352 UT, with a maximum electric field strength of about 187 μV m^{-1}. In comparison with the event in Figure 18 this event does not fit the ideal signature as well, since the onset time of the plasma oscillations at $f_p \simeq$ 17.8 kHz does not agree with the onset time of the radio emission at $2f_p \simeq$ 35.6 kHz. Nevertheless, the plasma oscillations do occur within the interval where substantial radio emission is being detected at $2f_p$.

By far the best example found to date of electron plasma oscillations associated with a type III radio burst is shown in Figure 20. This event, which occurred on day 92 (April 1), 1976, took place during a period of exceptional solar flare activity from day 83 to day 93, 1976. During this period a total of 11 separate type III radio bursts were detected by Helios 1 and 2. The type III event in Figure 20 is outstanding in that a very intense burst of plasma oscillations, with a maximum electric field strength of 5.26 mV m^{-1}, occurred during the radio burst. These electron plasma oscillations are the most intense ever detected by Helios and are much more intense than the typical electron plasma oscillation events discussed in the previous section. Although the onset of the plasma oscillations occurs somewhat later than the onset of the radiation at $2f_p$, the temporal correspondence is so good in this case that there can be essentially no doubt that the radio emission and plasma oscillations are closely associated. Preliminary comparisons with the data from the energetic particle and plasma experiments on Helios (E. Keppler and H. Rosenbauer, personal communication, 1976) confirm that intense fluxes of low-energy (1–20 keV) electrons of solar origin are present during this event. About 4 hours after the event in Figure 20, another type III radio burst occurred in which correspondingly intense electron plasma oscillations are observed. This event is shown in Figure 21. The electron plasma oscillations in this case are of much shorter duration than those in the event in Figure 20, consisting of only a few brief bursts, but are again unusually intense. The maximum electric field intensity of the plasma oscillations in this case is 2.35 mV m^{-1}.

Considered together, these four events provide substantial evidence confirming that electron plasma oscillations are associated with type III radio bursts. The events in Figures 20 and 21, with plasma oscillation intensities much larger than those in any of the other available data, provide particularly strong evidence of this association. The case is not quite as strong for the more moderate intensity (~200 μV m^{-1}) plasma oscillations observed during the events in Figures 18 and 19. One obvious interpretational difficulty is that comparable moderate intensity electron plasma oscillations often occur for which no type III radio emission can be detected. Several such cases are evident in Figure 14. Even though the absence of a one-to-one correspondence raises a question of interpretation, it does not conclusively prove that such moderate intensity plasma oscillations cannot in some cases be associated with the type III radio emission. For example, in cases where no radio emission is detected, it is possible that these plasma oscillations are essentially a localized instability occurring in a much smaller volume than the plasma oscillations associated with a type III radio burst. Direction-finding measurements show that the type III source is very large at low frequencies, subtending half angles as large as 45°–60° as viewed from the sun [*Baumback et al.*, 1977].

Summary and Discussion

The Helios 1 plasma wave measurements show that the electric field intensities in the solar wind are often very low, much lower than those for comparable plasma wave measurements near the earth. During the quiet periods which occur in the Helios 1 plasma wave data the only plasma wave activity

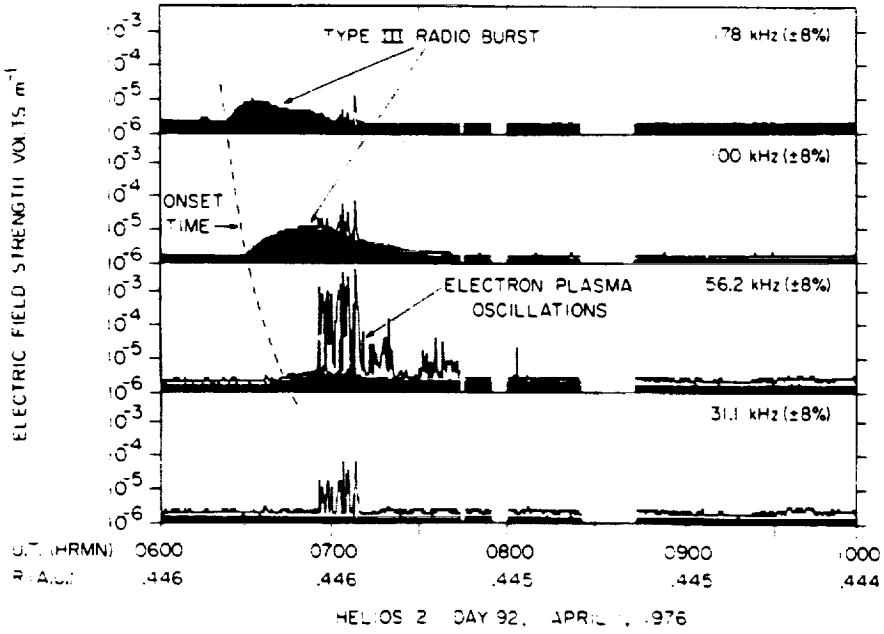

Fig. 20. A type III radio event occurring in association with very intense electron plasma oscillations at $f_p \simeq$ 56.2 kHz. The maximum intensity of the plasma oscillations in this case is 5.26 mV m^{-1}. These are the most intense electron plasma oscillations observed to date with the Helios plasma wave experiment.

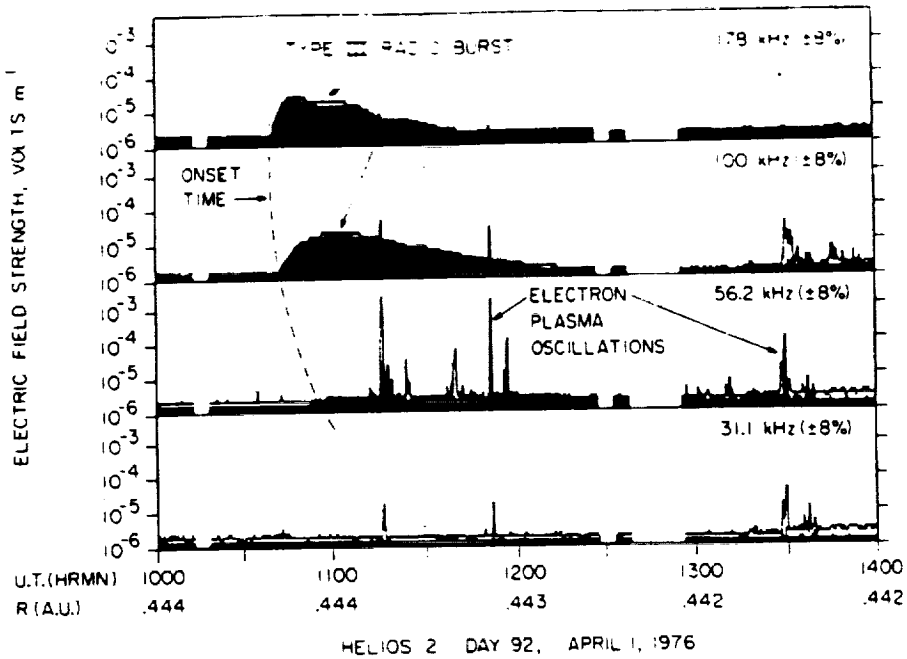

Fig. 21. A type III radio burst and associated electron plasma oscillations occurring a few hours after the event in Figure 20. The maximum intensity of the plasma oscillations in this case is 2.35 mV m^{-1}.

which can be detected is a slight enhancement of the noise levels in the frequency range from about 500 Hz to 3.0 kHz. The broadband electric field strength of these quiet time enhancements is very small, only about 10 μV m^{-1}. During more disturbed periods the most commonly observed plasma wave is a sporadic emission at frequencies between the electron and ion plasma frequencies, typically from about 1 to 10 kHz. These waves are referred to as $f_p^+ < f < f_p^-$ noise. The frequency spectrum of the $f_p^+ < f < f_p^-$ noise shows a systematic variation with radial distance from the sun, shifting toward higher frequencies closer to the sun. The electric field strength of this noise is very impulsive, consisting of many brief bursts lasting for only a few seconds or less with peak single-channel electric field strengths of a few hundred microvolts per meter. No pronounced variation in the electric field strength of this noise is evident with radial distance from the sun. Spin modulation measurements show that the electric field of this noise is closely aligned along the direction of the solar wind magnetic field. At higher frequencies, from about 20 to 100 kHz, narrow band electron plasma oscillations are occasionally detected at frequencies near the local electron plasma frequency. The electron plasma oscillations are more intense than the $f_p^+ < f < f_p^-$ noise, sometimes with electric field strengths as large as a few millivolts per meter, but occur very infrequently. The electric field of the electron plasma oscillations is usually very impulsive and is aligned approximately parallel to the direction of the solar wind magnetic field. The frequency of the electron plasma oscillations closely tracks the local electron plasma frequency as determined by the solar wind plasma experiment and shows a clear systematic variation with radial distance from the sun, increasing in frequency closer to the sun. In all of the available data a total of 18 type III radio bursts have been detected by Helios 1 and 2. Of these, four have simultaneously occurring electron plasma oscillations associated with the type III radio emission. In one of these cases the electron plasma oscillations are unusually intense, with a maximum electric field strength of about 5.26 μV m^{-1}.

In examining the origin of the various types of plasma waves detected by Helios 1 many interpretational questions must be considered. For the electron plasma oscillations the close tracking of the emission frequency with the local electron plasma frequency and the alignment of the electric field parallel to the solar wind magnetic field strongly support the identification of these waves as electron plasma oscillations. The electric field orientation specifically shows that these waves cannot be associated with the upper hybrid resonance, since waves associated with this resonance would have an electric field orientation perpendicular to the local magnetic field [*Stix*, 1962]. The basic two-stream instability responsible for the generation of electron plasma oscillations is well known and has been confirmed in some detail by *Gurnett and Frank* [1975]. The principal questions that remain concern the details of the double-peaked electron distribution function required to produce these waves and the origin of the streaming electrons causing the instability. In some cases, for example, in the event analyzed by *Gurnett and Frank* [1975] and the events in Figures 18–20 of this paper, it seems reasonably certain that the streaming electrons originate from solar flare activity at the sun. However, other cases occur in the Helios 1 data for which no specific solar flare activity is known to occur, and in these cases the streaming electrons may originate from local acceleration processes in the solar wind. Further studies and comparisons with the plasma measurements are needed to understand fully the conditions and circumstances which lead to the generation of electron plasma oscillations in the solar wind. Since electron plasma oscillations occur very infrequently, it seems unlikely that these waves play a significant role in the steady state properties of the solar wind. These waves may, however, play an important role in thermalizing the low-energy electron streams which sometimes occur in the solar wind. It is also of interest to comment on the very impulsive temporal variations frequently observed for the plasma oscillations detected by Helios. Although the origin of these amplitude fluctuations is not known, it is suggestive, particularly for the very intense events such as occur in Figure 20, that these impulsive variations may be related to a parametric

instability, such as the oscillating two-stream instability proposed by *Papadopoulos et al* [1974] to stabilize electron streams from solar flares.

The proper identification of the plasma wave mode responsible for the $f_p^- < f < f_p$ noise is more difficult. This noise almost certainly consists of electrostatic waves, since no comparable magnetic field noise has ever been detected in the solar wind. As was mentioned earlier, even though this noise occurs at frequencies between electron and proton plasma frequencies, it is not immediately certain that the noise has any direct relationship to either of these frequencies because of the large Doppler shifts which can occur in the solar wind. If the Doppler shifts are small, $\Delta f/f \ll 1$, the most obvious plasma wave mode which could be associated with this noise is the Buneman mode [*Buneman*, 1958] at $f_B \simeq (m^-/m^+)^{1/3} f_p^-$. However, for the typical solar wind parameters $T_e = (2\text{–}6)T_i$, the Buneman mode is not considered a very likely possibility for explaining this noise, since this mode has a higher instability threshold than the ion sound wave and requires a large electron drift velocity in relation to the ions to drive the instability. Although such large drift velocities may occur at discontinuities in the solar wind, it seems unlikely that this instability could occur over the large spatial regions for which the $f_p^- < f < f_p$ noise is observed.

If the Doppler shifts are large, the most likely possibility for explaining the $f_p^- < f < f_p$ noise is thought to be ion sound waves at $f \simeq f_p^-$ which are Doppler-shifted to frequencies above f_p^- (requires wave vectors **K** directed away from the sun). The possible occurrence of an ion sound wave instability in the solar wind has been previously suggested and discussed by *Forslund* [1970]. Because ion sound waves have relatively short wavelengths, the Doppler shift caused by the motion of the solar wind is large in comparison to the wave frequency of $\sim f_p^-$ in the rest frame of the plasma. The frequency detected in the spacecraft frame of reference is approximately

$$f' = f_p^- + (V/\lambda) \cos \theta_{KV}$$

where V is the solar wind velocity, λ is the wavelength, and θ_{KV} is the angle between **K** and **V**. Since θ_{KV} is typically not near $\pi/2$, the upper cutoff frequency of the observed frequency spectrum is mainly determined by the minimum wavelength ($f_{max} = V/\lambda_{min}$). The minimum wavelength is controlled by the onset of strong Landau damping and is approximately $\lambda_{min} = 2\pi\lambda_D$, where λ_D is the Debye length. For typical solar wind temperatures and densities at 1.0 AU, $T = 1.0 \times 10^5$ °K, and $n = 5\ \text{cm}^{-3}$, the minimum wavelength is approximately $\lambda_{min} = 61$ m. For a solar wind velocity of 400 km s^{-1} the corresponding f_{max} is 6.5 kHz, which is in good agreement with the observed upper cutoff frequency of the $f_p^- < f < f_p^-$ noise at 1.0 AU (compare with Figure 12). The increase in the upper cutoff frequency with decreasing radial distance from the sun and the apparent proportionality to f_p^- can be attributed to the density dependence of the Debye length, which gives $f_{max} \propto f_p^-$ if the electron temperature remains constant.

Another possible explanation of the $f_p^- < f < f_p^-$ noise is that it is caused by electron plasma oscillations at $f \simeq f_p^-$ which are Doppler-shifted to lower frequencies (**K** vectors directed toward the sun). This alternative is considered unlikely because for a two-stream instability, such plasma oscillations could only be produced by electrons streaming toward the sun from a source beyond 1.0 AU, which seems very implausible. Other possible plasma wave modes involving **K** vectors perpendicular to **B**, such as the electron Bernstein modes at $f \simeq nf_e^-$, appear to be ruled out because of the electric field direction, which is parallel to **B** (see Figure 13).

Of the various possible explanations of the $f_p^- < f < f_p$ noise we believe that the ion sound wave is the most likely mode which could be associated with this noise. If these waves are ion sound waves, then there remains the important question of how these waves are generated and what effect they may have on the macroscopic properties of the solar wind. Since these waves apparently occur over large regions of the solar wind and are not particularly associated with discontinuities or other small-scale features where large currents may be present, the best possibility for generating these waves appears to be the heat flux driven instability suggested by *Forslund* [1970]. Further detailed comparisons with the Helios plasma measurements are clearly needed to identify definitely the instability mechanism involved in the generation of these waves. Although the maximum intensity of $f_p^- < f < f_p$ noise is relatively small, with energy density ratios of typically $\epsilon_0 E^2/2nkT \simeq 10^{-5}$, this turbulence may nevertheless play a significant role in controlling the electron energy distribution in the solar wind, since these waves are present a large fraction (30–50%) of the time.

After several years of investigation [see *Gurnett and Frank*, 1975] the Helios plasma wave measurements have now finally provided clear evidence that intense electron plasma oscillations do occur in association with type III radio events. Rough estimates by *Gurnett and Frank* [1975] using the theory of *Papadopoulos et al.* [1974] indicate that electron plasma oscillations with field strengths of the order of 10 mV m^{-1} are required to explain low-frequency type III radio bursts. Field strengths nearly this large (5.26 mV m^{-1}) have now been found in association with a type III burst. Although the electron plasma oscillation model originally proposed by *Ginzburg and Zheleznyakov* [1958] can now be considered confirmed, there are still many questions remaining concerning the exact mechanism by which the plasma oscillations are converted to radio emissions. The most significant question is still concerned with the electric field strength of the plasma oscillations required to explain the power flux of the type III radio emission. If field strengths this large are always required to produce a significant level of radio emission, then it is surprising that such events are not found more often considering the large size of the type III radio source and the extensive measurements available from the Imp spacecraft near the earth [*Gurnett and Frank*, 1975]. Considerable future work is still needed to evaluate the various mechanisms for converting the plasma oscillation energy to radio emissions and to investigate further and understand the spatial structure of the type III radio emission.

When the Helios electric field measurements are compared with the previous Pioneer 8 and 9 results, it is apparent that a significant difference exists in the electric field spectrums and intensities detected by these two spacecraft. Of the two primary types of plasma waves detected by Helios (the $f_p^- < f < f_p^-$ noise and electron plasma oscillations) neither was detected by Pioneer 8 and 9. As can be seen by comparing the spectrums in Figures 12 and 15 with the instrument noise levels in Figure 4, the $f_p^- < f < f_p^-$ noise normally occurs with intensities too small to be detected by Pioneer 8 and 9. Unusually intense electron plasma oscillations, such as those in Figures 20 and 21, could have been detected by Pioneer 8 and 9; however, such large intensities occur so seldom that it is not surprising that events of this type were not observed. Thus insofar as comparisons are possible, there is no disagreement with the Pioneer measurements concerning the primary types

of plasma waves detected by Helios 1. However, when the waves and intensities detected by Pioneer 8 and 9 are compared with Helios measurements, significant differences are evident. In describing the Pioneer 8 and 9 results, *Scarf et al.* [1968] and *Scarf and Siscoe* [1971] discuss the occurrence of narrow band electric fields (at 400 Hz) of 1–10 mV m^{-1} and corresponding broadband (equivalent 100-Hz sine wave) amplitudes as large as 20–50 mV m^{-1}. In comparison, the peak electric field intensities detected by Helios are seldom larger than 1 mV m^{-1} and are more typically a few hundred microvolts per meter. As was described by *Siscoe et al.* [1971], Pioneer detects two principal types of plasma waves in the solar wind: noise bursts, or spikes, with durations of less than approximately 10 s and persistent long-duration events lasting typically 1 day or more. The short-duration noise bursts are shown to be closely correlated with discontinuities (such as shocks) in the solar wind, and the long-duration events are correlated with density enhancements preceding high-speed streams. The spectrums of both types of noise consist primarily of an intense low-frequency component at frequencies of $f < 400$ Hz. The short-duration noise bursts have intensities as large as 10 mV m^{-1} (1.6×10^{-6} V^2 m^{-2} Hz^{-1}) at 400 Hz, and the long-duration events frequently have broadband (equivalent 100-Hz sine wave) amplitudes exceeding 20 mV m^{-1}. In comparison, Helios 1, which has a threshold sensitivity nearly 40 dB better than Pioneer 8 and 9 at 400 Hz (see Figure 4), seldom detects any waves at all in the low-frequency ($f < 400$ Hz) channels, and even in cases where waves can be detected (Figure 8), the intensities are very low, typically not more than 10–30 μV m^{-1} in the 311- and 562-Hz channels. Although it is very difficult to compare the Helios multichannel measurements with the Pioneer broadband measurements, which involve certain assumptions regarding the shape of the spectrum [*Scarf et al.*, 1973], broadband intensities computed from the Helios peak spectrums, as shown in Figure 12, typically give broadband fields (0.3–1 mV m^{-1}) which are much smaller than the broadband amplitudes (20–50 mV m^{-1}) from Pioneer 8 and 9.

At the present time the difference in the low-frequency electric field intensities and characteristics given by Helios and Pioneer is not understood. Comments on two of the factors which could affect the comparisons between these two spacecraft are summarized below.

Solar activity. Because the primary Helios mission is being conducted during solar minimum conditions, whereas the Pioneer 8 and 9 measurements were made during a more active period of the solar cycle (1968–1969), it is possible that changes in the solar activity could account for some of the differences in the electric field intensities observed by Pioneer and Helios. This explanation could be important for the spike-like bursts and associated disturbances observed by Pioneer in association with interplanetary shocks, since the occurrence of interplanetary shocks has been very low during the period of the Helios observations. Many of the events discussed by *Scarf et al.* [1973] are closely associated with interplanetary shocks and have no counterpart in the Helios data currently available. In a few cases, electric field spectrums qualitatively similar to the shock-associated spikes and long-duration events detected by Pioneer 8 and 9 have been detected by Imp 6 and 8; however, the intensities in these cases also appear to be significantly smaller than the intensities observed by Pioneer 8 and 9.

Wavelengths shorter than the antenna length. When the plasma density is sufficiently large ($n \gtrsim 70$ cm^{-3} for $T_e \simeq 10^5$ °K), it is possible for the minimum wavelength of plasma waves in the solar wind, $\lambda_{min} = 2\pi\lambda_D$, to be less than the length of the Helios 1 antenna. If wavelengths this short occur, then the electric field strengths are underestimated, possibly by a large factor if $\lambda \ll l_{eff}$. Two tests can be performed with the Helios data to verify that the wavelengths being detected are longer than the antenna length. First, if the wavelengths are longer than the antenna, then the spin modulation pattern should be that of a simple dipole with two nulls per rotation. As is evident in Figures 13 and 17, both the $f_{p^-} < f < f_p$ noise and the electron plasma oscillations clearly satisfy this criterion. If $\lambda \ll l_{eff}$, then a much more complex spin modulation pattern should occur with several nulls per rotation. Second, if wavelengths of $\lambda \ll l_{eff}$ occur, then large Doppler shifts should be evident in the electric field spectrums (except for the unlikely case that **K** is exactly perpendicular to the solar wind velocity). For the Helios 1 antenna, with $l_{eff} = 8.0$ m, wavelengths this short would have Doppler shifts greater than 50 kHz if a solar wind speed of 400 km s^{-1} is assumed. Doppler shifts this large are never observed for the electron plasma oscillations detected by Helios, and only the very highest frequency components of the $f_{p^-} < f < f_p$ noise (see Figure 12) could possibly be associated with Doppler shifts this large (if we assume that the noise consists of ion sound waves). It should be noted that the intense low-frequency ($f < 400$ Hz) noise detected by Pioneer cannot be attributed to wavelengths too short to be detected by Helios, since the Doppler shift for these waves is not more than a few hundred hertz, implying wavelengths of 10^3 m or more. We conclude that the occurrence of wavelengths shorter than the Helios antenna length cannot account for the difference between Pioneer and Helios electric field measurements.

Acknowledgments. The authors wish to express their thanks to H. Rosenbauer, M. Montgomery, and R. Schwenn from the Max-Planck-Institut for their helpful discussions and assistance in providing the plasma density measurements and to F. Neubauer from the Technical University of Braunschweig for providing the magnetic field data used in this study. The research at the University of Iowa was supported by the National Aeronautics and Space Administration under contract NAS5-11279 and grant NGL-16-001-043. The research at the Max-Planck-Institut was supported by the Alexander von Humboldt Foundation.

The Editor thanks D. W. Forslund and F. L. Scarf for their assistance in evaluating this paper.

REFERENCES

Baumback, M. M., W. S. Kurth, and D. A. Gurnett, Direction-finding measurements of type III radio bursts out of the ecliptic plane, *Solar Phys.*, in press, 1977.

Belcher, J. W., and L. Davis, Jr., Large-amplitude Alfvén waves in the interplanetary medium, 2, *J. Geophys. Res.*, *76*, 3534, 1971.

Benediktov, E. A., G. G. Getmantsev, N. A. Mityakov, V. O. Rapoport, and A. F. Tarasov, Relation between geomagnetic activity and the sporadic radio emission recorded by the electron satellites, *Kosm. Issled.*, *6*, 946, 1968.

Buneman, O., Instability, turbulence and conductivity in a current-carrying plasma, *Phys. Rev. Lett.*, *1*, 8, 1958.

Burlaga, L. F., Hydromagnetic waves and discontinuities in the solar wind, *Space Sci. Rev.*, *12*, 600, 1971.

Coleman, P. J., Jr., Hydromagnetic waves in the interplanetary plasma, *Phys. Rev. Lett.*, *17*, 207, 1966.

Fainberg, J., L. G. Evans, and R. G. Stone, Radio tracking of solar energetic particles through interplanetary space, *Science*, *178*, 743, 1972.

Forslund, D. W., Instabilities associated with heat conduction in the solar wind and their consequences, *J. Geophys. Res.*, *75*, 17, 1970.

Fredricks, R. W., Electrostatic heating of solar wind ions beyond 0.1 AU, *J. Geophys. Res.*, *74*, 2919, 1969.

Ginzburg, V. L., and V. V. Zheleznyakov, On the possible mechanism of sporadic radio emission (radiation in an isotropic plasma), *Soc. Astron. A. J.*, *2*, 653, 1958.

Gurnett, D. A., The earth as a radio source: Terrestrial kilometric radiation, *J. Geophys. Res.*, *79*, 4227, 1974.

Gurnett, D. A., and L. A. Frank, The relationship of electron plasma oscillations to type III radio emissions and low-energy solar electrons, *Solar Phys.*, *45*, 477, 1975.

Haddock, F. T., and H. Alvarez, The prevalence of second harmonic radiation in type III bursts observed at kilometric wavelengths, *Solar Phys.*, *29*, 183, 1973.

Hartle, R. E., and P. A. Sturrock, Two-fluid model of the solar wind, *Astrophys. J.*, *151*, 1155, 1968.

Hatch, A. J., and H. B. Williams, The secondary electron resonance mechanism of low-pressure high-frequency gas breakdown, *J. Appl. Phys.*, *25*, 417, 1954.

Hatch, A. J., and H. B. Williams, Multipacting modes of high frequency gaseous breakdown, *Phys. Rev.*, *112*, 681, 1958.

Hollweg, J. V., Waves and instabilities in the solar wind, *Rev. Geophys. Space Phys.*, *13*, 263, 1975.

Kaiser, M. L., The solar elongation distribution of low-frequency radio bursts, *Solar Phys.*, *45*, 181, 1975.

Kurth, W. S., M. M. Baumback, and D. A. Gurnett, Direction-finding measurements of auroral kilometric radiation, *J. Geophys. Res.*, *80*, 2764, 1975.

Papadopoulos, K., M. L. Goldstein, and R. A. Smith, Stabilization of electron streams in type III solar radio bursts, *Astrophys. J.*, *190*, 175, 1974.

Parker, E. N., Dynamics of the interplanetary gas and magnetic fields, *Astrophys. J.*, *128*, 664, 1958.

Rodriguez, P., and D. A. Gurnett, Electrostatic and electromagnetic turbulence associated with the earth's bow shock, *J. Geophys. Res.*, *80*, 19, 1975.

Scarf, F. L., and G. L. Siscoe, The Pioneer 9 electric field experiment, 2, Observations between 0.75 and 1.0 AU, *Cosmic Electrodynamics*, *2*, 44, 1971.

Scarf, F. L., G. M. Crook, I. M. Green, and P. F. Virobik, Initial results of the Pioneer 8 VLF electric field experiment, *J. Geophys. Res.*, *73*, 6665, 1968.

Scarf, F. L., R. W. Fredricks, L. A. Frank, and M. Neugebauer, Nonthermal electrons and high-frequency waves in the upstream solar wind, 1, Observations, *J. Geophys. Res.*, *76*, 5162, 1971.

Scarf, F. L., R. W. Fredricks, and I. M. Green, Comparison of deep space and near-earth observations of plasma turbulence at solar wind discontinuities, Solar Wind, *NASA Spec. Publ. 308*, 421, 1972.

Scarf, F. L., I. M. Green, and J. S. Burgess, The Pioneer 9 electric field experiment, 3, Radial gradients and storm observations, *Astrophys. Space Sci.*, *20*, 499, 1973.

Schulz, M., and A. Eviatar, Electron temperature asymmetry and the structure of the solar wind, *Cosmic Electrodynamics*, *2*, 402, 1972.

Siscoe, G. L., F. L. Scarf, I. M. Green, J. H. Binsack, and H. S. Bridge, Very low frequency electric fields in the interplanetary medium: Pioneer 8, *J. Geophys. Res.*, *76*, 828, 1971.

Slysh, V. I., The measurement of cosmic radio emission at 210 and 2200 kilocycles per second to eight earth radii on the automatic interplanetary station Zond-2, *Kosm. Issled.*, *3*, 760, 1965.

Smith, D. F., Type III radio bursts and their interpretation, *Space Sci. Rev.*, *16*, 91, 1974.

Stix, T., *The Theory of Plasma Waves*, p. 32, McGraw-Hill, New York, 1962.

Sturrock, P. A., Spectral characteristics of type III solar radio bursts, *Nature*, *192*, 58, 1961.

Tidman, D. A., T. J. Birmingham, and H. M. Stainer, Line splitting of plasma radiation and solar radio outbursts, *Astrophys. J.*, *146*, 207, 1966.

(Received May 3, 1976;
accepted September 17, 1976.)

Stereoscopic Direction Finding Analysis of a Type III Solar Radio Burst: Evidence for Emission at $2f_p^-$

D. A. GURNETT AND M. M. BAUMBACK

Department of Physics and Astronomy, University of Iowa, Iowa City, Iowa 52242

H. ROSENBAUER[1]

Max-Planck-Institut für Physik und Astrophysik, Institut für extraterrestrische Physik 8046 Garching, Germany

Stereoscopic direction finding measurements from the Imp 8, Hawkeye 1, and Helios 2 spacecraft over base line distances of a substantial fraction of an astronomical unit are used to directly determine the three-dimensional trajectory of a type III solar radio burst. By comparing the observed source positions with the direct in situ solar wind plasma density measurements obtained by Helios 1 and 2 near the sun the relationship of the emission frequency to the local plasma frequency can be determined directly without any modeling assumptions. These comparisons show that the type III radio emission occurs near the second harmonic, $2f_p^-$, of the local electron plasma frequency. Other characteristics of the type III radio emission, such as the source size, which can be obtained from this type of analysis are also discussed.

INTRODUCTION

Stereoscopic direction finding measurements from the Helios 1 and 2 spacecraft, in orbit around the sun, and from the Imp 8 and Hawkeye 1 satellites, in orbit around the earth, are used to track a low-frequency (<1 MHz) type III solar radio burst in three dimensions, independent of modeling assumptions concerning the emission frequency as a function of radial distance from the sun. By combining these radio direction finding measurements with direct in situ measurements of the solar wind plasma density near the sun, the relationship between the emission frequency and the local electron plasma frequency f_p^- can be determined. This relationship is of fundamental importance for understanding the mechanism by which type III radio emissions are generated. As will be shown by a detailed analysis of a type III radio burst using this technique, the dominant emission occurs at the second harmonic, $2f_p^-$, of the electron plasma frequency.

Type III radio bursts are produced by electrons ejected from a solar flare and are characterized by an emission frequency which decreases with increasing time [*Wild*, 1950; *Alvarez et al.*, 1972; *Frank and Gurnett*, 1972; *Lin et al.*, 1973]. The decreasing emission frequency with increasing time is attributed to the decreasing electron density, hence electron plasma frequency f_p^- encountered by the solar flare electrons as they move outward through the solar corona. According to current ideas, the generation of type III radio emissions is a two-step process in which (1) electrostatic electron plasma oscillations are produced at f_p^- by a two-stream instability and (2) the plasma oscillations are converted to electromagnetic radiation by nonlinear wave-wave interactions [*Ginzburg and Zheleznyakov*, 1958; *Sturrock*, 1961; *Smith*, 1974; *Papadopoulos et al.*, 1974; *Gurnett and Anderson*, 1976]. At high frequencies, $\gtrsim$10 MHz, radiation at both the fundamental and the second harmonic of the electron plasma frequency can be detected in the frequency-time spectrums of type III radio bursts [*Wild et al.*, 1954]. At lower frequencies, $\lesssim$10 MHz, the dispersion characteristics of type III bursts are such that the fundamental and second harmonic components cannot be easily resolved. Current evidence based on statistical analyses of average burst properties and various modeling techniques indicates that for low frequencies the dominant emission is at the second harmonic [*Fainberg et al.*, 1972; *Haddock and Alvarez*, 1973; *Fainberg and Stone*, 1974; *Alvarez et al.*, 1975; *Kaiser*, 1975].

A determination of whether the radiation occurs at the fundamental or second harmonic can be made by accurate tracking of the trajectory of a type III burst. The first measurements of the trajectory of a low-frequency type III radio burst were obtained by *Fainberg et al.* [1972], using direction finding measurements from the Imp 6 spacecraft. The technique used consists of analyzing the spin modulation caused by the rotating antenna pattern to determine the direction of arrival of the radio emission. For an electric dipole antenna oriented perpendicular to the spacecraft spin axis the spin modulation gives the direction of arrival projected onto the plane of rotation of the antenna. Since only one angle of the direction of arrival is provided by this technique, additional assumptions must be made to determine a unique trajectory for the type III burst. Using a model for the average emission frequency as a function of radial distance from the sun derived from a statistical analysis of the dispersion characteristics of many type III bursts, Fainberg et al. were able to determine the projection of the type III bursts trajectory onto the ecliptic plane. Their results showed that the trajectories projected onto the ecliptic plane closely match the expected Archimedean spiral form of the magnetic field in the solar wind [*Parker*, 1958].

Since the spin axis of Imp 6 is oriented perpendicular to the ecliptic plane, no information could be obtained by Fainberg et al. on the component of the trajectory out of the ecliptic plane. Later measurements by *Baumback et al.* [1976 and *Fitzenreiter et al.* [1977], using two spacecraft with nearly orthogonal spin axis orientations, provided two coordinates of the direction of arrival so that the source position out of the ecliptic plane could also be determined. However, even with this technique it was still necessary to determine the radial distance of the source from the sun on the basis of an assumed model for the average emission frequency versus radial distance.

Although trajectories obtained by using the average emis-

[1] Now at Max-Planck-Institut für Aeronomie, D-3411 Katlenburg-Lindau 3, West Germany.

Paper number 7A0821.
0148-0227/78/027A-0821$03.00

sion frequency model have the correct qualitative characteristics, large errors can occur in individual events because of deviations of the solar wind density from the average model. Furthermore, comparisons of the emission frequency with the local electron plasma frequency cannot be performed with high accuracy because of the implicit requirement to assume a model for the emission frequency as a function of radial distance from the sun. As will be shown, the stereoscopic direction finding analyses used in this study completely eliminate the need for any a priori assumption regarding the emission frequency as a function of radial distance from the sun, thereby providing a more direct method for determining the relationship of the emission frequency to the local electron plasma frequency.

INSTRUMENTATION AND METHOD OF ANALYSIS

Radio wave and plasma density measurements from five spacecraft, Helios 1 and 2, Imp 7 and 8, and Hawkeye 1, are used in this study. Helios 1 and 2 are in eccentric solar orbits near the ecliptic plane with perihelion radial distances of 0.309 and 0.290 AU and aphelion radial distances of 0.985 and 0.983 AU, respectively. Imp 7 and 8 are in low-eccentricity earth orbits near the equatorial plane at geocentric radial distances ranging from about 23.1 to 46.3 R_E. Hawkeye 1 is in a highly eccentric earth orbit with the apogee located at a radial distance of 20.5 R_E over the north pole. The radio wave measurements presented are from very similar University of Iowa plasma wave instruments on the Helios 2, Imp 8, and Hawkeye 1 spacecraft. Details of these experiments are given by *Kurth et al.* [1975] and *Gurnett and Anderson* [1977].

The plasma density measurements used in this study are from the Max-Planck-Institut plasma experiments on Helios 1 and 2 and from the Los Alamos plasma experiments on Imp 7 and 8. Details of these instruments and the procedures used in the data analysis are given by *Schwenn et al.* [1975] and *Asbridge et al.* [1976].

In order to interpret the three-dimensional radio direction finding measurements presented in this study it is important to review briefly the method of analysis and the geometry used for determining the source position. The direction of arrival of a radio wave is determined by a least squares fit of the measured electric field intensities to a theoretical equation for a spin modulation envelope given by

$$\left(\frac{E}{E_0}\right)^2 = \left(1 - \frac{m}{2}\right) - \frac{m}{2}\cos\left[2(\varphi_A - \alpha)\right]$$

where E is the measured field strength and φ_A is the corresponding orientation angle of the electric antenna in the plane of rotation. The parameters determined by the fitting procedure, which is usually applied to a sequence of about 10 min of data, are the direction of arrival α, the modulation factor m, and the electric field strength E_0. As was mentioned earlier, it is only possible to determine the direction of arrival projected onto a plane perpendicular to the spacecraft spin axis. The spin axis directions of both Helios and Imp 8 are oriented perpendicular to the ecliptic plane as shown in Figure 1. Simultaneous direction finding measurements from Helios and Imp 8 therefore give the angles α_1 and α_2 shown in Figure 1, which uniquely determines the position of the source projected onto the ecliptic plane. The spin axis direction of Hawkeye 1, on the other hand, is oriented nearly parallel to the ecliptic plane, which gives the angle of arrival β_1 above the ecliptic plane. As shown in Figure 1, these three angles, α_1, α_2, and β_1, completely specify the position of the source. By performing this analysis as a function of frequency the three-dimensional trajectory of the type III burst can be determined.

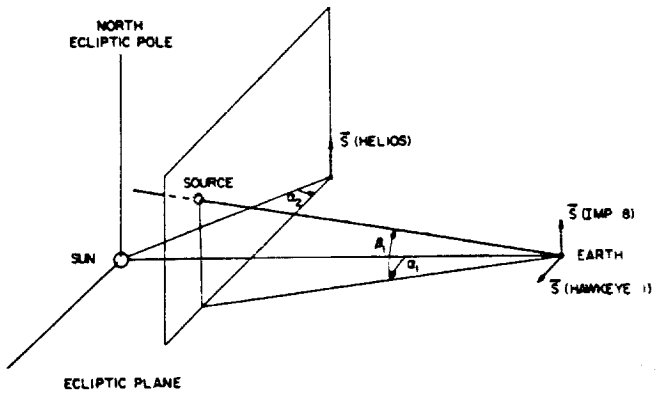

Fig. 1. The geometry used for the three-dimensional stereoscopic direction finding with Imp 8, Hawkeye 1, and Helios. The spin modulation gives the direction of arrival projected onto a plane perpendicular to the spacecraft spin axis. Imp 8 and Helios have their spin axes perpendicular to the ecliptic plane, which gives the angles α_1 and α_2, thereby determining the source position projected onto the ecliptic plane. Hawkeye 1 has its spin axis nearly parallel to the ecliptic plane, which gives the angle β_1, thereby determining the source position out of the ecliptic plane.

ANALYSIS OF THE TYPE III RADIO BURST ON MARCH 23, 1976

Because of the low occurrence of solar flare activity during solar minimum and various geometrical constraints the number of type III radio bursts which are currently available for a detailed analysis is very small. One event for which all of the spacecraft involved were in particularly favorable positions for analysis occurred on March 23, 1976. The onset of time of this event is at about 0843 UT as determined by ground high-frequency radio measurements [*NOAA*, 1976]. No Hα solar flare was detected at this time; however, a large X ray flare and a solar electron event consistent with this onset time were detected by both Helios 1 and Helios 2 (J. Trainor and A. Richter, personal communication, 1976). The type III radio emission associated with this event was first detected by Helios 2 at about 0850 UT. The corresponding radio intensities detected by Helios 2, Hawkeye 1, and Imp 8 are shown in Figure 2. At the time of this event, Helios 2 was east of the earth-sun line, at an earth-sun-probe angle of 1.38° and a heliocentric radial distance of 0.56 AU, and Helios 1 was west of the earth-sun line, at an earth-sun-probe angle of 28.8° and a heliocentric radial distance of 0.34 AU. The positions of Helios 1 and 2 projected onto the ecliptic plane are shown in Figure 3. The type III burst was not detected by Helios 1.

The direction of arrival measurements obtained for this event are summarized in Table 1. The time intervals used to obtain the parameters given in Table 1 were selected on the basis of a sliding average analysis, and only those intervals which give a consistent direction of arrival for several contiguous intervals were used in computing the average directions of arrival. Reliable fits were obtained for three frequencies, 500, 178, and 100 kHz, from Imp 8, for two frequencies, 178 and 100 kHz, from Helios 2, and for one frequency, 178 kHz, from Hawkeye 1. Although Table 1 shows results from Hawkeye 1 for 100 kHz, the standard deviation and fluctuations in the direction of arrival for this frequency are so large that this measurement was not used in the subsequent analysis.

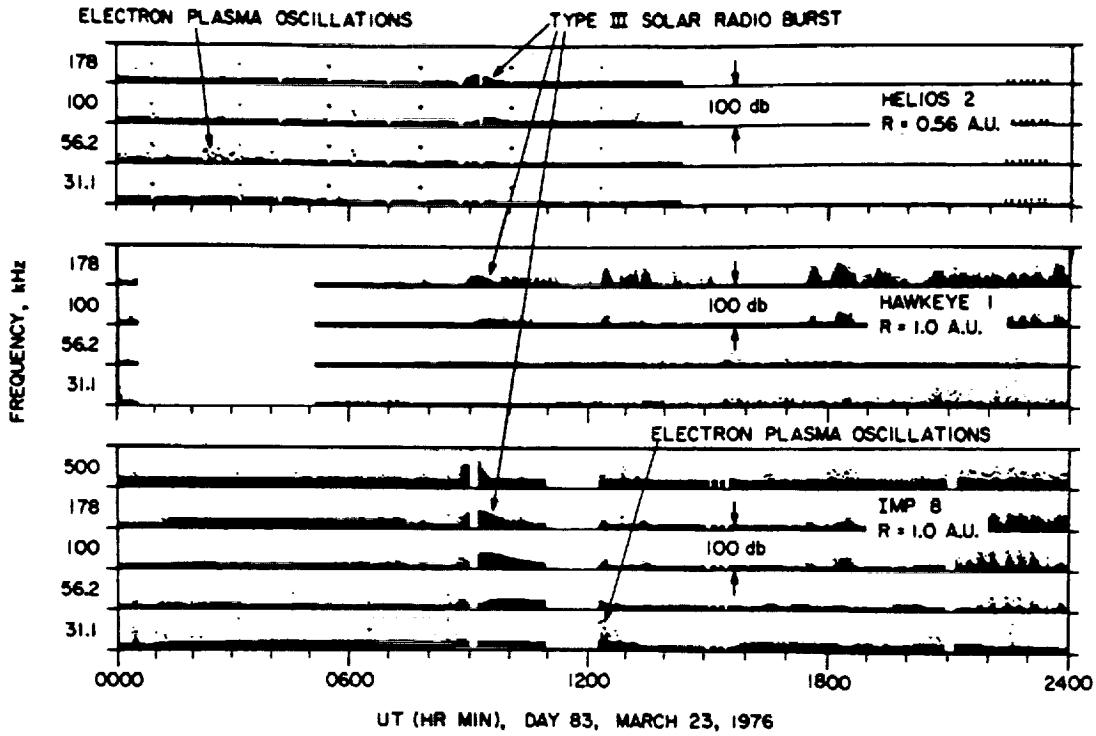

Fig. 2. The electric field intensities detected by Imp 8, Hawkeye 1, and Helios 2 for the type III radio burst on day 83, March 23, 1976. The larger intensities detected by Imp 8 are due to the longer antenna length, 121.8 m from tip to tip for the Imp 8 plasma wave experiment, compared to 42.45 m for Hawkeye 1 and 32.0 m for Helios 2.

For all frequencies below 100 kHz the intensities and modulation factors were too small to give a reliable fit.

The directions of arrival projected onto the ecliptic plane are shown in Figure 3 for each frequency analyzed. The source positions at 100 and 178 kHz are indicated by the corresponding intersections of the directions of arrival from Imp 8 and Helios 2 for these frequencies. The crosshatched regions give the uncertainty in the source positions as determined from the estimated errors in α_1 and α_2 (see Table 1). Both the Imp 8 and the Helios direction finding measurements clearly show a systematic eastward shift in the directions of arrival with decreasing frequency and increasing radial distance from the sun, characteristic of the typical Archimedean spiral trajectory of a type III burst. The best fit Archimedean spiral through the source positions is shown in Figure 3. The equation used for the Archimedean spiral is

$$\varphi = \varphi_0 - (\Omega/V_{SW})r$$

where φ and r are the heliographic longitude and radial distance, V_{SW} is the solar wind velocity, and Ω is the rotational velocity of the sun. The solar wind velocity is assumed to be 600 km s^{-1}. As will be discussed in the next section, this solar wind velocity is an approximate average value based on direct measurements by Helios 2 and Imp 8, with an appropriate delay to provide measurements in the source region. The trajectory of the type III burst in Figure 3 shows that the particles which produced the radio emission were emitted slightly east of the central meridian.

The trajectory of the type III burst out of the ecliptic plane, as determined by Hawkeye 1, is shown in the meridian plane projection of Figure 4. Unfortunately, accurate source positions in the meridian plane can only be obtained at one frequency, 178 kHz, for this event. Nevertheless, this measurement is important because it shows that the type III burst trajectory is very close to the ecliptic plane.

From the modulation factors given in Table 1 it is also possible to estimate the apparent size of the source. As can be easily shown, the modulation factor is sensitive to the angular width of the source projected in the plane of rotation of the antenna. The modulation factor is the largest for a point source and decreases monotonically with increasing source size. The modulation factor is also affected by the angular position of the source with respect to the spin plane of the

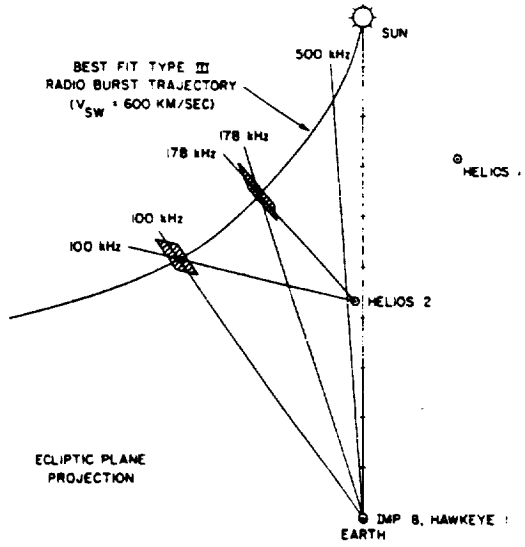

Fig. 3. The ecliptic plane projection of the source positions determined by triangulation from Imp 8 and Helios 2. The uncertainty in the centroid of the source position is indicated by the crosshatched regions at the intersections of the directions of arrival. The best fit trajectory is an Archimedean spiral through the observed source positions. The parameters of the Archimedean spiral have been selected to represent the expected configuration of the solar wind magnetic field for a solar wind velocity of 600 km/s.

TABLE 1. Direction of Arrival Measurements Obtained for the March 23, 1976, Type III Radio Burst

Frequency, kHz	Helios 2		Imp 8		Hawkeye 1	
	α_1, deg	m	α_1, deg	m	β_1, deg	m
500	...	...	3.9 ± 1.1	0.985	...	...
178	42.0 ± 0.4	0.444	17.4 ± 1.2	0.809	4.1 ± 0.6	0.448
100	78.0 ± 4.1	0.047	35.4 ± 0.6	0.521	24.7 ± 9.4	0.130

antenna. Since the detailed shape of the source cannot be determined from this type of analysis, some assumption must be made concerning the form of the source intensity distribution. For this analysis we have assumed that the source consists of a uniformly illuminated circular disk normal to the direction to the sun and centered on the source position determined from the triangulation measurements. Because of the geometric complexities the best fit source size must be determined by a computer fitting procedure which gives the best agreement with the measured modulation factors. For 178 and 500 kHz, which are the only frequencies analyzed, the half angles of the source regions as viewed from the earth are 36.5° and 10.5°. It is evident that the source region of the type III radio emission at these frequencies is quite large. These source sizes are probably larger than the true size of the radiating region because of scattering in the interplanetary medium.

COMPARISON WITH THE SOLAR WIND DENSITY

Since the trajectory of the radio burst has been determined without reference to any specific model for the emission frequency, these results can now be compared with the in situ plasma density measurements to determine the relationship of the emission frequency to the local electron plasma frequency. Fortunately, the trajectory of the type III burst passed very close to the ecliptic plane, since this is the only region in which plasma density measurements are available. For this event, plasma densities can be obtained over a wide range of heliocentric radial distances. Densities are available from Imp 7 and 8 at 1.0 AU, from Helios 2 at about 0.55 AU, and from Helios 1 at about 0.32 AU. As is shown in Figure 3, the trajectory of the type III burst passed eastward of all of these spacecraft. Therefore it is not possible to determine the plasma densities in the source region at the time of the burst. Instead the comparisons must be made a few days later, after the appropriate time delays for the solar rotation to bring the magnetic field line through the source region into coincidence with the spacecraft positions. The geometric considerations required to determine these time delays are illustrated in Figure 5, which shows the trajectories of Imp 7 and 8, Helios 2, and Helios 1 in a coordinate system fixed to the sun. The appropriate time delays are approximately 3.9 days for Imp 7 and 8, 2.6 days for Helios 2, and 8 days for Helios 1. Since the large-scale rotational structure of the solar wind is usually quite consistent and repeatable for several solar rotations during solar minimum conditions, it is believed that any temporal changes which may have occurred in the plasma density during this few-day period should be small. Fortunately, the shortest delay is for Helios 2, which passes the closest to the observed source locations (compare Figures 3 and 5).

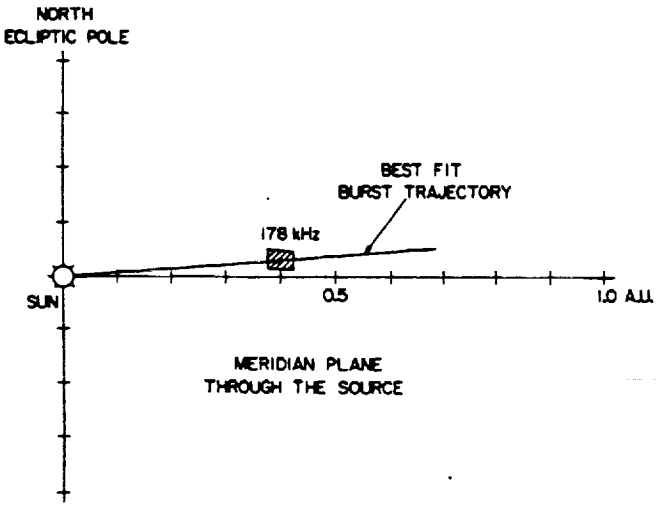

Fig. 4. The observed source position of the type III burst in the meridian plane. Unfortunately, reliable direction finding measurements can only be obtained for one frequency, 178 kHz, from Hawkeye 1 during this event. This one measurement does, however, show that the trajectory of the type III was very close to the ecliptic plane.

The solar wind plasma densities obtained from Imp 7 and 8, Helios 2, and Helios 1 are shown in Figure 6. Although the plasma instruments actually measure ion densities, the measurements shown are equivalent electron densities computed assuming the plasma to be electrically neutral. The time scales in Figure 6 are adjusted so that measurements obtained at the same heliographic longitude are aligned vertically. The points A, B, and C correspond to times when the spacecraft cross the best fit trajectory of the type III burst. Although large variations in the electron density are evident, particularly in the Imp 7 and 8 data, the density is relatively smooth and constant in the region near the type III burst trajectory. The density enhancement evident at all three radial distances (day 87 at Helios 1, days 83 and 84 at Helios, and days 85 and 86 at Imp 7 and 8) is evidently a corotating structure which has an Archimedean spiral structure similar to the type III burst but displaced approximately 20° westward in longitude. Comparisons with solar wind velocity measurements show that this density compression precedes the onset of a high-speed stream, following the well-known pattern discussed by *Hundhausen* [1973].

When the electron plasma frequencies obtained from these plasma densities are compared with the observed emission frequencies, consideration must be given to the uncertainties in the position of the source and the apparent size of the source. Although points A, B, and C in Figure 6 represent the best estimate of the type III trajectory, based on the Archimedean spiral fit, these intersections are somewhat uncertain because of our lack of knowledge of the exact structure of the solar wind magnetic field. Point C probably has the largest error because it represents an extrapolation by several tenths of an astronomical unit into a region where the Archimedean spiral angle is quite sensitive to the solar wind velocity. The solar wind velocity, V_{SW} = 600 km s^{-1}, used in the Archimedean spiral fit is in close agreement with the velocities measured by

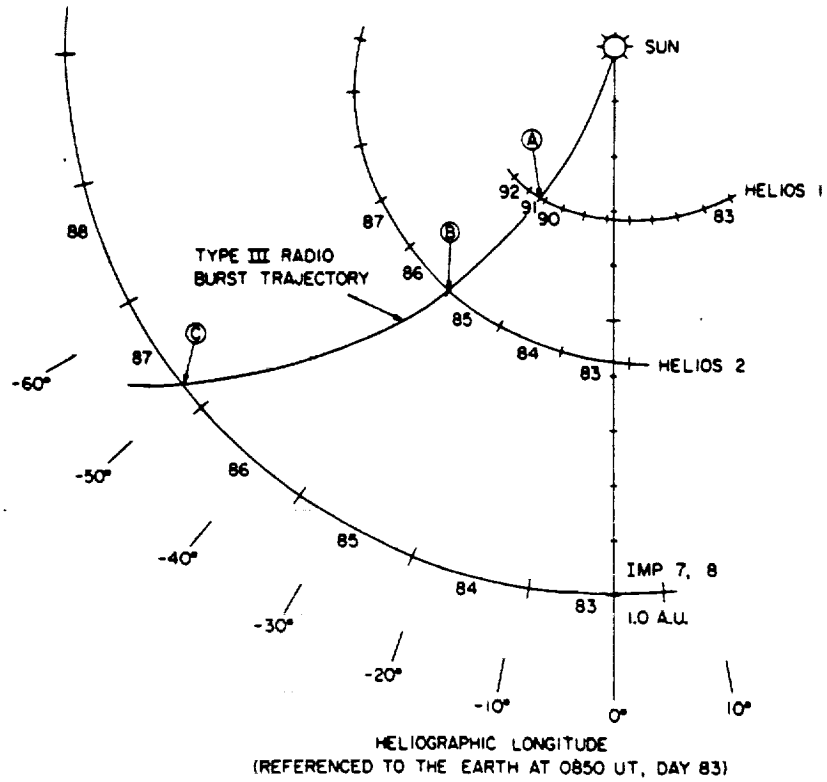

Fig. 5. The trajectories of Imp 7 and 8, Helios 2, and Helios 1 in a coordinate system fixed to the sun. The spacecraft intersect the best fit trajectory of the type III burst at the points marked A, B, and C. Point B represents the best position for comparisons with the local plasma frequency, since this intersection is the closest to the observed source positions (compare with Figure 3) and occurs at the shortest time (2.6 days) after the event.

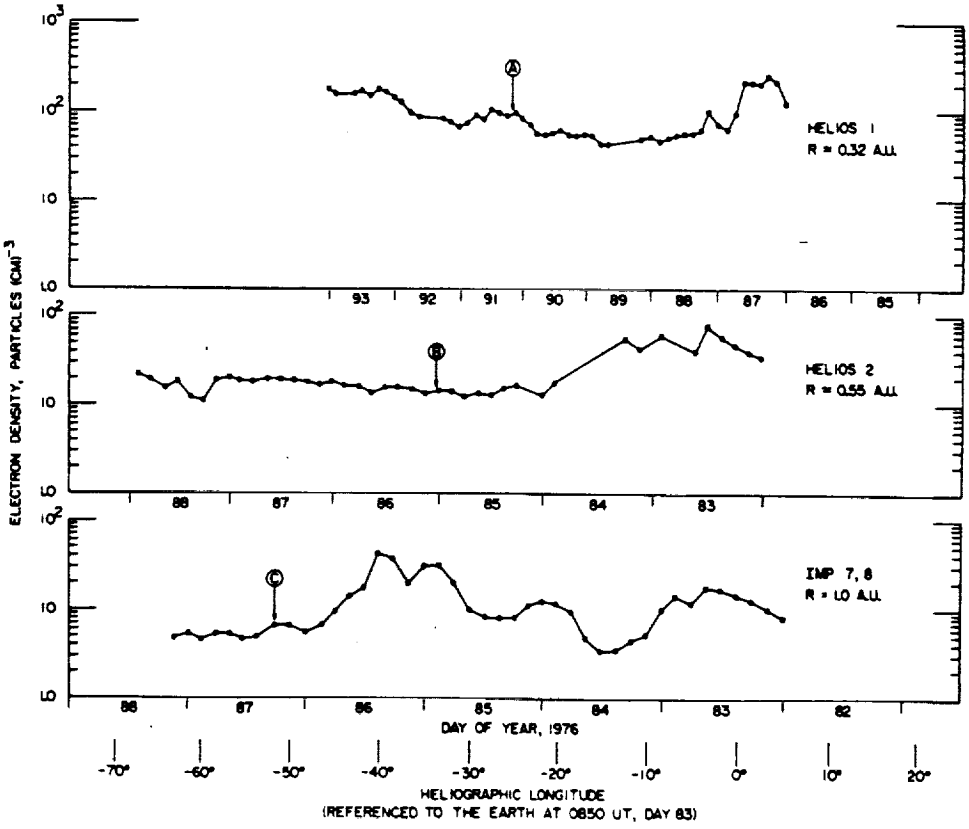

Fig. 6. The electron densities observed by Imp 7 and 8, Helios 2, and Helios 1 for the several-day period after the type III event on day 83. The intersections with the best fit trajectory occur at points A, B, and C, as determined from Figure 5.

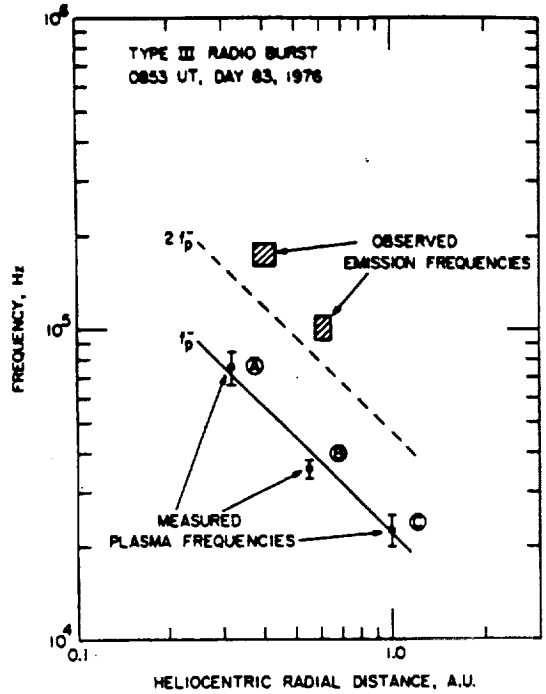

Fig. 7. A comparison of the observed emission frequencies of the type III burst and the measured electron plasma frequencies as a function of radial distance from the sun. Since the angular size of the source is rather large, as viewed from the earth, the electron plasma frequencies have been averaged over a longitude range of ±10° centered on the points A, B, and C in Figure 6. The error bars give the standard deviation of the electron plasma frequency over this interval.

Helios 2 and Imp 7 and 8. Point B, on the other hand, is probably very accurate, since it is determined by an interpolation between measured source positions less than 0.2 AU apart. Point A is also considered to be reasonably accurate, since the Archimedean spiral model for the magnetic field is less subject to errors close to the sun. Also, in the region close to the sun the direction finding measurements (500 kHz in Figure 3) show good qualitative agreement with the best fit Archimedean spiral, even though exact source positions cannot be determined by triangulation.

Because of the large apparent source size a choice must be made concerning the size of the region over which the electron densities are to be compared. Although the Imp 8 and Hawkeye 1 spin modulation measurements indicate that the source subtends a half angle of about 40°, as viewed from the sun, this source size is almost certainly determined by scattering and is too large. This viewpoint is supported by the Helios 2 measurements at 178 kHz which still have a sizable spin modulation (m = 0.44, which corresponds to a half angle of about 46° for a uniformly illuminated disk), even though the spacecraft is only 18° in heliographic longitude from the center of the source. These results suggest that the angular size of the source is of the order of 10°–15° half angle, as viewed from the sun, or possibly even smaller. On the basis of these estimates of the source size we have averaged the electron density measurements over a region of ±10° heliographic longitude on either side of the centroid of the source as determined by the points A, B, and C in Figure 6.

The average electron plasma frequencies within the ±10° regions centered on points A, B, and C are shown in Figure 7, plotted as a function of heliocentric radial distance. The standard deviation of the plasma frequency in each region is also shown by the error bars in Figure 7, to indicate the range of variability of the plasma frequency in the assumed source region. The electron plasma frequency is also considered to be uncertain by about ±15% because of instrumental limitations in the absolute density determination. Also shown in Figure 7 are the observed type III emission frequencies and their corresponding heliocentric radial distances, as determined from the triangulation measurements in Figure 3. The error limits on the emission frequencies and radial distances, indicated by the cross-hatched regions, are determined by the filter bandwidths (±7.5%) and the uncertainties in the triangulation measurements.

The systematic decrease in the solar wind plasma frequency and the type III emission frequency with increasing heliocentric radial distance is clearly evident in Figure 7. The electron plasma frequencies are seen to be in good agreement with the expected $1/R$ variation with radial distance, as indicated by the solid line. The emission frequencies are in all cases substantially above the local electron plasma frequency, too far removed to be consistent with generation of the radiation at f_p^-. For comparison the second harmonic of the electron plasma frequency, $2f_p^-$, is shown by the dashed line in Figure 7, based on the $1/R$ curve through the average plasma frequencies. The observed emission frequencies are seen to be in reasonably good agreement with the second harmonic, $2f_p^-$, much better than for the fundamental, f_p^-.

Summary and Discussion

By using long base line stereoscopic direction finding measurements from the Imp 8, Hawkeye 1, and Helios 2 spacecraft the three-dimensional trajectory of a type III solar radio burst has been determined and analyzed. In contrast to previous direction finding analyses of type III radio bursts the trajectory in this case was obtained completely independent of any modeling assumptions regarding the radial dependence of the emission frequency. Comparisons of the observed emission frequencies with the plasma densities measured along the trajectory were used to determine whether the radiation is generated at the fundamental, f_p^-, or second harmonic, $2f_p^-$, of the local electron plasma frequency. For the event analyzed the results show that the radio emission is generated near the second harmonic, $2f_p^-$, and not at the fundamental.

In considering possible uncertainties in our result, several factors must be considered. The primary uncertainties in the analysis are concerned with (1) the constancy of the solar wind density distribution from the time the event occurred until the time that the density measurements were obtained, (2) the size of the source, and (3) the plasma densities out of the ecliptic plane. The temporal stability of the rotating solar wind structure during the period of interest is supported by the close agreement between the solar wind velocity and density variations observed by Imp 7 and 8 near the earth and by Helios 1 and 2 closer to the sun and by the fact that the solar wind sector structure is relatively steady and repeatable for several solar rotations during solar minimum. The uncertainty regarding the source size arises because of the necessity for comparing a large-scale average property, the emission frequency, with a series of local measurements. Because of the presently unknown role of scattering in the interplanetary medium the actual source size is not easily related to the apparent source size given by the modulation factor measurements. Since the actual source size is not well known, except for an upper limit, the size of the region over which the electron density must be averaged to compute the 'average' electron plasma frequency is not accurately known. Fortunately, the spatial variations in

the plasma frequency are not so large that the basic conclusion is affected by the assumed size of the source region. Even if the source size is increased by a factor of 2 or more, the electron plasma frequencies detected by Helios 1 and 2 are not changed sufficiently to be consistent with generation of the radiation at the fundamental. Another limitation is that in situ plasma density measurements are only available near the ecliptic plane. It is of course possible that the plasma density is unexpectedly large in the region away from the ecliptic plane, in which case the radiation could be generated at the fundamental and still be consistent with our measurements. Since the centroid of the source is located very close to the ecliptic plane (see Figure 4), this hypothesis is not considered very likely, since it would require that the average plasma density increase symmetrically, by at least a factor of 4, within a few degrees on either side of the ecliptic plane. Considering the observed range of longitudinal variations, such large latitudinal variations of the plasma density away from the ecliptic plane seem quite unlikely.

The conclusion of this investigation, that the low-frequency type III radio emission is generated at $2f_p$, is consistent with and confirms the earlier results of *Fainberg et al.* [1972], *Haddock and Alvarez* [1973], *Fainberg and Stone* [1974], *Alvarez et al.* [1975], and *Kaiser* [1975]. The main advantage of this study is that the relationship is determined directly by comparisons with in situ measurements rather than relying on an assumed model for the radial dependence of the emission frequency and/or average statistical properties of the solar wind.

Acknowledgments. The authors express their thanks to William Feldman from the Los Alamos Scientific Laboratory for providing the Imp 7 and 8 plasma densities and velocities used in this study. The research at the University of Iowa was supported in part by NASA under contracts NAS5-11431, NAS1-13129, and NAS5-11279 and grant NGL-16-001-043 and by the Office of Naval Research.

The Editor thanks D. F. Smith for his assistance in evaluating this paper.

REFERENCES

Alvarez, H., F. T. Haddock, and R. P. Lin, Evidence for electron excitation of type III radio burst emission, *Solar Phys.*, *26*, 468, 1972.

Alvarez, H., R. P. Lin, and S. J. Bame, Fast solar electrons, interplanetary plasma and km-wave type-III radio bursts observed from the Imp-6 spacecraft, *Solar Phys.*, *44*, 485, 1975.

Asbridge, J. R., S. J. Bame, W. C. Feldman, and M. D. Montgomery, Helium and hydrogen velocity differences in the solar wind, *J. Geophys. Res.*, *81*, 2719, 1976.

Baumback, M. M., W. S. Kurth, and D. A. Gurnett, Direction finding measurements of type III radio bursts out of the ecliptic plane, *Solar Phys.*, *48*, 361, 1976.

Fainberg, J., and R. G. Stone, Satellite observations of type III solar radio bursts at low frequencies, *Space Sci. Rev.*, *16*, 145, 1974.

Fainberg, J., L. G. Evans, and R. G. Stone, Radio tracking of solar energetic particles through interplanetary space, *Science*, *178*, 743, 1972.

Fitzenreiter, R. J., J. Fainberg, R. R. Weber, H. Alvarez, F. T Haddock, and W. H. Potter, Radio observations of interplanetary magnetic field structures out of the ecliptic, *Solar Phys.*, *52*, 477, 1977.

Frank, L. A., and D. A. Gurnett, Direct observations of low-energy solar electrons associated with a type III solar radio burst, *Solar Phys.*, *27*, 446, 1972.

Ginzburg, V. L., and V. V. Zheleznyakov, On the possible mechanism of sporadic solar radio emission (radiation in an isotropic plasma) (in Russian), *Soc. Astron. AJ*, *2*, 653, 1958.

Gurnett, D. A., and R. R. Anderson, Electron plasma oscillations associated with type III radio bursts, *Science*, *194*, 1159, 1976.

Gurnett, D. A., and R. R. Anderson, Plasma wave electric fields in the solar wind: Initial results from Helios 1, *J. Geophys. Res.*, *82*, 632, 1977.

Haddock, F. T., and H. Alvarez, The prevalence of second harmonic radiation in type III bursts observed at kilometric wavelengths, *Solar Phys.*, *29*, 183, 1973.

Hundhausen, A. J., Nonlinear model of high-speed solar wind streams, *J. Geophys. Res.*, *78*, 1528, 1973.

Kaiser, M. L., The solar elongation distribution of low frequency radio bursts, *Solar Phys.*, *45*, 181, 1975.

Kurth, W. S., M. M. Baumback, and D. A. Gurnett, Direction-finding measurements of auroral kilometric radiation, *J. Geophys. Res.*, *80*, 2764, 1975.

Lin, R. P., L. G. Evans, and J. Fainberg, Simultaneous observations of fast solar electrons and type III radio burst emission near 1 AU, *Astrophys. J.*, *14*, L191, 1973.

NOAA, Solar Geophysical Data, vol. 385, part II, p. 22, Sept. 1976.

Papadopoulos, K., M. L. Goldstein, and R. A. Smith, Stabilization of electron streams in type III solar radio bursts, *Astrophys. J.*, *190*, 175, 1974.

Parker, E. N., Dynamics of the interplanetary gas and magnetic fields, *Astrophys. J.*, *128*, 664, 1958.

Schwenn, R., H. Rosenbauer, and H. Miggenrieder, Das Plasmaexperiment auf Helios (E1), *Raumfahrtforschung*, *19*(5), 226, 1975.

Smith, D. F., Type III radio bursts and their interpretation, *Space Sci. Rev.*, *16*, 91, 1974.

Sturrock, P. A., Spectral characteristics of type III solar radio bursts, *Nature*, *192*, 58, 1961.

Wild, J. P., Observations of the spectrum of high-intensity solar radiation at metre wavelengths, III, Isolated bursts, *Aust. J. Sci. Res.*, *A3*, 541, 1950.

Wild, J. P., M. D. Murray, and W. C. Rowe, Harmonics in the spectra of solar radio disturbances, *Aust. J. Phys.*, *7*, 439, 1954.

(Received April 4, 1977;
accepted August 30, 1977.)

Ion Acoustic Waves in the Solar Wind

D. A. GURNETT AND L. A. FRANK

Department of Physics and Astronomy, University of Iowa, Iowa City, Iowa 52242

Plasma wave measurements on the Helios 1 and 2 spacecraft have revealed the occurrence of electric field turbulence in the solar wind at frequencies between the electron and ion plasma frequencies. Wavelength measurements with the Imp 6 spacecraft now provide strong evidence that these waves are short-wavelength ion acoustic waves which are Doppler-shifted upward in frequency by the motion of the solar wind. Comparison of the Helios results with measurements from the earth-orbiting Imp 6 and 8 spacecraft shows that the ion acoustic wave turbulence detected in interplanetary space has characteristics essentially identical to those of bursts of electrostatic turbulence generated by protons streaming into the solar wind from the earth's bow shock. In a few cases, enhanced ion acoustic wave intensities have been observed in direct association with abrupt increases in the anisotropy of the solar wind electron distribution. This relationship strongly suggests that the ion acoustic waves detected by Helios far from the earth are produced by an electron heat flux instability, as was suggested by Forslund. Possible related mechanisms which could explain the generation of ion acoustic waves by protons streaming into the solar wind from the earth's bow shock are also considered.

INTRODUCTION

Plasma wave measurements on the solar-orbiting Helios 1 and 2 spacecraft [*Gurnett and Anderson*, 1977] have recently revealed the occurrence of significant levels of electric field turbulence in the solar wind at frequencies from about 1 to 10 kHz, between the electron and ion plasma frequencies. In this paper we expand the initial investigation of this turbulence and present evidence that this turbulence consists of short-wavelength ion acoustic waves below the ion plasma frequency which are Doppler-shifted upward in frequency by the motion of the solar wind. Measurements are presented both in interplanetary space, from Helios 1 and 2, and in the solar wind upstream of the earth's bow shock, from Imp 6 and 8. These data provide a comprehensive description of the spectrum, polarization, wavelength, and other essential characteristics of the turbulence. Comparisons are also made with the ambient plasma parameters under a variety of conditions to identify the origin of these waves. In interplanetary space, far away from the earth, the primary mechanism for producing the ion acoustic waves is believed to be the electron heat flux instability suggested by *Forslund* [1970]. Near the earth, however, the same types of waves are often observed to be associated with low-energy (1–10 keV) protons streaming toward the sun from the earth's bow shock. Thus more than one mechanism is apparently operative in the solar wind to destabilize the ion acoustic mode. As will be discussed, similar mechanisms, based on an induced drift between the solar wind electrons and protons, are believed to account for both the heat flux and the proton streaming instabilities.

In the initial description of the ion acoustic wave turbulence by *Gurnett and Anderson* [1977] this turbulence was called $f_p^+ < f < f_p^-$ noise. This terminology was chosen on a strictly observational basis, since the largest intensities usually occur in the frequency range between the electron and ion plasma frequencies f_p^- and f_p^+. As detected by Helios 1 and 2, the maximum single-channel (±10% bandwidth) electric field amplitudes of the $f_p^+ < f < f_p^-$ noise are typically a few hundred microvolts per meter. The electric field strength of this noise is very impulsive, consisting of many brief bursts lasting for only a few seconds. When it is viewed on a time scale of several hours or more, the $f_p^+ < f < f_p^-$ noise is present a large fraction (30–50%) of the time. The noise is observed over the entire range of the Helios orbits from about 0.3 to 1.0 AU. The frequency spectrum of the $f_p^+ < f < f_p^-$ noise shows a systematic variation with radial distance from the sun, shifting toward higher frequencies closer to the sun. Spin modulation measurements show that the electric field of the noise tends to be aligned along the direction of the magnetic field in the solar wind. Gurnett and Anderson discussed the possible plasma wave modes which could account for the $f_p^+ < f < f_p^-$ noise and concluded that the noise could be produced by either the *Buneman* [1958] mode or the ion acoustic mode, the ion acoustic mode being the most likely.

HELIOS OBSERVATIONS IN INTERPLANETARY SPACE

Since more data have now been analyzed from the Helios plasma wave experiments, a much more detailed analysis of the $f_p^+ < f < f_p^-$ noise detected by Helios in the interplanetary medium can be provided than was given in the initial survey by *Gurnett and Anderson* [1977]. For details of the Helios 1 and 2 plasma wave instrumentation, see the paper by *Gurnett and Anderson* [1977]. A typical example of the $f_p^+ < f < f_p^-$ noise detected by Helios 2 is shown in Figure 1. Helios 2 at this time is near the earth-sun line at a heliocentric radial distance of about 0.45 AU. The solid lines for each frequency channel in Figure 1 show the peak electric field intensities over 40.0-s intervals, and the vertical bars (solid black areas) indicate the corresponding average electric field intensities. The intensity scales are logarithmic with a total range of 100 dB from the bottom of one channel to the bottom of the next adjacent channel. The $f_p^+ < f < f_p^-$ noise is evident as a broad band of noise extending from about 1.0 to 17.8 kHz, roughly between the electron and ion plasma frequencies f_p^- and f_p^+, as indicated on the right-hand side of Figure 1. A typical spectrum, selected from Figure 1 at a time of nearly maximum intensity, is shown in Figure 2. The broad peak in the spectrum between the electron and ion plasma frequencies is clearly evident. The relationship to the local electron and ion plasma frequencies $f_p^+ < f < f_p^-$ is believed to be mainly fortuitous, since as will be shown later, the frequency spectrum is strongly Doppler-shifted by the motion of the solar wind. Both Figure 1 and Figure 2 show that the peak field strengths of the $f_p^+ < f < f_p^-$ noise are much larger than the average field strengths, indicating that the noise is very impulsive. The detailed temporal

Paper number 7A0723.
0148-0227/78/017A-0723$03.00

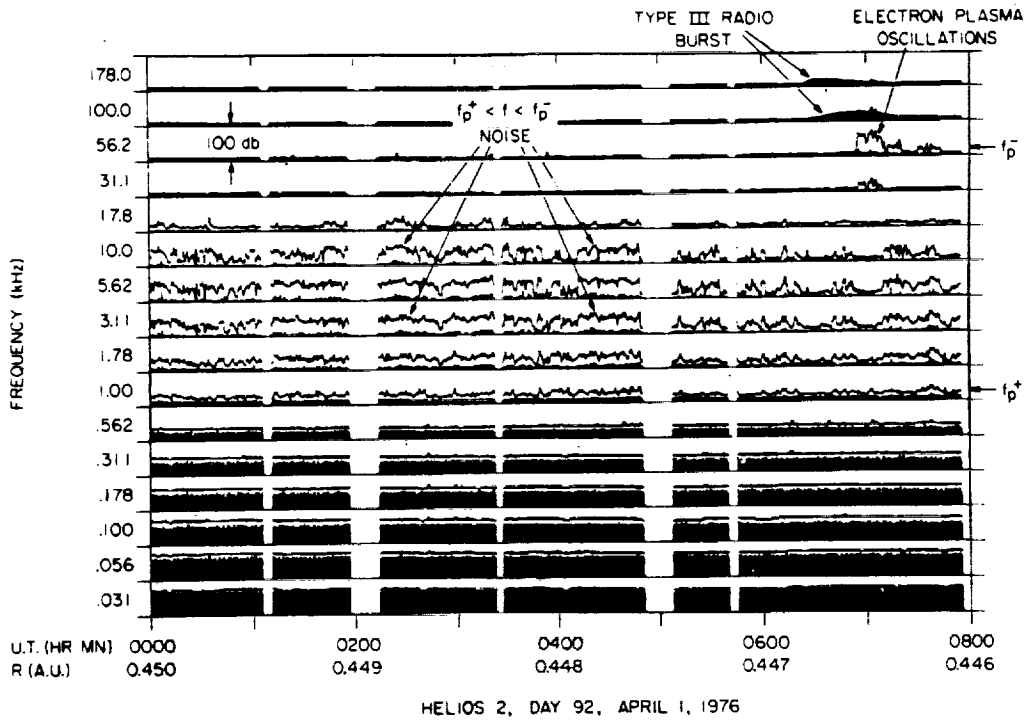

Fig. 1. Typical example of the $f_p^+ < f < f_p^-$ noise detected by the Helios 2 spacecraft at about 0.45 AU. The solid lines and the vertical bars (solid black areas) indicate the peak and average electric field strengths. The intense noise at low frequencies, ≤311 Hz, is caused by interference from the spacecraft solar array.

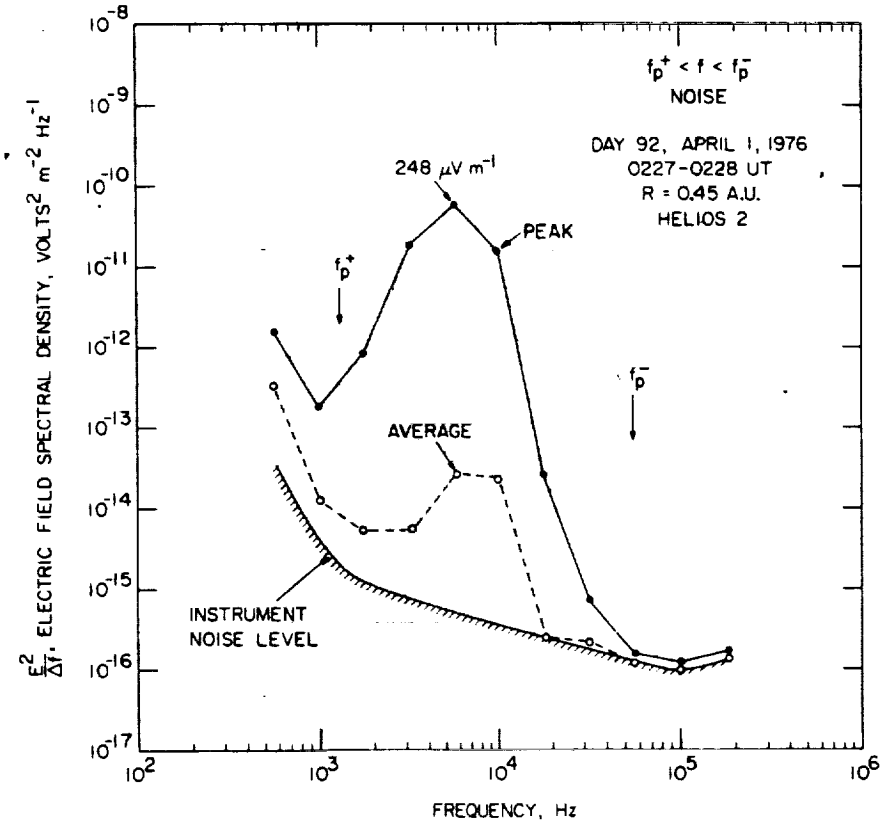

Fig. 2. Typical spectrum of the $f_p^- < f < f_p^-$ noise at a selected interval from Figure 1. Note the distinct peak in the spectrum at about $(2\text{–}10)f_p^-$ and the large ratio of the peak to the average electric field strength, indicative of very impulsive temporal variations.

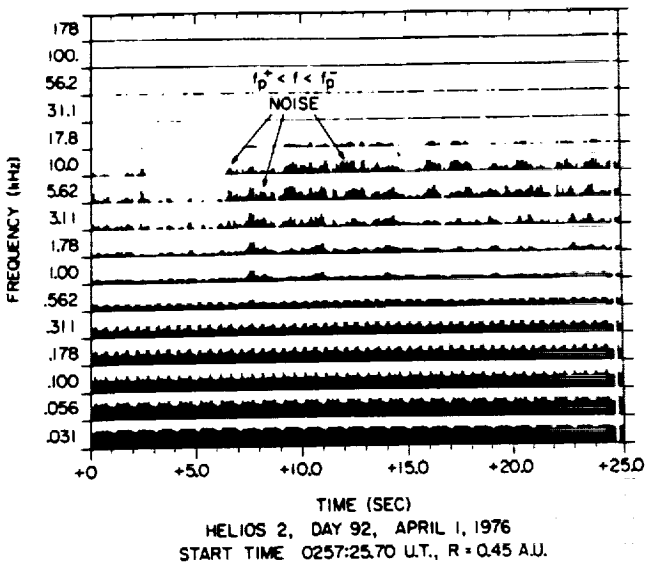

Fig. 3. Very high time resolution measurements from Figure 1, showing the impulsive burstlike temporal structure of the $f_p^+ < f < f_p^-$ noise.

variations are illustrated in Figure 3, which shows a very high time resolution snapshot of the electric field intensities stored in the spacecraft memory from the event in Figure 1, at about 0257 UT. These high time resolution measurements show that the $f_p^+ < f < f_p^-$ noise consists of many short bursts lasting only a few tenths of a second. The individual bursts have a very broad bandwidth and tend to occur simultaneously across a broad range of frequencies. Occasionally, high time resolution measurements, such as those in Figure 3, show distinct evidence of spin modulation caused by the rotation of the electric antenna. A brief period in which such spin modulation is apparent occurs from about +12 to +15 s in the 1.78-kHz channel in Figure 3. The spin modulation consists of two maxima and two minima in each 1-s rotation of the spacecraft. In most cases the extremely rapid temporal variations make it very difficult to determine the phase of the spin modulation accurately. However, by averaging a long series of measurements the detailed spin modulation pattern can usually be identified. An example of one such series of measurements is illustrated in Figure 4, which shows the electric field intensity distribution above a fixed percentage occurrence level (10 and 20%) as a function of the antenna orientation angle φ_{SE}^A. A long (1 hour) analysis interval is used to reduce statistical fluctuations. These data show that the maximum electric field intensity occurs when the antenna is oriented approximately parallel to the solar wind magnetic field. Individual high time resolution measurements of the spin modulation, such as those in Figure 3, also show the same relationship. From these measurements it is concluded that the electric field of the $f_p^+ < f < f_p^-$ noise is oriented approximately parallel to the static magnetic field in the solar wind.

To illustrate the approximate fraction of the time that the $f_p^+ < f < f_p^-$ noise is present in the solar wind, Figure 5 shows the peak and average field strengths for one complete solar rotation. The four frequencies shown in Figure 5 are selected to cover the range of frequencies in which the $f_p^- < f < f_p^-$ noise is normally observed. Here, as in Figure 1, the peak and average field strengths are shown by lines and vertical bars. A time interval of 36.0 min is used for both the peak and the average field strength calculations. It is evident from Figure 5 that peak electric field amplitudes of a few hundred microvolts per meter are present in the frequency range from 1.78 to 5.62 kHz a substantial fraction of the time. Occasionally, bursts of $f_p^+ < f < f_p^-$ noise are seen to extend into the 562-Hz and 17.8-kHz channels. Because of the long interval for the peak determination the compressed time scale presentation in Figure 5 tends to enhance the apparent occurrence of the $f_p^+ < f < f_p^-$ noise, since even one short burst during any given 36-min interval will register in the peak measurements. Nevertheless, these data show that bursts of $f_p^+ < f < f_p^-$ noise are a common feature of the solar wind, since during any given 36-min interval a few bursts are normally detected. Occasionally, quiet periods occur. However, some turbulence is usually detected in any given 36-min interval. Sometimes, distinct enhancements are evident for periods of several days, for example, from November 21 to November 23 and from November 27 to November 29.

To investigate the variation in the spectrum of the $f_p^+ < f < f_p^-$ with radial distance from the sun, a detailed statistical analysis has been performed on all of the available Helios 1 data, consisting of approximately two complete orbits around the sun. The results of this analysis are summarized in Figure 6, which shows the distribution of electric field strengths detected in each frequency channel as a function of radial distance. The electric field strengths used in this analysis are 36-min peak values, comparable to those in Figure 5. The electric field strength contours shown in Figure 6 correspond to intensities which are exceeded a fixed fraction (5 and 10%) of the time. The portion of the overall spectrum attributed to the $f_p^+ < f < f_p^-$ noise is indicated by the shaded areas. The steeply rising spectrum at low frequencies ($\lesssim$500 Hz) is caused by interference from the spacecraft solar array (also evident in Figure 1). The isolated peaks in the spectrum at high frequencies ($\gtrsim$30 kHz) are caused by narrow-band electron plasma

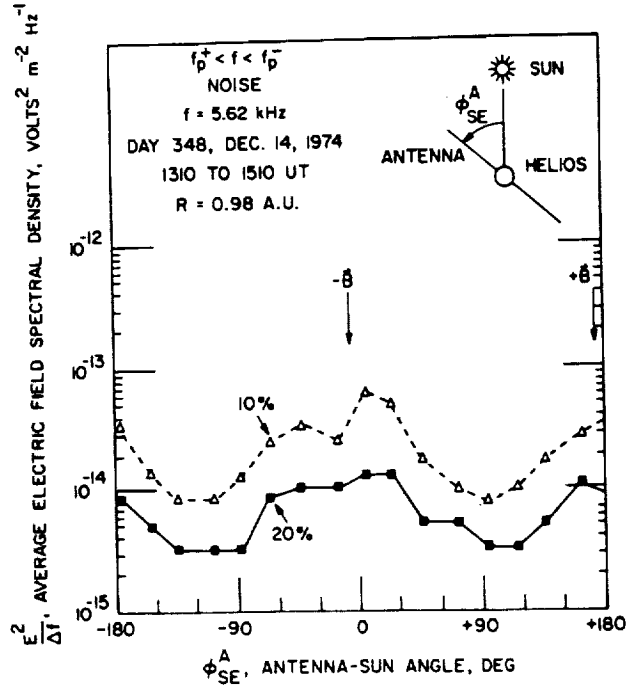

Fig. 4. Angular distribution of the electric field intensity of the $f_p^- < f < f_p^-$ noise, showing that the electric field of this noise is oriented approximately parallel to the solar wind magnetic field.

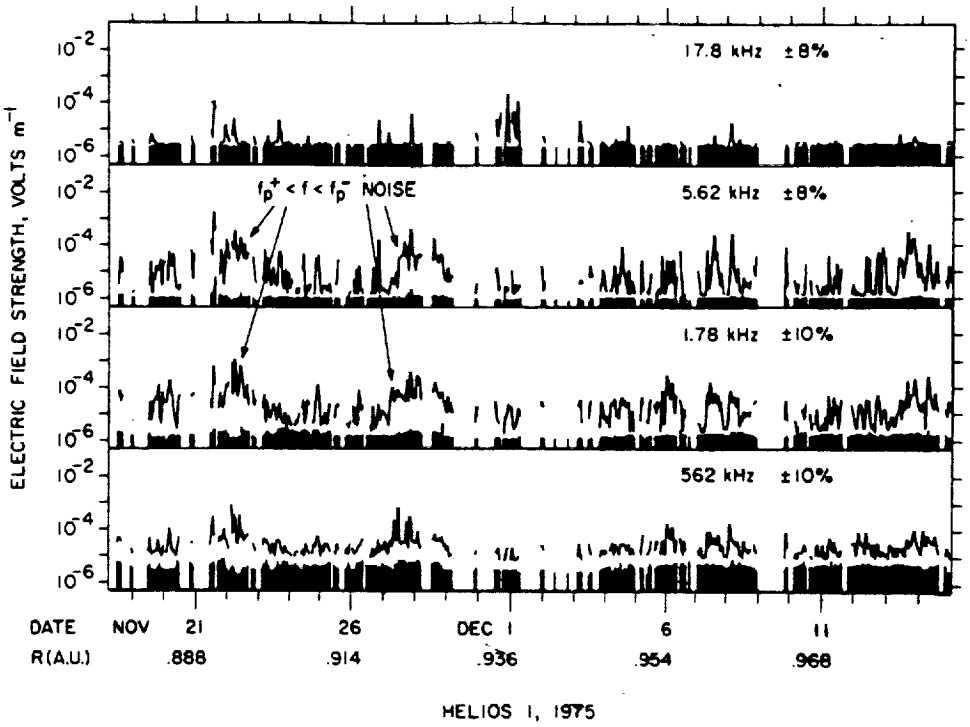

Fig. 5. Compressed time scale plot showing the electric field intensities for one solar rotation. Each peak and each average point represent a 36-min interval. These data show that a low level of $f_p^+ < f < f_p^-$ noise, at amplitudes of 10–100 μV m^{-1}, is present in the solar wind a substantial fraction of the time.

oscillations comparable to the event in Figure 1 at about 0700 UT. These plasma oscillations are directly associated with energetic electrons streaming outward from the sun [*Gurnett and Frank*, 1975] and are often directly associated with type III solar radio bursts [*Gurnett and Anderson*, 1976]. Although narrow-band electron plasma oscillations are easily distinguished from the $f_p^+ < f < f_p^-$ noise, no attempt was made to separate the two types of waves for the statistical analysis in Figure 6, since the plasma oscillations occur very infrequently. Figure 6 clearly shows that both the upper cutoff frequency and the intensity of the $f_p^+ < f < f_p^-$ noise increase with decreasing radial distance from the sun. A rough analysis indicates that the upper cutoff frequencies of the $f_p^+ < f < f_p^-$ noise and the frequency of the electron plasma oscillations vary approximately as $1/R$, where R is the heliocentric radial distance. The radial variation of the $f_p^+ < f < f_p^-$ noise intensity is shown in more detail in Figure 7, which gives the distribution of broadband electric field strengths as a function of the radial distance from the sun. The broadband electric field strengths used in this analysis are calculated by integrating the individual 36-min peak electric field spectrums from 562 Hz to 31.1 kHz. As can be seen from Figure 6, the main contribution to the $f_p^+ < f < f_p^-$ noise spectrum usually occurs in this frequency range. The frequency of occurrence contours in Figure 7 clearly show the increase in the $f_p^+ < f < f_p^-$ noise intensity with decreasing radial distance from the sun. A best fit analysis of the broadband field strength as a function of the radial distance, a power law radial distance dependence being assumed, indicates that the electric field strength also varies approximately as $1/R$.

IMP 6 AND 8 OBSERVATIONS UPSTREAM OF THE EARTH'S BOW SHOCK

Waves essentially identical to the $f_p^+ < f < f_p^-$ noise detected by Helios are also commonly observed by the Imp 6 and 8 spacecraft in the solar wind upstream of the earth's bow shock. See the description by *Gurnett* [1974] of the plasma wave instrumentation on Imp 6 and 8. As will be shown, some of the $f_p^+ < f < f_p^-$ noise bursts detected by Imp 6 and 8 are clearly of terrestrial origin, whereas others appear to be of interplanetary origin, as is true in the Helios observations. Figures 8, 9, and 10 illustrate some typical examples of the $f_p^+ < f < f_p^-$ noise detected by Imp 8 upstream of the bow shock. Figure 8 shows an example of an earth-related event in which a burst of $f_p^+ < f < f_p^-$ noise, from about 0920 to 1115 UT, is closely associated with the arrival of a stream of low-energy protons from the earth's bow shock. The corresponding charged particle measurements from the University of Iowa low-energy proton-electron differential energy analyzer (Lepedea) on Imp 8 are shown in Plate 1. Details of this spectrogram display of the charged particle intensities and the Lepedea instrumentation are given by *Frank et al.* [1976]. The sunward streaming 1- to 10-keV protons associated with the $f_p^+ < f < f_p^-$ noise are clearly evident in the second, third, and fourth spectrograms from the top in Plate 1, between about 0920 and 1115 UT, in almost exact coincidence with the burst of $f_p^+ < f < f_p^-$ noise. These spectrograms represent viewing directions looking toward local evening, local midnight, and local morning, respectively. The direction of motion of the protons can also be seen from the sector spectrogram in Plate 1, which shows that the protons are streaming toward the sun with directions of arrival in the range $120° \lesssim \varphi_{SE}{}^L \lesssim 300°$ (solar ecliptic coordinates). Imp 8 at this time is located upstream of the earth at a local time of about 14.5 hours and a geocentric radial distance of about 41 R_E. The observed directions of arrival correspond closely with the expected directions of motion for particles originating from the vicinity of the earth. The velocity distribution function for these protons, measured along directions approximately parallel to the earth-sun line, is shown in Figure 11, along with the ambient solar

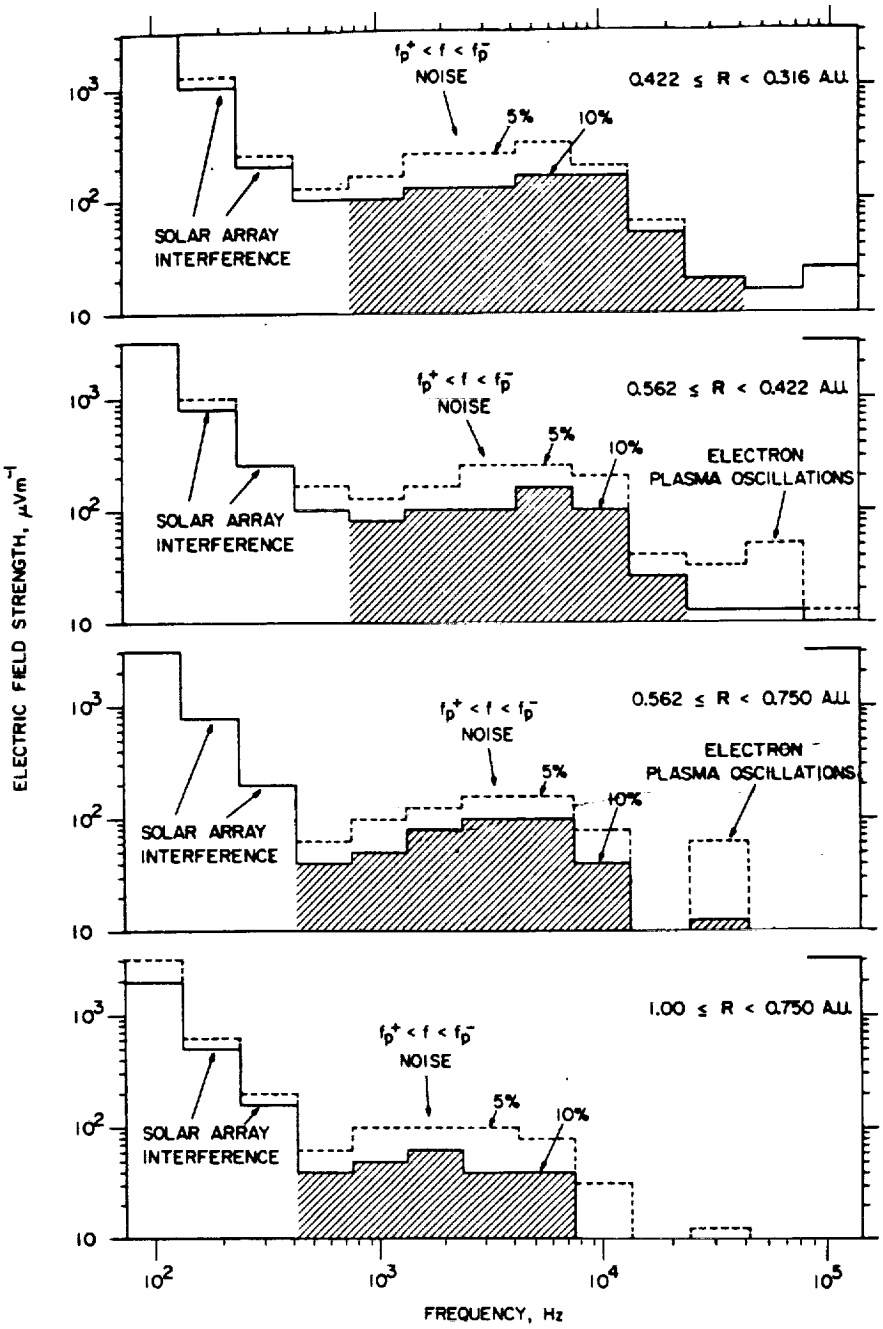

Fig. 6. Statistical survey of the 36-min peak field strength measurements of the type shown in Figure 5 for a total of two complete orbits around the sun. These data show that both the frequency and the amplitude of the $f_p^+ < f < f_p^-$ noise increase systematically with decreasing radial distance from the sun, with $f_{max} \propto 1/R$.

wind distribution determined from the Los Alamos plasma instrument on Imp 8 (W. Feldman, personal communication, 1977). As can be seen in Figure 11, the protons streaming into the solar wind produce a very pronounced double peak in the proton distribution function. Possible mechanisms by which these sunward streaming protons can generate $f_p^+ < f < f_p^-$ noise are considered later.

The upstream $f_p^+ < f < f_p^-$ noise associated with protons arriving from the earth's bow shock, such as that in Figure 8, almost certainly corresponds to the electrostatic noise first reported by *Scarf et al.* [1970] upstream of the bow shock from Ogo 5. In comparison to the $f_p^- < f < f_p^-$ noise detected by Helios the upstream waves detected by Imp 8 have essentially identical characteristics. In both cases the noise is electrostatic and extends with comparable intensities from about 562 Hz to 10 kHz, between the electron and ion plasma frequencies. The peak electric field strengths are much greater than the average electric field strengths, as is true in the Helios measurements, and angular distributions, such as those in Figure 12, show that the wave electric field is aligned approximately parallel to the solar wind magnetic field, also in agreement with the Helios observations. From all available evidence the electrostatic waves generated upstream of the earth by protons arriving from the bow shock are essentially identical to the $f_p^- < f < f_p^-$ noise detected by Helios far from the earth. These comparisons indicate that the same basic plasma wave mode is

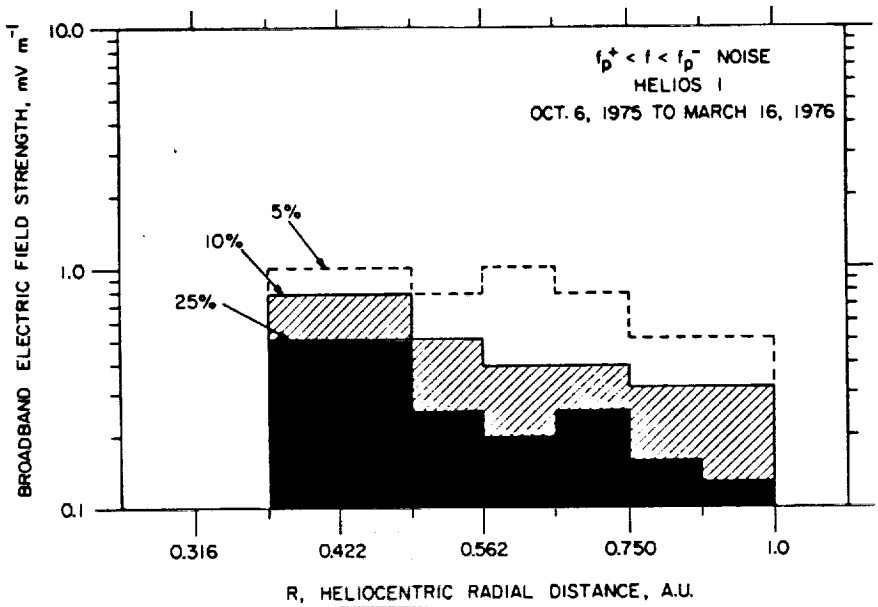

Fig. 7. More detailed analysis of the broadband electric field intensity as a function of the radial distance from the sun. The radial distance is plotted on a logarithmic scale, so that a power law dependence will be a straight line. The electric field amplitude varies approximately as $1/R$.

involved in both types of noise. The detailed mechanisms by which the noise is generated must, however, be quite different in the two cases, since protons from the earth's bow shock cannot possibly produce the waves detected by Helios far from the earth.

Not all of the $f_p^+ < f < f_p^-$ noise bursts detected by Imp 8 are associated with protons arriving from the bow shock. Figure 9, for example, shows a sequence of $f_p^+ < f < f_p^-$ noise events extending over an entire day which are not related to upstreaming protons. The corresponding Lepedea spectrograms in Plate 2 for the same day demonstrate that no sunward streaming protons are detectable during these events, except possibly for the event around 1300–1400 UT. The magnetic field during this day is often close to the ecliptic plane, so there is no possibility that the Lepedea, which scans viewing directions in the ecliptic plane, would not be able to detect protons streaming along the magnetic field from the bow shock. The corresponding electron spectrograms in Plate 2 also show no abrupt changes in the electron distribution function which can be clearly related to variations in the $f_p^+ < f < f_p^-$ noise intensity. Events of this type, for which no earth-related source can be identified, constitute about 30–50% of all of the $f_p^+ < f < f_p^-$ noise events detected by Imp 8 upstream of the bow shock. These events evidently correspond to the interplanetary $f_p^+ < f < f_p^-$ noise commonly detected by Helios far from the earth, since no earth-related source can be identified.

To try to identify the feature of the solar wind charged particle distribution which produces the interplanetary (non earth related) $f_p^+ < f < f_p^-$ noise, the Imp 8 Lepedea and plasma wave data have been examined for correlated events which would indicate the origin of the instability. Several events have been identified which strongly indicate that the anisotropy associated with the electron heat flux in the solar wind plays an important role in producing the $f_p^+ < f < f_p^-$ noise. One such event, which occurred during a disturbed period on July 5, 1974, is illustrated in Figure 10 and Plate 3. In this case a pronounced burst of $f_p^+ < f < f_p^-$ noise occurs from about 1645 to 1930 UT, preceded by a shorter burst from about 1540 to 1600 UT. The Lepedea spectrograms in Plate 3 clearly show that no protons are arriving from the earth's bow shock during this time, so these waves must correspond to the interplanetary $f_p^- < f < f_p^-$ noise. The enhanced background, evident in the proton spectrogram throughout the period shown in Plate 3, is caused by an energetic solar cosmic ray event. Close examination of the electron sector spectrogram in the second panel from the bottom in Plate 3 shows that the $f_p^+ < f < f_p^-$ noise occurs during a period when a substantial anisotropy is present in the solar wind electron distribution. The maximum intensities occur for Lepedea viewing directions in the range $0° \lesssim \varphi_{SE}{}^L \lesssim 90°$, which are approximately symmetrical with respect to the magnetic field direction, $\varphi_{SE}{}^B \simeq 45°$, during this period. This anisotropy is representative of a substantial streaming of electrons along the magnetic field away from the sun. The electron velocity distribution indicates that these electrons correspond to the high-temperature 'halo' electrons which provide the main contribution to the heat flux in the solar wind [*Feldman et al.*, 1974]. The anisotropy evident in Plate 3 corresponds to an unusually large electron heat flux away from the sun, directed along the solar wind magnetic field. The detailed variations of the electron velocity distribution function at a fixed energy and the corresponding 1.78-kHz electric field intensity variations are shown in Figure 13 near the beginning of the event. The electron distribution function is shown in two directions, $\varphi_{SE}{}^L = 34°$ and 124°, which are approximately parallel and perpendicular, respectively, to the average magnetic field directions projected onto the ecliptic plane during this period. The interpretation of these data is somewhat complicated by variations in the magnetic field direction. Before about 1610 UT the magnetic field is too far out of the ecliptic plane, $\theta_{SE}{}^B \gtrsim 60°$, for accurate measurements of the anisotropy parallel and perpendicular to the magnetic field. However, after about 1610 UT the magnetic field is sufficiently close to the ecliptic plane, $\theta_{SE}{}^B \lesssim 30°$, for good anisotropy measurements. As can be seen from Figure 13, after about 1650 the intensities at $\varphi_{SE}{}^L = 34°$, looking along

the magnetic field toward the sun, increase substantially above the intensities at $\varphi_{SE}{}^{L} = 124°$, perpendicular to the magnetic field. Comparisons with the 1.78-kHz electric field intensities show that the onset of the $f_p{}^{+} < f < f_p{}^{-}$ noise is closely correlated with the increase in the anisotropy of the electron distribution. The burst of noise at about 1550 UT is also seen to be correlated closely with the increase of electron intensities in the direction $\varphi_{SE}{}^{L} \simeq 34°$ at about 1552 UT. Even though $\theta_{SE}{}^{B}$ is large at this time, this burst must be associated with an anisotropic component streaming along the magnetic field, since the intensity perpendicular to the magnetic field, $\varphi_{SE}{}^{L} = 124°$, shows no comparable increase. The evidence that the $f_p{}^{+} < f < f_p{}^{-}$ noise is associated with the magnetic-field-aligned anisotropy in the electron flux is further supported by the velocity distributions shown in Figure 14, which are selected for times when $\theta_{SE}{}^{B} \simeq 0°$ and for viewing directions parallel ($\varphi_{SE}{}^{L} = 304°$ and 34°) and antiparallel ($\varphi_{SE}{}^{L} = 124°$ and 214°) to the magnetic field. The electron intensity measurements at 1252 UT (triangles), before the onset of the $f_p{}^{+} < f < f_p{}^{-}$ noise, show that the anisotropy is typically small, $\lesssim 20\%$, at all velocities. However, the measurements at 1720 UT (circles), after the onset of the $f_p{}^{+} < f < f_p{}^{-}$ noise, show that the anisotropy is very large, typically a factor of 3–5, over a broad range of velocities. These velocity distributions also show that other than the change in the anisotropy the electron distribution functions are nearly identical in the two regions, before and after onset of the noise. Comparison of these velocity distributions with the measurements of *Feldman et al.* [1975] clearly identifies this anisotropy with a greatly enhanced heat flux of the halo electrons, directed along the magnetic field line away from the sun. These and other similar observations provide strong evidence that the anisotropy associated with the electron heat flux in the solar wind plays an essential role in the generation of these waves. Close inspection of the electron angular distributions in Plate 2 also shows, for example, that a similar electron anisotropy is present during the period when the ion acoustic waves in Figure 9 are being observed. The variations in the $f_p{}^{+} < f < f_p{}^{-}$ noise intensity are not, however, as easily associated with changes in the electron distribution function in this case, possibly because the plasma is close to marginal stability, so that only very minor changes in the electron distribution or other parameters can trigger the growth or decay of the waves.

Identification of the $f_p{}^{+} < f < f_p{}^{-}$ Noise as Short-Wavelength Ion Acoustic Waves

Some of the factors involved in the identification of the plasma wave mode associated with the $f_p{}^{+} < f < f_p{}^{-}$ noise detected by Helios have already been discussed by *Gurnett and Anderson* [1977]. From the electrostatic character of the noise, all of the well-known electromagnetic modes of propagation, such as the whistler and magnetosonic modes, can be eliminated from consideration. The electric field orientation, parallel to the static magnetic field, further restricts the possibilities, eliminating, for example, the various types of ion cyclotron and Bernstein modes which propagate nearly perpendicular to the static magnetic field. Essentially only two plasma wave modes are known which could account for all of the observed characteristics. These modes are the ion acoustic mode at $f \lesssim f_p{}^{+}$ and the *Buneman* [1958] mode at $f_B \simeq (m^{-}/m^{+})^{1/3} f_p{}^{-}$. We also note that *Scarf et al.* [1970] identified the same modes as the best candidates for explaining the upstream electrostatic noise, which is now believed to be the same basic plasma wave mode detected by Helios far from the earth. Although *Gurnett and Anderson* [1977] argue that it is unlikely that the proper conditions exist in the solar wind for generating the Buneman

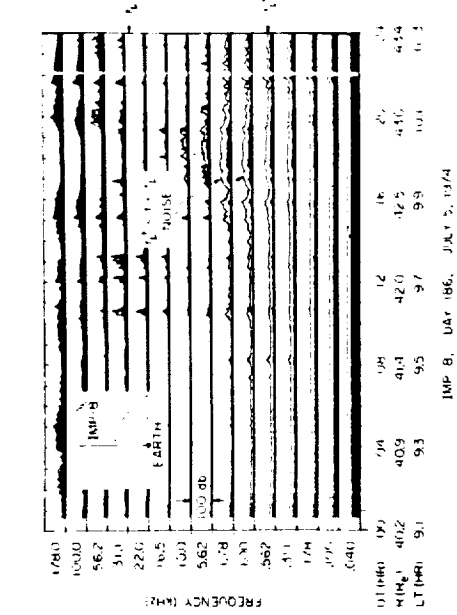

Fig. 10. Intense burst of $f_p{}^{+} < f < f_p{}^{-}$ noise detected during a period when a substantial anisotropy is evident in the low-energy electron distribution (see Plate 3).

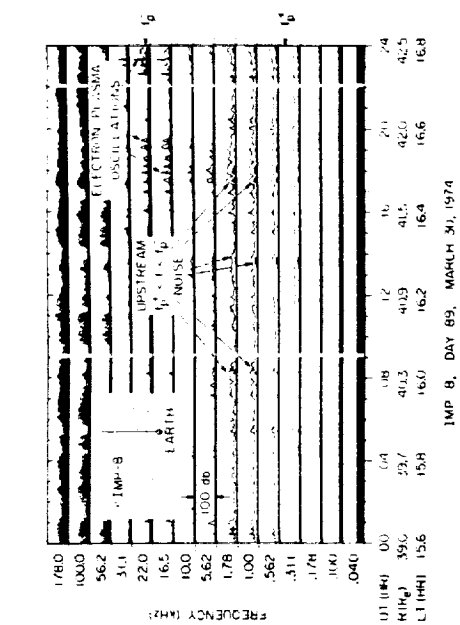

Fig. 9. Series of $f_p{}^{+} < f < f_p{}^{-}$ noise bursts detected by Imp 8 for which no protons can be detected arriving from the bow shock (see Plate 2). These waves evidently correspond to the interplanetary $f_p{}^{+} < f < f_p{}^{-}$ noise detected by Helios far from the earth.

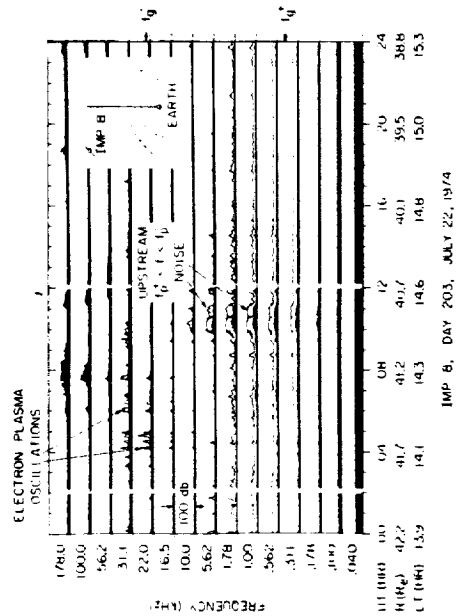

Fig. 8. Example of $f_p{}^{+} < f < f_p{}^{-}$ noise detected upstream of the earth's magnetosphere in association with an intense burst of 1- to 10-keV protons streaming into the solar wind from the bow shock (see Plate 1).

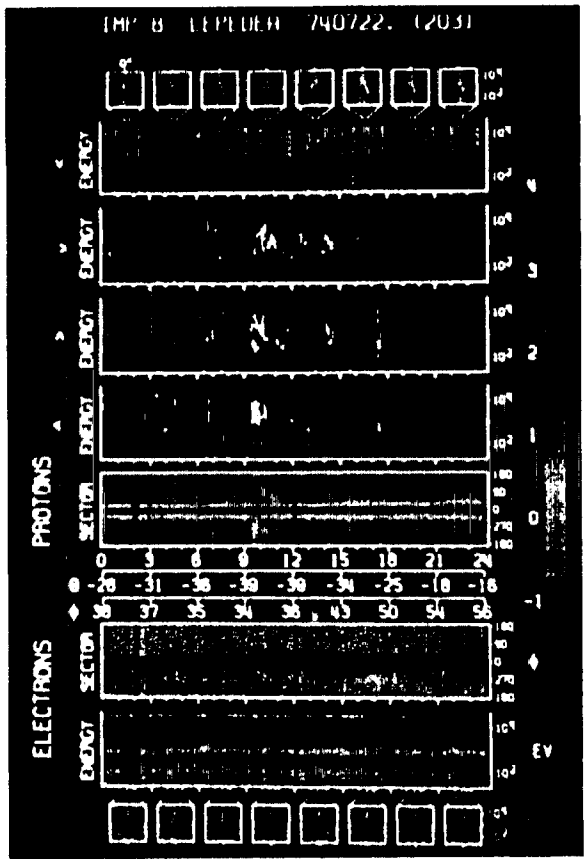

Plate 1. The Lepedea data corresponding to the electric field measurements in Figure 8, showing the occurrence of an intense burst of protons streaming toward the sun in direct correspondence with the burst of $f_p^- < f < f_p$ noise from about 0920 to 1115 UT. These protons propagate from the earth's bow shock.

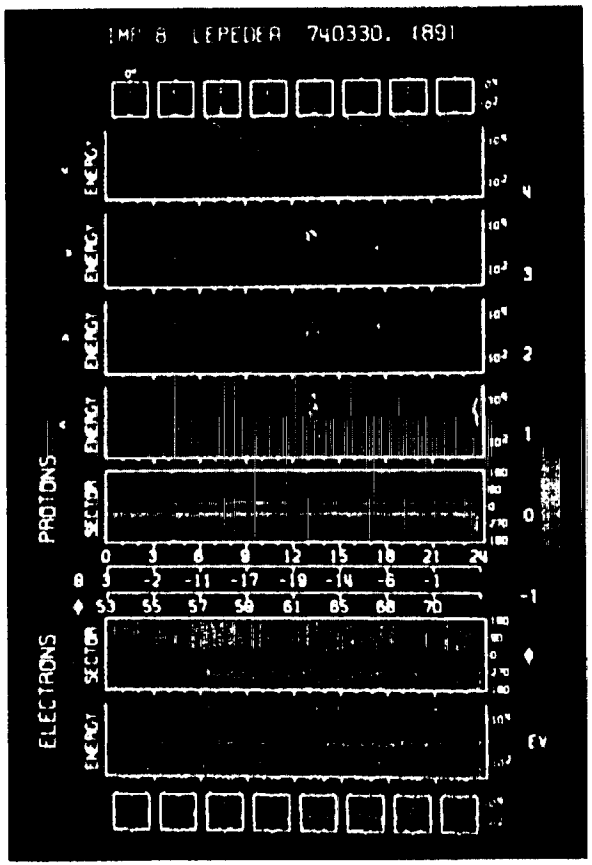

Plate 2. The Lepedea data corresponding to the electric field measurements in Figure 9, showing a series of $f_p^+ < f < f_p$ noise bursts for which no significant enhancement in either the electron or the proton intensities can be identified in association with the $f_p^+ < f < f_p^-$ noise.

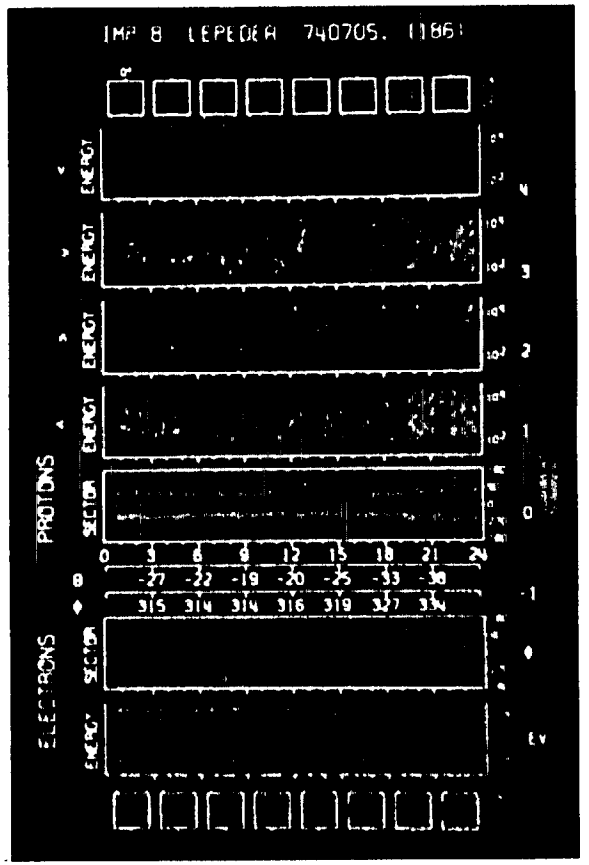

Plate 3. The Lepedea data corresponding to the electric field measurements in Figure 10, showing an event in which the $f_p^+ < f < f_p$ noise (from about 1540 to 1930 UT) is closely correlated with the occurrence of a greatly enhanced anisotropy in the low-energy solar wind electron distribution. This anisotropy is clearly evident in the electron sector spectrogram from about 1540 to 1900 UT.

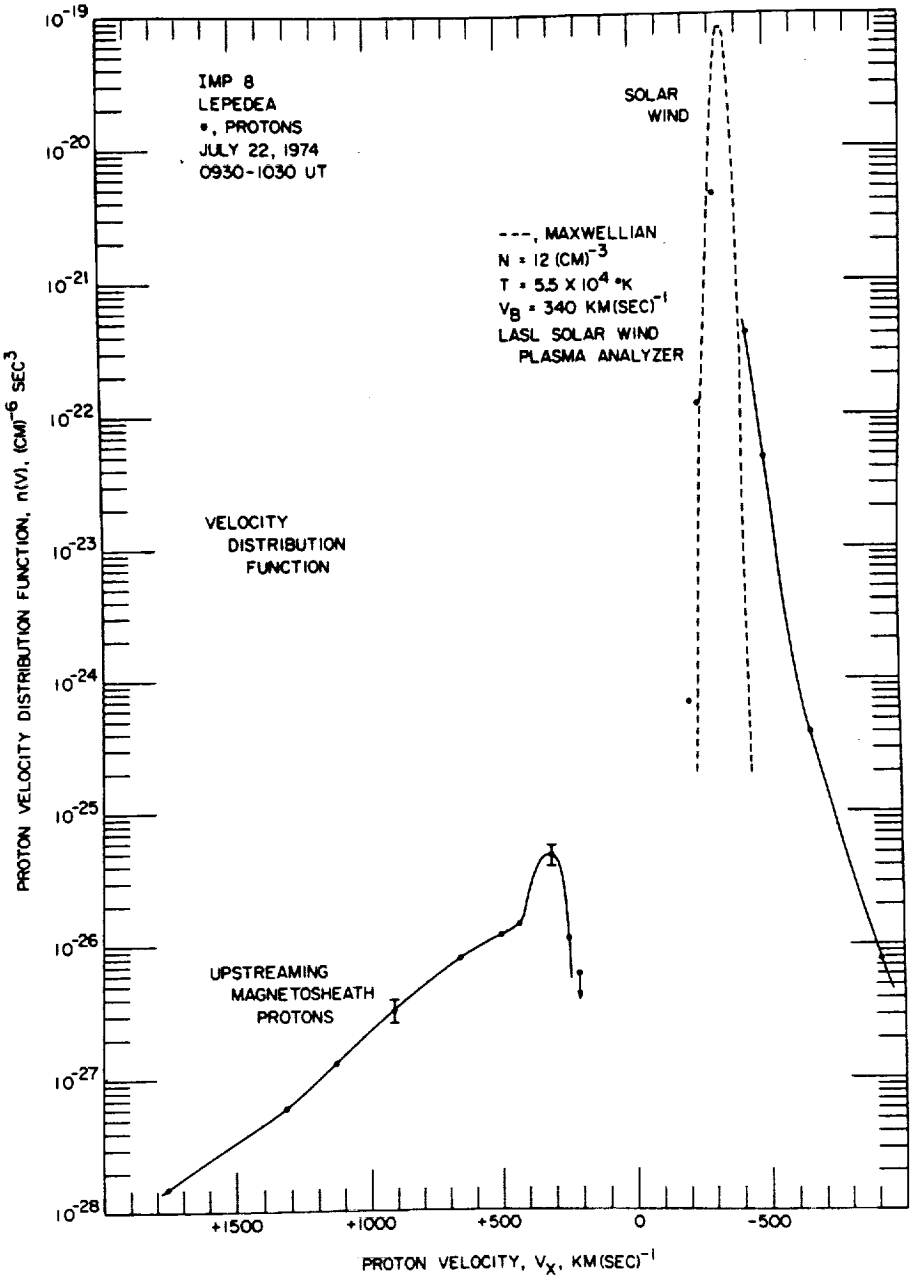

Fig. 11. Distribution function for the intense burst of protons observed streaming into the solar wind from the earth's bow shock from 0930 to 1030 UT in Plate 1. The $+V_x$ velocity axis is directed toward the sun. The dashed line gives the solar wind proton distribution function as determined from the Los Alamos plasma analyzer on Imp 8.

instability, no method was available to distinguish clearly between these two modes of propagation.

One way of distinguishing the Buneman mode from the ion acoustic mode is to measure the wavelength. The two modes differ fundamentally in the wavelengths required to account for the observed frequency spectrums. Since ion acoustic waves only occur at frequencies less than f_p^+ in the rest frame of the plasma, large Doppler shifts and correspondingly short wavelengths of tens to hundreds of meters are required to account for the frequency range, $(2\text{–}10)f_p^+$, in which the noise is usually observed. The Buneman mode, on the other hand, occurs at a frequency $f_B \simeq 3.49f_p^+$, which requires no Doppler shift to account for the observed frequency spectrum, implying wavelengths of several hundred meters or more.

Since only a single electric dipole antenna is used on Helios, the wavelength cannot be determined. However, the Imp 6 spacecraft, which also detects the same waves upstream of the bow shock, has two antennas of different lengths which can be used to estimate wavelengths. The technique used consists of comparing the measured antenna voltages V with the tip-to-tip lengths L of the antennas. For wavelengths longer than the antenna the antenna voltage is directly proportional to the antenna length, so that the computed electric field strength $E = 2V/L$ is the same for both antennas. However, for wavelengths λ comparable to or shorter than the antenna this proportionality no longer holds. In general, we expect that when $\lambda \lesssim L$, the measured electric field strength will be underestimated.

On Imp 6 the electric field antennas consist of two orthogonal dipoles with tip-to-tip lengths of $L_y = 92.5$ m and $L_x =$

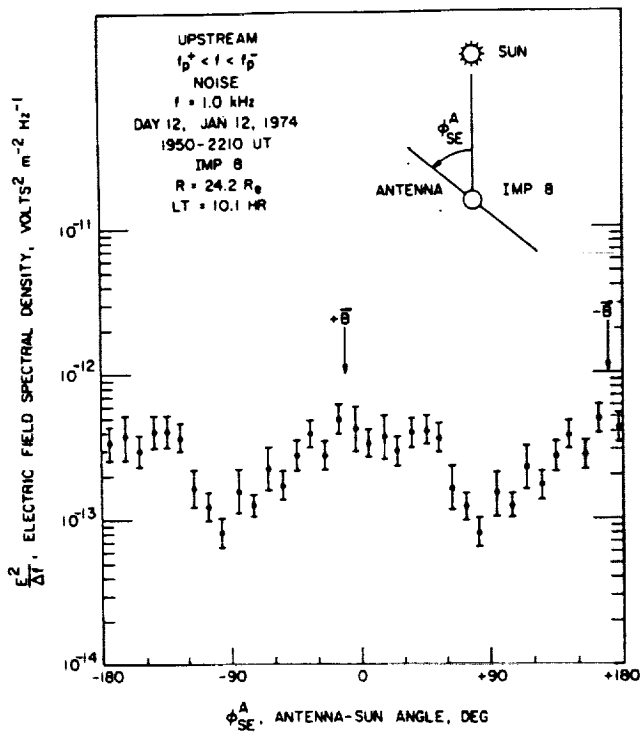

Fig. 12. Angular distribution of the electric field intensity for a burst of $f_p^+ < f < f_p^-$ noise produced by upstreaming magnetosheath protons. These data show that the electric field of the proton-driven $f_p^+ < f < f_p^-$ noise is parallel to the solar wind magnetic field, essentially identical to the $f_p^+ < f < f_p^-$ noise detected by Helios far from the earth (compare with Figure 4).

53.5 m [*Gurnett*, 1974]. The two antennas are mounted orthogonally to each other and to the spacecraft spin axis. The spin axis is directed normal to the ecliptic plane. Simultaneous measurements of the voltage spectrums from the two antennas are made with two identical spectrum analyzers. Because of their orientation the two antennas do not detect the same component of the electric field. However, for a steady state wave spectrum, comparisons can be made by averaging over many rotations of the spacecraft.

A case for which the wavelength of the interplanetary $f_p^+ < f < f_p^-$ noise has been estimated by using this technique is shown in Figure 15. During this period, Imp 6 is upstream of the bow shock at geocentric radial distances from about 19 to 26 R_E and local times from about 9.8 to 10.2 hours. A substantial level of $f_p^+ < f < f_p^-$ noise is present during this period. Some of these events can be associated with low-energy protons arriving from the bow shock, whereas other events, such as the intense bursts from about 0520 to 0610 UT, are of interplanetary origin. This period of enhanced activity occurs shortly after an abrupt increase in the solar wind density at about 0500 UT (see the top panel of Figure 15), which preceded the onset of a high-speed solar wind stream a few hours later (W. Feldman, personal communication, 1977).

The electric field spectrums obtained from the E_y and E_x antennas during the interval from about 0530 to 0602 UT are shown in the bottom panel of Figure 16. These spectrums give the median values of all of the peak intensities obtained during this interval, computed by using $E = 2V/L$. Each point represents the median of approximately 700 individual peak measurements. Because of the impulsive temporal fluctuations a large number of measurements are needed to reduce the statistical fluctuations to an acceptable level. The ratio of the E_y to the E_x field strengths, computed from these spectrums, is shown in the top panel of Figure 16, with estimates of the corresponding error limits (one standard deviation). As can be seen, the E_y/E_x ratio is approximately 1 at low frequencies, $f \lesssim 3$ kHz, but deviates substantially below 1 at high frequencies, $f \gtrsim 10$ kHz. The decrease in the E_y/E_x ratio at high frequencies indicates that the longer, E_y antenna is significantly underestimating the field strengths in comparison to the shorter, E_x antenna. This deviation of the E_y/E_x ratio indicates that wavelengths shorter than $L_y = 92.5$ m are being detected at frequencies above about 3 kHz.

To demonstrate the overall accuracy and reliability of this technique, a corresponding analysis was performed on a band of whistler mode plasmaspheric hiss detected in the earth's magnetosphere a few hours later. It is easily shown that the wavelengths of these whistler mode waves are very large, much larger than the dimensions of the Imp 6 electric antennas. The results of this analysis are shown in Figure 17. As can be seen, the E_y/E_x ratio stays very close to 1 at all frequencies, thereby confirming that the wavelengths are longer than the antenna length. These and many other similar comparisons for a wide variety of plasma wave phenomena demonstrate that significant deviations of the E_y/E_x ratio below 1, such as the deviation in Figure 16, are not instrumental effects and can only be attributed to wavelengths shorter than the antenna length.

Since the accuracy of the method has been confirmed, it is now of interest to compare the measurements in Figure 16 with the wavelengths to be expected if the waves are ion acoustic waves. For typical solar wind parameters $T^- \simeq 1.5 \times 10^5$ °K it is readily shown that the ion acoustic speed $C_s = (kT^-/m^+)^{1/2} \simeq 35.2$ km s^{-1} is much less than the solar wind velocity. For these conditions the frequency detected in the spacecraft frame of reference is, to a good approximation, given entirely by the Doppler shift (valid for $f \gg f_p^+$),

$$f = (V_{sw}/\lambda) \cos \theta_{kV} \tag{1}$$

where θ_{kV} is the angle between the propagation vector $\mathbf{k}$ and the solar wind velocity $\mathbf{V}_{sw}$. Even though the ion acoustic mode can propagate at a substantial angle to the magnetic field [*Stix*, 1962], the $f_p^+ < f < f_p^-$ noise is evidently generated with $\mathbf{k}$ vectors nearly parallel to the static magnetic field, since the electric field is always observed to be nearly parallel to the static magnetic field. Thus θ_{kV} can be determined from the measured magnetic field direction; i.e., $\theta_{kV} \simeq \theta_{BV}$. By solving (1) for λ by means of the appropriate solar wind speed $V_{sw} \simeq 360$ km s^{-1} from Figure 15 and by means of $\theta_{BV} \simeq 22°$ from the Imp 6 magnetometer data (D. Fairfield, personal communication, 1977) the wavelengths corresponding to each frequency can be calculated. These wavelengths are shown by the wavelength scale at the top of Figure 16 along with the lengths L_y and L_x of the two electric antennas. As can be seen, the E_y/E_x ratio starts to deviate below 1 as soon as the computed wavelength becomes significantly shorter than the antenna. These comparisons show that the wavelength computed from the Doppler shift formula is in excellent quantitative agreement with the wavelength estimated from the E_x/E_y ratio ($\lambda \simeq 92.5$ m at $f \simeq 3$ kHz).

Further evidence of short wavelengths is provided by the upper cutoff of the observed frequency spectrum and the variation of this cutoff with radial distance from the sun. It is well known that the shortest wavelength which can occur in a plasma is determined by the onset of strong Landau damping

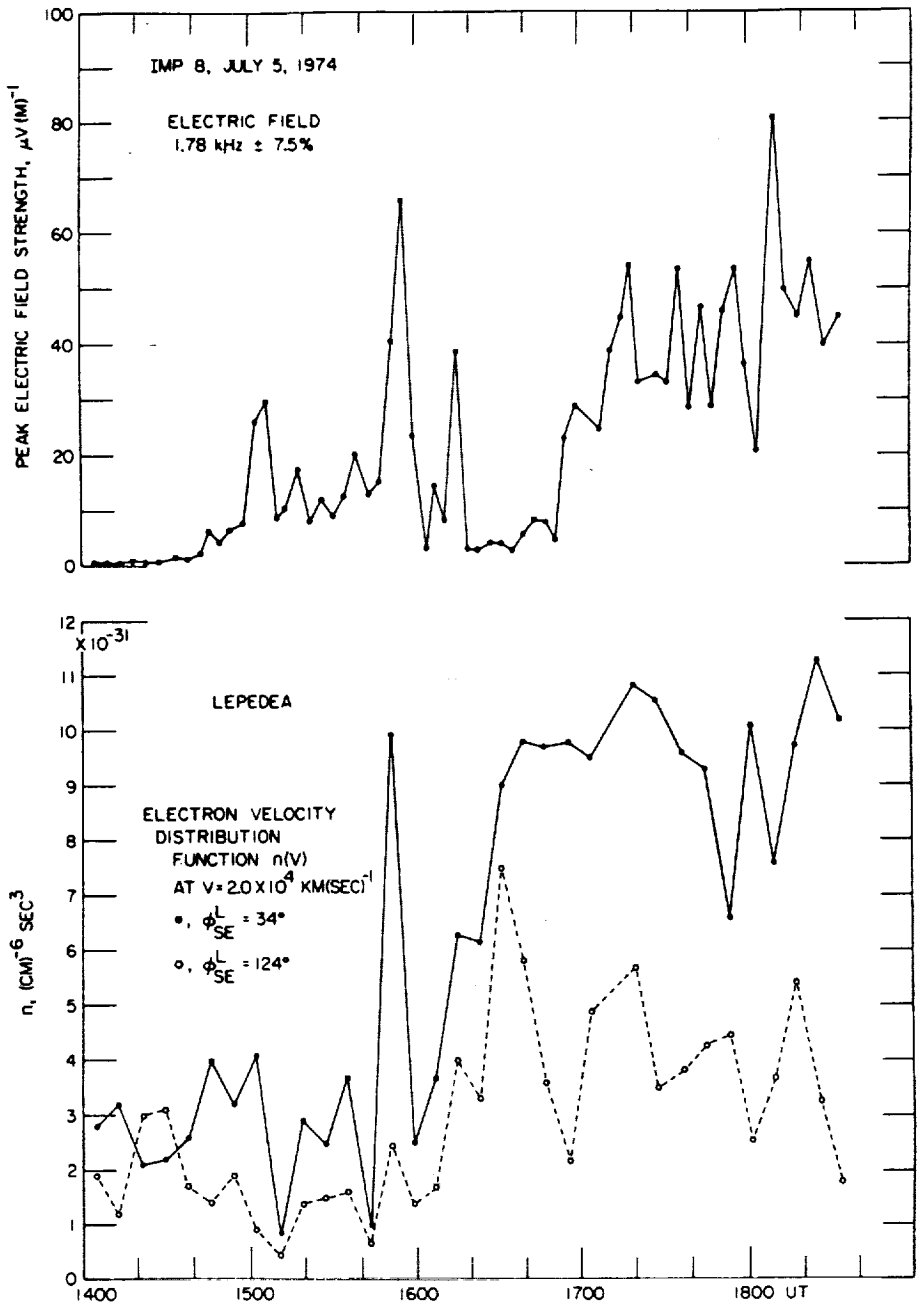

Fig. 13. Low-energy electron intensity variations associated with the burst of $f_p^+ < f < f_p^-$ noise shown in Figure 10. The dashed curve at $\varphi_{sE}{}^L = 124°$ gives the electron intensities perpendicular to the magnetic field, and the solid curve at $\varphi_{sE}{}^L = 34°$ gives the intensities looking generally toward the sun and along the ecliptic plane projection of the magnetic field. The $f_p^+ < f < f_p^-$ noise occurs during periods of substantial anisotropy in the low-energy electron intensities associated with the electron heat flux in the solar wind.

at a wavelength of about $2\pi\lambda_D$, where $\lambda_D{}^2 = \epsilon_0 kT/ne^2$ is the Debye length. The minimum wavelength $\lambda_{min} = 2\pi\lambda_D$, computed from the measured plasma density $n \simeq 35$ cm^{-3} and the temperature $T^- = 1.4 \times 10^5$ °K, is approximately 27.5 m, as is shown at the top of Figure 16. As can be seen, this minimum wavelength is in excellent agreement with the observed upper cutoff frequency of the electric field spectrum. The dependence of the minimum wavelength on the plasma density, $\lambda_{min} \propto \lambda_D \propto 1/n^{1/2}$, furthermore explains the tendency for the upper cutoff frequency $f_{max} \simeq (V_{sw}/\lambda_{min}) \propto n^{1/2}$ to increase with decreasing radial distance from the sun (see Figure 6), since the plasma density increases closer to the sun. When the plasma density scaling law $n \propto 1/R^2$, appropriate for the solar wind far from the sun, is used, the upper cutoff frequency should vary approximately as $f_{max} \propto 1/R$, which is seen to be in good agreement with the observed radial variation of the upper cutoff frequency illustrated in Figure 6. All these comparisons provide strong evidence that the low-frequency electrostatic waves detected in the solar wind by Imp 6, Imp 8, and Helios have short wavelengths and Doppler shifts consistent with the identification of these waves as ion acoustic waves.

Although short wavelengths are clearly evident for the event in Figure 16, in most cases the $f_p^+ < f < f_p^-$ noise detected by Imp 6 does not show these effects. The event in Figure 16 is

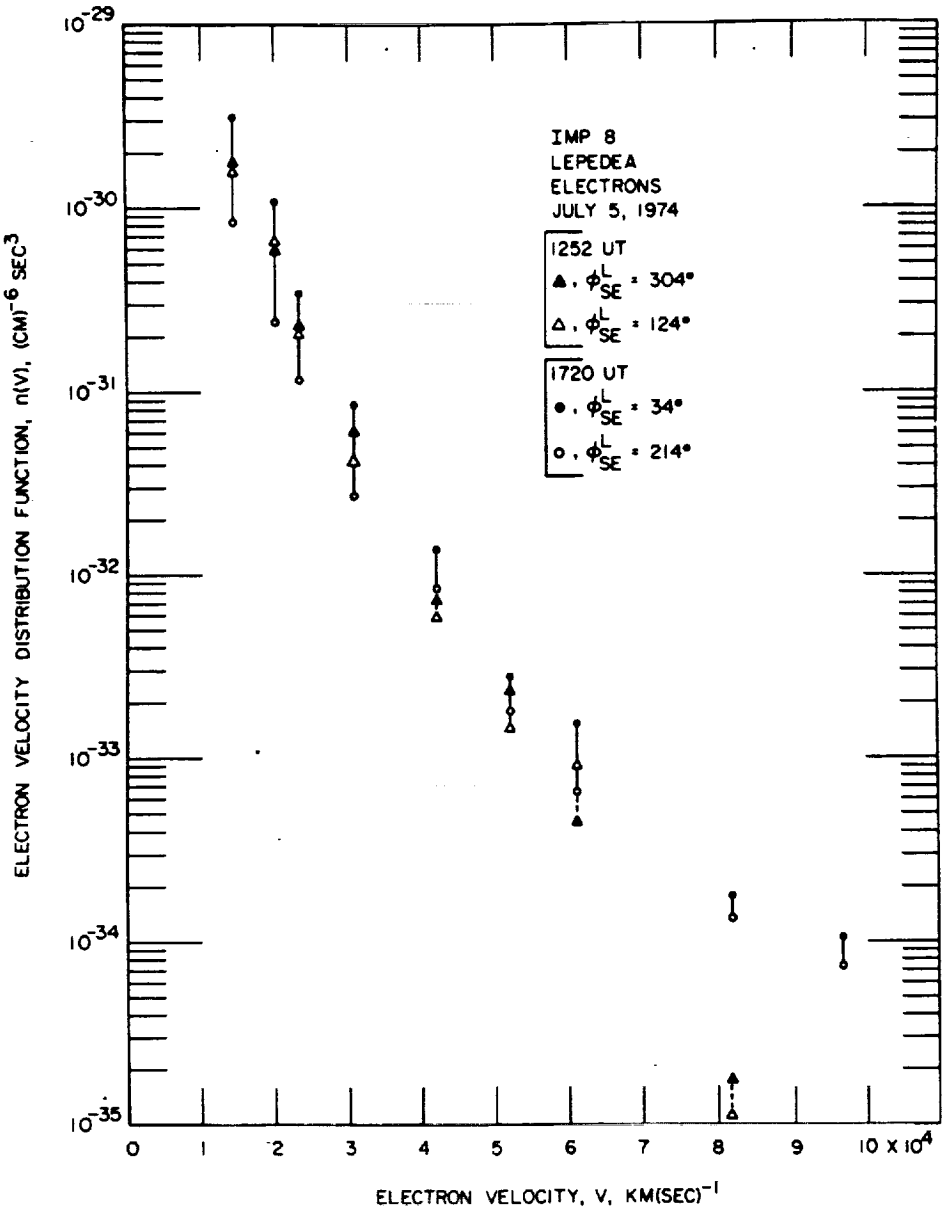

Fig. 14. Further details of the anisotropic electron distribution associated with the burst of $f_p^- < f < f_p^-$ noise shown in Figure 10, selected for times when the magnetic field is aligned parallel to the viewing direction of the Lepedea. At 1252 UT the anisotropy is very small, and no $f_p^- < f < f_p^-$ noise is present. At 1720 UT the anisotropy is large, particularly at the lower velocities, and the $f_p^- < f < f_p^-$ noise intensities are correspondingly large.

unusual in that the plasma density is very large, n = 35 cm^{-3}, and results in a minimum wavelength substantially less than the antenna length. For typical solar wind plasma densities at 1 AU, $n \simeq 5$ cm^{-3}, the minimum wavelength is approximately λ_m = 72 m, which is evidently sufficiently large to make short-wavelength effects undetectable even though wavelengths shorter than the Imp 6 antenna length, L_y = 92.5 m, could occur. Note from Figure 16 that most of the wave energy occurs at wavelengths substantially larger than $\lambda_{min} = 2\pi\lambda_D$ and that the intensity is strongly attenuated for wavelengths approaching λ_{min}. It should also be noted that because of the shorter length of the Helios antennas (L = 16 m for Helios 1, and L = 32 m for Helios 2), errors due to short-wavelength effects are not normally expected to be significant for the Helios measurements, except for unusually high densities.

ORIGIN OF THE SOLAR WIND ION ACOUSTIC WAVES

Having established that the $f_p^+ < f < f_p^-$ noise consists of short-wavelength ion acoustic waves, we now consider the mechanisms for generating these waves, both in the interplanetary medium and in the region upstream of the bow shock. The observed triggering of the ion acoustic waves by an increase in the electron heat flux provides strong evidence that the ion acoustic mode is being driven unstable by the electron heat flux in the solar wind, as was first suggested by *Forslund* [1970].

The basic mechanism proposed by *Forslund* [1970] is illustrated schematically in Figure 18, which shows the general form of the reduced one-dimensional electron and proton distribution functions in the solar wind. The reduced one-

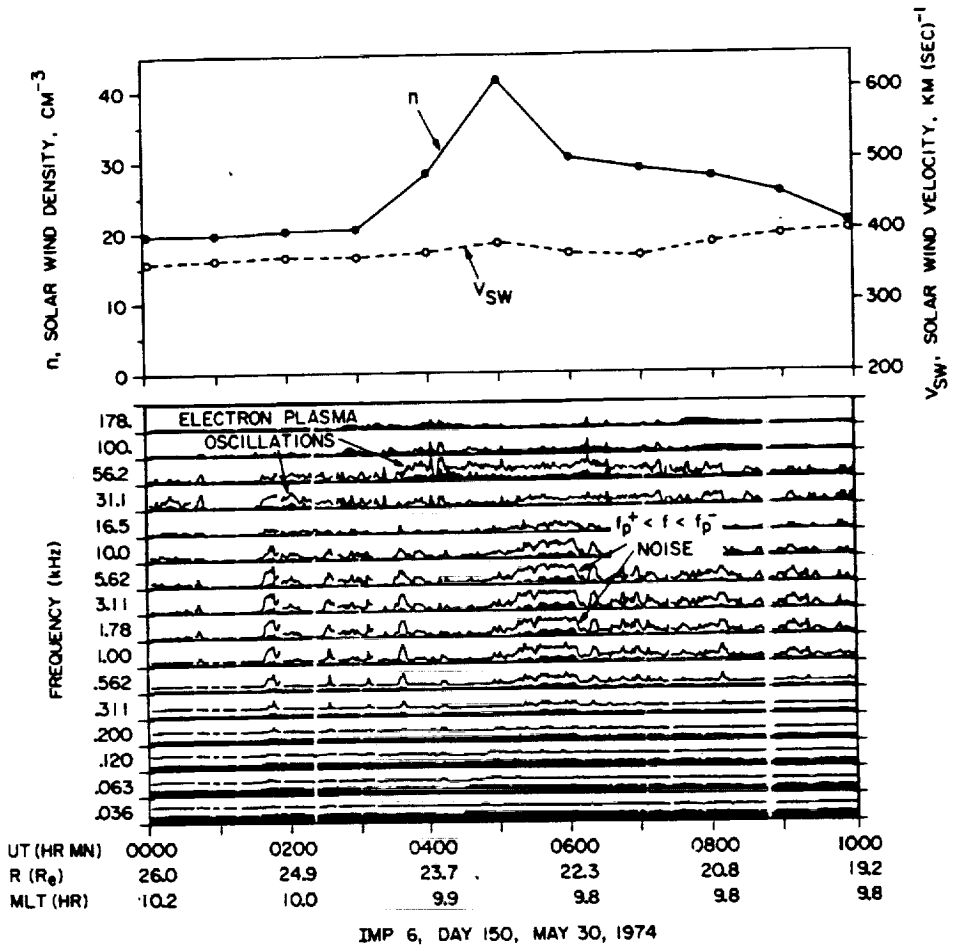

Fig. 15. Series of $f_p^- < f < f_p^-$ noise bursts detected by Imp 6 in association with a density compression preceding a high-speed solar wind stream.

dimensional distribution function $F(V)$ is defined by $F(V) = \int d\mathbf{V}_\perp f(\mathbf{V})$, where $f(\mathbf{V})$ is the three-dimensional distribution function and $d\mathbf{V}_\perp$ represents an integration over velocities perpendicular to the magnetic field. As is indicated, a substantial anisotropy is produced in the high-energy, or 'halo,' electrons by the electron heat flux flowing outward away from the sun [*Feldman et al.*, 1974, 1975]. Since the net current in the solar wind is essentially zero, except at discontinuities, the electron current associated with the antisunward drift of the energetic 'halo' electrons must be compensated by a sunward drift of the low-energy 'core' electrons. This drift velocity V_d is indicated in Figure 18. If the double peak in the combined velocity distribution function $F(V) = F^-(V) + (m^-/m^+)F^+(V)$ produced by this drift is sufficiently large, then the ion acoustic mode is unstable. Since the drift is parallel to the static magnetic field, the waves produced by this instability are expected to have their wave vectors and electric fields oriented approximately parallel to the static magnetic field. The condition for instability is given by the Penrose criterion

$$\int_{-\infty}^{\infty} \frac{F(V) - F(V_0)}{(V - V_0)^2}\, dV > 0 \qquad (2)$$

where V_0 is the velocity of the minimum in $F(V)$ [*Penrose*, 1960]. For equal electron and ion temperatures $T^- \simeq T^+$ the threshold drift velocity is very large, approximately $V_t = (kT^-/m^-)^{1/2}$, which is too large to be exceeded in the solar wind. However, if $T^- \gg T^+$, which is sometimes satisfied in the solar wind, then the threshold drift velocity for instability is greatly reduced, to approximately

$$V_t \simeq (kT^+/m^+)^{1/2} \qquad (3)$$

[*Krall and Trivelpiece*, 1973]. For a solar wind ion temperature of $T^+ \simeq 4.0 \times 10^4$ °K the threshold drift velocity is, for example, only $V_t = 18$ km s^{-1} ($T^- \gg T^+$ being assumed). For electron temperatures only moderately larger than the ion temperature the threshold drift velocity is larger than (3) by a factor which depends on T^-/T^+ [see *Krall and Trivelpiece*, 1973]. On the basis of his analysis, *Forslund* [1970] concluded that the ion acoustic mode should be driven unstable by the electron heat flux whenever the electron to ion temperature ratio is sufficiently large.

Both the observed electric field orientation and the association of enhanced ion acoustic wave activity with increases in the electron anisotropy provide substantial evidence for the mechanism proposed by *Forslund* [1970]. The detailed arguments in support of this mechanism are, however, more involved, since all other types of double-peak distribution functions which could possibly generate ion acoustic waves must be eliminated from consideration. Charged particle measurements, such as those in Plates 2 and 3, clearly show that ion

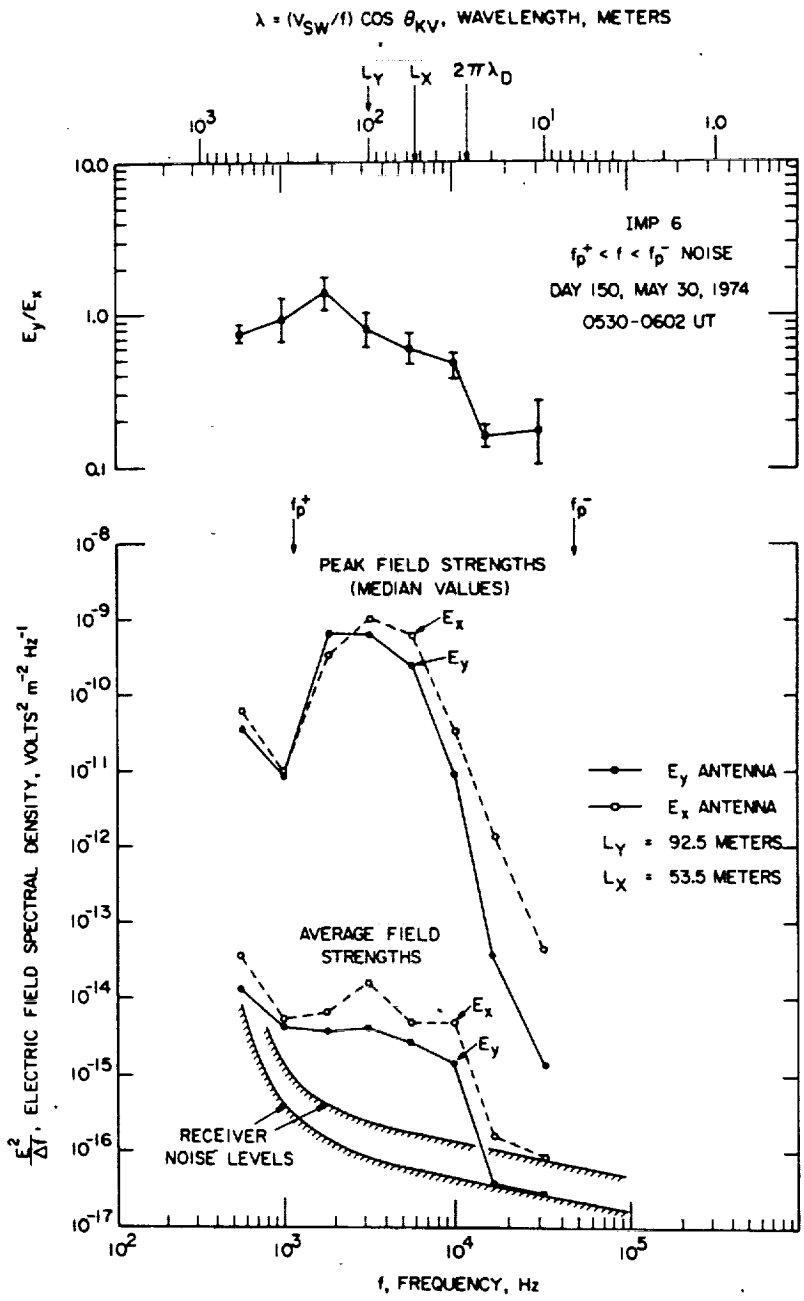

Fig. 16. Comparison of the electric field amplitudes for the burst of $f_p^- < f < f_p^-$ noise from 0530 to 0602 UT in Figure 15 using antennas of two different lengths. The deviation of the E_y/E_x ratio below 1 indicates that the wavelengths of the waves are shorter than the longest antenna, L_y = 92.5 m, at frequencies above about 3 kHz. The scale at the top of the illustration indicates the wavelength which would occur if the observed frequencies were entirely due to Doppler shifts. Note the close correspondence of the upper frequency cutoff to the minimum wavelength $2\pi\lambda_D$ caused by Landau damping.

acoustic waves occur during times when no secondary peak is detectable in either the electron or the proton distribution functions, within the energy range (50 eV $\lesssim E \lesssim$ 45 keV) and resolution of the Lepedea. Although electron energies less than 100 eV were not investigated, it is almost completely certain, on the basis of the results of *Feldman et al.* [1975], that double peaks do not occur in the electron distribution function at energies less than 100 eV. It is possible that closely spaced double peaks could occur in the ion distribution, such as the double proton streams reported by *Feldman et al.* [1973*a*], and still be unresolved in the Lepedea data. Comparisons with published examples of double proton streams [*Feldman et al.*, 1973*a*] do not show a close correspondence with the occurrence of ion acoustic waves; however, further detailed studies are needed to investigate whether double proton streams can under some circumstances generate ion acoustic waves. On the assumption that the ion distribution functions do not generally have the double-peaked form required to produce an instability, essentially the only possibility left is the double peak produced by a velocity shift between the peaks in the electron and ion distributions, as illustrated in Figure 18. The presence of such a velocity shift in the solar wind has now been amply demonstrated by *Feldman et al.* [1974, 1975]. It only remains to be demonstrated that this shift is sufficiently large to exceed

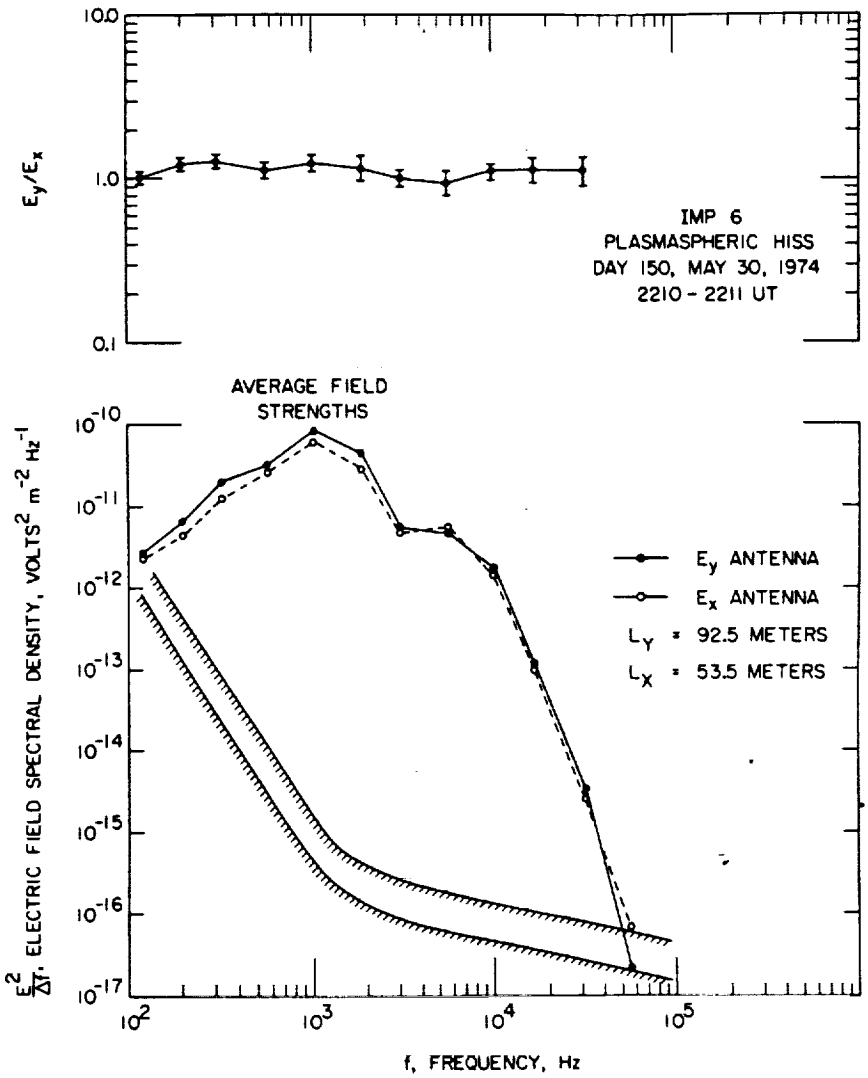

Fig. 17. Comparison of the E_y/E_x ratio for a broadband plasmaspheric hiss emission observed a few hours after the event in Figure 16. Plasmaspheric hiss has wavelengths much longer than the antenna length. The close correspondence of the E_y/E_x ratio to 1 confirms the overall accuracy of this technique for detecting short-wavelength effects.

the threshold for generating ion acoustic waves. The magnitude of the velocity shift, which is difficult to measure directly, can be estimated from the anisotropy in the halo electron distribution. For the event in Figure 14 at 1720 UT the flux of electrons along the magnetic field (first moment) is estimated to be 1.50×10^8 el $(\text{cm}^2\,\text{s})^{-1}$. When the measured local plasma density of $n = 10.1$ el cm^{-3} is used, this flux must be compensated by a sunward drift of the core electrons at a velocity of about 150 km s^{-1}. The ratio of this drift velocity to the electron thermal speed ($T^- = 1.5 \times 10^5$ °K being used) is about 0.1. Whether this drift velocity exceeds the threshold drift velocity for the ion acoustic wave instability is critically dependent on the electron to ion temperature ratio. For the period of interest the ion temperature measured by the Los Alamos plasma probe on Imp 8 is $T^+ = 7.1 \times 10^4$ °K. When a typical temperature of $T^- = 1.5 \times 10^5$ °K is used for the core electrons, the temperature ratio is $T^-/T^+ = 2.14$. For this relatively low electron to ion temperature ratio the ion acoustic mode should be stable according to the curves given by *Stringer* [1964]. On the other hand, if a typical halo temperature of $T^- = 7.0 \times 10^5$ °K is used, which gives $T^-/T^+ = 10$, the threshold drift velocity given by equation (3), $V_t = 23$ km s^{-1} (valid when $T^- \gg T^+$), is exceeded by a substantial factor. Since no computer calculations of the threshold drift velocity are available for a realistic combination of core and halo electron distributions, the stability of the ion acoustic mode cannot be accurately determined. However, since the correct effective electron to ion temperature ratio is probably somewhere in between the two extremes given by the core and halo temperatures, it seems likely that the ion acoustic mode is unstable in this case. Further detailed analyses of the exact instability conditions are needed for realistic models of the solar wind electron distribution to answer this question clearly.

For the ion acoustic waves generated by protons streaming into the solar wind from the bow shock there is no question about which particles are responsible for the instability. However, considerable uncertainty still remains concerning the detailed mechanism by which the proton stream produces the instability. In considering the origin of the instability, two distinctly different mechanisms can be identified: (1) the instability may be caused directly by the double peak in the proton

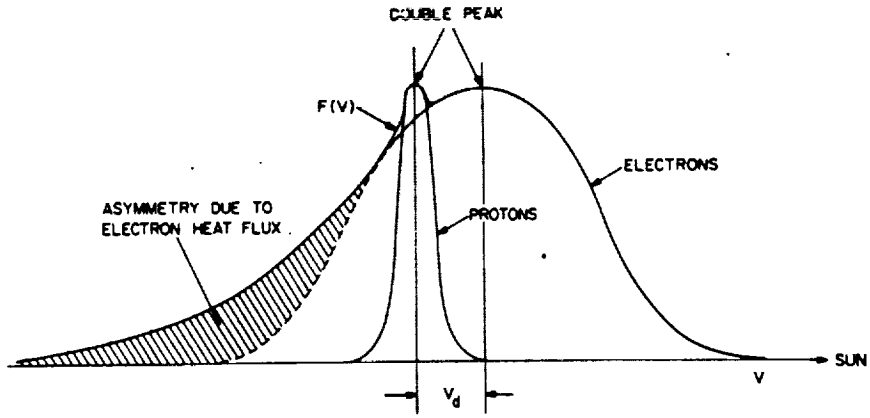

Fig. 18. Illustration showing the velocity shift V_d between the low-energy electrons and the solar wind protons, required to maintain zero net current when a substantial electron heat flux is present. If the velocity shift is sufficiently large, the resulting double peak in the combined electron and proton distribution function $F(V)$ can cause the ion acoustic mode to become unstable.

distribution (see Figure 11), or (2) the instability may be caused indirectly by the shift in the velocity of the core electrons required to maintain zero net current, similar to the heat flux mechanism. Of these two possibilities the second mechanism is believed to be dominant. For the first mechanism, rough estimates show that the peak in the proton distribution function due to the upstreaming protons is simply too small to be unstable according to the Penrose criterion. Note that the contribution of the proton stream to $F(V)$ is greatly reduced by the factor (m^-/m^+) in the combined one-dimensional distribution function, in addition to the fact that the distribution function for this stream is nearly 6 orders of magnitude below the peak due to the solar wind beam (see Figure 11). On the other hand, the proton flux associated with the upstreaming protons can be quite substantial, $\sim 5 \times 10^8$ protons $(\text{cm}^2\ \text{s})^{-1}$. The upstreaming protons must therefore cause a shift in the velocity of the core electrons with respect to the solar wind protons in order to maintain zero net current. If this shift is large enough to produce instability, this mechanism will explain why the ion acoustic waves driven by the upstreaming protons are so similar to the interplanetary ion acoustic waves, since the mechanisms are essentially identical. Note that halo electrons streaming away from the sun and sunward streaming protons both contribute in the same sense to the current imbalance. Detailed comparisons, however, often show that the intensities of the upstreaming protons are too small, by factors of 10–100, to produce velocity shifts exceeding the threshold for the ion acoustic wave instability using a simple Maxwellian distribution for the core electrons. The detailed explanation of this discrepancy is not known; however, one possibility is that the electron heat flux maintains the plasma near marginal stability for ion acoustic waves, so that only a small current imbalance is needed to trigger the instability. Also, *Feldman et al.* [1973*b*] have shown that protons streaming into the solar wind from the earth's bow shock produce substantial perturbations in the ambient solar wind electron distribution. These perturbations and their effect on the instability condition given by the Penrose criterion must be studied in greater detail before the generation mechanism of the upstream ion acoustic waves can be completely resolved.

Numerous investigators have suggested possible roles which ion acoustic turbulence may play in determining the large-scale properties of the solar wind. It has been suggested that plasma waves can heat the solar wind ions [*Fredricks*, 1969], regulate the electron heat flux in the solar wind [*Forslund*, 1970; *Schulz and Eviatar*, 1972], and thermally couple the electron and ion distributions [*Perkins*, 1973]. The extent to which the ion acoustic waves detected by Helios and Imp 6 and 8 play any significant role in these processes remains to be determined. At 1 AU the maximum intensities of the ion acoustic turbulence are relatively small, energy density ratios being approximately $\epsilon_0 E^2/2nkT \simeq 10^{-5}$. The turbulence is, however, present a large fraction of the time and increases rapidly in intensity with decreasing radial distance from the sun. These factors all suggest that the presence of these waves must be given serious consideration in the overall understanding of the solar wind, particularly in relation to the regulation of the solar wind heat flux.

SUMMARY AND CONCLUSION

Plasma wave measurements on the solar-orbiting Helios spacecraft have previously shown that sporadic bursts of electrostatic turbulence are commonly observed in the solar wind at frequencies between the electron and ion plasma frequencies [*Gurnett and Anderson*, 1977]. In this paper we have expanded the earlier investigation of these waves using the Helios data and have compared the Helios results with similar measurements from the earth-orbiting Imp 6 and 8 spacecraft. Wavelength measurements with the Imp 6 spacecraft now provide strong evidence that these waves are short-wavelength ion acoustic waves at $f \lesssim f_{p^+}$ which are Doppler-shifted upward in frequency by the motion of the solar wind. The upper cutoff frequency and the variation of this cutoff frequency with radial distance from the sun, $f_{max} \propto 1/R$, are in close agreement with the short-wavelength cutoff expected for ion acoustic waves.

Comparison with the Imp 6 and 8 data reveals that a substantial fraction, 50–70%, of the ion acoustic wave turbulence detected in the solar wind near the earth is caused by suprathermal protons streaming into the solar wind from the earth's bow shock. These waves, which correspond to the upstream electrostatic waves first reported by *Scarf et al.* [1970], are observationally indistinguishable from the ion acoustic waves detected by Helios. Although both the upstream proton-driven waves and the waves detected by Helios are evidently ion acoustic waves, some distinctly different source is required to explain the Helios observations, since protons from the earth's bow shock cannot possibly account for the waves detected by Helios far from the earth. Examina-

C-2

tion of the Imp 6 and 8 data reveals many examples of ion acoustic turbulence during periods when no protons can be detected coming from the earth's bow shock. These events evidently correspond to the waves detected by Helios far from the earth. Usually in these cases there is no evidence of significant suprathermal electron or proton fluxes other than the quiescent solar wind distribution. In a few events, variations in the ion acoustic wave intensity were found which are closely correlated with changes in the anisotropy of the solar wind electron distribution. These events suggest that the ion acoustic turbulence is driven by the anisotropy associated with the electron heat flux in the solar wind, as was suggested by *Forslund* [1970]. Although it seems reasonably certain that the electron heat flux is in some cases involved in the generation of the interplanetary ion acoustic waves, the association of ion acoustic waves with suprathermal protons from the bow shock suggests that the solar wind ion distributions should be investigated in greater detail to see if double ion streams and other nonthermal solar wind ion distributions could also be involved in the generation of these waves.

Acknowledgments. The authors express their thanks to William Feldman from the Los Alamos Scientific Laboratory for providing the Imp 8 plasma density and temperature measurements used in this report. The research at the University of Iowa was supported in part by NASA under contracts NAS5-11279, NAS5-11431, and NAS5-11064 and grants NGL-16-001-002 and NGL-16-001-043 and by the Office of Naval Research.

The Editor thanks W. Bernstein and F. L. Scarf for their assistance in evaluating this paper.

REFERENCES

Buneman, O., Instability, turbulence and conductivity in a current-carrying plasma, *Phys. Rev. Lett.*, *1*, 8, 1958.

Feldman, W. C., J. R. Asbridge, S. J. Bame, and M. D. Montgomery, Double ion streams in the solar wind, *J. Geophys. Res.*, *78*, 2017, 1973*a*.

Feldman, W. C., J. R. Asbridge, S. J. Bame, and M. D. Montgomery, Solar wind heat transport in the vicinity of the earth's bow shock, *J. Geophys. Res.*, *78*, 3697, 1973*b*.

Feldman, W. C., M. D. Montgomery, J. R. Asbridge, S. J. Bame, and H. R. Lewis, Interplanetary heat conduction—Imp 7 results, in *Solar Wind Three*, p. 334, Institute of Geophysics and Planetary Physics, University of California, Los Angeles, Calif., 1974.

Feldman, W. C., J. R. Asbridge, S. J. Bame, M. D. Montgomery, and S. P. Gary, Solar wind electrons, *J. Geophys. Res.*, *80*, 4181, 1975.

Forslund, D. W., Instabilities associated with heat conduction in the solar wind and their consequences, *J. Geophys. Res.*, *75*, 17, 1970.

Frank, L. A., K. L. Ackerson, and R. P. Lepping, On hot tenuous plasmas, fireballs, and boundary layers in the earth's magnetotail, *J. Geophys. Res.*, *81*, 5859, 1976.

Fredricks, R. W., Electrostatic heating of solar wind ions beyond 0.1 AU, *J. Geophys. Res.*, *74*, 2919, 1969.

Gurnett, D. A., The earth as a radio source: Terrestrial kilometric radiation, *J. Geophys. Res.*, *79*, 4227, 1974.

Gurnett, D. A., and R. R. Anderson, Electron plasma oscillations associated with type III radio bursts, *Science*, *194*, 1159, 1976.

Gurnett, D. A., and R. R. Anderson, Plasma wave electric fields in the solar wind: Initial results from Helios 1, *J. Geophys. Res.*, *82*, 632, 1977.

Gurnett, D. A., and L. A. Frank, The relationship of electron plasma oscillations to type III radio emission and low-energy solar electrons, *Solar Phys.*, *45*, 477, 1975.

Krall, N. A., and A. W. Trivelpiece, *Principles of Plasma Physics*, p. 482, McGraw-Hill, New York, 1973.

Penrose, O., Electrostatic instability of a uniform non-Maxwellian plasma, *Phys. Fluids*, *3*, 258, 1960.

Perkins, F., Heat conduction, plasma instabilities, and radio star scintillations in the solar wind, *Astrophys. J.*, *179*, 637, 1973.

Scarf, F. L., R. W. Fredricks, L. A. Frank, C. T. Russell, P. J. Coleman, Jr., and M. Neugebauer, Direct correlations of large-amplitude waves with suprathermal protons in the upstream solar wind, *J. Geophys. Res.*, *75*, 7316, 1970.

Schulz, M., and A. Eviatar, Electron-temperature asymmetry and the structure of the solar wind, *Cosmic Electrodynamics*, *2*, 402, 1972.

Stix, T. H., *The Theory of Plasma Waves*, p. 215, McGraw-Hill, New York, 1962.

Stringer, T. E., Electrostatic instabilities in current-carrying and counterstreaming plasmas, *Plasma Phys.*, *6*, 267, 1964.

(Received April 4, 1977;
accepted August 1, 1977.)

The Heliocentric Radial Variation of Plasma Oscillations Associated With Type III Radio Bursts

D. A. GURNETT, R. R. ANDERSON, F. L. SCARF,[1] AND W. S. KURTH

Department of Physics and Astronomy, University of Iowa, Iowa City, Iowa 52242

A survey is presented of all of the electron plasma oscillation events found to date in association with low-frequency type III solar radio bursts using approximately 9 years of observations from the Imp 6 and 8, Helios 1 and 2, and Voyager 1 and 2 spacecraft. Plasma oscillation events associated with type III radio bursts show a pronounced increase in both the intensity and the frequency of occurrence with decreasing heliocentric radial distance. This radial dependence explains why intense electron plasma oscillations are seldom observed in association with type III radio bursts at the orbit of the earth. Possible interpretations of the observed radial variation in the plasma oscillation intensity are considered.

1. INTRODUCTION

The currently accepted model for the generation of type III solar radio bursts is that these radio emissions are produced by nonlinear processes involving electron plasma oscillations excited by solar flare electrons streaming outward through the solar corona. The electron plasma oscillation mechanism, first proposed by *Ginzburg and Zheleznyakov* [1958], has become the basic element of essentially all theories of type III radio bursts, with suitable refinements to account for various types of nonlinear interactions [*Sturrock*, 1961; *Tidman et al.*, 1966; *Papadopoulos et al.*, 1974; *Smith*, 1974]. Although the plasma oscillation mechanism has been widely accepted for many years, only in the past two years have measurements been obtained which definitely establish the existence of these electron plasma oscillations. Initially, studies by earth-orbiting satellites failed to detect electron plasma oscillations in association with type III radio bursts [*Kellogg and Lin*, 1976]. After searching through nearly 4 years of data from the earth-orbiting Imp 6 and 8 satellites, only one type III event was identified with clearly associated electron plasma oscillations [*Gurnett and Frank*, 1975]. However, the intensity of this event, $\sim 100\ \mu V\ m^{-1}$, was much too small to account for the observed radio emission intensities. The first observations of electron plasma oscillations with intensities sufficiently large to explain type III radio emissions were obtained from the Helios 1 and 2 solar probes, in orbit around the sun at radial distances ranging from 0.29 to 1.00 AU [*Gurnett and Anderson*, 1976, 1977]. In the initial survey of the Helios 1 and 2 plasma wave data, three events were found with electron plasma oscillation intensities exceeding 1 $mV\ m^{-1}$. All of these events occurred relatively close to the sun, at heliocentric radial distances of less than 0.45 AU.

Since the initial survey of the Helios 1 and 2 data the quantity of data available for analysis has increased considerably, and several more intense electron plasma oscillation events have been identified in association with type III radio bursts. Approximately 12 months of plasma wave data are also available from the Voyager 1 and 2 spacecraft at radial distances of from 1.0 to 2.2 AU. A description of the plasma wave instrumentation on the Voyager 1 and 2 spacecraft is given by *Scarf and Gurnett* [1977]. From these data it is found that the most intense electron plasma oscillations, ~ 1–$10\ mV\ m^{-1}$, are usually detected relatively close to the sun, at heliocentric radial distances of less than 0.5 AU, and that only weak events, $\sim 100\ \mu V\ m^{-1}$, are detected near and beyond 1.0 AU. These observations indicate the presence of a strong radial variation in the electron plasma oscillation intensities associated with type III radio bursts, decreasing rapidly with increasing radial distance from the sun. The purpose of this paper is to survey the characteristics of all of the electron plasma oscillation events observed to date in association with type III bursts and to investigate the variation in intensity of these events with radial distance from the sun.

2. SURVEY OF EVENTS ANALYZED

Up to the present time a total of 18 type III solar radio bursts have been detected with clearly associated electron plasma oscillations. The total quantity of data surveyed to identify these events consists of approximately 4 years of observations from Imp 6 and 8 [*Gurnett and Frank*, 1975], 4 years of observations from Helios 1 and 2, and 12 months of observations from Voyager 1 and 2. These data include 153 type III radio bursts which were detectable at frequencies below 178 kHz. Since only 18 of these events occur in association with plasma oscillations, it is evident that the chance of detecting the plasma oscillations responsible for a type III radio burst is quite small, approximately 12%.

The typical characteristics of the events detected are illustrated in Figures 1 and 2, which show the electric field strength in four adjacent frequency channels for each of the 18 events. The solid line in each plot gives the maximum electric field strength, and the solid black area (or vertical lines in the case of days 208 and 209) gives the average electric field strength. The spectrum analyzers on Imp 6, Imp 8, Helios 1, and Helios 2 all have continuously active channels with peak detection so that any signal within the time resolution of the instrument (~ 50 ms) is always detected by the peak field strength measurement. The maximum field strength shown in each channel is the largest peak field strength in the interval since the previous point plotted. For Voyager 1, which does not have peak detection, the maximum field strength is computed from all of the average field strengths available in each interval plotted. The type III radio bursts in Figures 1 and 2 are in most cases easily identified by the smooth increase in the field strength over a period of several tens of minutes and by the characteristic decrease in the emission frequency with increasing time. The electron plasma oscillations associated with these events usually consist of a series of brief but very intense narrow band

[1] Now at TRW Defense and Space Systems Group, Redondo Beach, California 90278.

Paper number 8A0436.
0148-0227/78/098A-0436$01.00

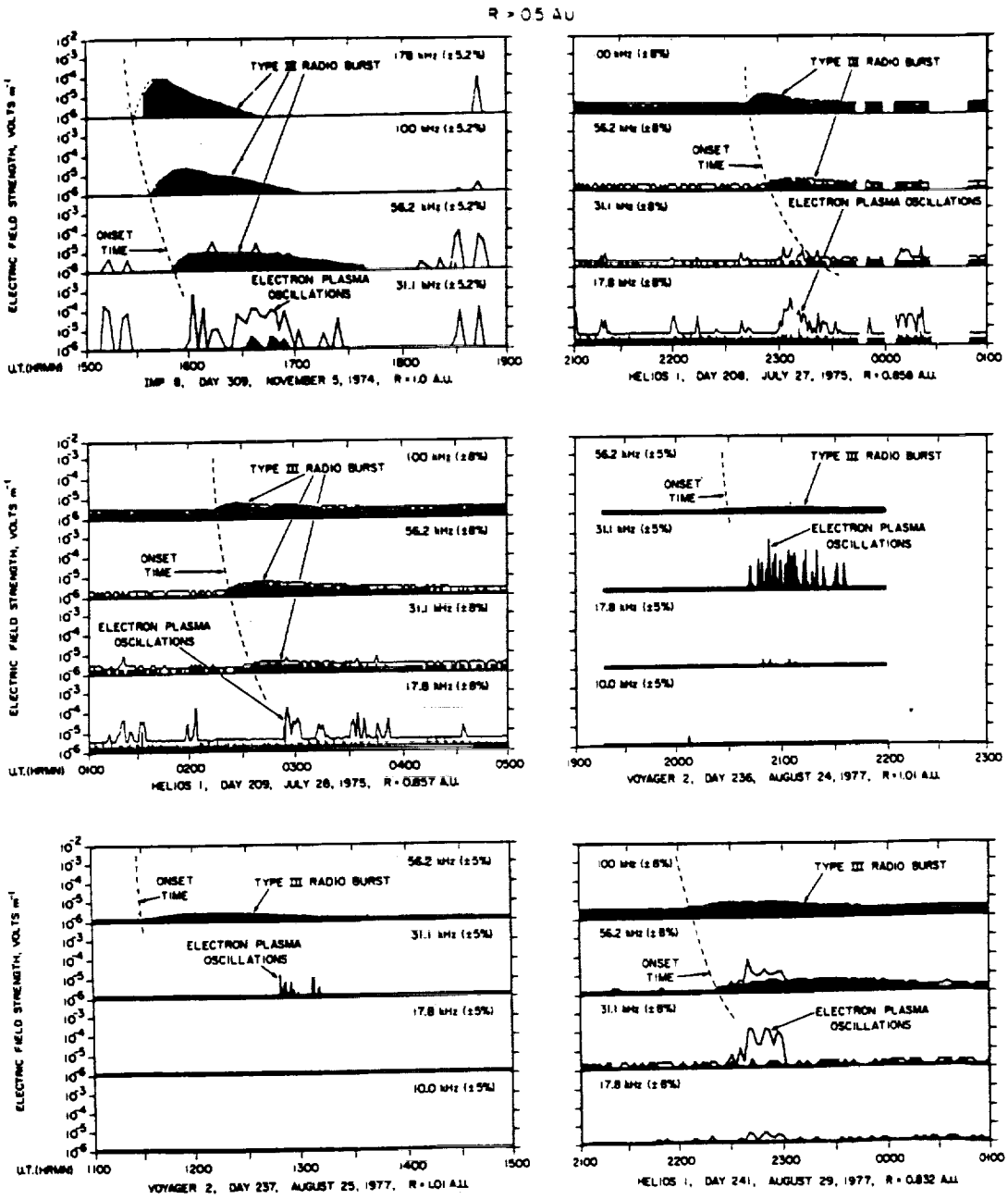

Fig. 1*a*

Fig. 1. All of the type III radio noise bursts and associated electron plasma oscillation events observed to date at heliocentric radial distances beyond 0.5 AU. The solid line gives the maximum electric field intensity, and the solid black areas (or vertical bars for days 208 and 209) give the average electric field intensity. The plasma oscillations beyond 0.5 AU are generally very weak, typically $\sim 100\,\mu V\ m^{-1}$, and occur very infrequently in comparison with the total number of type III bursts.

bursts at the local electron plasma frequency. These bursts usually occur shortly after the onset of the type III radio emission in the next higher frequency channel. The maximum electric field intensity is always much larger than the average electric field intensity, indicating that the plasma oscillations consist of many short impulsive bursts. The impulsive intensity variations of the plasma oscillations are illustrated in greater detail in Figure 3, which shows a high-time resolution snapshot of the plasma oscillation intensities associated with the day 92, 1976, event. The most intense burst detected during this interval lasted only a few tenths of a second. Large temporal variations are evident on time scales comparable to the time resolution (50 ms) of the instrument.

To illustrate the variation in plasma oscillation intensity with heliocentric radial distance, the events in Figures 1 and 2 have been arranged with all of the events at radial distances greater than 0.5 AU in Figure 1 and all of the events at radial distances less than 0.5 AU in Figure 2. Comparison of these illustrations shows that the plasma oscillations are more intense in the region closer to the sun. Although more events have been detected beyond 0.5 AU than inside of 0.5 AU, considerations of the relative observing times in the two regions show that the frequency of occurrence of plasma oscillations is significantly higher in the region closer to the sun. Because of the eccentric orbits of the Helios spacecraft, with aphelion near 1.0 AU and perihelion near 0.3 AU, the frac-

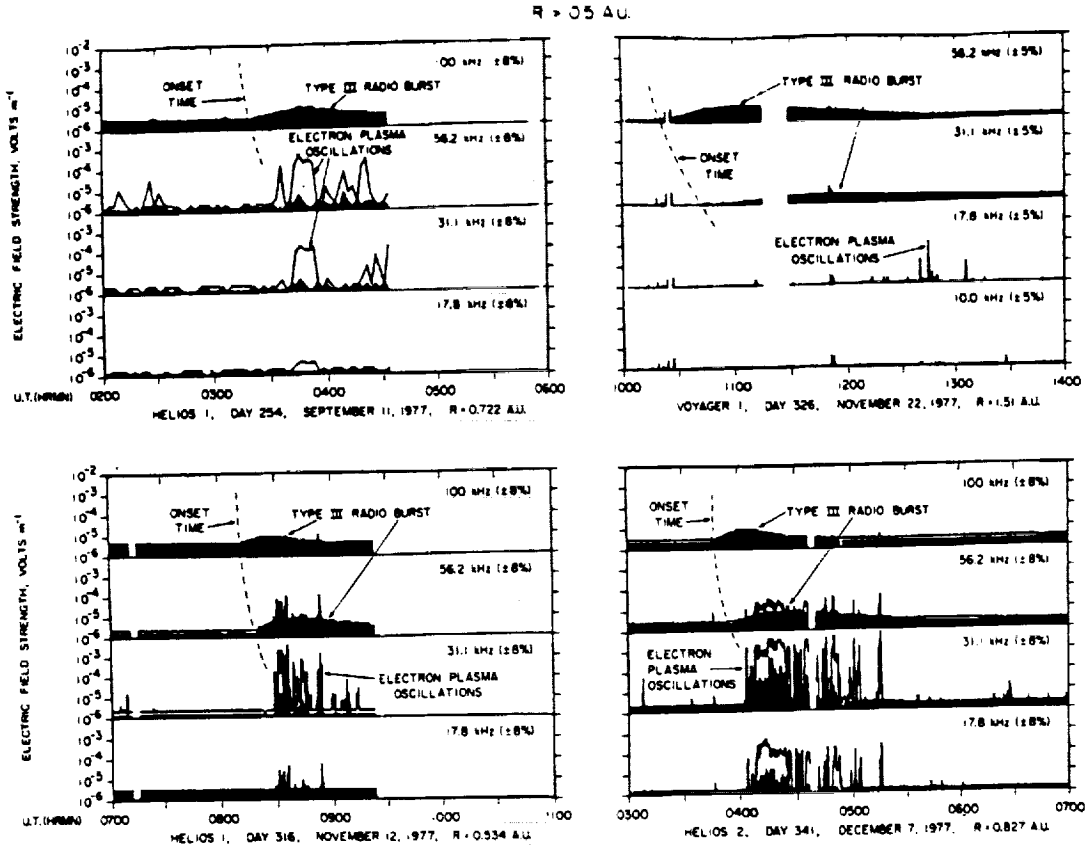

Fig. 1*b*

tional observing time inside of 0.5 AU is only about 25%. It is estimated that only about 1 year of total observing time is available inside of 0.5 AU, compared with 8 years of combined observing time outside of 0.5 AU. Since eight events have been detected in only 1 year at $R \leq 0.5$ AU, compared with ten events in 8 years at $R > 0.5$ AU, we estimate that the chance of detecting plasma oscillations in association with a type III radio burst is almost 10 times larger in the region inside of 0.5 AU than in the region beyond 0.5 AU.

As can be seen from Figure 1, most of the plasma oscillation events beyond 0.5 AU are quite weak, typically only a few hundred microvolts per meter. In many of these cases it is probably questionable whether these weak plasma oscillations could be responsible for the observed radio emission intensities, even though the close time coincidence indicates that they are produced by the same particles which are responsible for the type III radio emission. Probably the only events in Figure 1 which are strong enough to account for the observed type III radio emission intensities, according to current theories, are on days 316 and 341, 1977. As is evident in Figure 2, the plasma oscillations inside of 0.5 AU are generally much more intense, typically 1–10 mV m^{-1}. According to the estimates of *Gurnett and Frank* [1975], plasma oscillations in this intensity range are required to explain the observed type III radio emission intensities. For the intense events the onset of the plasma oscillations is usually very abrupt, as it is on days 92, 108, 112, 278, and 279, and consistently occurs about 10–30 min after the onset of the radio burst in the next higher frequency channel. Detailed comparisons show, however, that the onset time is usually a little too late to be consistent with generation of the type III radio emission at the second harmonic of the electron plasma frequency [*Fainberg and Stone*, 1974; *Kaiser*, 1975; *Gurnett et al.*, 1978]. If the radiation is generated at the second harmonic, as is widely believed, then the plasma oscillations should start when the frequency of the type III radio emission reaches the second harmonic, $2f_p^-$, of the local electron plasma frequency. As can be seen for the events on days 91, 92, 108, 112, and 341, the plasma oscillations start well after the frequency of the type III emission drops below $2f_p^-$. The disagreement in these cases may indicate that the radiation was being generated at the fundamental rather than the second harmonic, that plasma oscillations were present but on time scales too small (<50 ms) to be detected, or that the plasma oscillations were occurring in small regions or filaments which by chance were not encountered until well after the leading edge of the emission region had swept past the spacecraft. The events on day 341 in Figure 1 and day 108 in Figure 2 also show another interesting effect, which is a nearly constant peak electric field amplitude for time intervals of almost half an hour. These nearly constant electric field amplitudes are almost certainly the result of some nonlinear saturation mechanism which limits the maximum attainable electric field amplitude.

The radial variation of the maximum electric field amplitude with radial distance from the sun is shown in Figure 4. This illustration shows the maximum electric field amplitude for each of the 18 plasma oscillation events shown in Figures 1 and 2. A best fit power law through all of the points indicates that the electric field amplitude varies approximately as $(1/R)^{2.5}$. Although the limited number of events strongly restricts the accuracy with which the detailed radial dependence can be determined, the general trend toward decreasing field strength with increasing radial distance from the sun is unmistakable, especially when consideration is given to the much greater observing time near 1.0 AU compared with regions closer to the sun.

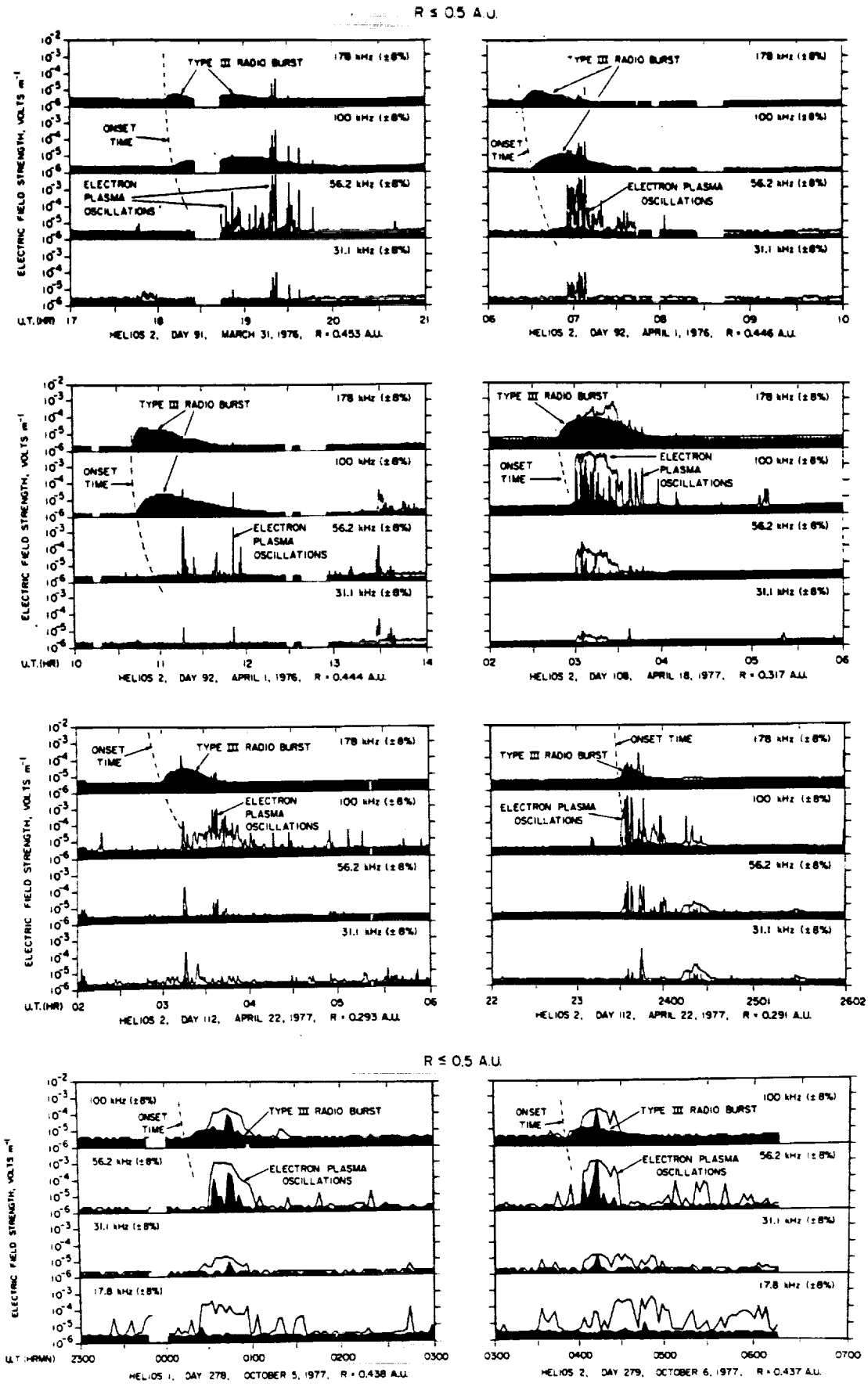

Fig. 2. All of the type III radio noise bursts and associated plasma oscillation events observed to date at heliocentric radial distances of less than 0.5 AU. The plasma oscillations closer to the sun, inside of 0.5 AU, are generally much more intense, typically 1–10 mV m^{-1}, and occur much more frequently than those beyond 0.5 AU. Note the large ratio of the maximum (solid line) to the average (solid black area) field strength, indicating that the plasma oscillations consist of many brief impulsive bursts.

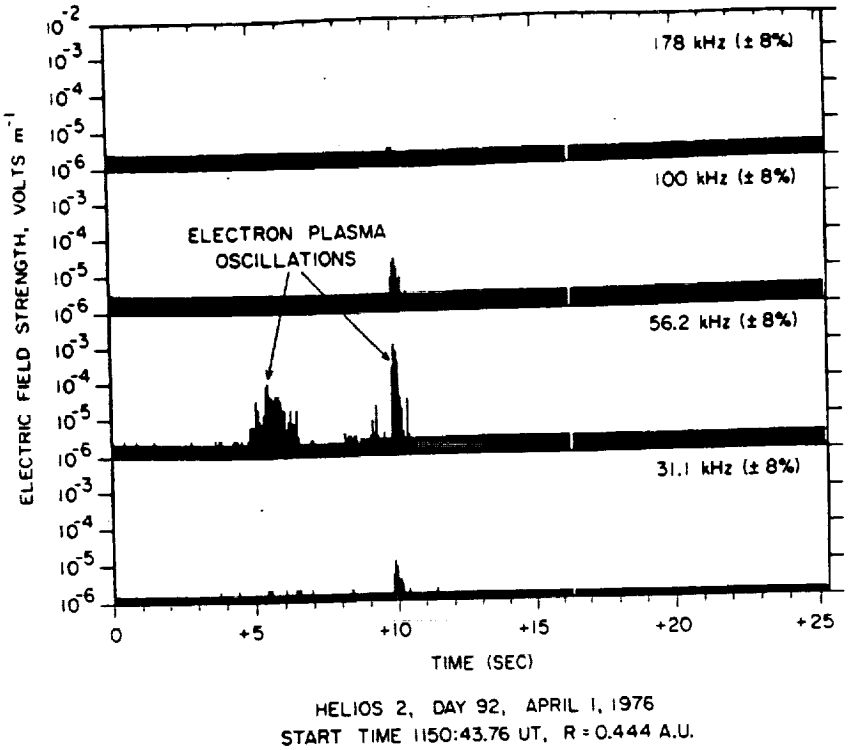

Fig. 3. A high-time resolution snapshot of the electron plasma oscillations associated with the event on day 92, 1976, in Figure 2. The plasma oscillations are seen to occur in short intense bursts lasting only a few tenths of a second. In some cases the temporal variations occur on time scales which approach the time resolution (50 ms) of the instrument.

3. Discussion

These measurements show that the electric field strength of electron plasma oscillations associated with type III radio bursts decreases rapidly with increasing radial distance from the sun. This radial variation provides a partial answer to the question of why electron plasma oscillations are so seldom observed in association with type III radio bursts at the orbit of the earth. Evidently, by the time the beam of electrons which produces the type III radio emission reaches the earth, the velocity distribution function has evolved to the point that the plasma oscillations are only weakly unstable or not unstable at all. Closer to the sun the distribution function is evidently more unstable, leading to more intense plasma oscillations. The observed radial variation of plasma oscillation intensities is also consistent with the frequency spectrums of type III radio bursts, which usually decrease in intensity with decreasing frequency, indicating a decreasing emissivity (hence plasma oscillation intensity) with increasing radial distance from the sun.

Qualitatively, the decreasing plasma oscillation intensity with increasing distance from the sun fits in reasonably well with what one would expect, since the temporal dispersion of the emitted electron beam tends to intensify the unstable part of the electron velocity distribution function in the region closer to the sun, causing larger electric field amplitudes. A quantitative understanding of the observed radial variation, however, will require a detailed understanding of the nonlinear effects which saturate or limit the growth of the plasma oscillations and of the wave-particle interactions which influence the evolution of the electron beam as it propagates outward from the sun. Saturation effects are usually characterized by the dimensionless ratio of the electric field to plasma energy density, $E^2/8\pi nkT$, which for a given distribution function reaches an approximately constant asymptotic value after the instability has grown into the nonlinear regime. Numerical simulations [*Armstrong and Montgomery*, 1967] for strongly unstable distributions typically show that after several hundred plasma periods the energy density ratio $E^2/8\pi nkT$ approaches a constant asymptotic value characteristic of the initial beam intensity. Since the plasma density increases with decreasing distance from the sun approximately as $n \propto (1/R)^2$ and the temperature T remains nearly constant, the electric field strength would be expected to vary as $E \propto (1/R)$ if the asymptotic energy density ratio remains constant, independent of the radial distance. On the basis of the results in Figure 4 it is seen that the electric field strength varies much more rapidly than $(1/R)$, which means that changes in the electron beam characteristics are significantly modifying the asymptotic value of the saturation energy density ratio between 0.3 and 1.0 AU. Typical values for the energy density ratio vary from about $E^2/8\pi nkT \simeq 10^{-6}$ at 0.3 AU to about 5×10^{-9} at 1.0 AU.

Because of the complex evolution and interaction of the electron beam with the background plasma, numerical simulations are clearly needed to understand these radial dependences. Calculations of the propagation of solar electron streams have been performed by *Magelssen and Smith* [1977], assuming that the plasma oscillation intensities are controlled by quasi-linear interactions [*Smith and Fung*, 1971]. Overall, the results of Magelssen and Smith predict the correct general behavior, with approximately the right plasma oscillation amplitudes. However, detailed comparisons show significant disagreements with observations. The observed radial variation in the electric field energy density (in Figure 4) decreases more rapidly than predicted by the computer simulation, and the observed rapid spikelike variations in the plasma oscillation intensities have no resemblance to the smooth intensity variations predicted by the quasi-linear model. Further simulations using more complex models for the nonlinear beam plasma interactions, such as those discussed by *Papadopoulos et al.*

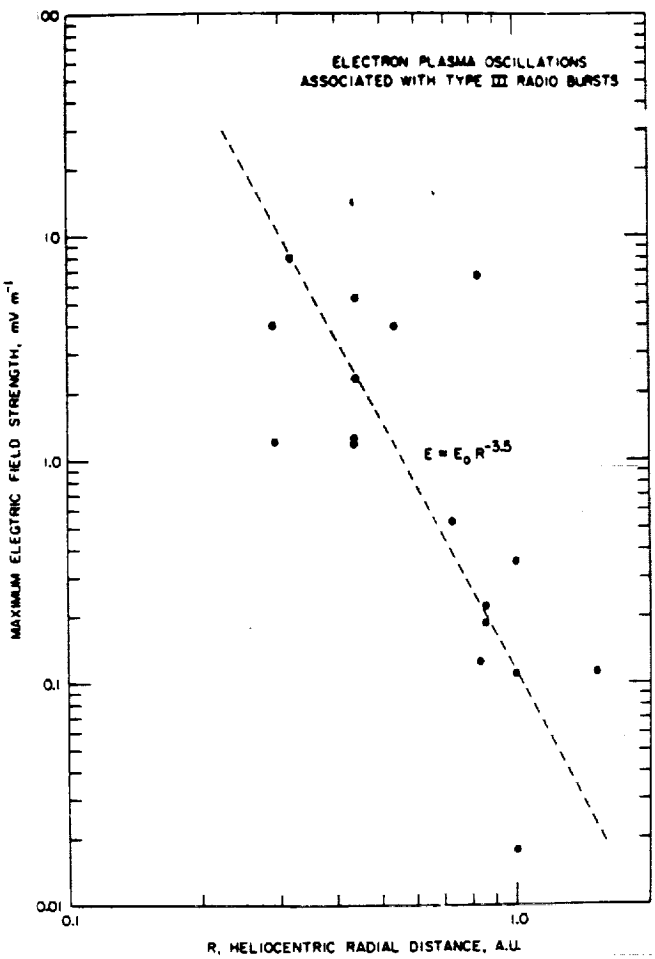

Fig. 4. A scatter plot of the maximum electric field strengths of the plasma oscillations in Figures 1 and 2 as a function of heliocentric radial distance. The electric field strength of the plasma oscillations decreases rapidly with increasing radial distance from the sun, varying approximately as $R^{-3.5}$.

[1974], *Bardwell and Goldman* [1976], and *Rowland and Papadopoulos* [1977], need to be performed to see if more complex models of the beam stabilization mechanism provide better agreement with the observations.

Acknowledgments. The research at the University of Iowa was supported by the National Aeronautics and Space Administration through grants NGL-16-001-002 and NGL-16-001-043 and through contract NAS5-11279 with Goddard Space Flight Center and contract 954013 with the Jet Propulsion Laboratory. The research at TRW was supported by the National Aeronautics and Space Administration through contract 954012 with the Jet Propulsion Laboratory.

The Editor thanks R. G. Stone and P. Kellogg for their assistance in evaluating this paper.

REFERENCES

Armstrong, T. P., and D. Montgomery, Asymptotic state of the two-stream instability, *J. Plasma Phys., 1*, 425, 1967.

Bardwell, S., and M. W. Goldman, Three-dimensional Langmuir wave instabilities in type III solar radio bursts, *Astrophys. J., 209*, 912, 1976.

Fainberg, J., and R. G. Stone, Satellite observations of type III solar radio bursts at low frequencies, *Space Sci. Rev., 16*, 145, 1974.

Ginzburg, V. L., and V. V. Zheleznyakov, On the possible mechanism of sporadic radio emission (radiation in an isotropic plasma), *Sov. Astron., AJ 2*, 653, 1958.

Gurnett, D. A., and R. R. Anderson, Electron plasma oscillations associated with type III radio bursts, *Science, 194*, 1159, 1976.

Gurnett, D. A., and R. R. Anderson, Plasma wave electric fields in the solar wind: Initial results from Helios 1, *J. Geophys. Res., 82*, 632, 1977.

Gurnett, D. A., and L. A. Frank, The relationship of electron plasma oscillations to type III radio emissions and low-energy electrons, *Solar Phys., 45*, 477, 1975.

Gurnett, D. A., M. M. Baumback, and H. Rosenbauer, Stereoscopic direction finding analysis of a type III solar radio burst: Evidence for emission at $2f_p^-$, *J. Geophys. Res., 83*, 616, 1978.

Kaiser, M. L., The solar elongation distribution of low frequency radio bursts, *Solar Phys., 45*, 181, 1975.

Kellogg, P. J., and R. P. Lin, Generation of solar type III bursts at the second harmonic (abstract), *Solar Phys., 447*, 1976.

Magelssen, G. R., and D. F. Smith, Nonrelativistic electron stream propagation in the solar atmosphere and type III radio bursts, *Solar Phys., 55*, 211, 1977.

Papadopoulos, K., M. L. Goldstein, and R. A. Smith, Stabilization of electron streams in type III solar radio bursts, *Astrophys. J., 190*, 175, 1974.

Rowland, H. L., and K. Papadopoulos, Simulations of nonlinearly stabilized beam-plasma interactions, *Phys. Rev. Lett., 39*, 1276, 1977.

Scarf, F. L., and D. A. Gurnett, A plasma wave investigation for the Voyager mission, *Space Sci. Rev., 21*, 289, 1977.

Smith, D. F., Type III radio bursts and their interpretation, *Space Sci. Rev., 16*, 91, 1974.

Smith, D. F., and P. C. Fung, A weak turbulence analysis of the two-stream instability, *J. Plasma Phys., 5*, 1, 1971.

Sturrock, P. A., Spectral characteristics of type III solar radio bursts, *Nature, 192*, 58, 1961.

Tidman, D. A., T. J. Birmingham, and H. M. Stainer, Line splitting of plasma radiation and solar radio outbursts, *Astrophys. J., 146*, 207, 1966.

(Received February 7, 1978;
revised April 17, 1978;
accepted April 17, 1978.)

Plasma Wave Turbulence Associated With an Interplanetary Shock

D. A. GURNETT

Department of Physics and Astronomy, The University of Iowa, Iowa City, Iowa 52242

F. M. NEUBAUER

Institut für Geophysik und Meteorologie der Technischen Universität Braunschweig, 33 Braunschweig, West Germany

R. SCHWENN

Max-Planck-Institut für Physik und Astrophysik, 8046 Garching, West Germany

In this paper we give a brief summary of the interplanetary shocks detected and analyzed to date from the Helios 1 and 2 spacecraft and present a detailed analysis of the plasma wave turbulence associated with one particular shock, on March 30, 1976. This event was selected because a very clearly defined burst of plasma wave turbulence occurs at the shock with otherwise quiet conditions in the solar wind upstream and downstream of the shock. The shock is an oblique shock and the upstream parameters are characterized by a low Mach number, a low beta, and an unusually large electron to ion temperature ratio. Three types of plasma waves are detected in association with this shock: (1) electron plasma oscillations, (2) electrostatic ion-acoustic or Buneman mode turbulence from about 1 to 30 kHz, and (3) whistler-mode magnetic noise. Because of the high velocity of the shock and the quiet conditions in the solar wind this event provides a particularly good determination of the scale size and characteristics of the precursor waves upstream of the shock and the electric and magnetic field turbulence in the wake behind the shock. The primary burst of electric and magnetic field noise at the shock occurs a few seconds after the jump in the magnetic field, with a broad maximum in the electric field intensities at about 3 kHz and a monotonically decreasing magnetic field spectrum below about 1 kHz. Many of the characteristics of this shock are found to be closely similar to, and are compared with, previous observations of plasma wave turbulence associated with the earth's bow shock.

1. INTRODUCTION

For many years the investigation of shocks in collisionless plasmas has received considerable attention in both laboratory and space plasmas. Upstream of the earth's magnetosphere a collisionless shock wave is known to form in the solar wind as it flows past the earth at supersonic velocities. Because this region can be readily studied by eccentric earth orbiting spacecraft substantial progress has been made in understanding and characterizing the earth's bow shock for a wide range of plasma parameters. The current state of knowledge of the earth's bow shock has recently been reviewed by *Greenstadt and Fredricks* [1978]. Within the shock transition region it has been established [*Fredricks et al.*, 1968; *Olson et al.*, 1969] that intense electric and magnetic field turbulence is generated by plasma instabilities. This plasma wave turbulence acts to heat the incoming plasma as it flows across the shock boundary and plays a role similar to collisions in an ordinary collision-dominated shock. Electric field measurements in the transition region [*Fredricks et al.*, 1968, 1970*a*, *b*] show that the electric field turbulence is closely correlated with magnetic field gradients, indicating the presence of a current-driven instability [*Wu and Fredricks*, 1972]. Detailed studies of the dependence of the turbulence amplitude on the upstream parameters have been presented by *Rodriguez and Gurnett* [1975, 1976].

Collisionless shocks similar to the earth's bow shock also occur in the interplanetary medium in response to changes induced in the solar wind flow by solar rotation and by transient events (flares) near the sun (see, for example, *Smith and Wolfe* [1976] and *Dryer et al.* [1976]). In comparison to the earth's bow shock near the subsolar point interplanetary shocks are usually weaker. Studies of these shocks can, therefore, provide information on shock characteristics for ranges of parameters which often are not observed in the earth's bow shock. Interplanetary shocks are also of interest because of their role in the acceleration of energetic charged particles in the interplanetary medium [*Sarris and Van Allen*, 1974]. Because of the infrequent occurrence of interplanetary shocks and the absence until recently of suitable instrumentation on interplanetary spacecraft the study of plasma wave turbulence associated with interplanetary shocks is in a relatively early stage of investigation. Electric field observations associated with an interplanetary shock have been reported by *Scarf et al.* [1974] and magnetic field observations have been reported by *Neubauer et al.* [1977]. For a review of these and other observations see *Scarf* [1978]. The purpose of this paper is to give a brief survey of the plasma wave turbulence observed in association with interplanetary shocks detected by the solar-orbiting Helios 1 and 2 spacecraft and to present a detailed analysis of one particular event, on March 30, 1976.

The Helios 1 and 2 spacecraft, which were launched on December 10, 1974, and January 15, 1976, are in eccentric solar orbits near the ecliptic plane with initial perihelion radial distances of 0.309 and 0.290 AU and aphelion radial distances of 0.985 and 0.983 AU, respectively. The plasma wave electric field measurements presented in this study are from the University of Iowa electric field experiment on Helios 1 and 2. This experiment uses a dipole antenna for electric field measurements and provides electric field intensities in 16 filter channels from 31.1 kHz to 178 kHz. A detailed description of this experiment is given by *Gurnett and Anderson* [1977]. The wave magnetic field measurements are from the Technical University of Braunschweig search-coil magnetometer experiment on Helios 1 and 2. This experiment is described by *Dehmel et al.* [1975] and *Neubauer et al.* [1977*a*, *b*]. Briefly the experiment

Paper number 8A0987.
0148-0227/79/008A-0987$01.00

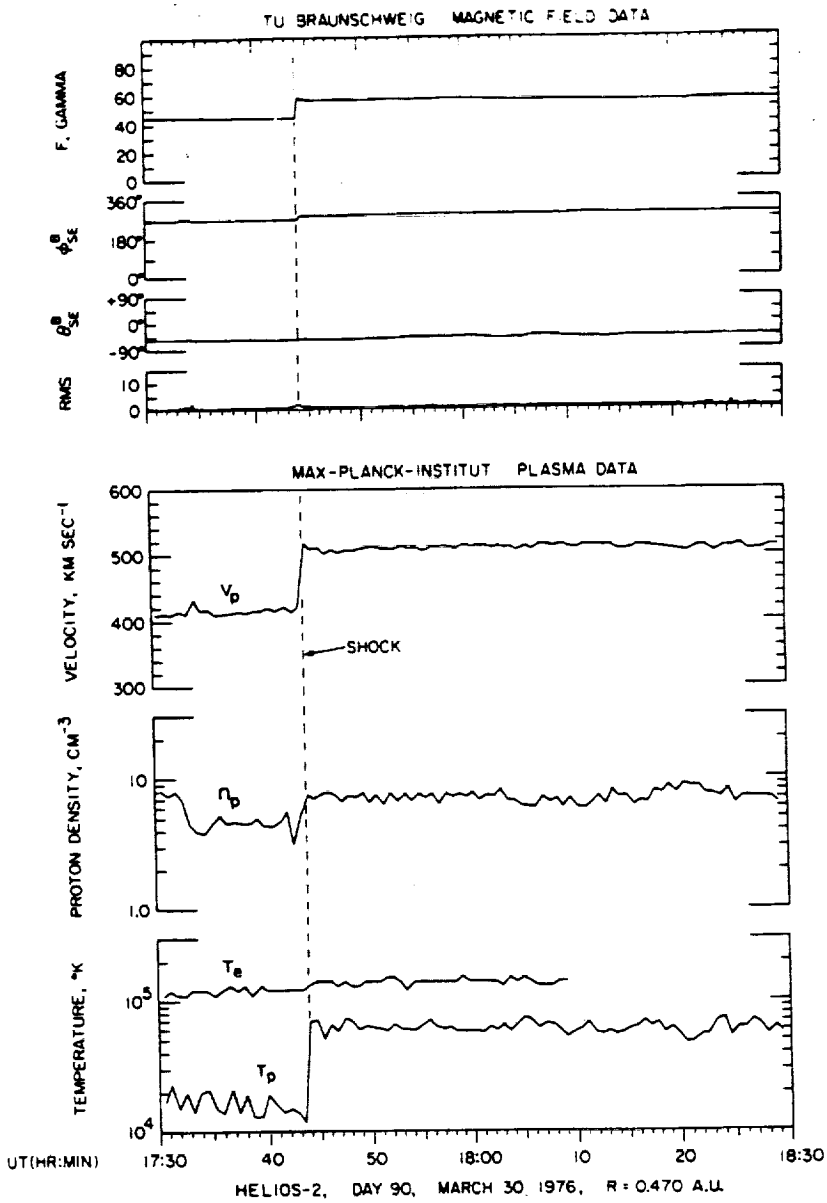

Fig. 1. The Helios 2 magnetic field and solar wind plasma data for the interplanetary shock on March 30, 1976. Note the relatively quiet conditions in the solar wind upstream and downstream of the shock.

consists of three orthogonal search-coil magnetic field sensors mounted on a boom at a distance of 4.6 m from the center of the spacecraft. Magnetic field spectral densities are determined in eight logarithmically spaced filter channels (frequency bands 4.7–10 Hz, 10–22 Hz, etc., up to 1–2.2 kHz) for each of two axes, one parallel to the spin axis and the other perpendicular to the spin axis. Both experiments provide peak as well as average spectral densities. The solar wind magnetic field measurements are from the TU Braunschweig flux-gate magnetometer described by *Musmann et al.* [1975] and *Gliem et al.* [1976]. This experiment provides measurements of three orthogonal components of the magnetic field with an accuracy of ±0.2 gamma. The solar wind plasma measurements are from the Max-Planck-Institut für Physik und Astrophysik plasma analyzer described by *Schwenn et al.* [1975]. This experiment provides a full 3-dimensional ion distribution function over the energy range from 155 eV to 15.3 keV every 40.5 seconds (for bit rates above 256 bps) and electron measurements scanning the ecliptic plane over the energy range from 0.5 eV to 1.66 keV.

2. Brief Survey of the Shocks Detected by Helios and the Event Selected for Analysis

Because of the low level of solar activity during the solar minimum period the total number of shocks available for analysis in the Helios data is quite small. For the data analyzed to date, during the primary mission of Helios 1 and 2, only 5 interplanetary shocks have been identified. All of these events have enhanced levels of magnetic turbulence at the shock boundary and in the downstream region behind the shock. The intensity of this turbulence usually decreases monotonically with increasing frequency and is detectable at frequencies up to several hundred Hz. A typical example of this magnetic turbulence is discussed by *Neubauer et al.* [1977*a*, *b*]. Although the intensity and spectrum of the magnetic field turbulence vary somewhat from event to event, the noise is always ob-

served in association with a shock at intensities substantially above the threshold of the search coil magnetometer.

In comparison to the magnetic turbulence, the electric field turbulence associated with interplanetary shocks is much more highly variable. In some cases the electric field amplitudes associated with an interplanetary shock are so small that the shock-related fields cannot be distinguished from other types of waves, such as ion-acoustic waves [*Gurnett and Frank*, 1978], which are commonly observed in the solar wind. In other cases, strong bursts of broad-band electrostatic noise, similar to the earth's bow shock, are observed in association with the shock.

Because of the limited number of events which are currently available for analysis we have not yet attempted to determine which parameters control the large variations in the plasma wave turbulence associated with interplanetary shocks. Instead, we have selected one particular event, on March 30, 1976, for analysis. This event was selected because it has a very clearly defined burst of plasma wave turbulence in both the electric and magnetic field data, and because the conditions in the solar wind upstream and downstream of the shock were relatively quiet and uncomplicated. Comparisons with other solar and geophysical observations [*Pinter*, 1977] indicate that this shock probably was associated with the type 1B solar flare at 1905 UT on March 28, 1976, and the subsequent geomagnetic SSC (indicative of an interplanetary shock) at 0255 UT on April 1, 1976. At the time the shock was detected by Helios 2 the spacecraft was near the ecliptic plane approximately 9.6° west of the earth-sun line at a radial distance of 0.470 AU from the sun.

TABLE 1. Plasma and Magnetic Field Parameters for the March 30, 1976, Shock

Upstream	Downstream
$\mathbf{B}_1 = (-0.2, -24.9, -35.6)\,\gamma$	$\mathbf{B}_2 = (10.2, -32.2, -44.5)\,\gamma$
$\mathbf{v}_1 = (-419.3, -7.9, 4.0)$ km/s ((−417.4, −0.7, −1.4) km/s)	$\mathbf{v}_2 = (-507.2, -7.8, -8.9)$ km/s
$n_{p1} = 6.8$ cm^{-3} (5.6 cm^{-3})	$n_{p2} = 8.8$ cm^{-3}
$n_{\alpha 1} = 1.6$ cm^{-3} (1.3 cm^{-3})	$n_{\alpha 2} = 2.1$ cm^{-3}
$T_{p1} = 15{,}000$ K	$T_{p2} = 66{,}000$ K
$T_{e1} = 105{,}000$ K	$T_{e2} = 125{,}000$ K
$T_{\alpha 1}/T_{p1} \approx 1$, $T_{e1}/T_{p1} = 7.0$	$T_{\alpha 2}/T_{p2} \approx 1$, $T_{e2}/T_{p2} \approx 1.9$
Derived Quantities	
$\beta_1 = \sum_i n_{i1} K T_{i1}/B_1^2/8\pi = 0.016$	$\beta_2 = 0.023$
$\alpha_1 = \angle \mathbf{B}_1, \mathbf{v}_1 = 89.6°$	$\alpha_2 = 99.2°$
$\theta_1 = \angle \mathbf{n}, \mathbf{B}_1 = 47.5°$	$\theta_2 = 58.4°$
$V_{A1} = \lvert\mathbf{B}_1\rvert/(4\pi\rho_1)^{1/2} = 259$ km/s	$V_{A2} = 294$ km/s
Mach Numbers	
$M_{A1} = \lvert\mathbf{v}_1\rvert/V_{A1} = 1.62$	$M_{A2} = 1.73$
$A_{n,1} = v_{n,1}/B_n/(4\pi\rho_1)^{1/2} = 1.80$	$A_{n,2} = 1.60$
$M_{f,1} = v_{n,1}/c_{f,1} = 1.20$	$M_{f,2} = v_{n,2}/c_{f,2} = 0.80$
Characteristic Frequencies	
$f_{cp1} = 0.67$ Hz	$f_{cp2} = 0.86$ Hz
$f_{ce1} = 1.23$ kHz	$f_{ce2} = 1.58$ kHz
$f_{pe1} = 26$ kHz	$f_{pe2} = 29.6$ kHz
$f_{pp1} = 611$ Hz	$f_{pp2} = 691$ Hz
Characteristic Length Scales	
$c/\omega_{pe1} = 1.8$ km	$c/\omega_{pe2} = 1.6$ km
$c/\omega_{pp1} = 77$ km	$c/\omega_{pp2} = 69$ km
$\lambda_{D1} = 5.52$ m	$\lambda_{D2} = 4.75$ m
Propagation Parameters	
shock speed: 627 km/s	
shock normal: $\mathbf{n} = -(0.738, 0.334, 0.586)$	

3. Macroscopic Analysis of the March 30, 1976, Shock

The magnetic field and solar wind plasma data from Helios 2 for the period of interest, from 1730 to 1830 UT, on March 30, 1976, are illustrated in Figure 1. The top four panels show the magnetic field magnitude, direction and RMS fluctuations from the flux-gate magnetometer, and the bottom three panels show the proton velocity, proton density, and electron and proton temperatures from the solar wind plasma experiment. The polar and azimuthal angles of the magnetic field direction, $\theta_{SE}{}^B$ and $\varphi_{SE}{}^B$, are given in the usual solar ecliptic coordinates. For the time interval under consideration the sampling rate for the magnetic field measurements was one vector per second. The magnetic field data shown in Figure 1 are 8 second averages. The time resolution of the plasma measurements in Figure 1 is 40.5 seconds, which is the highest resolution available.

The high time resolution magnetic fields data show that the primary jump in the magnetic field magnitude occurred in less than one second, at 1744:00.5 UT ±0.5 s. The plasma data show that the jump in the solar wind velocity occurred between 1743:52 and 1744:11 UT, which is consistent with the magnetic field measurements. On the time scale shown in Figure 1 the solar wind on both sides of the shock is extremely quiet, making this event well suited for a detailed analysis of the upstream and downstream plasma parameters. Averaging the magnetic field components over 240 seconds and the plasma parameters over seven spectrums (283.5 seconds) gives the quantities shown in Table 1. Parameters upstream and downstream of the shock are denoted by subscripts 1 and 2, respectively. Because the proton temperature in front of the shock is unusually low the plasma parameters are subject to substantial errors. This is particularly true for the proton density, n_{p1}, and the proton temperature, T_{p1}. This problem does not exist for the downstream plasma. In order to obtain optimum plasma parameters both the magnetic field vectors and the measured downstream plasma parameters have been used to compute the upstream parameters and at the same time to check the consistency of the shock parameters (speed and normal) with the MHD-Rankine-Hugoniot relations [*Jeffrey and Taniuti*, 1964]. Where a computed value is considered to be more accurate than the observed one, it is used in Table 1 with the observational value given in brackets. All upstream and downstream quantities not included in brackets are measured quantities.

Since the magnetic field changes direction quite significantly at the shock the coplanarity theorem can be used to obtain the shock normal, $\mathbf{n} = -(0.738, 0.334, 0.586)$, in solar-ecliptic ($x$, y, z) coordinates. The shock is therefore coming from the NE-quadrant of the sun as seen from the spacecraft. The angles between magnetic field and the shock normal are $\theta_1 = 47.5°$ and $\theta_2 = 58.4°$, respectively, indicating an oblique shock. Because of the unusually low density and large magnetic field strength at 0.47 AU the plasma beta is extremely small, $\beta_1 = 0.016$ and $\beta_2 = 0.023$, even behind the shock. Using β_2, θ_1 and θ_2, the expected density ratio can be computed across the shock, leading to a theoretical value of $n_{p1} = 6.8$ cm^{-3}. The experimental value $n_{p1} = 5.6$ cm^{-3} is shown in brackets and is well within the expected experimental error (~±20%) for the

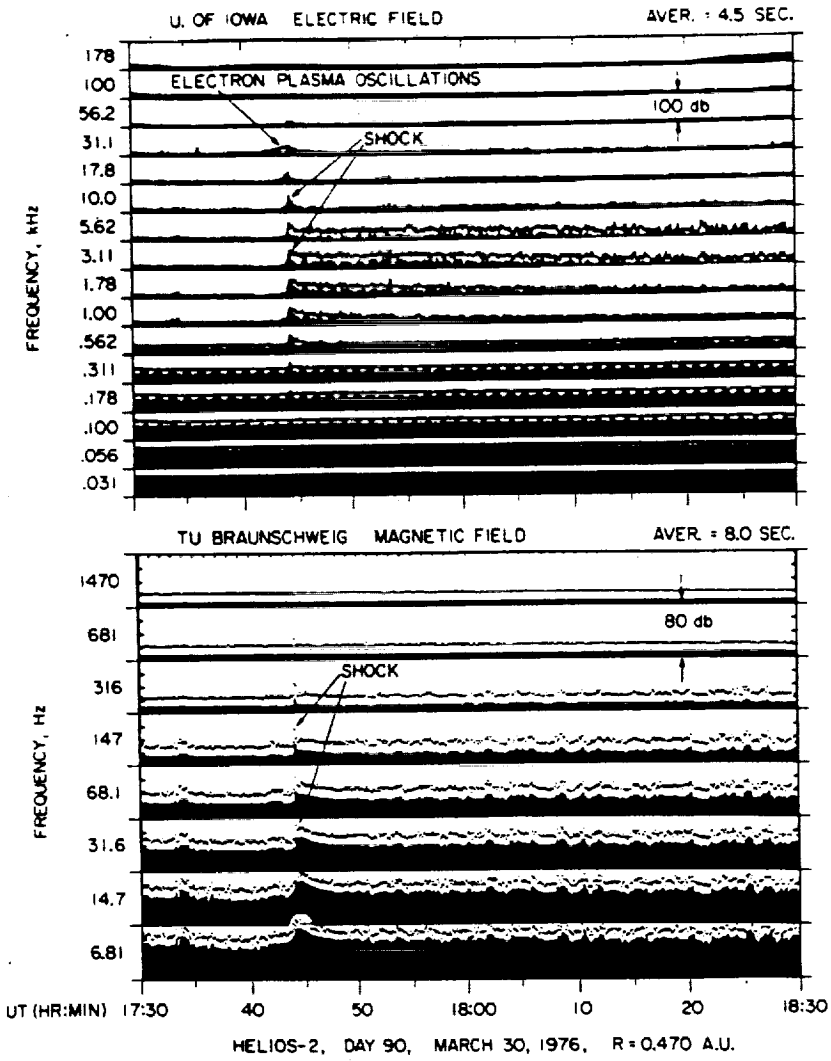

Fig. 2. The electric and magnetic field intensities associated with the shock on March 30, 1976, on a time scale corresponding to Figure 1. The shock occurred at 1744:00.5 UT ±0.5 s. Note the narrow band electron plasma oscillations upstream of the shock, the abrupt burst of noise at the shock, and the broad band of electric and magnetic field turbulence in the wake region downstream of the shock.

density determination. The shock is unusual because of the extremely large α-particle to proton ratio, $n_\alpha/n_i = 0.24$, which is the same on both sides of the shock, and the large electron to ion temperature ratio, $T_{e1}/T_{p1} = 7$, in the upstream region.

The Alfvén Mach numbers A_n computed from the normal components V_n of the velocity vectors in the shock frame and the magnetic field are $A_{n,1} = 1.8$ and $A_{n,2} = 1.6$ which are greater than one as required for a fast MHD-shock. The fast Mach numbers M_f based on the fast magnetoacoustic speed $C_f(\theta)$ turn out to be $M_{f,1} = 1.2 > 1$ and $M_{f,2} = 0.8$ respectively. The Alfvén Mach numbers M_{A1} and M_{A2}, with $M_A = |\mathbf{V}|/V_A$ where V_A is the Alfvén speed, are also given for later use. Using these parameters the Rankine-Hugoniot relations also yield an independent determination of the upstream velocity vector $\mathbf{V}_1 = (-419.3, -7.9, 4.0)$ km/s, which is in very good agreement with the observationally determined quantity in brackets. The propagation speed of the shock in the direction of the normal is 627 km/s.

4. Plasma Wave Turbulence Associated With the March 30, 1976, Shock

The plasma wave electric and magnetic field intensities associated with the March 30, 1976, shock are shown in Figure 2, on a time scale corresponding to the magnetic field and plasma data in Figure 1. The electric field intensities are given in 16 frequency channels from 31.1 Hz to 178 kHz and the z-axis magnetic field intensities are given in 8 frequency channels from 6.81 Hz to 1.47 kHz. The intensity scale is logarithmic with a range of 100 dB, from approximately 1 μV/m to 0.1 V/m, for the electric field measurements and a range of 80 dB, from 10^{-5} to 10^{-1} gamma/Hz$^{1/2}$, for the magnetic field measurements. The solid lines for the electric field measurements and the dots for the magnetic field measurements show the peak field intensity over each measurement interval and the vertical bars (solid black areas) show the average field intensities. For the period of interest the sampling rate is one complete spectrum of peak and average field intensities every 4.5 seconds. The electric field intensities in Figure 1 are plotted on 4.5 second intervals and the magnetic field intensities are plotted on 8 second intervals, after appropriate averaging of the individual data points. The rapid increase of the electric field background at low frequencies is caused by electrical interference from the spacecraft solar array [see *Gurnett and Anderson*, 1977]. The enhanced background noise level in the low frequency magnetic field channels ahead of the shock is caused by low level magnetic field fluctuations which are essen-

tially always present in the solar wind [see *Neubauer et al.*, 1977*b*].

Because interplanetary shocks can provide unique information on the large scale structure of a shock, with less uncertainty concerning the motion of the shock compared to studies of the earth's bow shock, we first concentrate on describing the large scale features of the plasma wave turbulence upstream and downstream of the March 30, 1976, shock. Upstream of the shock electrostatic electron plasma oscillations at the local electron plasma frequency (f_{pe} = 26 kHz) are clearly evident in Figure 2, starting about 5 minutes before the shock and increasing exponentially in intensity as the shock approaches. These upstream plasma oscillations are qualitatively similar to the electron plasma oscillations commonly found upstream of the earth's bow shock in association with suprathermal electrons streaming into the solar wind from the shock [*Scarf et al.*, 1977]. Using the shock velocity of 627 km/s from Table 1 it is estimated that the *e*-folding distance of the electron plasma oscillations upstream of this shock is about 1.9 × 10^5 km.

Electron plasma oscillations are also evident with somewhat reduced intensities in the downstream region behind the shock. The presence of plasma oscillations in the region behind the shock differs from the usual situation in the earth's bow shock, for which electron plasma oscillations are seldom detected downstream of the shock [*Rodriguez and Gurnett*, 1975].

In the region behind the shock both the electric and magnetic field data in Figure 2 show the occurrence of a long extended region of plasma wave turbulence. For the electric field this wake turbulence is mainly concentrated in the frequency range from 1 to 10 kHz, with maximum intensity at about 3 kHz. For the magnetic field the turbulence is mainly at frequencies below about 500 Hz, somewhat below the electron gyrofrequency, increasing rapidly in intensity with decreasing frequency. After the initial large burst at the shock both the electric and magnetic field intensities are seen to have a remarkably linear decrease in intensity with increasing time. For the semilogarithmic scale used this variation corresponds to a simple exponential decay, $e^{-x/L}$, where x is the distance nor-

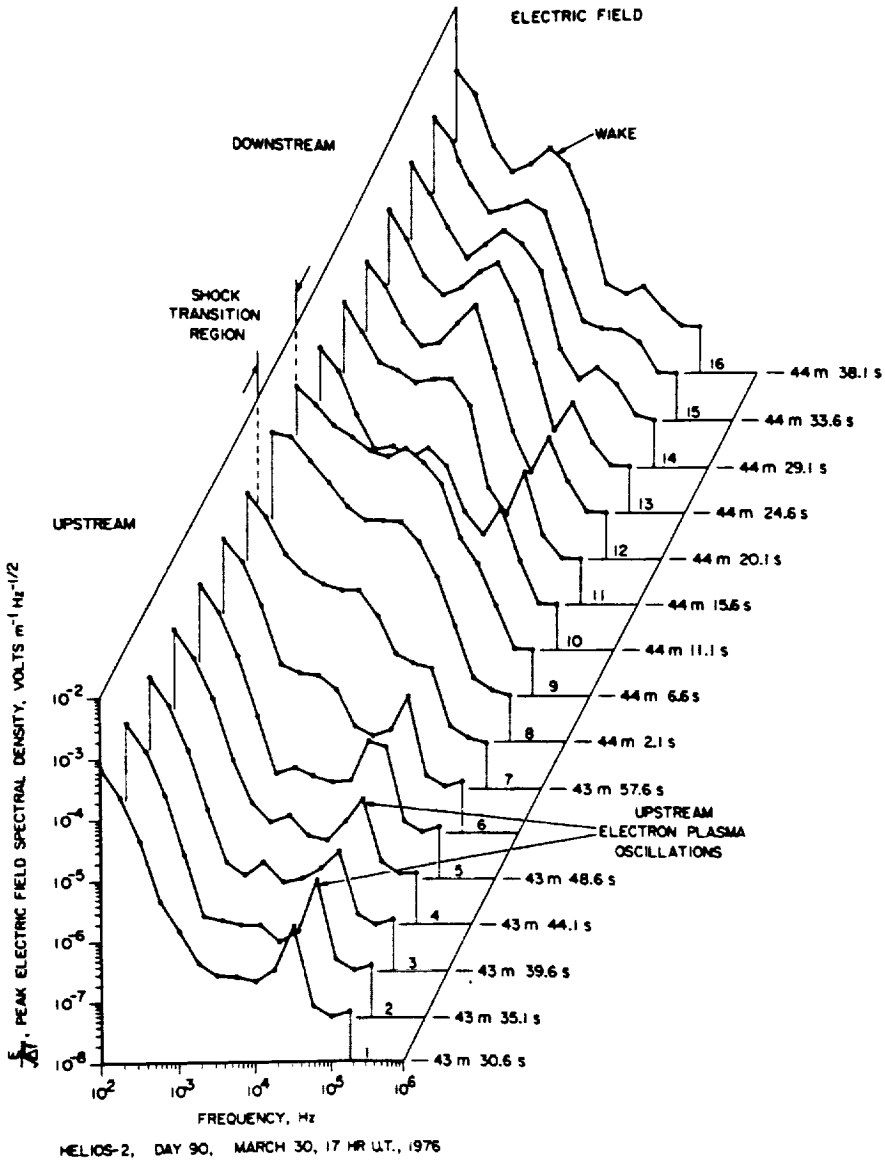

Fig. 3. A sequence of electric field spectrums through the shock transition with the highest time resolution available. Each spectrum gives the peak field intensity over the 4.5 s interval since the preceding spectrum. The jump in the magnetic field strength at the shock occurs at 44 min 0.5 s (see Figure 5).

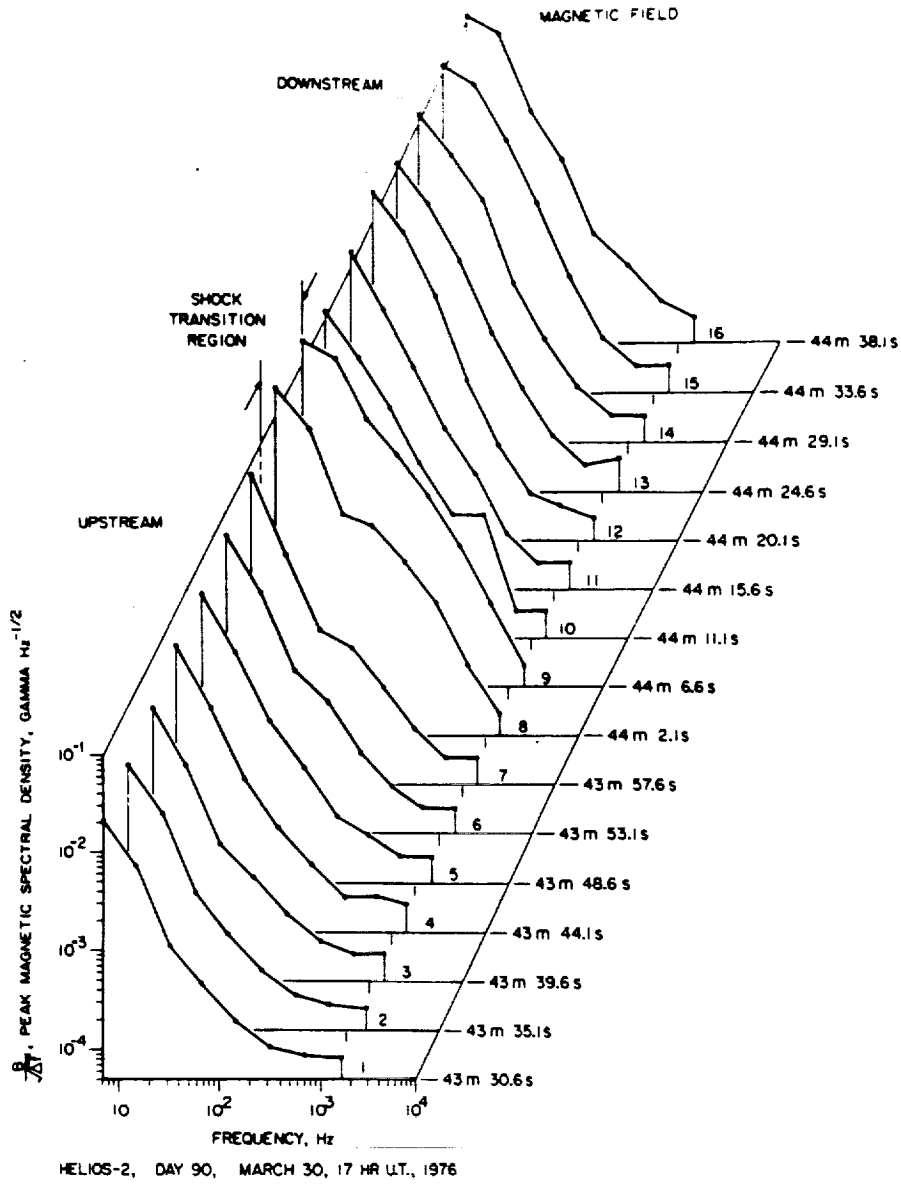

Fig. 4. A sequence of magnetic field spectrum through the shock transition on a time scale corresponding to Figure 3. The intensities are again peak values, however the times correspond to the center of each 4.5 s peak sampling interval.

mal to the shock and L is a characteristic e-folding length. For the magnetic field the e-folding length increases slightly with increasing frequency. Using the shock speed and shock normal direction from Table 1 the e-folding lengths for the magnetic field turbulence are found to vary from about $L \simeq 1.3 \times 10^5$ km at 6.81 Hz to $L \simeq 2.5 \times 10^6$ km at 147 Hz. The e-folding lengths for the electric field turbulence are significantly longer than for the magnetic field turbulence and have a distinct maximum at a frequency of about 3 to 5 kHz. The e-folding lengths for the electric field turbulence at 3.11, 5.62 and 10.0 kHz are about 3.8×10^6 km, 1.9×10^6 km, and 1.6×10^4 km, respectively.

Since the waves constituting the downstream turbulence are evidently being reabsorbed by the plasma, it is of interest to consider whether these waves provide a significant energy input into the plasma. At 1745:50 UT, shortly after the shock crossing, the normalized electric (>178 Hz) and magnetic (>4.7 Hz) field energy density ratios are approximately $E^2/(8\pi nkT) \simeq 7.7 \times 10^{-9}$ and $B^2/(8\pi nkT) \simeq 9.2 \times 10^{-6}$. These ratios show that the wave absorption provides a negligible energy input to the total plasma energy, although the waves may nonetheless play an important role in thermalizing the plasma.

Having discussed the regions upstream and downstream of the shock we now consider the plasma wave turbulence in the vicinity of the transition region. Figure 2 shows that the peak electric and magnetic field intensities near the shock are much larger than the average intensities. The large peak to average field strength ratios indicate that the turbulence in the transition region is very impulsive, consisting of one or more brief bursts with durations short compared to the sampling interval (4.5 seconds). The spectrum variations are illustrated in greater detail in Figures 3 and 4, which show a sequence of contiguous electric and magnetic field spectrums through the transition region. A corresponding plot of the magnetic field strength for the same interval is shown in Figure 5. The spectrums in Figures 3 and 4 are numbered, with the sampling times for the spectrums indicated at the top of Figure 5. The spectrum intensities are the maximum value of the square root of the power spectrum density, $(E^2/\Delta f)^{1/2}$ and $(B^2/\Delta f)^{1/2}$, for

each 4.5 second sampling interval. Because of differences in the internal timing of the experiments, the time for the electric field spectrums correspond to the end of each sampling interval, whereas the times for the magnetic field spectrums correspond to the midpoints of each sampling interval. The electric field spectrums in Figure 3 clearly show the upstream electron plasma oscillations, the intense burst of broadband electrostatic noise in the transition region and the relaxation to a nearly steady level of noise from 1 to 10 kHz in the downstream region. A few weak bursts of electron plasma oscillations are also evident in the downstream region, gradually merging into the broadband 1 to 10 kHz noise. The magnetic field spectrums in Figure 4 are less complex and show a relatively featureless monotonic frequency variation, decreasing in intensity with increasing frequency. Upstream of the shock low frequency precursor waves associated with the shock are present in the low frequency channels, increasing gradually in intensity as the shock approaches. These precursor waves are also evident at even lower frequencies in Figure 5.

In the shock transtition region the magnetic field intensities abruptly increase by a substantial factor at all frequencies up to 1 kHz, and then shift down to a relatively steady level in the downstream region. Although the primary jump in the magnetic field at the shock occurs in less than 1 second, both the electric and magnetic field data show very large turbulence levels for two successive 4.5 second intervals (spectrums 8 and 9) following the jump. Thus, the intense plasma wave turbulence associated with the shock occurs behind the magnetic field jump and extends over a region substantially thicker than the current sheet associated with the ramp in the magnetic field. This region of greatly enhanced turbulence is referred to as the 'shock transition region' in Figures 3, 4, and 5. Detailed analyses show that the most intense electric and magnetic field turbulence occurs during spectrum interval number 9, which starts 1.1 seconds after the magnetic field jump for the electric field measurements and 3.4 seconds after the jump for the magnetic field measurements. The electric and magnetic field spectrums for this interval are shown in greater detail in Figures 6 and 7, along with selected spectrums from the precursor and wake regions. The peak broadband rms electric field strengths for the shock spectrum in Figure 6, integrated from 311 Hz to 100 kHz, is 2.12 mV m. The primary contribution to the broadband field strength occurs in the frequency range from about 2 to 5 kHz. The average magnetic field intensity for the shock spectrum in Figure 7 fits a power law, $B/(\Delta f)^{1/2} = 0.4 f^{-1.3}$ gamma/$Hz^{1/2}$, to a good approximation over the frequency range, 4.7 Hz $\lesssim f \lesssim$ 50 Hz. At high frequencies the slope of the spectrum increases, with the power law index varying from about 1.3 at 50 Hz to about 2.5 at 500 Hz.

Further information on the nature of the magnetic field jump at the shock can be obtained from an analysis of the search-coil magnetic field data. Because of the spacecraft rotation the Z component of the magnetic field is best suited for this purpose. According to Table 1 the absolute change in the Z-component of the magnetic field is $\Delta B_z = 8.9$ gammas. As is shown in more detail by *Neubauer et al.* [1977*a*] the contribution from the frequency range 4.7 Hz to 2.2 kHz to the rms value of $\dot{B}_z = dB_z/dt$, i.e., $(\dot{B}_z^2)^{1/2}$, can be obtained from the average magnetic field spectrum. In this case $(\dot{B}_z^2)^{1/2}$ for the 4.5 second analysis interval which includes the shock is 10.9 gamma/s over the frequency range 4.7 Hz to 1.0 kHz. To obtain $(\dot{B}_z^2)^{1/2}$ over the frequency range 0 to 1.0 kHz the contribution from the 4 Hz bandwidth of the flux-gate magnetometer has been added to the search-coil data to give $(\dot{B}_z^2)^{1/2}$ = 16.0 gamma/s. Considering the shock to be a ramp of duration Δt, we obtain $\Delta t = \Delta B_z/(4.5 \text{ s } (\dot{B}_z^2)) = 0.07$ s, using equation 4 from *Neubauer et al.* [1977*a*]. This time corresponds to a length scale of 44 km. In other words, if a ramp leading to $\Delta B_z = 8.9$ gammas occurred in less than 44 km the frequency integrated power spectral density of B_z would give the observed value. Of course, for the real case the contribution from wave fields must be added to the magnetic field spectrum produced by the ramp. The shock thickness must then be greater than 44 km. Theoretically, it is expected that the shock should have a thickness of several $c/\omega_{pp} = V_A/\omega_{cp}$, where V_A is the Alfvén speed and ω_{pp} and ω_{cp} are the proton plasma and proton cyclotron frequencies, respectively [*Galeev*, 1976]. From Table 1 the characteristic length c/ω_{pp} for this shock is estimated to be about 70 km, which is in reasonably good agreement with the shock thickness, $\gtrsim$44 km, estimated from the magnetic field data.

Although the time resolution is not adequate to determine

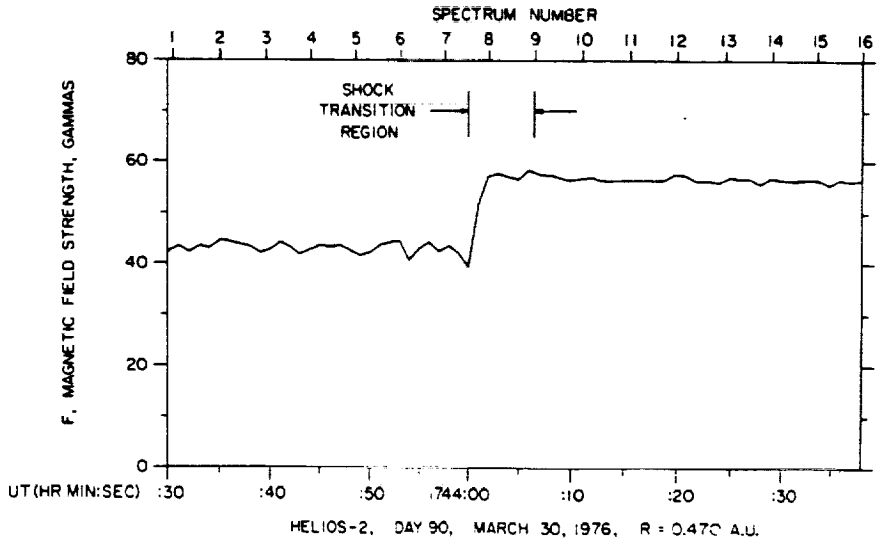

Fig. 5. The detailed magnetic field variations for the same interval as Figures 3 and 4, with the times for the corresponding spectrum numbers shown at the top. The most intense electric and magnetic field turbulence occurs in the region labeled shock transition region, a few seconds after the jump in the magnetic field.

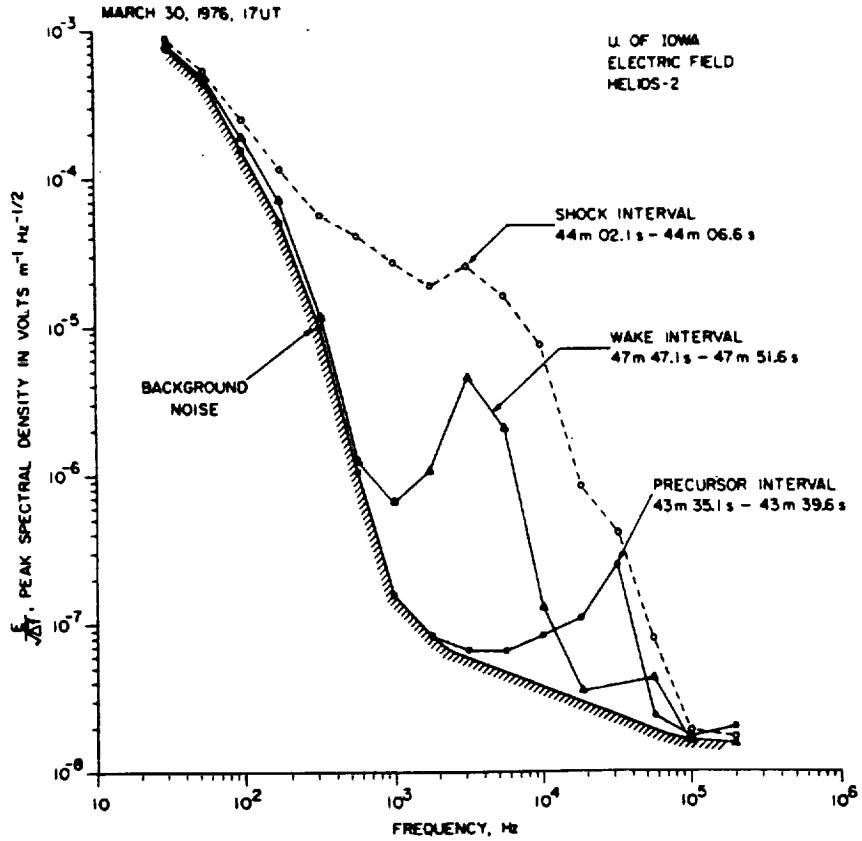

Fig. 6. Selected peak electric field spectrums in the precursor region upstream of the shock, in the transition region, and in the wake downstream of the shock. The shock spectrum (number 9 in Figure 3) corresponds to the time of maximum broadband field strength.

the polarization of the plasma wave turbulence in the transition region, some information can be obtained on the polarization of the electric fields in the wake. Figure 8 shows the angular distribution of the electric field intensities in the downstream region at 3.11 kHz, near the peak in the spectrum of the broadband electric field turbulence. This angular distribution was obtained by sorting the electric field intensities into 16 equally spaced angular sectors, based on the antenna orientation angle $\varphi_{SE}{}^{A}$ in solar ecliptic coordinates, and computing the frequency of occurrence of field intensities above fixed threshold levels. Figure 8 gives the angular variation of the electric field intensity at a constant frequency of occurrence of 20%. Since the electric field noise is very impulsive a long accumulation interval, from 1745 to 1759 UT, was necessary to reduce the statistical fluctuations to an acceptable level. The angular distribution in Figure 8 clearly shows a pronounced spin modulation, with maximum intensities at about $\varphi_{SE}{}^{A} \simeq -75°$ and $+105°$ and sharp nulls at $\varphi_{SE}{}^{A} \simeq -165°$ and $+15°$. For comparison the average direction of the magnetic field, $+\mathbf{B}$ and $-\mathbf{B}$, projected onto the ecliptic plane, $\varphi_{SE}{}^{B} \simeq -80°$ and $+100°$, are shown in Figure 8. The electric field intensities clearly have a symmetric distribution with respect to the solar wind magnetic field direction, with the maximum intensity when the antenna axis is parallel to the projected magnetic field and sharp nulls perpendicular to the magnetic field. Although the spin modulation only provides information on the electric field direction projected onto the spin plane, the sharp nulls, by about a factor of 10, together with the expected azimuthal symmetry of the electric field distribution around the magnetic field direction, provides strong evidence that the electric field of these waves is very closely aligned along the direction of the solar wind magnetic field, probably to within less than 5°. Similar results are obtained at 1.78 and 5.62 kHz.

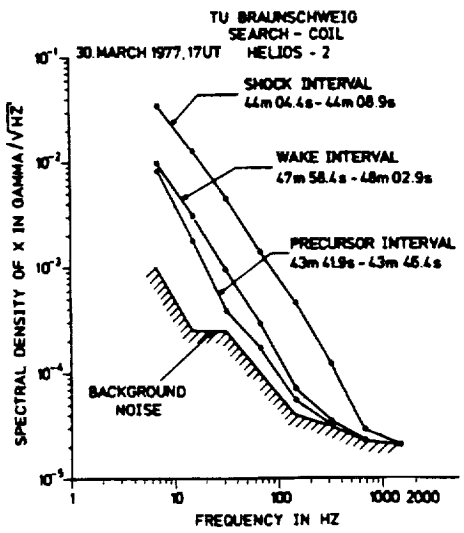

Fig. 7. Selected average magnetic field spectrums in the precursor region upstream of the shock, in the transition region, and in the wake downstream of the shock. The shock spectrum (number 9 in Figure 4) corresponds to the time of maximum broadband field strength.

5. Summary and Discussion

Because of the low level of solar activity during the solar minimum, interplanetary shocks have been relatively rare in the Helios data. Up to the present time only 5 events have been identified and analyzed. These events show a large variability

in the intensity and characteristics of the plasma wave turbulence associated with the shock, particularly for the electric fields. In some cases only very weak electric field enhancements, $\lesssim 10$ μV m, are present in association with the shock, whereas in other cases very intense bursts, $\gtrsim 1$ mV/m of electric field turbulence occurs at the shock and in the regions upstream and downstream from the shock. To illustrate the types of plasma waves which can occur in association with an interplanetary shock one particular event, on March 30, 1976, was selected for analysis. This event was selected because it displayed a very substantial and well-defined burst of electric and magnetic field noise at the shock, with usually quiet conditions in the solar wind upstream and downstream of the shock. The shock is an oblique shock ($\theta_{Bn,1} = 47.5°$) and is characterized by a low Mach number ($A_{n,1} = 1.80$, $M_{f,1} = 1.2$), a low beta ($\beta_1 = 0.016$) and an unusually large electron to ion temperature ratio ($T_{e1}/T_{p1} = 7.0$) upstream of the shock.

Three distinctly different types of plasma waves can be identified in association with this shock, (1) narrow-band electron plasma oscillations, (2) a broad band of electrostatic noise from about 1 to 30 kHz, and (3) a monotonic spectrum of low frequency magnetic noise extending up to frequencies of about 1 kHz. The observation of electron plasma oscillations in association with an interplanetary shock is apparently new and unique, since none of the other shocks detected by Helios have electron plasma oscillations and no events of this type have been previously reported. These observations of electron plasma oscillations associated with an interplanetary shock are possibly of importance to the understanding of type II and type IV solar radio bursts, since for many years it has been postulated that these radio emissions are generated by electron plasma oscillations produced by shock waves in the solar corona [*Kundu*, 1965]. In fact, the solar flare responsible for the shock analyzed is accompanied by a complex type II radio burst at frequencies from about 25 to 200 MHz, starting at 1921 UT on March 28, 1976 [*Maxwell*, 1977]. Although Helios is too far from the sun to directly detect the plasma oscillations associated with these high frequency radio emissions, the observation of electron plasma oscillations at 0.47 AU strongly suggests that similar plasma oscillations, probably with even greater intensities, are present closer to the sun. No locally generated radio emissions were detected from the plasma oscillations observed by Helios, evidently because of their low intensities, which are only about 35 μV/m.

Electron plasma oscillations, similar to the March 30, 1976, event are also commonly observed upstream of the earth's magnetosphere [*Scarf et al.*, 1971], in association with suprathermal, 100 eV to 10 keV, electrons streaming into the solar wind from the shock. It is presumed that the plasma oscillations detected by Helios are generated by essentially the same mechanism. Although it is known that the electron beams which generate plasma oscillations upstream of the earth's bow shock can propagate at least several earth radii, no definite determination has been made of the scale length over which these waves are generated. The Helios observations clearly show that the plasma oscillation intensity increases

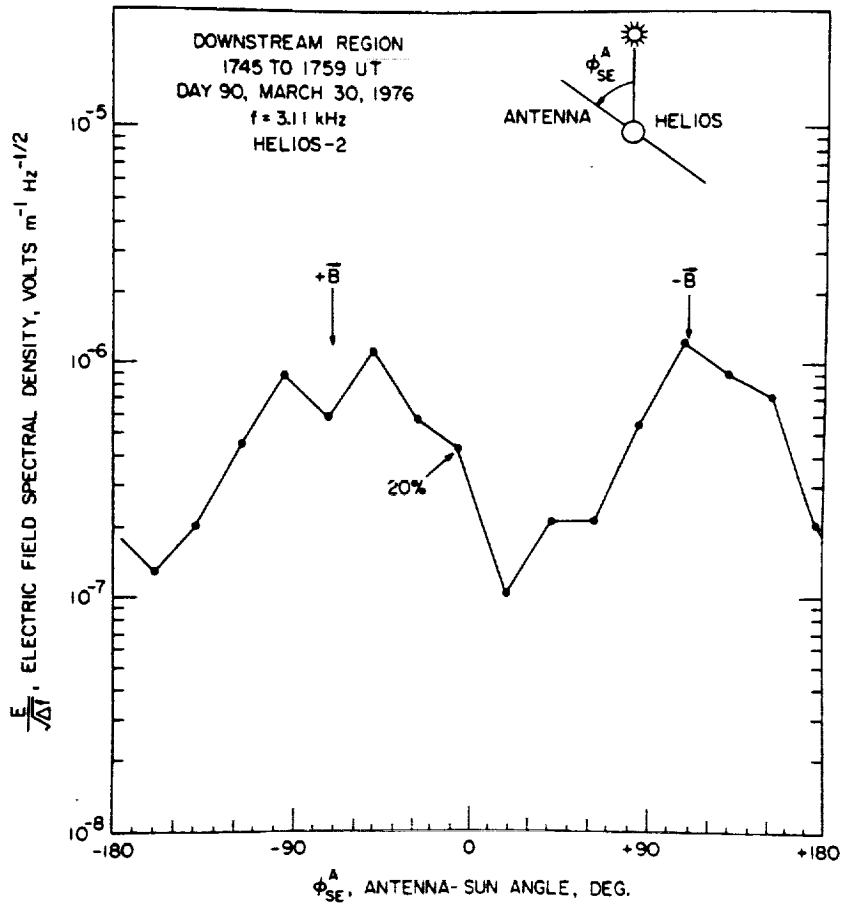

Fig. 8. The angular distribution of electric field intensities at 3.11 kHz in the wake region behind the shock. The sharp nulls when the antenna is aligned parallel to **B** and $-$**B** indicates that the electric field turbulence in the wake is aligned very closely along the direction of the solar wind magnetic field.

exponentially with decreasing distance from the shock. The e-folding distance is found to be about 190,000 km, which is consistent with our current knowledge of plasma oscillations associated with the earth's bow shock. This scale length presumably represents the combined effects of the growth rate of the plasma oscillation and the attenuation of the electron beam by wave-particle interactions as the beam propagates into the undisturbed plasma ahead of the shock.

Detailed comparisons of the transition region electric field spectrum in Figure 6 with spectrums given by *Rodriguez and Gurnett* [1975, 1976] from the earth's bow shock show a very close similarity. Of particular interest is the broad peak in the spectrum at about 3 kHz, which is a characteristic feature of the electric field spectrums in the earth's bow shock, although usually at somewhat lower frequencies, typically from 200 to 800 Hz. A comparable broad peak is also evident in the spectrum of the September 15, 1974, interplanetary shock investigated by *Scarf* [1978]. The unusually large electric field intensities for the shock analyzed in this paper, compared to the other events detected by Helios, also appear to be consistent with the correlations found by *Rodriguez and Gurnett* [1976], which show that large electric field intensities tend to be associated with large electron to ion temperature ratios, T_{e1}/T_{p1}, upstream of the shock. As mentioned earlier, T_{e1}/T_{p1} was unusually large for the shock analyzed. Because of the possibility of large Doppler shifts and the unknown wave number distribution in the transition region the exact identification of the waves modes responsible for the transition region electric field turbulence remains difficult. In accordance with the discussion of *Greenstadt and Fredricks* [1978] the most likely plasma wave mode responsible for this turbulence is the ion-acoustic mode, although other possibilities such as the Buneman mode [*Buneman*, 1958] cannot be completed ruled out.

The broad band of electrostatic turbulence from 1 to 10 kHz observed by Helios downstream of the transition region has features broadly similar to the electrostatic turbulence in the magnetosheath, downstream of the earth's bow shock. As described by *Rodriguez and Gurnett* [1975], the magnetosheath electrostatic turbulence has a spectrum similar to the transition region, with a broad peak at a few kHz and intensities about 1 to 2 orders of magnitude smaller than the transition region. The electric field of the magnetosheath electrostatic turbulence is also aligned parallel to the magnetic field [*Rodriguez*, 1979], in agreement with the electric field polarization determined from Helios (see Figure 8) downstream of the shock. Because of the high velocity of the shock relative to the spacecraft the Helios observations provide a determination of the large scale structure of the wake region which cannot be easily obtained from studies of the earth's bow shock. Most remarkable is the very nearly exponential decay of the electric field intensities in the wake and the occurrence of a distinct peak in the spectrum at about 3 to 5 kHz. The exponential decay and the emergence of a characteristic frequency strongly suggests that this turbulence consists of a weakly damped electrostatic mode excited by the shock which is slowly decaying in amplitude as the plasma carries the waves downstream of the shock. The impulsive variations indicated by the large ratio of peak to average field strengths (see Figure 2) suggests that these waves occur in small isolated packets or clumps which are encountered by the spacecraft on a more or less random basis.

When considering the possible plasma wave modes which could account for these waves two possibilities naturally come to mind, the ion-acoustic mode and the Buneman mode [*Buneman*, 1958]. Since ion-acoustic waves are thought to play an important role in the transition region [*Greenstadt and Fredricks*, 1978], it is reasonable to propose that the wake turbulence simply consists of slowly decaying ion-acoustic waves. Since the ion-acoustic mode can only propagate at frequencies below the ion plasma frequency, f_{pp}, which from Table 1 is only about 691 Hz, very large Doppler shifts are required to explain the observed frequency spectrum, which has a distinct peak at about 3.11 kHz (see Figure 6). Fortunately, a reasonably accurate estimate of the Doppler shift can be made in this case. The Doppler shift is given by

$$\Delta f = \frac{V}{\lambda} \cos \theta_{kV}$$

where V is the solar wind velocity, λ is the wavelength, and θ_{kV} is the angle between the solar wind velocity and the wave vector $\mathbf{k}$. Since the wake electric field turbulence is purely electrostatic the wave vector direction is parallel to the electric field. As shown earlier the electric field of this noise is very nearly parallel to the magnetic field. Therefore, θ_{kV} is approximately equal to the angle between the magnetic field and the solar wind velocity, which from Table 1 gives $\theta_{kV} \simeq \alpha_2 = 99.2°$. To compute the Doppler shift an assumption must be made concerning the wavelength of the ion-acoustic waves. For wave frequencies approaching the ion plasma frequency, the wavelength of the ion-acoustic mode approaches the minimum wavelength for waves in a plasma, which is given approximately by $\lambda_{min} = 2\pi\lambda_D$, where λ_D is the Debye length [*Stix*, 1962]. Using $\lambda_{D2} = 4.75$ m, $V_2 = 507.2$ km/s and $\theta_{kV} = 99.2°$ the corresponding Doppler shift is $\Delta f = -2.72$ kHz. The frequency in the spacecraft frame of reference would be $f' \simeq |f_p + \Delta f| = 2.03$ kHz. As can be seen from Figure 6 this frequency is in reasonably good agreement with the frequency of maximum intensity (3.11 kHz) of the wake turbulence. Thus, the wake electric field turbulence can be accounted for by ion-acoustic waves which have wavelengths very close to the minimum wavelength, $k\lambda_D \sim 1$. One difficulty with this interpretation is that significant wave intensities are still observed at frequencies as high as 10 kHz (see Figure 6), which would imply wavelengths somewhat shorter than the minimum wavelength $2\pi\lambda_D$. This difficulty also occurs for ion-acoustic waves in the transition region, since the electric field spectrum in this region has significant intensities up to frequencies as high as 56 kHz, which is too high to be accounted for by the maximum possible Doppler shift, even if we let $\theta_{kV} = 0°$. *Scarf* [1978] has noted a similar problem in his analysis of the September 15, 1974, event. Although troublesome, this difficulty is probably not serious since the wavelengths would only have to be smaller than the minimum wavelength by a modest factor and the minimum wavelength condition is only an approximate limit caused by the onset of strong Landau damping as $k\lambda_D \to 1$. Also the Debye length in Table 1 is somewhat uncertain because of the non-Maxwellian component of the solar wind electron distribution.

It is also of interest to consider the interpretation of the wake electric field turbulence in terms of the Buneman mode [*Buneman*, 1958]. For the Buneman mode the phase velocity is much larger than the solar wind velocity, so Doppler effects are unimportant. The characteristic frequency of the Buneman mode is $f_B = (m_e/m_p)^{1/3} f_{pe}$, which for the parameters given in Table 1 is approximately $f_B = 2.40$ kHz in the downstream region. This frequency is also seen to be in good agreement

with the frequency of maximum electric field intensity in the wake region (see Figure 6). Since the Buneman mode is a very rapidly growing instability, with growth rates comparable to the frequency, the frequency spectrum of the waves produced by this instability is expected to be very broad and impulsive, possibly comparable to the observed spectrum. The Buneman mode, however, has the difficulty that very large currents (electron-ion drift velocities comparable to the electron thermal speed) are needed to drive this instability. Since neither the plasma measurements nor the magnetic field measurements give any indication of such large currents in the relatively quiescent wake region, it is difficult to see how the Buneman mode could be driven unstable in this region, or why the resulting electric fields should display the exponential decay clearly evident in Figure 2. In the absence of any satisfactory explanation for the generation of the Buneman mode in the wake, we believe that short wavelength ion-acoustic waves provide the most satisfactory explanation of the electric field turbulence downstream of this shock.

In constrast to the uncertainty concerning plasma wave mode responsible for the electric field turbulence, the magnetic field turbulence near the shock must be propagating in the whistler mode since no other electromagnetic mode of propagation exists at frequencies between the electron and ion cyclotron frequencies. The interpretation of the magnetic field turbulence for this event is greatly simplified because of the unusually low Doppler shifts for most parts of the electromagnetic waves spectrum. The low Doppler shifts in this case are due firstly to the relatively small values of the Alfvén Mach numbers ($M_{A1} = 1.62$ and $M_{A2} = 1.73$) and secondly to the fact that the magnetic field is aligned very nearly perpendicular to the solar wind velocity ($\alpha_1 = 89.6°$ and $\alpha_2 = 99.2°$). For example, a wave propagating with a phase speed equal to the Alfvén speed along the magnetic field will undergo fractional Doppler shifts of only +1% and +28% upstream and downstream of the shock, respectively. Since for the R-mode [*Stix*, 1962] the phase speed is greater than the Alfvén speed except near the electron cyclotron frequency, f_{ce}, Doppler shifts are generally negligible for parallel propagation. For other propagation directions the Doppler shifts are still reasonably small except near resonances. Hence, the magnetic field spectrums in Figure 7 may be interpreted as lying close to the frequencies in the shock rest frame. Since the electron cyclotron frequencies range from about 1.23 to 1.58 kHz, it can be seen from Figure 7 that the magnetic field noise extends with appreciable intensities up to about $f_{ce}/2$ in the shock transition region. The approximately exponential decrease in the low frequency, $\lesssim 10$ Hz, magnetic field intensities in either direction from the shock suggests that whistler-mode turbulence generated in the shock can propagate freely away from the shock and is gradually absorbed by cyclotron damping in the upstream and downstream regions. Measurements of the e-folding lengths for this damping give a scale length for the cyclotron damping of a few hundred thousand km. At higher frequencies, $\gtrsim 10$ Hz, most of whistler-mode radiation tends to be directed into the downstream region.

In this paper we have attempted to present a detailed analysis of one particular event for which a substantial level of plasma wave turbulence was present. It is clear from our initial investigations that the details of the plasma wave turbulence associated with a shock vary considerably from event to event. This case should therefore not be regarded as necessarily typical of all interplanetary shocks. In the future, after more events have been detected and analyzed, we plan to present a more detailed study of the range of variability of the turbulence associated with interplanetary shocks and to try to provide a better determination of the parameters which cause this variability.

Acknowledgments. The research at the University of Iowa was supported by NASA under contract NAS5-11279 and grant NGL-16-001-043. The research at the TU Braunschweig and MPI Garching was supported by the German Bundesministerium für Forschung und Technologie.

The Editor thanks E. J. Smith and R. W. Fredricks for their assistance in evaluating this paper.

References

Buneman, O., Instability, turbulence and conductivity in a current carrying plasma, *Phys. Rev. Lett.*, *1*, 8, 1958.

Dehmel, G., F. M. Neubauer, D. Lukoschus, J. Wawretzko, and E. Lammers, Das Induktionsspulen-Magnetometer-Experiment (E4), *Raumfahrtforschung*, *19*, 241, 1975.

Dryer, M., A. Eviatar, A. Frohlich, A. Jacobs, J. H. Joseph, and E. J. Weber, Interplanetary shock waves and comet brightness fluctuations during June–August 1972, *J. Geophys. Res.*, *80*, 2001, 1975.

Fredricks, R. W., C. F. Kennel, F. L. Scarf, G. M. Crook, and I. M. Green, Detection of electric-field turbulence in the earth's bow shock, *Phys. Rev. Lett.*, *21*, 1761, 1968.

Fredricks, R. W., F. V. Coroniti, C. F. Kennel, and F. L. Scarf, Fast time-resolved spectra of electrostatic turbulence in the earth's bow shock, *Phys. Rev. Lett.*, *24*, 994, 1970*a*.

Fredricks, R. W., G. M. Crook, C. F. Kennel, I. M. Green, and F. L. Scarf, Ogo 5 observations of electrostatic turbulence in bow shock magnetic structures, *J. Geophys. Res.*, *75*, 3751, 1970*b*.

Galeev, A. A., Collisionless shocks, in *Physics of Solar Planetary Environments*, vol. 1, edited by D. J. Williams, p. 464, AGU, Washington, D. C., 1976.

Gliem, F., G. Dehmel, G. Musmann, C. Türke, U. Krupstedt, and R. P. Kugel, Die Bordrechner der Helios-Magnetometer-Experimente E2 and E4, *Raumfahrtforschung*, *20*, 16, 1976.

Greenstadt, E. W., and R. W. Fredricks, Shock systems in collisionless plasmas, in *Solar System Plasma Physics: A Twentieth Anniversary Overview*, North-Holland, Amsterdam, in press, 1978.

Gurnett, D. A., and R. R. Anderson, Plasma wave electric fields in the solar wind: Initital results from Helios 1, *J. Geophys. Res.*, *82*, 632, 1977.

Gurnett, D. A., and L. A. Frank, Ion acoustic waves in the solar wind, *J. Geophys. Res.*, *83*, 58, 1978.

Jeffrey, A., and T. Taniuti, *Non-Linear Wave Propagation*, Academic, New York, 1964.

Kundu, M. R., *Solar Radio Astronomy*, Interscience, New York, 1965.

Maxwell, A., Solar radio burst of spectral type II recorded at Fort Davis, Texas, during the period 20 March–2 May 1976, in *Collected Data Reports for STIP Interval II, Rep UAG-61*, edited by H. E. Coffey and J. A. McKinnon, p. 97, National Oceanic and Atmospheric Administration, Boulder, Colo., 1977.

Musmann, G., F. M. Neubauer, A. Maier, and E. Lammers, Das Förstersonden-Magnetofeldexperiment (E2), *Raumfahrtforschung*, *12*, 232, 1975.

Neubauer, F. M., H. J. Beinroth, R. Barnstorf, and G. Dehmel, Initial results from the Helios-1 search-coil magnetometer experiment, *J. Geophys.*, *42*, 599, 1977*a*.

Neubauer, F. M., G. Musmann, and G. Dehmel, Fast magnetic fluctuations in the solar wind: Helios 1, *J. Geophys. Res.*, *82*, 3201, 1977*b*.

Olson, J. V., R. E. Holzer, and E. J. Smith, High-frequency magnetic fluctuations associated with the earth's bow shock, *J. Geophys. Res.*, *74*, 4601, 1969.

Pinter, S., Velocities of propagation of March/April 1976 coronal and interplanetary shock waves, in *Collected Data Reports for STIP Interval II, Rep. UAG-61*, edited by H. E. Coffey and J. A. McKinnon, p. 127, National Oceanic and Atmospheric Administration, Boulder, Colo., 1977.

Rodriguez, P., Magnetosheath electrostatic turbulence, *J. Geophys. Res.*, in press, 1978.

Rodriguez, P., and D. A. Gurnett, Electrostatic and electromagnetic turbulence associated with the earth's bow shock, *J. Geophys. Res.*, *80*, 19, 1975.

Rodriguez, P., and D. A. Gurnett, Correlation of bow shock plasma

wave turbulence with solar wind parameters, *J. Geophys. Res.*, *81*, 2871, 1976.

Sarris, E. T., and J. A. Van Allen, Effects of interplanetary shock waves on energetic charged particles, *J. Geophys. Res.*, *79*, 4157, 1974.

Scarf, F. L., Wave-particle interaction phenomena associated with shocks in the solar wind, in *Proceedings of the De Feiter Memorial Symposium on the Study of Traveling Interplanetary Phenomena*, D. Reidel, Hingham, Mass., in press, 1978.

Scarf, F. L., R. W. Fredricks, L. A. Frank, and M. Neugebauer, Nonthermal electrons and high-frequency waves in the upstream solar wind, 1, Observations, *J. Geophys. Res.*, *76*, 5162, 1971.

Scarf, F. L., R. W. Fredricks, I. M. Green, and G. M. Crook, Observations of interplanetary plasma waves, spacecraft noise, and sheath phenomena on Imp 7, *J. Geophys. Res.*, *79*, 73, 1974.

Schwenn, R., H. Rosenbauer, and H. Miggenrieder, Das Plasma-experiment auf Helios (E1), *Raumfahrtforschung*, *19*, 226, 1975.

Smith, E. J., and J. H. Wolfe, Observations of interactions regions and corotating shocks between one and five AU: Pioneers 10 and 11, *Geophys. Res. Lett.*, *3*, 137, 1976.

Stix, T. H., *The Theory of Plasma Waves*, McGraw-Hill, New York, 1962.

Wu, C. S., and R. W. Fredricks, Cyclotron drift instability in the bow shock, *J. Geophys. Res.*, *77*, 5585, 1972.

(Received March 23, 1978;
revised September 9, 1978;
accepted September 13, 1978.)

Ion Acoustic Waves and Related Plasma Observations in the Solar Wind

D. A. GURNETT

Department of Physics and Astronomy, The University of Iowa, Iowa City, Iowa 52242

E. MARSCH, W. PILIPP, AND R. SCHWENN

Max-Planck-Institut für Physik und Astrophysik, Institut für extraterrestrische Physik 8046 Garching, West Germany

H. ROSENBAUER

Max-Planck-Institut für Aeronomie, 3411 Katlenburg-Lindau 3, West Germany

This paper presents an investigation of solar wind ion acoustic waves and their relationship to the macroscopic and microscopic characteristics of the solar wind plasma. Comparisons with the overall solar wind corotational structure show that the most intense ion acoustic waves usually occur in the low-velocity regions ahead of high-speed solar wind streams. Of the detailed plasma parameters investigated, the ion acoustic wave intensities are found to be most closely correlated with the electron to proton temperature ratio T_e/T_p and with the electron heat flux. Investigations of the detailed electron and proton distribution functions also show that the ion acoustic waves usually occur in regions with highly non-Maxwellian distributions characteristic of double-proton streams. The distribution functions for the double-proton streams are usually not resolved into two clearly defined peaks, but rather they appear as a broad shoulder on the main proton distribution. Two main mechanisms, an electron heat flux instability and a double-ion beam instability, are considered for generating the ion-acoustic-like waves observed in the solar wind. Both mechanisms have favorable and unfavorable features. The electron heat flux mechanism can account for the observed waves at moderate to large ratios of T_e/T_p but has problems when T_e/T_p is small, as sometimes occurs. The ion beam instability appears to provide more flexibility in the T_e/T_p ratio; however, detailed comparisons using observed distribution functions indicate that the ion beam mode is usually stable. Possible resolutions of these difficulties are discussed.

1. INTRODUCTION

Plasma wave observations on the Helios and Voyager spacecraft [*Gurnett and Anderson*, 1977; *Gurnett and Frank*, 1978; *Kurth et al.*, 1979] have demonstrated that short-wavelength electrostatic waves are frequently present in the solar wind at frequencies between the ion and electron plasma frequencies, $f_p^+ < f < f_p^-$. The primary characteristics of these waves are that they occur in brief monochromatic bursts with a rapidly varying center frequency. The frequency spectrum of these bursts varies systematically with radial distance from the sun, as is illustrated in Figure 1, decreasing in frequency with increasing radial distance. The upper and lower frequency limits of the spectrum are approximately f_p^+ and f_p^-. The electric field of the waves tends to be aligned along the direction of the solar wind magnetic field, within approximately 15° or less. The waves tend to occur in distinct 'storms' lasting from a few hours to several days, separated by intervals of a few days during which little or no activity is detected.

Only three types of plasma wave modes are known which can account for the characteristics of the electrostatic waves detected by Helios and Voyager. These modes are the Buneman mode [*Buneman*, 1958] at $f_B \simeq (m^-/m^+)^{1/3} f_p^-$, the ion acoustic mode at $f \lesssim f_p^+$, and electron plasma oscillations at $f \simeq f_p^-$. Both the ion acoustic mode and the electron plasma oscillations require large Doppler shifts to explain the observed frequency spectrum. At the present time the existing evidence suggests that short-wavelength ion acoustic waves, Doppler shifted to frequencies $f_p^- < f < f_p^-$, provide the most likely explanation for the waves detected by Helios and Voyager. This identification is based on the wavelength measurements of *Gurnett and Frank* [1978], who showed that the observed wavelengths provide the correct Doppler shift to account for the observed frequency spectrum. In this case the fact that the frequency spectrum falls in the range $f_p^+ < f < f_p^-$ is purely coincidental, since the overall proportionality to f_p^+ and f_p^- can be explained in terms of the density dependence of the Debye length λ_D, which determines the minimum wavelength and the maximum Doppler shift. Electron plasma oscillations, Doppler shifted downward in frequency, are not considered a very likely possibility for explaining these waves, since such oscillations could only be excited by relatively energetic particles streaming back toward the sun, which have not been observed. Similarly, the Buneman mode is not considered a very likely possibility because of the very large relative drift velocities, and hence currents, which are required to drive this instability. Although a complete understanding of the instability mechanism and mode of propagation has not yet been achieved, we will continue to refer to these waves as ion acoustic waves, following our previous terminology.

The primary objective of this paper is to present a study of the relationship between the interplanetary ion acoustic waves detected by Helios and the macroscopic and microscopic characteristics of the solar wind plasma. For details of the Helios 1 and 2 plasma wave and plasma instruments used in this study, see *Gurnett and Anderson* [1977], *Schwenn et al.* [1975], and *Rosenbauer et al.* [1977]. Special emphasis is placed on determining which plasma parameters play the primary role in controlling the intensity and occurrence of ion acoustic waves in the solar wind. Because it is well known that the ion acoustic instability is very sensitive to the electron to ion temperature ratio [*Stix*, 1962], special attention is given to this parameter. The detailed electron and proton velocity distribution func-

Paper number 9A0110.
0148-0227/79/009A-0110$01.00

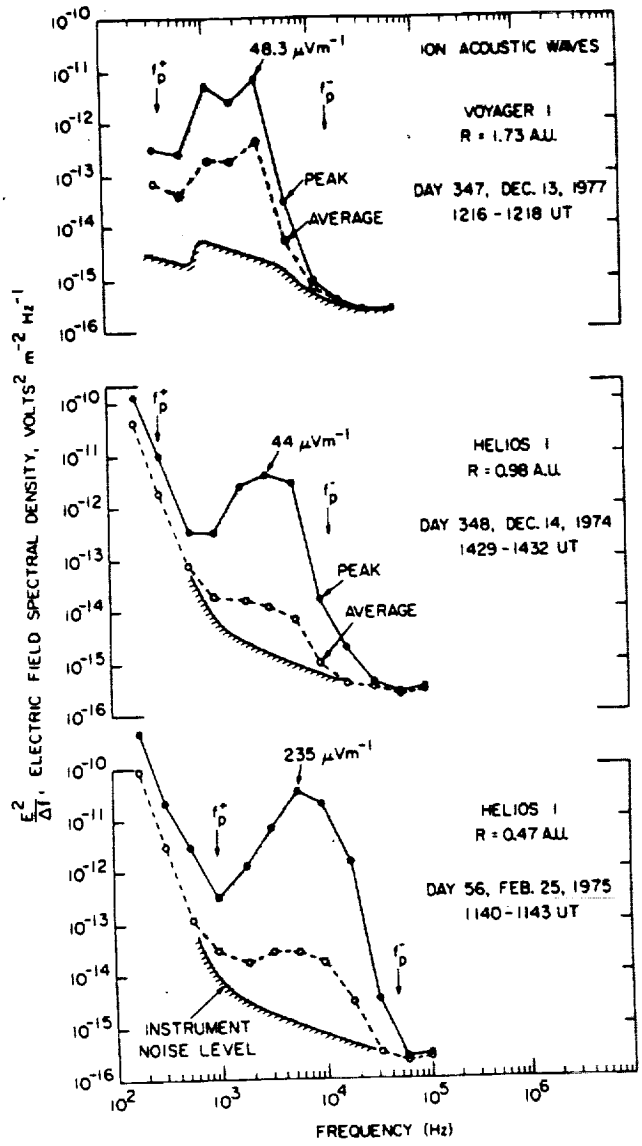

Fig. 1. A series of spectra of the interplanetary ion acoustic waves detected by Helios and Voyager at progressively closer distances to the sun (from top to bottom). The increase in the intensity and the frequency of these waves with decreasing radial distance from the sun is clearly evident.

tions are also examined to try to establish the source of free energy which drives the ion acoustic waves. Both the electron heat flux mechanism of *Forslund* [1970] and the double-ion beam mechanism of *Gary* [1978a] are considered.

2. Relationship to Solar Wind Stream Structure

To investigate the relationship between periods of enhanced ion acoustic wave activity and the large-scale corotational structure of the solar wind, a series of combined plots of the plasma wave and plasma data have been made for each solar rotation during the Helios 1 and 2 mission. Three representative plots of this type are shown in Figures 2, 3, and 4. Each plot shows one complete solar rotation. The abscissa is the Carrington longitude of the spacecraft. The day number and heliocentric radial distance are also shown for reference at the bottom of each plot. The top panels give the proton flow speed V_p, density n_p, and temperature T_p as obtained from the Max-Planck plasma instrument. The middle panels give the electric field intensities from the University of Iowa plasma wave instrument in 11 frequency channels extending from 311 Hz to 100 kHz. The solid line in each channel gives the peak electric field intensity, and the vertical bars (black areas) give the average electric field intensity. The dynamic range for each channel is 100 dB, extending from about 10^{-8} to 10^{-1} V m^{-1}. The bottom panels give the electron heat flux Q_e (in units of ergs cm^{-2} s^{-1}) and the electron to proton temperature ratio T_e/T_p.

Two types of waves can be identified in the electric field measurements of Figures 2, 3, and 4: (1) ion acoustic waves in the frequency range from about 1 to 10 kHz and (2) narrow band electron plasma oscillations in the frequency range from about 31.1 to 56.2 kHz. Both the ion acoustic waves and the electron plasma oscillations vary considerably during a solar rotation. Usually, two or three periods of enhanced ion acoustic wave activity occur during each solar rotation, separated by periods of relatively low intensity. The periods of enhanced ion acoustic wave activity usually last from a few hours to several days and are most pronounced in the peak intensity measurements. It should be noted that the peak intensity measurements, which are computed over time intervals of 36.0 min, are extremely sensitive to even very low levels of activity, since even a single burst of noise with a duration greater than 50 ms during any 36.0-min sampling interval will be indicated. Even

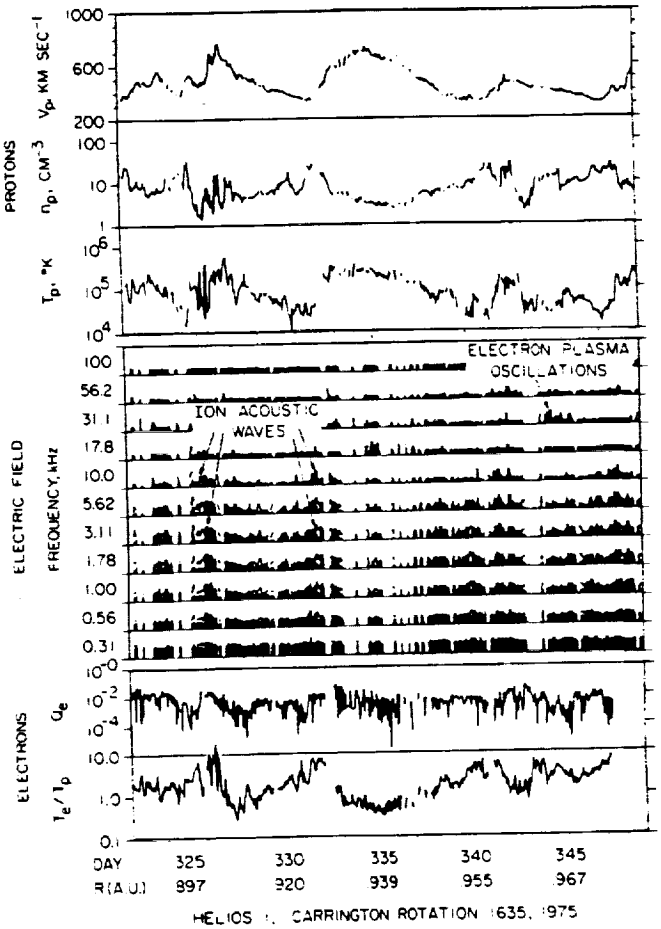

Fig. 2. The plasma wave electric field intensities and solar wind electron and proton parameters for one complete solar rotation, plotted as a function of the Carrington longitude of the spacecraft. Some sporadic ion acoustic wave activity is present nearly all of the time. However, the most intense ion acoustic waves tend to occur in the low-velocity regions ahead of high-speed streams, where T_e/T_p is large, and in regions of large electron heat flux Q_e.

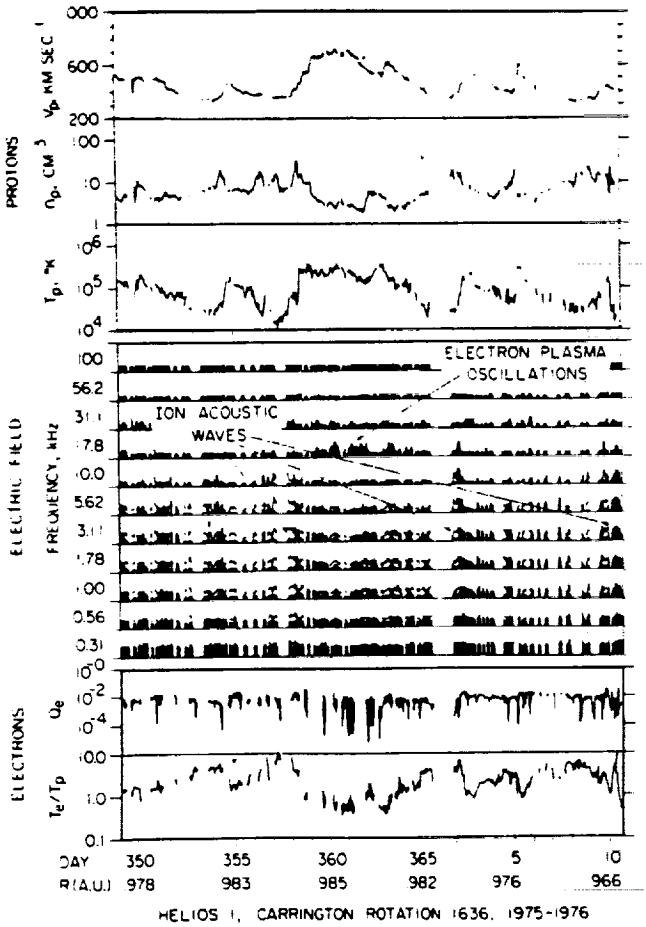

Fig. 3. The plasma wave and solar wind plasma data for the next solar rotation following that of Figure 2. The same general trend, toward large ion acoustic wave intensities ahead of high-speed streams and in regions of large T_e/T_p and Q_e, is again evident.

during quiet periods a low level of ion acoustic wave activity can usually be detected with peak intensities of about 1–10 μV m^{-1}. During more active periods, such as those on day 326 in Figure 2 and days 71–75 in Figure 4, the peak intensities in a given channel (~10% bandwidth) are typically 50–200 μV m^{-1}. The peak intensities are always much larger than the average intensities. The large ratio of peak to average field strengths indicates that the ion acoustic waves consist of many impulsive bursts, with a time interval between the bursts which is much larger than the duration of the bursts.

When the ion acoustic wave intensities are compared with the solar wind velocity measurements, a fairly consistent pattern can be identified in Figures 2, 3, and 4. Whenever a well-defined high-speed stream onset is evident in the proton flow speed V_p, this onset is usually preceded by a period of enhanced ion acoustic wave activity ahead of the high-speed stream. Examples of this relationship can be seen for the high-speed stream onsets on days 327 and 333 in Figure 2, days 357 and 2 in Figure 3, and days 74 and 84 in Figure 4. The ion acoustic waves therefore tend to occur in the low-speed region immediately preceding a high-speed stream interface. Within the high-speed stream regions, where the velocities are greater than about 500 km s^{-1}, the ion acoustic wave intensities are usually quite low. The relationship between the ion acoustic wave intensities and the high- and low-speed stream regions can be placed on a more quantitative basis by computing the average of the 36.0-min peak electric field intensities as a function of the proton flow speed using all of the available data, which include approximately 4 years of observations. The result of this correlation analysis is illustrated in Figure 5, which shows the electric field intensities at 5.62 kHz, roughly in the center of the ion acoustic wave spectrum, averaged in a sequence of contiguous solar wind velocity windows. A negative correlation is clearly evident between the ion acoustic wave intensities and the solar wind velocity, showing that on the average the wave intensities are large in the low-speed solar wind regions. Although Figure 5 indicates a definite negative correlation, a large amount of scatter is also present which tends to reduce the correlation in comparison with what one would expect on the basis of a visual examination of Figures 2, 3, and 4. This scatter usually results from periods, such as the period from day 86 to day 92 in Figure 4, that have a complex structure not simply resolved into low- and high-speed streams.

A more detailed illustration of the electrostatic wave activity observed near a high-speed stream interface is shown on an expanded time scale in Figure 6. This example is for the high-speed stream interface in Figure 4 at about 0940 UT on day 74, 1976. The interface in this case is characterized by a clearly defined tangential discontinuity [*Gosling et al.*, 1978] showing an abrupt increase in the proton flow speed and temperature and a corresponding decrease in the plasma density, which maintains an approximate pressure balance, across the interface. The region of high plasma density, characteristic of the

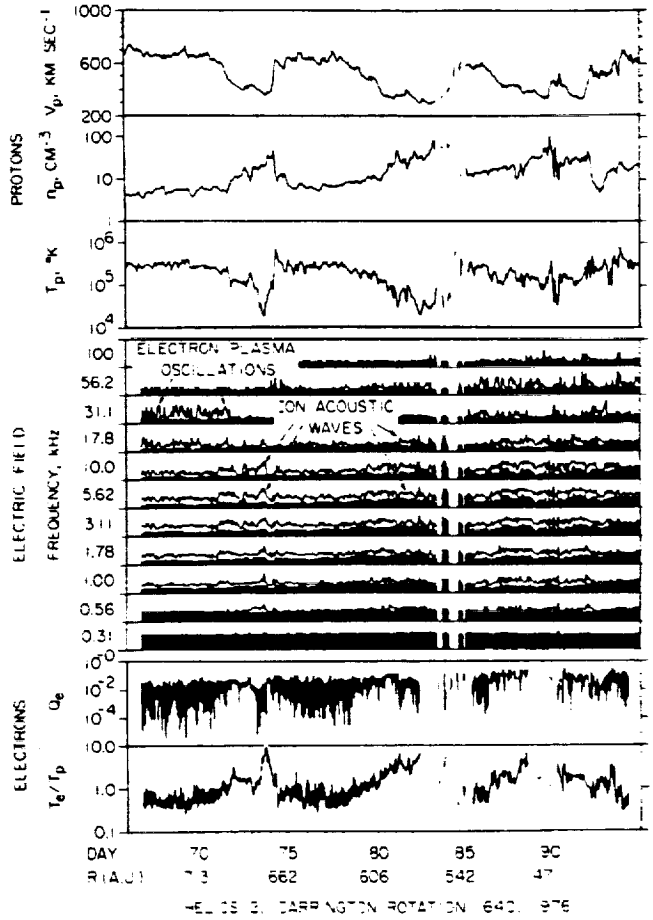

Fig. 4. The plasma wave and solar wind plasma data for another solar rotation similar to Figures 2 and 3. The ion acoustic wave intensities associated with the high-speed stream onset on days 73 and 74 are shown in greater detail in Figure 6.

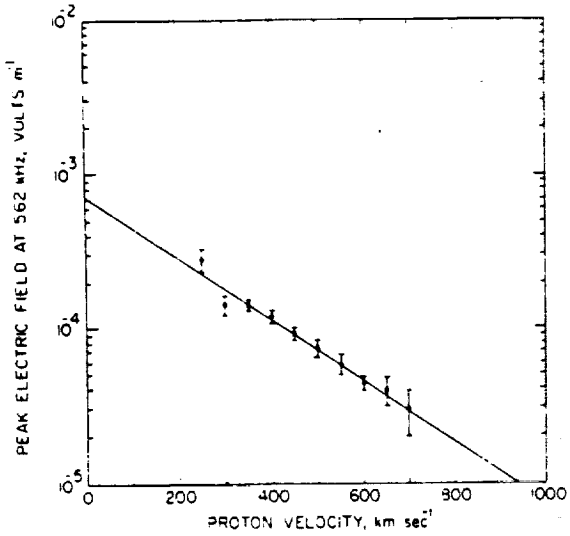

Fig. 5. A plot of the average of the peak 36-min electric field intensities at 5.62 kHz as a function of the solar wind velocity using all of the available Helios 1 and 2 data. The error bars are the standard deviation of the average solar wind velocity in each interval. This illustration shows the general trend toward increasing ion acoustic wave intensities with decreasing solar wind velocity.

compression zone ahead of the high-speed stream (see, for example, *Hundhausen* [1972]), is clearly evident in Figures 4 and 6. As can be seen in Figure 4, several periods of sporadic ion acoustic wave activity are evident for nearly 3 days before the onset of the high-speed stream. These waves reach their highest intensities from about 1200 to 2400 UT on day 73, about 16 hours ahead of the stream interface. A few sporadic bursts of ion acoustic waves are also evident from about 0940 to 1130 UT on day 74, immediately after the stream interface but before the proton flow speed has reached its maximum value. Electron plasma oscillations are also evident in this same region.

3. Correlation With T_e/T_p

A well-known characteristic of the ion acoustic mode is that the damping, and hence stability, of this mode is strongly influenced by the electron to ion temperature ratio T_e/T_i [*Stix*, 1962]. For values of T_e/T_i less than 1, the phase velocity of the ion acoustic mode is comparable to the thermal velocity of the ions, and the wave is strongly damped by Landau damping. As T_e/T_i increases above 1, the phase velocity increases, and the number of resonant ions, and hence the damping, rapidly decreases. The ion acoustic mode is therefore difficult to drive

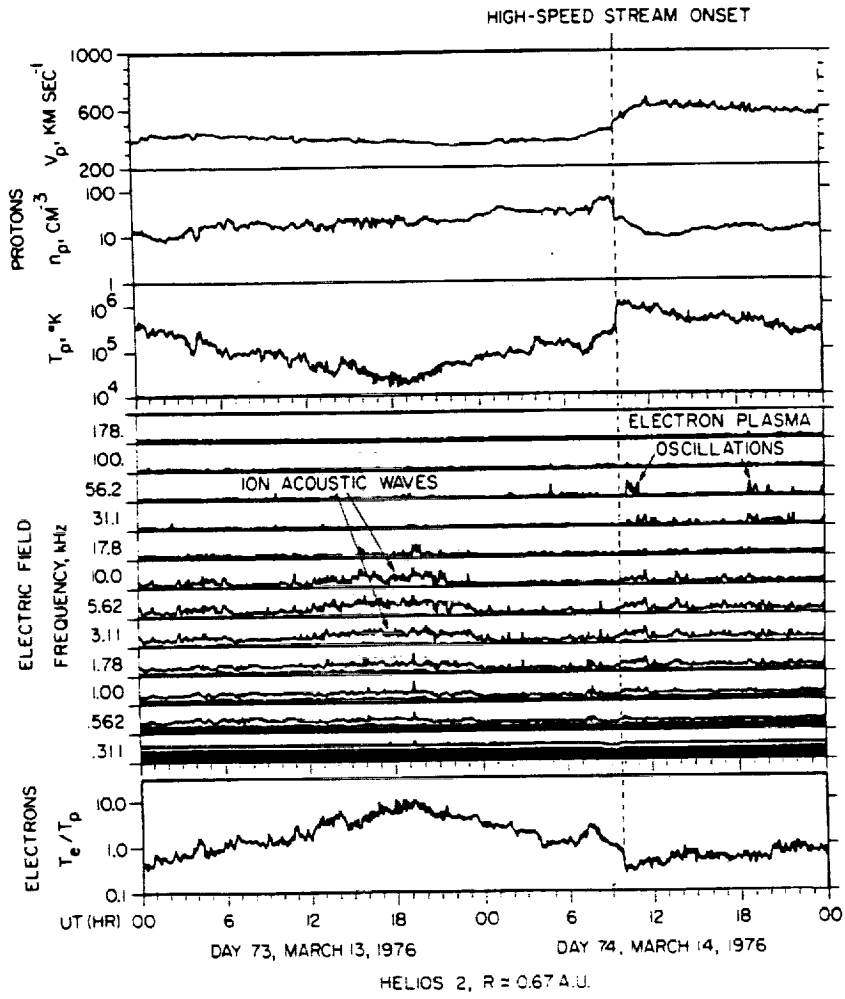

Fig. 6. Details of the plasma wave electric field intensities and solar wind plasma parameters for the high-speed solar wind stream onset on day 74, 1976, from Figure 4. The largest ion acoustic wave intensities during this period occur in the region of large T_e, T_p immediately preceding the high-speed stream onset.

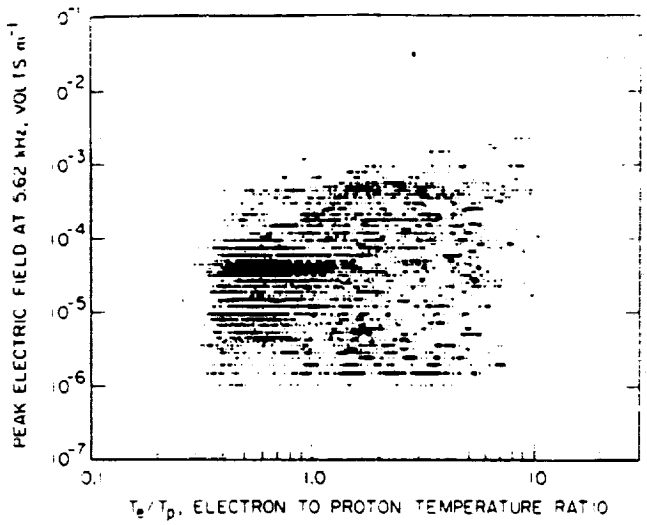

Fig. 7. A scatter plot of the ion acoustic wave electric field intensities as a function of T_e/T_p for the three solar rotations shown in Figures 2, 3, and 4. Although a considerable amount of scatter exists in these data, the general trend toward increasing electric field intensity with increasing T_e/T_p is clearly evident.

unstable for values of T_e/T_i less than or comparable to 1. Because the electrostatic waves under consideration are thought to be caused by an ion acoustic instability, it is of considerable interest to investigate the relationship between the intensity of these waves and the corresponding electron to ion temperature ratios.

Because of the non-Maxwellian anisotropic character of the solar wind plasma, several different methods can be used to compute the electron and proton temperatures. For this study, all temperatures have been computed from the second moment of the velocity distribution function $f(\mathbf{V})$:

$$nk\mathrm{T} = \tfrac{1}{2}m\int f(\mathbf{V})(\mathbf{V} - \mathbf{U})^2\, d^3V$$

where k is Boltzmann's constant, m is the particle mass, and $\mathbf{U}$ is the bulk velocity. Since the solar wind ion acoustic waves are known to be propagating approximately parallel to the magnetic field, ideally one should use the temperature parallel to the magnetic field. However, since the angular field of view of the electron instrument is restricted to a 18° wide disk in the ecliptic plane, it is not possible to measure parallel electron temperatures if the magnetic field is more than about ±10° from the ecliptic plane. To provide the best estimate of the parallel temperature, the electron temperature has been computed along a direction parallel to the projection of the magnetic field in the ecliptic plane. The proton temperature has been computed along the spacecraft-sun line. Comparison with the temperature tensor resulting from a complete analysis of the three-dimensional proton measurements shows reasonable agreement provided the **B** vector is within a 45° cone around the radial direction. In addition, since the temperature anisotropies are normally less than a factor of 2, the errors introduced by this simplified analysis are not expected to be large. In any case, these temperatures are considered adequate for this initial survey. More detailed analyses of the electron and proton distribution functions for a specific case are presented later.

As can be seen from the T_e/T_p plots in Figures 2, 3, and 4, the temperature ratio varies considerably during any given solar rotation, from about 0.5 to greater than 10. These variations are mainly due to changes in the proton temperature, since the electron temperature tends to remain relatively constant at about (1–2) × 10^5 °K. Comparisons of the T_e/T_p variations with the ion acoustic wave intensities generally show a good correlation, with a strong tendency for the wave intensities to be large when T_e/T_p is large. For example, the large increases in T_e/T_p centered on days 326, 331, and 341 in Figure 2, on days 357, 2, and 10 in Figure 3, and on days 73, 82, and 88 in Figure 4 are all associated with periods of enhanced ion acoustic wave activity. The correlation with T_e/T_p can be seen in further detail in Figure 6, which shows that the intense burst of ion acoustic waves from about 1200 to 2400 UT on day 73 is centered on a region of unusually large T_e/T_p, with $T_e/T_p \simeq 10$ at 1900 UT.

The correlation between the ion acoustic wave intensities and T_e/T_p is presented on a more quantitative basis by the scatter plot in Figure 7. This illustration shows the peak electric field intensities at 5.62 kHz, approximately in the center of the ion acoustic wave spectrum, and the corresponding T_e/T_p values for all of the data in Figures 2, 3, and 4. Although a fair amount of scatter exists, the general trend toward larger electric field intensities at larger values of T_e/T_p is clearly evident. This correlation can be demonstrated even more clearly if the peak electric field intensities are averaged and plotted as a function of T_e/T_p, as is shown in Figure 8. As can be seen, the average ion acoustic wave intensities increase by about a factor of 7, from 70 to 500 μV m^{-1}, as the electron to proton temperature ratio increases from 1.0 to 10.

The T_e/T_p correlation described above also fits in well with the overall morphology of the ion acoustic wave activity and the relationship to the high-speed stream structure discussed in the preceding section. A well-established observational feature of the solar wind plasma flow is that the proton temperature tends to be largest in the high-speed streams and drops substantially in the low-speed regions [*Hundhausen*, 1972]. Sometimes the proton temperature in the region immediately ahead of the high-speed stream drops to extremely low values, ~10^4 °K, as is illustrated by the example in Figure 6. Since the electron temperature does not change by very much across the stream interface, this pattern usually results in large T_e/T_p values ahead of the high-speed stream interface, in the region where the ion acoustic waves tend to be most intense.

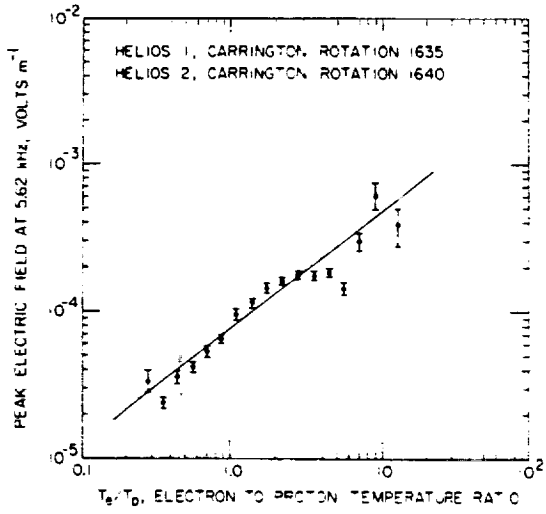

Fig. 8. A further detailed analysis of the data in Figure 7, showing the average of the 36-min peak electric field intensities as a function of T_e/T_p. The error bars give the standard deviation of the average T_e/T_p in each interval. The ion acoustic wave intensity increases by about a factor of 7 as T_e/T_p increases from 1 to 10.

Overall, the observed correlation of the electrostatic wave intensities with T_e/T_p supports the view that these waves are an ion-acoustic-like mode. One unexplained feature of this correlation is the fact that although the electric field intensities tend to increase as T_e/T_p increases, substantial ion acoustic wave intensities sometimes occur even when T_e/T_p is quite small. For example, in Figure 6 a moderately intense burst of ion acoustic waves can be seen from about 0930 to 1130 UT on day 74, in a region where T_e/T_p is approximately 0.3. Since the ion acoustic mode should be strongly damped under these conditions, an important question arises as to how the ion acoustic mode can be unstable in regions such as this and what feature of the proton and electron velocity distribution is responsible for the instability. The presence of electron plasma oscillations in this same region suggests that some unusual suprathermal particle distributions are probably present immediately following the high-speed stream interface which may also be responsible for generating these waves.

4. Comparisons With Electron and Proton Distribution Functions and Related Parameters

Since the generation of the solar wind ion acoustic waves must involve some suitable source of free energy, detailed comparisons have been made with the electron and proton distribution functions to try to identify the primary feature of the distribution function which is responsible for these waves. A typical example of these comparisons is illustrated by the electron distribution function in Figure 9. This distribution function was selected from the period of very intense ion acoustic wave activity in Figure 6.

The top panel of Figure 9 shows a contour diagram of the electron distribution function at about 1702:50 UT on day 73, near the time of maximum wave intensity. The electron distribution functions are measured by using a detector viewing radially outward from the spacecraft spin axis. The spin axis is oriented perpendicular to the ecliptic plane. The contour diagram in the top panel of Figure 9 therefore represents a cut through the distribution function parallel to the ecliptic plane. To assure that all possible pitch angles with respect to the magnetic field are contained within such a cut, the measurement in Figure 9 was selected at a time when the magnetic field direction was nearly parallel, $\theta_B = -9.8°$, to the ecliptic plane. The magnetic field direction projected onto the ecliptic plane is indicated by the dashed line in the top panel of Figure 9. A one-dimensional cross section of the electron distribution function along the direction of the magnetic field, with positive velocities away from the sun, is shown in the bottom panel of Figure 9. The best fit Maxwellian distribution function for the core electrons is also indicated in Figure 9. The core temperature, parallel to the magnetic field, in this case is $T_\parallel = 1.4 \times 10^5$ °K. A detailed description of the methods used to compute these distribution functions will be given elsewhere.

As can be seen from Figure 9, the electron distribution function is a monotonically decreasing function of velocity in all directions with respect to the magnetic field and shows no evidence of a double peak in the distribution function over the entire energy range, 10 eV to 1.6 keV, for which measurements are available. Measurements at even higher energies, >20 keV, (E. Keppler, personal communication, 1978) also show no evidence of a double peak. The only identifiable feature of the distribution function which could contribute to the free energy available for generating waves is the slight asymmetry, parallel and antiparallel to the magnetic field, caused by the electron heat flux. The computed heat flux in this case is $Q_e = 2.2 \times 10^{-2}$ erg cm^{-2} s^{-1}. The relative drift induced between the core electrons and the solar wind protons by this heat flux has been suggested by *Forslund* [1970] as a possible mechanism for producing ion acoustic waves in the solar wind.

To provide an overall evaluation of the possible role of the electron heat flux as the source of the interplanetary ion acoustic waves, the electron heat flux has been plotted in the bottom panels of Figures 2, 3, and 4. Whenever possible, the electron parameters were computed when the magnetic field was within ±10° from the ecliptic plane. Large variations in the electron heat flux are clearly evident, even on relatively short time scales. Detailed comparisons with the ion acoustic wave intensities show that the heat flux is usually relatively large, 10^{-2} to 10^{-1} erg cm^{-2} s^{-1}, in the region where the ion acoustic waves occur. This relationship is illustrated in better detail by the scatter diagram in Figure 10, which shows the electric field intensity at 5.62 kHz as a function of electron heat flux Q_e for the three solar rotations in Figures 2, 3, and 4. As can be seen, the electric field intensities show a very clear correlation with Q_e, increasing in intensity with increasing heat flux. Since the physically relevant parameter for the electrostatic heat flux instability is the skewness of the electron velocity distribution

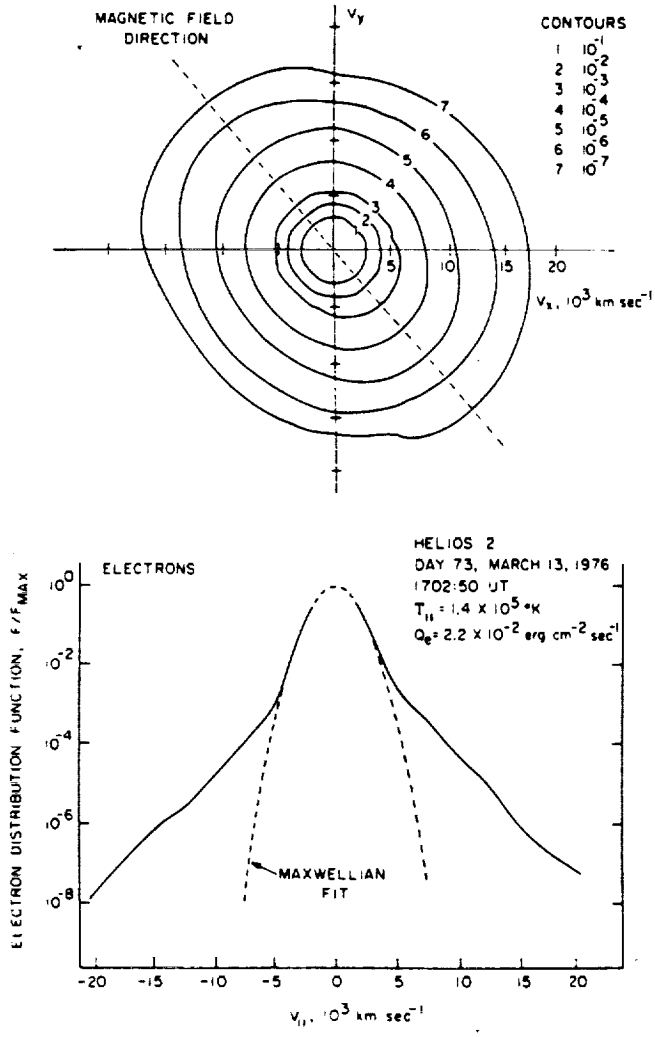

Fig. 9. The electron distribution function for the period of intense ion acoustic wave activity in Figure 6 at about 1702:50 UT on day 73. The only source of free energy evident in the electron velocity distribution which could drive the ion acoustic waves is the asymmetry due to the electron heat flux.

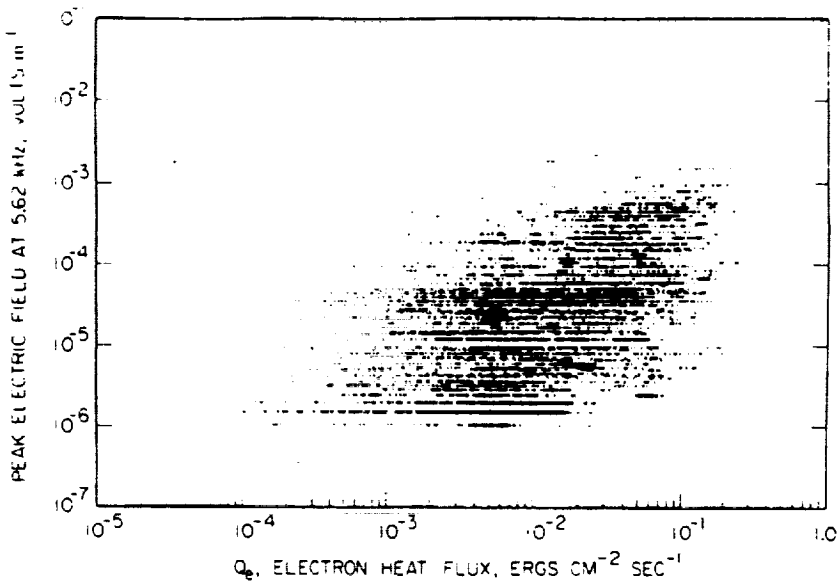

Fig. 10. A scatter plot of the ion acoustic wave electric field intensities as a function of the electron heat flux for the three solar rotations shown in Figures 2, 3, and 4. The electric field intensity shows a clear correlation with the heat flux, increasing with increasing Q_e.

function [*Forslund*, 1970; *Gary*, 1978*b*], the average electric field intensities have also been computed as a function of the normalized electron heat flux, $Q_e/n_e m_e V_{th}^3$, where V_{th} is the core electron thermal velocity. The results of this analysis are illustrated in Figure 11, which shows a rapid increase in the electric field intensities as the normalized electron heat flux increases. Of particular interest is the rapid increase in the electric field strength when the normalized heat flux exceeds about 0.1, which suggests an approximate threshold condition for the ion acoustic instability.

To investigate the possible relationship with the solar wind proton distributions, Figure 12 shows a representative proton distribution function selected from a period of intense ion acoustic wave activity. This distribution function is from about 1700:08 UT on day 73, nearly simultaneous with the electron distribution function in Figure 9. Since the plasma instruments on Helios measure the full three-dimensional distribution function of the solar wind protons, cuts and projections of the proton distribution function can be made in any desired plane. The top panel of Figure 12 shows a cross section of the proton distribution function in a plane containing the magnetic field and the spacecraft-sun line. The positive V_x axis is directed toward the sun, and the magnetic field direction is indicated by the dashed line. The bottom panel shows the reduced one-dimensional distribution function $F(V)$ obtained by integrating over velocities perpendicular to the magnetic field. Details of the procedures used to compute these distribution functions are given by *Marsch et al.* [1979].

As can be seen from Figure 12, the proton distribution function in the region where the intense ion acoustic waves are observed displays a marked asymmetry with respect to velocities parallel and antiparallel to the magnetic field. This asymmetry is caused by the presence of a double-proton stream of the type discussed by *Feldman et al.* [1973*a*, *b*] and *Rosenbauer et al.* [1977]. The secondary proton stream in this case has a velocity shift of about 80 km s^{-1} with respect to the main solar wind stream and a relative density of about 3%. Although the shoulder on the distribution function is caused by the secondary stream, the distribution function does not have a clearly resolved double peak, at least not within the velocity resolution of the instrument, which is about 30 km s^{-1}.

The fact that a double-proton stream is present in the region of intense ion acoustic waves is of considerable interest, since *Gary* [1978*a*] has proposed that these waves are caused by an 'ion-acoustic-like' instability driven by a double-ion beam. Whether or not the double-proton stream in Figure 12 can actually produce this instability is a question which will be discussed later. Observationally, detailed inspection of the proton distribution function for cases in which ion acoustic waves are present nearly always shows some evidence of a double-proton stream. However, in most cases the secondary proton stream is not resolved into a separate peak, but rather appears as a shoulder on the main proton distribution, as in Figure 12.

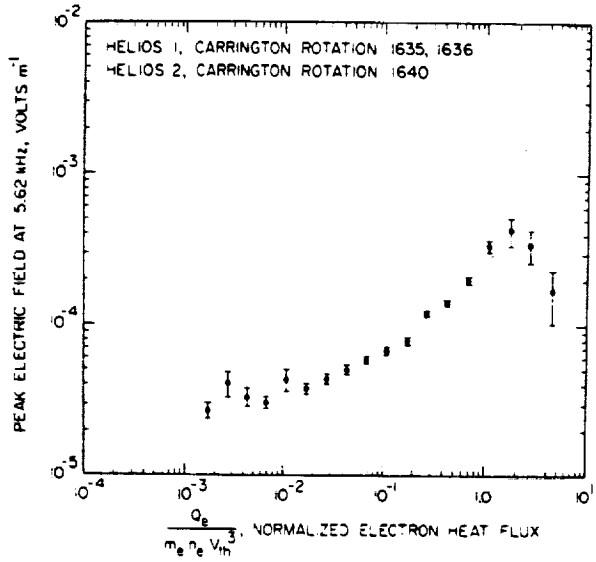

Fig. 11. The average of the peak 36-min electric field intensities as a function of the normalized electron heat flux, $Q_e/n_e m_e V_{th}^3$, where V_{th} is the electron thermal velocity. The error bars give the standard deviation of the average electron heat flux in each interval.

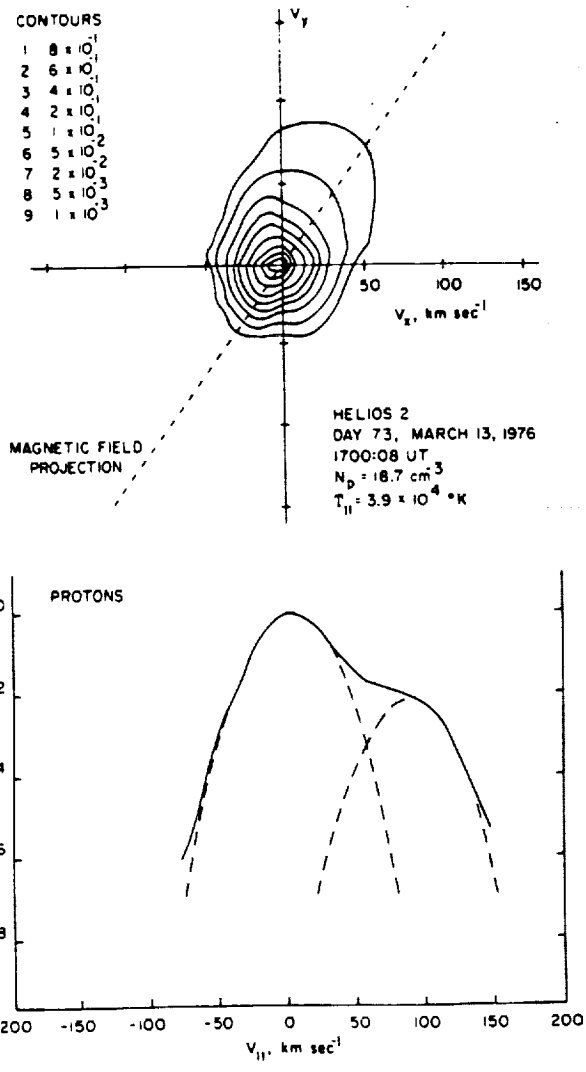

Fig. 12. The proton distribution function for the period of intense ion acoustic waves in Figure 6 at about 1700:08 on day 73, very close to the time for the electron spectrum in Figure 9. The large asymmetry in the reduced one-dimensional distribution function is caused by a double-proton stream. Double-proton streams of this type, usually consisting of a broad shoulder on the main solar wind proton distribution, are usually present in the regions where the ion acoustic waves are observed.

At the present time it is difficult to put the correlation with double-proton streams on a clear quantitative basis, since it is very time consuming and costly to compute individual stream parameters from the three-dimensional measurements for a large quantity of data, such as would be required for a detailed statistical analysis. To provide a rough quantitative indication of the level of correlation, we have compared the ion acoustic wave intensities with the one-dimensional fit parameter χ^2, which indicates how well the radial proton flux fits a Maxwellian velocity distribution. The main utility of the χ^2 parameter is that it is readily available for all of the plasma data and that any deviation from a simple Maxwellian, such as one due to a double-proton stream, is indicated by an increase in χ^2. The main disadvantages are that the fit parameter does not detect deviations from a Maxwellian in directions transverse to the radial direction and that other types of deviations, not attributable to double-proton streams, can affect χ^2. Practically, although a large χ^2 does not uniquely identify the presence of a double-proton stream, our experience from investigating individual cases is that a large χ^2, $\gtrsim 100$, provides a reasonably reliable indication of a double-proton stream. A plot of the average 5.62-kHz electric field intensities as a function of χ^2 is shown in Figure 13, using all of the available data. As can be seen, the electric field intensities show a moderately good correlation with χ^2, thereby indicating that double-proton streams are usually present when the ion acoustic wave intensities are large. The correlation of the ion acoustic wave intensities with double-proton streams also fits in well with the overall morphology of the ion acoustic wave activity, since, as is discussed by *Feldman et al.* [1973*b*], double-ion streams tend to occur in the low-velocity regions between high-speed streams, which is where the ion acoustic wave intensities are usually the largest. Although a correlation with double-proton streams clearly exists, it is still by no means certain that double-proton streams provide the free energy to generate the ion acoustic waves, since the double-peaked proton distribution required for the ion beam instability is usually not observed.

5. Summary and Discussion

In this paper we have investigated the relationship of interplanetary ion acoustic waves to the large-scale corotational structure of the solar wind and to various detailed plasma parameters. The results of this study show that the ion acoustic waves usually occur with the greatest intensity and frequency of occurrence in the low-speed regions immediately preceding the onset of a high-speed stream. Comparisons with the detailed plasma parameters show that the ion acoustic waves have a good correlation with the electron to proton temperature ratio, increasing in intensity by about a factor of 7 as the electron to proton temperature ratio increases from 1.0 to 10.0. The electron velocity distribution functions in the region where the ion acoustic waves occur are usually monotonic over a large range of energies and do not show any evidence of a double peak which could drive an electrostatic instability. The only source of free energy which can be identified in the

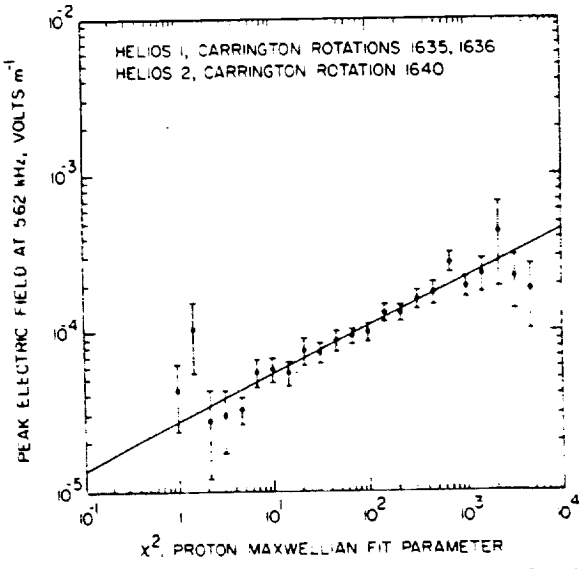

Fig. 13. The average ion acoustic wave intensities as a function of the Maxwellian fit parameter χ^2 for all of the available Helios 1 and 2 data. Large values of χ^2 indicate large deviations of the proton distribution from a Maxwellian, such as occur when a double-proton stream is present. The positive correlation between χ^2 and the ion acoustic wave intensities indicates that the ion acoustic waves tend to occur in regions where a double-proton stream is present.

electron velocity distribution function is the asymmetry caused by the electron heat flux. Detailed comparisons show that the ion acoustic wave intensities have a good correlation with the electron heat flux, increasing by about a factor of 10 as the normalized heat flux increases from 0.1 to greater than 1.0. The only source of free energy that can be identified in the proton distribution function is the occurrence of double-proton streams. Examination of the proton distribution function in the regions where the ion acoustic waves are observed usually shows evidence of a double-proton stream. Detailed statistical analyses also show a good correlation with the χ^2 parameter, which indicates the presence of a double-proton stream. The secondary proton stream is, however, almost never clearly resolved into a separate peak, but rather appears as a shoulder on the main solar wind proton distribution.

Although an extensive study has been undertaken to try to identify the primary features of the plasma distribution responsible for the solar wind ion acoustic waves, it has become increasingly clear that a combination of parameters controls the generation of these waves and that at the present time a definitive identification of the instability mechanism is probably not possible. One inherent problem is that because of the complex interdependence of the various solar wind parameters, it is very difficult with a statistical analysis to identify conclusively the relevant parameters that control the generation of these waves. Nonetheless, the results of this study do provide important limitations on the possible instability mechanisms and provide a quantitative basis for further theoretical analysis.

When the possible mechanisms for generating the ion acoustic waves are considered, there appear at the present time to be three general possibilities: (1) the waves are ion acoustic waves driven by the electron heat flux, as has been suggested by *Forslund* [1970]; (2) the waves are an ion-acoustic-like mode driven by a double-proton stream, as was suggested by *Gary* [1978*a*]; or (3) the waves are driven by a yet undetected feature of the velocity distribution function. The favorable and unfavorable features associated with each of these possibilities are now considered in detail.

The good correlation of the ion acoustic wave intensities with the electron heat flux and with T_e/T_p provides substantial support for the suggestion of *Forslund* [1970] that ion acoustic waves could be driven unstable in the solar wind by the electron heat flux. As was pointed out by *Gary* [1978*a*], the principal difficulty with the electron heat flux mechanism is that for typical values of T_e/T_p the relative drift velocity induced between the core electrons and the solar wind protons is too small to drive the ion acoustic instability. If we take favorable cases, such as the case in Figure 6 at about 1800 UT, where $T_e/T_p \simeq 10$, then it can be demonstrated that the ion acoustic mode is very close to instability. For example, by using the measured electron heat flux Q_e, the relative drift velocity v_{oc} between the core electrons and the solar wind protons can be estimated by using equation (4) of *Feldman et al.* [1975]:

$$Q_e = \frac{5}{2} n v_{oc} k T_e \left(\frac{T_h}{T_c} - 1 \right) \qquad (1)$$

where T_c and T_h are the electron core and halo temperature and k is the Boltzmann constant. Using the measured values of $Q_e = 2.2 \times 10^{-2}$ erg cm^{-2} s^{-1}, $T_c = 1.4 \times 10^5$ °K, and $T_h = 8.4 \times 10^5$ °K, (1) above gives $v_{oc} = 47$ km s^{-1}. Using the measured electron temperature of $T_e = 1.4 \times 10^5$ °K, the ratio of the relative drift velocity to the electron thermal speed is $v_{oc}/v_{th} = 3.2 \times 10^{-2}$. Using the plot of the critical drift velocity for electrostatic instability given by *Freid and Gould* [1961] and $T_e/T_i = 10$, it can be shown that the drift velocity is close to instability, within about a factor of 2. Thus in this case the electron heat flux mechanism provides a reasonable explanation for the observed.

However, in other cases, such as can be seen in Figure 6, ion acoustic waves with substantial intensities are still present when $T_e/T_p \simeq 1$. The observations of ion-acoustic-like waves at such low values of T_e/T_p represent a serious problem for the electron heat flux mechanism. Nonetheless, various possibilities exist for improving this situation which need to be further explored. For example, the proton temperatures in this study are a best fit to the entire proton distribution, including any double-proton stream contribution, and are therefore somewhat too large for purposes of computing the ion acoustic instability thresholds. Also, deviations of the proton distribution from a Maxwellian may occur in such a way as to reduce the proton Landau damping. Further consideration of these effects involves very detailed computer analyses using the measured distribution functions and will be discussed in a future paper [*Dum et al.*, 1979].

The frequent observation of double-proton streams in association with the solar wind ion acoustic waves also gives substantial support for the proposal of *Gary* [1978*a*] that these waves are produced by an electrostatic double-ion beam instability. However, detailed modeling calculations using the observed proton distribution functions show that it is difficult to satisfy the instability criterion for the ion beam mode. The basic reason for this difficulty is that the double-proton streams usually are not well enough resolved to produce a two-stream instability. Typically, the proton beam only appears as a shoulder on the main proton distribution as in Figure 12. The absence of a clearly defined double peak probably cannot by itself be taken as evidence against this mechanism, since the instrument resolution of about 30 km s^{-1} may in some cases smear out the minimum between the two peaks. Also, wave-particle interactions may act to fill in the minimum in such a way as to produce a marginally stable distribution. If we ignore the fact that the minimum usually does not exist and try to fit observed proton distributions to two Maxwellians, some rough comparisons can be made with Gary's instability threshold calculations. For example, the two Maxwellian distributions indicated by the dashed lines in Figure 10 give a ratio of the beam density to the main stream density of $n_b/n_m = 0.03$, a ratio of the beam temperature to the main stream temperature of $T_b/T_m = 1.1$, a ratio of the electron temperature to the main proton stream temperature of $T_e/T_m = 6.67$, and a ratio of the beam velocity to the main stream thermal velocity of $V_o/V_m = 3.0$. Comparison of these parameters with the ion beam instability calculations in Figure 4 of *Gary* [1978*a*] shows that the ion beam mode should be stable for these conditions. These results are in agreement with the recent comparisons of *Lemons et al.* [1979], in which it was also concluded that the ion beam mode is stable, although not by a large factor. The main advantage of the ion beam instability in comparison to the electron heat flux instability is that for a given T_e/T_p the ion beam instability can occur at a lower relative drift speed between the core electrons and the main proton stream. In this sense, the ion beam mode seems to offer the best possibility for explaining the existence of these waves, although the detailed reasons for the discrepancy in the instability threshold are not understood. Many possible explanations for the observed discrepancies can be offered, including, for example, the occurrence of small-scale spatial irregularities in the proton distribu-

tion function which cannot be resolved or large velocity space irregularities in the beam which cannot be detected by the plasma analyzer.

Because of the uncertainties in establishing the mechanism responsible for the interplanetary ion acoustic waves, other possible sources of free energy should be mentioned which could possibly be responsible for these waves. One possible nonthermal effect which could have escaped observation by Helios is the low-energy ($5 \lesssim E \lesssim 50$ keV) protons observed by *Frank* [1970] in the interplanetary medium. These suprathermal proton streams occur sporadically for periods of a few days every few weeks, with a frequency of occurrence comparable to the solar wind ion acoustic waves. The possibility that such proton streams could cause the interplanetary ion acoustic waves is also supported by the fact that somewhat similar proton streams from the earth's bow shock, although of higher intensity, are known to produce waves similar to the ion acoustic waves detected by Helios far from the earth [*Gurnett and Frank*, 1978]. Waves of this type have also been observed by Voyager in association with interplanetary shocks [*Kurth et al.*, 1979]. Since Helios does not have instrumentation suitable for detecting protons in this energy range ($5 \lesssim E \lesssim 50$ keV), nothing is currently known about the possible association of the ion acoustic waves with these low-energy proton streams.

In conclusion, the results of this study provide support for both the electron heat flux and the double-ion beam mechanisms for generating the solar wind ion acoustic waves, although each mechanism has problems under certain conditions, particularly for low values of T_e/T_p. The positive correlation with T_e/T_p and the electron heat flux is expected for both the electron heat flux and double-ion mechanisms. The main difficulty with the double-ion beam mechanism is that the proton distributions usually do not have the clearly resolved double peak required for instability. This difficulty could be the result of insufficient velocity or spatial resolution to resolve the two peaks. It is also possible that more than one mechanism could be operative in the solar wind to produce these waves. From the electric field measurements alone it is impossible to distinguish between the various mechanisms which can produce electrostatic waves propagating parallel to the magnetic field with wavelengths near $2\pi\lambda_D$, since the large Doppler shifts essentially destroy all information on the frequency spectrum in the rest frame of the plasma. It is hoped that in the future, more detailed studies of the plasma distribution functions, and their implications with regard to the various instability mechanisms, will provide a definitive determination of the plasma instability mechanism responsible for these waves.

Acknowledgments. The authors would like to express their appreciation to C. Dum and P. Gary for their helpful comments and suggestions during the preparation of this manuscript and to R. Anderson, K. Muhlhauser, and G. Voots for their assistance in the data analysis. We also thank F. Neubauer from the Technischen Universitat Braunschweig for providing the magnetic field data used in this study. The research at the University of Iowa was supported by NASA under contract NAS5-11279 and grant NGL-16-001-043. The research at the Max-Planck-Institut was supported by the Deutsches Bundeministerium für Forschung und Technologie.

The Editor thanks R. W. Fredricks and D. S. Lemons for their assistance in evaluating this paper.

REFERENCES

Buneman, O., Instability, turbulence and conductivity in a current-carrying plasma, *Phys. Rev. Lett.*, *1*, 8, 1958.

Dum, C. T., E. Marsch, W. Pilipp, and D. A. Gurnett, Ion sound turbulence in the solar wind, in *Solar Wind 4*, Springer, New York, in press, 1979.

Feldman, W. C., J. R. Asbridge, S. J. Bame, and M. D. Montgomery, Double ion streams in the solar wind, *J. Geophys. Res.*, *78*, 2017, 1973*a*.

Feldman, W. C., J. R. Asbridge, S. J. Bame, and M. D. Montgomery, On the origin of solar wind proton thermal anisotropy, *J. Geophys. Res.*, *78*, 6451, 1973*b*.

Feldman, W. C., J. R. Asbridge, S. J. Bame, M. D. Montgomery, and S. P. Gary, Solar wind electrons, *J. Geophys. Res.*, *80*, 4181, 1975.

Forslund, D. W., Instabilities associated with the heat conduction in the solar wind and their consequences, *J. Geophys. Res.*, *75*, 17, 1970.

Frank, L. A., On the presence of low-energy protons ($5 \lesssim E \lesssim 50$ keV) in the interplanetary medium, *J. Geophys. Res.*, *75*, 707, 1970.

Freid, B. D., and R. W. Gould, Longitudinal ion oscillations in a hot plasma, *Phys. Fluids*, *4*, 139, 1961.

Gary, S. P., Ion-acoustic-like instabilities in the solar wind, *J. Geophys. Res.*, *83*, 2504, 1978*a*.

Gary, S. P., Electrostatic heat flux instabilities, *J. Plasma Phys.*, *20*, 47, 1978*b*.

Gosling, J. T., J. R. Asbridge, S. J. Bame, and W. C. Feldman, Solar wind interfaces, *J. Geophys. Res.*, *71*, 1401, 1978.

Gurnett, D. A., and R. R. Anderson, Plasma wave electric fields in the solar wind: Initial results from Helios 1, *J. Geophys. Res.*, *82*, 632, 1977.

Gurnett, D. A., and L. A. Frank, Ion acoustic waves in the solar wind, *J. Geophys. Res.*, *83*, 58, 1978.

Hundhausen, A. J., *Coronal Expansion and Solar Wind*, Springer, New York, 1972.

Kurth, W. S., D. A. Gurnett, and F. L. Scarf, High-resolution spectrograms of ion acoustic waves in the solar wind, *J. Geophys. Res.*, *84*, in press, 1979.

Lemons, D. S., J. R. Asbridge, S. J. Bame, W. C. Feldman, S. P. Gary, and J. T. Gosling, The source of electrostatic fluctuations in the solar wind, *J. Geophys. Res.*, *84*, this issue, 1979.

Marsch, E., W. Pilipp, H. Rosenbauer, R. Schwenn, K.-H. Mühlhäuser, Characteristics of the three-dimensional proton distribution in the solar wind observed by Helios between 0.3 and 1 AU, in *Solar Wind 4*, Springer, New York, in press, 1979.

Rosenbauer, H., R. Schwenn, E. Marsch, B. Meyer, H. Miggenrieder, M. D. Montgomery, K. H. Mühlhäuser, W. Pilipp, W. Voges, and S. M. Zink, A survey on initial results of the Helios plasma experiment, *Z. Geophys.*, *42*, 561, 1977.

Schwenn, R., H. Rosenbauer, and H. Miggenrieder, Das Plasmaexperiment auf Helios (E1), *Raumfahrtforschung*, *19*(5), 226, 1975.

Stix, T. H., *The Theory of Plasma Waves*, McGraw-Hill, New York, 1962.

(Received October 19, 1978;
revised January 4, 1979;
accepted January 4, 1979.)

PLASMA OSCILLATIONS AND THE EMISSIVITY OF TYPE III RADIO BURSTS

D. A. Gurnett, R. R. Anderson and R. L. Tokar
Department of Physics and Astronomy
The University of Iowa
Iowa City, Iowa 52242

ABSTRACT

Plasma wave electric field measurements with the solar orbiting Helios spacecraft have shown that intense electron plasma oscillations occur in association with type III solar radio bursts, thereby confirming a well known mechanism for generating solar radio emissions first proposed by Ginzburg and Zheleznyakov in 1958. In this paper we review the principal characteristics of these plasma oscillations and compare the observed plasma oscillation intensities with recent measurements of the emissivity of type III radio bursts. The observed emissivities are shown to be in good agreement with two current models for the conversion of electrostatic plasma oscillations to electromagnetic radiation.

INTRODUCTION

As known from early studies of Wild [1950] type III radio bursts are produced by particles ejected from a solar flare and are characterized by an emission frequency which decreases with increasing time. The decreasing emission frequency with increasing time is attributed to the decreasing electron plasma frequency, f_p, encountered by the solar flare particles as they move outward through the solar corona. Emission can occur at either the fundamental, f_p, or harmonic, $2f_p$, of the local electron plasma frequency, although at low frequencies, $\lesssim 1$ MHz, the harmonic emission appears to be the dominant component [Fainberg, 1974; Kaiser, 1975; Gurnett et al., 1978]. The particles responsible for the type III radio emissions are electrons with energies ranging from a few Kev to several tens of Kev. According to current ideas, the generation of the type III radiation is a two-step process in which (i) electron plasma oscillations are first produced at f_p by a two-stream instability excited by the solar flare electrons and (ii) the plasma oscillations are converted to electromagnetic radiation by nonlinear wave-particle interactions. This mechanism, first proposed by Ginzburg and Zheleznakov [1958] and refined by numerous investigators [Tidman et al., 1966;

M.R. Kundu and T.E. Gergely (eds.), Radio Physics of the Sun, 369-379.

Kaplan and Tystovich, 1968; Papadopoulos et al., 1974; Smith, 1977], is illustrated in Figure 1, which shows the expected conversion of the electron stream energy to electron plasma oscillations, and the subsequent conversion to electromagnetic radiation at either the fundamental, f_p^-, or the harmonic, $2f_p^-$. The radiation at the fundamental is caused by interactions of the plasma oscillations with ion sound waves, and the radiation at the harmonic is caused by interactions between oppositely propagating electron plasma oscillations.

Since electron plasma oscillations are local plasma wave phenomena which cannot be detected remotely, in situ measurements must be used to confirm the presence of these oscillations. The first observations of electron plasma oscillations associated with a type III solar radio burst were obtained by Gurnett and Anderson [1976, 1977] using measurements from the Helios 1 and 2 spacecraft which are in orbit around the sun between about 0.3 to 1.0 A.U. The Helios observations are important not only because they confirm a basic radio emission mechanism proposed over twenty years ago, but also because they provide important new information on nonlinear plasma processes of considerable current interest. In this paper we review the principal results of the Helios plasma oscillation observations, including many new events which have been recently detected. The plasma oscillation intensities are also compared with the recent type III radio emissivity measurements given by Tokar and Gurnett [1979], to provide a quantitative evaluation of proposed emission mechanisms.

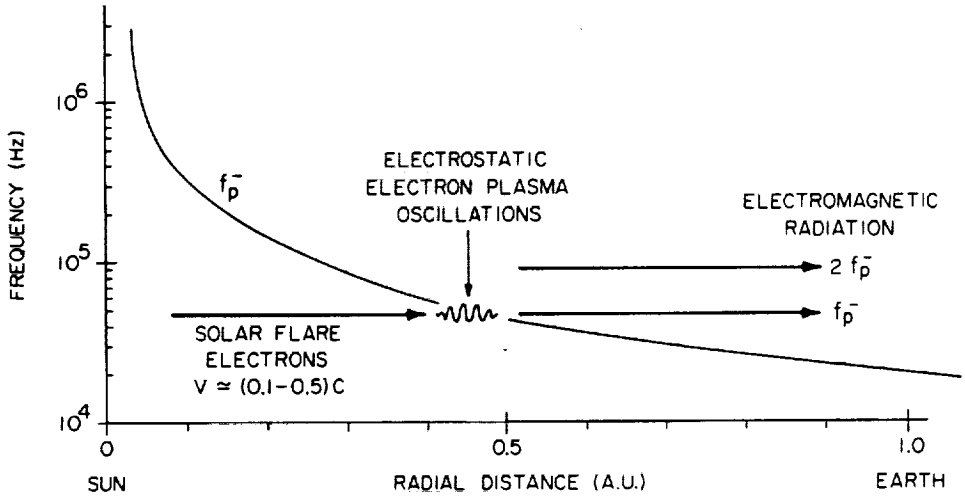

Figure 1. A representative radial profile of the electron plasma frequency in the solar wind illustrating the generation of electron plasma oscillations and the subsequent conversion to electromagnetic radiation at f_p^- and $2f_p^-$.

SURVEY OF PLASMA OSCILLATION CHARACTERISTICS

Only a small fraction, approximately 15%, of all the type III radio bursts detected by Helios can be associated with electron plasma oscillations. The relatively small occurrence of plasma oscillation events is almost certainly due to the fact that the radio emissions can be detected at large distances from the source, whereas the plasma oscillations can only be detected within the source region. Up to the present time a total of ninety electron plasma oscillation events have been identified in all the data available, which includes Helios 1 and 2, Voyager 1 and 2, and IMP 8. All but four of these events were detected by Helios 1 and 2.

A plasma oscillation event illustrating most of the features commonly observed is shown in Figure 2. The type III radio emission can be clearly identified in the 178 and 100 KHz channels by the rapid smooth rise to peak intensity followed by a somewhat longer smooth decay. The characteristic shift toward decreasing frequency with increasing time is also clearly evident. The intense narrow-band emissions in the 56.2 KHz channel, starting at about 1023 UT and ending about 1055 UT, are the associated electron plasma oscillations. The solid line is the peak

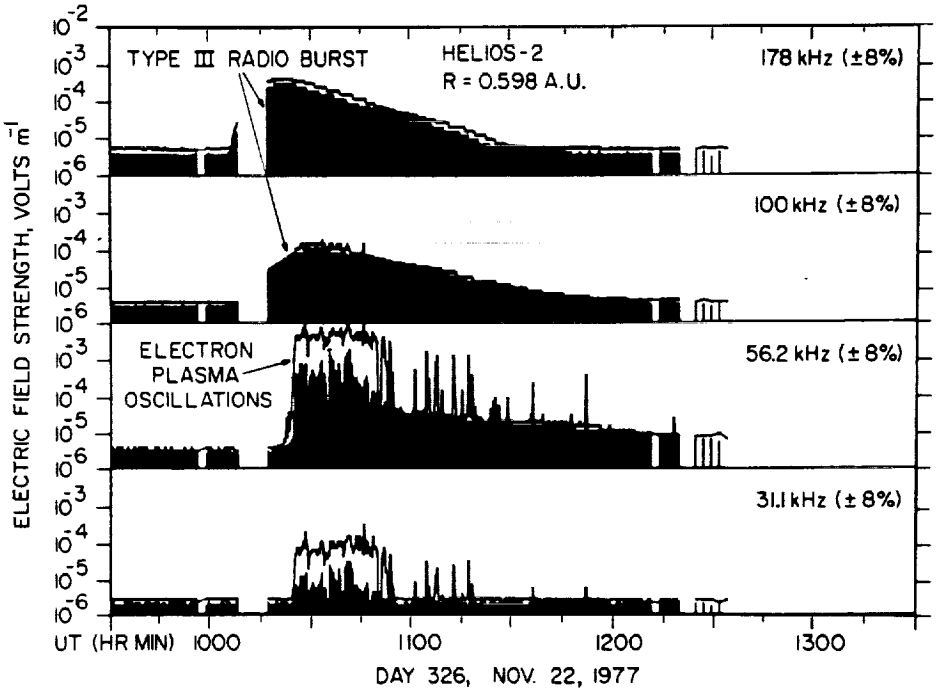

Figure 2. Intense electron plasma oscillations at $f_p \approx 56$ kHz detected by Helios 2 in association with a type III radio burst.

electric field intensity and the solid dark area is the average electric field intensity. As can be seen the peak electric field intensity is much larger than the average electric field intensity indicating that the plasma oscillations are extremely impulsive, consisting of many short intense bursts. High time resolution measurements show that the bursts often occur on time scales approaching the time resolution of the instrument, which is about 50 msec. The occurrence of such short bursts has been suggested as indicating the presence of strong turbulence processes such as soliton collapse, which would occur on spatial scales of only a few Debye lengths [Nicholson et al., 1978]. Unfortunately, structures with such a small spatial scale are swept by the spacecraft on a time scale less than 1 msec., which is too small to be resolved by the Helios instrumentation. Therefore no definitive statement can be made concerning the possible occurrence of solitons from the Helios observations. Although the plasma oscillations are very impulsive, it is interesting to note that the peak amplitudes in Figure 2 remain very nearly constant at a level of about 3 to 5 mVm^{-1} for nearly half an hour. Not all events display this flat top characteristic; however it occurs sufficiently often to suggest that the plasma oscillation intensities are being limited by some nonlinear saturation mechanism.

To investigate the variation in the electron plasma oscillation intensities with radial distance from the sun, the maximum electric field strength for each of the ninety events currently available for analysis is shown as a function of heliocentric radial distance in Figure 3. This plot is an update of an earlier report by Gurnett et al. [1978] with a substantial increase in the number of data points, mainly due to the greatly increased solar activity in the last year and one half, as solar maximum approaches. Figure 3 clearly shows that the electric field strength of the plasma oscillations decreases with increasing radial distance from the sun. The best fit power law through all of the data points is shown by the dashed line. The current best estimate for the power law index is -1.4 ± 0.5. This index has changed substantially from the earlier results of Gurnett et al. [1978] as more events have been analyzed. The trend toward decreasing plasma oscillation intensity with increasing radial distance from the sun is consistent with the expected radial variation of the saturation field strength. If the electric field to plasma energy density ratio, $E^2/8\pi nkT$, at saturation is constant, then E should vary approximately as $(1/R)^{1.14}$, since the electron density, n, varies as $(1/R)^2$ and the temperature, T, varies as $(1/R)^{2/7}$ [Hundhausen, 1972]. A representative maximum value for $E^2/8\pi nkT$, shown by the solid line at the top of Figure 3, is about 2×10^{-5}.

COMPARISON WITH TYPE III EMISSIVITIES

To compare the plasma oscillation intensities in Figure 3 with existing theories, it is necessary to determine the typical emissivity of a type III radio burst, particularly in the radial distance range

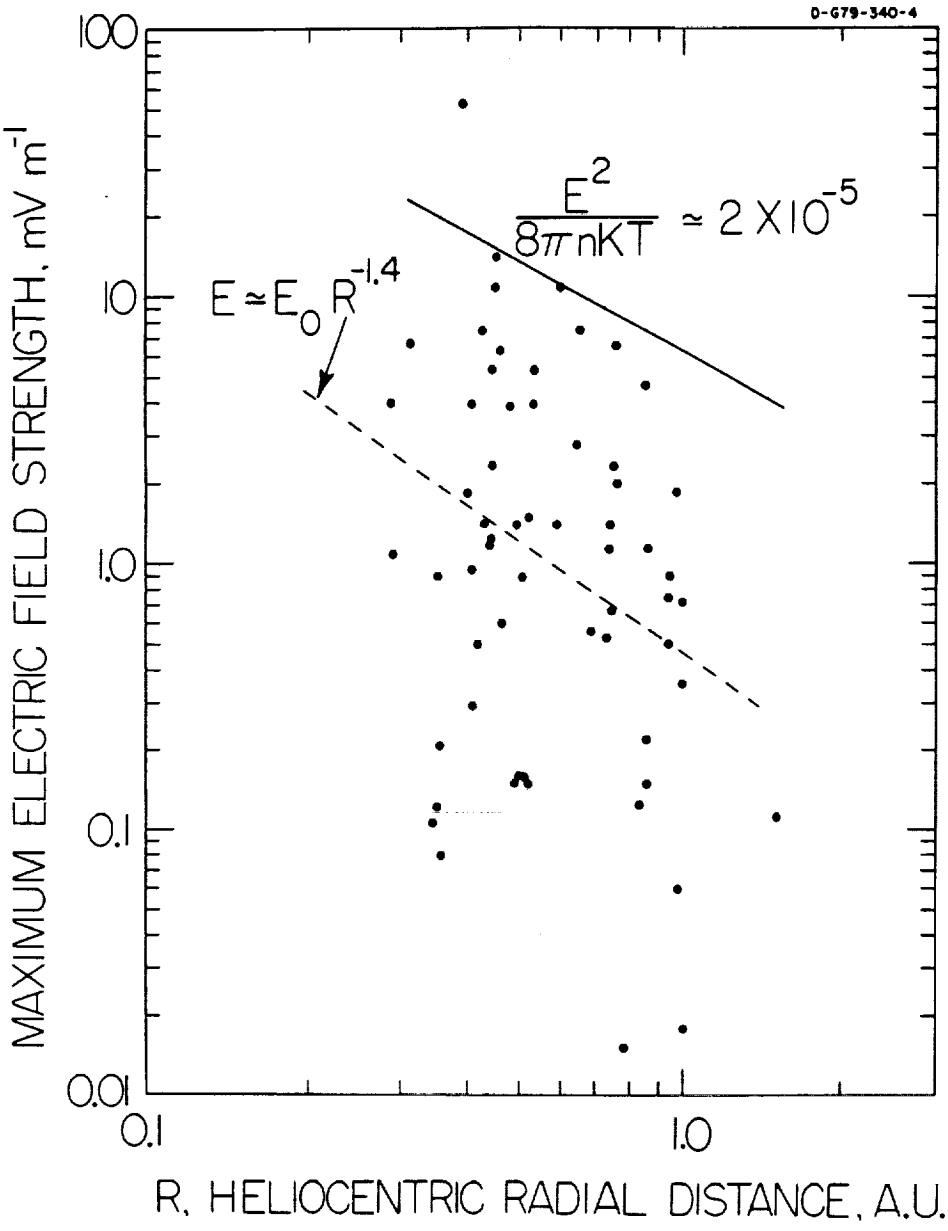

Figure 3. A plot of the peak electric field strength for all of the plasma oscillation events with type III bursts detected to date as a function of radial distance from the sun.

from about 0.3 to 1.0 A.U. where in situ measurements of plasma observations are available. In principle, a comparison of the radial variation of the plasma oscillation intensities and the type III emissivity provides a powerful test, since any given mechanism implies a specific relationship between these two parameters. Recently Tokar and Gurnett [1979] have completed an analysis of the radial variation of the emissivity of low frequency type III radio bursts. The technique used consists of computing the power ΔP emitted in volume ΔV with the emissivity defined as $J(2f_p) = \Delta P/4\pi\Delta V$, where it is assumed, for simplicity, that the radiation is emitted isotropically over a solid angle of 4π. The power is computed from $\Delta P = 4\pi r^2 I \Delta f$, where r is the distance from the source to the spacecraft, Δf is the bandwidth and I is the power flux, in watts $m^{-2}Hz^{-1}$, at the spacecraft. The volume is computed from $\Delta V = R^2 \Delta R \Omega$, where Ω is the solid angle of the emitting region as viewed from the sun. Since it is usually not possible to directly determine Ω, we have assumed that the source subtends a half-angle of 45.0° as viewed from the sun, which is consistent with the results of Baumback et al. [1976]. The center of the source volume is assumed to follow the magnetic field line through the originating flare location using the magnetic field model of Parker [1958] with a solar wind velocity of 400 km s^{-1}. The emission frequency is assumed to be at the harmonic of plasma frequency, following the radial variation given by Fainberg and Stone [1974]. The results of this analysis, as applied to thirty-six type III radio bursts, are shown in Figure 4. Because of the uncertainty in the solid angle Ω the absolute value of J probably has a substantial uncertainty, perhaps as much as a factor of 2 or 3. This uncertainty is, however, small compared to the variations from event to event. Except for certain special cases, for example when the source passes close to the spacecraft, the radial dependence tends to be rather independent of the assumptions used. In all cases the emissivity decreases monotonically with increasing radial distance from the sun and a power law provides a good fit to the radial variation. The average power law index for all of the events analyzed is -6.0 ± 0.3. The best fit power law through all of the data points is shown by the dashed curve in Figure 4.

Having established the radial dependence and absolute intensity of both the plasma oscillations and the radio emissivity, comparisons can now be made with specific models for the generation of type III radio bursts. Two models will be evaluated, the coherent parametric (oscillating two-stream) mechanism of Papadopoulos et al. [1974], and the incoherent induced scattering mechanism of Smith [1977]. The emissivity given by Papadopoulos et al. [1974], converted to MKS units and evaluating constants (using $\alpha = 0.1$), is

$$J(2f_p) = 5.83 \times 10^{-15} \left(\frac{T}{T_o}\right)^{3/2} \frac{E^4}{\sqrt{n}}, \text{ watts } m^{-3}sr^{-1}, \qquad (1)$$

where E is the electric field strength of the plasma oscillations in Volts m^{-1}, n is the electron density in cm^{-3}, T is the electron

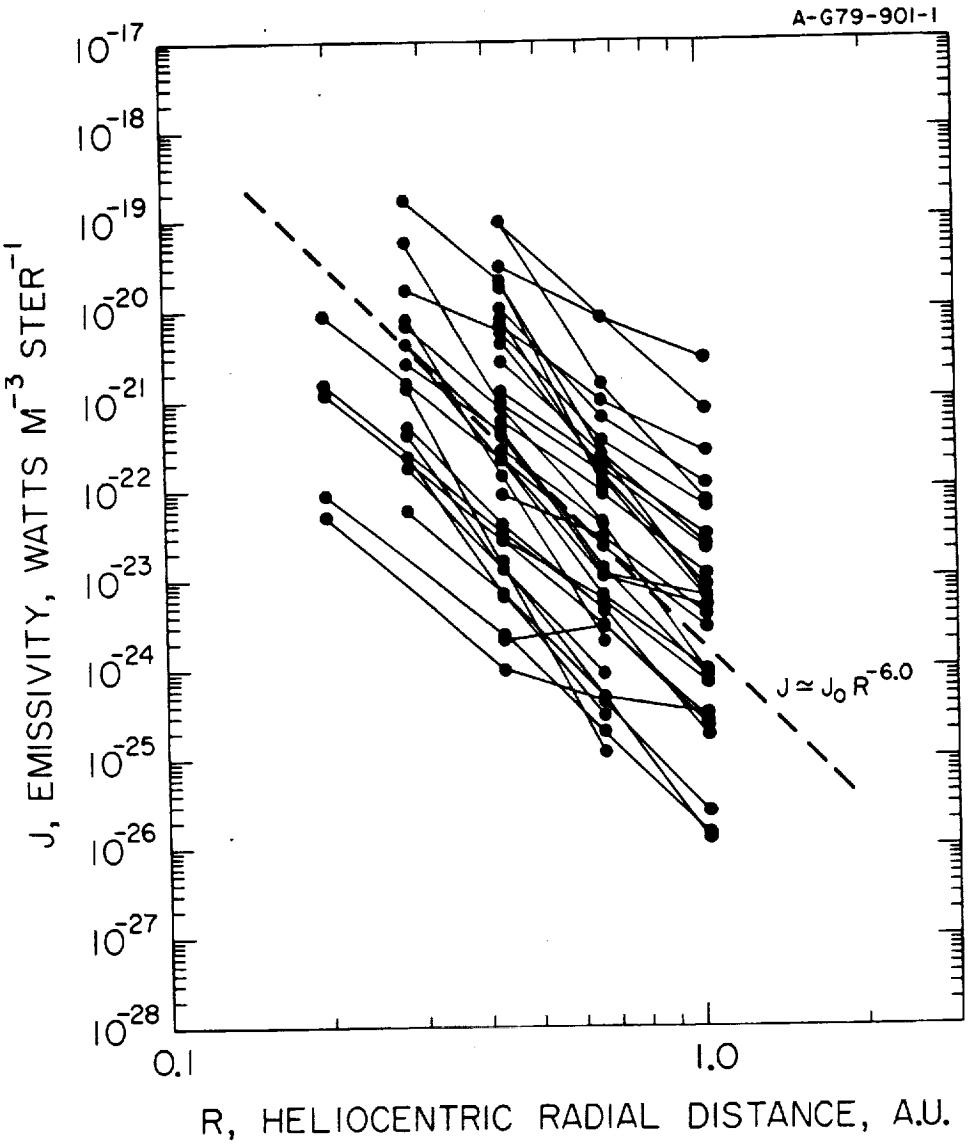

Figure 4. The emissivity as a function of radial distance from the sun determined from thirty-six type III radio bursts detected by IMP 8 and ISEE 1.

temperature in ^{o}K, and T_o is the electron temperature at 1 A.U., $\sim$1.2 X 10^{5}^{o}K. The corresponding emissivity given by Smith [1977] is

$$J(2f_p^-) = 1.12 \times 10^{-13} \frac{E^4}{\sqrt{n}}, \text{ watts } m^{-3}sr^{-1}, \qquad (2)$$

where E is again in Volts m^{-1}, and n is in cm^{-3}. Both the coherent and incoherent mechanisms have essentially the same dependence on the electric field strength and electron density, and differ only slightly in the temperature dependence. As can be seen the dominant dependence, by far, is on the electric field strength of the plasma oscillations. Since the electron density and temperature in the solar wind vary as $n \sim (1/R)^2$ and $T \sim (1/R)^{2/7}$, and since J varies as $(1/R)^{6.0 \pm 0.3}$, the expected radial variation of E from Equation 1 for the model of Papadopoulos et al. [1974] should be $(1/R)^{1.64 \pm 0.1}$. For the model of Smith [1977] the corresponding radial variation of E from Equation 2 should be $(1/R)^{1.75 \pm 0.1}$. Both of these predictions compare very favorably with the observed radial variation for E of $(1/R)^{1.4 \pm 0.5}$.

In addition to comparing the radial variations with the theoretical predictions the absolute values of the emissivity can also be compared. From Figure 3 it is seen that the largest plasma oscillation field strength at 1 A.U. is about $E \approx 5$ mVm^{-1}. Using this maximum field strength, the corresponding emissivities given by Papadopoulos et al. [1974], using Equation 1, and Smith [1977], using Equation 2, are 1.63×10^{-24} and 3.13×10^{-23} watts $m^{-3}sr^{-1}$, respectively. Comparing these emissivities with Figure 4 it is seen that the emissivity computed from Smith's model would be able to account for about 85% of all the events observed at 1.0 A.U., whereas Papadopoulos' model would be able to account for only about 30% of the events observed. Thus, it appears that for the largest plasma oscillation intensities observed the incoherent model of Smith [1977] is able to account for the emissivity of all but the most intense radio bursts, whereas the model of Papadopoulos et al. [1974] is not able to account for a burst of average intensity. It should also be pointed out that Smith [1977] has already demonstrated in a specific case that the incoherent mechanism can account for the simultaneously observed radio emission intensities with a substantial margin. The case considered by Smith [1977] was, however, a particularly intense plasma oscillation event, with an intensity (14.8 mVm^{-1}) near the upper limits of the events shown in Fig 3. If instead of taking the most intense plasma oscillation event, one takes more typical intensities representative of, for example, the best fit power law (dashed line) in Figure 3, then the emissivity is drastically reduced because of the E^4 dependence in Equations 1 and 2. For these more typical plasma oscillation intensities, both the models of Papadopoulos et al. [1974] and Smith [1977] give emissivities well below the best fit curve (dashed line) shown in Figure 4. These difficulties are further complicated by the fact that the actual volume of the source is probably substantially smaller than has been assumed in Equations 1 and 2 because of the impulsive variations in the amplitude of the plasma oscillations. In summary it appears that the radial variation of the plasma oscillation intensities and type III emissivity are in good agreement with the current theoretical models but that in all except for the most intense plasma oscillation events the emissivity given by the theory is somewhat smaller than the observed emissivity. Several explanations can be advanced to account for this discrepancy in the absolute emissivity. Probably

the most likely possibility is that the plasma oscillations have substantial temporal fluctuations on a time scale short compared to the 50 msec. averaging time of the Helios instrument. If the fluctuations are very impulsive, as seems to be the case, then because of the E^4 dependence of the emissivity the radiation intensity may be substantially underestimated on the basis of the average electric field intensity. Another possibility is that the intense plasma oscillations are confined to very small spatial regions which are very unlikely to be encountered by the spacecraft, thereby tending to bias the electric field intensity measurements, as in Figure 3, more heavily toward lower intensities.

CONCLUSION

These comparisons of plasma oscillation intensities and the emissivity of type III radio bursts show good overall agreement with current theories for the conversion of electron plasma oscillations to electromagnetic radiation at $2f_p$. The primary questions remaining involve the fine time scale structure of the plasma oscillations and the relative importance of incoherent and coherent (soliton collapse) processes. Although the absolute emissivities computed in this study tend to favor the incoherent process, it is probably not possible to determine which mechanism is most important because of the uncertainty about the fine time scale variations in the plasma oscillation intensity. Further progress in understanding the possible role of soliton collapse processes in the generation of type III radio emissions will require much higher time resolution measurements than are currently available.

ACKNOWLEDGEMENTS

The authors wish to thank Drs. D. Smith and D. Papadopoulos for their assistance in the interpretation of these results, and A. Persoon for her help in analyzing the data. This research was supported by NASA through Grant NGL-16-001-043 and Contracts NAS5-11279, NAS5-11431, and NAS5-20093 with the University of Iowa. Part of this research was also conducted while one of us (D. Gurnett) was on leave at the Institute of Geophysics and Planetary Physics, University of California, Los Angeles.

REFERENCES

Baumback, M.M., Kurth, W.S., and Gurnett, D.A.: 1976, Solar Phys. 48, p. 361.
Fainberg, J., and Stone, R.G.,: 1974, Space Sci. Rev. 16, p. 145.
Ginzburg, V.L., and Zheleznyakov, V.V.: 1958, Sov. Astron. AJ2, p. 653.
Gurnett, D.A., Baumback, M.M., and Rosenbauer, H.: 1978, J. Geophys. Res. 83, p. 616.
Gurnett, D.A., and Anderson, R.R.: 1976, Science 194, p. 1159.

Gurnett, D.A., and Anderson, R.R.: 1977, J. Geophys. Res. 82, p. 632.
Hundhausen, A.J.: 1972, Coronal Expansion and Solar Wind, Springer, Berlin Heidelberg N. York, p. 58.
Kaiser, M.L.: 1975, Solar Phys. 45, p. 181.
Kaplan, S.A., and Tsytovich, V.N.: 1968, Sov. Astron. AJ 11, p. 956.
Nicholson, D.R., Goldman, M.V., Hoyng, P., and Weatherall, J.C.: 1978, Ap. J. 223, p. 605.
Papadopoulos, K., Goldstein, M.L., and Smith, R.A.: 1974, Astrophys. J. 190, p. 175.
Parker, E.N.: 1958, Ap. J. 128, p. 664.
Smith, D.F.: 1970, Adv. Astr. Ap. 7, p. 147.
Smith, D.F.: 1977, Astrophys. J. 216, p. L53.
Tidman, D.A., Birmingham, T.J., and Stainer, H.M.: 1966, Astrophys. J. 146, p. 207.
Tokar, R.L., and Gurnett, D.A.: 1979, J. Geophys. Res., submitted for publication.
Wild, J.P.: 1950, Aust. J. Sci. Ser. A3, p. 541.

DISCUSSION

Stewart: Type II bursts show both fundamental and second harmonic structure at kilometric wavelengths. Your observation that the plasma waves are delayed with respect to the radio waves supports, as you say, the hypothesis that fundamentals also occur in type III bursts at kilometric wavelengths, despite what the theorists say.

Gurnett: We can't resolve the fundamental and the second harmonic on the basis of the radio data alone at these frequencies because of the dispersion in time of the emission.

Stewart: Is the radio emission coming from the same place?

Gurnett: Well of course at higher frequencies its coming in closer to the sun and its source is moving out and the situation is that plasma oscillations usually start about the time the radio emission frequency approaches the local plasma frequency. Definitely after the time where it passes the second harmonic.

Stone: Not all information suggesting second harmonic radiation at long wavelengths comes from direction finding. Indeed we can make direct comparisons between the in situ plasma density measurements. We find in all cases looked at thus far that the radio emission is observed at $2f_p$. There is a wealth of other observational data to support the second harmonic radiation. Moreover some isolated cases of fundamental have also been reported.

Gurnett: Let me say that I personally have done direction finding measurements in two spacecrafts that also seem to confirm that emission is coming from the second harmonic. Perhaps in these cases we are right near the source so that we can begin to see the fundamental; its a puzzle I really don't know the answer to this question.

Benz: I have some interest in your observation of ion-acoustic waves since we postulate them in our type I model. What is the energy density of these waves you see in interplanetary space? What do you suggest as their origin?

Gurnett: The plasma energy density is about 10^{-6} to 10^{-7} the electric field energy density or the magnetic field energy density. The question of why they are there is a very puzzling one. There are two theories on this. One is that they are driven by the electron heat flux in the solar wind and of course the real issue is the electron-ion temperature ratio and I have shown that these ion acoustic waves are correlated with the T_e/T_i and tend to occur in regions that have rather high T_e/T_i. The other model is that they are driven by ion streams in the solar wind.

JOURNAL OF GEOPHYSICAL RESEARCH, VOL. 85, NO. A5, PAGES 2227-2242, MAY 1, 1980

Interplanetary Particles and Fields, November 22 to December 6, 1977: Helios, Voyager, and Imp Observations Between 0.6 and 1.6 AU

L. BURLAGA,[1] R. LEPPING,[1] R. WEBER,[1] T. ARMSTRONG,[2] C. GOODRICH,[3] J. SULLIVAN,[3] D. GURNETT,[4] P. KELLOGG,[5] E. KEPPLER,[6] F. MARIANI,[7] F. NEUBAUER,[8] H. ROSENBAUER,[9] AND R. SCHWENN[9]

In the period November 22 to December 6, 1977, three types of interplanetary flows were observed: a corotating stream, a flare-associated shock wave, and a shock wave driven by ejecta. Helios 2, Imp 7, 8, and Voyager 1, 2 were nearly radially aligned at ≈0.6, 1, and 1.6 AU, respectively, while Helios 1 was at ≈0.6 AU and 35° east of Helios 2. The instruments on these spacecraft provided an exceptionally complete description of the particles and fields associated with the three flows and corresponding solar events. Analysis of these data revealed the following results. (1) A corotating stream associated with a coronal hole was observed at 0.6 and 1 AU, but not at 1.6 AU. The stream interface corotated and persisted with little change in structure even though the stream disappeared. A forward shock was observed ahead of the interface and moved from Helios 2 at 0.6 AU to Voyager 1, 2 and 1.6 AU; although the shock was ahead of a corotating stream and interface, the shock was not corotating, because it was not seen at Helios 1, probably because the corotating stream was not stationary. (2) An exceptionally intense type III burst was observed in association with a 2B flare of November 22. The exciter of this burst (a beam of energetic electrons) and plasma oscillations (presumably caused by the electron beam) were observed by Helios 2. (3) A nonspherical shock was observed in association with the November 22 flare. This shock interacted with another shock between 0.6 and 1 AU, and they coalesced to form a single shock that was identified at 1 and at 1.6 AU. (4) A shock driven by ejecta was studied. In the ejecta the density and temperature were unusually low, and the magnetic field intensity was relatively high. This region was preceded by a directional discontinuity at which the magnetic field intensity dropped appreciably. The shock appeared to move globally at a uniform speed, but locally, there were fluctuations in speed and direction of up to 100 km/s and 40°, respectively. (5) Three types of electrostatic waves were observed at the shocks, in different combinations. The detailed wave profiles differed greatly among the shocks, even for spacecraft separations of ≤0.2 AU, indicating a strong dependence on local conditions. However, the same types of fluctuations were observed at 0.6 and at 1.6 AU. (6) Energetic (50–200 keV) protons were accelerated by the shocks. The intensities and durations of the fluxes varied by a factor of 12 over longitudinal distances of ≈0.2 AU. The intensities were higher, and the durations were lower, at 1.6 than at 0.6 AU, suggesting a cumulative effect. (7) Energetic (≈50 keV) protons from the November 22 flare were observed by all the spacecraft. During the decay, Helios 1 observed no change in intensity when the interface moved past the spacecraft, indicating that particles were injected and moved uniformly on both sides of the interface. Helios 2 observed an increase in flux not seen by Helios 1, reaching maximum at the time that a shock arrived at Helios 2. The intensity dropped abruptly when the interface moved past Helios 2, indicating that the 'extra' particles seen by Helios 2 did not penetrate the interface.

1. INTRODUCTION

It is customary to speak of three types of flows in the solar wind, which *Chapman* [1964] called streams, flare shells, and solar wind. We shall refer to these as (1) corotating streams (also known as corpuscular streams, stationary streams, and high-speed streams), (2) ejecta (also called nascent streams, flare ejecta, jets, active wind, drivers, and pistons), and (3) slow flows (also called quiet wind, ambient wind, and structureless wind), respectively. The term piston has been applied both to corotating streams [e.g., *Dryer and Steinolfson*, 1976] and to ejecta [e.g., *Dryer et al.*, 1972]. Corotating flows are separated from slow flows by a thin boundary called a stream interface [*Belcher and Davis*, 1971; *Burlaga*, 1974], which in some cases is a tangential discontinuity [*Burlaga*, 1974; *Gosling et al.*, 1978]. Ejecta are presumed to be separated from slow flows by a thin boundary called a contact surface [*Lee and Chen*, 1968; *Dryer*, 1980]; this too is called a piston by some authors [e.g., *Dryer*, 1980]. Both corotating streams and ejecta may be preceded by a shock.

There are numerous studies of the above phenomena based on observations from just one spacecraft, but these cannot separate spatial variations from temporal changes. Data from two or more widely separated spacecraft are needed to study nonstationary corotating streams, transient ejecta, and interacting flows. There have been relatively few such observational studies [e.g., *Dryer et al.*, 1972; *Gosling et al.*, 1976; *Intriligator*, 1976; *Lazarus et al.*, 1970; *Schwenn et al.*, 1978, 1980; *Smith and Wolfe*, 1977, 1979; *Vaisberg and Zastenker*, 1976]. Some attempts have been made to model multipoint observations [*Gosling et al.*, 1976; *Dryer et al.*, 1978*a*, *b*].

In the period November 22 to December 6, 1977, Helios 1 and 2, Imp 7 and 8, and Voyager 1 and 2 were aligned very favorably for the investigation of solar outputs (Figure 1), and during this period, which was part of Study of Travelling Interplanetary Phenomena (STIP) interval IV from October 15

[1] NASA Goddard Space Flight Center, Laboratory for Extraterrestrial Physics, Greenbelt, Maryland 20771.
[2] Department of Physics, University of Kansas, Lawrence, Kansas 66044.
[3] Massachusetts Institute of Technology, Cambridge, Massachusetts 02139.
[4] Department of Physics and Astronomy, University of Iowa, Iowa City, Iowa 52242.
[5] Department of Physics, University of Minnesota, Minneapolis, Minnesota 55455.
[6] Max-Planck-Institut fur Aeronomie, Lindau/Harz, Federal Republic of Germany.
[7] Istituto Fisica G. Marconi, Citta Universita, Rome, Italy.
[8] Institut fur Geophysik der Technische Universität, Federal Republic of Germany.
[9] Max-Planck-Institut fur Aeronomie, Katlenburg-Lindau 3, Federal Republic of Germany.

Paper number 80A0172.
0148-0227/80/080A-0172$01.00

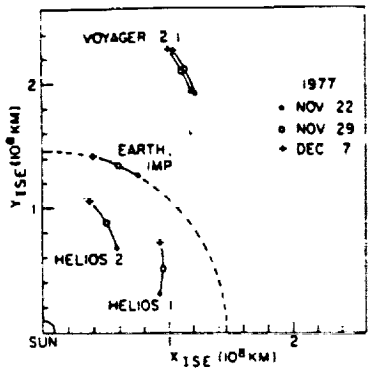

Fig. 1. Ecliptic plane projection of the trajectories of Helios 1, 2 and Voyager 1, 2 shown in the inertial solar ecliptic coordinate system for the interval November 22 to December 6, 1977.

to December 15, 1977, several significant solar events occurred. Recognizing that this interval (and a similar interval in September-October 1977) offered a unique opportunity for a comprehensive study of interplanetary shocks, flows, magnetic fields, and energetic particle phenomena, a workshop was organized to bring together experimenters from the Helios, Voyager, and Imp programs. The meeting was organized by S. M. Krimigis with the support of the Voyager and Helios team leaders. This paper is based on some of the results of that workshop. The purpose of this paper is to present a description and an analysis of the principal interplanetary events that were observed in the period November 22 to December 6, 1977, by Helios 1, 2, Voyager 1, 2, and Imp 7, 8.

Three flow systems were observed in the period under consideration: (1) a corotating stream and a stream interface associated with a coronal hole, (2) a shock wave and an energetic particle event associated with a 2B flare, and (3) an isolated shock wave whose origin is uncertain.

This paper is based on data from 28 experiments from six spacecraft. The experiments and the corresponding principal investigators are listed in Table 1. Nearly complete measurements of solar wind plasma, magnetic fields, and plasma waves are available from all spacecraft. Radio waves, plasma waves, and energetic electrons associated with the November 22 event are available from Helios 1, 2 and Voyager 1, 2. Data describing low-energy protons associated with the November 22 event are available from Helios 1, 2 and Voyager 1, 2.

We begin in section 2 by discussing the corotating stream and its associated shock and interface; this flow system was relatively simple, and the other two events interacted with it. Section 3 discusses the particles, fields, and flows associated with the flare of November 22. Section 4 analyses a relatively simple, isolated shock wave that passed all of the spacecraft in the early days of December 1977. Plasma waves at the shocks in the three events are discussed qualitatively in section 5. Energetic protons accelerated by the shocks and injected by the November 22 flare are described in section 6. Section 7 summarizes the results.

2. Corotating Stream, Interface, and Shock

A stream that was observed successively by Helios 1, Helios 2, Imp 7, 8, Voyager 1, and Voyager 2 is shown in Figure 2, which shows bulk speeds from the experiment of Rosenbauer on Helios 1, 2 and from the experiments of Bridge on Imp 7, 8 and Voyager 1, 2. Sixteen-minute averages of V are plotted versus time, and the phase is chosen such that the arrival time of the stream interface at each spacecraft is coincident with the vertical line marked 'interface.' The stream interface is readily identified as an abrupt decrease in density and an abrupt increase in temperature at the front of a stream [*Belcher and Davis*, 1971; *Burlaga*, 1974, 1975]. In this case the interface at each spacecraft can be seen in Figure 3, where the time profiles of 16-min averages of the density n and temperature T are plotted. Figure 2 shows that the interface and stream arrived at Helios 1 on November 23, at Helios 2 on November 25, at earth on November 27, and at Voyager 1 and 2 on November 29. The 2-day interval between successive encounters of the interface is approximately that which is expected for a 'corotating spiral' corresponding to a streamline with a speed of 400 km/s, as illustrated at the bottom of Figure 2.

The precise corotation times of the interface from one spacecraft to the next are shown in Table 2, together with the 'predicted' corotation times computed from the equation $t_2 - t_1 = (r_2 - r_1)/V + (\phi_2 - \phi_1)/\Omega_s$, with allowance for the spacecraft motions (here Ω_s is the sidereal rotation period of the sun; V is the solar wind speed; ϕ_1 and ϕ_2 are the longitudes of the spacecraft at time t_1 (when the interface passed the first spacecraft) and a later time t_2 (when the interface passed the second spacecraft), respectively; and r_1 and r_2 are the radial distances from the sun of the two spacecraft at t_1 and t_2.) Table 2 shows that the predicted corotation times are close to the observed corotation times, the difference being $\lesssim 15^{\circ}$c in the three largest time intervals. These small differences may be due to small irregularities in the shape of the surface of the interface. Thus we conclude that the interface was a corotating feature, and we infer that the stream which followed it was likewise corotating.

The low densities in the stream (Figure 3) and the fact that it was corotating suggest that its source was a coronal hole [*Hundhausen*, 1977; *Burlaga*, 1979]. A coronal hole, tentatively identified in the Kitt Peak He 10830-Å maps, passed central meridian on November 24, 25. The observed peak speed of the stream in question was ≈500 km/s; thus if its source was the coronal hole and if it propagated at nearly constant speed, the stream should have arrived at the earth on November 27, which, in fact, it did.

The dynamical evolution of the corotating stream in Figure

TABLE 1. Principal Investigators

	Plasma Analyzer	Magnetometer	Magnetometer	Radio Waves	Plasma Waves	Plasma and Radio Waves	Energetic Particles
Helios 1	Rosenbauer	Neubauer	Mariani/Ness	Stone	Gurnett	Kellogg	Keppler
Helios 2	Rosenbauer	Neubauer	Mariani/Ness	Stone	Gurnett	Kellogg	Keppler
Voyager 1	Bridge	Ness			Gurnett		Krimigis
Voyager 2	Bridge	Ness			Gurnett		Krimigis
Imp 7	Bridge	Ness			Gurnett		
Imp 8	Bridge	Ness			Gurnett		

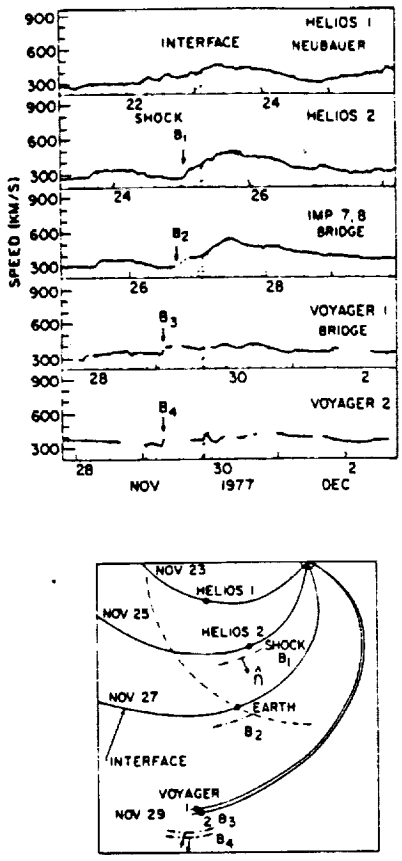

Fig. 2. Corotating interface. The top panel shows the associated stream relative to the interface at each spacecraft. The bottom panel shows the intersection of the interface with the ecliptic plane at the time that it passed each of the spacecraft. The dashed circular arc passing through earth represents the earth's orbit. The position of shock B is also shown, and its orientation is illustrated in the bottom panel.

2 is surprising and significant. Helios 1 and 2 observed similar profiles of $V(t)$, $n(t)$, and $T(t)$ following the interface, with a time delay of ≈53 hours, consistent with corotation. At the earth, Imp 7 and Imp 8 also saw the stream with approximately the expected corotation delay. The surprising result is that the stream appears to have been absent (or much slower) at Voyager 1 and 2 (Figure 2), even though both spacecraft observed the stream interface (Figure 3). This is probably not a latitude effect like that reported by *Schwenn et al.* [1978], since the latitudes of Voyager 1 and earth differed by only 1.5° (the latitude of Voyager 2 was ≈5.2° higher than that of earth). The heliographic latitudes of Voyager 1 and earth were 3° and 1°, respectively; these are well within the latitudinal range of the coronal hole (−2° to 10°) tentatively identified in solar geophysical data [*U.S. Department of Commerce*, 1978].

A numerical model is needed to show quantitatively that a stream can evolve near 1 AU as just described, and this will be discussed in another paper. One can understand the result qualitatively as follows. Ahead of the stream the density and hence the momentum flux were high (Figure 3). Inside the stream the density was low, and the speed of the stream itself was relatively low; the momentum flux of the stream did not greatly exceed that of the flow ahead of it. As the stream evolved, stress was relieved somewhat by shear at the interface. Nevertheless, two compression waves formed, moving toward and away from the sun with respect to the interface. The wave moving toward the sun (i.e., into the stream) decelerated the stream. The wave moving away from the sun (i.e., ahead of the stream) evolved into a forward shock (see discussion below). The importance of momentum flux in corotating stream dynamics has been discussed quantitatively by *Pizzo* [1980*a*, *b*] for some conventional stream profiles. A decrease of V with increasing distance has been discussed by *Dryer and Steinolfson* [1976].

The structure of the stream interface observed by Voyager 1 and 2 is shown in Figure 4. In both cases the density and temperature transitions occurred in ≈30 min, consistent with the durations of some of the interfaces observed at 1 AU by *Burlaga* [1974]. The n, T profiles observed at Helios 1, 2 are very similar to those in Figure 4. The magnetic field intensity reached a maximum at the interface (see Figure 4), as is usually the case [*Burlaga*, 1974; *Siscoe*, 1972]. In this case there was a large change in magnetic field direction across the interface at both Voyager 1 and Voyager 2. It is significant that all of the parameters just described (n, T, V, and **B**) had nearly the same profile at Voyager 2 as at Voyager 1, despite the separation of ≈0.2 AU; this shows that the internal structure of a stream interface can be coherent over a relatively large distance. Plasma wave observations at the interface at Voyager 2 (Figure 4) show no significant wave emission in the frequency range 10–562 Hz, suggesting that the interface was relatively stable. Similar observations of a different interface described by *Gurnett et al.* [1979*b*] showed the same result.

A 'corotating shock' (which we label shock B) was observed by Voyager 1 and 2; this is shown at high resolution in Figure 5. The identification of the disturbance as a shock is based on the simultaneous, abrupt increases in V, N_p, T_p, and $F \equiv |\mathbf{B}|$ and on the simultaneous change in the characteristics of the plasma waves. The observation of a shock at Voyager 1 and 2 is not surprising, since models of corotating streams [e.g., *Hundhausen*, 1973; *Hundhausen and Burlaga*, 1975; *Gosling et al.*, 1976; *Steinolfson et al.*, 1975; *Dryer et al.*, 1978*b*] predict the development of corotating shocks as streams evolve with distance from the sun, and many such shocks have been observed beyond 1 AU [*Smith and Wolfe*, 1977]. The shock normals computed from the Voyager plasma and magnetic field data using the method of *Lepping and Argentiero* [1971] were directed 9° and 14° west of radial, respectively (see Table 3 and Figure 2), consistent with corotation. At Voyager 2 the angle between the shock normal and the upstream magnetic field was 14.6°; the corresponding angle at Voyager 1 was 15.8°. The local shock speed was 400 ± 10 km/s relative to a fixed frame shock at both Voyager 1 and Voyager 2 (Table 3). This speed and the computed shock normals imply a time delay between Voyager 1 and Voyager 2 of 4.5 ± 1.3 hours. This compares favorably with the observed time delay of 5 hours 17 min.

Shock B probably passed Helios 2 and Imp 8 on November 25 and 26, respectively (see Table 3). This is significant, because shocks are rarely observed ahead of corotating streams at ≲1 AU [*Ogilvie*, 1972]. The identification of shock B at Helios 1 is based on the observations that (1) the magnetic field intensity measured by Neubauer's instrument increased from ≈7 to ≈15 γ within 2 min (it increased from 7.7 to 11.5 γ in 64 s) and (2) the plasma speed density and temperature increased between 0122 and 0205 UT (see Figures 2 and 3). The shock normal computed from the magnetic field data using the coplanarity theorem is $\lambda_n = 60°$, $\theta_n = 14°$, which is close to that expected for corotation in a 300-km/s wind, namely, $\lambda_n = 50°$, $\theta_n = 0$; here λ_n is the heliographic longitude, which is

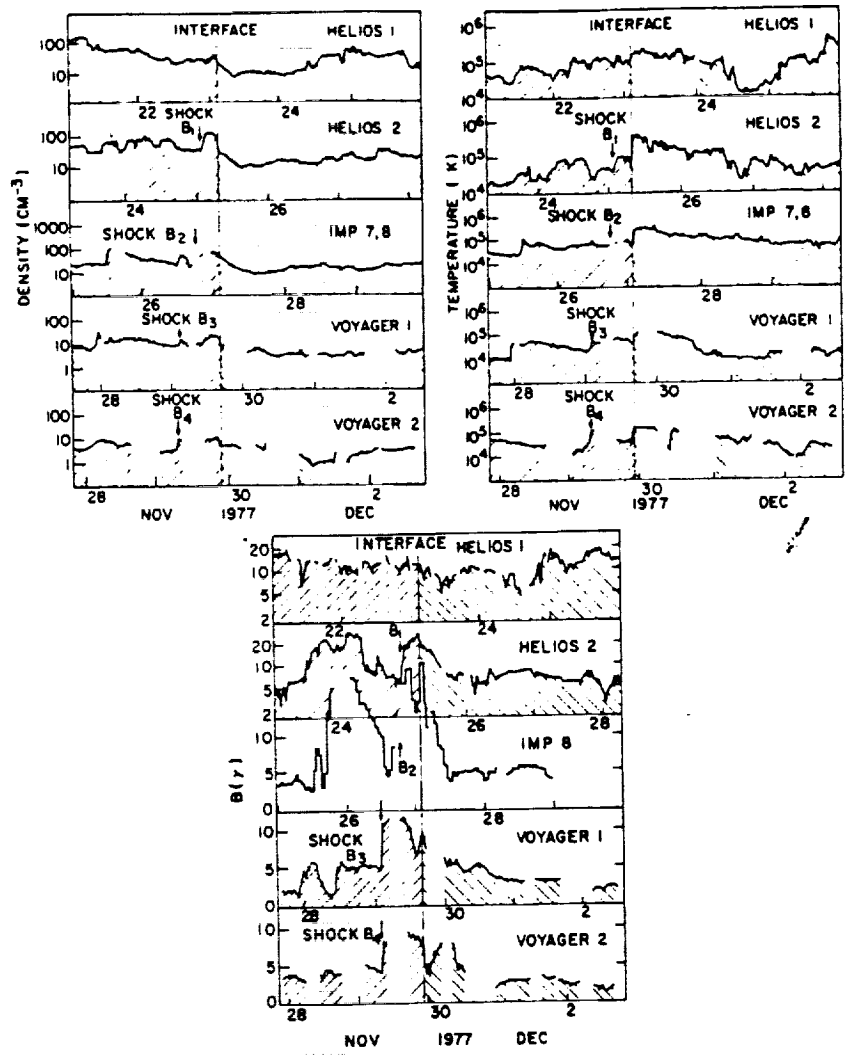

Fig. 3. The corotating stream interface (top) seen by each of the spacecraft. The interface is defined by the abrupt decrease in density and the corresponding increase in temperature. Times have been shifted so that the interfaces are aligned vertically, allowing a comparison of the density, temperature, and magnetic field intensity profiles (bottom).

taken to be zero for a vector pointing radially away from the sun, and θ_n is the latitude with respect to the ecliptic plane. The shock speed computed from the observed densities and bulk speeds using the coplanarity normal is 300 km/s, or 540 km/s in the radial direction. This implies that the shock should have arrived at earth 41 hours after it passed Helios 2 (if it moved at constant speed), that is, at hour 19 on November 26. A ssc was reported at 1704 UT on November 26, in good agreement with the prediction. Imp 8 was in the solar wind on November 26, but there are data gaps at the time of the ssc. Nevertheless, the magnetic field intensity nearly doubled at some time in a 2-hour interval centered about the ssc (Figure 3), and the plasma density, temperature, and speed increased at some time in a 5-hour data gap which included the time of the ssc (Figures 2 and 3). Thus the Imp 8 data are consistent with the presence of a shock at earth at 1704 on November 26. Altogether, the data from Helios 2, Imp 8, and the ssc give fairly convincing evidence for a shock driven by a corotating stream, which moved nearly radially from 0.6 to 1 AU and on to Voyager 1, 2 at 1.6 AU. Figure 3 shows that the shock moved away from the interface during the time that it moved from 0.6 to 1.6 AU.

It is customary to refer to a shock ahead of a corotating stream as a corotating shock. This is not appropriate for shock

TABLE 2. Stream Interface Corotation

From	To	$(\phi_2 - \phi_1)$, deg	$(r_2 - r_1)$, AU	$(t_2 - t_1)$, hours	
				Predicted	Observed
Helios 1 (Nov. 23, 0245)	Helios 2 (Nov. 25, 0721)	35.2	−0.029	57	53
Helios 2	Imp (Nov. 27, 0200 ± 0100)	8.2 ± 0.1	0.353	51	43 ± 1
Imp	Voyager 1 (Nov. 29, 1600 ± 0015)	−1.7 ± 0.8	0.605	60 ± 3	62 ± 1
Voyager 1	Voyager 2 (Nov. 29, 2125)	0.9	0.012	3	5

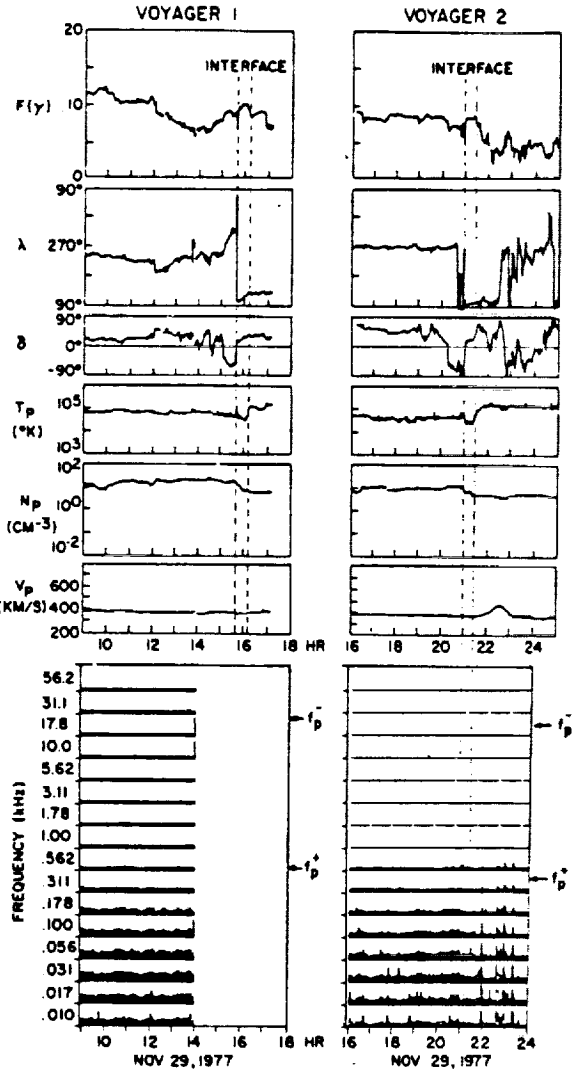

Fig. 4. Structure of the interface, shown by a plot of high-resolution magnetic field and plasma data (top) and corresponding plasma wave observations. The interface is relatively broad (30 min), its structure does not change appreciably over the 0.2-AU separation between Voyager 1 and Voyager 2, and there is no evidence of an instability that might produce waves $\lesssim f_p^+$ at Voyager 2.

B, however. If shock B were corotating, then it should have been detected at Helios 1 ≈50–60 hours before it was observed at Helios 2 (i.e., late on November 23), because Helios 1 was at the same radial distance as Helios 2 and ≈35° to the east. Although the Helios 1 observations are nearly complete and continuous, there is no evidence of a shock at Helios 1 (see Figures 2 and 3). A possible explanation is that the stream which produced the shock was corotating but not stationary. For example, the stream may have been produced by a coronal hole that rotated with the sun but whose physical characteristics changed on a scale of 1 day, producing a time-varying stream profile. Indeed, Figure 2 shows that the speed profile measured by Helios 2 differs in some details from that measured by Helios 1, indicating some time variations in this case. Evidence for nonstationary, corotating streams was presented earlier by *Burlaga et al.* [1978]. (A model of nonstationary flows was presented by *Wu et al.* [1979], but this does not include the dynamical effects of the sun's rotation.) Shock B was seen at Helios 2, Imp 8, and Voyager 1, 2 because those spacecraft were near a radial line; once formed at ≤0.6 AU, the shock persisted and was convected past the other spacecraft. But apparently, conditions were different at the time the stream was at Helios 1, 35° east of Helios 2, and were not favorable for the production of a shock.

3. Events Associated With a Flare

On November 22, 1977, a 2B flare at N23, W40 in McMath plage region 15031 was observed in Hα starting at 0946 UT and reaching maximum intensity at 1006 UT. *Chambon et al.* [1978] observed hard X rays and γ rays from the flare starting at ≈1000 UT. It produced a SID, a type IV burst (starting at 1002), a type III burst (beginning at 0959 UT), an interplanetary shock wave, and an energetic particle event. Thus the event displayed a wide range of phenomena that one associates with a great flare [*Dryer*, 1974].

Type III bursts. The type III solar radio burst produced by the flare is the most intense observed to date by Helios 1 and 2. Helios 2 radio observations of the November 22 burst are shown in Figure 6. They are from the University of Minnesota (52, 77, and 203 kHz) and Goddard Space Flight

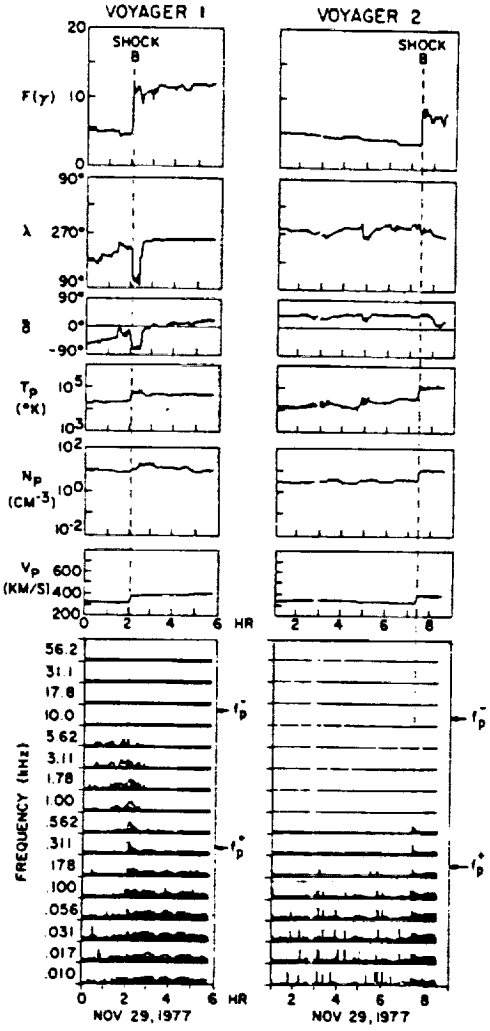

Fig. 5. Shock B, showing the high-resolution magnetic field and plasma data (top panel) and plasma wave observations (bottom panel) near the shock. The flow and field parameters are steady before and after the shock front, allowing accurate determination of its normal and speed. Whistler wave turbulence is observed at $f < f_p^+$ behind the shock; a short burst of broadband turbulence is observed at the shock; and 'ion acoustic' waves are observed at $f_p^+ < f < f_p^-$ ahead of the shock.

TABLE 3. Shock B

	Helios 2	ssc	Voyager 1	Voyager 2
Shock	B_1	B_2	B_3	B_4
Date	Nov. 25	Nov. 26	Nov. 29	Nov. 29
Time, UT	0147	1704	0204	0721
r, 10^8 km	0.944	1.476	2.373	2.390
Normal λ_n, deg	60		9.1	14.9
Normal δ_n, deg	14		−0.7	21.2
V, km/s	300		409	395
V_n, km/s	540		409	423

Center experiments. Electron observations from the Max-Planck-Institut fur Aeronomie experiment are also displayed in Figure 6, showing that electrons in and near the 20- to 65-keV energy range were present, consistent with the idea that low-frequency type III solar radio emission is caused by electrons with energies 10–100 keV [*Lin et al.*, 1973]. Despite the data gap around 1010 UT, it is clear that the radio burst was double peaked at the higher frequencies, possibly due to two separate bursts; however, there was only a single peak at lower frequencies. The first peak reached maximum intensity at 1001 UT for 3 MHz, and the merged peak is observed at 1032 UT for 77 kHz. Much of this delay corresponds to the transit time for the energetic electrons from a heliocentric distance of 0.05 AU (3-MHz level) out to 0.8 AU (77-kHz level), indicating an outward speed greater than $0.2c$ for the exciter. A few minutes of the delay arise from the difference in propagation time of the electromagnetic waves from the source levels to Helios 2, located at 0.6 AU.

Flux densities observed for this burst by Helios 2 reached maximum values exceeding 10^{-15} W m^{-2} Hz^{-1} for frequencies from 77 to 255 kHz; they decreased to approximately 10^{-16} W m^{-2} Hz^{-1} at 3 MHz, the highest Helios observing frequency. The 52-kHz channel, which shows strong electrostatic noise from 1025 to 1050 UT, is at the peak of the electrostatic noise spectrum, and it is within 1–2 kHz of the local plasma frequency determined from the measured density. Similar bursts were reported by *Gurnett et al.* [1978] and *Gurnett and Anderson* [1977]. The electrostatic bursts might be short in comparison to the sampling time of the tuned receiver. The bandwidth of the receiver is about 5 kHz, and its rise time therefore is about 0.2 ms, which is instantaneous in comparison to the detector integration time of 50 ms. As a consequence, for signals whose duration is more than 0.2 ms, the measurement gives the input voltage averaged over 50 ms.

The 77-kHz channel is the lowest frequency which did not show electrostatic noise. Burst radio emission has been reported to be generated at twice the local plasma frequency [*Alvarez et al.*, 1972]. Consequently, the 77-kHz electromagnetic waves detected at 0.60 AU by Helios 2 were propagating backward toward the sun from a source level near 0.8 AU, where the plasma frequency is half of 77 kHz.

This burst and the associated electron beam were also observed by the Voyager 1 and 2 planetary radio astronomy experiment and low-energy particle experiment, respectively. The burst arrival directions, found by the spinning Helios 1 and 2 antennas, together with the Helios and Voyager electron data, show that the exciter extends over a wide (>75°) range of solar longitudes. Analysis of the relative intensities and positions observed by Helios 1 and 2 also indicates that the centroid of the burst passed between these two spacecraft. Assuming a source longitude of 40°W and a spiral field configuration, a best fit to the intensity versus frequency data obtained by Helios 1 and 2 is obtained for a solar wind speed of 300 km/s. This is consistent with the speeds measured by the Helios plasma instruments, which were near 300 km/s for several days.

Interplanetary shocks and flows. The interplanetary shock wave produced by the flare was observed directly by Helios 1 and 2, Imp 8, and Voyager 1 and 2; it was also observed indirectly as a ssc at the earth (see Table 4 and Figure 7). The shock might have been driven by ejecta, as is suggested by the sketch in Figure 8, but the ejecta were not actually observed, because no spacecraft was suitably positioned.

If one tries to determine the motion of the shock by using a radial distance versus time plot (Figure 9) and the customary assumption of spherical symmetry, one encounters difficulties that would have been overlooked if there were fewer spacecraft. One difficulty is that the speed determined from the time delay between Imp 8 and Voyager 1 is 418 km/s, whereas the speed determined from the time delay between Imp 8 and Voyager 2 is 568 ± 20 km/s (the uncertainty is due to a data gap at Voyager 2 between 0600 and 0900 UT). This discrepancy is large, considering that Voyager 1 and Voyager 2 were separated by only 0.005 AU in the radial direction and by 0.2 AU in the transverse direction.

A second and more extreme example of the inadequacy of the assumption of spherical symmetry for computing shock speeds is the speed determined from the time delay between Voyager 1 and Voyager 2: 14 ± 2 km/s! This is obviously

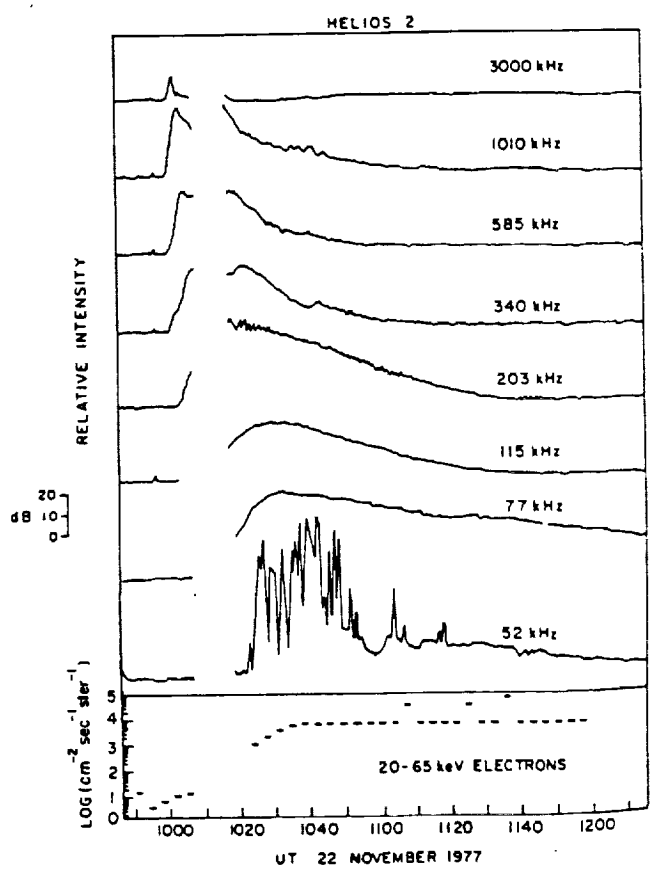

Fig. 6. A type III burst (77–3000 kHz), the beam of electrons (20–65 keV) which produced the burst, and plasma waves (at the local plasma frequency, 52 kHz) produced locally by the electron beam. The profiles at 52, 77, and 203 kHz are from the University of Minnesota experiment; the others are from the Goddard Space Flight Center experiment on Helios 2.

TABLE 4. Shock A

	Helios 2	Helios 2	Helios 1	Imp 8	Voyager 2	Voyager 1
Shock	A_1	A_2	A_3	A_4	A_5	A_n
Date	Nov. 23	Nov. 24	Nov. 25	Nov. 25	Nov. 27	Nov. 27
Time, UT	1610	0611	2228	1213	0730 ± 0130	2226
r, 10^8 km	0.916	0.927	1.018	1.476	2.361	2.533
Normal λ_n, deg	16	−15	4			−34
Normal θ_n or δ_n, deg	$\theta_n = -14$	$\theta_n = -48$	$\theta_n = 25$			$\delta_n = -10$
V, km/s	330	304	352			302
V_n, km/s	353	467	390	−418		369

wrong, and it is far from the speed determined from the analysis of the shock data at Voyager 1 (Figure 10), namely, 302 km/s. The shock normal and speed computed from the Voyager 1 data by using the method of *Lepping and Argentiero* [1971] were ($\lambda_n = -34°$, $\theta_n = -10°$) and $V_n = 302$ km/s, respectively (see Table 4). Using these numbers, assuming that the shock was plane between Voyager 1 and Voyager 2, and considering the inertial solar ecliptic positions of Voyager 1 (r_1 = (2.280, −0.274, 0.115) × 10^8 km) and Voyager 2 (r_2 = (2.285, −0.533, 0.267) × 10^8 km), one finds that the predicted time delay between Voyager 1 and Voyager 2 is 11 hours 13 min, which is reasonably close to the observed delay, (15 ± 1.5) hours. (The ±1.5-hour uncertainty is due to a data gap.) The small discrepancy may be attributed to uncertainties in the shock normal and to curvature of the shock surface. By contrast, the time delay predicted by using the assumption of spherical symmetry is only 36 min. We conclude that the use of time delays and assumption of spherical symmetry do not always give accurate shock speeds, whereas the use of local jump conditions and observations did give reasonably accurate estimates of the shock speed and direction in this case. The observed orientation of the shock is consistent with that

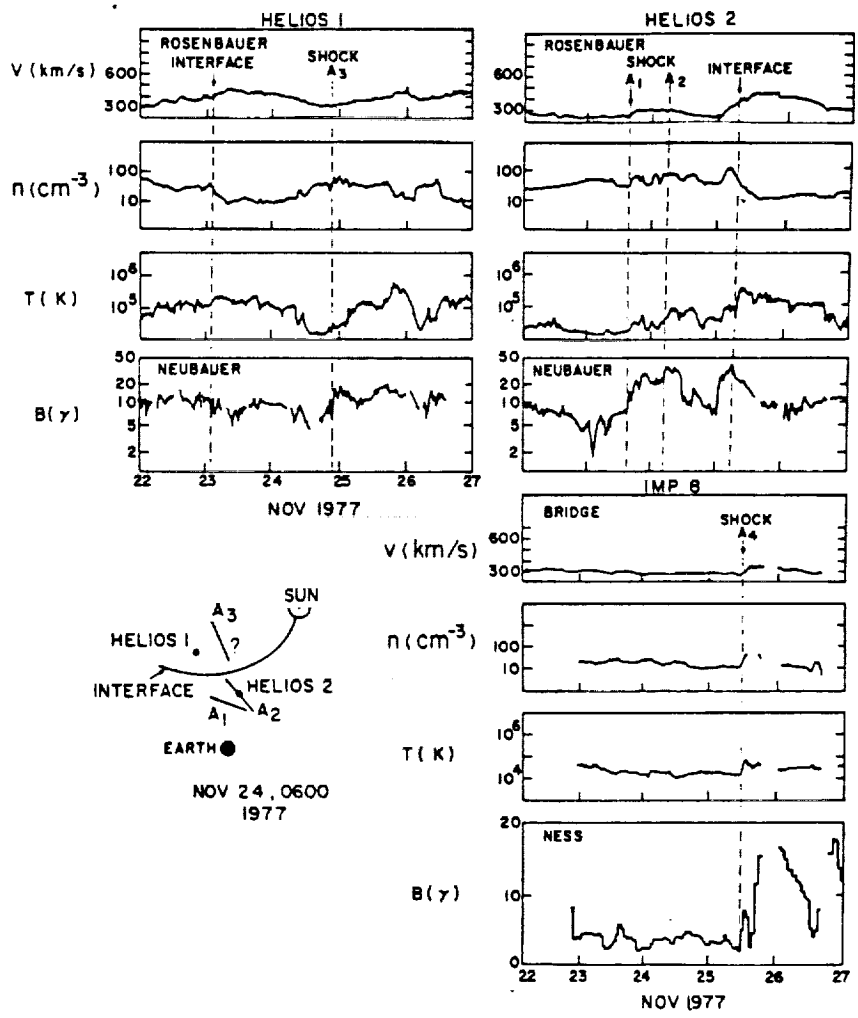

Fig. 7. Shocks A_1, A_2, and A_3 and the stream interface. At 0600 UT, November 24, 1977, the interface had passed Helios 1 but had not reached Helios 2. One shock (A_3) was approaching Helios 1 and arrived at Helios 1 late on November 24. Two shocks were observed by Helios 2. One (A_2) arrived at Helios 2 at 0611 UT on November 24, and another was a short distance ahead of it. A_1 and A_2 coalesced into one shock (A_4) as they moved from Helios 1 to earth, where A_4 was detected by Imp 8.

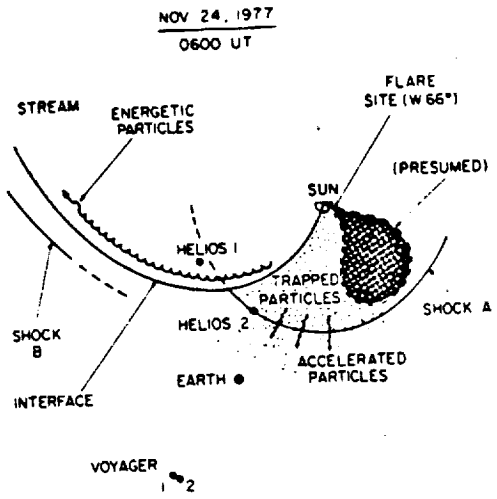

Fig. 8. A sketch, approximately to scale, showing the position of shock B, the stream interface, and shock A_2 at 0600 UT, when A_2 was approaching Helios 2. The positions of the spacecraft and the flare site at that time are also shown. The hypothetical ejecta were not observed. The flare produced energetic protons which escaped freely through the stream. Shock A_2 accelerated particles locally and perhaps trapped some of the flare particles, producing a local maximum in counting rates at the shock observed by Helios 2. These shock-accelerated particles did not penetrate the stream interface and were not observed by Helios 1.

expected for a shock with a radius of curvature less than 1.6 AU, originating at the flare site.

Helios 2 observed two shocks (A_1 and A_2, at 1610 UT on November 23 and at 0611 UT on November 24, respectively (see Figures 7 and 11)). However, Imp 8, which was at nearly the same latitude and longitude and which was only 0.36 AU away from Helios 2, observed only one shock (A_4 at 1213 UT on November 25 (see Figures 7 and 10)). We cannot unambiguously determine why two shocks passed Helios 2 (several origins can be imagined), but we can suggest why only one shock was subsequently observed at Imp 8 and at Voyager 1 and 2. The radial speed of shock A_1, determined from the local plasma and magnetic field observations of the shock by method MD1 of *Abraham-Shrauner and Yun* [1976], was 353 km/s. The corresponding speed of A_2 was 467 km/s. Thus although A_2 followed A_1 (i.e., it was closer to the sun (see Figure 7)), it was moving faster than A_1. Consequently, A_2 should have overtaken A_1 at some point; assuming constant speeds, this point was at 1.08 AU on the Helios 2–sun line. If the computed shock normals (Table 4 and Figure 7) are even approximately correct, the shocks should have interacted along the earth-sun line before they reached Imp 8 near the earth. The observation of only one shock at Imp 8 suggests that when the shocks interacted, they coalesced. This is in agreement with gas dynamic theory, where the overtaking of one shock (A_1) by a following one (A_2) leads to a coalesced shock moving forward and a reverse rarefaction fan, which because of its spreading is difficult to observe. (In MHD the interaction leads to seven distinct MHD structures, the most prominent ones of which are a forward fast shock and a reverse fast rarefaction wave.) The resultant shock propagated to Voyager 1, which was close to the earth-sun line. Its radial speed at Voyager 1, which was close to the earth-sun line. Its radial speed at Voyager 1, determined from the shock observations by using the method of *Lepping and Argentiero* [1971], was 369 km/s, which is in reasonable agreement (considering typical normal errors) with the speed determined from the time delay between Imp 8 and Voyager 1, namely, 427 km/s. Evidence for shock coalescence in Pioneer data has been reported by *Smith et al.* [1977]. A second alternative would be a sufficient weakening of one shock before it interacted with the other one. (Note that the very weak shock would still have to interact with the second shock.) This possibility is ruled out by the following two arguments: A_2 cannot be the weakened shock, since it fits very nicely into the propagation diagram (Figure 9) in contrast to shock A_1. We rule out a large weakening of shock A_1, since it is followed by a long-lasting region of increased momentum and energy flux as shown in Figure 7.

A remaining aspect which requires clarification is the observation of one shock only at Helios 1. A possible explanation for this observation may be the presence of the stream interface and an interaction region between Helios 1 and Helios 2 [*Burlaga and Scudder*, 1975]. If we approximate the interface as a tangential discontinuity, its interaction with A_1 may lead to the latter's disappearance [e.g., *Neubauer*, 1976].

4. THE DECEMBER SHOCK

During the Helios-Voyager-Imp workshop it was noted that a shock was observed by Helios 1 and 2 on December 1 and by Voyager 1 and 2 on December 2, and it was decided to include this event in the joint study. The interplanetary data are nearly complete for Helios 1, as is shown in Figure 12. However, the solar data do not show any large flare which might have produced the shock. One candidate is an SN flare at S24, E85 which began in Hα at 0338 UT on November 30 and reached a maximum at 0350 UT. This small flare was associated with an X ray burst (starting at 0330 UT, with a maximum at 0348 UT) and a SID (starting at 0334 UT, with a maximum at 0349 UT). This implies deceleration of the shock within 0.6 AU [see *Gosling et al.*, 1968]. In view of the uncertainty concerning the source of the shock our discussion emphasizes the interplanetary observations.

Postshock conditions. The density and temperature profiles in Figure 12 suggest that the shock observed by Helios 1 was followed by ejecta in which the density and temperature were low. There is also evidence for enhanced magnetic field intensities in the ejecta. Helios 2 may also have observed the

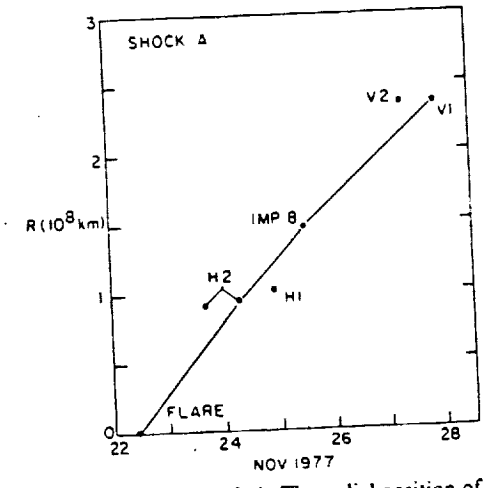

Fig. 9. Propagation of shock A. The radial position of the shock is shown at the times that the shocks arrived at Helios 1 (H1), Helios 2 (H2), Imp 8, Voyager 1 (V1), and Voyager 2 (V2). The two shocks observed by H2 coalesced into the one shock observed by Imp 8. Departures from spherical symmetry of shock A are indicated by the scatter of the points about a straight line.

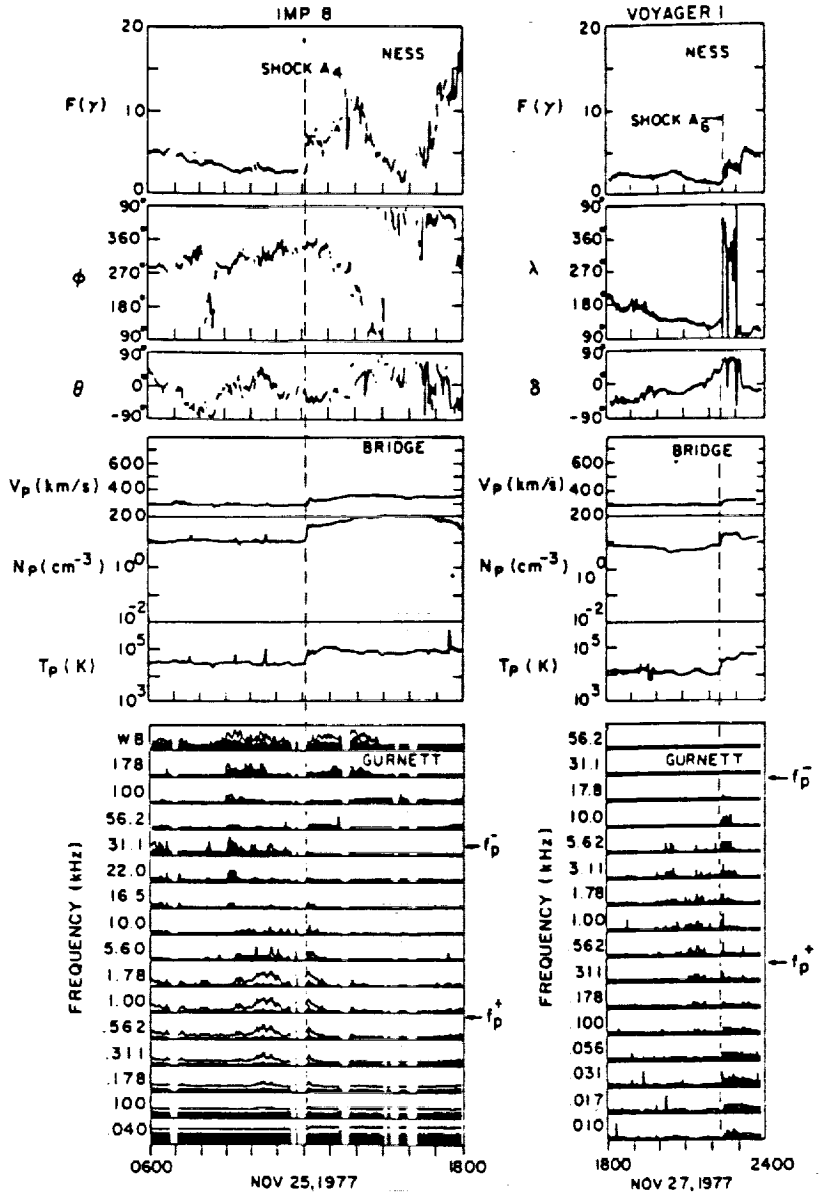

Fig. 10. High-resolution magnetic field and plasma data showing that A_4 (at Imp 8) and A_6 (at Voyager 1) are shocks. A narrow, broadband burst of electrostatic noise was observed at the time of the shock by both spacecraft. 'Ion acoustic' waves between f_p^- and f_p^+ were observed upstream by both spacecraft. Voyager 1 also observed whistler mode turbulence at $f < f_p^+$ behind the shock.

ejecta (Figure 13), but this is less certain because of a data gap. The shock was also detected by Voyager 1 and 2 (see Figures 13 and 14), but they did not encounter ejecta like that seen by Helios 2. (Voyager 1 observed a small depression in density on December 4 and a small increase in B on December 4–5; this was probably a local phenomenon, since it was not seen by Voyager 2, which was near by. This signature is clearly different from that seen by Helios 1, so we do not identify it as ejecta.) Thus the evidence is that the shock had a wide longitudinal extent (≳40° (see Figure 15)) and was driven by ejecta less broad, originating east of the Voyager-sun line.

Note that Voyager 2 observed a nearly monotonic decrease in speed, density, temperature, and magnetic field strength behind the shock (Figure 13). Many authors have interpreted such a signature as evidence for a blast wave, generally on the basis of observations from just one satellite [see *Hundhausen*, 1972]. However, the observation of ejecta at Helios 1 indicates that this was probably not a blast wave; it was a driven shock. Voyager 2 saw the shock, but it did not encounter the ejecta owing to its more limited longitudinal extent. This shows that the signature of the postshock flow is not sufficient to identify the type of a shock wave. This point was made previously by *Ogilvie and Burlaga* [1974] and by *Rosenau and Frankenthal* [1978]; it has recently been demonstrated very clearly by *Acuna et al.* [1980]. The concept of a broad shock driven by narrow ejecta is not new, although it is often forgotten or ignored. It dates back at least to *Gold* [1959].

Shock motion. Figure 16 gives a plot of radial distance versus time, showing the shock positions and times determined from the observations of Helios 1, 2 and Voyager 1, 2 and from a sudden commencement at earth. The points lie very close to a straight line with a slope corresponding to a speed of 555 km/s. Considering that Helios 1 was 19° east of the Voyager 2-sun line and that earth was 17° west of that line the straight line in Figure 16 suggests a nearly spherical

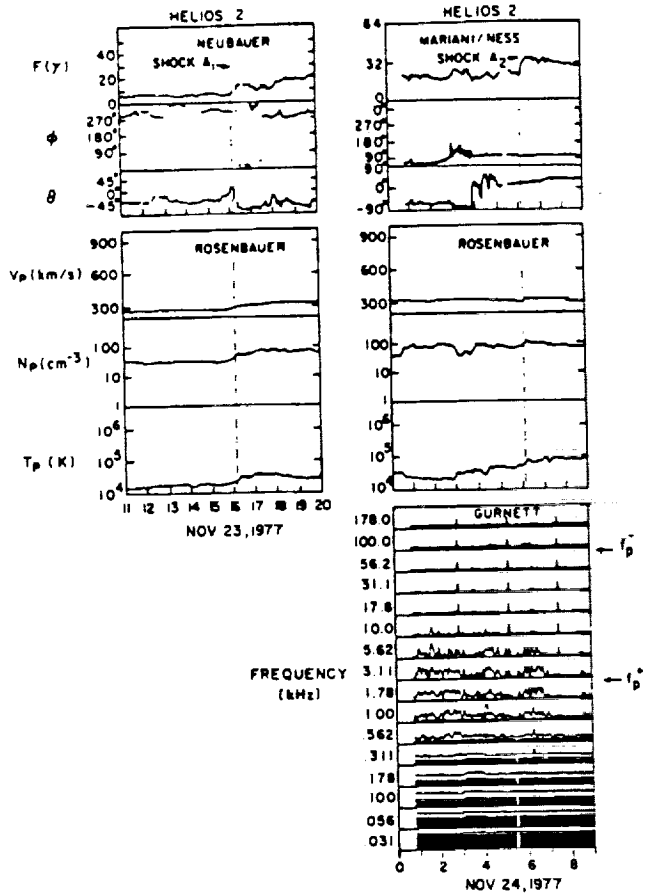

Fig. 11. High-resolution magnetic field and plasma data showing that A_1 and A_2 are shocks (or steep compressive waves). Electrostatic plasma wave data from Helios 2 show that the shock was imbedded in a broad region of Doppler-shifted 'ion acoustic' waves. A narrow spike was observed at 562 and 311 Hz at the time of the shock.

shock front moving at a constant speed between 0.6 and 1.6 AU. Similar results for the August 1972 events were reported by *Smith et al.* [1977] and *Dryer et al.* [1976]. However, examination of the local shock speeds and normals reveals a more complicated picture. Since Voyager 2 and Helios 2 were nearly radially aligned and since Figure 16 suggests a spherical shock, one expects that Voyager 2 and Helios 2 should have observed essentially the same shock speed and direction, the radial component of velocity being close to 555 km/s. The local jump conditions give rather different results (Table 5): (1) the local speeds were substantially less than the speed determined from the average speed determined from the time delay; and (2) the shock normal at Helios 2 ($\lambda_n = -3°$, $\theta_n = 17°$) was very different from that at Voyager 2 ($\lambda_n = 38°$, $\theta_n = -6°$). These differences are too large to be attributed to uncertainties in the computation of the local shock speed and direction. The field and plasma parameters were relatively steady before and after the shock, the field direction change was relatively large (18° at Helios 2), and we used both magnetic field and plasma observations, so we expect the uncertainty in speed to be $\lesssim$20 km/s and the uncertainty in direction to be $\lesssim$10° [*Abraham-Shrauner and Yun*, 1976; *Lepping and Argentiro*, 1971]. Thus the observations suggest that locally the shock surface may have been distorted such that the normal was not radial, although the normal may have been radial on average. Likewise, locally the shock may have been accelerated or decelerated, giving local speeds higher than average in one place, lower than average in a second place, and near average in a third place [*Heineman and Siscoe*, 1974; *Burlaga and Scudder*, 1975]. For example, the radial component of the local velocity at Voyager 2 (530 km/s) is consistent with the average speed determined from time delay (555 km/s) within the experimental uncertainties, but the radial component of the local velocity at Helios 2 (460 km/s) is substantially less than the average value. Since Helios 2 and Voyager 2 were nearly radially aligned, this suggests that the radial component of the shock velocity may have fluctuated as much as $\simeq \pm 100$ km/s and its direction may have fluctuated as much as $\pm 40°$ as it moved between 0.6 and 1.6 AU. The alternative is to postulate very large azimuthal variations.

5. Plasma Waves at Shocks

Helios 1, 2 and Voyager 1, 2 carried plasma wave instruments (see *Gurnett and Anderson* [1977] and *Scarf and Gurnett* [1977], respectively, for a discussion of the instruments), which provided an extensive set of observations of waves near the interplanetary shocks discussed above. These observations were used as a means of searching for and confirming the identity of the shocks. More important, however, they provide an exceptionally large and complete record which forms a basis for a comparative study of waves at interplanetary shocks. Only a few papers discussing plasma wave electric fields at interplanetary shocks have been published [*Scarf*, 1978; *Scarf et al.*, 1979; *Gurnett et al.*, 1979*a*, *b*]. Here

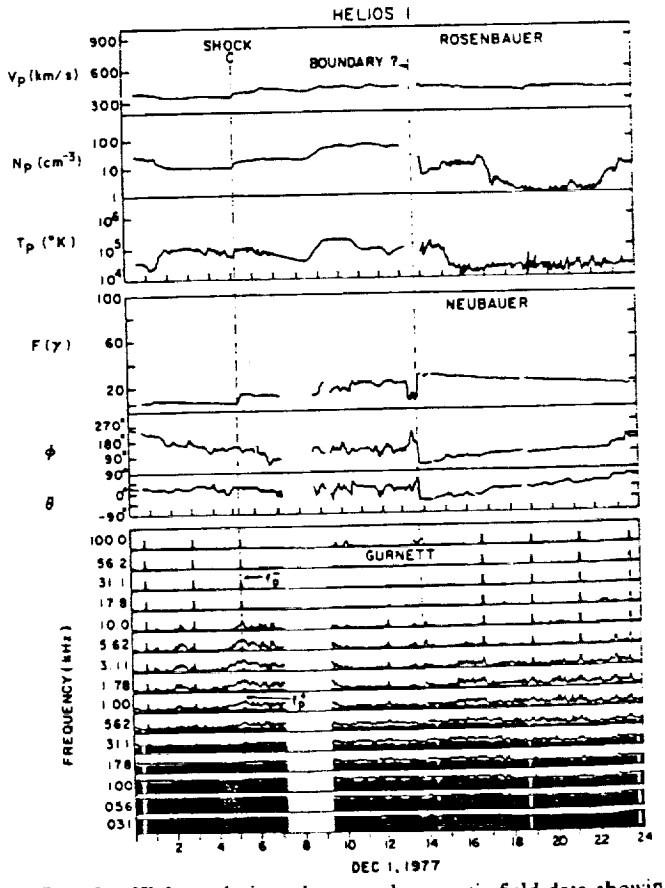

Fig. 12. High-resolution plasma and magnetic field data showing shock C and a boundary behind it, which might be the boundary of the ejecta (contact surface). Note the depression in magnetic field intensity at the boundary. Electrostatic plasma waves are observed between f_p^- and f_p^+ at the shock, but no significant waves are observed at the contact surface.

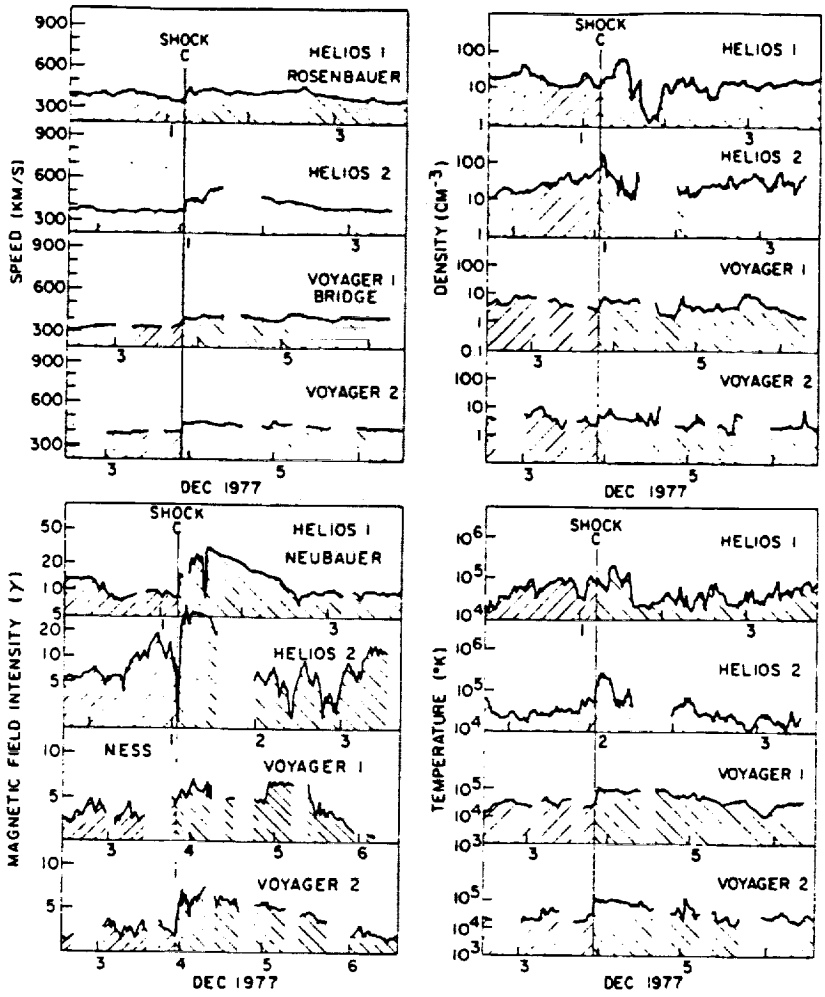

Fig. 13. Sixteen-minute averages of the speed, density, temperature, and magnetic field intensity, showing shock C, the preshock and postshock conditions, and the postshock conditions at Helios 1, 2 and at Voyager 1, 2. Note the drop in density and temperature and the high magnetic field intensities behind the shock at Helios 1 and 2, suggesting entry into the ejecta. The parameters slowly decrease behind the shock at Voyager 2, to the preshock levels, indicating that this spacecraft did not penetrate the ejecta.

we shall present only a qualitative discussion stressing the remarkable variety of signatures. A more comprehensive physical discussion is deferred to another paper.

The wave data are given together with the plasma and magnetic field observations of the shocks in Figures 5, 10, 11, 12, and 14. The electric field intensity is plotted versus time for each of several frequency channels on a logarithmic scale with a range of 100 dB for each channel. The electric field strength ranges from about 1 μV m^{-1} at the bottom of the scale to 100 mV m^{-1} at the top of the scale. The solid lines represent peak electric field amplitudes, and solid black areas (or vertical solid lines in some cases) represent the average electric field amplitude.

Let us consider the individual shock observations in the order in which shocks were introduced above, beginning with shock B. This shock had not developed at the position of Helios 1, but it was observed at both Voyager 1 and Voyager 2 (Figure 5), which were at essentially the same radial distance (1.6 AU) and separated by $\approx$0.2 AU. The Voyager 1 plasma wave observations show at least three different types of emissions: (1) turbulence extending downstream of the shock at frequencies of $\lesssim f_p^+$, identified as whistler mode turbulence; (2) waves extending upstream at frequencies from about 1.0 to 5.62 kHz, tentatively identified as ion acoustic waves; and (3) a short, well-defined broadband burst at the shock at frequencies from 10 Hz to 5.62 kHz. These types of emissions have been discussed by *Scarf et al.* [1970], *Gurnett and Frank* [1978], and *Gurnett et al.* [1979*a*]. Voyager 2 also observed the whistler mode turbulence extending downstream from the shock, and it observed a peak corresponding to the broadband emissions at the shock. There are no Voyager 2 data above 1 kHz, probably because of a failure in the spacecraft data system which reduced the sensitivity of these channels.

Plasma waves at shock A were observed by Helios 2 (Figure 11) and by Imp 8 and Voyager 1 (Figure 10). Whistler waves were not observed downstream of the shock at Helios 2 and Imp 8, but they were observed downstream of the shock at Voyager 1. The shock at Helios 2 is almost totally obscured by a broad region of ion acoustic wave turbulence from about 562 Hz to 10 kHz; these waves are not necessarily all associated with the shock [*Gurnett and Frank*, 1978]. Imp 8 and Voyager 1 (Figure 10) observed ion acoustic waves upstream of the shock between f_p^+ and f_p^-. Helios 2 (Figure 11) observed a sharp burst of noise in the 311- and 562-Hz channels coincident with the passage of shock; Imp 8 found some evidence of a corresponding noise burst below f_p^+, and Voyager 1 observed a noise burst at the shock in the range 31 Hz to $\approx$1.78 kHz.

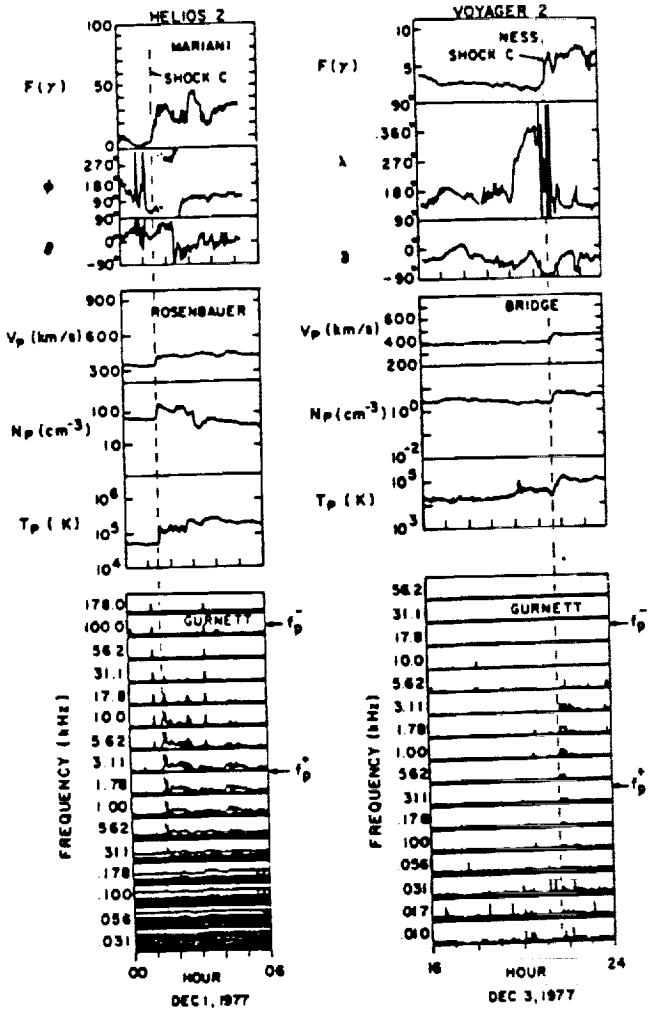

Fig. 14. High-resolution magnetic field data showing shock C. The plasma wave data show a short broadband burst at Helios 2 but not at Voyager 2. Electrostatic waves were observed behind shock C at frequencies between 311 Hz and 17.8 kHz by Helios 2 and over a more limited frequency range (178 Hz to 5.62 kHz) by Voyager 2.

Shock C was observed by Helios 1 and 2 and by Voyager 2 (Figures 12–14). None of the spacecraft observed intense whistler mode turbulence behind the shock. Helios 1 and Helios 2 observed an enhancement in electric field intensity in

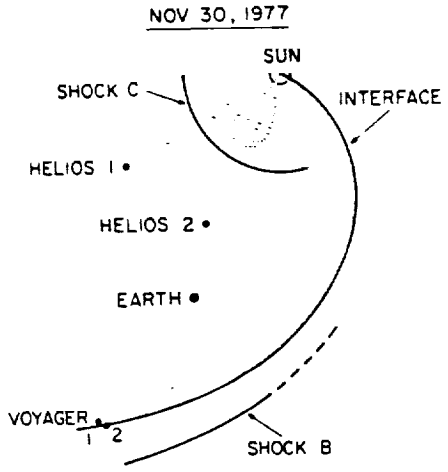

Fig. 15. A sketch, drawn approximately to scale, illustrating the position of shock B, the corresponding stream interface, the position of shock C and the corresponding ejecta at hour 0 on November 30, 1977. The positions of Helios 1, 2, Voyager 1, 2, and earth at this time are also shown.

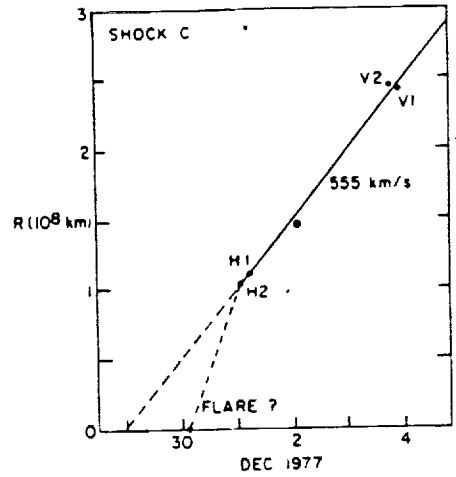

Fig. 16. Propagation of shock C. The radial distances at the times that the shock passed each of the spacecraft are shown. The straight-line fit suggests a uniform speed of 555 km/s and spherical symmetry, but local observations indicate appreciable scatter about those values

the range 562 Hz to 10 kHz with a large peak to average ratio, probably due to Doppler-shifted ion acoustic waves [*Gurnett and Frank*, 1978]. The waves extended both upstream and downstream at Helios 1 but only downstream at Helios 2. Voyager saw only weak emission of such waves, downstream of the shock. A sharp, intense (1–5 mV m^{-1}) broadband burst of electric field turbulence was observed at Helios 2, but it was absent at Voyager 2 and missing or obscured by the ion acoustic waves at Helios 1.

We conclude that at least three types of emissions (in various combinations) may be observed at an interplanetary shock, namely, downstream 'whistler mode turbulence,' upstream 'ion acoustic' waves, and a brief broadband noise burst coincident with the shock. In some cases, only one or two of these are observed. In addition, the shock may be embedded in a broad region of ion acoustic waves not necessarily caused by the shock. The combination of wave types and the characteristics of each wave mode seen at one spacecraft may be very different from those observed by another spacecraft nearby. Apparently, the plasma waves at a shock depend strongly on the local characteristics of the medium. This is not surprising, since it has been observed in the case of the earth's bow shock [*Greenstadt et al.*, 1973]. However, the basic types of emissions are the same at 0.6 AU as they are at 1.6 AU.

6. Energetic Protons

In the interval November 22 to December 6, 1977, Helios and Voyager instruments observed energetic protons (≈50–200 keV) produced by at least two mechanisms: local shock acceleration and acceleration in a flare. It is convenient to begin by discussing the former, since shock-accelerated particles are less complicated by propagation effects.

Shock acceleration. Protons accelerated by a shock are seen most clearly in the case of shock C, which was relatively isolated and uncomplicated, as was discussed in section 4. Recall that Voyager 1 and 2 observed a shock behind which the flow parameters and magnetic field intensity dropped gradually to the preshock values; there was no evidence of ejecta like those observed by Helios 1. Figure 17 shows enhancements in the counting rate of protons at Voyager 1 and 2 in the energy range ≈50 to ≈138 keV; the maximum intensity occurred at or just behind the shock. At Voyager 2 the peak counting rate was ≈100 times the ambient value, and at Voy-

TABLE 5. Shock C

	Helios 2	Helios 1	Imp 7	Voyager 2	Voyager 1
Shock	C_1	C_2	C_3	C_4	C_5
Date	Dec. 1	Dec. 1	Dec. 2	Dec. 3	Dec. 3
Time, UT	0129	0514	0215	2141	2318
r, 10^8 km	1.042	1.111		2.455	2.445
Normal λ_n, deg	−3	3		38.3	
Normal θ_n, deg	17	−34		−6	
V, km/s	441	417		415	
V_n, km/s	460	501		530	

ager 1 the enhancement was somewhat smaller. The enhancement began ≈15 hours ahead of the shock at both Voyager 1 and Voyager 2. It persisted for ≈32 hours behind the shock at Voyager 1 and ≈28 hours behind the shock at Voyager 2. There were small differences in the shapes of the profiles which might be due to differences in the local magnetic field configurations. Basically, however, the proton enhancement at Voyager 1 was similar to that at Voyager 2. This may be due to the simple geometry of the shock near Voyager 1 and 2 and to their relatively small separation (0.2 AU).

The situation at Helios 1 and 2 was quite different. Both spacecraft observed an enhancement in counting rate of protons (Figure 17). The maximum enhancement at Helios 2 was only ≈20 times the background counting rate, and it occurred at the shock. Two maxima were observed by Helios 1, and the shock occurred between them. A compression wave was observed at the time of the second maximum (Figure 12), but the time resolution was not adequate to determine whether or not it was a shock. The counting rate dropped abruptly approximately 6 hours after the shock at both Helios 1 and Helios 2, in contrast to the more gradual, longer-lasting decline at Voyager 1 and 2. This might be due, at least in part, to the presence of ejecta at Helios 1 and at Helios 2, which were not observed by Voyager 1 and 2. (There is no accepted signature for the boundary of ejecta, and we cannot be certain that we have identified one. The vertical line behind the shock in Figure 17 corresponds to an abrupt decrease in density observed behind the shocks in Figures 12 and 13). The enhancement began ≈6 hours ahead of the shock at Helios 2 and a few hours ahead of the shock at Helios 1; the slight difference could be due to different acceleration efficiencies of the two shocks and/or to different upstream magnetic field conditions which gave connection to the shocks at slightly different times. There is a curious enhancement at Helios 1, occurring several hours ahead of the shock-associated enhancement but closely resembling it. One can imagine that this was due to a magnetic field geometry which provided a good connection between the observer and the shock for several hours before the shock arrived.

The differences between the enhancements at Helios 1 and Helios 2 and the differences between the enhancements at Voyager 1 and Voyager 2 indicate that local conditions do influence the intensity profile somewhat. Note, however, that the Voyager 1, 2 profiles have a greater maximum enhancement and a greater upstream extent than the Helios 1, 2 profiles. One possible reason for this (but not the only one) is that Voyager 1, 2 were farther from the sun than Helios 1, 2, so that the shock at Voyager 1, 2 had been accelerating particles for a longer time and perhaps accelerated and accumulated more particles than it had when it was at the positions of Helios 1 and 2.

Flare-accelerated particles. Now let us discuss the low-energy (≈25–200 keV) protons ejected by the flare of November 22, 1977 (see section 3 for a discussion of the flare characteristics and the corresponding interplanetary flows). Helios 1 and 2 observed very different intensity-time profiles during the decay in intensity (Figure 18), even though they were at nearly the same radial distance and were separated in longitude by only 32° (see Figures 1 and 8). At Helios 1 the intensity decreased smoothly and monotonically for at least 3 days (Figure 18). The corotating stream discussed in section 2 was east of Helios 1 at the beginning of the event, and the interface

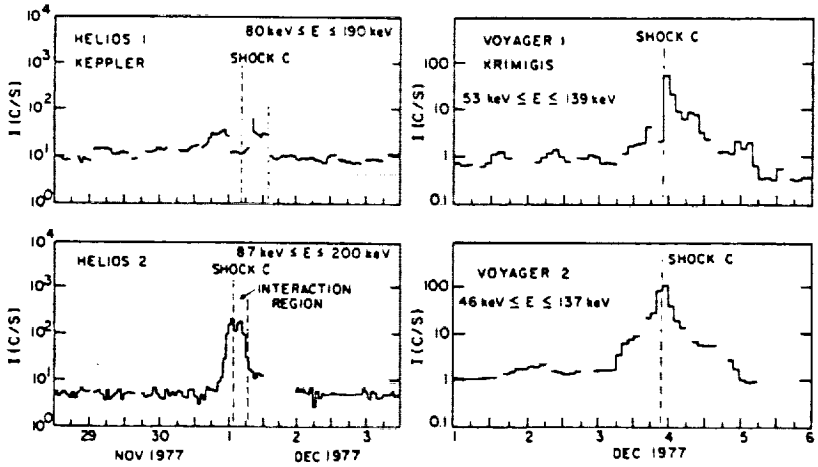

Fig. 17. Counting rates of energetic protons near shock C, observed by Helios 1, 2 and Voyager 1, 2. The broad, intense fluxes of particles at Voyagers 1 and 2 closely resemble one another, but they differ appreciably from the narrower, less intense fluxes observed by Helios 1 and 2. The Helios 2 profile differs appreciably from that of Helios 1. The abrupt decrease in counting rates behind the shock observed by Helios 1 and Helios 2 may be due to a flow boundary (e.g., a piston) behind the shock.

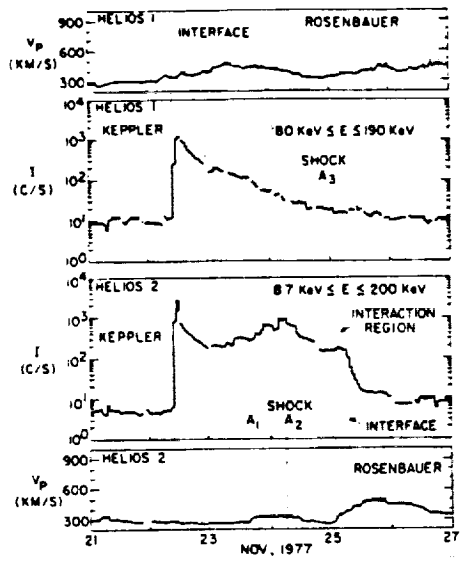

Fig. 18. Counting rates of energetic protons produced by the November 22 flare and by shock A, as observed by Helios 1 and 2. The speed profiles are shown as an aid in describing the corresponding flows. Helios 1 and Helios 2 observed similar intensity-time profiles during the initial stage of the decay. Helios 1, which was in the corotating stream, continued to observe an uninterrupted, monotonic decay to the background level 3 days later. Helios 2 observed a second increase of flux. The intensity dropped abruptly when the interface arrived, because the accelerated particles did not penetrate the interface.

passed the spacecraft ≈16 hours later with only a small perturbation on the intensity-time profile. Apparently, the flare injected particles over a broad range of longitudes near the sun, so that the intensity versus longitude was nearly uniform across the corotating interface. The particles in the slow flow ahead of the interface decayed freely (e.g., by diffusing to infinity [*Kurt et al.*, 1978]) for at least 16 hours after the flare, and the particles in the corotating stream decayed similarly for at least 3 days after the flare. In particular, particles in the corotating stream were unaffected by the flare-associated shock wave (shock A) and the postshock flow (see section 3 and Figure 8).

The intensity-time profile at Helios 2 was quite different from that at Helios 1, probably because it was influenced by the flare-associated shock and postshock flow. The early part of the decay seen by Helios 2 was very similar to that observed by Helios 1 (Figure 18), the flux decreasing monotonically for at least 12 hours. As shock A_1 (produced by the flare) approached Helios 2, the counting rate of energetic protons began to increase, reaching a maximum at the time that shock A_2 reached Helios 2. The maximum flux was 4×10^6 ions cm^{-2} s^{-1} sr^{-1} MeV^{-1}. The maximum counting rate was ≈25 times that measured by Helios 1 at the same time, that is, comparable to the increase which Helios 2 observed at shock C, as described above. This increase may be due to (1) particles accelerated by the shock, (2) flare particles trapped behind the shock, and/or (3) energetic storm particles. Following the shock the counting rate again decreased until the interaction region of the corotating stream arrived at Helios 2, at which time there was a slight increase in the counting rate, perhaps due to compression in the interaction region. When the interface arrived, the counting rate at Helios 2 dropped rapidly (exponentially with a time scale of 3 hours) to approximately the same level that Helios 1 recorded. Apparently, particles accelerated by shock A could not penetrate the stream interface, and many were trapped in a region bounded by the interface on one side and the shock on another side. The ejecta from the flare might have provided the third boundary. The scenario that has been described is represented schematically in Figure 8.

Voyager 1 and 2 observed intensity-time profiles of protons in the energy range ≈50–138 keV (Figure 19) which resemble the profile recorded by Helios 2. During the early stage of the decay both spacecraft observed a monotonic decrease in counting rate lasting ≈16 hours. (The initial increase in counting rate and the first hour or two of the decay include an uncertain contribution to energetic, omnidirectional particles.) The counting rate then increased gradually during the next 8 days, reaching a maximum counting rate at the time that shock A arrived. (Recall that there was a data gap at Voyager 2 between 0600 and 0900 UT, so the shock was not observed directly.) This gradual increase lasted too long to be due to particles accelerated by the shock alone. Probably, energetic storm particles were present. The rapid increase several hours ahead of the shock at Voyager 1 and 2, however, is probably a contribution due to shock acceleration. The enhancement is relatively small, no more than about 16 times the ambient

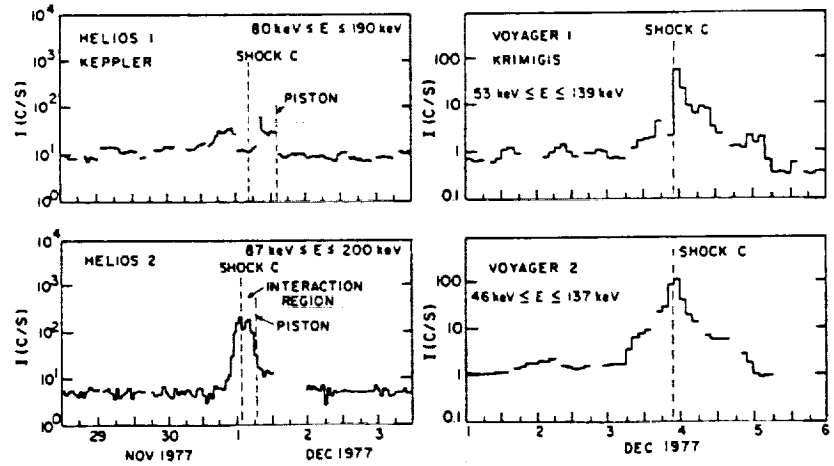

Fig. 19. Counting rates of energetic protons observed by Voyager 1 and 2. Speed profiles are shown to indicate the flow conditions. Both Voyager 1 and Voyager 2 observed flare particles on November 22. The broad increase between November 27 and 29 may be due to energetic storm particles. Locally accelerated particles are observed at the transient shock A, but there is no significant increase at the stationary shock B.

value. It did not extend above 0.5 MeV for protons. No modulation of electrons in the range 0.03–1.5 MeV was observed. At the time of the shock, Voyager 1 observed a strong anisotropy (3.5:1), the particles flowing away from the sun. Shortly after the shock passed, the anisotropy direction reversed, and particles were observed to be streaming toward the sun, consistent with the hypothesis that most of the particles observed near the shock were accelerated by the shock. Following the shock the counting rate decreased, rapidly at first and then more slowly. Shock B (see section 2) arrived at Voyager 1 and 2 during the decline in intensity, on November 29, and the corotating stream interface arrived several hours later. A very small increase in the counting rate of low-energy protons was observed by Voyager 2, and an even smaller increase by Voyager 1, but these were insignificant in comparison to the other shock-associated enhancements described above. A small increase in counting rate was observed in the interaction region ahead of the interface (Figure 19), analogous to that observed on November 25 by Helios 2 when it encountered the interaction region (Figure 18).

7. SUMMARY

We have presented a wealth of data obtained at ≈0.6, 1, and 1.6 AU, describing the evolution and interactions of particles, flows, and fields in the period November 22 to December 6, 1977. Some of the principal results of our analysis of these data are as follows:

1. A small, corotating stream, originating in a coronal hole, was observed to disappear as it moved from 0.7 to 1.6 AU. A forward shock (shock B) was produced by the stream and observed by Helios 2 (0.6 AU), Imp 8 and earth (1 AU), and Voyager 1, 2, which were nearly radially aligned; however, the shock was not corotating because it was not seen at Helios 1, 35° east of Helios 2. Apparently, the flow was corotating but nonstationary. The stream interface corotated from 0.7 to 1.6 AU and persisted even though the stream had dissipated; it was stable, and its structure remained essentially the same at all positions.

2. An exceptionally intense type III burst, produced by the November 22, 1977, flare, was observed by Helios 1 and 2. The electron beam which caused it and plasma oscillations excited by the beam were observed at 0.6 AU.

3. The shock produced by the flare of November 22 (shock A) was nonspherical, pointing 34° to the east and 10° south of the radial direction at 1.6 AU. It interacted with another shock beyond 0.6 AU, and they coalesced, forming a single shock that was observed at 1 and at 1.6 AU.

4. A shock of uncertain origin (shock C) was observed by five spacecraft at radial distances from the sun ranging from 0.6 to 1.6 AU and with longitudinal separations of up to 36°. The radial distances versus time diagram suggested a spherical shock moving at a constant speed, but analysis of data at the shocks showed local fluctuations of up to 100 km/s in speed and 40° in direction.

5. One or more of three types of electrostatic waves were observed at interplanetary shocks: upstream waves with $f_p^- \lesssim f < f_p^+$, downstream waves with $f < f_p^-$, and broadband noise at the shock. These three types of emission were observed at 1.6 AU as well as 0.6 AU. The specific pattern varied greatly among the shocks observed, even for the same shock observed at closely separated (≲0.2 AU) spacecraft, indicating a strong dependence on local shock and solar wind parameters.

6. Energetic protons (≈50–200 keV) were observed to be accelerated at shocks. The maximum and half widths of the flux profiles at a shock differed by approximately a factor of 2 over distances of a few tenths of an astronomical unit, indicating a dependence on local conditions. The data suggest a tendency for the fluxes to become broader and more intense with increasing distance from the sun.

7. Energetic protons (≈50 keV) from the November 22, 1977, flare were observed. Helios 1 observed that their intensity decayed monotonically in the corotating stream, with little change across the stream interface. Helios 2, 30° to the west of the interface, observed a very different profile, with a second increase to a maximum at the time that the shock produced by the flare arrived. These 'extra' particles apparently did not penetrate the interface, for the intensity at Helios 2 dropped abruptly to the intensity observed at Helios 1 when the interface corotated past Helios 2.

Acknowledgments. This paper was made possible by the efforts of many people. The project leaders—H. Porsche, J. Trainor, A. Kutzer (DFVLR/ERNO), and F. Kochendorfer (NASA/HQ) representing Helios and E. Stone and M. Mitz (NASA/HQ) representing Voyager—made special efforts to coordinate the acquisition of Helios and Voyager data and to provide nearly complete data sets for the unique interval that we studied. The workshop was proposed and organized by S. Krimigis. Four principal investigators, not listed as authors, generously provided us their data, which were essential for this study—H. Bridge, S. Krimigis, N. Ness, and R. Stone. The shocks were identified by the workshop participants in presentations and round table discussions. M. Denskat and P. Volkmer provided the data on the shock seen at Helios 2 on November 25.

The Editor thanks M. Dryer and W. C. Feldman for their assistance in evaluating this paper.

REFERENCES

Abraham-Shrauner, B., and S. H. Yun, Interplanetary shocks seen by Ames plasma probe on Pioneer 6 and 7, *J. Geophys. Res.*, *81*, 2097, 1976.

Acuna, M. H., L. F. Burlaga, R. P. Lepping, and N. F. Ness, Initial results from the Voyagers 1, 2 magnetic field experiments, in *Lecture Notes in Physics*, Springer, New York, in press, 1980.

Alvarez, H., F. Haddock, and R. P. Lin, Evidence for electron excitation of type III radio burst emission, *Solar Phys.*, *26*, 468, 1972.

Belcher, J., and L. Davis, Jr., Large-amplitude Alfven waves in the interplanetary medium, 2, *J. Geophys. Res.*, *76*, 3534, 1971.

Burlaga, L. F., Interplanetary system interfaces, *J. Geophys. Res.*, *79*, 3717, 1974.

Burlaga, L. F., Interplanetary streams and their interaction with the earth, *Space Sci. Rev.*, *17*, 327, 1975.

Burlaga, L. F., Magnetic fields, plasmas, and coronal holes: The inner solar system, *Space Sci. Rev.*, *23*, 201, 1979.

Burlaga, L. F., and J. D. Scudder, Motion of shocks through interplanetary streams, *J. Geophys. Res.*, *80*, 4004, 1975.

Burlaga, L. F., N. Ness, F. Mariani, B. Bavassano, U. Villante, H. Rosenbauer, R. Schwenn, and J. Harvey, Magnetic fields and flows between 1 and 0.3 AU during the primary mission of Helios 1, *J. Geophys. Res.*, *83*, 5167, 1978.

Chambon, G., K. Hurley, M. Niel, R. Talon, G. Vendrenne, O. B. Likine, A. V. Kovznetsov, and I. V. Estovline, A hard X-ray and gamma ray observation of the 22 November, 1977 solar flare, *Colloq. Int. Cent. Nat. Rech.*, *282*, 1978.

Chapman, S., *Solar Plasma, Geomagnetism, and Aurora*, p. 48, Gordon and Breach, New York, 1964.

Dryer, M., Interplanetary shock waves generated by solar flares, *Space Sci. Rev.*, *15*, 403, 1974.

Dryer, M., Solar-generated disturbances and their propagation through the interplanetary medium, in *Lecture Notes in Physics*, Springer, New York, in press, 1980.

Dryer, M., and R. S. Steinolfson, MHD solution of interplanetary disturbances generated by simulated velocity perturbations, *J. Geophys. Res.*, *81*, 5413, 1976.

Dryer, M., Z. K. Smith, G. H. Endrud, and J. H. Wolfe, Pioneer 7 ob-

servations of the August 29, 1966, interplanetary shock-wave ensemble, *Cosmic Electrodynamics*, *3*, 184, 1972.
Dryer, M., Z. K. Smith, R. S. Steinolfson, J. D. Mihalov, J. H. Wolfe, and J. K. Chao, Interplanetary disturbances caused by the August 1972 solar flares as observed by Pioneer 9, *J. Geophys. Res.*, *81*, 4651, 1976.
Dryer, M., C. Candelaria, Z. Smith, R. Steinolfson, E. J. Smith, J. H. Wolfe, J. D. Mihalov, and P. Rosenau, Dynamic MHD modeling of the solar wind disturbances during the August 1972 events, *J. Geophys. Res.*, *83*, 532, 1978*a*.
Dryer, M., Z. K. Smith, E. J. Smith, J. D. Mihalov, J. H. Wolfe, R. S. Steinolfson, and S. T. Wu, Dynamic MHD modeling of solar wind corotating stream interaction regions observed by Pioneer 10 and 11, *J. Geophys. Res.*, *83*, 4347, 1978*b*.
Gold, T., Plasma and magnetic fields in the solar system, *J. Geophys. Res.*, *64*, 1665, 1959.
Gosling, J. T., J. R. Asbridge, S. J. Bame, A. J. Hundhausen, and I. B. Strong, Satellite observations of interplanetary shock waves, *J. Geophys. Res.*, *73*, 43, 1968.
Gosling, J. T., A. J. Hundhausen, and S. J. Bame, Solar wind evolution at large heliocentric distances: Experimental demonstration and the test of a model, *J. Geophys. Res.*, *81*, 2111, 1976.
Gosling, J. T., J. R. Asbridge, S. J. Bame, and W. C. Feldman, Solar wind stream interfaces, *J. Geophys. Res.*, *83*, 1401, 1978.
Greenstadt, E. W., M. Dryer, and Z. K. Smith, Field-determined structure of interplanetary shocks, in *Flare Produced Shock Waves in the Corona and in Interplanetary Space*, p. 245, High Altitude Observatory, National Center for Atmospheric Research, Boulder, Colo., 1973.
Gurnett, D. A. and R. R. Anderson, Plasma wave electric fields in the solar wind: Initial results from Helios 1, *J. Geophys. Res.*, *82*, 632, 1977.
Gurnett, D. A., and L. A. Frank, Ion acoustic waves in the solar wind, *J. Geophys. Res.*, *83*, 58, 1978.
Gurnett, D. A., M. M. Baumback, and H. Rosenbauer, Stereoscopic direction finding analysis of a type III solar radio burst: Evidence for emission at $2f_p$, *J. Geophys. Res.*, *83*, 616, 1978.
Gurnett, D. A., F. M. Neubauer, and R. Schwenn, Plasma wave turbulence associated with an interplanetary shock, *J. Geophys. Res.*, *84*, 541, 1979*a*.
Gurnett, D. A., E. Marsch, W. Pilipp, R. Schwenn, and H. Rosenbauer, Ion acoustic waves and related plasma observations in the solar wind, *J. Geophys. Res*, *84*, 2029, 1979*b*.
Heineman, M. A., and G. L. Siscoe, Two-dimensional simulation of flare-associated disturbances in the solar wind, *J. Geophys. Res.*, *79*, 1349, 1974.
Hundhausen, A. J., *Coronal Expansion and Solar Wind*, Springer, New York, 1972.
Hundhausen, A. J., Nonlinear model of high-speed solar wind streams, *J. Geophys. Res.*, *78*, 1528, 1973.
Hundhausen, A. J., An interplanetary view of coronal holes, in *Coronal Holes and High Speed Solar Wind Streams*, edited by J. B. Zirker, p. 298, Colorado Associated Universities Press, Boulder, 1977.
Hundhausen, A. J., and L. F. Burlaga, A model for the origin of solar wind stream interfaces, *J. Geophys. Res.*, *80*, 1845, 1975.
Intriligator, D. S., The August 1972 solar-terrestrial events: Solar wind plasma observations, *Space Sci. Rev.*, *19*, 629, 1976.
Kurt, V. G., Yu. I. Logacher, V. G. Stolpovskii, N. F. Pissarenko, M. Gros, A. Ranart, L. Trieger, and T. Gombosi, Analysis of energetic particle events following solar flares of September 24 and November 22, 1977, *Tech. Rep. KFKI-1978-37*, Cent. Res. Inst. for Phys., Budapest, Hungary, 1978.
Lazarus, A. J., K. W. Ogilvie, and L. F. Burlaga, Interplanetary shock observations by Mariner 5 and Explorer 34, *Solar Phys.*, *13*, 232, 1970.
Lee, T. S., and T. Chen, Hydromagnetic interplanetary shock waves, *Planet. Space Sci.*, *16*, 1483, 1968.
Lepping, R. P., and P. D. Argentiero, Single spacecraft method of estimating shock normals, *J. Geophys. Res.*, *76*, 4349, 1971.
Lin, R. P., L. G. Evans, and J. Fainberg, Simultaneous observations of fast electrons and type III radio burst emissions near 1 AU, *Astrophys. Lett.*, *14*, 191, 1973.
Neubauer, F. M., Nonlinear interaction of discontinuities in the solar wind and the origin of slow shocks, *J. Geophys. Res.*, *81*, 2248, 1976.
Ogilvie, K. W., Corotating shock structures, Solar Wind, *NASA Spec. Publ. SP-308*, 1972.
Ogilvie, K. W., and L. F. Burlaga, A discussion of interplanetary postshock flows with two examples, *J. Geophys. Res.*, *79*, 2324, 1974.
Pizzo, V., An evaluation of corotating solar wind stream models, in *Lecture Notes in Physics*, Springer, New York, in press, 1980*a*.
Pizzo, V., A three-dimensional model of corotating streams in the solar wind, 2, Hydrodynamic streams, *J. Geophys. Res.*, *85*, 727–743, 1980*b*.
Rosenau, P., and S. Frankenthal, Propagation of magnetohydrodynamic shocks in a thermally conducting medium, *Phys. Fluids*, *21*, 559, 1978.
Scarf, F. L., Wave-particle interaction phenomena associated with shocks in the solar wind, in *Proceedings of the De Feiter Memorial Symposium on the Study of Traveling Interplanetary Phenomena*, D. Reidel, Hingham, Mass., 1978.
Scarf, F. L., and D. A. Gurnett, A plasma wave investigation for the Voyager mission, *Space Sci. Rev.*, *21*, 289, 1977.
Scarf, F. L., R. W. Fredricks, L. A. Frank, C. T. Russell, P. J. Coleman, Jr., and M. Neugebauer, Direct correlations of large-amplitude waves with suprathermal protons in the upstream solar wind, *J. Geophys. Res.*, *75*, 7316, 1970.
Scarf, F. L., D. A. Gurnett, W. S. Kurth, and R. R. Shaw, Voyager 1, 2, plasma wave observations for the September 1977 storm period, UAG Report on the September 1977 and November 1977 Solar-Geophysical Activity, World Data Center A, Boulder, Colo., 1979.
Schwenn, R., M. D. Montgomery, H. Rosenbauer, H. Miggenrieder, K. H. Mulhauser, S. J. Bame, W. C. Feldman, and R. T. Hansen, Direct observations of the latitudinal extent of a high-speed stream in the solar wind, *J. Geophys. Res.*, *83*, 1011, 1978.
Schwenn, R., K. H. Mulhauser, and H. Rosenbauer, Two states of the solar wind at the time of solar activity minimum, I, Boundary layers between fast and slow streams, *Lecture Notes in Physics*, Springer, New York, in press, 1980.
Siscoe, G. L., Structure and orientation of solar wind interaction fronts: Pioneer 6, *J. Geophys. Res.*, *77*, 27, 1972.
Smith, E. J., and J. H. Wolfe, Pioneer 10, 11 observations of evolving solar wind streams and shocks beyond 1 AU, in *Study of Traveling Interplanetary Phenomena 1977*, edited by M. A. Shea et al., pp. 227–257, D. Reidel, Hingham, Mass., 1977.
Smith, E. J., and J. H. Wolfe, Fields and plasmas in the outer solar system, *Space Sci. Rev.*, *23*, 217, 1979.
Smith, E. J., L. Davis, Jr., P. J. Coleman, Jr., D. S. Colburn, P. Dyal, and D. E. Jones, August 1972 solar-terrestrial events: Observations of interplanetary shocks at 2.2 AU, *J. Geophys. Res.*, *82*, 1077, 1977.
Steinolfson, R. S., M. Dryer, and Y. Nakagawa, Numerical MHD simulation of interplanetary shock pairs, *J. Geophys. Res.*, *80*, 1223, 1975.
U.S. Department of Commerce, Solar-geophysical data 401, part I, p. 7, Boulder, Colo., Jan. 1978.
Vaisberg, O. L., and G. N. Zastenker, Solar wind and magnetosheath observations at earth during August 1972, *Space Sci. Rev.*, *19*, 687, 1976.
Wu, S. T., S. M. Han, and M. Dryer, Two-dimensional, time dependent MHD description of interplanetary disturbances, 1, Simulation of high-speed solar wind interactions, *Planet. Space Sci.*, [illegible] 255, 1979.

(Received September 5, 1979;
revised November 29, 1979;
accepted January 3, 1980.)

JOURNAL OF GEOPHYSICAL RESEARCH, VOL. 85, NO. A5, PAGES 2353–2356, MAY 1, 1980

The Volume Emissivity of Type III Radio Bursts

ROBERT L. TOKAR AND DONALD A. GURNETT

Department of Physics and Astronomy, The University of Iowa, Iowa City, Iowa 52242

The volume emissivity has been calculated for thirty-six type III solar radio bursts obtained from approximately 6.5 years of Imp 8 and ISEE 1 satellite data. Although the emissivities for these events vary over a large range, all the emissivities decrease rapidly with increasing heliocentric radial distance. The best fit power law for the emissivity, using the average power law index for all events analyzed, is $J = J_0 R^{-6.0}$, with $J_0 = 1.5 \times 10^{-24}$ W m^{-3} sr^{-1}. This best fit emissivity is used to estimate the expected radial variation of the plasma oscillations responsible for the type III radio emission.

INTRODUCTION

Type III solar radio bursts are characterized by an emission frequency which decreases with increasing time. These bursts are produced by solar flare electrons traveling away from the sun along the interplanetary magnetic field lines. The decreasing emission frequency with increasing time is attributed to the decreasing electron plasma frequency encountered by the exciter electrons as they move outward away from the sun [*Wild*, 1950; *Lin*, 1970; *Alvarez et al.*, 1972]. The generation of type III radio bursts is thought to be a two-step process in which electrostatic electron plasma oscillations are first produced by the energetic electron stream and are then converted to electromagnetic radiation by nonlinear interactions [*Ginzburg and Zheleznyakov*, 1958; *Sturrock*, 1961; *Tidman et al.*, 1966; *Papadopoulos et al.*, 1974; *Smith*, 1974]. For a review of low-frequency type III bursts, see, for example, *Fainberg and Stone* [1974]. Plasma oscillations associated with type III bursts are described by *Gurnett and Anderson* [1976, 1977] and *Gurnett et al.* [1978a].

The volume emissivity, which is the power emitted per unit volume per unit solid angle, is a fundamental quantity which characterizes all radio emission processes, including type III radio bursts. Because of the recent observations of electron plasma oscillations in association with type III bursts it is now possible to conduct quantitative evaluations of various mechanisms for generating the radio emission. Since little is known concerning the emissivity of type III bursts, particularly in the low-frequency range where direct comparisons with plasma oscillations are possible, it is the purpose of this paper to investigate the emissivity of some representative type III radio bursts. Particular attention will be given to the variation of the emissivity with heliocentric radial distance, since this variation can be directly compared with various generation mechanisms.

The type III events analyzed in this study were obtained from the earth-orbiting Imp 8 and ISEE 1 satellites. The plasma wave instrumentation onboard Imp 8 and ISEE 1 are described by *Gurnett* [1974] and *Gurnett et al.* [1978c], respectively.

METHOD OF CALCULATING THE EMISSIVITY

The emissivity is calculated by using the sun-centered coordinate system shown in Figure 1. The emissivity is defined as

$$J = \frac{\Delta P}{\Delta V \Delta \omega} \text{ W m}^{-3} \text{ sr}^{-1} \tag{1}$$

where ΔP is the power radiated in volume ΔV into a solid angle $\Delta\omega$. Since the angular distribution of the emitted radiation is not known, we will assume that the radiation is emitted isotropically (i.e., $\Delta\omega = 4\pi$). To determine J we measure the spectral power flux at the earth and compute ΔP using a $1/r^2$ law for the radial variation of the emitted radiation. The isotropy assumption and the simple propagation model used of course introduce an error, since any radiation propagating toward the sun will be reflected, thereby producing an anisotropy in the emitted radiation pattern. The error introduced is, however, at most a factor of 2, which is small in comparison with the wide range of intensities observed from event to event. Also, the isotropy assumption does not affect the radial variation of the emissivity, since sources at all radial distances are treated equivalently.

To compute the power ΔP, the distance from the source to the earth must be determined. Since the source position cannot, in most cases, be determined by direct measurement, a simple model is used for the trajectory of the type III source. The source is assumed to follow the magnetic field in the solar wind starting from the flare location at the sun. The magnetic field model used is that of *Parker* [1958]: in the solar equatorial plane the magnetic field lines are Archimedian spirals, whereas in the meridian plane the field lines stay on a cone of constant heliographic latitude. The heliographic longitude of the associated flare, ϕ_0, gives the heliographic longitude of the source region, ϕ, through the Archimedian spiral equation

$$\phi = \phi_0 - (\omega / V_{sw}) R \tag{2}$$

Here ω is the rotational velocity of the sun, V_{sw} is the solar wind velocity, taken as 400 km/s, and R is the heliocentric radial distance to the source. R is related to the observed emission frequency by using the emission level scale given by *Fainberg and Stone* [1974],

$$f = 66.8 R^{-1.315} \text{ MHz} \tag{3}$$

where f is the observed frequency of the type III burst and R is the heliocentric radial distance in solar radii. The position of the earth above the solar equatorial plane is determined from a simple model for the earth's orbit around the sun.

From the measured radiation intensity I at the time of maximum intensity the power radiated from the source, ΔP, in frequency interval Δf is calculated from

$$\Delta P = (4\pi r^2) I \Delta f \tag{4}$$

Paper number 80A0197.
0148-0227/80/080A-0197$01.00

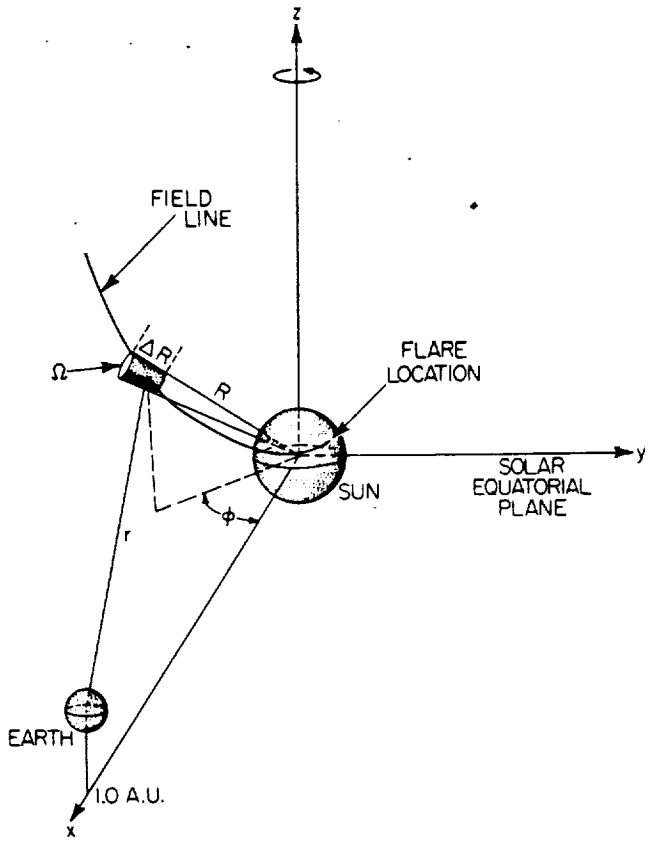

Fig. 1. A perspective drawing showing the geometry used to calculate the emissivity of a type III burst source region. The spectral power flux at the earth gives the power radiated out of the source region and this together with the volume of the source region gives the emissivity.

where r is the radial distance from the source to the earth (see Figure 1). The volume of the source is determined by two factors, the angular size of the source as viewed from the sun, Ω, and the radial thickness ΔR. Since the electrons which produce the radio emission closely follow the interplanetary magnetic field lines, the angular size of the source as viewed from the sun is essentially constant, independent of radial distance from the sun. Since it is often not possible to determine the source size because of geometric considerations, we have assumed a half angle for the source of 45° as viewed from the sun. The corresponding solid angle is $\Omega = 1.84$ sr. This source size is comparable to the source sizes measured by *Baumback et al.* [1976] and *Gurnett et al.* [1978*b*] and is considered a reasonable estimate, since both radio and charged particle measurements indicate that the source must be quite large. The relation of the radial thickness ΔR to the frequency interval Δf can be determined from (3), which gives $\Delta R/R = 1.315\,(\Delta f/f)$. By combining all of these factors the volume of the source becomes

$$\Delta V = \Omega R^2 \Delta R = 1.315 \Omega R^3 (\Delta f/f) \tag{5}$$

and the emissivity is given by

$$J = (r^2 f/1.315 \Omega R^3) I \tag{6}$$

Since the emissivity is determined by using average values for the solar wind parameters and since significant deviations from the average parameters may occur in specific cases, the approach taken is to analyze a large number of events and compute an average best fit emissivity, thereby hopefully averaging out the variations which may be present in individual cases. Although the absolute emissivity is probably uncertain by about a factor of 2, mainly due to the difficulty in estimating the angular size of the source, the radial dependence of the emissivity is much more accurately determined, since most of the parameters assumed are nearly independent of radial distance.

Results and Discussion

Approximately 5 years of Imp 8 data and 1.5 years of ISEE 1 data were surveyed for type III bursts suitable for analyzing the emissivity. While type III bursts were frequently observed, two main factors limited the number of events used in this study: (1) clear burst maximums needed to be observed in at least three channels in order to give a reasonably accurate indication of the radial variation of the emissivity; and (2) for each event an associated solar flare had to be found in order to determine the trajectory of the source. Of a total of 117 events which showed clear burst maxima, 54 had associated solar flares. Of these, 13 events were common to both satellites. Restricting the study to heliocentric distances less than 1.0 AU eliminated 3 events, while 2 events were eliminated as being inconsistent. Consequently, 36 events were suitable for analysis. Table 1 contains the date, onset time, and flare coordinates for each event.

For each event the emissivity J was calculated as a function of the heliocentric radial distance R and fit to a power law of the form $J = J_0 R^{\alpha}$. In most cases a power law provided a good least squares fit to the radial dependence, although in a few cases a substantial deviation from a power law was observed. In all cases the power law index α was negative, indicating a decreasing emissivity with increasing radial distance from the sun. Consult Table 1 for the derived J_0 and α values. The distribution of the power law indices obtained is shown by the histogram of Figure 2. The highest frequency of occurrence of an α falls in the interval from -4.0 to -6.0, and the average value of all the indices measured is $\bar{\alpha} = -6.0 \pm 0.3$. The standard deviation of the sample is 1.9. Figure 3 shows a composite summary of the emissivity for all the events analyzed. Points common to the same event are connected by a line. As can be seen, the emissivity varies over a large range from event to event. The dashed line shows the best fit of $\log J$ to $\log J_0 R^{-6.0}$. The best fit value for J_0 is 1.5×10^{-24} W m^{-3} sr^{-1}.

It is clear from these results that the emissivity of low-frequency type III radio bursts decreases very rapidly with increasing radial distance from the sun, with an average power law index of about -6.0. This decrease in the emissivity must be related to a corresponding decrease in the plasma oscillation intensity with increasing radial distance from the sun. From the currently available evidence on type III radio bursts the dominant emission at low frequencies is thought to be at the harmonic, $2f_p^-$, of the local electron plasma frequency [*Fainberg et al.*, 1972; *Haddock and Alvarez*, 1973; *Kaiser*, 1975; *Gurnett et al.*, 1978*b*]. In all current theories for harmonic emission the essential dependence of the emissivity on the electric field strength E of the plasma oscillations is $J \propto E^4$. Neglecting for the moment other weaker radial dependences, the $R^{-6.0}$ dependence of J would imply a $R^{-1.5}$ variation of E with radial distance from the sun. This radial variation of the plasma oscillation intensities is not nearly as steep as the $R^{-3.5}$ dependence reported recently by *Gurnett et al.* [1978*a*]. However, the plasma oscillation intensities given by *Gurnett et al.*

TABLE 1. The 36 Events Analyzed, With Associated Flare Coordinates and Calculated J_0 and α Values

Date	Onset Time, UT	Flare Coordinates (Heliographic)		J_0, W m^{-3} sr^{-1}	α
		Latitude	Longitude		
Dec. 23, 1973	0800	16°S	35°W	6.84×10^{-25}	− 5.8
Jan. 18, 1974	0230	4°N	65°W	3.22×10^{-25}	− 2.5
April 5, 1974	1800	11°S	35°W	5.73×10^{-25}	− 4.4
May 8, 1974	0100	16°S	3°E	2.57×10^{-26}	− 4.5
May 9, 1974	2300	5°S	45°W	1.41×10^{-26}	− 5.3
Sept. 18, 1974	0530	9°N	37°W	2.17×10^{-25}	− 5.4
Sept. 18, 1974	1130	10°N	42°W	2.16×10^{-25}	− 5.2
Jan. 4, 1977	1720	22°S	72°W	1.47×10^{-23}	− 6.2
Oct. 10, 1977	2035	6°N	10°E	9.51×10^{-25}	− 6.8
Nov. 22, 1977	1000	23°N	41°W	3.25×10^{-24}	− 8.7
Dec. 7, 1977	0330	22°S	16°W	7.42×10^{-23}	− 5.3
Dec. 9, 1977	0650	24°S	41°W	2.48×10^{-26}	− 9.8
Dec. 23, 1977	0630	23°N	6°E	8.93×10^{-28}	−11.0
Dec. 24, 1977	1840	22°N	12°W	2.10×10^{-25}	− 7.6
Jan. 6, 1978	0730	35°N	4°W	3.52×10^{-24}	− 3.7
Jan. 8, 1978	0710	12°S	85°W	2.92×10^{-25}	− 5.6
Feb. 11, 1978	1430	14°N	6°E	5.12×10^{-23}	− 8.5
March 4, 1978	1200	18°N	39°E	4.88×10^{-24}	− 9.3
March 12, 1978	0210	20°N	69°W	9.15×10^{-24}	− 4.7
April 11, 1978	1410	22°N	56°W	5.06×10^{-23}	− 4.4
April 18, 1978	0100	14°N	45°W	6.10×10^{-22}	− 5.6
May 6, 1978	1635	19°N	53°W	2.20×10^{-24}	− 5.1
May 13, 1978	0750	28°S	70°W	1.90×10^{-23}	− 5.6
May 22, 1978	0200	27°S	44°W	1.96×10^{-21}	− 2.8
May 31, 1978	1620	21°N	56°W	4.21×10^{-24}	− 8.4
June 1, 1978	1330	21°N	17°W	1.81×10^{-22}	− 3.8
July 1, 1978	1145	21°N	65°E	1.35×10^{-25}	− 4.3
July 11, 1978	1050	20°S	28°W	2.95×10^{-24}	− 5.9
Sept. 8, 1978	1815	15°N	64°W	2.39×10^{-24}	− 4.7
Sept. 23, 1978	1010	34°N	50°W	5.01×10^{-23}	− 4.6
Oct. 5, 1978	1405	18°S	4°E	1.31×10^{-26}	− 7.5
Oct. 13, 1978	1235	18°S	1°W	7.29×10^{-25}	− 6.5
Oct. 31, 1978	0915	20°N	36°W	2.70×10^{-26}	− 7.3
Dec. 18, 1978	1630	11°N	17°E	2.62×10^{-24}	− 5.4
Feb.18, 1979	0650	19°N	16°E	7.57×10^{-27}	− 7.8
Feb. 18, 1979	1640	18°N	16°W	5.77×10^{-24}	− 6.6

[1978*a*] are based on so few points it is probably not possible to make a meaningful quantitative comparison until more plasma oscillation events are analyzed. Such a study is currently under way. Nevertheless, it is interesting to note that the $R^{-1.5}$ variation implied by the above considerations agrees reasonably well with what would be expected for the saturation amplitude of plasma oscillations in the solar wind. Saturation effects are usually characterized by a dimensionless ra-

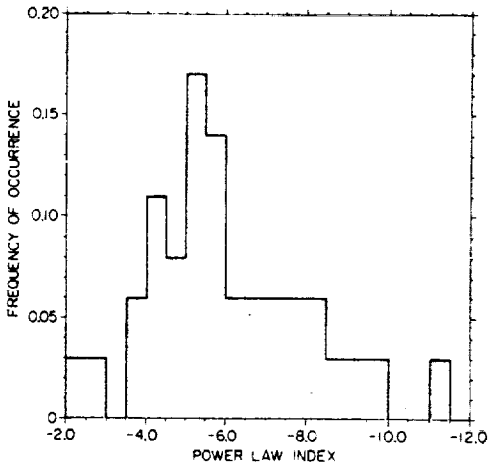

Fig. 2. A histogram of the power law indexes obtained from the 36 events analyzed. The highest frequency of occurrence is in the interval −4.0 to −6.0, and the average index is -6.0 ± 0.3. The standard deviation of the sample is 1.9.

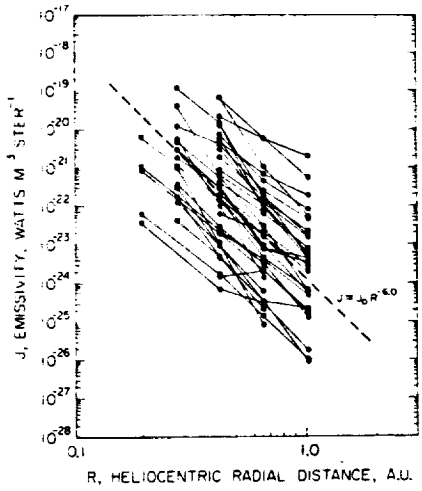

Fig. 3. A composite plot of the emissivity for the 36 events used in this study. Points common to one event are connected by a solid line, and the best fit power law is shown by a dashed line. This plot shows that the emissivity decreases rapidly with increasing radial distance from the sun.

tio of the electric field to plasma energy density, $E^2/8\pi nkT$, which reaches an approximately constant asymptotic value after the instability has grown into the nonlinear regime. Since the electron density varies approximately as $n \propto 1/R^2$, and the electron temperature varies approximately as $T \propto R^{-0.28}$ [*Hundhausen*, 1972], the saturation electric field strength should vary approximately as $E \propto R^{-1.14}$ if $E^2/8\pi nkT$ is constant, which is very close to the radial dependence estimated from the emissivity.

Acknowledgments. This research was supported by the National Aeronautics and Space Administration through contracts NAS5-11431 and NAS5-20093 and grant NGL-16-001-043 and by the U.S. Office of Naval Research.

The Editor thanks J. Fainberg for his assistance in evaluating this paper.

REFERENCES

Alvarez, H., F. T. Haddock, and R. P. Lin, Evidence for electron excitation of type III radio burst emission, *Solar Phys., 26,* 468, 1972.

Baumback, M. M., W. S. Kurth, and D. A. Gurnett, Direction-finding measurements of type III radio bursts out of the ecliptic plane, *Solar Phys., 48,* 361, 1976.

Fainberg, J., and R. G. Stone, Satellite observations of type III solar radio bursts at low frequencies, *Space Sci. Rev., 16,* 145, 1974.

Fainberg, J., L. G. Evans, and R. G. Stone, Radio tracking of solar energetic particles through interplanetary space, *Science, 178,* 743, 1972.

Ginzburg, V. L., and V. V. Zheleznyakov, On the possible mechanism of sporadic solar radio emission (radiation in an isotropic plasma), *Sov. Astron., AJ2,* 653, 1958.

Gurnett, D. A., The earth as a radio source: Terrestrial kilometric radiation, *J. Geophys. Res., 79,* 4227, 1974.

Gurnett, D. A., and R. R. Anderson, Electron plasma oscillations associated with type III radio bursts, *Science, 194,* 1159, 1976.

Gurnett, D. A., and R. R. Anderson, Plasma wave electric fields in the solar wind: Initial results from Helios 1, *J. Geophys. Res., 82,* 632, 1977.

Gurnett, D. A., R. R. Anderson, F. L. Scarf, and W. S. Kurth, The heliocentric radial variation of plasma oscillations associated with type III radio bursts, *J. Geophys. Res., 83,* 4147, 1978*a*.

Gurnett, D. A., M. M. Baumback, and H. Rosenbauer, Stereoscopic direction finding analysis of a type III solar radio burst: Evidence for emission at $2f_p^-$, *J. Geophys. Res., 83,* 616, 1978*b*.

Gurnett, D. A., F. L. Scarf, R. W. Fredricks, and E. J. Smith, The ISEE-1 and ISEE-2 plasma wave investigation, *Geosci. Electron., GE-16,* 225, 1978*c*.

Haddock, F. T., and H. Alvarez, The prevalence of second harmonic radiation in type III bursts observed at kilometric wavelengths, *Solar Phys., 29,* 183, 1973.

Hundhausen, A. J., *Coronal Expansion and Solar Wind,* p. 57, Springer, New York, 1972.

Kaiser, M. L., The solar elongation distribution of low frequency radio bursts, *Solar Phys., 45,* 181, 1975.

Lin, R. P., The emission and propagation of 40 keV solar flare electrons, *Solar Phys., 12,* 266, 1970.

Papadopoulos, K., M. L. Goldstein, and R. A. Smith, Stabilization of electron streams in type III solar radio bursts, *Astrophys. J., 190,* 175, 1974.

Parker, E. N., Dynamics of the interplanetary gas and magnetic fields, *Astrophys. J., 128,* 664, 1958.

Smith, D. F., Type III radio bursts and their interpretation, *Space Sci. Rev., 16,* 91, 1974.

Sturrock, P. A., Spectral characteristics of type III solar radio bursts, *Nature, 192,* 58, 1961.

Tidman, D. A., T. J. Birmingham, and H. M. Stainer, Linc splitting of plasma radiation and solar radio outbursts, *Astrophys. J., 146,* 207, 1966.

Wild, J. P., Observations of the spectrum of high-intensity solar radiation at metre wavelengths, III, Isolated bursts, *Aust. J. Sci. Res., Ser. A, 3,* 541, 1950.

(Received November 14, 1979;
revised February 8, 1980;
accepted February 11, 1980.)

Correction

In the paper 'The Volume Emissivity of Type III Radio Bursts' by Robert L. Tokar and Donald A. Gurnett (*Journal of Geophysical Research, 85*(A5), 2353–2356, 1980) there is an error in the equation immediately preceding (5). It should read $\Delta f/f = 1.315\Delta R/R$. This changes (5) to $\Delta V = (\Omega R^3/1.315)(\Delta f/f)$ and (6) to $J = (1.315r^2 f/\Omega R^3)I$. As a result, the best fit value of J_0 is now 2.6×10^{-24} W m^{-3} sr^{-1}, and the J_0 values given in Table 1 should be multiplied by $(1.315)^2 = 1.73$. Also, any J values taken from Figure 3 should be multiplied by 1.73. These changes do not affect our conclusions.

(Received May 23, 1980;
accepted May 28, 1980.)

Paper number 80A0863.
0148-0227/81/080A-0863$01.00

Gurnett and Anderson: A Summary of Progress in Space Physics Made with Helios Plasma Wave Instrument Data (E5a)

A SUMMARY OF PROGRESS IN SPACE PHYSICS MADE WITH HELIOS PLASMA WAVE INSTRUMENT DATA (E 5a)

P.I.: D.A. Gurnett

Co.I.: R.R. Anderson

Department of Physics and Astronomy, University of Iowa
Iowa City, Iowa U.S.A.

Many significant advances in the study of plasma waves in the solar wind have been made with data from the University of Iowa Plasma Wave Instruments on Helios-1 and -2. The first observations of intense electron plasma oscillations associated with Type III solar radio bursts were made with data from these instruments. These observations confirmed the basic electron plasma oscillation mechanism proposed by Ginzburg and Zheleznyakov in 1958 for the generation of the Type III solar radio emissions. A study of electron plasma oscillation events associated with Type III solar radio bursts, using data from Helios-1 and -2, IMP-6 and -8 and Voyager 1 and 2, found that these events showed a pronounced increase in both intensity and frequency of occurrence with decreasing heliocentric radial distance. Only the Helios spacecraft, with their close approaches to the Sun, have been able to provide in situ measurements of these events in the region of their highest occurrence.

The Type III solar radio burst itself has been studied extensively using data from the Helios spacecraft. Stereoscopic radio direction-finding measurements from the Helios-1 and -2, IMP-8 and Hawkeye 1 spacecraft were used to track a Type III solar radio burst in three dimensions, independent of modeling assumptions concerning the emission frequency as a function of radial distance from the Sun. By combining these radio direction-finding measurements with direct in situ measurements of the solar wind plasma density near the Sun, it was found that the dominant emission occurs at the second harmonic, $2\ f_p$, of the electron plasma frequency. The results of this study confirmed earlier results by other investigations which had to rely on assumed models for the radial dependence of the emission frequency or on average statistical properties of the solar wind.

Further work has also been done on the association of Type III solar radio bursts and electron plasma oscillations in order to provide important new information on nonlinear plasma processes of considerable current interest. A study of the volume emissivity of Type III solar radio bursts showed that although the emissivities varied over a large range, all the emissivities decreased rapidly with increasing heliocentric radial distance. The best fit power law for the events analyzed found the emissivity J proportional to $R^{-6.0\pm0.3}$. When the observed electron plasma oscillation intensities and variation with radial distance (E was proportional to $R^{-1.4\pm0.5}$) were used in two current models for the conversion of electrostatic plasma oscillations to electromagnetic radiation, the observed emissivities were shown to be in good agreement with the predicted emissivities.

The most commonly occurring plasma wave detected by Helios is a sporadic emission between the electron and ion plasma frequencies. These waves are thought to be ion acoustic waves which are Doppler-shifted upwards in frequency from below the ion plasma frequency by the motion of the solar wind. Wavelength measurements from IMP-6 support this conclusion. Comparison of Helios results with measurements from this Earth-orbiting spacecraft show that the ion acoustic wave turbulence detected in interplanetary space has characteristics essentially identical to those of bursts of electrostatic turbulence generated by protons streaming into the solar wind from the Earth's bow shock. In a few cases, ion acoustic wave enhancements have been observed in direct association with abrupt increases in the anisotropy of the solar wind electron distribution. Comparisons with the overall solar wind corotational structure show that the most intense ion acoustic waves usually occur in the low-velocity regions ahead of high-speed solar wind streams. Of the detailed plasma parameters investigated, the ion acoustic wave intensities are found to be most closely correlated with the electron-to-proton temperature ratio, T_e/T_p, and with the electron heat flux. Investigations of the detailed electron and proton distribution functions also show that the ion acoustic waves usually occur in regions with highly non-Maxwellin distributions characteristic of double-proton streams. Two main mechanisms, an electron heat flux instability and a double-ion beam instability have been studied as possible generation mechanisms for the ion-acoustic-like waves observed in the solar wind.

Plasma wave turbulence associated with interplanetary shocks has also been studied using the Helios plasma wave data. Three types of plasma waves are usually detected in association with a strong interplanetary shock: (1) electron plasma oscillations, (2) electrostatic ion-acoustic or Buneman mode turbulence from about 1 to 30 kHz and (3) whistler-mode magnetic noise. The primary burst of electric and magnetic field noise at the shock occurs a few seconds after the jump in the magnetic field, with a broad maximum in the electric field intensities at a few kHz and a monotonically decreasing magnetic field spectrum below about 1 kHz. Many of the characteristics of strong interplanetary shocks are found to be closely similar to previous observations of plasma wave turbulence associated with the Earth's bow shock.

The Helios-1 and -2 Plasma Wave Instruments continue to operate satisfactorily and are returning valuable scientific data. As solar maximum approaches, the number of solar radio bursts and interplanetary shock waves detected has increased dramatically. This increase in activity provides many valuable opportunities for correlative studies with ISEE-1, -2 and -3 to provide triangulation measurements of Type III solar radio bursts and other plasma wave events. Current research efforts are concentrating on the study of plasma waves associated with interplanetary shocks using a large number of events to investigate the dependence of the plasma wave intensities on the Mach number, magnetic field direction and shock normal angle. Other studies of electron plasma oscillations associated with Type III solar radio bursts and electron plasma oscillations and ion acoustic waves in the solar wind are continuing.

S LAR WIND, VOL. 4, MAX PLANCK INSTITUT REPORT NO. MPAE-2-100-81-31, LINDAU, GERMAMY, PAGE 286, 198

Gurnett: Plasma Waves in the Solar Wind: A Review of Observations

PLASMA WAVES IN THE SOLAR WIND: A REVIEW OF OBSERVATIONS

D. A. Gurnett
Department of Physics and Astronomy, The University of Iowa
Iowa City, Iowa, USA

Abstract. A review is presented of the current experimental and theoretical understanding of plasma waves in the solar wind, with comments on the possible effect these waves may have on the macroscopic structure of the solar wind. Only short wavelength waves at frequencies above the magnetohydrodynamic regime are considered. These waves include electron plasma oscillations, ion-acoustic waves, whistler-mode waves, and ion-cyclotron waves. Waves associated with interplanetary shocks are also discussed.

I. INTRODUCTION

In the past few years significant advances have been made in our knowledge and understanding of plasma instabilities in the solar wind. The purpose of this paper is to survey the current status of solar wind plasma wave observations and to comment on the various plasma instability mechanisms which are thought to be responsible for these waves. To limit the scope of this review only short wavelength instabilities driven by microscopic, local processes in the solar wind are considered. For a review of long wavelength, Alfvén and magnetohydrodynamic (MHD) waves involving interactions on time scales comparable to the expansion time of the solar wind, see for example, Hollweg [1975]. Since this review covers all waves above the MHD range, the frequencies of interest extend across the entire range of local characteristic frequencies of the plasma, from the ion-cyclotron frequency to the electron plasma frequency.

Since the earliest work of Parker [1958], it has been thought that plasma instabilities play an important role in the dynamical evolution of the solar wind. As is well-known, waves generated by instabilities in a collisionless plasma play a role similar to collisions in an ordinary gas by providing the scattering and momentum transfer necessary to drive the plasma towards thermal equilibrium. Since the collisionless solar wind plasma can be described in many respects by fluid-like equations involving approximate local thermal equilibrium, wave-particle interactions must be involved in determining the equilibrium particle distributions. It has been suggested, for example, that wave-particle interactions play a role in controlling the heat flux in the solar wind [Forslund, 1970; Gary et al., 1975], in heating the solar wind protons [Fredricks, 1969], in thermalizing double-ion streams [Montgomery et al., 1975; Lemons et al., 1978], in accelerating alpha particles in the solar wind [Hollweg and Turner, 1978], and in controlling the evolution of energetic electrons emitted by solar flares [Papadopoulos et al., 1974; Magelssen and Smith, 1977].

Up to the present time the primary solar wind plasma wave measurements which are available for analysis are from the Pioneer 8 and 9 [Scarf et al., 1968], Helios 1 and 2 [Gurnett and Anderson, 1977; Neubauer et al., 1977] and Voyager 1 and 2 [Scarf and

Gurnett, 1978] spacecraft. Because of the low sensitivity, the early Pioneer 8 and 9 measurements are mainly confined to large amplitude electric fields associated with shocks and other solar wind discontinuities. The higher sensitivity measurements from the more recently launched Helios and Voyager spacecraft have in the meantime provided a comprehensive survey of all the plasma waves which occur in the solar wind from about 0.3 to 3 AU, even at very low intensities.

The main types of plasma waves observed in the solar wind are, in order of decreasing frequency (1) electron plasma oscillations (Langmuir waves) at the local electron plasma frequency, f_p^-, (2) ion-acoustic waves at frequencies below the ion plasma frequencies, f_p^+, (3) whistler-mode waves at frequencies below the electron gyrofrequency, f_g^-, and (4) ion-cyclotron waves at frequencies below the proton cyclotron frequency f_g^+. The approximate frequency range and radial variation of the characteristic frequency associated with each of these waves are shown in Figure 1. For future reference, Figure 2 shows the corresponding dispersion relation, phase velocity vs. frequency, for typical solar wind parameters at 1 AU. In this review, electrostatic and electromagnetic waves are discussed separately since the instability mechanism and interaction with the plasma tends to be quite different for these two cases. In addition, plasma waves associated with interplanetary shocks are discussed in a separate section since these events are of a somewhat specialized nature.

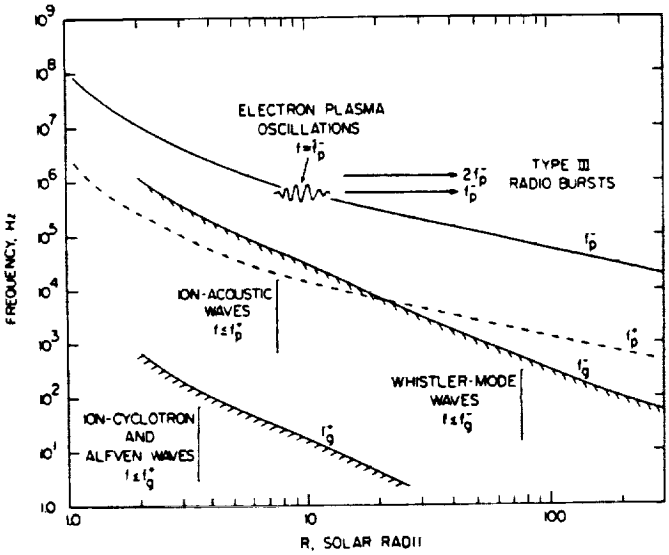

Figure 1. The radial variation of the most important characteristic frequencies of the solar wind plasma.

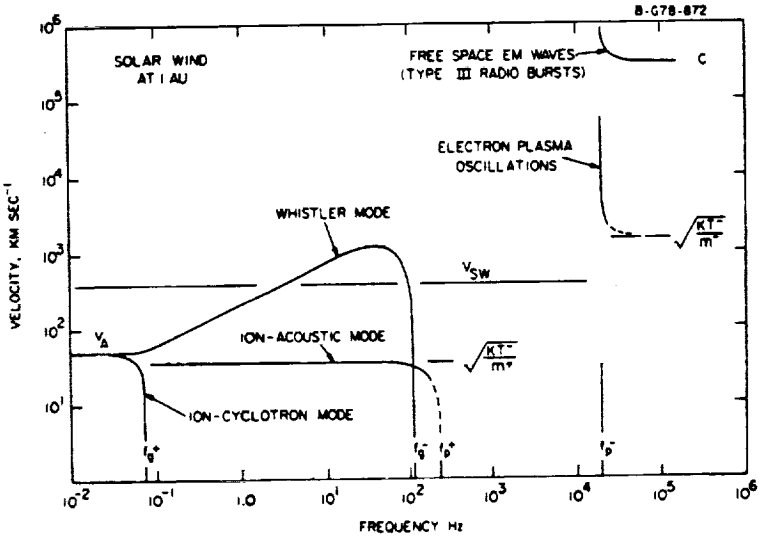

Figure 2. The phase velocity of the various plasma wave modes which occur in the solar wind at 1 AU.

II. ELECTROSTATIC WAVES

A. Electron Plasma Oscillations

Intense narrow-band electrostatic emissions near the electron plasma frequency, f_p^-, are occasionally detected by both the Helios and Voyager spacecraft. Polarization measurements with the Helios spacecraft [Gurnett and Anderson, 1977] show that the electric field of these waves is parallel to the static magnetic field, which together

with the oscillation frequency, uniquely identifies these waves as electron plasma oscillations. Electron plasma oscillations usually occur in association with solar flares and type III radio bursts, although occasionally no relationship to solar activity is apparent. A typical example of electron plasma oscillations detected by Helios in association with a type III radio burst is shown in Figure 3, from Gurnett and Frank [1978]. The solid lines in this illustration give the peak electric field strengths and the vertical bars (solid black areas) give the average field strengths. The intensity scale for each frequency channel is logarithmic, with a dynamic range of 100 db, extending from about 1 $\mu V\ m^{-1}$ to 100 $mV\ m^{-1}$. The local electron plasma frequency, f_p^-, at the time of the burst is indicated in Figure 3. As can be seen, the largest electric field strength occurs in the 31.1 kHz channel, in almost exact coincidence with the electron plasma frequency. Since the phase velocity of these waves is substantially larger than the solar wind velocity, V_{sw}, Doppler shifts due to the solar wind motion are small (see Figure 2). The very large ratio of peak-to-average field strengths, $\sim 10^3$, evident in Figure 3 indicates that the plasma oscillations consist of many short very intense bursts, with a relatively long dead time between bursts. As shown by Gurnett and Anderson [1977], the time scale for an individual burst is often extremely short, sometimes comparable to the time resolution (50 msec.) of the instrument. The observation of such spiky bursts has led to the suggestion that these waves may be involved in strong turbulence effects, such as the oscillating two-stream instability [Papadopoulos et al., 1974] and soliton collapse [Nicholson et al., 1978]. At the present time, however, support for such processes is only qualitative since the field strengths involved, $E^2/8\pi nkT \simeq 10^{-5}$, are only marginal for the onset of strong turbulence effects, and the time resolution is not adequate to resolve the intense fields associated with a collapsing soliton [Smith and Nicholson, 1978].

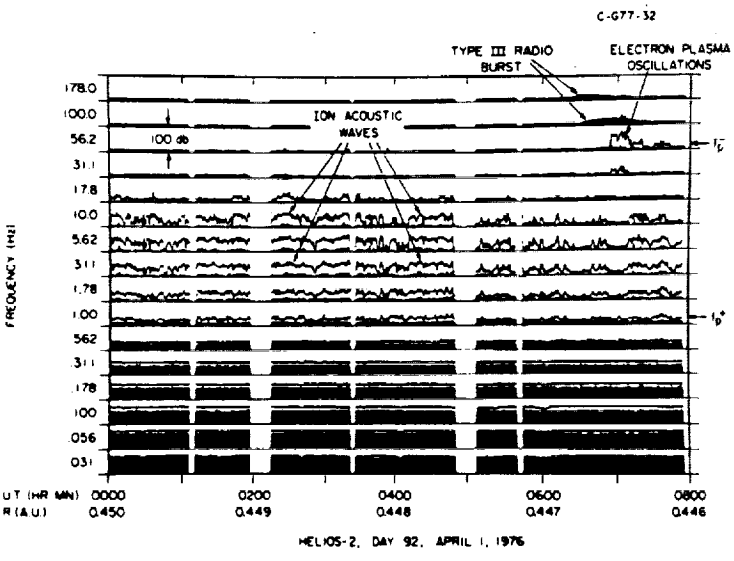

Figure 3. Typical examples of electron plasma oscillations and ion-acoustic waves detected by Helios 2 at 0.45 AU.

The Helios observations of electron plasma oscillations in direct association with type III solar radio bursts [Gurnett and Anderson, 1976] provides a convincing verification of the mechanism, first proposed by Ginzburg and Zheleznyakov [1958] nearly twenty years ago, that these radio bursts are caused by intense electron plasma oscillations generated by a two-stream instability. As indicated in Figure 1, nonlinear interactions can produce radio emission at both the fundamental, f_p^-, and second harmonic, $2f_p^-$, of the electron plasma frequency. The characteristic

decreasing frequency with increasing time of a type III radio burst is produced by the decreasing electron plasma frequency excited by the solar flare electrons as they sweep outward away from the sun. Various techniques show that the dominant radio emission at low frequencies (< 1 MHz) is at the second harmonic [Fainberg et al., 1972; Kaiser, 1975; Gurnett et al., 1978a].

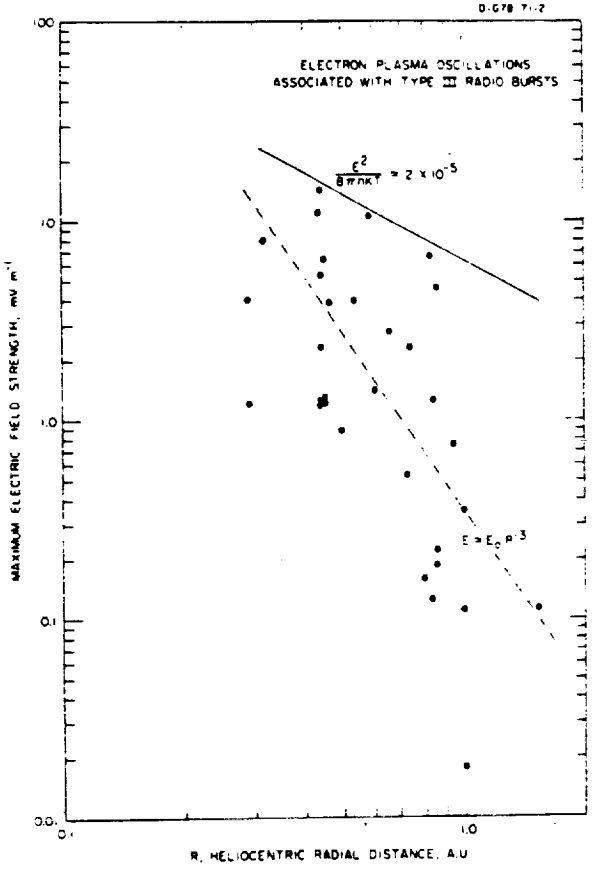

Figure 4. The heliocentric radial variation of electron plasma oscillation intensities associated with type III radio bursts.

When plasma oscillations are associated with a type III radio burst they are often very intense, as in Figure 3, and show a clear tendency for a saturation effect which limits the maximum field strength of the oscillations. Studies of numerous events at various radial distances from the sun show a systematic decrease in the saturation field strength with increasing radial distance. This radial dependence is illustrated in Figure 4, from Gurnett et al. [1978b], which shows the maximum plasma oscillation field strengths for all of the type III events detected to date with electron plasma oscillations. A best fit power law through all of the points indicates that the electric field amplitude varies approximately as $1/R^3$. Although the small number of events limits the accuracy to which the power law index can be determined, the general trend toward decreasing field strength with increasing radial distance from the sun is clearly evident. An approximate upper bound to the electric field to plasma energy density ratio, $E^2/8\pi nkT$, is approximately 2×10^{-5}, as indicated by the solid line in Figure 4.

B. Ion-Acoustic Waves

One of the early discoveries from the Helios plasma wave experiment was the observation of moderately intense electrostatic waves at frequencies between the ion and electron plasma frequencies, $f_p^+ < f < f_p^-$. These waves were initially referred to $f_p^+ < f < f_p^-$ noise [Gurnett and Anderson, 1977]. Subsequent investigations by Gurnett and Frank [1978] showed that these waves have very short wavelengths, $\lambda \simeq 2\pi\lambda_D$ where λ_D is the Debye length. Polarization measurements showed that the electric field is closely aligned along the direction of the static magnetic field. Considerations of the possible short wavelength electrostatic modes which can occur in a plasma strongly

suggest that these waves are short wavelength ion-acoustic waves or waves with very similar characteristics.

An example of the ion-acoustic waves detected by Helios is shown in Figure 3. The ion-acoustic waves usually extend over a relatively broad range of frequencies and consist of many short impulsive bursts, as indicated by the large ratio of peak-to-average field strengths. The frequency spectrum of these bursts shows a systematic variation with radial distance from the sun, decreasing in intensity and frequency with increasing radial distance from the sun. This radial dependence is illustrated in Figure 5 which shows two typical spectrums from Helios at 0.47 and 0.98 AU and one spectrum from Voyager at 1.73 AU. The upper frequency cutoff of the spectrum is consistent with the maximum frequency expected for Doppler shifted ion-acoustic waves [Gurnett and Anderson, 1977],

$$f_{max} \simeq f_p^+ + \left(\frac{V_{SW}}{2\pi\lambda_D}\right) \cos \theta_{kV} ,$$

where θ_{kV} is the angle between the wave vector and the solar wind velocity. As indicated in Figure 2, large Doppler shifts are expected for ion-acoustic waves, since the solar wind velocity is much larger than the ion-acoustic velocity, $\sqrt{kT^-/m^+}$. The radial variation in the upper frequency cutoff is mainly due to the radial variation in the Debye length which varies approximately as $\lambda_D \propto 1/R$. According to this interpretation the apparent relationship of the upper and lower cutoffs of the spectrum to f_p^+ and f_p^- is purely coincidental.

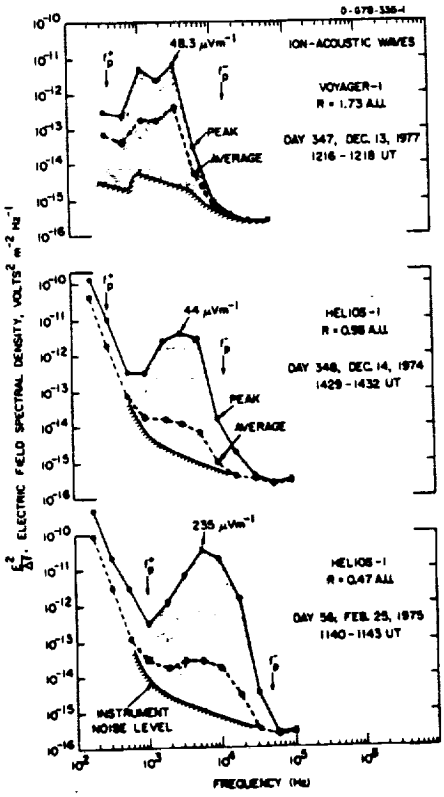

Figure 5. A sequence of ion-acoustic wave spectrums showing the decrease in the intensity and frequency with increasing radial distance from the sun.

High-time resolution spectrum measurements from the Voyager spacecraft, shown in Figure 6 from Kurth et al. [1979], provide very detailed information on the frequency-time structure of these waves. As can be seen from Figure 6, the ion-acoustic wave bursts consist of narrow-band emissions with a rapidly varying center frequency, sometimes displaying the inverted-U form evident in Figure 6. The rapid frequency variations explains why the peak field strength spectrums from Helios, as in Figure 3, appear so broad, since the frequency of a single burst usually sweeps through several channels. The duration of the bursts is usually very short, only a few tenths of a second to about one second.

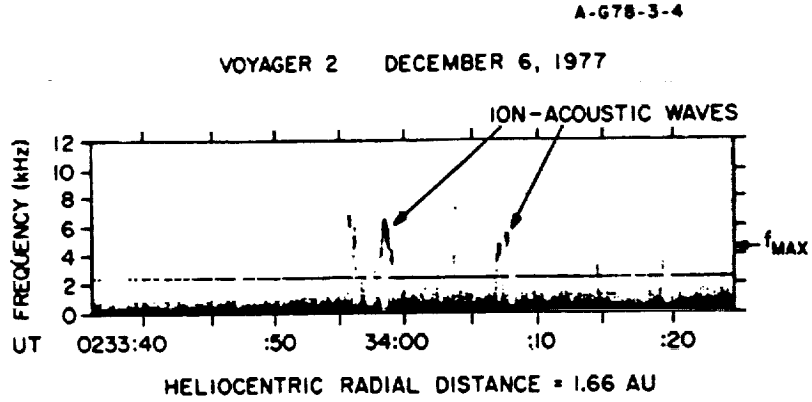

Figure 6. High-time resolution spectrogram of an ion-acoustic wave burst detected by Voyager 1.

The occurrence of ion-acoustic-like waves in the solar wind is not surprising, since at least two investigators predicted their occurrence before the Helios observations. Fredricks [1969] predicted that current-driven ion-acoustic waves should be observed in association with shocks and other discontinuities, and Forslund [1970] proposed that ion-acoustic waves should be generated by an electron heat flux instability whenever the electron-to-ion temperature ratio, T_e/T_i, is sufficiently large. More recent attempts to account for the detailed characteristics of the ion-acoustic waves detected by Helios and Voyager have concentrated on a double-ion beam instability proposed by Gary [1978] and on refinements of Forslund's electron heat flux mechanism [Dum et al., 1979]. At the present time the exact mechanism responsible for these waves, and even the precise identification of the waves as ion-acoustic waves, has not been definitely established. A thorough study of the relationship of these waves to the plasma parameters measured simultaneously by Helios has recently been given by Gurnett et al. [1979]. Im summary, both the electron heat flux and double-ion beam mechanisms have elements of support in the experimental data. The principal difficulty with the electron heat flux mechanism is that occasionally waves are observed at T_e/T_i ratios which are too small to predict instability. Similarly the proton distribution functions usually do not display a sufficiently separated double peak to produce an ion beam instability. Overall, the observed correlation of the wave intensity with T_e/T_i and the electron heat flux seem to favor the electron heat flux mechanism, although other mechanisms involving double-ion beams or suprathermal proton streams [which cannot be detected by Helios in the energy range from about 1.6 to 50 keV) cannot be ruled out.

III. ELECTROMAGNETIC WAVES

A. Whistler-Mode Waves

Measurements with high sensitivity search-coil magnetometers on Helios [Neubauer et al., 1977a] have shown that a weak background of low frequency magnetic field turbulence is nearly always present in the solar wind at frequencies extending up to approximately the local electron gyrofrequency. The upper frequency cutoff near the local electron gyrofrequency, f_g^-, provides substantial evidence that this turbulence is caused by electromagnetic whistler-mode waves. As shown in Figure 1, the whistler mode has an upper frequency cutoff at f_g^-. Fortunately, the phase velocity of the whistler mode (see Figure 2) is usually comparable or larger than the solar wind

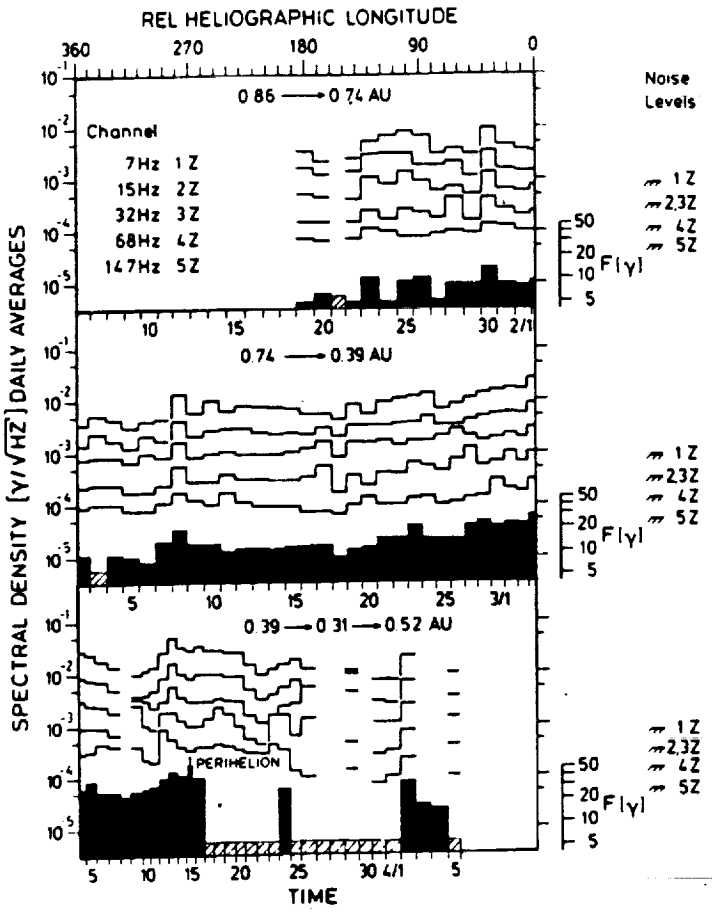

Figure 7. Magnetic field spectral densities of whistler-mode turbulence during the primary mission of Helios 1 [from Neubauer et al., 1977a].

velocity, so that the upper cutoff frequency is not strongly modified by Doppler shifts. A typical example of the magnetic field intensities associated with this whistler-mode turbulence is shown in Figure 7, from Neubauer et al. [1977a]. As can be seen, the intensity of this turbulence increases rapidly with decreasing frequency and with decreasing radial distance from the sun. Other types of discrete whistler-mode emissions have also been reported by Neubauer et al. in association with discontinuities in the solar wind.

Several possible mechanisms for generating unstable whistler-mode waves in the solar wind have been proposed, including thermal anisotropies in the ion distribution function [Scarf et al., 1967] and instabilities driven by the electron heat flux [Gary et al., 1975]. At the present time it seems most likely that the whistler-mode turbulence detected in the solar wind by Helios is produced by an electron heat flux instability, although other possibilities such as the nonlinear cascading of long wavelength large amplitude Alfvén waves cannot be entirely ruled out. Since whistler-mode waves can interact resonantly with electrons it is possible that this turbulence could play an important role in the pitch angle scattering of solar wind electrons or in controlling the thermal conductivity of the solar wind [Gary and Feldman, 1977]. For a review of these and other kinetic processes in the solar wind, see Feldman [1978].

B. Ion-Cyclotron Waves

As shown in Figure 1 electromagnetic ion-cyclotron waves are expected in the solar wind at frequencies below the proton cyclotron frequency, f_g^+. Because of the decreasing proton gyrofrequency with increasing radial distance from the sun, ion-cyclotron waves are generated as a natural consequence of the outward propagation of Alfvén waves from the sun, as in the "magnetic beach" model discussed by Stix [1962]. Ion-cyclotron waves can also be generated by a locally driven instability when $T_{\parallel} > T_{\perp}$ [Gary et al., 1976].

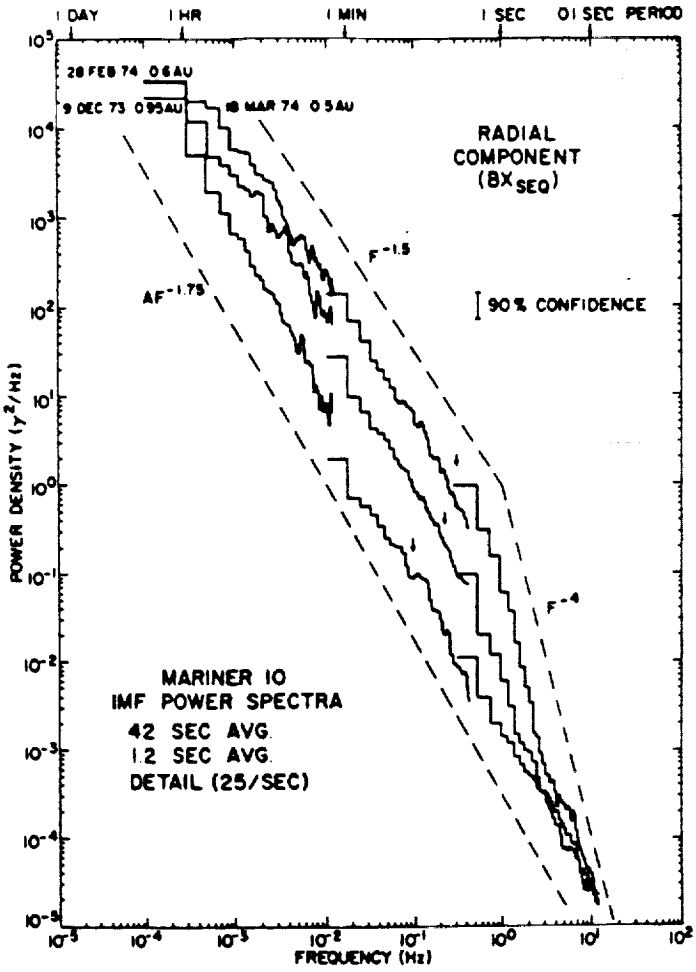

Figure 8. Typical magnetic field spectrums from Mariner 10 [Behannon, 1976] showing the break in the spectral slope near the proton gyrofrequency, possibly attributed to ion-cyclotron waves.

Because of the large Doppler shifts expected for the ion-cyclotron mode and the presence of whistler-mode turbulence in the same frequency range (see Figure 2), conclusive identification of ion-cyclotron waves in the solar wind is difficult. Magnetic field spectrum measurements such as in Figure 8, from Behannon [1976], consistently show a break in the spectral slope near the proton gyrofrequency which may indicate the presence of ion-cyclotron waves. Behannon has also reported nearly monochromatic left-hand polarized magnetic field oscillation at frequencies near the proton gyrofrequency which he tentatively identifies as ion-cyclotron waves. Further measurements with improved plasma diagnostics are needed to provide a firm identification of these waves as ion-cyclotron waves. Since ion-cyclotron waves can interact resonantly with protons, alpha particles and other heavy ions, it is thought that these waves may play an important role in the acceleration of solar wind ions [Hollweg and Turner, 1978].

IV. WAVES ASSOCIATED WITH INTERPLANETARY SHOCKS

As is the case for the earth's bow shock large plasma wave turbulence levels are expected in association with interplanetary shocks. This turbulence is necessary to provide the collisionless interactions required to heat the plasma at the shock boundary. The first observations of plasma wave electric fields associated with interplanetary shocks were obtained from Pioneer 7 and 8 [Scarf et al., 1968; Scarf and Siscoe, 1971; Siscoe et al., 1971]. Other shocks which have been investigated include measurements from IMP-7 [Scarf, 1977], Helios 1 and 2 [Neubauer et al., 1977b], Gurnett et al., 1979], and Voyager 1 [Kurth et al., 1979]. Because of the limited number of events which have been examined and the wide variability from event to event, it is difficult to summarize the characteristics observed, other than to comment that most of the wave modes discussed in the previous two sections are also present in association with shocks.

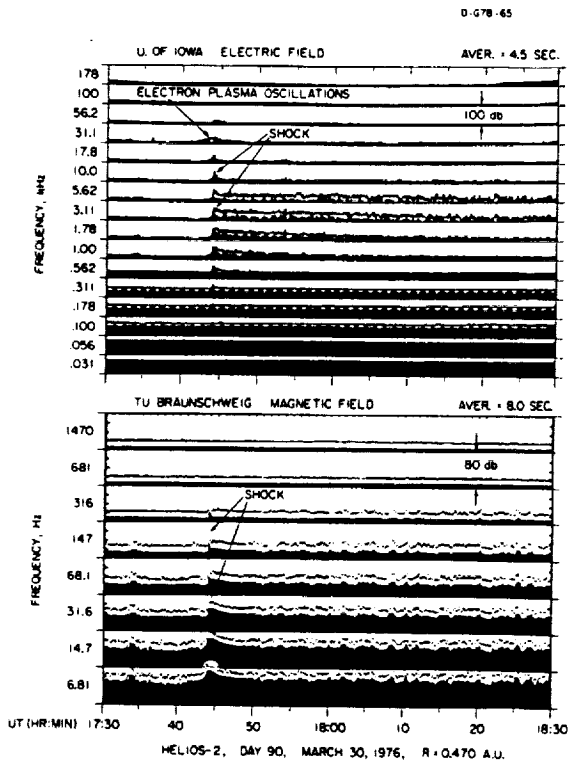

Figure 9. The electric and magnetic field intensities detected by Helios 2 for an interplanetary shock observed on March 30, 1976.

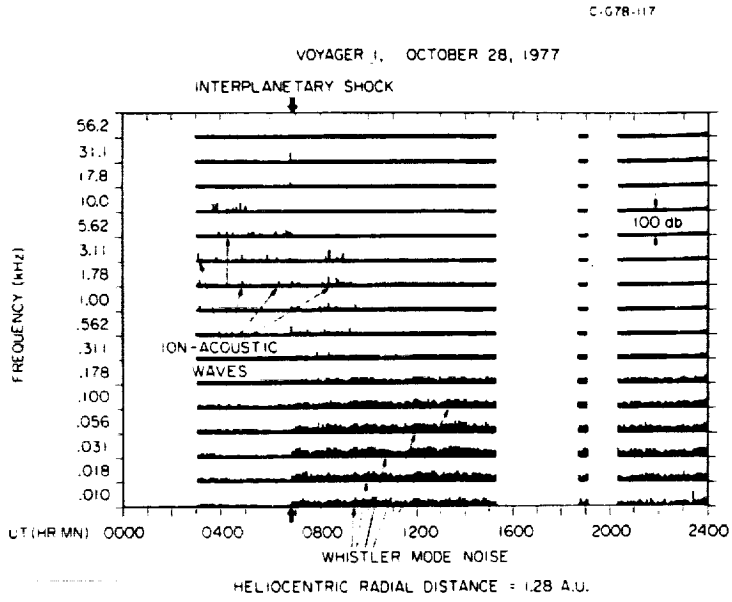

Figure 10. The electric field intensities detected by Voyager 1 for an interplanetary shock observed on October 28, 1977.

To illustrate the types of plasma wave turbulence usually observed, Figures 9 and 10 show two interplanetary shocks, one from Helios 2 [Gurnett et al., 1979] and the other from Voyager 1 [Kurth et al., 1979]. The shock in Figure 9 is a low Mach number, low beta, shock which has a very clearly defined enhancement in the electric and magnetic field intensities at the shock boundary. The electric field spectrum in the transition region and downstream from the shock is qualitatively similar to the spectrum of the ion-acoustic waves discussed in Section II. A weak burst of electron plasma oscillations can also be seen upstream of the shock. The magnetic field noise in and near the transition region is believed to be whistler-mode turbulence.

The Voyager 1 shock in Figure 10 differs from the shock in Figure 9 in several respects. In this case, only very small electric field intensities are observed in the transition region. Instead, a broad region of electrostatic wave turbulence similar to the ion-acoustic waves discussed in Section II is observed for several hours ahead of the shock. It seems likely that these upstream ion-acoustic-like waves are driven by suprathermal protons streaming out ahead of the shock, as occurs for the earth's bow shock. No electron plasma oscillations are observed in association with this shock. Whistler-mode turbulence qualitatively similar to Figure 9 is present in a broad region downstream of the shock.

These and other shocks studied show that there is a great deal of variability in the electrostatic noise intensities associated with shocks. Since so many parameters, such as the Mach number, the magnetic field direction with respect to the shock normal and the electron-to-ion temperature ratio, can affect the kinetic structure of a shock it is not possible with the limited number of events analyzed to give any general conclusions regarding the control which these parameters have on the plasma wave turbulence levels associated with a shock. Further studies are clearly needed.

V. CONCLUSION

This review has shown that considerable progress has been made in the experimental study and understanding of plasma waves in the solar wind during the past few years. Continued measurements by the Helios spacecraft during the solar maximum, by the Voyager spacecraft at large distances from the sun and by the ISEE-C spacecraft at the libration point upstream of the earth, promise to provide further improvements in our knowledge of solar wind plasma waves during the next few years. Although significant advances will be made, additional attention needs to be given to certain types of measurements. Of particular importance is the need for much higher time resolution, both for the plasma wave measurements and for the corresponding plasma distribution functions. As can be seen, many of the plasma wave phenomena observed in the solar wind occur on extremely short time scales, sometimes as short as a few tens of milliseconds or less. The reason why such impulsive fine structure occurs in, for example, electron plasma oscillations and ion-acoustic waves is not known, and probably cannot be fully resolved until higher time resolution measurements are available. Another area of particular importance is to extend these measurements in much closer to the sun. Essentially every plasma instability studied shows a clear tendency to increase rapidly in intensity with decreasing radial distance from the sun. This trend, along with various theoretical considerations, suggests that the most important microinstability processes which occur in the solar wind probably occur close to the sun, for example, near the sonic point in the solar wind flow and in the region of maximum solar wind heating. Direct *in situ* measurements close to the sun, such as may someday be obtained from a solar probe mission, are clearly needed to fully understand these processes.

ACKNOWLEDGEMENTS

This research was supported by the National Aeronautics and Space Administration under Grant NGL-16-001-043 with NASA Headquarters, Contract 11279 with Goddard Space Flight Center, and Contract 954013 with the Jet Propulsion Laboratory.

REFERENCES

Behannon, K., Observations of the interplanetary magnetic field between 0.46 and 1 AU by the Mariner 10 spacecraft, GSFC Preprint X-692-76-2, Greenbelt, MD, 1976.

Dum, C. T., E. Marsch, W. Pilipp, D. A. Gurnett, Ion sound turbulence in the solar wind, Solar Wind 4, edited by H. Rosenbauer, Springer, N. York-Heidelberg-Berlin, 1979.

Fainberg, J., L. G. Evans, and R. G. Stone, Radio tracking of solar energetic particles through interplanetary space, Science, 178, 743, 1972.

Feldman, W. C., Kinetic processes in the solar wind, Solar System Plasma Processes--A Twentieth Anniversary Review, edited by C. F. Kennel and L. J. Lanzerotti, North-Holland, Amsterdam, (in press), 1978.

Forslund, D. S., Instabilities associated with heat conduction in the solar wind and their consequences, J. Geophys. Res., 75, 17, 1970.

Fredricks, R. W., Electrostatic heating of solar wind ions beyond 0.1 AU, J. Geophys. Res., 74, 2919, 1969.

Gary, S. P. and W. C. Feldman, Solar wind heat flux regulation by the whistler instability, J. Geophys. Res., 82, 1087, 1977.

Gary, S.P., W. C. Feldman, D. W. Forslund, and M. D. Montgomery, Electron heat flux instabilities in the solar wind, Geophys. Res. Lett., 2, 79, 1975.

Gary, S. P., W. C. Feldman, D. W. Forslund and M. D. Montgomery, Heat flux instabilities in the solar wind, J. Geophys. Res., 80, 4197, 1975.

Gary, S. P., M. D. Montgomery, W. C. Feldman, and D. W. Forslund, Proton temperature anisotrophy instabilities in the solar wind, J. Geophys. Res., 81, 1241, 1976.

Ginzburg, V. L. and V. V. Zheleznyakov, On the possible mechanism of sporadic radio emission (radiation in an isotropic plasma), Sov. Astrom. A. J., 2, 653, 1958.

Gurnett, D. A. and R. R. Anderson, Electron plasma oscillations associated with type III radio bursts, Science, 194, 1159, 1976.

Gurnett, D. A. and R. R. Anderson, Plasma wave electric fields in the Solar wind: Initial results from Helios 1, J. Geophys. Res., 82, 632, 1977.

Gurnett, D. A., R. R. Anderson, F. L. Scarf, and W. S. Kurth, The heliocentric radial variation of plasma oscillations associated with type III radio bursts, J. Geophys. Res., 83, 4147, 1978b.

Gurnett, D. A., M. M. Baumback, and H. Rosenbauer, Steroscopic direction finding analysis of a type III solar radio burst: Evidence for emission at $2f_p$, J. Geophys. Res., 83, 616, 1978a.

Gurnett, D. A., and L. A. Frank, Ion-acoustic waves in the solar wind, J. Geophys. Res., 83, 58, 1978.

Gurnett, D. A., F. M. Neubauer, and R. Schwenn, Plasma wave turbulence associated with an interplanetary shock, J. Geophys. Res., (accepted for publication), 1979.

Gurnett, D. A., E. Marsch, W. Philipp, R. Schwenn, H. Rosenbauer, Ion-acoustic waves and related plasma observations in the solar wind, J. Geophys. Res., (submitted for publication), 1979.

Hollweg, J. V., Waves and instabilities in the solar wind, Rev. Geophys. Space Phys., 13, 263, 1975.

Hollweg, J. V.,and J. M. Turner, Acceleration of solar wind He^{++}: 3. Effects of resonant and non-resonant interactions with transverse waves, J. Geophys. Res., 83, 97, 1978.

Kaiser, M. L., The solar elongation distribution of low frequency radio bursts, Solar Phys., 45, 181, 1975.

Kurth, W. S., D. A. Gurnett, and F. L. Scarf, High resolution spectrograms of ion-acoustic waves in the solar wind, J. Geophys. Res., (accepted for publication), 1979.

Lemons, D. S., J. R. Asbridge, S. J. Bame, W. C. Feldman, S. P. Gary, and J. T. Gosling, The source of electrostatic fluctuations in the solar wind, J. Geophys. Res., (submitted for publication), 1978.

Magelssen, G.R., and D. F. Smith, Nonrelativistic electron stream propagation in the solar atmosphere and type III radio bursts, Solar Phys., 55, 211, 1977.

Montgomery, M. D., D. P. Gary, D. W. Forslund, and W. C.Feldman, Electromagnetic ion-beam instabilities in the solar wind, Phys. Rev. Lett., 35, 667, 1975.

Neubauer, F. M., H. J. Beinroth, H. Barnstorf, and G. Dehmel, Initial results from the Helios 1 search coil magnetometer experiment, J. Geophys. Res., 42, 599, 1977a.

Neubauer, F. M., G. Musmann, and G. Dehmel, Fast magnetic fluctuations in the solar wind: Helios 1, J. Geophys. Res., 82, 3201, 1977b.

Nicholson, D. R., M. V. Goldman, P. Hoyng, and J. C. Weatherall, Nonlinear Langmuir waves during type III solar radio bursts, Astrophys. J., 223, 605, 1978.

Papadopoulos, K., M. L. Goldstein, and R. A. Smith, Stabilization of electron streams in type III solar radio bursts, Astrophys. J., 190, 175, 1974.

Parker, E. N., Dynamics of the interplanetary gas and magnetic fields, Astrophys. J., 128, 664, 1958.

Scarf, F. L., Wave-particle interaction phenomena associated with shocks in the solar wind, edited by M. A. Shea, Study of Travelling Interplanetary Phenomena, D. Reidel, Dordrecht, 259, 1977.

Scarf, F. L., G. M. Crook, I. M. Green, and P. L. Virobik, Initial results of the Pioneer 8 VLF electric field experiment, J. Geophys. Res., 73, 6665, 1968.

Scarf, F. L. and D. A. Gurnett, A plasma wave investigation for the Voyager mission, Space Sci. Rev., 21, 289, 1977.

Scarf, F. L. and G. L. Siscoe, The Pioneer 9 electric field experiment, 2, Observations between 0.75 and 1.0 AU, Cosmic Electrodynamics, 2, 44, 1971.

Scarf, F. L., J. H. Wolfe, and R. W. Silva, A plasma instability associated with thermal anisotropies in the solar wind, J. Geophys. Res., 72, 993, 1967.

Siscoe, G. L., F. L. Scarf, I. M. Green, J. H. Binsack, and H. S. Bridge, Very low frequency electric fields in the interplanetary medium: Pioneer 8, J. Geophys. Res., 76, 828, 1971.

Smith, D. F., and D. R. Nicholson, Nonlinear effects involved in the generation of type III solar radio bursts, Proceedings of the URSI Conf. on Wave Instabilities in Space Plasmas, D. Reidel, Dordrecht, 1979.

Stix, T., The theory of plasma waves, McGraw-Hill, New York, 1962.

S LAR WIND, VOL. 4, MAX PLANCK INSTITUT REPORT NO. MPAE-2-100-81-31, LINDAU, GERMANY, PAGE 299, 198

ION SOUND TURBULENCE IN THE SOLAR WIND

C.T. Dum, E. Marsch, W. Pilipp
Max-Planck-Institut für Physik und Astrophysik,
Institut für extraterr. Physik, 8046 Garching, FRG
and
D.A. Gurnett
Dept. of Physics and Astronomy, University of Iowa
Iowa City, Iowa 52242, U.S.A.

Abstract: A stability analysis for ion sound is carried out which directly uses detailed measured particle distributions, rather than model distributions. Correlation with measured wave activity is satisfactory. Valuable information about the instability mechanism, transport processes and the accuracy of measured distributions can be obtained by this method.

Recently, electrostatic fluctuations have been measured in the solar wind, over a wide range of radial distances (0.3 - 3 AU) from the sun (Gurnett, 1978). The wave vectors tend to be aligned with the magnetic field (heat flux) and satisfy $k\lambda_D \lesssim 1$ (λ_D Debye length). Waves occur in bursts of a few tenths of a second and activity lasts from several hours to several days. These wave characteristics and the correlation of wave activity with macroscopic parameters such as the electron-ion temperature ratio and the electron heat flux strongly indicate that the modes may be identified with ion sound waves (Gurnett et al., 1978). The stability of unmagnetized electrostatic modes depends on the reduced distribution function in the direction of wave propagation. Accepting that electrons have no net drift with respect to the ions or low energy double peaks, there are basically only two free energy sources for ion sound, a drift of low energy electrons (core) relative to the ions as is characteristic of a skewed distribution carrying a heat flux, and resolved double peaks in the reduced ion distribution (Gary, 1978; Lemons et al., 1978). Nonlinear excitation by coupling to other modes may also be possible. The question regarding the mechanism responsible for the observed fluctuations is still open. An answer to this problem is also important for a stuy of the anomalous transport effects connected with the wave activity (Dum, 1978a, b). We hope to contribute to a resolution of this issue, by a linear stability analysis which directly uses detailed measured particle distributions rather than model distribution functions, and compares the results with measured wave activity.

A numerical code which resolves the measured distribution functions into spherical harmonics,

$$f(\underline{v}) = \sum_{l,m} f_l^m(\underline{v})\, Y_l^m(\underline{\hat{v}}); \qquad \underline{\hat{v}} = \underline{v}/v = (\theta,\phi) \tag{1}$$

in an appropriately chosen coordinate system, and then determines the dispersion relation for arbitrary speed dependence of the f_l^m, can be used most efficiently for our purposes (Dum et al., 1978). One may, for example, isolate a particular free energy source for instability, by arbitrarely turning off various measured anisotropies, corresponding to heat flux ($l = 1$), viscous pressure ($l = 2$) or higher order terms required to describe the electron anisotropy at high speeds or the strong speed dependent ion anisotropies. We are not biased by the rigid speed dependence and anisotropies of the various model distributions generally used in stability analysis and thus are able to extract the maximum information from data, such as obtained from the Helios space crafts (Rosenbauer et al., 1978).

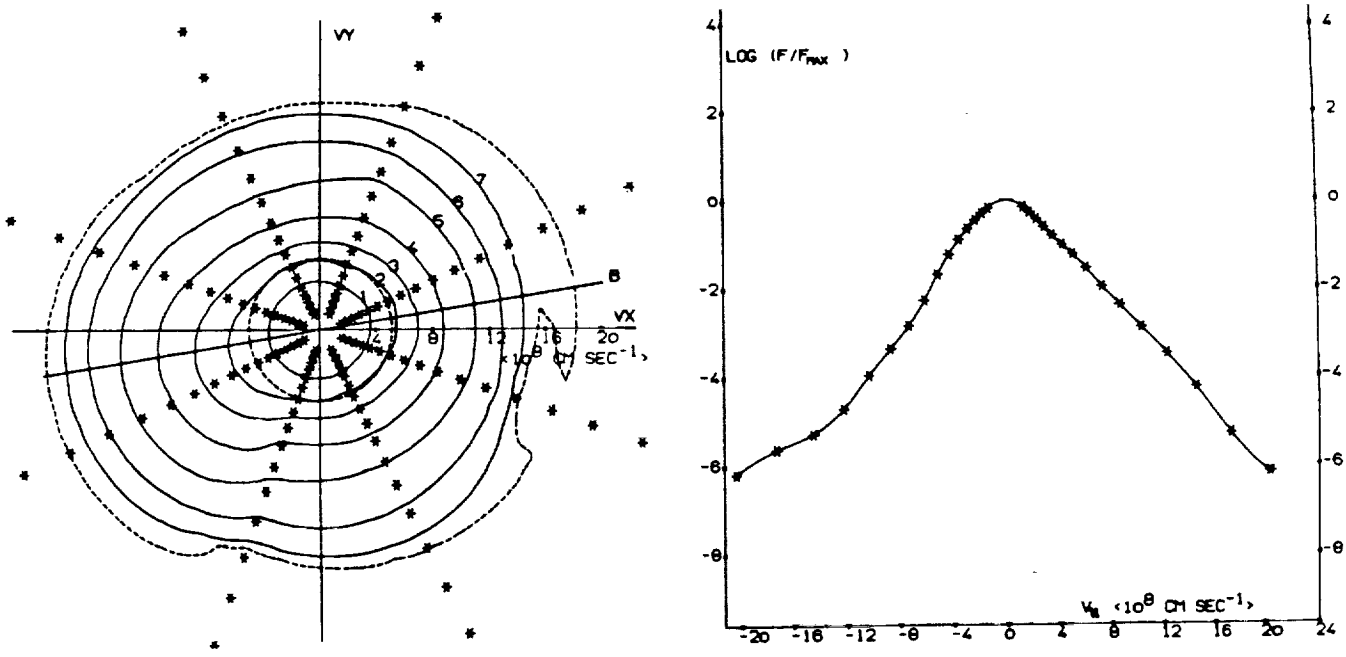

Fig. 1. Electrons: Contour lines (10^{-n}, n = 1,2..) of a cut in the ecliptic plane and reduced distribution function along the magnetic field. (Solar direction: $v_x > 0$, $v_{||} < 0$).

The intrinsic limitations of the stability analysis imposed by the finite resolution and accuracy of the measurements can be analyzed by our method. We may also find out how the ambiguity in fitting various models to measured distribution functions affects the outcome of conventional stability analysis. The fact that there is an apparently strong positive correlation between observed wave activity and the least square deviation from a Maxwellian fit to the ions (Gurnett et al., 1978) should be noted in this connection. For electrons, more sophisticated core-halo fits by two bi-Maxwellians, also become poor for increased anisotropies, characteristic of heat flux, despite the large number of parameters that need to be determined (Feldman et al., 1976).

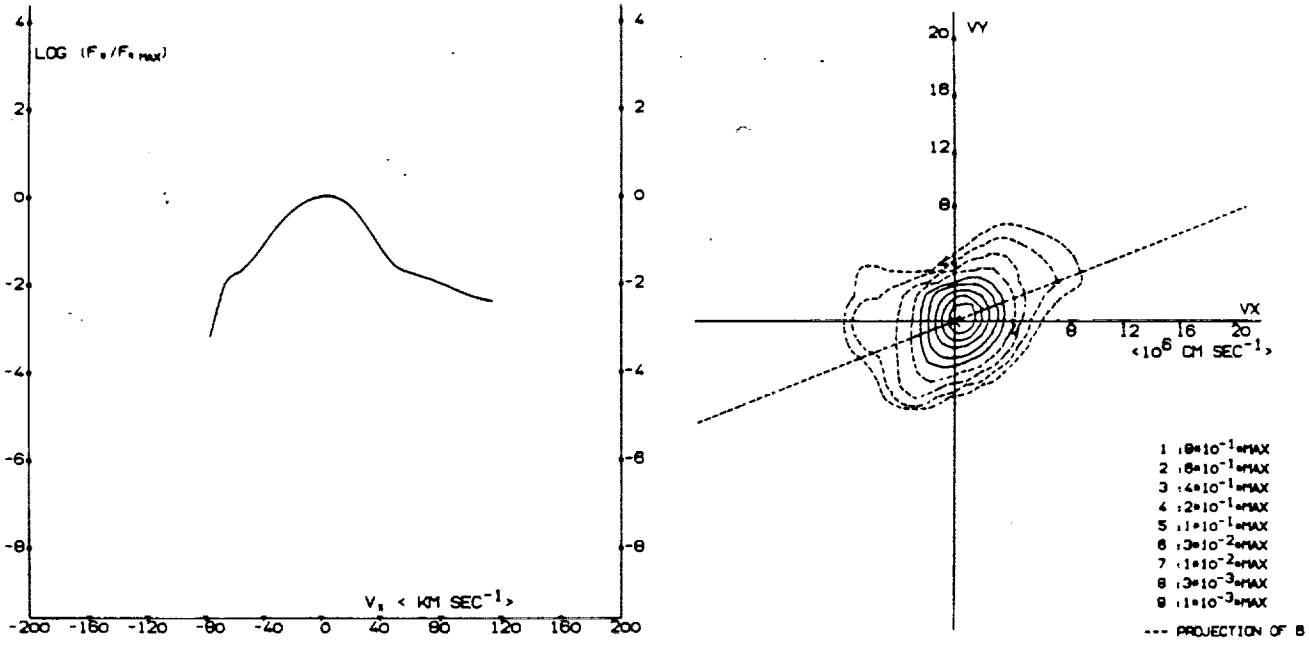

Fig. 2. Ions: Reduced distribution along the magnetic field and contour lines of a cut in the plane formed by magnetic field and bulk speed. (Solar direction: $v_x < 0$, $v_{\parallel} < 0$). Measurements are by Helios 1 at UT 289:14:12:32 and distance 0.57 AU from the sun.

A stability analysis using a combination of drifting Maxwellians is very instructive (Gary, 1978; Lemons et al., 1978) but appears somewhat artificial for the measured distributions. The features of non-Maxwellian distributions relevant to ion sound have been analyzed in detail (Dum, 1978a, b). The dispersion relation may be written in the form

$$(kv_i/\omega_i)^2 = -[(T_i/T_e)\hat{\varepsilon}_e(\underline{k},\omega) + \hat{\varepsilon}_i(\underline{k},\omega)] \qquad (2)$$

where the dielectric constants are normalized by introducing the plasma frequencies $\omega_j^2 = 4\pi n_j e_j^2/m_j$ and characteristic thermal velocities $v_j^2 = T_j/m_j$, $j = e, i$ defined by the second moments of the distributions in the (common) rest frame $\underline{w} = \underline{v}-\underline{u}$. The quasi-neutrality condition $n_e = n_i = n$ is also used, but not for the fluctuations. For phase velocities $(\omega/k) \ll v_e$ the electron contribution to (2) depends primarily on low speed particles, roughly with the weight factor w^{-2}, although particles of all speeds $w > (\omega/k)$ contribute to the resonance $\omega - \underline{k}\cdot\underline{w} = 0$. The dielectric constant may be written in a form resembling the result for a drifting Maxwellian

$$\hat{\varepsilon}_e(\underline{k},\omega) = a_{-2} + i(\pi/2)^{1/2} a_{-3}\, v_e^{-1}[(\omega/k) - u^*(\underline{k})] \qquad (3)$$

where the form factors $a_{-2} = v_e^2 \int d\,\underline{w}\, f_e(\underline{w}) w^{-2} = T_e/T_e^*$ and $a_{-3} = (2\pi v_e^2)^{3/2} f_e(0)$ define the effective electron temperature and slope respectively, and are equal to

unity for a Maxwellian. The effective drift velocity is determined by the odd l anisotropies, also weighted with the factor w^{-2}. Thus, $u^*(\underline{k})$ is not directly related to the mean-velocity (<w> = 0 in the rest frame) or the heat flux ($\sim w^3$) but rather to the rate of momentum transfer with an effective collision frequency $\nu \sim w^{-3}$, corresponding to electron-ion collisions or ion sound turbulence (Dum, 1978b). A unique relationship between u^*, heat flux q_e and temperature gradient ∇T_e exists only for the nearly Maxwellian distributions of classical transport. The dependence on the angle α between wave vector $\underline{k}$ and anti-heat flux direction $-\underline{q}$ may also differ from a cos α law. In fact, we find that in the presence of a strong "Strahl", u^* generally peaks at substantial angles to $-\underline{q}$. In the low temperature approximation $(\omega/kv_i) >> 1$ for the ions, the real part of the dielectric constant may be expanded in terms of the usual moments, density, pressure tensor, heat flux tensor etc. Each term also yields a dependence on the direction $\underline{k}$, corresponding to definite values of l in expansion (1) (Dum et al., 1978). Stability analysis must account for the very different behaviour of electrons and ions, just discussed. If model distributions are used, the fit parameters should at least be determined from measured distributions with appropriate weight factors, rather than from simple least square fits.

For ion sound in the solar wind, the approximation $(\omega/kv_e) << 1$ is excellent. The condition $(\omega/kv_i)^2 >> 1$ is not very well satisfied, however. In fact, the temperature ratio is often not as large as demanded by conventional stability analysis. From Fig. 2 we may guess that the effective ion temperatures for the sound velocity, $c_s^2 = (T_e^* + 3\,T_i^*)/m$, and for Landau damping also differ from the moment T_i. No analytic reduction such as (3) is possbile, however, for finite (ω/kv_i) and the dielectric constant must be computed directly from the measured distribution. For resonant instabilities, the imaginary part of the dielectric constant depends on details of the distribution functions and thus must always be computed by the full numerical code. For small growth rates the range of phase velocities $(\omega/k) + i0$ is determined by the condition that $Re\hat{\varepsilon}_i$ be sufficiently negative to compensate $(T_i/T_e)Re\hat{\varepsilon}_e \approx T_i/T_e^*$ in (2). The imaginary part of (2) determines then the rate of dissipation or the growth rate $\gamma_{\underline{k}}$. We introduce the normalization

$$\hat{\gamma}_{\underline{k}} = -(1/2)(\omega/kv_i)^2 \left[(T_i/T_e)Im\,\hat{\varepsilon}_e + Im\hat{\varepsilon}_i\right] \qquad (4)$$

corresponding to $\hat{\gamma}_{\underline{k}} \approx \gamma_{\underline{k}}/\omega_{\underline{k}}$ for low temperature ions. The distributions in Figs. 1, 2 correspond to observed ion sound activity. We find $T_i/T_e^* = 0.187$, a maximum phase speed $(\omega/k) = 46$ km/sec corresponding to $k\lambda_D \approx 0$ and $\gamma_{\underline{k}} = -3.8 10^{-2}\,[-3.8 + 4.8] = -3.8 10^{-2}$ in the direction $-\underline{q}$. The damping is larger in other directions and increases rapidly with decreasing phase speed. Less than three minutes later the electrons are more anisotropic and give the largest destabilizing term at $\alpha \approx 45^0$. We also found a few destabilizing double ion peaks. So far, however, we have not found positive net growth

rates by either mechanism. For periods of observed wave activity the computed damping rates are very small, whereas for passive periods the damping is large. We consider this correlation satisfactory, since for active periods we only expected to find conditions close to marginal stability. It is well known from laboratory and computer experiments that self-regulatory quasi-linear effects in a collisionless plasma limit ion sound turbulence to short temporal or spatial bursts, with a width and (much longer) repetition period depending on macroscopic conditions (Dum, 1978a, b). High resolution wave observations in the solar wind agree with this picture. The period required for a complete measurement of particle distributions, however, is much longer than the duration of the bursts, hence it should be dominated by the decay and recovery phase, $\gamma_\kappa \lesssim 0$, of the bursts (Lemons et al., 1978). From the very low excitation levels and the short duration of the bursts, we may conclude that during active periods the plasma actually remains extremely close to marginal stability. Rather than looking for unstable distributions, it thus appears to be more promising to study possible modifications of the distributions, consistent with the constraints imposed by the marginal stability condition, quasi-linear effects and particle measurements. Comparing with Coulomb collisions we find for electrons that even for fluctuation levels $\langle E^2\rangle/8\pi nT$ as low as 10^{-7}, turbulence completely dominates isotropization. Inelastic turbulent scattering is much slower but still dominates for speeds $w \leq w_0 = 0(v_e)$ and leads to a flattening of the electron distribution in this range. The form factor a_{-3} decreases very rapidly (Fig. 1; Dum, 1978a) and a_{-2} also decreases for an electron distribution self-consistent with ion sound. Because of contamination by photoelectrons and distortions by the spacecraft potential the electron distribution below the thermal velocity is not measured but extrapolated, using a Maxwellian fit to core electrons. Simply using a flat topped distribution in this range, instead, leads to negligible changes in total temperature and density but reduces the form factors for the core component from unity to $a_{-3} = 0.63$ and $a_{-2} = 0.83$. Varying the space craft potential by $\pm$ 2 Volts from the estimated value changes $\mathrm{Im}\hat{\varepsilon}_e$ by a few percent. Cold ions, on the one hand favor ion sound instability, but on the other hand, the measured fluxes are then above the one count level only in relatively few channels of the ion instrument. The spacing of channels in velocity may become comparable or even larger than the ion thermal velocity. These uncertainties affect primarily the imaginary part $\mathrm{Im}\hat{\varepsilon}_i$. The net growth rate, of course, is affected even more strongly, since near marginal stability it is the difference of two comparable terms.

We have demonstrated the feasibility of a stability analysis which directly uses measured distributions. More extensive data surveys are under way, including also electromagnetic instabilities. Stability analysis for periods of observed ion sound activity should give valuable information about the instability mechanism, transport processes and particle distributions.

ACKNOWLEDGEMENTS

The research at the University of Iowa was supported by NASA grant NGL-16-001-043 and contract NAS5-11279.

REFERENCES

Dum, C.T., Anomalous heating by ion sound, Phys. Fluids, 21, 945-55, 1978a.

Dum, C.T., Anomalous electron transport equations for ion sound and related turbulent spectra, Phys. Fluids, 21, 956-69, 1978b.

Dum, C.T., E. Marsch, and W. Pilipp, Determination of wave growth from measured distributions or transport theory, J. Plasma Phys., submitted, 1978.

Feldman, W.C., J.R. Asbridge, S.J. Bame, S.P. Gary, and M.D. Montgomery, Electron Parameter Correlations in High-Speed Streams and Heat Flux Instabilities, J. Geophys. Res., 81, 2377-82, 1976.

Gary, S.P., Ion-Acoustic-Like Instabilities in the Solar Wind, J. Geophys. Res., 83, 2504-8, 1978.

Gurnett, D.A., Microinstabilities in the Solar Wind: a review of observations, Solar Wind 4, this volume, 1978.

Gurnett, D.A., E. Marsch, W. Pilipp, R. Schwenn, and H. Rosenbauer, Ion-Acoustic Waves and Related Plasma Observations in the Solar Wind, J. Geophys. Res., submitted 1978.

Lemons, D.S., J.R. Asbridge, S.J. Bame, W.C. Feldman, S.P. Gary, and J.T. Gosling, The source of electrostatic fluctuations in the solar wind, J. Geophys. Res., submitted, 1978.

Rosenbauer, H., R. Schwenn, E. Marsch, B. Meyer, H. Miggenrieder, M.D. Montgomery, K.-H. Mühlhäuser, W. Pilipp, W. Voges, and S.M. Zink, A Survey on Initial Results of the Helios Plasma Experiment, J. Geophys., 42, 561-80, 1977.

INTERNATIONAL UNION OF GEODESY AND GEOPHYSICS, INTERNATIONAL ASSOCIATION OF GEOMAGNETISM AND AERONOMY, BULLETIN NO. 48, AUGUST 1983

Kikuchi et al.: Solar Radio Bursts and Electron Plasma Oscillations Associated with Interplanetary Shocks Waves and Energetic Protons

PHYSICS OF THE INNER HELIOSPHERE (submitted for publication), 1984

Denskat and Gurnett: Physics of the Inner Heliosphere: Waves and Discontinuities

PHYSICS OF THE INNER HELIOSPHERE:

WAVES AND DISCONTINUITIES*

by

K. U. Denskat and D. A. Gurnett

January 1984

Department of Physics and Astronomy
The University of Iowa
Iowa City, IA 52242

*Draft contribution by D. A. Gurnett

I. INTRODUCTION

To fully understand the macroscopic fluid-like behavior of the solar wind it is first necessary to understand the microscopic processes that control the fluid properties of the plasma. In a collisionless plasma such as the solar wind it is now widely recognized that the relevant microscopic processes are plasma instabilities. As dynamical interactions occur between various elements of the plasma velocity space gradients, $\partial f/\partial v_\perp$ and $\partial f/\partial v_\parallel$, are produced in the distribution function that lead to the growth of waves. As the waves grow to large amplitude, wave-particle interactions occur that tend to eliminate the velocity space gradients causing the instability. Plasma instabilities thereby play a role similar to collision in an ordinary gas by controlling and preventing large deviations from thermal equilibrium.

The principal plasma wave modes of importance in the solar wind are summarized in Figure 1, which shows a plot of the phase velocity, ω/k, as a function of frequency for typical solar wind conditions at 1 AU. For simplicity, only waves propagating parallel to the magnetic field are shown. At low frequencies the relevant characteristic speeds of the plasma are the Alfven speed, $V_A = B/\sqrt{\mu_o \rho_m}$, and the sound speed, $V_s = \sqrt{\gamma \kappa T/m}$, where ρ_m is the mass density, γ is the adiabatic compression constant, T is the temperature and m is the ion mass. At

radial distances beyond about ten solar radii, the solar wind speed, V_{sw}, is substantially greater than either of these speeds. At low frequencies three modes exist. These modes are called the fast, intermediate and slow Alfven waves. At higher frequencies the three Alfven modes merge into the whistler mode, the ion-acoustic mode, and the ion-cyclotron mode. The whistler mode has a resonance (zero phase velocity) at the electron cyclotron frequency, f_c^-, and the ion-cyclotron mode has a resonance at the ion cyclotron frequency, f_c^+. These two modes are electromagnetic and are driven unstable by anisotropies in the electron and ion distribution functions [Kennel and Petschek, 1966]. At frequencies above the ion cyclotron frequency the ion-acoustic mode is almost completely electrostatic and has many properties similar to a sound wave in an ordinary gas. This mode is strongly damped by Landau damping unless the electron temperature, T_e, is much greater than the ion temperature, T_i. If $T_e >> T_i$, then the ion-acoustic mode can be driven unstable by a variety of processes, including currents [Stix, 1962], electron heat conduction [Forslund, 1970] and ion beams [Lemons et al., 1979]. At higher frequencies, near the electron plasma frequency, f_p^-, two more modes appear. One of these modes is a purely electrostatic oscillation at the electron plasma frequency and is called an electron plasma oscillation. Electron plasma oscillations are produced by electron beams or a region of positive slope, $\partial f/\partial v_\parallel > 0$, in the electron distribution function. The other mode is the free space electromagnetic mode. This mode only propagates at frequencies above the electron plasma frequency. When only linear effects are considered the free

space electromagnetic mode is completely independent of the other plasma wave modes. However, when nonlinear effects are included the free space mode is coupled to other modes such as the electron plasma oscillation. These modes can then transfer energy to the free space mode, producing electromagnetic radiation that can escape from the plasma. The radial variation in the frequency range of these various plasma wave modes is summarized in Figure 2 for typical solar wind conditions.

To investigate plasma waves in the inner heliosphere the Helios-1 and -2 spacecraft were equiped with a set of triaxial flux gate amd search coil magnetometers for measuring magnetic fields, and a 30-meter tip-to-tip electric dipole antenna for measuring electric fields. The flux gate magnetometers measure magnetic fields at frequencies less than ____ Hz, and the search coil magnetometers measure magnetic fields at higher frequencies, from ____ Hz to ___ Hz. Complete descriptions of the Helios magnetic field instruments are given by Musmann et al. [1975] and Dehmel et al. [1975]. The electric field instrument provides measurements of electric fields in sixteen channels over the frequency range from 30 Hz to 178 kHz. A complete description of the plasma wave electric field instrument on Helios is given by Gurnett et al. [1975].

II. ELECTROSTATIC WAVES

The Helios plasma wave instrument detected two primary types of electrostatic waves: electron plasma oscillations and ion acoustic waves. Examples of both types of waves are illustrated in Figure 3 which shows a 16-channel plot of the electric field intensities detected by Helios 2 at a heliocentric radial distance of about 0.45 AU. The solid line in each frequency channel gives the peak electric field strength and the upper edge of the solid black band gives the average field strength. The time resolution for the peak and average field strength measurements vary with bit rate and in this case is 40 seconds. The electron plasma oscillations occur in the 56.2 kHz channel during the interval from about 0650 to 0740 UT, and the ion acoustic waves occur in the frequency range from about 1.0 to 17.8 kHz for the entire 8 hour duration of the plot. Because these two types of emissions usually occur independently and have different characteristics, they will be discussed separately.

A. Electron Plasma Oscillations

Electron plasma oscillations are easily identified in the Helios electric field data because they usually occur in only one or two frequency channels near the local electron plasma frequency, f_p. Electron plasma oscillations are often associated with type III solar radio bursts of the type shown in Figure 3, although they also occur

separately. Type III radio bursts are produced by flares and active regions on the sun and have an easily identified frequency-time variation, with the frequency decreasing monotonically with increasing time [Wild, 1950]. The Helios observations of electron plasma oscillations associated with type III radio bursts [Gurnett and Anderson, 1976] confirmed a long standing theory for the origin of these ratio bursts. According to this theory, first proposed by Ginzburg and Zheleznakov [1958], the generation of type III radio bursts is a two-step process in which (1) electron plasma oscillations are first produced by energic electrons from a solar flare, and (2) the energy in the plasma oscillations is converted to electromagnetic radiation via nonlinear coupling to the free space electromagnetic mode. Because the electrons are impulsively released by the flare a region of positive slope, $\partial f/\partial v_{\parallel} > 0$, is generated near the leading edge of the energetic electron stream due to time-of-flight considerations. The temporal evolution of the reduced one-dimensional distribution function, $f(v_{\parallel})$, is illustrated in Figure 4 for an electron plasma oscillation event detected by the ISEE 3 spacecraft at 1 AU [Lin et al., 1981]. Since the growth rate of the plasma oscillations is proportional to $\partial f/\partial v_{\parallel}$ [Stix, 1962; Krall and Trivelpiece, 1973], waves are only generated during the interval when $\partial f/\partial v_{\parallel}$ is positive. This interval is usually about 1 hour at 1 AU, decreasing to about 20 minutes at 0.3 AU. Because the region of positive slope is only present near the leading edge of the electron stream, the plasma oscillations are confined to a localized region that moves outward from the sun at a speed comparable to the energetic electron stream, typically 0.1 c to 0.5 c. As the region of intense plasma

oscillations moves outward from the sun electromagnetic radiation is generated at f_p^- and $2f_p^-$, producing the decreasing emission frequency with increasing time that is characteristic of type III radio bursts. This radio emission process is illustrated in Figure 2. At low frequencies, below about 1 MHz, the strongest radiation is at the seconmd second harmonic, $2f_p^-$, [Fainberg and Stone, 1974; Kaiser, 1975; Gurnett et al., 1978]. Because the electromagnetic radiation propagates freely away from the source, the type III radiation is typically detected 10 to 20 minutes before the region of intense plasma oscillations arrives at the spacecraft.

By using a large number of electron plasma oscillation events detected over a several year period, the variation of the electric field strength of the plasma oscillations can be determined as a function of radial distance from the sun [Gurnett et al., 1980]. This variation is shown in Figure 5. As can be seen, the electric field strength tends to decrease with increasing heliocentric radial distance, varying approximately as $R^{-1.4 \pm 0.5}$. This decrease is expected because the electric field to plasma energy density ratio, $E^2/8\pi nkT$, which controls the saturation intensity, is approximately constant. For a constant energy density ratio the maximum electric field E is expected to vary approximately as $R^{-8/7}$, since the number density n varies as R^{-2} and the temperature T varies as $R^{-2/7}$ [Hundhausen, 1972]. The observed radial variation is seen to be reasonably consistent with the expected radial variation. Typical maximum values for $E^2/8\pi nkT$ are about 2×10^{-5}.

The radial variation of the field strength of the plasma oscillations can also be compared with the emissivity of the type III radiation, which varies as approximately R^{-6} [Tokar and Gurnett, 1980]. For most second harmonic emission mechanisms the emissivity varies as E^4. This dependence occurs because the radiating current at the second harmonic is proportional to the product of the field strength of two interacting plasma oscillations. Since the power radiated is proportional to the square of the current, a fourth power dependence on the electric field strength is expected. Since the emissivity varies approximately as R^{-6}, the electric field intensity should then vary as $R^{-1.5}$. This radial variation is also in reasonable quantitative agreement with the observed radial variation.

High time resolution measurements of electron plasma oscillations detected by Helios [Gurnett and Anderson, 1977] show that the electric field intensity is very spiky, with rapid intensity variations down to time scales of 70 msec, or less. This very spiky electric field structure accounts for the very large peak to average field strength ratio evident in Figure 3. Consideration of the nonlinear interactions that stabilize the electron beam has led a number of investigators to predict that the electric field structure should be very spiky [Papadopoulos et al., 1974; Galeev et al., 1975; Bardwell and Goldman, 1976; Papadopoulos, 1978; Nicholson et al., 1978; Freud and Papadopoulos, 1980; Goldman et al., 1980]. The origin of the spiky structure involves a focusing effect that causes the plasma oscillation intensity to increase in regions of decreased plasma density. If the wave intensity is sufficiently large the electric field pressure causes the plasma density to decrease

further, increasing the focusing and eventually forming a soliton-like structure that collapses down to a spatial scale of only a few Debye lengths. Collapsed plasma oscillation structures of this type, sometimes referred to as "spiky turbulence", have been observed in the laboratory [Wong and Quon, 1975]. For the receiver averaging time constant of the Helios instrument, ~ 50 msec, it is not possible to follow intensity fluctuations down to the time scales, hundreds of μsec, required to resolve soliton-like structures. The maximum plasma oscillation field strengths detected by Helios, typically only 5 to 10 mV/m, are too small to reach the threshold electric field strength, $E^2/8\pi n\kappa T \gtrsim (k\lambda_D)^2 \approx 10^{-2}$ to 10^{-3}, required for soliton collapse. However, because of the relatively long, 50 msec, averaging interval it is still possible that such large field strengths could be occurring on short time scales. Evidence of soliton-like intensity fluctuation have been reported by Gurnett et al. [1981] for electron plasma oscillations detected in the solar wind upstream of Jupiter's bow shock.

B. Ion Acoustic Waves

The second type of electrostatic noise detected in the solar wind by Helios is a band of sporadic emissions between the proton and electron plasma frequencies, f_p^+ and f_p^-. Because of the frequency range involved, these emissions were initially referred to as $f_p^+ < f < f_p^-$ noise [Gurnett and Anderson, 1977]. In their initial interpretation of this noise, Gurnett and Anderson suggested that the emissions are ion acoustic waves which are Doppler-shifted into the frequency range $f_p^+ < f < f_p^-$ by the motion of the solar wind. Although the full understanding of the origin of these waves is not yet complete, considerable evidence now exists

indicating that the waves are either ion acoustic waves, or a closely related ion-acoustic-like mode. For this reason, we will refer to the emissions as ion acoustic waves. The reasons for this identification will be discussed shortly.

A typical example of the ion-acoustic waves detected by Helios is shown in Figure 3. The noise does not occur continuously, but rather in episodes lasting for periods ranging from a few hours to several days. Episodes of enhanced ion acoustic wave activity usually occur a few times per month, and tend to be more frequent and more intense closer to the sun. The periods of enhanced ion acoustic wave activity often recur on successive solar rotations, particularly ahead of high-speed solar wind streams [Gurnett et al., 1979] and ahead of interplanetary shocks [Kennel et al., 1982]. The ratio of the peak to average electric field strength is large, typically greater than 40 db, indicating that the noise is very impulsive and sporadic on time scales of a few seconds, or less. When the intensities are averaged over several minutes the spectrum appears very broad, usually extending from near f_p^+ to slightly below f_p^-. The cutoffs at f_p^+ and f_p^- are not rigid cutoffs, and as will be discussed shortly, it is probably coincidental that the spectrum falls in this frequency range. As shown by Gurnett and Frank [1978] and Gurnett et al. [1979] both the intensity and frequency of the noise tend to increase with decreasing radial distance. This tendency is illustrated in Figure 6, which shows representative electric field spectrums of the ion acoustic noise at three heliocentric radial distances: 1.73 AU from Voyager 1, 0.98 AU from Helios 1 and 0.47 AU from Helios 1. A statistical study of the radial dependence shows that the broadband electric field strength varies approximately

as 1/R, varying from about 1 mV/m (10% quartile) at 0.33 AU, to about 0.3 mV/m at 1 AU. Although Helios had no capability for obtaining electric field waveforms, wideband measurements from Voyager 2 [Kurth et al., 1979] show that the ion acoustic waves consist of nearly monochromatic emissions whose center frequencies vary over a wide range on a time scale of a few seconds. A typical high resolution frequency-time spectrogram of the ion-acoustic waves detected by Voyager 2 is shown in Figure 7. Because of the rapid fluctuations in the center frequency of the emission, the spectrum appears to be very broad when averaged over longer intervals, as in Figure 6, even though it is nearly monochromatic on short time scales.

The evidence that the $f_p^+ < f < f_p^-$ noise detected by Helios is caused by ion acoustic waves is somewhat indirect and is based mainly on comparisons with very similar waves observed upstream of the Earth's bow shock. Because ion acoustic waves have very short wavelengths, the Doppler-shift caused by the motion of the solar wind is substantial. When the Doppler shift is included the frequency of an ion-acoustic wave in the spacecraft frame of rest is given by

$$\omega = \frac{C_s k}{\sqrt{1 + k^2 \lambda_D^2}} + V_{sw} k \cos \theta_{kv} \quad ,$$

where $C_s = \sqrt{\kappa T_e / m_i}$ is the ion acoustic speed, k is the wave number, θ_{vk} is the angle between the wave vector and the solar wind velocity, and λ_D is the Debye length. The rest frame frequency of the ion acoustic

wave is given by the first term and the Doppler shift is given by the second term. For typical solar wind parameters the Doppler shift is much larger than the rest frame frequency. Therefore, to a good approximation $\omega \simeq V_{sw}k \cos \theta_{kv}$. Because of the onset of strong Landau damping at short wavelengths, k has a maximum value of $k\lambda_D \simeq 1$. The maximum frequency is then given by $\omega_{max} = V_{sw}/\lambda_D$. For typical solar wind parameters at 1 AU ($n = 5$ cm^{-3}, $T = 1.5 \times 10^5$°K, $V_{sw} = 400$ km/s) the maximum frequency is approximately $f_{max} \simeq 8.0$ kHz, which is in good agreement with the observed upper frequency limit (see Figure 6). Since the electron temperature is nearly independent of radial distance [Hundhausen, 1972] and since both V_{sw}/λ_D and f_p^- vary as the square root of the electron density, it is easy to verify that f_{max} is proportional to f_p^-. This relationship explains why the frequency of the ion acoustic waves appears to vary in direct proportion to f_p^- (see Figure 6). However, in this interpretation the upper cutoff frequency actually has no direct relationship to f_p^-. It is only coincidental that f_{max} is near f_p^-.

Although the upper cutoff frequency of the $f_p^+ < f < f_p^-$ noise is consistent with an ion-acoustic wave interpretation, it does not uniquely identify the noise as ion acoustic waves because other short wavelength mode also exist with cutoffs near $k\lambda_D \simeq 1$. These modes would also have an upper frequency cutoff at $\omega_{max} = V_{sw}/\lambda_D$. The evidence that the noise is due to ion acoustic waves rests on other observations. First, a well-known characteristic of the ion acoustic mode is that the damping is very sensitive to the electron to ion temperature ratio, T_e/T_i. Ion acoustic waves are weakly damped if $T_e/T_i \gg 1$,

and strongly damped if $T_e/T_i \approx 1$. Using solar wind plasma measurements from Helios, Gurnett et al. [1979] have shown that the electric field intensity of the $f_p^+ < f < f_p^-$ noise increases as the T_e/T_i ratio increases, as would be expected for an ion acoustic instability. Second, Gurnett and Frank [1978] have pointed out that the ion acoustic noise detected by Helios has essentially identical characteristics to a band of low frequency electric field noise detected upstream of the Earth's bow shock between about 1 to 10 kHz. By using techniques not available on Helios, Fuselier and Gurnett [1984] have been able to to measure the wavelength of the waves. By measuring both the wavelength and the frequency, the dispersion relation can be determined. An example of these measurements is shown in Figure 8. Although the polar angle θ of the wave vector is a free parameter, the basic shape of the dispersion curve, including the break at $k\lambda_{De} \approx 1$ and the upper frequency limit at ω_{pi}, are all in excellent agreement with the ion acoustic dispersion relation. Although this type of measurement is not available for the waves detected by Helios, these measurements strongly suggest that the waves detected by Helios far from the Earth are also ion acoustic waves.

Given that the waves detected by Helios are ion acoustic waves, the question arises as to how these waves are generated. This is a difficult question that has not yet been completely answered. Upstream of the Earth's bow shock it is now well established [Scarf et al., 1970; Gurnett and Frank, 1978; Anderson et al., 1981] that the ion acoustic waves are closely associated with energetic, 1 to 10 keV, proton beams arriving from the bow shock. Since ion acoustic waves are

also observed ahead of interplanetary shocks [Kennel et al., 1982] one might think that the ion acoustic waves detected by Helios far from the Earth are produced by a comparable type of ion beam in the solar wind. Lemons et al. [1979], for example, suggested that the waves are produced by an ion-beam instability. Despite the reasonableness of this line of thinking, to date no definite relationship has been established between ion beams in the interplanetary medium and ion acoustic waves. This failure could be in part due to the absence of suitable energetic ion measurements on Helios. However, attempts to establish a relationship using the more complete measurements available on ISEE 3 at 1 AU have also not been successful.

Many years ago, even before the discovery of the solar wind ion acoustic waves, it was suggested by Forslund [1970] that the conduction of heat away from the sun by electrons could produce ion acoustic waves in the solar wind. This instability occurs because if no current is allowed to flow then the presence of a third moment (heat flux) in the electron distribution function produces a shift between the peaks of the electron and ion distribution functions. If the heat flux is sufficiently large, this shift produces a double hump in the reduced distribution function that makes the ion acoustic mode unstable. Comparative studies of the Helios plasma and plasma wave data [Gurnett et al., 1979] show that the ion acoustic wave intensities are closely correlated with the electron heat flux. This correlation is shown in Figure 9. Detailed studies of electron and ion distribution functions by Dum et al. [1981] also show that the electron heat flux can account for the ion acoustic waves observed by Helios. The electron heat flux

instability therefore seems to provide a reasonable basis for understanding how these waves are generated. However, there are still unresolved difficulties. In some cases ion acoustic waves are observed when T_e/T_i is near one. Under these conditions the ion acoustic mode should be strongly damped. Also, in a few of the cases analyzed by Dum et al. [1981] the ion acoustic mode was found to be stable even though waves were present. The origin of the instability under these unusual conditions remains unresolved. Marsch and Chang et al. [1983], for example, have suggested that an entirely different instability such as the electrostatic lower hybrid instability may be required to explain the origin of the noise under these conditions.

The possible macroscopic consequences of the solar wind ion acoustic waves detected by Helios is unknown. Forslund [1970] suggested that ion acoustic waves in the solar wind could have important consequences for controlling heat conduction in the solar wind. Usually the ion acoustic waves detected by Helios are very weak. The ratio of the electric field energy density to the plasma energy density, $E^2/8\pi nkT$, is only about 10^{-5} to 10^{-7} during intense bursts, and much smaller on the average. Whether such low intensities can have significant macroscopic effects on the solar wind has not been adequately explored.

ACKNOWLEDGEMENTS

The research at the University of Iowa has been supported by NASA through contract NAS5-11279 with Goddard Space Flight Center, Grants NGL-16-001-002 and NGL-16-001-043 with NASA Headquarters, and by the Office of Naval Research through contract N00014-76-C-0016.

REFERENCES

Anderson, R. R., C. C. Harvey, M. M. Hoppe, B. T. Tsurutani, T. E. Eastman, and J. Etcheto, Plasma waves near the magnetopause, J. Geophys. Res., 87, 2087, 1982.

Bardwell, S., and M. V. Goldman, Three-dimensional Langmuir wave instabilities in type III solar radio bursts, Astrophys. J., 209, 912, 1976.

Dehmel, G., F. M. Neubauer, D. Lukoschus, J. Wawretzko, and E. Lammers, Das Induktionsspulen-Magnetometer-Experiment (E4), Raumfahrtforschung, 19, 241, 1975.

Dum, C. T., E. Marsch, W. Pilipp, and D. A. Gurnett, Ion sound turbulence in the solar wind, Solar Wind Four, ed. by H. Rosenbauer, Max-Planck-Institut Report MPAE W100-81-31, Lindau, Germany, 299, 1981.

Fainberg, J., and R. G. Stone, Satellite observations of type III solar radio bursts at low frequencies, Space Sci. Rev., 16, 145, 1974.

Forslund, D. S., Instabilities associated with heat conduction in the solar wind and their consequences, J. Geophys. Res., 75, 17, 1970.

Freud, H. P., and K. Papadopoulos, Oscillating two-stream and parametric decay instability in a weakly magnetized plasma, Phys. Fluids, 23, 139, 1980.

Fuselier, S. A., and D. A. Gurnett, Short wavelength ion waves upstream of the Earth's bow shock, J. Geophys. Res., 89, 91, 1984.

Galeev, A. A., R. Z. Sagdeev, Yu. S. Sigov, V. D. Shapiro, and V. I. Shevchenko, Nonlinear theory for the modulation instability of plasma waves, Sov. J. Plasma Phys. Engl. Transl., 1, 5, 1975.

Ginzburg, V. L., and V. V. Zheleznyakov, On the possible mechanism of sporadic radio emission (radiation in an isotropic plasma), Sov. Astron., AJ 2, 653, 1958.

Goldman, M. V. G. F. Reiter, and D. R. Nicholson, Radiation from a strongly turbulent plasma: Application to electron beam-excited solar emission, Phys. Fluids, 23, 388, 1980.

Gurnett, D. A., and R. R. Anderson, Electron plasma oscillations associated with type III radio bursts, Science, 194, 1159, 1976.

Gurnett, D. A., and R. R. Anderson, Plasma wave electric fields in the solar wind: Initial results from Helios 1, J. Geophys. Res., 82, 632, 1977.

Gurnett, D. A., R. R. Anderson, and D. L. Odem, The University of Iowa HELIOS solar wind plasma wave experiment, [E5a], Raumfahrtforschung, 5, 245, 1975.

Gurnett, D. A., R. R. Anderson, F. L. Scarf, and W. S. Kurth, The heliocentric radial variation of plasma oscillations associated with type III radio bursts, J. Geophys. Res., 83, 4147, 1978.

Gurnett, D. A., R. R. Anderson, and R. L. Tokar, Plasma oscillations and the emissivity of type III radio bursts, Radio Physics of the Sun, ed. by M. Kundu and T. Gergely, IAU, 369, 1980.

Gurnett, D. A., M. M. Baumback, and H. Rosenbauer, Stereoscopic direction finding analysis of a type III solar radio burst: Evidence for emission at $2f_p$, J. Geophys. Res., 83, 616, 1978.

Gurnett, D. A., and L. A. Frank, Ion acoustic waves in the solar wind, J. Geophys. Res., 83, 58, 1978.

Gurnett, D. A., J. E. Maggs, D. L. Gallagher, W. S. Kurth, and F. L. Scarf, Parametric interaction and spatial collapse of beam-driven Langmuir waves in the solar wind, J. Geophys. Res., 86, 8833, 1981.

Gurnett, D. A., E. Marsch, W. Pilipp, R. Schwenn, and H. Rosenbauer, Ion acoustic waves and related plasma oscillations in the solar wind, J. Geophys. Res., 84, 2029, 1979.

Hundhausen, A. J., Coronal Expansion and Solar Wind, Springer, Berlin, Heidelberg, N. York, 1972.

Kaiser, M. L., The solar elongation distribution of low frequency radio bursts, Solar Physics, 45, 181, 1975.

Kennel, C. F., and H. E. Petschek, A limit on stably-trapped fluxes, J. Geophys. Res., 71, 1, 1966.

Kennel, C. F., F. L. Scarf, F. V. Coroniti, E. J. Smith, and D. A. Gurnett, J. Geophys. Res., 87, 17, 1982.

Kurth, W. S., D. A. Gurnett, and F. L. Scarf, High-resolution spectrograms of ion acoustic waves in the solar wind, J. Geophys. Res., 84, 3413, 1979.

Krall, N. A., and A. W. Trivelpiece, Principles of Plasma Physics, McGraw-Hill, 1973.

Lemons, D. S., J. R. Asbridge, S. J. Bame, W. C. Feldman, S. P. Gary, and J. T. Gosling, The source of electrostatic fluctuations in the solar wind, J. Geophys. Res., 84, 2135, 1979.

Lin, R. P., D. W. Potter, D. A. Gurnett, and F. L. Scarf, Energetic electrons and plasma waves associated with a solar type III radio burst, Astrophys. J., 251, 364, 1981.

Marsch, E., and T. Chang, Lower hybrid waves in the solar wind, J. Geophys. Res., 88, 6869, 1983.

Musmann, G., F. M. Neubauer, A. Maier, and E. Lammers, Das Förstersonden-Magneticfeldexperiment (E2), Raumfahrtforschung, 19, 232, 1975.

Papadopoulos, K., On the physics of strong turbulence for electron plasma waves, Proc. Varenna School on Plasma Physics, Pergamon, N.Y., 355, 1978.

Papadopoulos, K., M. L. Goldstein, and R. A. Smith, Stabilization of electron streams in the type III solar radio bursts, Astrophys. J., 190, 175, 1974.

Scarf, F. L., R. W. Fredricks, L. A. Frank, C. T. Russell, P. J. Coleman, Jr., and M. Neugebauer, Direct correlations of large amplitude waves with suprathermal protons in the upstream solar wind, J. Geophys. Res., 75, 7316, 1970.

Scarf, F. L., E. Marsch, W. Pilipp, and D. A. Gurnett, Ion sound turbulence in the solar wind, Solar Wind Four, ed. by H. Rosenbauer, Max-Planck-Institut Report MPAE W100-81-31, Lindau, Germany, 299, 1981.

Stix, T., The Theory of Plasma Waves, McGraw-Hill, N. York, 1962.

Tokar, R. L., and D. A. Gurnett, The volume emissivity of type III radio bursts, J. Geophys. Res., 85, 2353, 1980.

Wild, J. P., Observations of the spectrum of high-intensity solar radiation at meter wavelengths, Aust. J. Sci. Res., 3, 541, 1950.

Wong, A. Y., and B. H. Quon, Spatial collapse of beam-driven plasma waves, Phys. Rev. Lett., 34, 1499, 1975.

FIGURE CAPTIONS

Figure 1 A plot showing the phase velocity of various plasma wave modes in the solar wind for propagation parallel to the magnetic field. Modes with phase velocities below the solar wind velocity, V_{sw}, are strongly Doppler shifted.

Figure 2 The characteristic frequencies of the plasma as a function of radial distance from the sun.

Figure 3 A representative plot of the electric field intensities from Helios-2 showing an electron plasma oscillation event associated with a type III solar radio burst and a period of enhanced ion-acoustic wave activity.

Figure 4 A sequence of reduced one-dimensional electron distribution functions from ISEE 3 [Lin et al., 1981] showing energetic electrons arriving from a solar flare. Electron plasma oscillations occur during the times when the distribution function has a region of positive slope, $\partial f/\partial v_{\parallel} > 0$.

Figure 5 The electric field strength of plasma oscillation events detected by Helios-1 and -2 in association with type III radio bursts. The best fit power law through these points varies as $R^{-1.4 \pm 0.5}$. The solid line shows the electric field intensity corresponding to an electric field to plasma energy density ratio of $E^2/8\pi nkT \simeq 2 \times 10^{-5}$.

Figure 6 Peak and average electric field spectral densities for ion acoustic waves at three representative radial distances from the sun. The spectrum increases in intensity and moves to higher frequencies with decreasing radial distance, usually staying in the range $f_p^+ < f < f_p^-$.

Figure 7 A high resolution frequency-time spectrogram of ion acoustic waves detected by Voyager 2 at 1.66 AU. The ion-acoustic emissions consist of a nearly monochromatic tone with a rapidly varying center frequency.

Figure 8 Measurements of the frequency and wave number of ion acoustic noise detected by ISEE-1 upstream of the Earth's bow shock. The solid curves show the dispersion relation for the ion acoustic mode as a function of the polar angle θ of the wave vector, which is unknown.

Figure 9 A plot of simultaneous measurements of the electric field intensity of ion acoustic waves and the electron heat flux. The field intensity clearly tends to increase as the heat flux increases, suggesting that the ion acoustic waves may be driven by an electron heat flux instability.

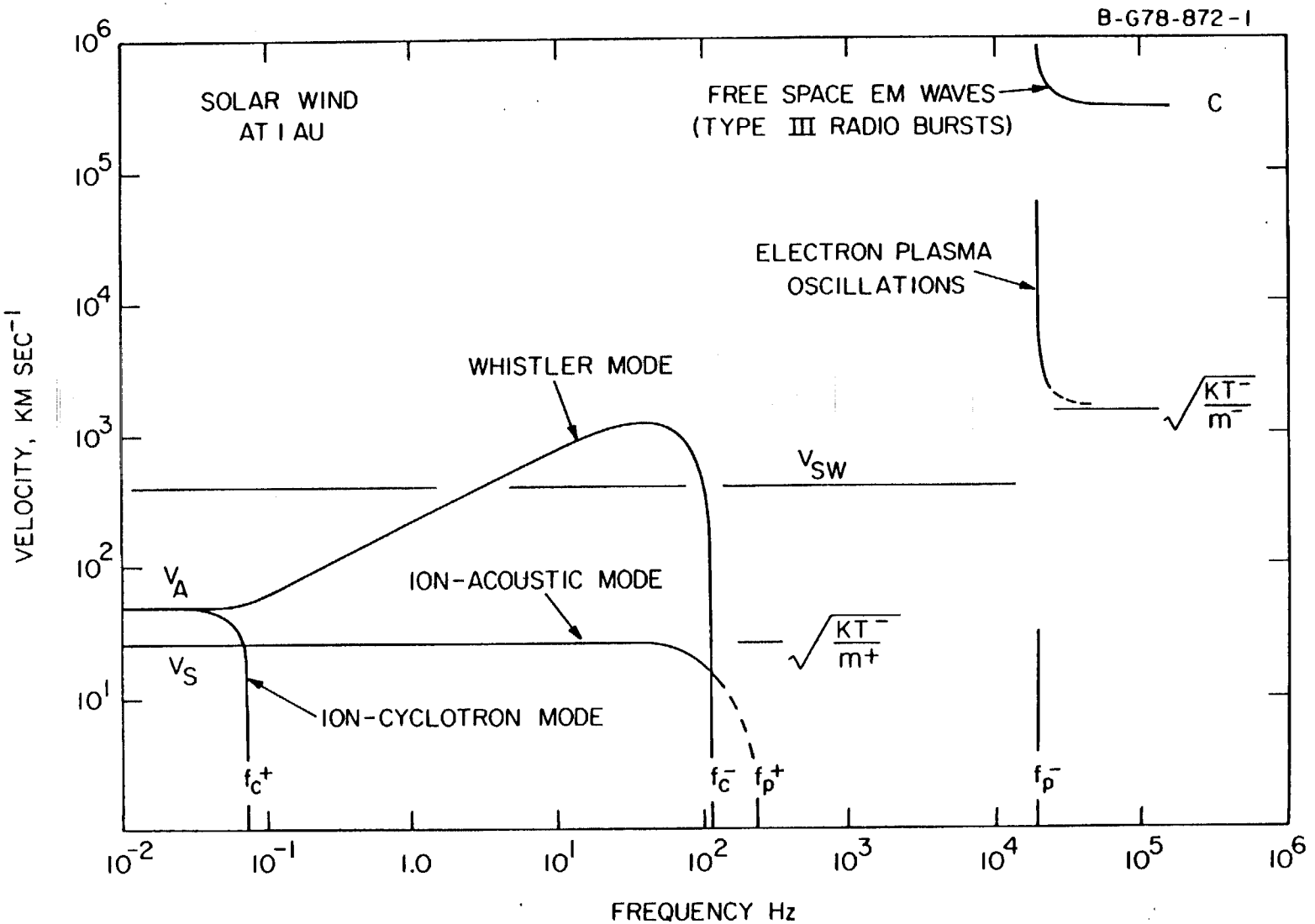
B-G78-872-1
SOLAR WIND
AT 1 AU
FREE SPACE EM WAVES
(TYPE III RADIO BURSTS)
C
ELECTRON PLASMA
OSCILLATIONS
WHISTLER MODE
$\sqrt{\frac{KT^-}{m^-}}$
V_{SW}
V_A
ION-ACOUSTIC MODE
$\sqrt{\frac{KT^-}{m^+}}$
V_S
ION-CYCLOTRON MODE
f_c^+
f_c^-
f_p^+
f_p^-
VELOCITY, KM SEC^{-1}
10^6
10^5
10^4
10^3
10^2
10^1
10^{-2}
10^{-1}
1.0
10^1
10^2
10^3
10^4
10^5
10^6
FREQUENCY Hz

Figure 1

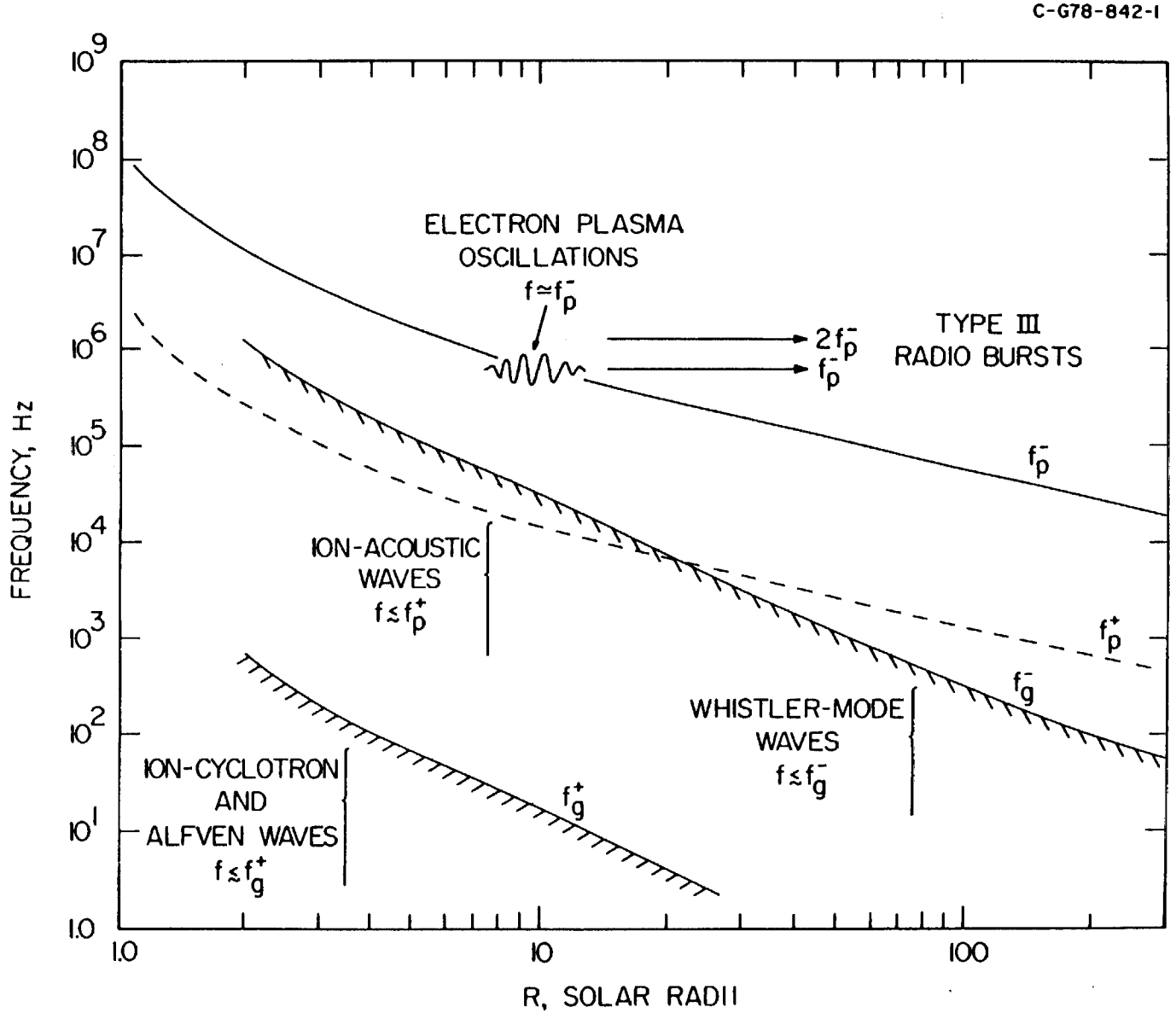
C-G78-842-I
FREQUENCY, Hz
R, SOLAR RADII
ELECTRON PLASMA OSCILLATIONS
$f \simeq f_p^-$
$2f_p^-$
f_p^-
TYPE III RADIO BURSTS
f_p^-
ION-ACOUSTIC WAVES
$f \lesssim f_p^+$
f_p^+
f_g^-
WHISTLER-MODE WAVES
$f \lesssim f_g^-$
ION-CYCLOTRON AND ALFVEN WAVES
$f \lesssim f_g^+$
f_g^+

Figure 2

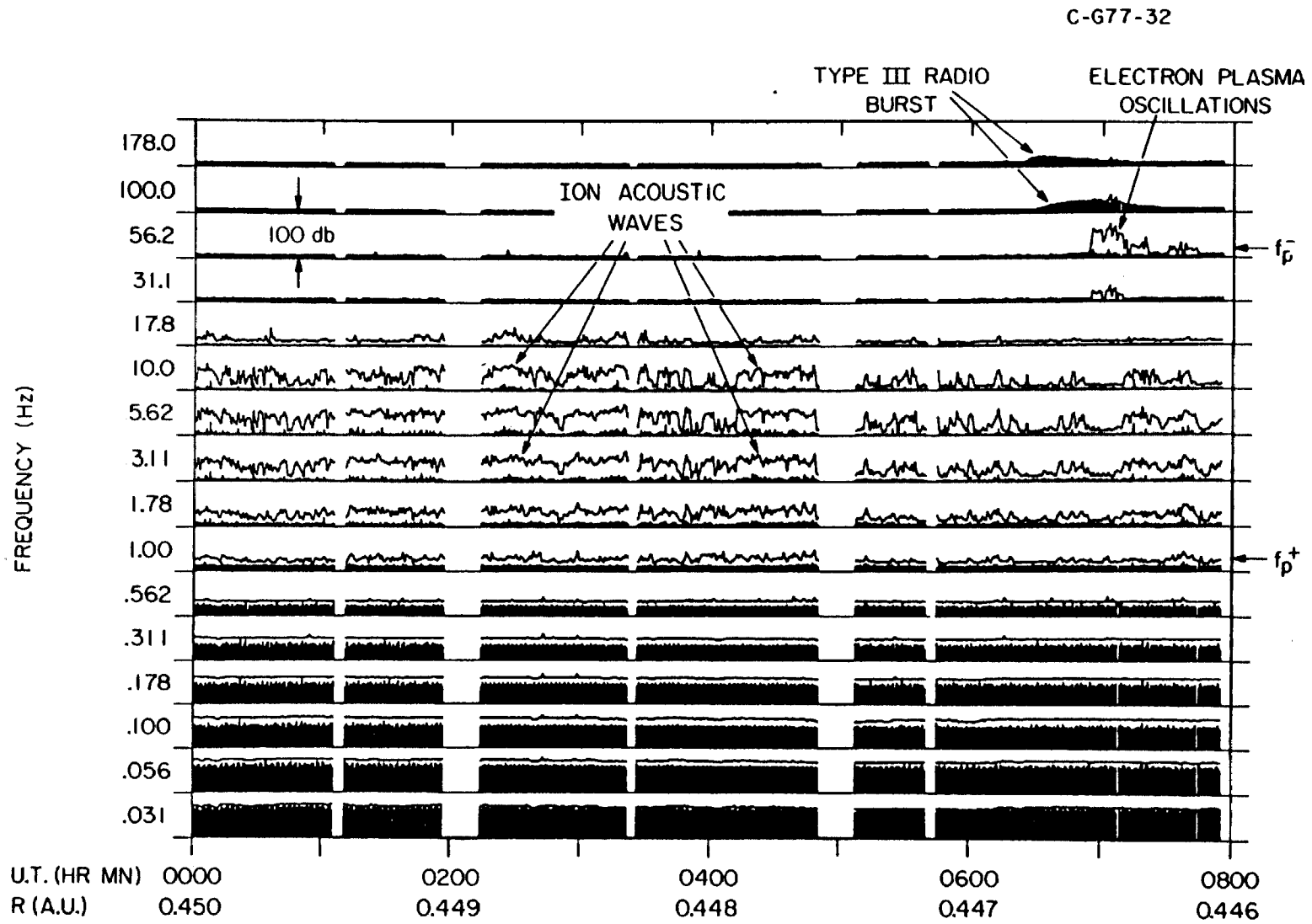
C-G77-32
TYPE III RADIO BURST
ELECTRON PLASMA OSCILLATIONS
ION ACOUSTIC WAVES
100 db
178.0
100.0
56.2
31.1
17.8
10.0
5.62
3.11
1.78
1.00
.562
.311
.178
.100
.056
.031
FREQUENCY (Hz)
f_p^-
f_p^+
U.T. (HR MN) 0000 0200 0400 0600 0800
R (A.U.) 0.450 0.449 0.448 0.447 0.446
HELIOS-2, DAY 92, APRIL 1, 1976

Figure 3

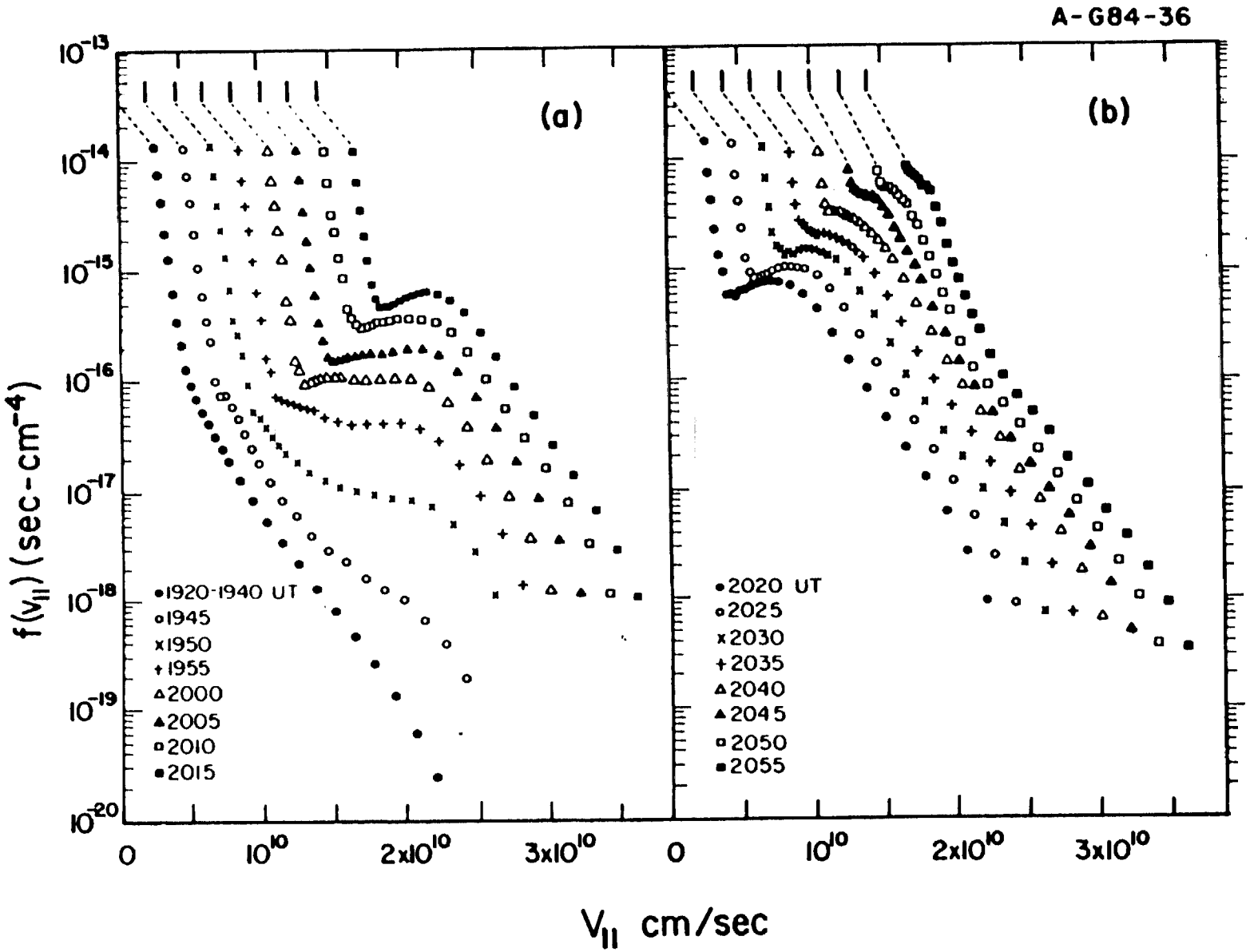
A-G84-36
(a)
(b)
10^{-13}
10^{-14}
10^{-15}
10^{-16}
10^{-17}
10^{-18}
10^{-19}
10^{-20}
$f(v_{||})$ (sec-cm^{-4})
•1920-1940 UT
o1945
x1950
+1955
△2000
▲2005
▫2010
▪2015
•2020 UT
o2025
x2030
+2035
△2040
▲2045
▫2050
▪2055
0
10^{10}
2×10^{10}
3×10^{10}
$V_{||}$ cm/sec

Figure 4

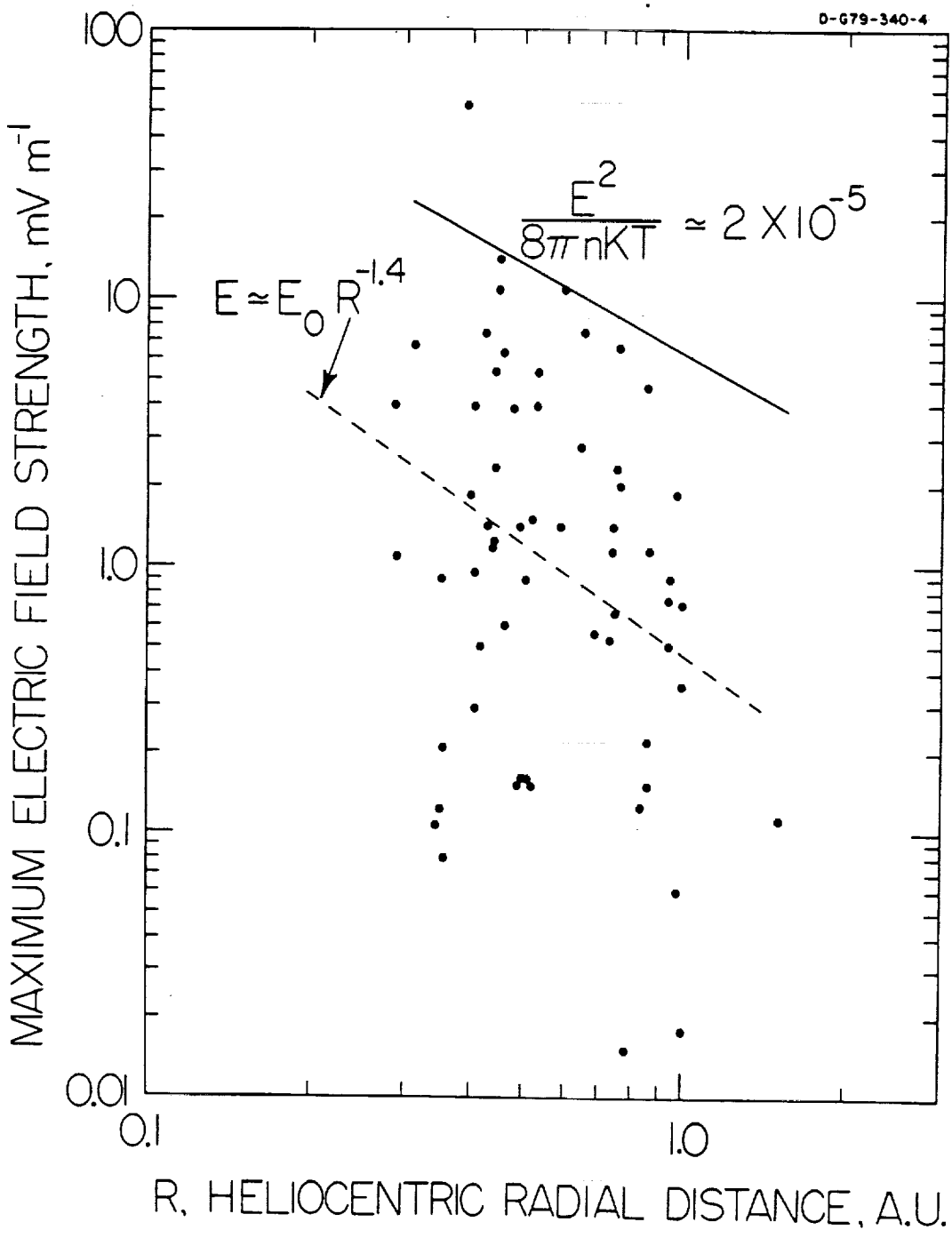
D-G79-340-4
100
10
1.0
0.1
0.01
0.1
1.0
MAXIMUM ELECTRIC FIELD STRENGTH, mV m⁻¹
R, HELIOCENTRIC RADIAL DISTANCE, A.U.
E ≈ E₀ R^-1.4
E²/8πnKT ≈ 2 X 10^-5

Figure 5

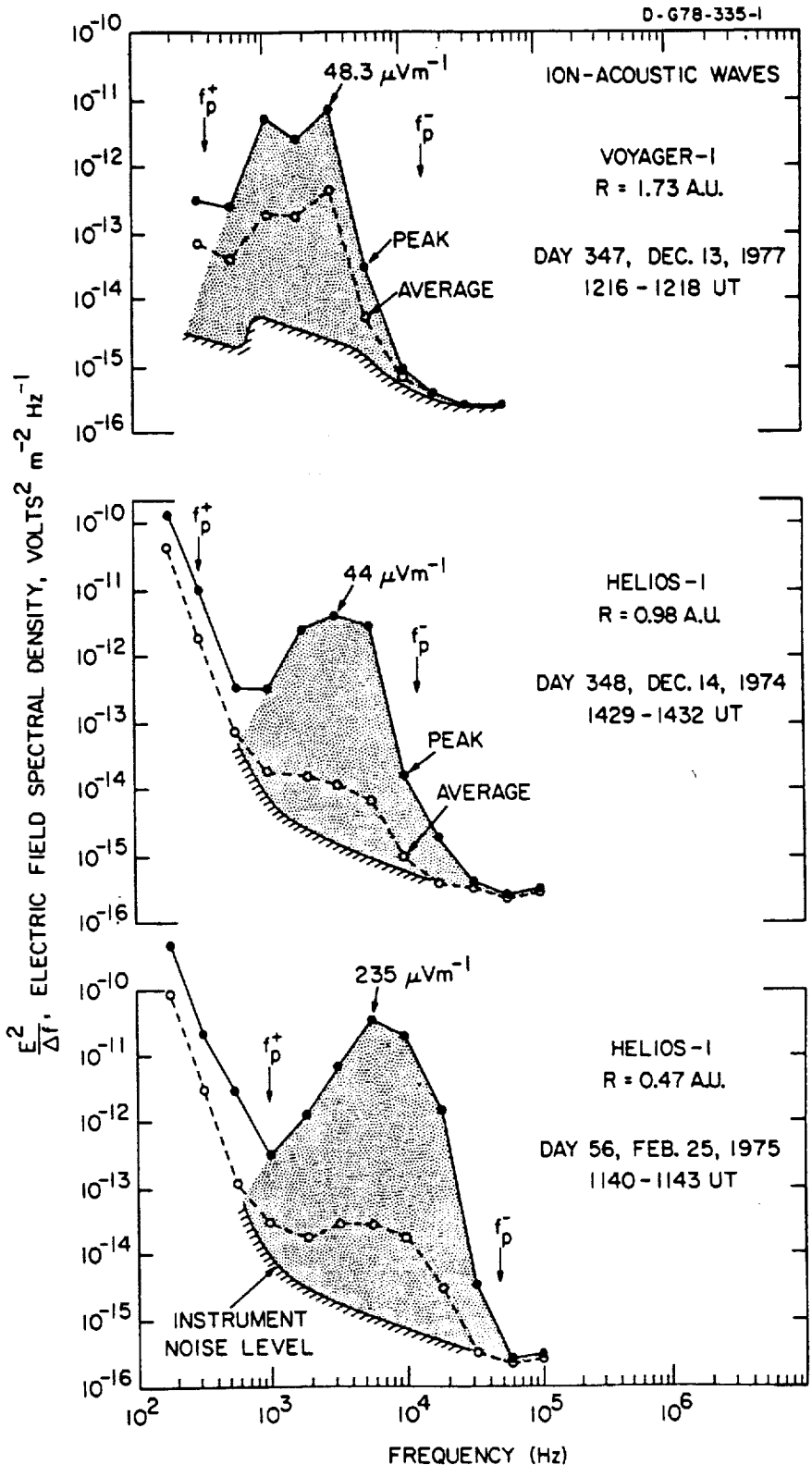
D-G78-335-1
ION-ACOUSTIC WAVES
48.3 μVm⁻¹
f_p^+
f_p^-
VOYAGER-1
R = 1.73 A.U.
PEAK
AVERAGE
DAY 347, DEC. 13, 1977
1216 - 1218 UT
44 μVm⁻¹
HELIOS-1
R = 0.98 A.U.
DAY 348, DEC. 14, 1974
1429 - 1432 UT
235 μVm⁻¹
HELIOS-1
R = 0.47 A.U.
DAY 56, FEB. 25, 1975
1140 - 1143 UT
INSTRUMENT
NOISE LEVEL
$\frac{E^2}{\Delta f}$, ELECTRIC FIELD SPECTRAL DENSITY, VOLTS^2 m^{-2} Hz^{-1}
FREQUENCY (Hz)

Figure 6

A-G78-3-4

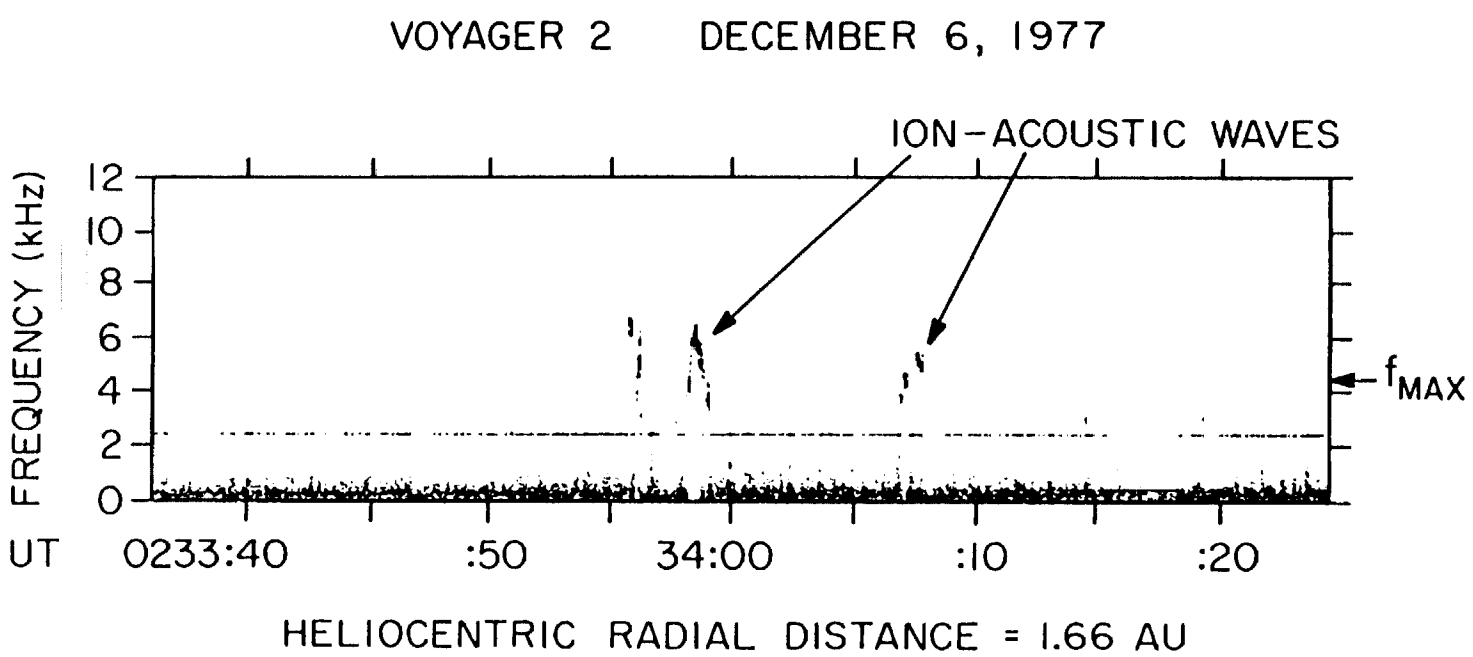

Figure 7

B-G83-233-2

NORMALIZED FREQUENCY VERSUS NORMALIZED WAVE NUMBER
FOR ION ACOUSTIC WAVES

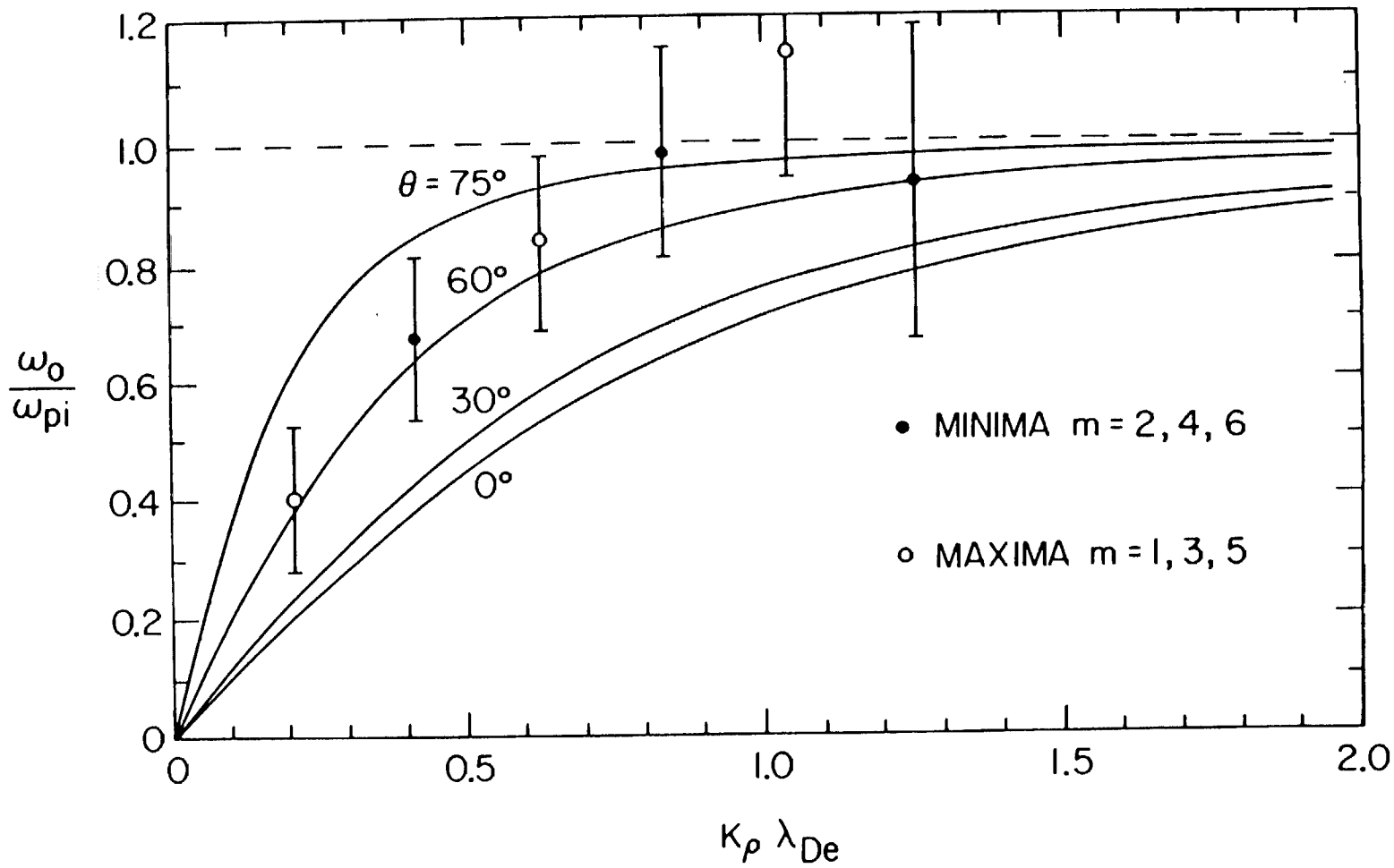

Figure 8

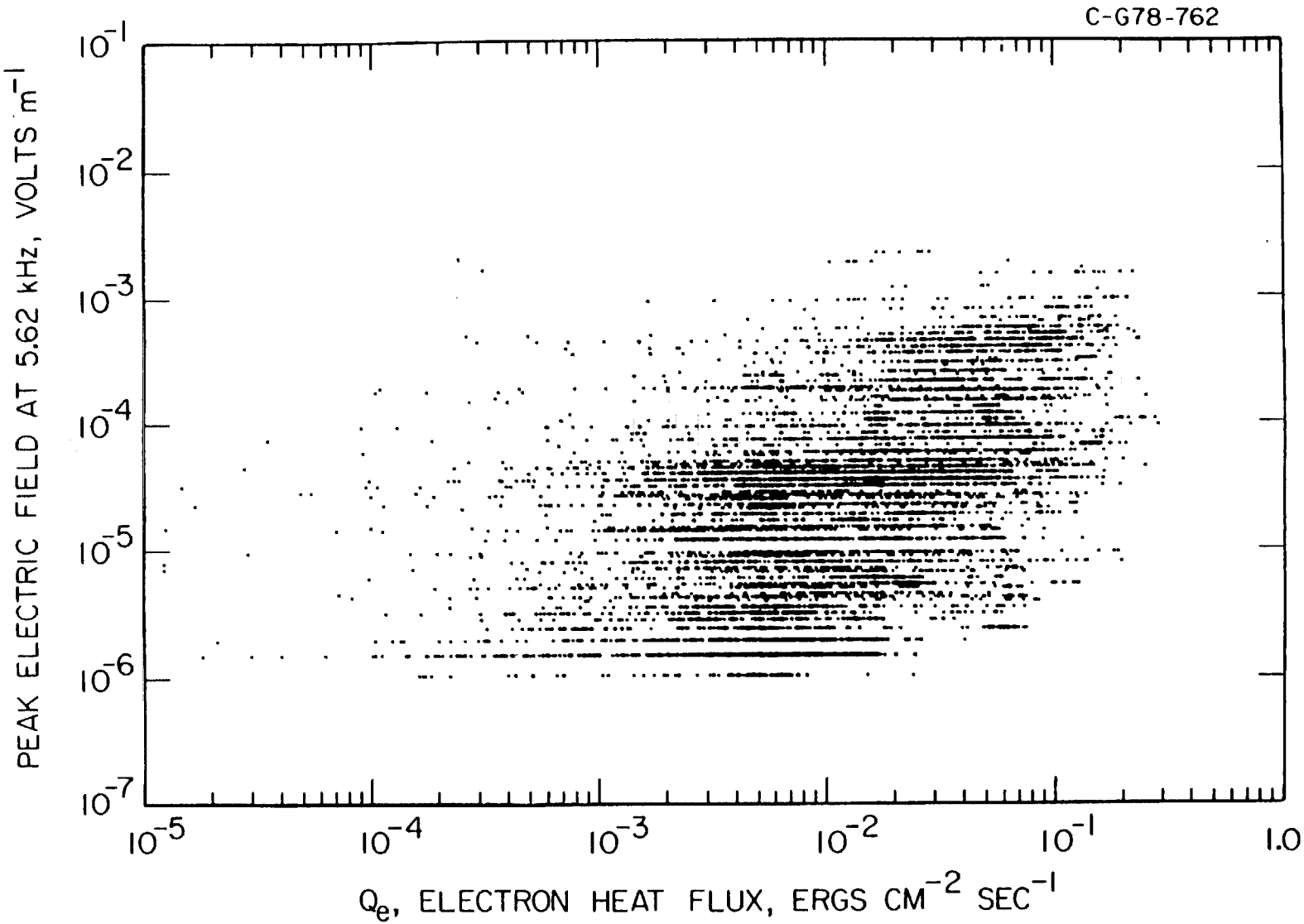
C-G78-762
PEAK ELECTRIC FIELD AT 5.62 kHz, VOLTS m^{-1}
10^{-1}
10^{-2}
10^{-3}
10^{-4}
10^{-5}
10^{-6}
10^{-7}
10^{-5}
10^{-4}
10^{-3}
10^{-2}
10^{-1}
1.0
Q_e, ELECTRON HEAT FLUX, ERGS CM^{-2} SEC^{-1}

Figure 9

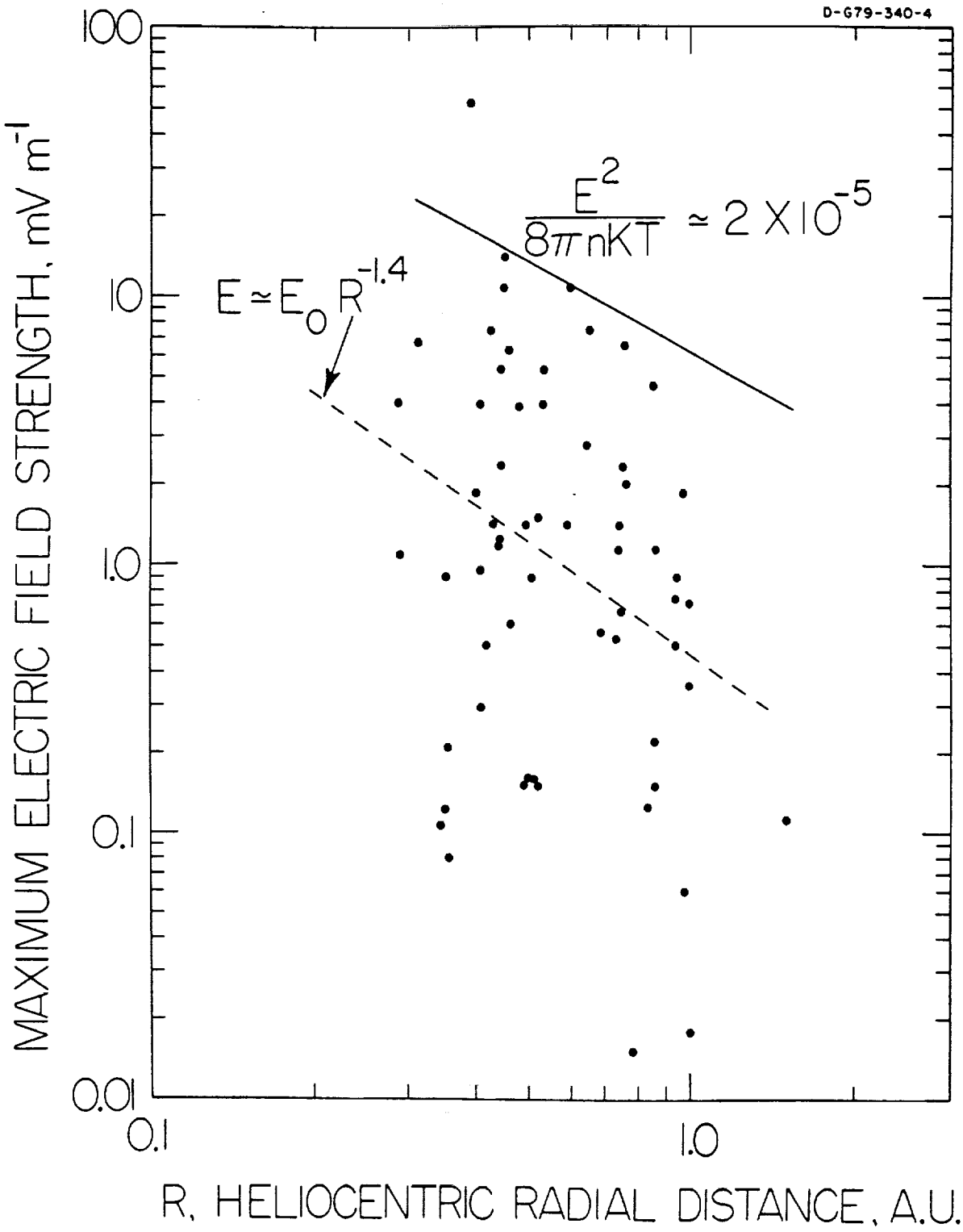
D-G79-340-4
100
10
1.0
0.1
0.01
0.1
1.0
MAXIMUM ELECTRIC FIELD STRENGTH, mV m⁻¹
R, HELIOCENTRIC RADIAL DISTANCE, A.U.
E ≃ E₀ R^-1.4
E²/8πnKT ≃ 2 X 10^-5

10 Jahre HELIOS

10 Years HELIOS

Festschrift aus Anlaß des
10. Jahrestages des Starts der
Sonnensonde HELIOS
am 10. Dezember 1974

Publication Celebrating the 10th Anniversary of the Launch of HELIOS on December 10, 1974

Herausgeber: Herbert Porsche,
Deutscher Projektwissenschaftler HELIOS
im Auftrag des Bundesministers
für Forschung und Technologie

Editor: Herbert Porsche
German HELIOS Project Scientist
on behalf of the Federal Minister
for Research and Technology

BMFT MPG DFVLR MBB JPL GSFC NASA

10 Jahre HELIOS 10 Years
Herausgeber: DFVLR Oberpfaffenhofen,
im Auftrag des Bundesministers für Forschung und Technologie
Redaktion: Herbert Porsche, DFVLR Oberpfaffenhofen
Einbandentwurf: Enno Kaczmierczak, DFVLR Oberpfaffenhofen, nach einer Vorlage von Fa. MBB
Karikaturen: Enno Kaczmierczak
Graphiken: Andreas Hart, DFVLR Oberpfaffenhofen
Für die freundliche Überlassung von Abbildungen wird gedankt:
S. 17, Hirmer-Verlag, München
S. 18, Staatl. Verwaltung Schloß Nymphenburg (Photo: Van der Mülben)
S. 19, Cecile Moessner, München
S. 14, 21, 22, 23, 27, 28, 29, 30, 31, Baader-Planetarium, München
S. 20, Holzforschungsinstitut d. Universität München
Gesamtherstellung: Wenschow Franzis Druck GmbH, München

Oberpfaffenhofen 1984
ISBN 3-88135-156-6

Gurnett

Anderson

Plasma Waves in the Solar Wind: 10 Years of HELIOS Observations

D. A. Gurnett and R. R. Anderson
Department of Physics and Astronomy
The University of Iowa
Iowa City, IA 52242

Elektronen und Ionen sind im Plasma des interplanetaren Raums frei beweglich. Sie können in vielfältiger Weise Schwingungen ausführen und dabei Wellen anregen. Solche Schwingungen und Wellen übernehmen in dem sehr dünnen Plasma, in dem gegenseitige Stöße zwischen den Teilchen höchst selten sind, die Rolle von Energieüberträgern und sorgen für Temperaturausgleich. Um solche Schwingungen und Wellen beobachten zu können, ist HELIOS mit einer 32m langen Meßantenne ausgestattet. Sie ist der Wellensensor für drei Empfänger, die den Frequenzbereich von ungefähr 10 Hz bis 3 MHz abdecken (Experimente 5a, 5b und 5c). Die Antenne spricht auf elektrische Feldschwingungen an. Magnetische Feldschwingungen werden vom Induktionsspulen-Magnetometer (E4) registriert.

Drei prinzipielle Typen von Plasmawellen wurden von der Meßantenne empfangen: (1) elektromagnetische Wellen, die sich durch den freien Raum hindurch ausbreiten, (2) Elektronen-Plasma-Schwingungen, (3) ionenakustische Schwingungen und Wellen.

Elektromagnetische Wellen (1) sind als Licht oder als Radiowellen – je nach ihrer Frequenz und Wellenlänge – allgemein bekannt. Im Plasma können sie sich nur dann fortpflanzen, wenn ihre Frequenz höher ist als eine Grenzfrequenz f_{pe} die man Plasmafrequenz nennt. Sie breiten sich mit Lichtgeschwindigkeit aus. Nur wenn ihre Frequenz knapp über der Plasmafrequenz liegt, wird die Wellengeschwindigkeit (Phasengeschwindigkeit) höher als die Lichtge-

I. Introduction

Previously in this book the reader has been introduced to the idea of a plasma, and to a solar plasma called the solar wind.

Because both the electrons and ions are free to move in a plasma, a wide variety of waves can exist in the solar wind. These waves are called plasma waves. Since the early days of the discovery of the solar wind it has been thought plasma waves play an important role in controlling dynamical processes in the solar wind. Because collisions are extremely rare in the tenuous solar wind, plasma waves play a role similar to collisions in an ordinary gas by scattering particles and providing the dissipation necessary to achieve thermal equilibrium. To detect plasma waves the HELIOS spacecraft included a 32 meter tip-to-tip dipole antenna for the electric field of plasma waves, and a search coil magnetometer for detecting magnetic fields. The signals from the electric antenna were analyzed by three instruments which covered the frequency range from about 10 Hz to 3 MHz. Another instrument analyzed the signals from the search coil magnetometer. In this paper we review results obtained from the HELIOS electric field measurements.

Before discussing the results, it is useful to review the types of waves that can exist in a plasma. Three principal types of plasma waves were detected by the electric field instruments on HELIOS: (1) the free space electromagnetic mode, (2) the electron plasma oscillation mode, and (3) the ion acoustic mode.

The free space electromagnetic mode is the usual electromagnetic mode in free space, of which light and radio waves are common examples.

The electron plasma oscillation is an almost purely oscillatory mode in which the electrons vibrate around their equilibrium position while the ions remain at rest. The resulting charge oscillation produces an electric field but no magnetic field. For this reason these waves are sometimes called electrostatic waves.

The ion acoustic mode is very similar to a sound wave in an ordinary gas, except that the electric field transfers the wave momentum instead of collisions. In contrast to electron plasma oscillations, both the electrons and ions participate in the wave motion. Because of the large inertia of the ions, the propagation speed of the ion acoustic mode is quite slow, normally much less than the solar wind speed, which is typically about 400 km/sec. As in the case of electron plasma oscillations the ion-acoustic mode is electrostatic, with no magnetic field.

Because the electron density decreases with increasing heliocentric radial distance, the laws of physics require that both the electron and ion plasma frequencies decrease with increasing radial distance from the sun. The resulting radial variation is shown in figure page 101. As can be seen the electron plasma frequency, which is the characteristic frequency of electron plasma oscillations and the low frequency limit of the free space electromagnetic mode, increases from

schwindigkeit. Die Plasmafrequenz hängt von der Zahlendichte der Elektronen im Plasma ab. In Erdbahnnähe liegt die Plasmafrequenz bei ungefähr 20kHz, also im Bereich der längsten Radiowellen.

Bei den Elektronen-Plasma-Schwingungen führen die Elektronen Oszillationen um die als ruhend angenommenen, viel schwereren Ionen des Plasmas aus. Die resultierenden Schwingungen der elektrischen Ladung erzeugen elektrische, aber keine magnetischen Felder (elektrostatische Wellen).

Ionenakustische Wellen haben ähnliche Eigenschaften wie Schallwellen in einem Gas, abgesehen davon, daß das elektrische Feld für den Wellenimpuls verantwortlich ist und nicht die gegenseitigen Teilchenstöße. Im Gegensatz zu den Elektronen-Plasma-Schwingungen nehmen an den ionenakustischen Wellen Elektronen und Ionen teil. Die Geschwindigkeit ist niedrig, normalerweise viel kleiner als die Sonnenwindgeschwindigkeit. Ionenakustische Wellen können sich ausbreiten, solange ihre Frequenz kleiner ist als die Ionen-Plasmafrequenz f_{pi}, die ihrerseits im allgemeinen nur 1/20 der Elektronen-Plasmafrequenz f_{pe} ausmacht.

Mit wachsendem Abstand von der Sonne nimmt die Plasmadichte ab. Dadurch werden sowohl die Elektronen-Plasmafrequenz f_{pe} als auch die Ionen-Plasmafrequenz f_{pi} beeinflußt. Die ungefähre Änderung mit dem Abstand gibt Abb. Seite 101. Gegen die Sonne hin wächst die Elektronen-Plasmafrequenz von etwa 20 kHz bis zu mehreren hundert MHz in der Nähe der Sonnenoberfläche an, entsprechend 500 Hz bis einige MHz für die Ionen-Plasmafrequenz.

Durch starke Elektronen-Plasmaschwingungen, die besonders dann entstehen, wenn ein größerer Schwarm schneller Elektronen von der Sonne aus durch den Raum und damit durch das Plasma fliegt, werden elektromagnetische Wellen angeregt (Wellenausbrüche vom Typ III; von Kellogg genauer beschrieben im nächsten Kapitel). Abb. Seite 102 oben zeigt Elektronen-Plasmaschwingungen, die im Zusammenhang mit einem Typ-III-Ausbruch beobachtet wurden. Wie

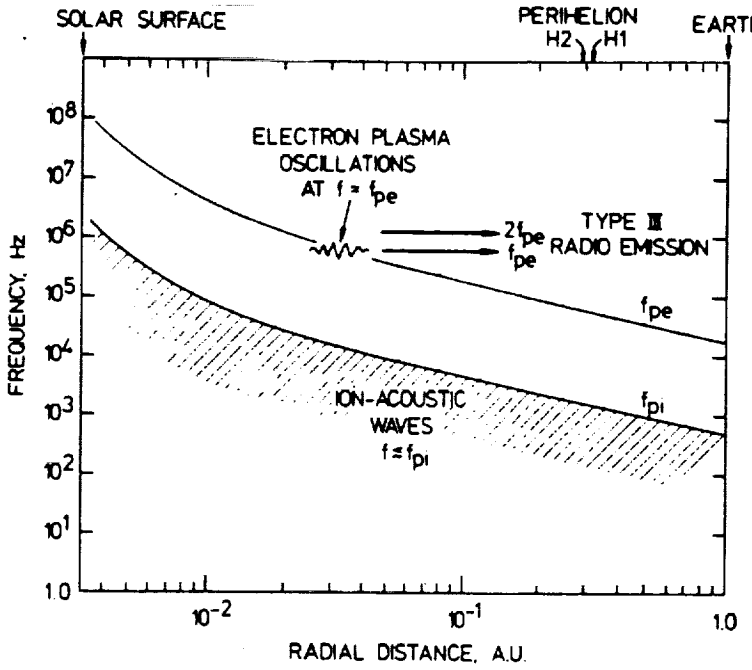

Darstellung der Änderung der Elektronen-Plasmafrequenz f_{pe} und der Ionen-Plasmafrequenz f_{pi} mit dem Abstand von der Sonne für typische Sonnenwindverhältnisse zwischen Sonnenoberfläche und Erdbahn.

A plot of the radial variation of the electron plasma frequency, f_{pe}, and the ion plasma frequency, f_{pi}, for a representative solar wind model from the surface of the sun to the orbit of the earth.

about 20 kHz at the earth's orbit to several hundred MHz at the solar surface. The ion plasma frequency, which is the upper frequency limit of the ion acoustic mode, varies from about 500 Hz at the earth's orbit to a few MHz at the solar surface.

II. Electron Plasma Oscillations and Type III Radio Bursts

Type III solar radio bursts are produced by solar flares at the sun and are characterized by an emission frequency that decreases with increasing time according to a long standing theory, first proposed by Ginzburg and Zheleznyakov (1958), the generation of type III bursts is a two-step process in which (1) electron plasma oscillations are first produced by energetic electrons ejected from a solar flare, and (2) the energy in the plasma oscillation is converted to electromagnetic radiation via a nonlinear coupling process. One of the first notable accomplishments of the HELIOS plasma wave experiment was the confirmation of this basic mechanism.

An example from HELIOS 2 illustrating the simultaneous occurrence of a type III radio burst, electron plasma oscillations, and energetic (20 – 65 keV) electrons from a solar flare is shown in figure on page 102 top. This event occurred on November 22, 1977, following a solar flare that started at 09:46 UT.

According to current ideas the electron plasma oscillations are excited by a beam-plasma instability as the high speed solar wind electrons stream outward from the sun. These plasma oscillations then produce radio waves at a fundamental frequency and the second harmonic via nonlinear coupling to the free space electromagnetic mode. This process is indicated schematically in figure page 101. For a further discussion of the generation of type III bursts, see the accompanying paper by Kellogg.

During the first 10 years of HELIOS observations a total of 238 electron plasma oscillation events were observed in association with type III radio bursts. Most of these events occurred around the time of maximum solar activity, from about 1977 to 1982. The frequency of the plasma oscillation shows a clear tendency to increase with decreasing radial distance from the sun, as would be expected from figure page 101. This trend is

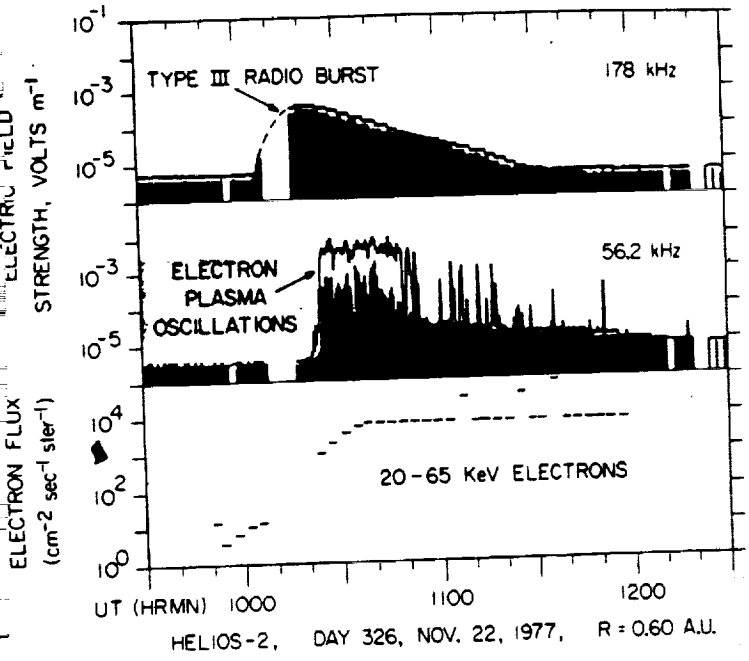

Beispiel für das gleichzeitige Auftreten eines solaren Radio-Ausbruchs vom Typ III, von Elektronen-Plasmaschwingungen und höherenergetischen Elektronen einer Sonneneruption. Man nimmt an, daß die Elektronen-Plasmaschwingungen durch Wechselwirkungen zwischen dem von der Sonne ausgestoßenen Elektronenstrahl und dem Sonnenwindplasma hervorgerufen werden. Die Radiowellen des Ausbruchs sind eine Folge der Plasmaschwingungen, verursacht durch komplizierte Wechselwirkungsprozesse.

An example illustrating the simultaneous detection of a type III solar radio burst, electron plasma oscillations, and energetic electrons arriving from a solar flare. The electron plasma oscillations are believed to be produced via a beam-plasma instability caused by the energetic electrons streaming out from the sun, and the type III radio emission is produced from the electron plasma oscillations via a nonlinear coupling process.

sehr die Frequenz der Elektronen-Plasmaschwingungen bei Annäherung an die Sonne zunimmt, zeigt Abb. Seite 102 unten. Auch die Intensität der Elektronen-Plasmaschwingungen scheint bei Annäherung an die Sonne anzusteigen. Solche Plasmaschwingungen treten nicht notwendigerweise nur dann auf, wenn ein Typ-III-Strahlungsausbruch beobachtet wird. Weit häufiger sind eng lokalisierte Schwingungsgebiete; sie treten gelegentlich mehrmals am Tag auf und stehen nicht in Verbindung mit der Aussendung von elektromagnetischen Wellen.

In den ersten Monaten der Mission HELIOS I wurden erhöhte elektrische Feldintensitäten im Sonnenwind entdeckt. Die Frequenzen lagen zwischen der Ionen- und der Elektronen-Plasmafrequenz in Perioden, die zwischen einigen Stunden und mehreren Tagen lagen. In Abb. Seite 103 sind die Frequenzspektren für drei verschiedene Abstände von der Sonne aufgetragen (die oberste der drei Kurven ist von einer VOYAGER-Beobachtung entliehen, um die Abhängigkeit vom Sonnenabstand besser darstellen zu können). Der Trend ist klar erkennbar.

illustrated in figure page 102 bottom which shows the spectrum of electron plasma oscillation events detected at 0.86, 0.68, and 0.32 AU. The decrease in the electron plasma frequency with increasing radial distance accounts for the decreasing emission frequency of the type III burst as the solar flare electrons move outward from the sun. The intensity of the electron plasma oscillation also tends to increase with decreasing radial distance from the sun. The increase in the field strength with decreasing radial distance probably explains why type III radio bursts tend to be more intense at higher frequencies, which are generated closer to the sun.

Electron plasma oscillations are also observed that are not associated with any detectable type III radio emission. These types of plasma oscillations occur quite frequently, sometimes several times per day. The absence of a detectable radio emission from these events indicates that the plasma oscillations are probably quite localized, and not occurring simultaneously over a large volume of the solar wind, as in the case of the type III related events.

Spektrale Messungen des elektrischen Felds zeigen die Änderung der Elektronen-Plasmafrequenz mit dem radialen Abstand von der Sonne.

Electric field spectrum measurements showing the variation of the electron plasma frequency with radial distance from the sun.

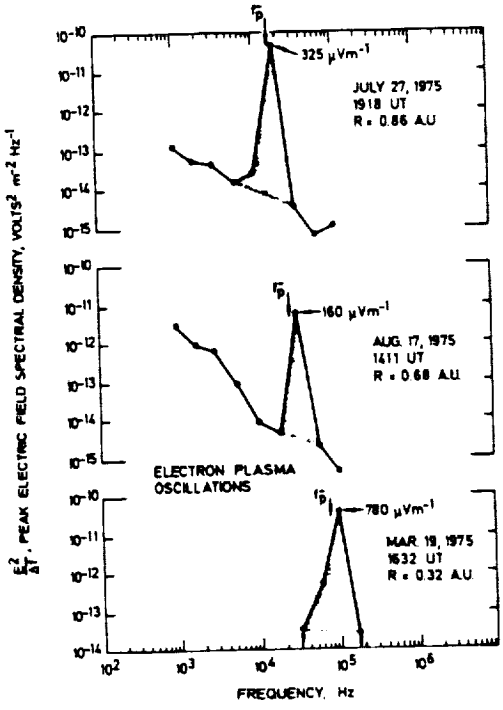

Über die zehn Jahre seit der Entdeckung dieser Art Rauschen konnte überzeugend nachgewiesen werden, daß es sich dabei um ionenakustische Wellen handelt. Diese müßten immer im Frequenzbereich unter der Ionen-Plasmafrequenz liegen, während sie von HELIOS bei Frequenzen registriert wurden, bei denen sie sich eigentlich nicht ausbreiten können. Die Lösung des Problems bietet der Doppler-Effekt. Er ist dafür verantwortlich, daß die Relativbewegung zwischen Sender und Empfänger zu Frequenzverschiebungen führt. Im vorliegenden Fall ist der Sender das Plasma, das die fraglichen Wellen erzeugt. Berücksichtigt man die Sonnenwindgeschwindigkeit und die Bahngeschwindigkeit von HELIOS und rechnet die zu erwartende Frequenzverschiebung aus, so ergeben sich tatsächlich Frequenzen, die geringer sind als die Ionen-Plasmafrequenz. Trotz des langen, ausgedehnten Studiums dieses Phänomens sind noch nicht alle Einzelheiten des Entstehens ionenakustischer Wellen klar. Zwei Faktoren scheinen besonders wichtig zu sein, das Verhältnis der Temperatur der Elektronen zu der der Ionen T_e/T_i (die beiden können stark verschieden sein, weil so gut wie keine Stöße zwischen einzelnen Teilchen auftreten), und der Wärmefluß der Elektronen Q_e. Falls sich herausstellen sollte, daß tatsächlich der Wärmefluß der entscheidende Anregungsfaktor dieser Wellen ist, so muß folgen, daß ionenakustische Wellen eine wichtige Rolle spielen für den Wärmetransport des Sonnenwinds.

Abb. Seite 104 zeigt eine interplanetare Stoßwelle, wie sie von einem der Radiowellenempfänger registriert wurde. Wie bereits auf den Seiten 74 bis 78 und 86 geschildert, stellen Stoßwellen drastische Störungen der sonst einigermaßen geordneten Verhältnisse im interplanetaren Raum dar. In den ersten Monaten der Mission traten sehr wenige solcher Ereignisse auf. Später jedoch, besonders im Maximum des Sonnenfleckenzyklus, waren sie recht häufig.

Die Stoßwelle von Abb. Seite 104 wurde am 30. März 1976, 17:44:00.5 Uhr registriert. In den meisten Frequenzkanälen setzte plötzlich starke

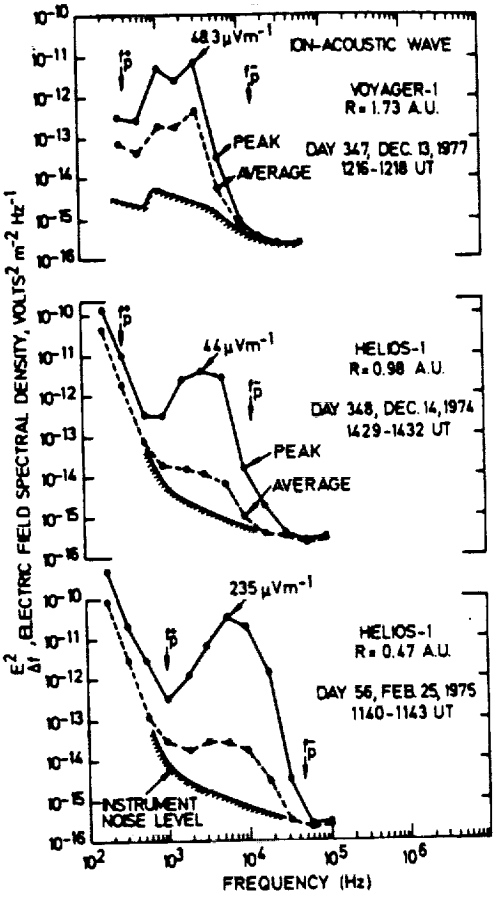

Typische Spektren der Feldstärke ionenakustischer Wellen in verschiedenen Abständen von der Sonne. Man beachte die Anstiegstendenz der Frequenz und der Intensität bei der Annäherung an die Sonne.

Typical spectra of the electric field strength of ion acoustic waves at various distances from the sun. Note the tendency for the frequency and intensity to increase closer to the sun.

III. Ion Acoustic Waves in the Solar Wind

In the first few months of operation of HELIOS 1, enhanced electric field intensities were discovered in the solar wind at frequencies between the ion and electron plasma frequencies. Typically, two or three periods of enhanced electric field intensities occur during each solar rotation, separated by periods of relatively low intensity. The periods of enhanced activity usually last from a few hours to several days. Subsequent investigations showed that the frequency spectrum of the electric field fluctuation depended on the radial distance from the sun, generally increasing in frequency, intensity and occurrence with decreasing distance from the sun. A representative set of electric field spectrums taken at 1.73, 0.98, and 0.47 AU, is shown in figure page 103. The spectrum at 1.73 AU is from VOYAGER 1. The trend toward increasing intensity and frequency with decreasing heliocentric radial distance is clearly evident.

Over 10 years since the discovery of this noise, a fairly convincing case has been made that these waves are ion acoustic waves. At first glance it does not appear that the spectrum is consistent with an ion acoustic wave interpretation, since the peak in the spectrum occurs well above the ion plasma frequency, whereas the ion acoustic mode can only propagate at frequencies below the ion plasma frequency. This difficulty was resolved by Gurnett and Anderson. Because the solar wind velocity is much greater than the ion acoustic speed, they concluded that the frequency should be almost entirely determined by the Doppler shift caused by the motion of the solar wind. The Doppler shift depends on wavelength and is given by $f = V/\lambda$, where λ is the wavelength of the waves.

The minimum wavelength varies from about 60 meters at the orbit of the earth to 20 meters at the HELIOS perihelion. The corresponding maximum frequencies, assuming a nominal solar wind velocity of 400 km/sec, are 6.6 and 20 kHz. These maximum frequencies are seen to be in excellent agreement with the upper cutoff frequency of the observed electric field spectrum.

Even after ten years of study the origin of the solar wind ion acoustic waves is not yet clearly established. Two factors, the electron to ion temperature ratio, T_e/T_i, and the electron heat flux, Q_e, seem to control the intensity of the ion acoustic waves.

These dependences support a theory, first by Forslund (1970), in which the ion acoustic waves are excited by the electron heat flux in the solar

...llenintensität ein. Bemerkenswert ist jedoch, ß bei Frequenzen um 30kHz bereits vor dem ...ntreffen der eigentlichen Stoßwelle erhöhte Feldstärken registriert wurden. Diese erhöhte ...tivität wird als Elektronen-Plasmaschwin... ng gedeutet ähnlich der, die auch bei Typ-III-Ausbrüchen beobachtet wird. Anscheinend strö... n einige Elektronen noch schneller als die ...ßwelle in das umgebende Plasma des Son...nwinds hinein. Die Schwingungen, die danach breitbandig in den meisten Frequenzkanä... einsetzen, sind ihrer Natur nach ionen...ustische Wellen. Ihre Intensität ist jedoch wesentlich höher als die der vorher besproche... n Wellen dieses Typs. Gelegentlich treten auch ...che Wellen bereits vor der eigentlichen Stoßwelle auf. Ihr Auftreten hängt von der Richtung ...s Magnetfeldes ab: steht es ungefähr senkrecht ...r Stoßwellenfront, so können auch Ionen in ...n Bereich vor der Front eindringen und dort Schwingungen anregen. Steht das Magnetfeld ...gefähr parallel, so ist dieser Fluß von Teil...en unterbunden; es treten keine ionenakustischen Wellen vor der Stoßfront auf. Der genaue ...echanismus der Anregung ionenakustischer ...ellen vor der Stoßfront ist allerdings noch nicht in allen Einzelheiten bekannt. Man kann jedoch von HELIOS I weitere Meßdaten erhof... n, die dazu beitragen werden, einige der vie...n offenen Fragen der Dynamik des interplanetaren Raums zu lösen.

...ispiel von Plasmawel...len, hervorgerufen durch ...e interplanetare Stoß...lle. Man nimmt an, daß ...ektronen-Plasma...schwingungen von Elektronen stammen, die in ...n Bereich vor der Stoß...mt strömen. Der plötzli...che Anstieg, der in den meisten Frequenzkanälen ...Augenblick des Eintref...s der Stoßfront regi...iert wird, ist auf ionen...akustische Wellen zurück...zuführen. Diese Wellen ...rden für die stoßwellen...dingte Aufheizung des Plasmas verantwortlich gemacht.

An example of plasma waves produced by an interplanetary shock. The electron plasma oscillations are believed to be produced by electrons streaming into the region ahead of the shock. The intense burst of noise at the shock crossing are believed to be ion acoustic waves. These waves are thought to heat the plasma at the shock.

wind. If the electron heat flux is the origin of enhanced acoustic wave intensities, it is possible that these waves may play an important role in regulating the thermal conduction of heat away from the sun by the solar wind!

IV. Waves Associated with Interplanetary Shocks

Solar flares often produce shock waves that propagate through the solar wind out to the orbit of the earth. These shock waves are called interplanetary shocks and are almost always accompanied by enhanced plasma emissions. During the early part of the HELIOS mission interplanetary shocks were quite rare. However, later, around solar maximum, from about 1977 to 1982, many shocks were observed. The plasma wave signatures associated with these shocks are highly variable and depend on the detailed stucture of the shock. A representative example is shown in figure page 104. This shock was detected by HELIOS 2 on March 30, 1976. The plasma wave signature in this case is quite straightforward and consists of a burst of electron plasma oscillations upstream of the shock and an abrupt broadband burst of electric field noise at the shock crossing, which was at 17:44:00.5 UT ±0.5 sec. The broadband burst of noise gradually decays downstream of the shock over a period of half an hour or more.

Electron plasma oscillations are frequently observed upstream of the earth's bow shock and are known to be caused by a beam of electrons streaming into the solar wind from the shock. The mechanism of exciting the plasma oscillations is essentially the same as the oscillations associated with type III radio bursts, except that the electrons originate from the shock instead of the solar flare. In the region close to the sun, electron plasma oscillations of this type are believed to cause type II and type IV solar radio bursts via a nonlinear coupling process very similar to the generation of type III radio bursts. Interestingly enough, shock-associated electron plasma oscillations are quite rare in the HELIOS data. The March 30, 1976 event is one of the few shocks with upstream electron plasma oscillations. The reasons for the relatively low occurence of upstream electron plasma oscillations ahead of interplanetary shocks is not completely understood, but is probably related to the lower Mach number of interplanetary shocks.

The intense broadband burst of electric field noise at the shock is observed on essentially every interplanetary shock detected by HELIOS. The shape of the spectrum of this noise is very similar to the spectrum of the ion acoustic noise described previously, but is usually more intense, sometimes reaching peak broadband field

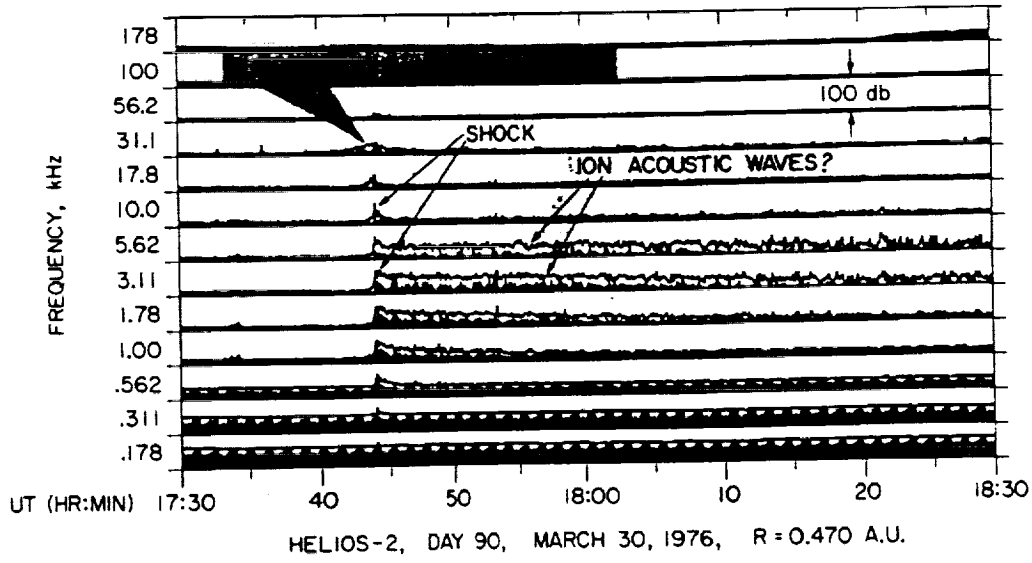

strengths of several mV/m. Because of the similarity to the ion acoustic wave spectrum, it is generally believed that this noise is caused by ion acoustic waves generated in the shock. Studies of similar turbulence in the earth's bow shock indicate that this noise probably plays an important role in heating the plasma at the shock. Because particle collisions in the tenuous solar wind are extremely rare, some type of turbulent process must be present to provide dissipation and to heat the plasma at the shock.

V. Conclusions

This summary of results from the HELIOS plasma wave experiment demonstrates that this investigation has produced many important new results over the 10 year period since HELIOS 1 was launched. This investigation confirmed a basic theory for the generation of type III radio bursts that was first proposed over 20 years ago, and it revealed the existence of enhanced levels of ion acoustic wave turbulence in the solar wind. The long duration of the observations and the extended radial distance coverage provided a vast quantity of data on the temporal and radial variation of these and other plasma wave phenomena over almost an entire solar cycle. The results obtained show that the plasma processes occurring in the solar wind are very complicated and many important questions still remain to be answered. Hopefully, with the continued operation of HELIOS 1 and further study of the existing data some of these questions can be answered.